



Seals/Secondary Fluid Flows Workshop 1997

NASA STI Program . . . in Profile

Since its founding, NASA has been dedicated to the advancement of aeronautics and space science. The NASA Scientific and Technical Information (STI) program plays a key part in helping NASA maintain this important role.

The NASA STI Program operates under the auspices of the Agency Chief Information Officer. It collects, organizes, provides for archiving, and disseminates NASA's STI. The NASA STI program provides access to the NASA Aeronautics and Space Database and its public interface, the NASA Technical Reports Server, thus providing one of the largest collections of aeronautical and space science STI in the world. Results are published in both non-NASA channels and by NASA in the NASA STI Report Series, which includes the following report types:

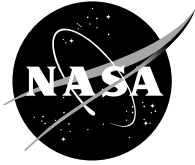
- **TECHNICAL PUBLICATION.** Reports of completed research or a major significant phase of research that present the results of NASA programs and include extensive data or theoretical analysis. Includes compilations of significant scientific and technical data and information deemed to be of continuing reference value. NASA counterpart of peer-reviewed formal professional papers but has less stringent limitations on manuscript length and extent of graphic presentations.
- **TECHNICAL MEMORANDUM.** Scientific and technical findings that are preliminary or of specialized interest, e.g., quick release reports, working papers, and bibliographies that contain minimal annotation. Does not contain extensive analysis.
- **CONTRACTOR REPORT.** Scientific and technical findings by NASA-sponsored contractors and grantees.

- **CONFERENCE PUBLICATION.** Collected papers from scientific and technical conferences, symposia, seminars, or other meetings sponsored or cosponsored by NASA.
- **SPECIAL PUBLICATION.** Scientific, technical, or historical information from NASA programs, projects, and missions, often concerned with subjects having substantial public interest.
- **TECHNICAL TRANSLATION.** English-language translations of foreign scientific and technical material pertinent to NASA's mission.

Specialized services also include creating custom thesauri, building customized databases, organizing and publishing research results.

For more information about the NASA STI program, see the following:

- Access the NASA STI program home page at <http://www.sti.nasa.gov>
- E-mail your question via the Internet to help@sti.nasa.gov
- Fax your question to the NASA STI Help Desk at 301-621-0134
- Telephone the NASA STI Help Desk at 301-621-0390
- Write to:
NASA STI Help Desk
NASA Center for AeroSpace Information
7121 Standard Drive
Hanover, MD 21076-1320



Seals/Secondary Fluid Flows Workshop 1997

Proceedings of a conference held at and sponsored by
Glenn Research Center
Cleveland, Ohio
October 15–16, 1997

National Aeronautics and
Space Administration

Glenn Research Center
Cleveland, Ohio 44135

This research was originally published internally as AST 028 in October 1998.

Note that at the time of writing, the NASA Lewis Research Center was undergoing a name change to the NASA John H. Glenn Research Center at Lewis Field. Both names may appear in this report.

This report contains preliminary findings, subject to revision as analysis proceeds.

Contents were reproduced from the best available copy as provided by the authors.

Contents were reproduced from author-provided presentation materials.

Trade names and trademarks are used in this report for identification only. Their usage does not constitute an official endorsement, either expressed or implied, by the National Aeronautics and Space Administration.

Level of Review: This material has been technically reviewed by technical management.

Available from

NASA Center for Aerospace Information
7121 Standard Drive
Hanover, MD 21076-1320

National Technical Information Service
5285 Port Royal Road
Springfield, VA 22161

Available electronically at <http://gltrs.grc.nasa.gov>

The 1997 Seals Workshop was divided into

- Program Needs and Overviews
- Seals/Secondary Air Management Developments
- Interactive Seals/Secondary/Power stream flows
- Engine Externals
- High Speed Research Sealing Needs
- Engine Design Development Margins, a short course.

The high speed civil transport anticipated sealing needs are published as NASA CP214329/Volume 2

The materials presented in the Programs Overviews covering the High Speed Civil Transport, IHPTET, and the Industrial Gas Turbine developments were not materially different than those presented in the 1996 Seals Workshop, NASA CP-10198, Vol. 1, Oct. 1997; and are not repeated herein. In that same light, the presentation on Advanced Metallic Seals for High Temperature Applications (Layer, Nolan, Swenson) can also be found in NASA CP-10198, Vol.1, p. 307.

The Allison/Rolls-Royce work on the high surface speed application of mechanical seals in engine rim and cavity configurations extends the mechanical sealing effort initiated by Ludwig et al. and Allison Engine in the late 1960's. The much quoted Mechanical Engineering articles by Ludwig and Greiner Nov.and Dec. 1978 still provide a critical path for development.

Development continues on several new sealing concepts as the leaf (EGG), finger (Allied Signal), air/oil (Allied Signal), floating brush (B&C Engr.), rope (NASA), brushes (Westinghouse, Boeing-Rocketdyne, NASA), and floating-T-buffer (Shapiro Assoc.). Each affords its own unique advantages and with the exception of the rope seals, applicable to high speed interfaces. The air/oil seal work represents the only two-phase flow work presented, however there are large opportunities here with the environmental 'O-leakage' sealing requirements, (see also NASA CP 10136, 1993 Seals Workshop, p67).

The work at Pratt-Whitney captures some of the efforts on application of controlled vortices and flow pre-swirl in controlling blade/disc thermal effects. Pre-swirl has been studied extensively as a means of controlling seal rotordynamics (NASA CP series 2133, 2250, 2338, 2409, 2443, 3122, 3344).

Westinghouse continues the successful applications of seal components to industrial gas turbines under the DOE-ATS program with the efficiencies of the 501-G combined cycle approaching 60%.

Boeing/Rocketdyne continues a NASA initiated concept (NASA CP 3092 Vol.II,p78) of applying brush seals to cryogenic turbomachinery.

Miller delineated a multitude of problems associated with engine externals as a secondary air flow problem (1996 Seals Workshop, NASA CP 10198 Vol. 2 , p 477). Engine externals include all components of engine fluid systems, sensors and their support structures. The clean features of the nacelle belie the minefield of opportunities that lie within. The Boeing group presented a discussion of the nacelle compartment venting and its effects on the airplane aerodynamics that continued to explore components in ever increasing details of the engine/nacelle/aircraft system. Pratt-Whitney provided component mounting and operations methods to mitigate in-flight shutdowns and relieve maintenance problems.

Chuck Bentz, Universal Technology Corp., Dayton OH, provided the short course on Engine Development Design Margins. The materials presented rely heavily on many years of experience with military engines their procurement, development problems, maintenance and overall costing. The problems usually stem from application of design margins, available materials and aggressive marketing. Chuck Bentz provided an outline demonstration of these materials and recommends the associated use of the code GASTURB for Windows 95.

TABLE OF CONTENTS

Volume I

ADVANCED SEALS AND SECONDARY AIRFLOW SYSTEMS FOR ALLISON AST John Munson, Allison Engine Company	1
FINGER SEAL: A NOVEL APPROACH TO AIR TO AIR SEALING Gul Arora, AlliedSignal Engines; and Bruce Steinetz and Margaret Proctor, NASA Lewis.....	21
MODELING AND FULL-SCALE TESTING OF AN ASPIRATING FACE SEAL Norman A. Turnquist, GE Corporate Research and Development	39
AIR/OIL SEALS R&D AT ALLIEDSIGNAL M. Rifat Ullah, AlliedSignal Engines.....	59
NASA HIGH TEMPERATURE TURBINE SEAL RIG DEVELOPMENT Bruce M. Steinetz and Margaret P. Proctor, NASA Lewis.....	69
EFFECTS OF 'COOLED' COOLING AIR ON PRE-SWIRL NOZZLE DESIGN J.A. Scricca and K.D. Moore, Pratt & Whitney.....	83
ROTATING BRUSH SEAL S.B. Lattime, M.J. Braun, and F.K. Choy, B&C Engineering Associates, Inc.; and R.C. Hendricks and B.M. Steinetz, NASA Lewis.....	93
EFFECTS OF COMPRESSION, STAGING, AND BRAID ANGLE ON BRAIDED ROPE SEAL PERFORMANCE Bruce M. Steinetz, NASA Lewis; and Patrick H. Dunlap, Jr. and Michael L. Adams, Modern Technologies Corp.	103
ADVANCED METALLIC SEAL FOR HIGH TEMPERATURE APPLICATIONS Terence Nolan, Jeff Swensen, and Jeff Layer, EG&G Pressure Science.....	115
DEVELOPMENT OF A THIN GAUGE METALLIC SEAL FOR GAS TURBINE ENGINE APPLICATIONS TO 1700°F Raymond O. England, EG&G Mechanical Components Research and Development Center	121
LM2500+ BRUSH SEAL CASE STUDY Fred G. Haaser, GE Aircraft Engines	123
ADVANCED SEAL DEVELOPMENT FOR LARGE INDUSTRIAL GAS TURBINES Raymond E. Chupp, Westinghouse Electric Corporation.....	147
BRUSH SEAL ARRANGEMENT FOR THE RS-68 TURBOPUMP SET D. Nunez, D. Ransom, and G. Prueger, Boeing, Rocketdyne Propulsion and Power.....	165
AN ADVANCED HELIUM BUFFER SEAL FOR THE SSME, ATD OXYGEN PUMP Wilbur Shapiro, WSA, Inc.....	197
STABILITY OF THE WAVE BEARING ON AN ELASTIC SUPPORT Florin Dimofte and Theo G. Keith, Jr., The University of Toledo	235
OPTIMIZATION OF TURBINE RIM SEALS J.H. Wagner, D.E. Tew, G.M. Stetson, and J.S. Sabnis, Pratt & Whitney.....	253

NUMERICAL METHODOLOGY FOR COUPLED TIME-ACCURATE SIMULATIONS OF PRIMARY AND SECONDARY FLOWPATHS IN GAS TURBINES A.J. Przekwas and M.M. Athavale, CFD Research Corporation; and R.C. Hendricks and B.M. Steinetz, NASA Lewis.....	269
UNSTEADY ANALYSIS OF TURBINE MAIN FLOW COUPLED WITH SECONDARY AIR FLOW Chunill Hah, NASA Lewis	293
LIQUID ANNULAR SEAL CFD ANALYSIS FOR ROTORDYNAMIC FORCE PREDICTION Jeff Moore and Alan Palazzolo, Texas A&M.....	295
TURBOFAN ENGINE CORE COMPARTMENT VENT AERODYNAMIC CONFIGURATION DEVELOPMENT METHODOLOGY Leonard J. Hebert, The Boeing Company.....	339
ADAPTING ANALYSIS TOOLS TO ENGINE EXTERNALS ANALYSIS Ken Dunkelberg, The Boeing Company.....	363
COMMERCIAL AIRCRAFT MAINTENANCE EXPERIENCE RELATING TO ENGINE EXTERNAL HARDWARE Sharon M. Soditus, United Airlines, San Francisco International Airport	381
737/CFM56-7 AIRCRAFT ENGINE SYSTEMS Steve Wright and Justin Shiosaki, The Boeing Company	397
THE IMPORTANCE OF ENGINE EXTERNAL'S HEALTH Barry L. Stoner, Pratt & Whitney	435
ENGINE DEVELOPMENT DESIGN MARGINS BRIEFING CHARTS Chuck Bentz, Universal Technology Corporation	445

ADVANCED SEALS AND SECONDARY AIRFLOW SYSTEMS FOR ALLISON AST

John Munson
Allison Engine Company
Indianapolis, Indiana

The author will present results obtained to date of a secondary flow study currently being conducted. The purpose of the study is to investigate and report all the ramifications of introducing advanced sealing technology into gas turbine engine secondary flow systems. In addition to detailed cost / benefit results we will also derive seal operational requirements which can be fed into a subsequent advanced seal development program.

Using the current Allison AE3007 engine as a model / baseline we have examined 6 different advanced seal variations. We have settled on a design with 2 advanced seals which results in a savings of 2% in chargeable cooling. The introduction of these advanced seals has resulted in substantial changes to surrounding engine components which will be reported.

SEALS & SECONDARY FLOW WORKSHOP

BACKGROUND

- Completed NASA study, Innovative Seal Technology for Next Generation Subsonic Aircraft - 1994
- Studied current and advanced versions of both T800 and AE3007
- Large gains in both T/W and simultaneous decrease in SFC possible with development and use of advanced seals
- Study provided sealing technology development roadmap
- Study indicated that advanced low leakage seals cannot be readily adapted into existing secondary airflow systems - greater gains were probably possible with a new approach
- Other issues: flight safety, cost, etc., needed to be addressed
- Systems level preliminary design study is currently underway as part of NASA/Allison AST initiative

Background

Allison completed a prior Task Ordered study for NASA Lewis Research Center wherein the potential beneficial effects of incorporating advanced sealing technology into advanced engines was investigated. The LHTEC T801 engine and the Allison AE3007 engines were used as the base line for the study the T801 is a small 1400HP class turboshaft engine, while the AE3007 is a 7000 pound thrust class turbofan. The study was conducted using existing secondary airflow models which were altered slightly to incorporate advanced seals into specific locations which were identified as high leakage areas. Turbine rim blade to vane locations, compressor discharge, etc. were identified as high value areas for advanced seals. Leakage data obtained from rig testing of advanced film riding seals was substituted for existing seals at the selected locations. We found that even the use of as few as 2 advanced seals greatly upset the existing flow systems. A great deal of "tweaking" was required to bring the flow system back into balance, and eliminate excess leakage at other locations so that a comparison could be made between configurations with current and advanced seals. The performance gains that resulted from the use of as few as 4 advanced seals were substantial.

In some cases the adjusted seal clearances could not be achieved in practice. An obvious conclusion was that it would have been better to start the flow system design assuming that the advanced seals would be available for use. The study focused on highlighting the potential benefits of advanced seals and presented a development road map.

The present work underway under the NASA Advanced Subsonic Transport (AST) initiative takes this earlier study one step forward, and will attempt to address other issues such as flight safety in the event of a single or multiple seals failures, cost, weight, and other collateral effects on the engine. The engine cycle being used for the study corresponds to an advanced version of the Allison AE3007.

SEALS & SECONDARY FLOW WORKSHOP

SECONDARY AIRFLOW PD STUDY

- Addresses most issues raised in previous NASA study
- Directed at Allison AE3007/301X - medium size turbofan
- PD study focuses on GG, particularly HP turbine
- **Rules of Engagement:** No change to flow path, blade cooling or LP circuit
- Study goals:
 - Determine operating requirements for advanced seals: pressure, temp., speed deflections/distortion of sealing faces
 - Analytically demonstrate safety of advanced system
 - Identify other potential benefits/concerns which may also accrue as a result of advanced seals/flow system - weight, cost, component life, blade tip clearance etc.

Secondary Airflow Study

The first task of Allison's AST seals task is to expand the scope of the previous study and do a preliminary design of an advanced flow system for the AE3007 engine which incorporates advanced seals. This study will include physical and mechanical constraints. One of the purposes of doing the study is to determine operating requirements i.e. pressures, temperatures, speeds, axial and radial motions, etc., which must be incorporated into the design of the advanced seals.

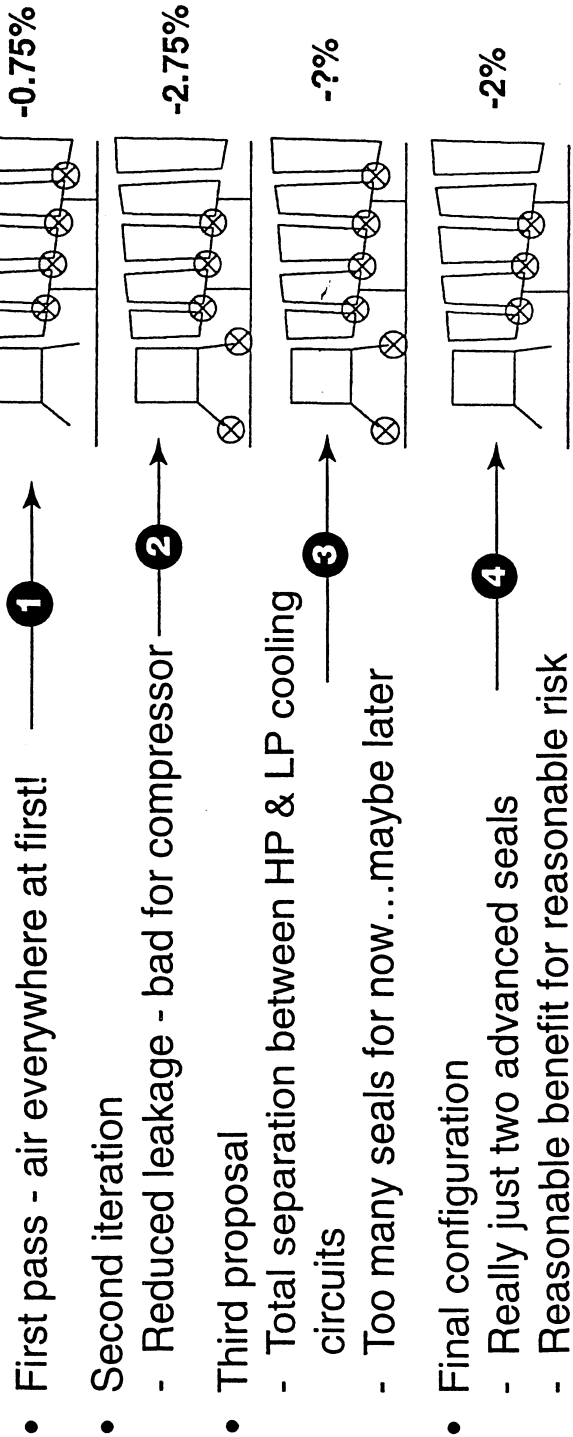
The engine being used for the study is an advanced version of the present Allison AE3007, a medium size turbofan. For the purposes of this study no changes are planned to the flow path aerodynamics. Blade cooling flows will be assumed to be adequate as currently planned, and will remain unchanged for this study. This study is also being confined to the gasifier section of the engine since the earlier study showed that most of the payoffs were in the HP turbine. Our intent is to leave the LP cooling circuit unchanged.

Another purpose of the study is to reveal the effects that use of the advanced seals might have on the rest of the engine HP rotor. We intend to report on cost and weight differences between the present system and the advanced. Flight safety will be addressed as well as the response of the HP rotor to transient operating conditions. What is planned is a systems level study which is as realistic as possible of the planned advanced flow system versus the current.

SEALS & SECONDARY FLOW WORKSHOP

SECONDARY FLOW SYSTEM DESIGN

- Have completed 3 1/2 major iterations with several minor iterations within each to accommodate input from hot section design, flow systems, seal systems, seal technology, heat transfer, lb. stress



Secondary Flow System Design

After several iterations through the proposed advanced secondary flow system we've selected a final design which balances complexity and risk against the benefits of reduced leakage. We are in the final stages of finishing up a detailed assessment of this final design configuration.

Four turbine rim seals were planned initially. These were placed into the secondary flow model with no other adjustments made to the flow system relative to the existing AE3007. This resulted in a net leakage reduction of 0.75%. It was clear we could do better. Much higher pressures were present in the rotor cavities. This caused large air leakage in places which in some cases had ingress from the gas path. In addition a large amount of high pressure air was leaking into the low pressure cooling circuit. Adjustments were made to reduce airflow into the HP turbine cooling circuit, as well as changes from segmented to solid cover plates.

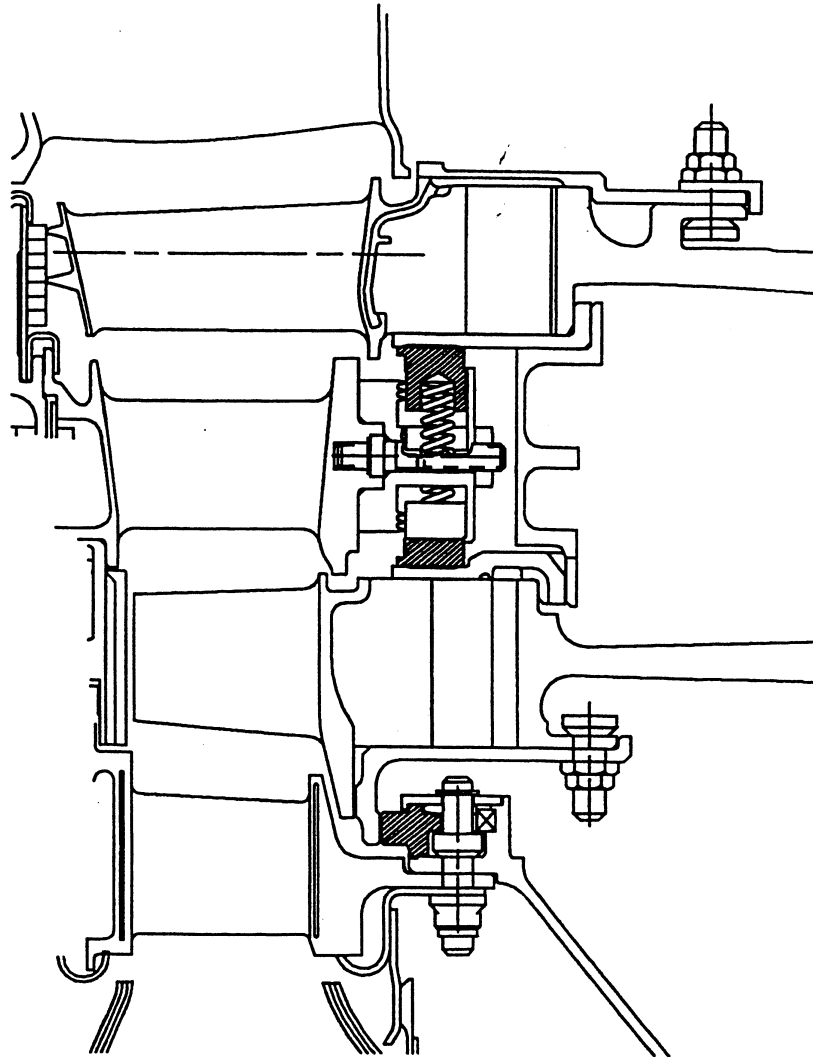
A second major iteration removed the 2B-3V rim seal, and added 2 film riding face seals. This was an effort to prevent leakage of the HP air into the LP cooling circuit. This produced an overall leakage reduction of approximately 2.75% and did totally separate the HP and LP cooling circuits. Unfortunately the amount of air required through the compressor ID rotor bleed to feed the LP circuit was excessive.

A third proposal shown in the figure would have conceivably solved the compressor problem. Although this probably would have resulted in even greater leakage reduction the proposal was not evaluated due to flight safety concerns, and the sheer complexity and risk trying to introduce so many advanced seals at one time into the engine.

The result was the forth configuration which balances risk and benefits. Allison has concentrated on developing this final configuration.

SEALS & SECONDARY FLOW WORKSHOP

MECHANICAL CONFIGURATION



Mechanical Design

While the secondary airflow iterations were being accomplished, mechanical design / layout work was done in parallel to assure that the proposed seals could in fact be incorporated into the planned locations. All the advanced seals considered for this engine were various forms of film riding seals. Shown in the figure are both face and circumferential type film riding seals. Also shown in the figure, but not so obvious are other adaptations which had to be made to accommodate the seals, and maintain the low leakage capability of the advanced seals. The use of solid cover plates, instead of segmented is one of the major adaptations required. These are used both to reduce airflow between the blades, and in some cases to provide a contiguous mating surface as well for the seals.

This is also a good place to also note that the current configuration also satisfies the initial requirement that the airfoils be unchanged. Blades and vanes get their cooling air separately from the interstage cavity purge air. The new flow system has been designed so that a single or multiple seal failure will not effect airfoil cooling thus satisfying at least in part the requirement for flight safety.

Allison has estimated that if blade cooling flows are excluded that it presently takes approximately 4% of cycle air to keep the HP turbine cavities purged. The arrangement shown in the figure saves approximately 50% of this flow.

SEALS & SECONDARY FLOW WORKSHOP

RIM SEAL REQUIREMENTS

Turbine rim seals:

	1V - 1B	1B - 2V <i>2V</i>	1V - 1B <i>2V - 2B</i>
Temp. °F (max source)	1048	1108	1108
ΔP (max. psid)	25.9	28.8	115.8
ΔP (min. psid)	0.02	0.57	6.28
Radial excursion (in)	.04 - .09	.08 - .13	.02 - .08
Axial excursion (in)	-.04 - +.20	-.03 - +.13	-.04 - +.19
Max speed (ft/sec)	1150	1050	1050

- Table shows total excursions due to thermal, mechanical, tolerance, etc.
- Less radial excursion than axial, but axial and/or radial must be accommodated in mechanical design
- Need to define acceptable leakage

Seal Requirements

As the study proceeds, we expect to derive in some detail requirements for the advanced seals which can then be used to guide subsequent development activities. At present we have been able to determine some gross operating parameters for the seals based on the expected pressures and temperatures for the mechanical configuration previously indicated.

The figures given in the table are derived from the secondary flow model, heat transfer results, and AE3007 engine limit stack analysis and are therefore believed to be very representative of an engine with advanced seals installed. Not yet defined are more detailed results of potential distortions of the initially flat, rotating, seal mating rings. We expect that due to thermal gradients, rotation, loading from blades, etc. the initially flat seal mating rings will not remain that way. The result will certainly be some amount of coning, and circumferential out of flatness which the seals will have to accommodate. We plan on obtaining these results from a structural finite element analysis of these parts. This work is presently underway.

It is clear from the differential pressure values presented in the table that a purely hydrostatic seal will not be practical for these proposed applications. While adequate differential pressure is available at the maximum power point, it is essentially zero at idle. An aircraft, particularly a regional airliner would be expected to spend about 30% of its time in what is essentially an idle mode, e.g. ground idle, taxiing, flight idle for descent, etc. The conclusion is that a hydrodynamic seal capable of dealing with relatively large distortions is required to be successful in the proposed applications.

SEALS & SECONDARY FLOW WORKSHOP

HEAT TRANSFER STUDY

- Utilized existing AE3007 models for basis of study
- Modified model to simulate geometry and flows resulting from new seals
- Adjusted secondary flows until no ingress predicted anywhere
- Starting point for analysis
 - Effective seal leakage increased via bypass holes to provide required flows
 - Analysis shows large temperature reductions throughout rim cavity area - over cooled
- Tried parametric analysis
 - Ran analysis at design seal flow
 - Ran at mid point between first two points
- OK from heat transfer to run at leakage flows expected from seals. Some local hot spots created, but manageable within present design and materials

Heat Transfer Study

Existing AE3007 heat transfer models were used for thermal modeling of the HP turbine rotor areas effected by the new seals. Although it does not show in the geometry output files, these models have been modified to simulate the new advanced seal configuration.

The starting point for this work was again the secondary airflow model. Interstage cavity purge airflows were increased until the model no longer predicted ingress. This required bypass holes around the advanced seals, as they could not be made to provide the increased flow the model predicted would be required. The heat transfer model indicated that we could get by with a great deal less airflow. We were predicting temperature reductions of almost 200°F less than the current AE3007 in some locations.

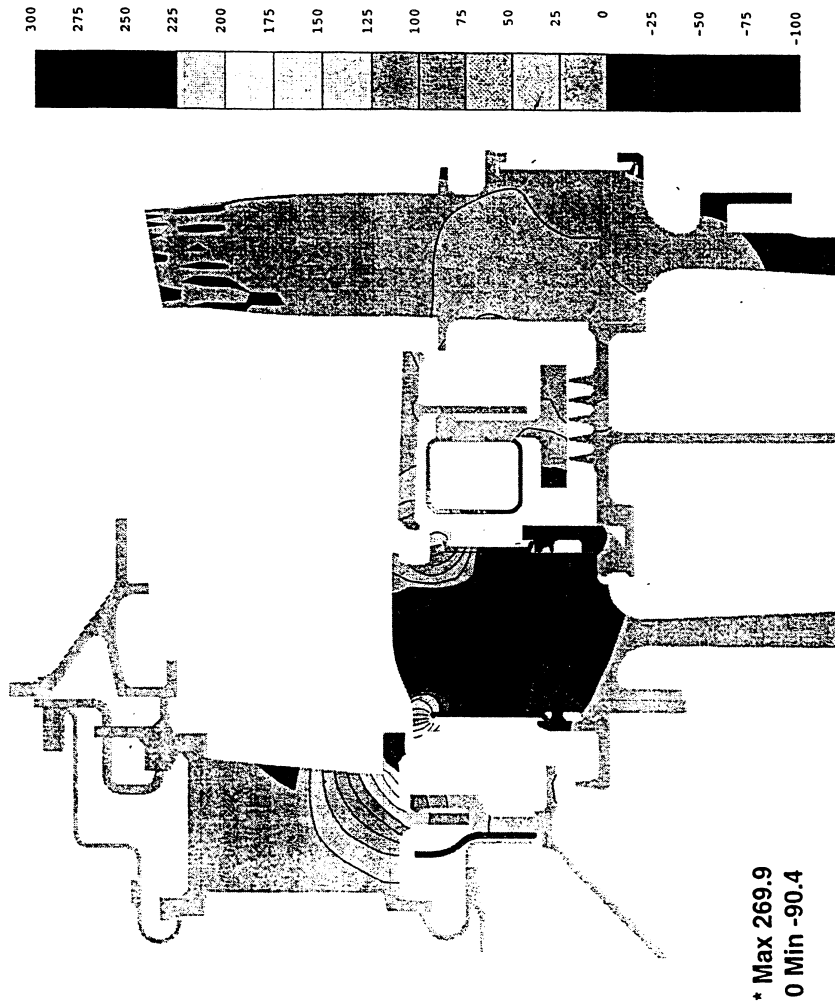
We next ran a case with airflow reduced to an intermediate level halfway between the predicted no ingress airflows, and the airflows which would result with as predicted advanced seal leakages. This result also showed that we were in some cases still over cooling and wasting air. However it also pointed out that air was escaping through the second row of blades via the still segmented rear cover plate.

A final iteration was done using the as predicted seal leakages with no bypass holes. Secondary flow revised the airflow predictions based on a solid 2B rear cover plate. This final result was deemed acceptable. Leakage was reduced by approximately 2% versus the current AE3007. Temperatures throughout the HP rotor are essentially unchanged versus the current design with 2 exceptions.

SEALS & SECONDARY FLOW WORKSHOP

HEAT TRANSFER RESULTS

AST HP Turbine Temperatures
 Minus AE3007 HP Turbine Temperatures
 Steady State MTO, SLS, 73F Day, 175KCAS



Heat Transfer Results

The chart depicts predicted temperatures for the HP rotor relative to the existing AE3007 at a maximum power point. Large areas of the turbine are essentially unchanged with respect to temperatures with the exception of the 1B attachment, and the 1V platform. The current AE3007 experiences slight ingress at the 1B attachment area. Higher rotor air pressure resulting from use of the advanced seals completely reverses the situation from slight ingress to slight leakage. This in turn results in a decrease in temperature in this area of approximately 90°F.

On the other hand the low leakage provided by the 1V-1B rim seal results in increased ingress in this now tiny interstage cavity. This ingress results in a predicted increase of approximately 270°F of the trailing edge of the 1V platform. This was judged to be acceptable as the current vane is operating well within accepted material limits on the current AE3007.

Based on the results, heat transfer finds the current configuration, seal leakages, and air flows acceptable.

SEALS & SECONDARY FLOW WORKSHOP

REMAINING TASKS

- Determine rotating component lives due to new thermal distribution in parts
- Determine expected seal distortion to feed into future seal design work
- Run transient analysis to determine effect on blade tip clearance during engine transients
- Run failed seal condition
 - Present flow system designed around leakage characteristics of advanced seals
 - Recognizes that potential ingress due to failed seal is not immediately fatal - need to reliably detect failed seal condition
 - Flows to airfoils will be unaffected by single or multiple seal failures
- Compile results and report

Remaining Work

Most of the remaining work involves determination of stresses and deflections in the HP turbine rotor components. The estimated deflections of the seal mating surfaces can be used as design requirements for future advanced seal development activities. We also plan to run a 0-max-0 type transient to determine what effects the new seals / flow system design have on turbine blade tip clearances. There had been some concern that the new design would have a tendency to thermally isolate the turbine rotor and would aggravate the tip clearance control problem. Based on the results so far, however it does not appear that the bulk turbine rotor temperatures are much different than the current AE3007, so this may not be a problem.

Another remaining task is to run a multiple seal failure case. These analyses will enable us to determine the potential effects of a seal failure relative to flight safety concerns. The best outcome would be that the engine would simply experience an increase in leakage which would be detectable as a sudden increase in fuel consumption. The engine design group has allowed that any detectable failure which does not cause immediate catastrophic consequences, i.e. the engine could continue to operate at least to the end of the planned flight, is an acceptable failure mode. The present flow system design does insure the integrity of the airfoils in the event of seal failure.

SEALS & SECONDARY FLOW WORKSHOP

SUMMARY

- Have demonstrated mechanical feasibility
- Have demonstrated thermal feasibility
- Advanced seals had only minor effect on engine emissions
- Slightly higher NOx predicted, but lower CO and unburned hydrocarbons
 - Higher CDT and longer combustor residence time mostly responsible for effect on emissions
 - NOx increase almost offset by decrease in fuel flow due to less parasitic leakage

Summary of Results to Date

At this point we have demonstrated that it is feasible to place advanced film riding seals close to the HP turbine blade / vane overlap gaps and thus directly control leakage through these points. This is a fundamental change to the way ingress is prevented in all present gas turbine engines.

We have also completed a parametric thermal model of the proposed mechanical arrangement and determined that predicted temperatures are within acceptable limits for the current materials. We note that in some areas the advanced seals and new secondary airflow system have resulted in large (>25°F) changes in predicted metal temperatures. We plan to take this analysis one step further and determine what effect the changed temperature changes have if any on component life.

Finally we have tried to assess the effect on emissions due to introduction of the advanced seals into the engine. We adjusted the AE3007 engine cycle to reflect the predicted reduction in leakage due to the advanced seals at the 4 ICAO points. These points were then used in an emissions model and the results compared to the existing AE3007. We found that there was only a slight effect on emissions due to advanced seals. Higher CDT and longer combustor residence time increased NOx (0.72%), which was partly offset by a reduction in fuel flow. CDT and longer residence time resulted in reduced CO (3.47%) and unburned hydrocarbons (2.91%). The predicted SAE smoke number was not effected since it is already small, and prediction accuracy is only $\pm 3\%$.

FINGER SEAL: A NOVEL APPROACH TO AIR TO AIR SEALING

Gul Arora
AlliedSignal Engines
Phoenix, Arizona

and

Bruce Steinetz and Margaret Proctor
NASA Lewis Research Center
Cleveland, Ohio

The gas turbine industry uses a variety of sealing mechanisms to contain and direct secondary flows into and around components for cooling, and to limit leakage into and from bearing and disk cavities. The function of these seals is very important to the component efficiencies and attendant engine performance.

Most of these seals are labyrinth seals, which are high-leakage seals that are costly to manufacture. In recent years, brush seals have been introduced which have demonstrated significantly reduced leakage, although they are still expensive and have exhibited wear and hysteresis difficulties. A new innovative concept called finger seal, patented by AlliedSignal, has demonstrated leakage similar to brush seals and is cheaper. The finger seal is comprised of a stack of precision photo-etched sheet metal elements, which allows intricate features to be made at very low cost and with the potential to resist wear and provide the compliance necessary to accommodate rotor excursions. Initial testing in the high-speed/high-temperature seal test facility, at the NASA Lewis Research Center, has corroborated the finger seal performance. The testing also revealed hysteresis problems with the current design.

A NASA funded research project is in progress to correct the functional deficiencies of the finger seal and to refine its features to provide sufficient seal life for commercial transport engines and other long-life applications. This research will benefit the aeronautical gas turbine industry as a whole in terms of fuel consumption, operational characteristics, and cost.

The first phase of this research to reduce finger seal hysteresis has been in progress for the last one year. This paper presents the results of this research to date.

In future the research program will address seal performance, manufacturing, cost and life issues. The research program is expected to be completed by December 1998.

FINGER SEAL IS A REVOLUTIONARY NEW CONCEPT IN SEALING TECHNOLOGY

KEY FEATURES

- o LOW AIR LEAKAGE SIMILAR TO BRUSH SEALS
- o AIR LEAKAGE 20 TO 40 PERCENT THAT OF A LABYRINTH SEAL
- o LOW COST: ABOUT 20 TO 50 PERCENT THAT OF A CONVENTIONAL LABYRINTH OR BRUSH SEAL
- o HIGH SPEED, PRESSURE AND TEMPERATURE CAPABILITY

EXPECTED SYSTEM BENEFITS TO PROPULSION ENGINES

- o 1 TO 2 PERCENT SAVING IN ENGINE AIR FLOW
- o 0.7 TO 1.4 PERCENT REDUCTION IN SPECIFIC FUEL CONSUMPTION
- o 0.35 TO 0.7 PERCENT REDUCTION IN DIRECT OPERATING COST

UNCLASSIFIED

UNCLASSIFIED

ALLIEDSIGNAL IS DEVELOPING FINGER SEALS UNDER TWO CONTRACTS

NASA CONTRACT GOALS:

- o LOW COST: 20 % THAT OF BRUSH SEAL
- o AIR TEMPERATURE: 1000 F
- o DIFFERENTIAL PRESSURE: 100 PSID
- o SURFACE SPEED: 1100 FT/ SEC

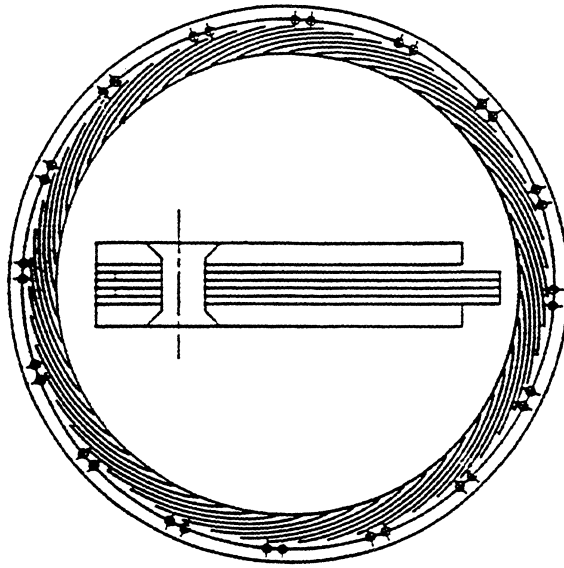
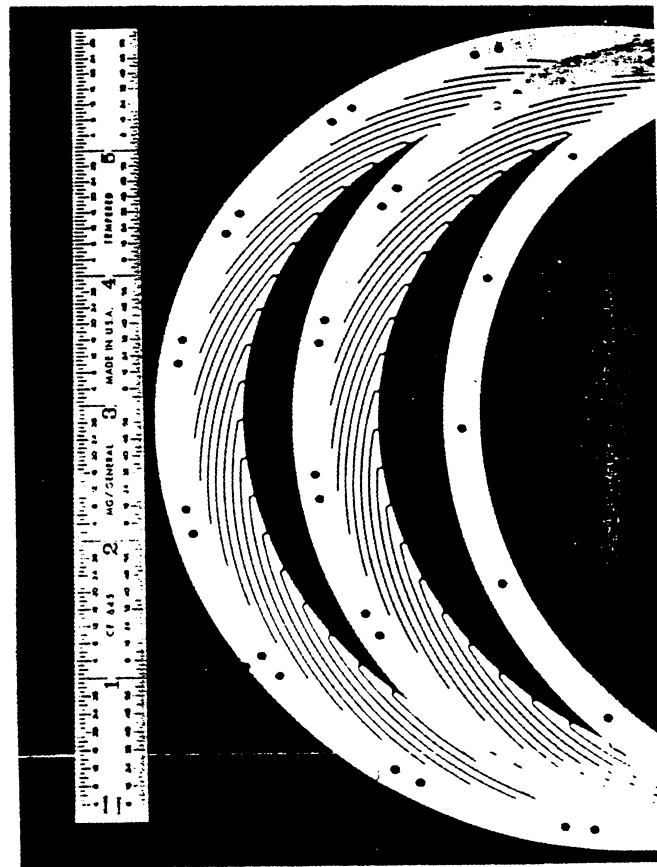
NAVY CONTRACT SOALS

- o LOW COST: 20-50 % THAT OF BRUSH SEAL
- o AIR TEMPERATURE: 1500 F
- o DIFFERENTIAL PRESSURE: 160 PSID
- o SURFACE SPEED: 1500 FT/ SEC

UNCLASSIFIED

UNCLASSIFIED

FINGER SEAL CONFIGURATION

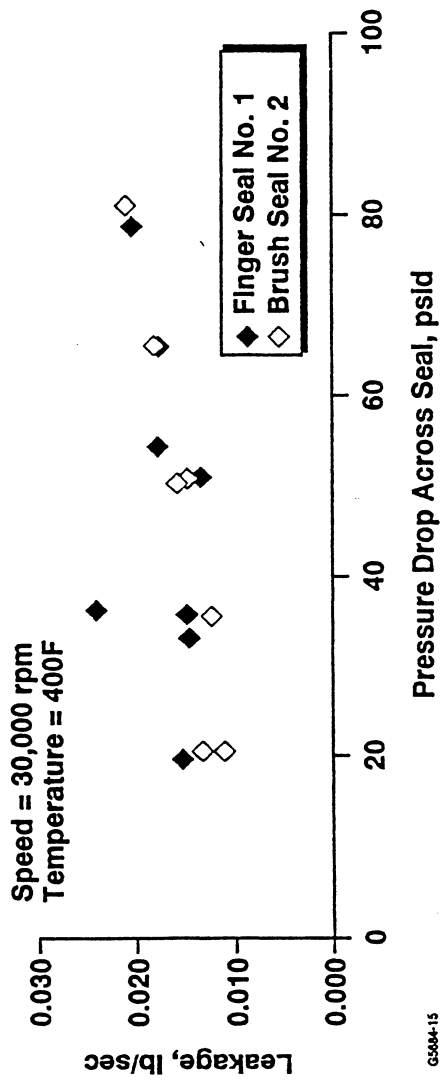


UNCLASSIFIED

UNCLASSIFIED

UNCLASSIFIED

FINGER SEAL HAS DEMONSTRATED AIR LEAKAGE SIMILAR TO A BRUSH SEAL



UNCLASSIFIED

UNCLASSIFIED

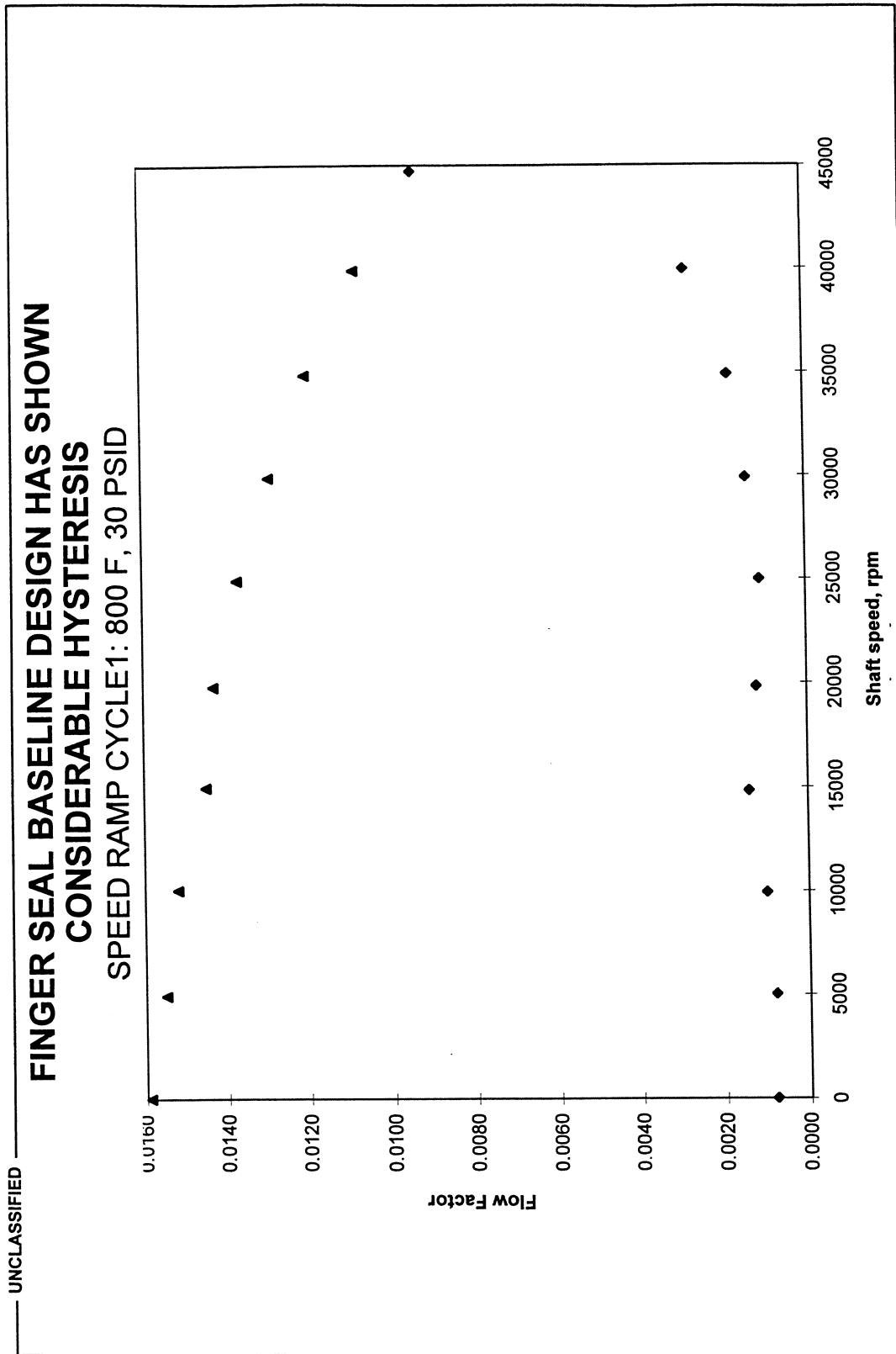
UNCLASSIFIED

FLOW FACTOR DEFENITION

- FLOW FACTOR PHI IS DEFINED AS
- $$\text{PHI} = (\dot{m} \cdot \sqrt{T_{\text{avg}} + 459.67}) / (P_u \cdot D_i)$$
-
- where, \dot{m} = Air leakage flow rate, lbm / sec
- T_{avg} = Average air temperature upstream of the seal, F
- P_u = Air pressure upstream of the seal, psia
- D_i = Outside diameter of the seal rotor, inch

UNCLASSIFIED

UNCLASSIFIED



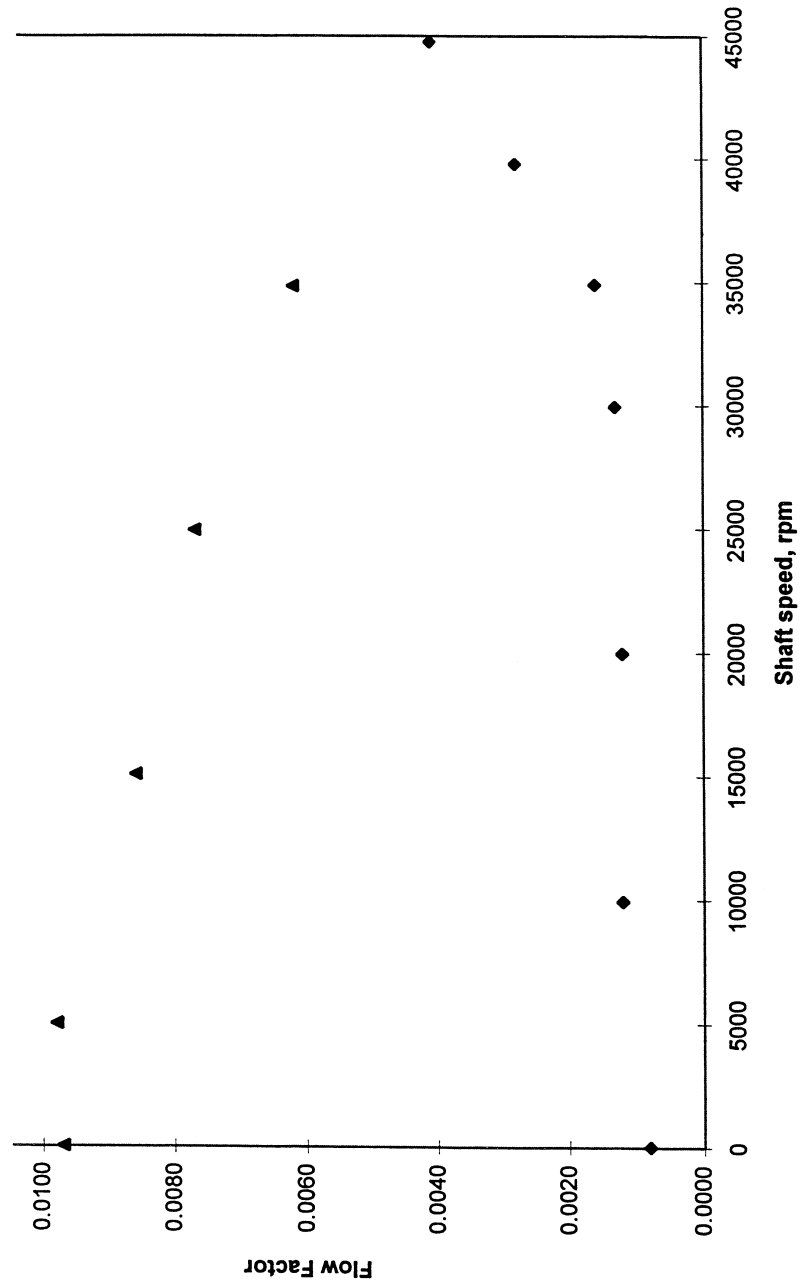
UNCLASSIFIED

UNCLASSIFIED

UNCLASSIFIED

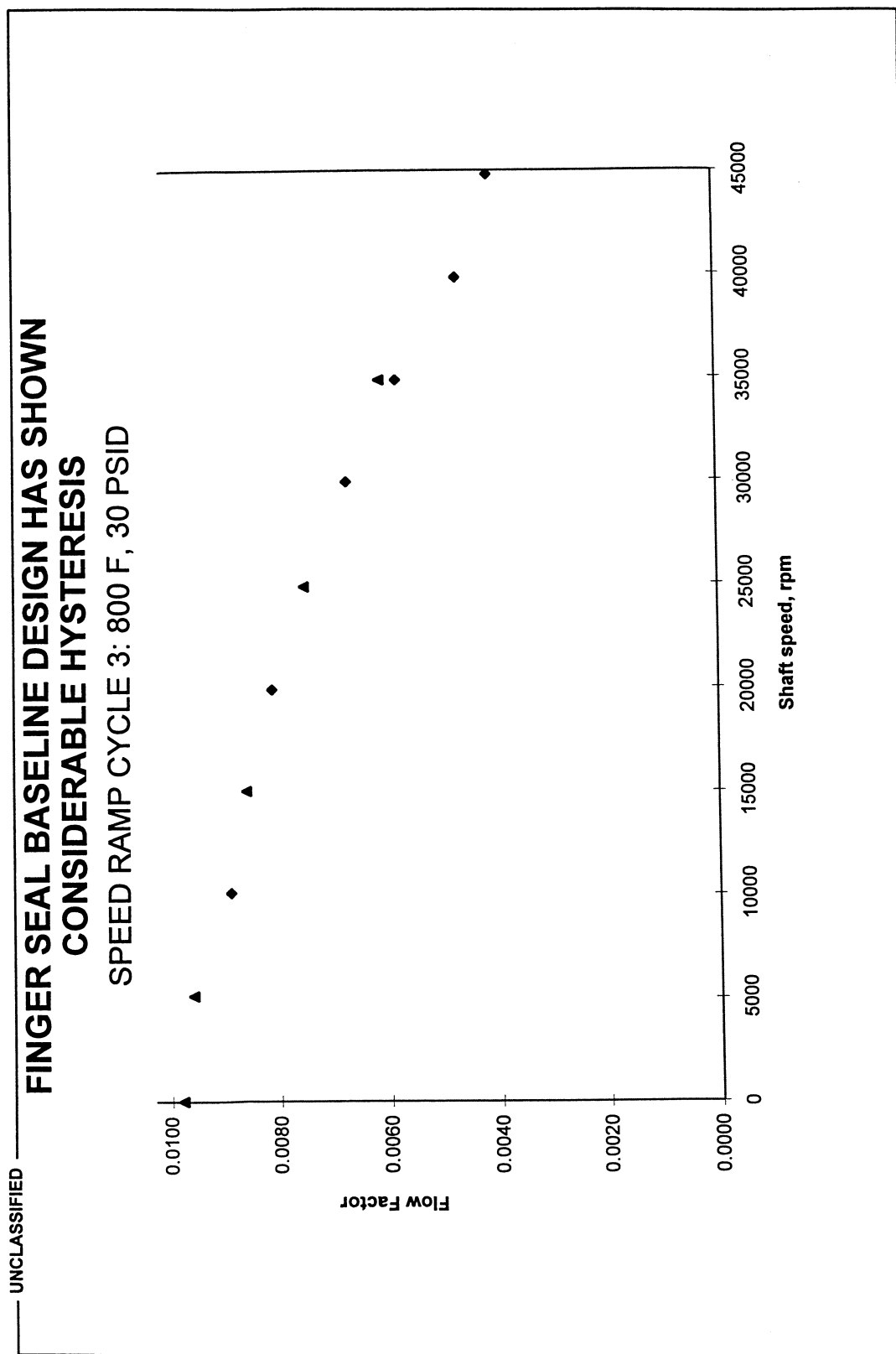
FINGER SEAL BASELINE DESIGN HAS SHOWN CONSIDERABLE HYSTERESIS

SPEED RAMP CYCLE 2: 800 F, 30 PSID

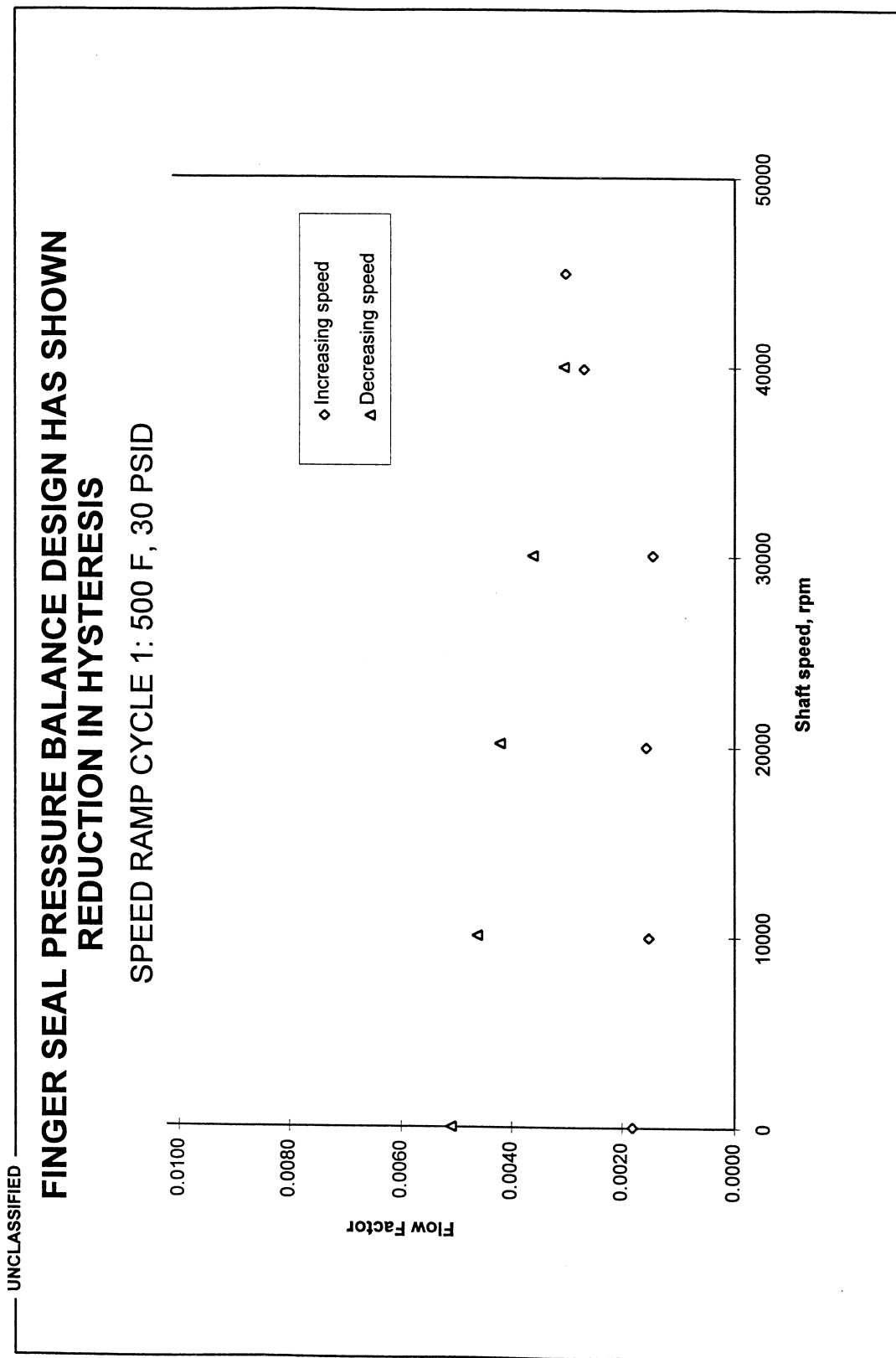


UNCLASSIFIED

UNCLASSIFIED



UNCLASSIFIED

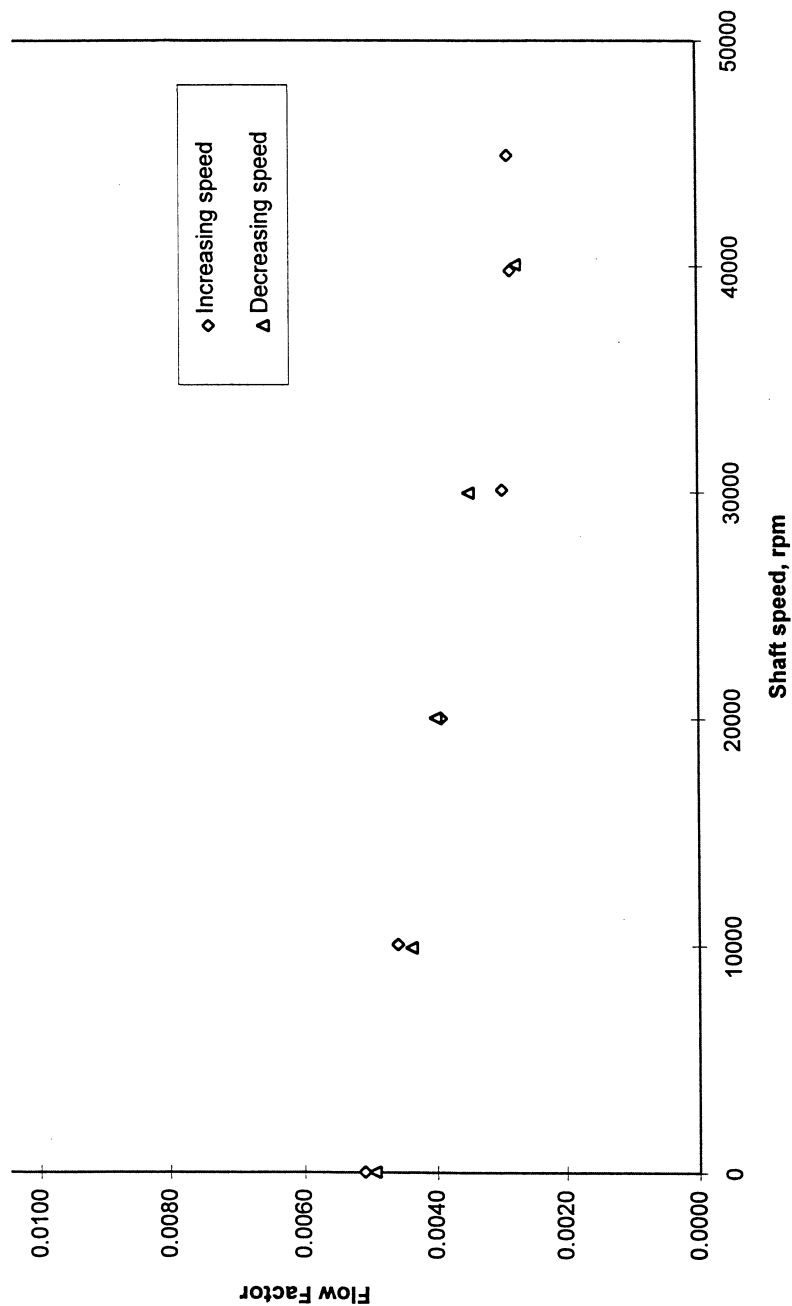


UNCLASSIFIED

UNCLASSIFIED

FINGER SEAL PRESSURE BALANCE DESIGN HAS SHOWN REDUCTION IN HYSTERESIS

- SPEED RAMP CYCLE 2: 500 F, 30 PSID



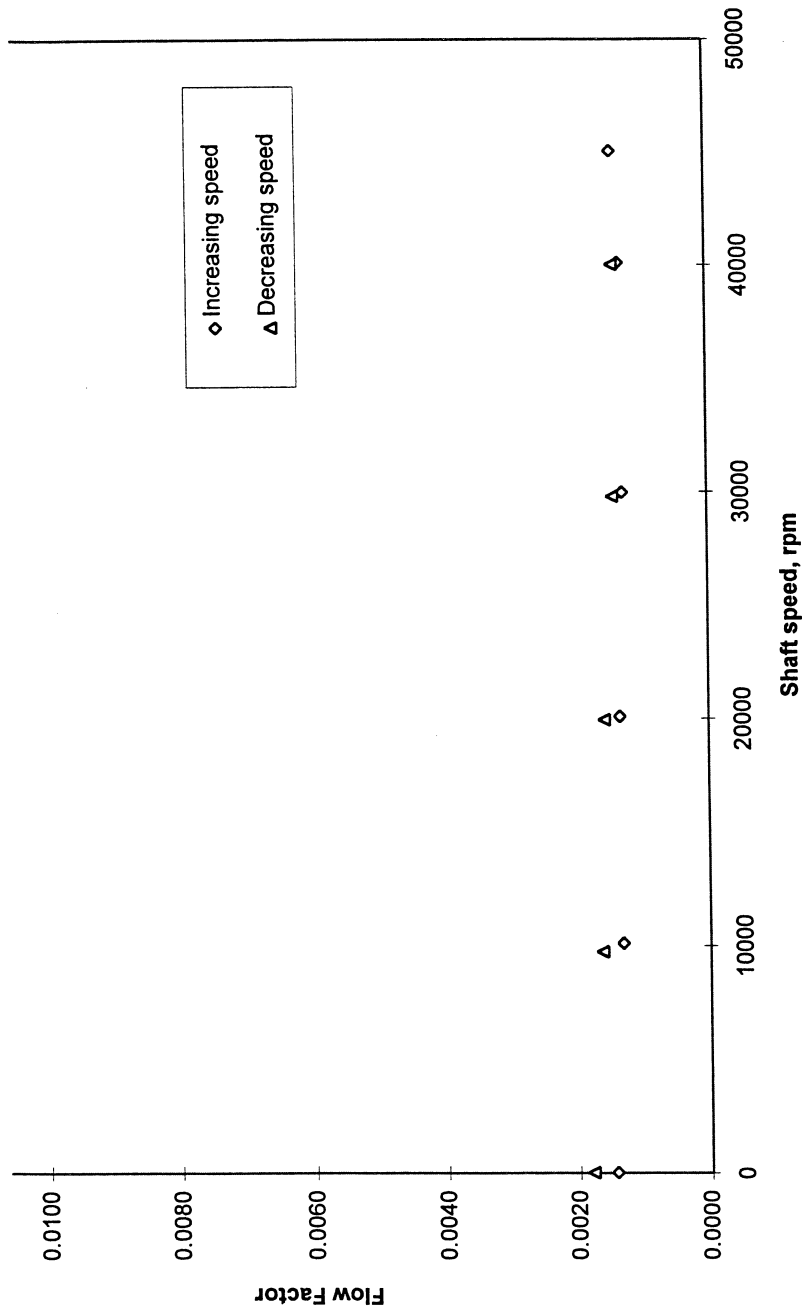
UNCLASSIFIED

UNCLASSIFIED

UNCLASSIFIED

FINGER SEAL PRESSURE BALANCE DESIGN HAS SHOWN REDUCTION IN HYSTERESIS

- SPEED RAMP CYCLE 1: 500 F, 60 PSID



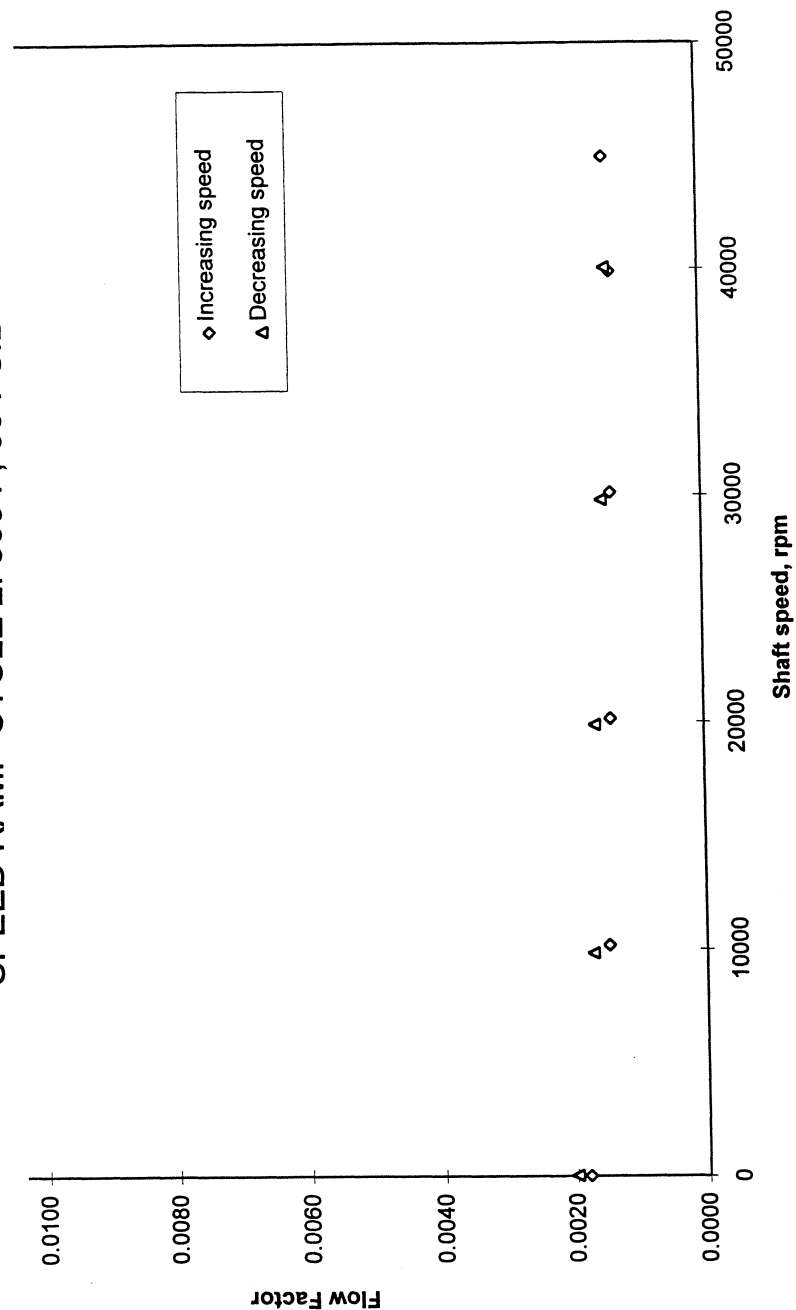
UNCLASSIFIED

UNCLASSIFIED

UNCLASSIFIED

FINGER SEAL PRESSURE BALANCE DESIGN HAS SHOWN REDUCTION IN HYSTERESIS

- SPEED RAMP CYCLE 2: 500 F, 60 PSID



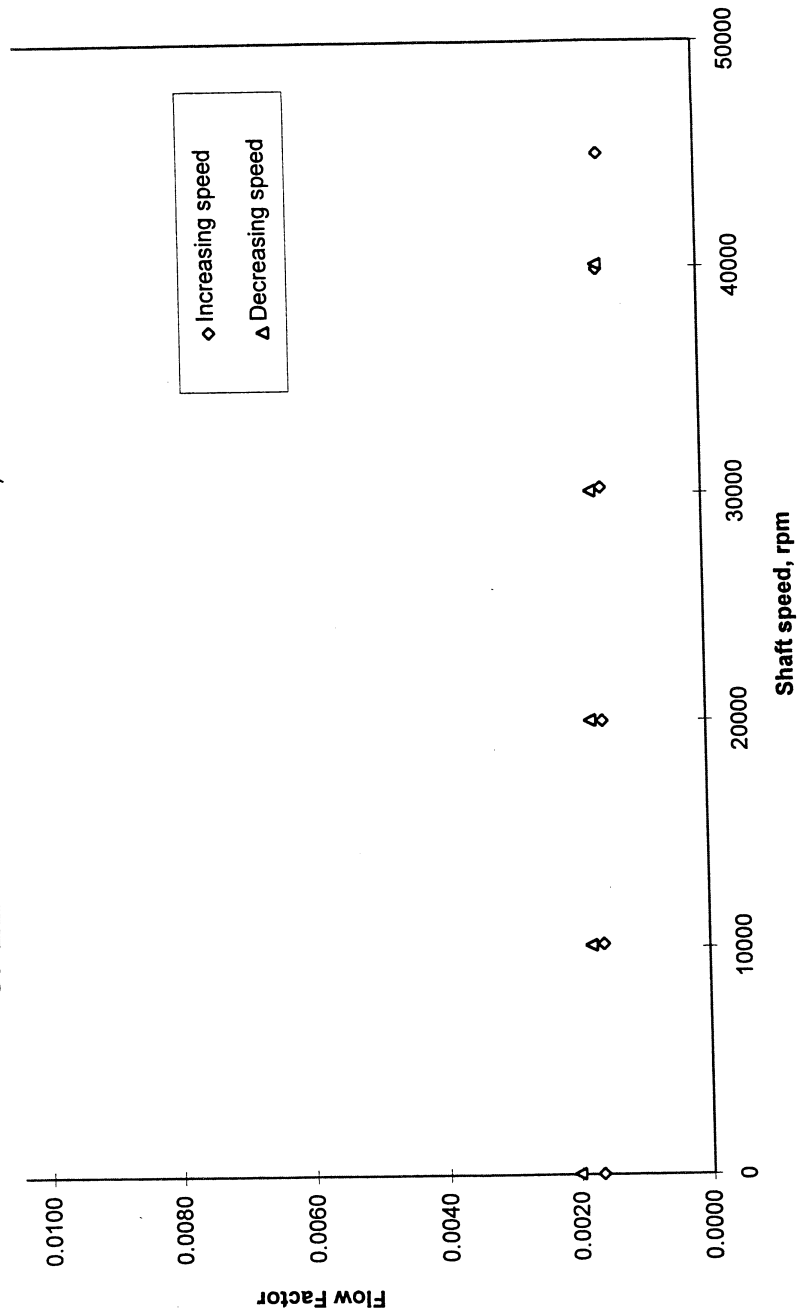
UNCLASSIFIED

UNCLASSIFIED

UNCLASSIFIED

FINGER SEAL PRESSURE BALANCE DESIGN HAS SHOWN REDUCTION IN HYSTERESIS

- SPEED RAMP CYCLE 1: 500 F, 90 PSID



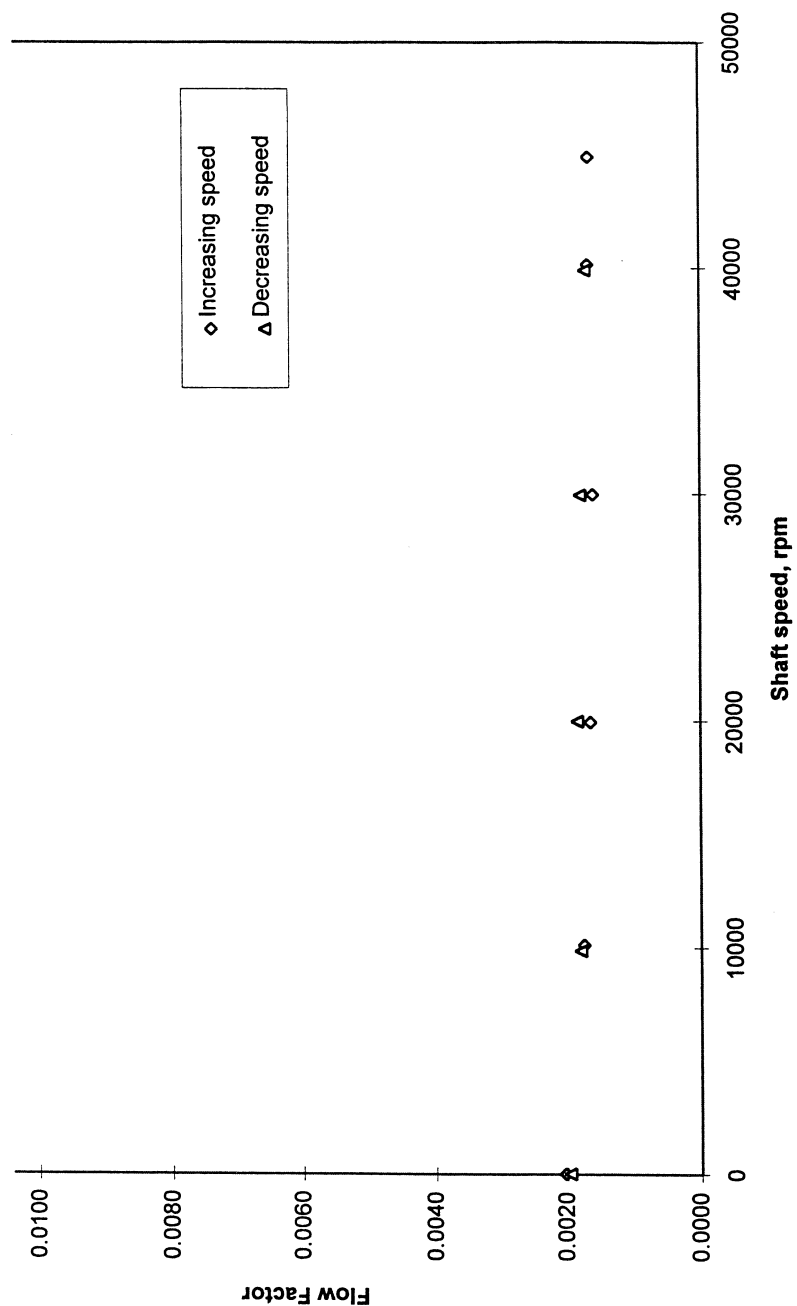
UNCLASSIFIED

UNCLASSIFIED

UNCLASSIFIED

FINGER SEAL PRESSURE BALANCE DESIGN HAS SHOWN REDUCTION IN HYSTERESIS

- SPEED RAMP CYCLE 2: 500 F, 90 PSID



UNCLASSIFIED

UNCLASSIFIED

UNCLASSIFIED

SUMMARY

- FINGER SEAL LEAKAGE IS SIMILAR TO A BRUSH SEAL
- FINGER SEAL COST GOAL IS 20 TO 50 PERCENT THAT OF BRUSH SEAL
- PRESSURE BALANCE DESIGN HAS SHOWN PROMISE IN REDUCING HYSTERESIS

UNCLASSIFIED

FINGER SEAL IS A REVOLUTIONARY NEW CONCEPT IN SEALING TECHNOLOGY

KEY FEATURES

- o LOW AIR LEAKAGE SIMILAR TO BRUSH SEALS
- o AIR LEAKAGE 20 TO 40 PERCENT THAT OF A LABYRINTH SEAL
- o LOW COST: ABOUT 20 TO 50 PERCENT THAT OF A CONVENTIONAL LABYRINTH OR BRUSH SEAL
- o HIGH SPEED, PRESSURE AND TEMPERATURE CAPABILITY

EXPECTED SYSTEM BENEFITS TO PROPULSION ENGINES

- o 1 TO 2 PERCENT SAVING IN ENGINE AIR FLOW
- o 0.7 TO 1.4 PERCENT REDUCTION IN SPECIFIC FUEL CONSUMPTION
- o 0.35 TO 0.7 PERCENT REDUCTION IN DIRECT OPERATING COST

MODELING AND FULL-SCALE TESTING OF AN ASPIRATING FACE SEAL

Norman A. Turnquist
GE Corporate Research and Development
Niskayuna, New York

A 36" diameter aspirating face seal for aircraft engine application has undergone extensive testing and analysis. Previous testing indicated that the seal tended to seek equilibrium at axial rotor clearances that were larger than expected. Parameter studies were conducted on several seal design parameters to evaluate effect on seal performance. Mixing of air flows from the air dam and air bearing regions of the seal was shown to have a significant impact on the seal's performance. Two methods of minimizing this flow interaction were studied both analytically and experimentally. The first method is to reduce the labyrinth tooth clearance, thereby limiting flow to the air dam itself. The second method involves utilizing a flow deflector between the air dam and air bearing regions of the seal in order to prevent radial flow from the air dam from disrupting the formation of a hydrostatic film at the air bearing. Both methods were shown to be effective design enhancements, allowing seal closure to be achieved. In both cases, the seal seeks an equilibrium position 0.0015" from the rotor surface, with correspondingly low leakage rates.

Description of Slides

1. Title slide
2. Objectives and Motivation for Aspirating Face Seal Modeling and Full Scale Testing
3. Cross-section of the 36" Diameter Aspirating Face Seal, showing seal components
4. Cross-section of the Full Scale Test Rig, in the Fully Assembled and Open Vessel Configurations
5. The Aspirating Seal Test Plan
6. Test Results - Seal/rotor Air Gap and Flow vs. % of Open Air Bearing Orifice Holes for 5 psid
7. Test Results - Seal/rotor Air Gap and Flow vs. Pressure Differential with 50% of Air Bearing Holes blocked
8. Axisymmetric Analytical Model of the Aspirating Seal, showing seal Degrees of Freedom and Forces
9. Wire Frame of the 3-D CFD Model
10. Test Results - Static Leakage for seal with 0.035" and 0.085" labyrinth tooth clearance, both with and without flow deflector in place between Air Dam and Air Bearing
11. Analytical Results - Flow fields for Base Design at 0.016" and 0.003" seal/rotor air gaps
12. Analytical Results - Flow fields for Base Design and Modified labyrinth tooth clearance of 0.035"; both for measured 0.016" seal/rotor air gap
13. Analytical Results - Flow fields for Base Design and Modified seal with flow deflector in place between air dam and air bearing; both for measured 0.016" seal/rotor air gap
14. Analytical Results - Pressure profiles for Base Design and Modified labyrinth tooth clearance of 0.035"; both for measured 0.016" seal/rotor air gap
15. Analytical Results - Pressure profiles for Base Design and Modified seal with flow deflector in place between air dam and air bearing; both for measured 0.016" seal/rotor air gap
16. Test Results - Flow vs. Pressure Differential at 0 RPM and Flow vs. Speed at 20 psid for the Aspirating Seal with a modified labyrinth tooth clearance of 0.035". Seal opened at 38 psid and 0 RPM, and at 20 psid and 1000 RPM.
17. Test Results - Flow vs. Pressure Differential at 0 RPM for 0.035" labyrinth tooth clearance and flow deflector in place between air dam and air bearing
18. Test Results - Flow vs. Pressure Differential at 0 RPM for 0.085" labyrinth tooth clearance and flow deflector in place between air dam and air bearing; deflector found to be damaged upon completion of test
19. Conclusions

Aspirating Face Seal Modeling and Full Scale Testing

Objectives

Develop an Aspirating Face Seal design for use in the GE90 aft outer LPT seal location, and other new and existing engines.

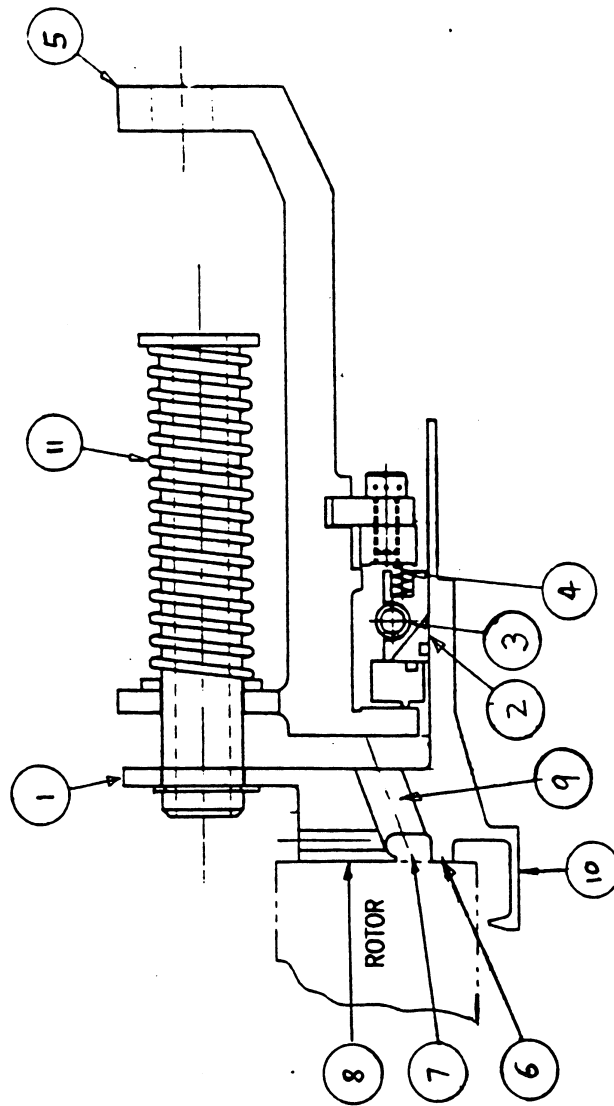
Motivation

Reduced secondary flow leakages result in SFC improvements
Non-contact seal results in longer seal life, no performance degradation

Outline

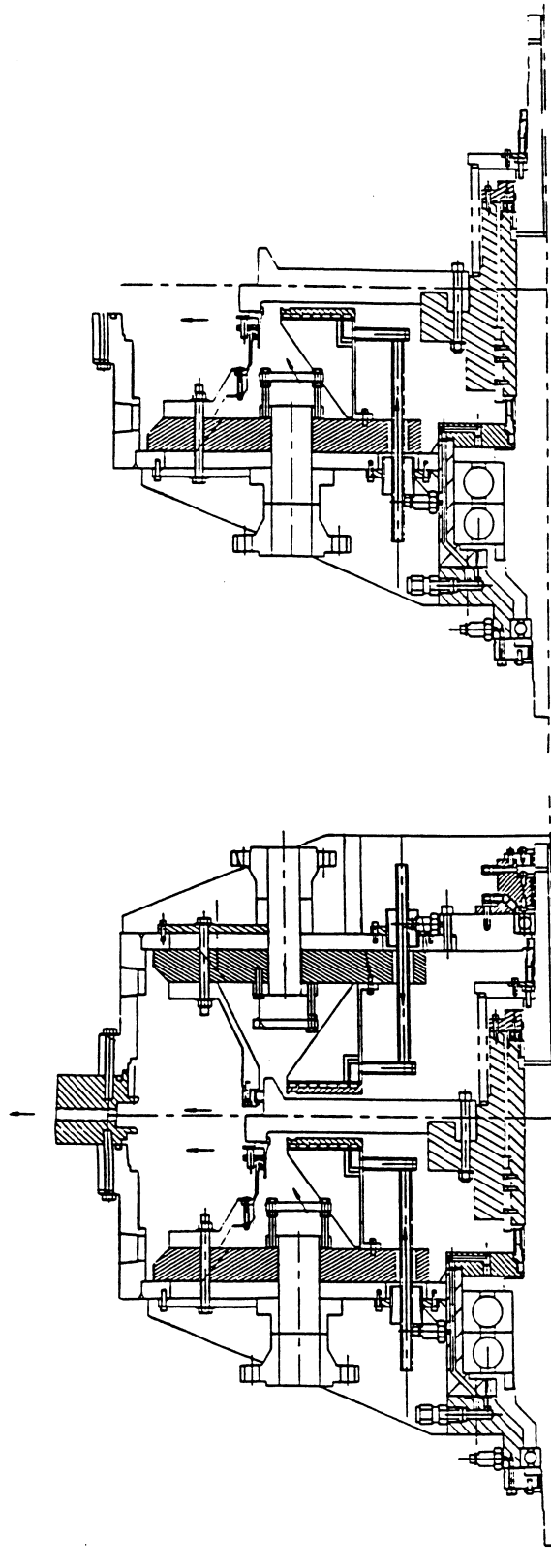
Seal Overview
Full Scale Test Rig
Test Plan
Test Results
Analytical Results
Conclusions

The 36" Diameter Aspirating Face Seal



- Hydrostatic gas bearing while closed
- Single tooth labyrinth while retracted
- Seal is normally retracted
- Non-contact
- All metal design
- Designed for 0.002" film thickness at operating pressure

The Full Scale Test Rig



**Open Vessel Test
Configuration**

**Fully Assembled
Rig Configuration**

The Test Plan

Plan must address all conditions seal is likely to encounter

1. Dust Ingestion

- 14.7" seal
- 0-10 micron particles at 1/3000 lb/sec

2. Static Leakage

- leakage performance up to 100 psid

3. Tracking

- 0.75" relative axial motion

4. Dynamic Leakage

- leakage performance up to 100 psid, 2400 rpm, 750° F

5. Rotor Runout

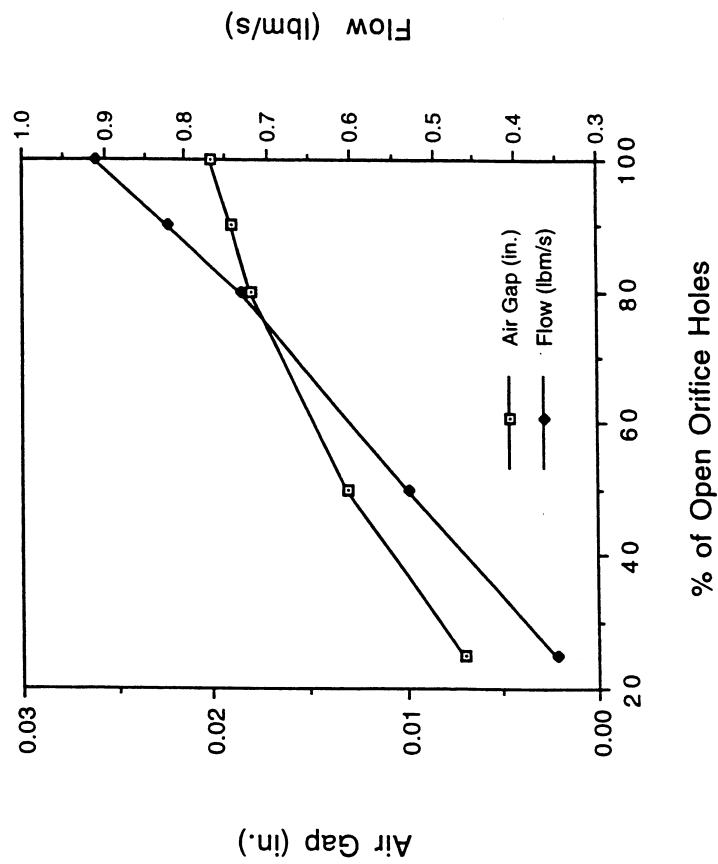
- leakage performance up to 100 psid, 2400 rpm with 0.005 and 0.010" TIR

6. Seal Tilt

- leakage performance up to 100 psid, 2400 rpm with 0.27° tilt

Test Results

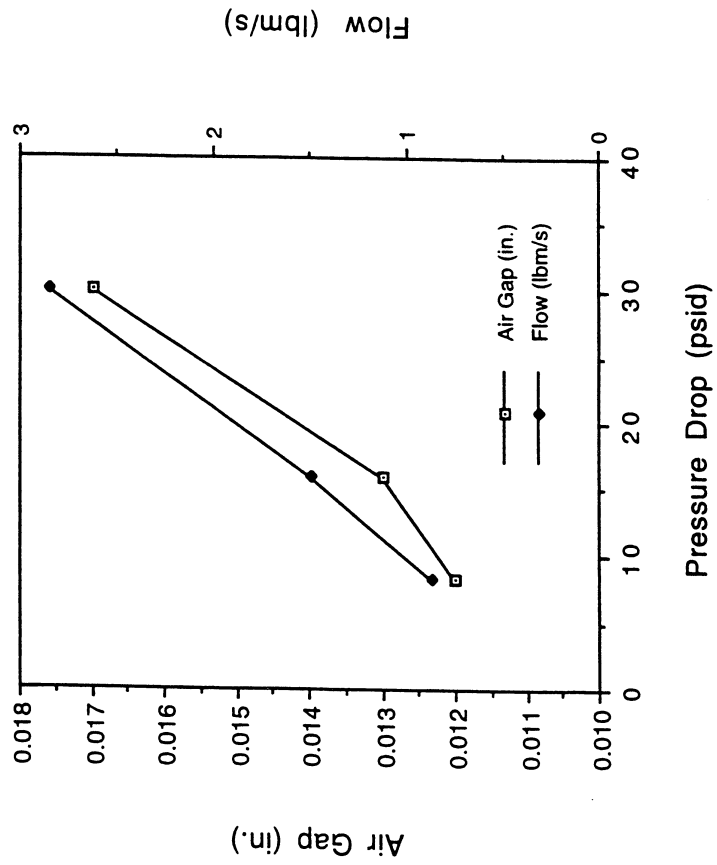
Static leakage with % of open orifice holes varied - 5 psid



- Larger than expected air gap and seal leakage
- Orifice holes strongly influence seal equilibrium position
- Larger number of holes yields larger air gap and leakage

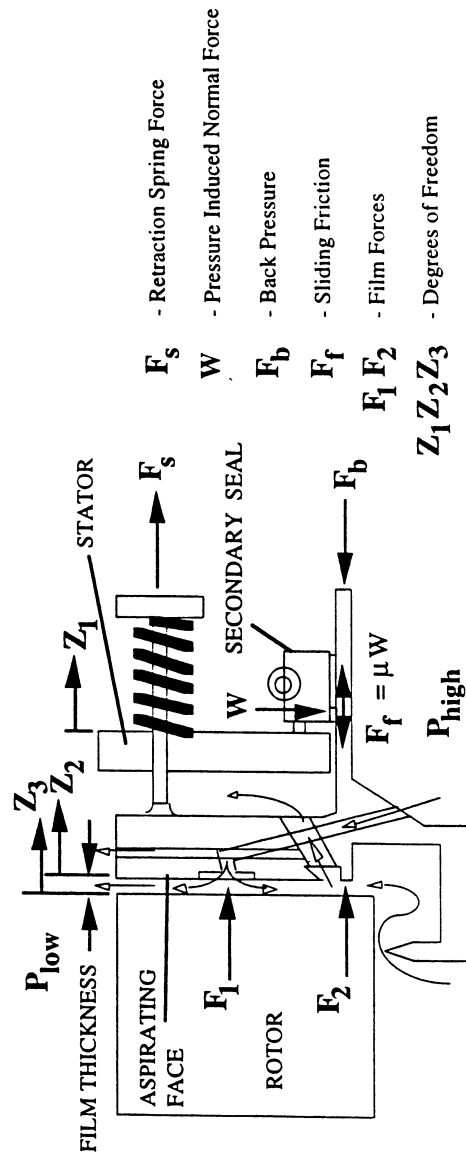
Test Results

Static leakage vs. Pressure differential; 50% of holes blocked



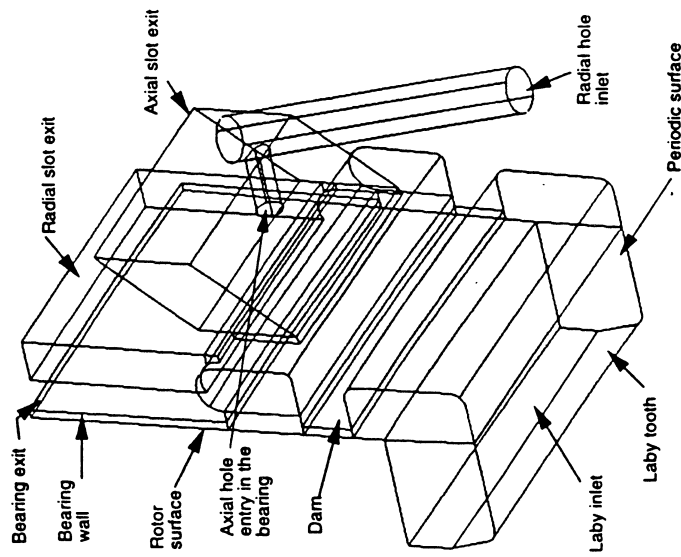
- Air gap increases with increasing seal differential pressure
- Seal observed closing at 3 psid

The Axisymmetric Model



- Force balance establishes seal equilibrium position

The CFD Model



- 3-D Pie Sector of seal
- Includes labyrinth tooth, air dam, and hydrostatic air bearing
- Captures effect of discrete orifice holes in air bearing face

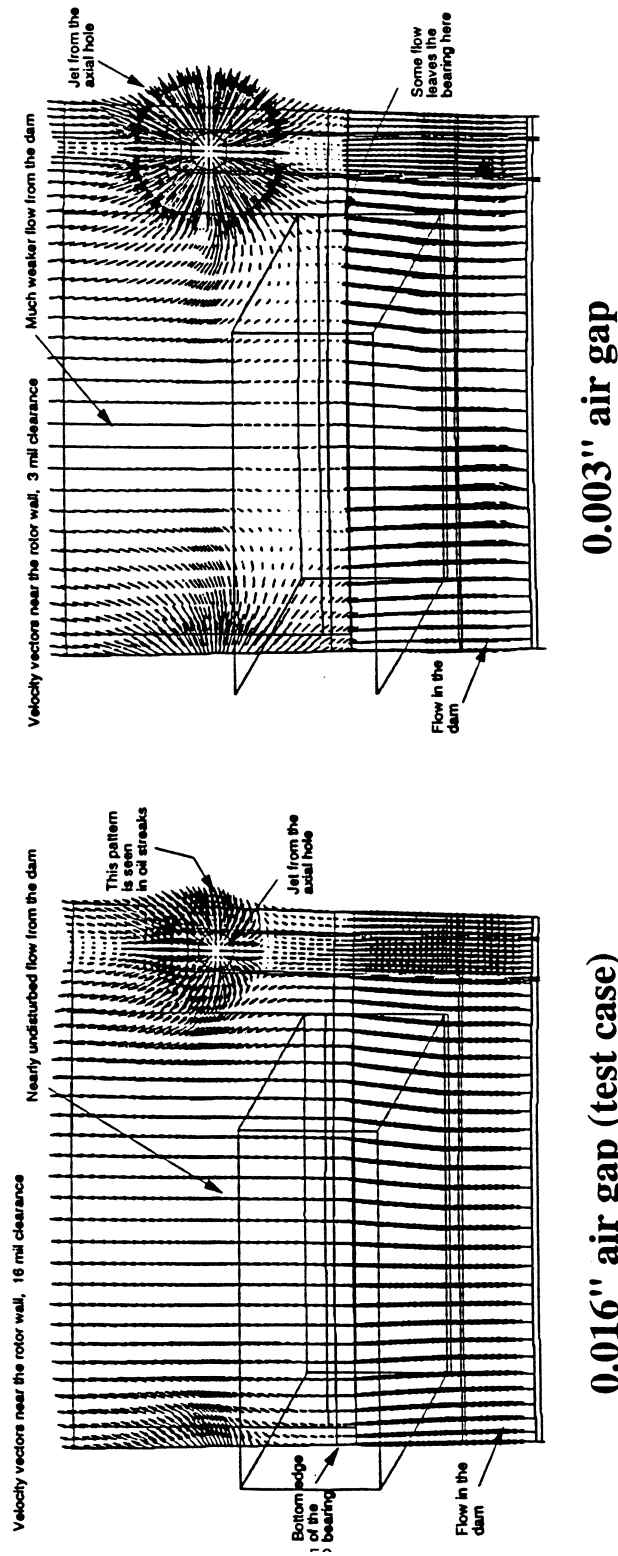
Aspirating Seal Test Results - Static Leakage

<u>Test</u>	<u>Flow Deflector</u> (Y/N)	<u>Labyrinth Tooth</u> <u>Clearance (in.)</u>	<u>Seal/Rotor Air</u> <u>Gap (in.)</u>	<u>Mass Flow</u> (lbm/s)
1	Y	0.035	0.001-0.002	0.15 @ 7.0 psid 0.20 @ 12.3 psid
2	Y	0.085	0.001-0.002	0.16 @ 7.3 psid 0.20 @ 12.3 psid
3	N	0.085	0.015-0.018	0.94 @ 6.2 psid 1.24 @ 10.0 psid
4	N	0.035	0.001-0.002	0.11 @ 4.8 psid 0.20 @ 12.4 psid
5*	N	0.085	0.016-0.020	1.00 @ 7.6 psid 0.93 @ 6.0 psid

* Test 5 is a repeat of Test 3

Analytical Results

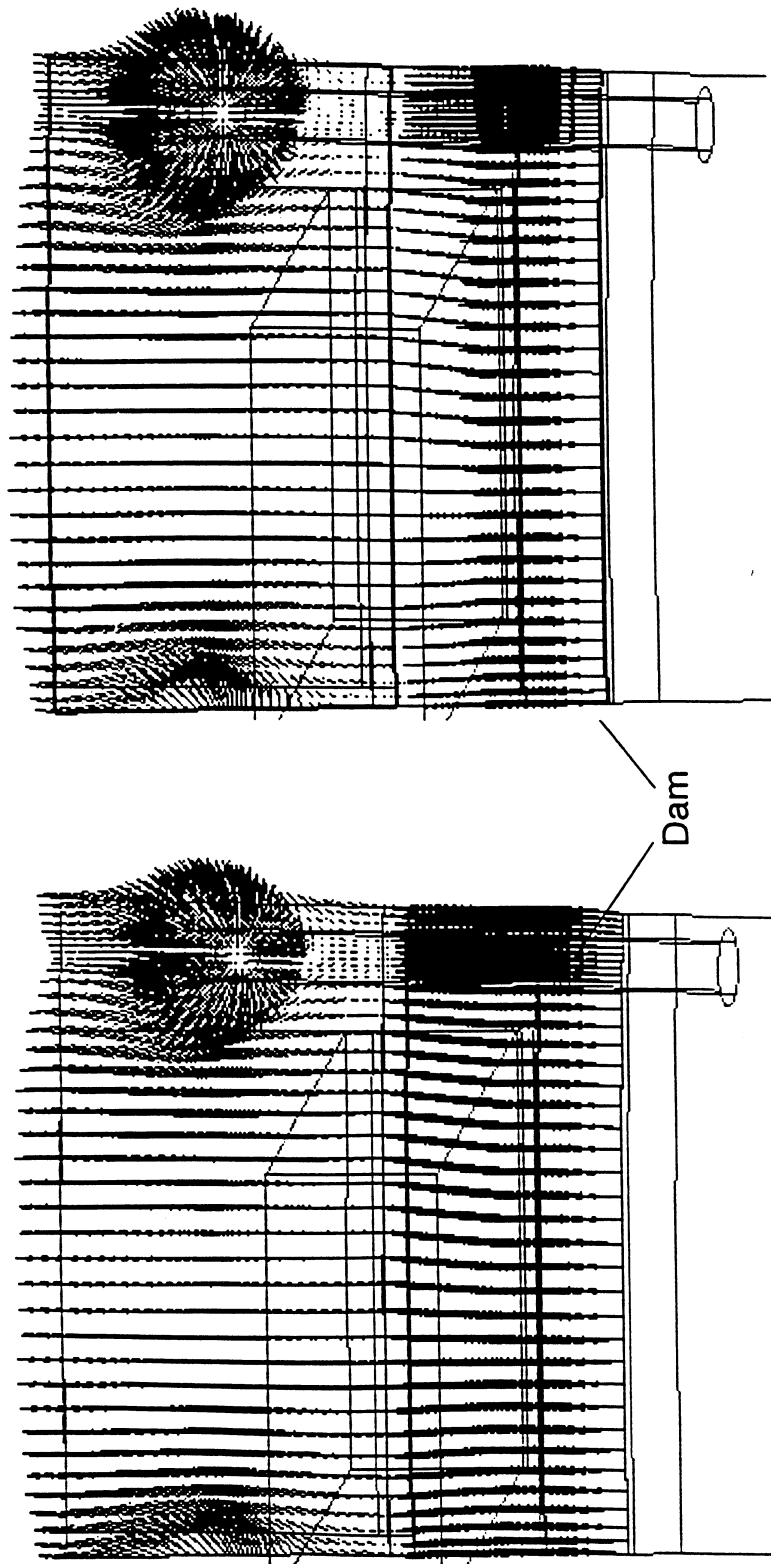
Axial view of flow fields - 0.016" and 0.003" air gaps



- Flow pattern at holes consistent with test observation for 0.016" gap
- Radial flow from the dam dominates the flow in air bearing region
- Even at clearance of 0.003", orifice flow is highly localized

Velocity Vector Plot

Plane near the rotor wall

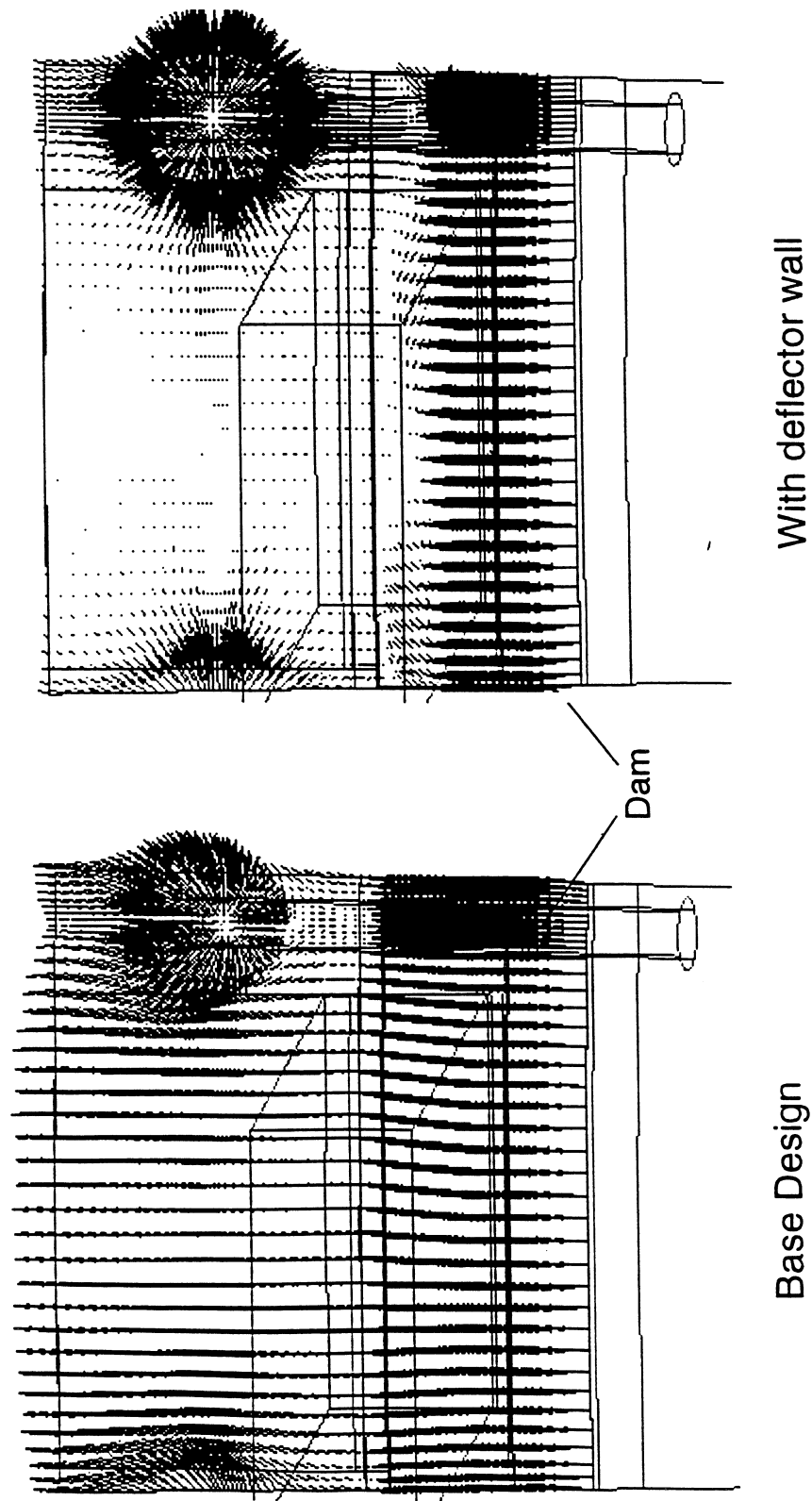


Base Design

Laby clearance 35 mils

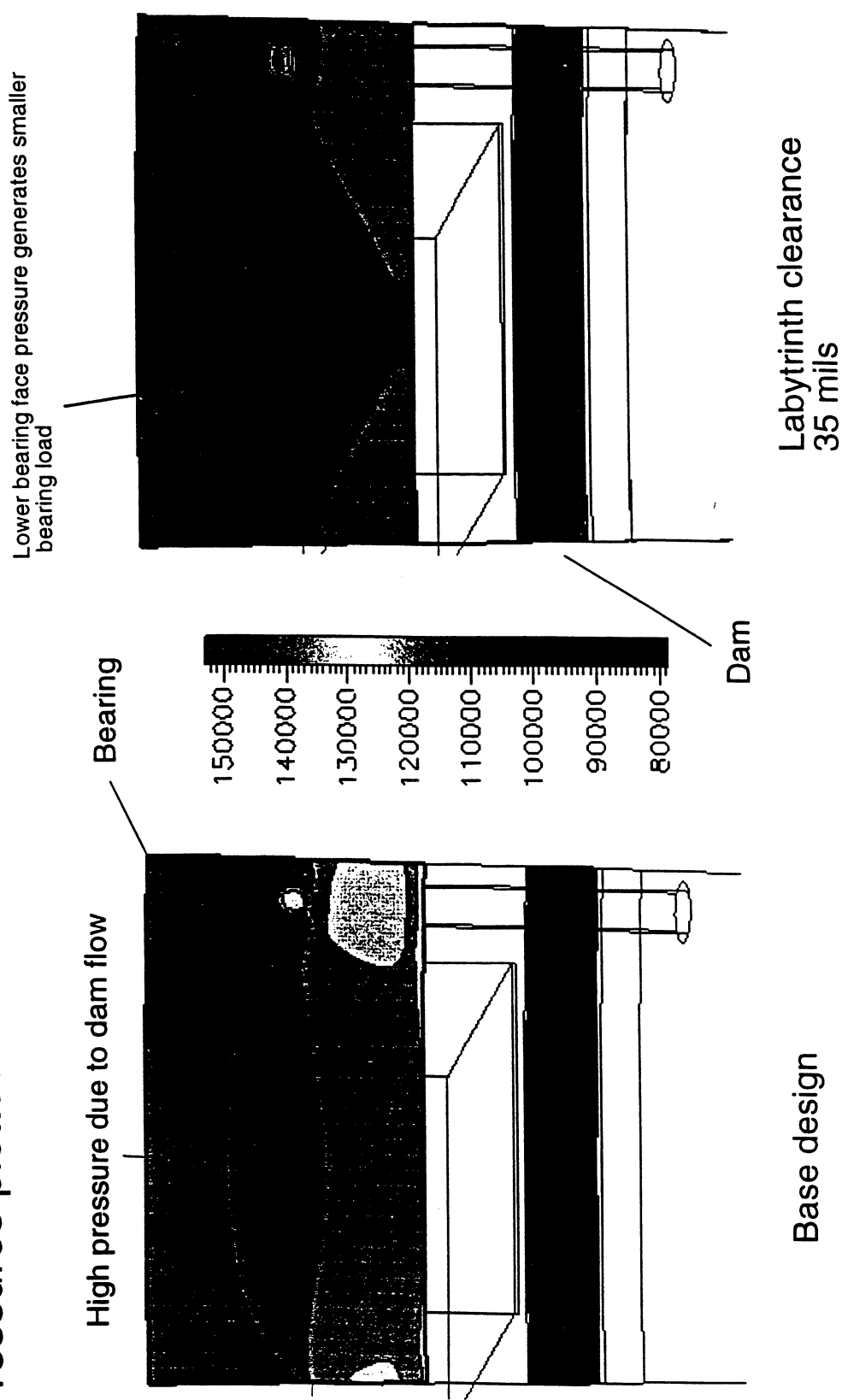
Velocity Vector Plot

Plane near the rotor wall



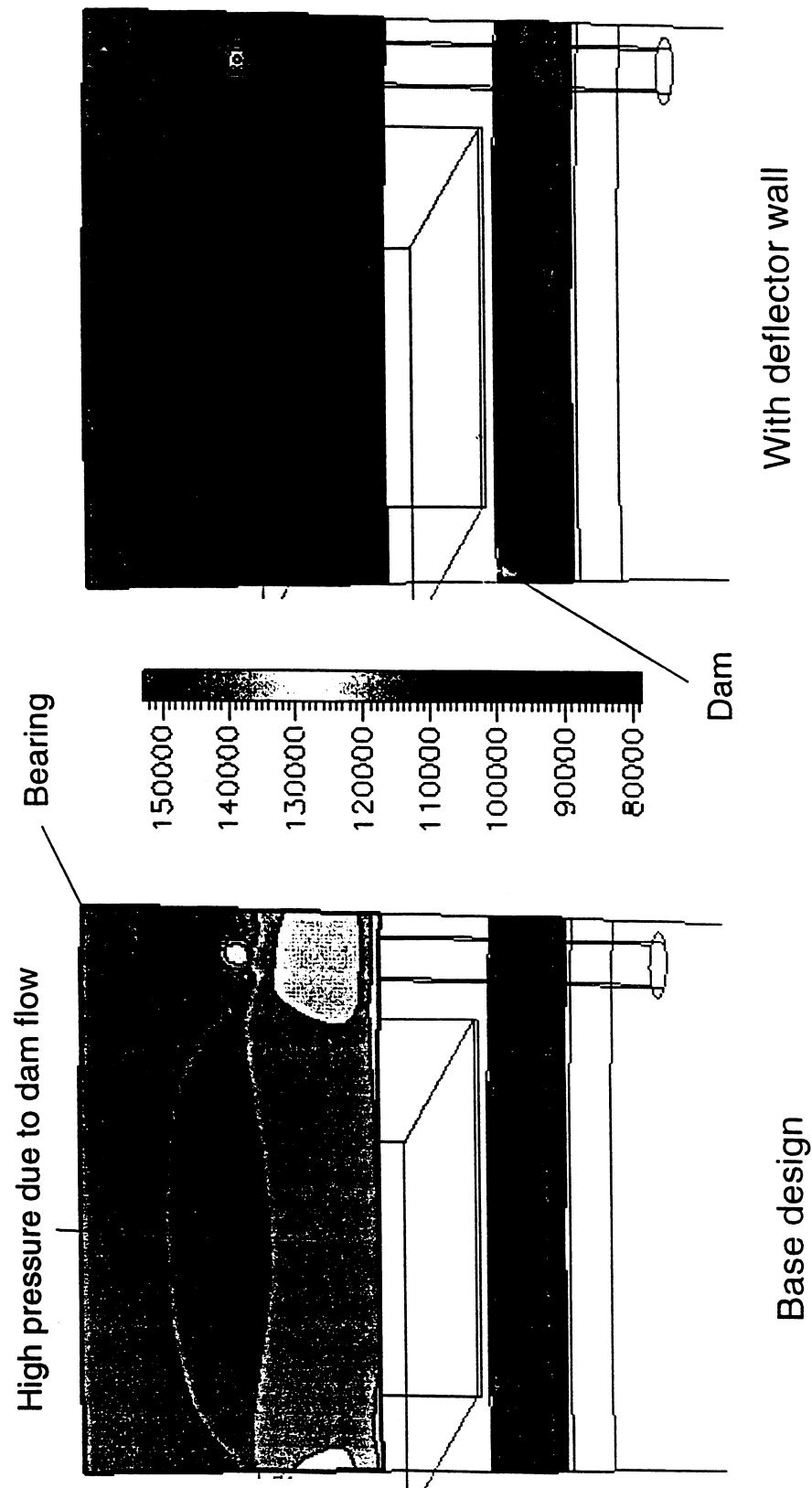
Surface Static Pressure Plot

Pressures plotted on the seal surfaces



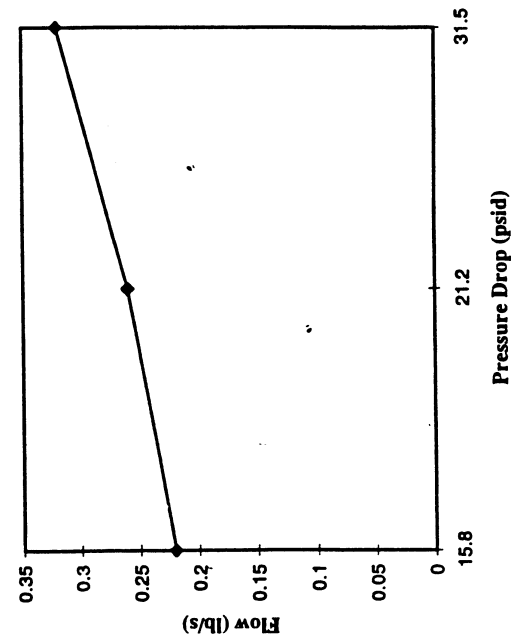
Surface Static Pressure Plot

Pressures plotted on the seal surfaces

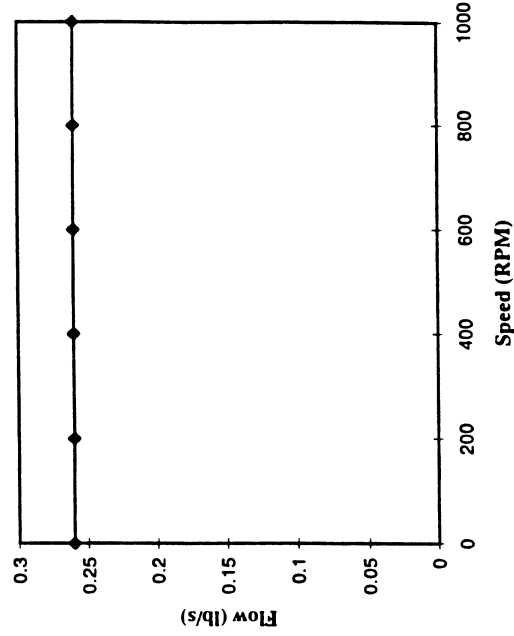


Nominal clearance 16 mils

Aspirating Seal Test Results - Static and Dynamic



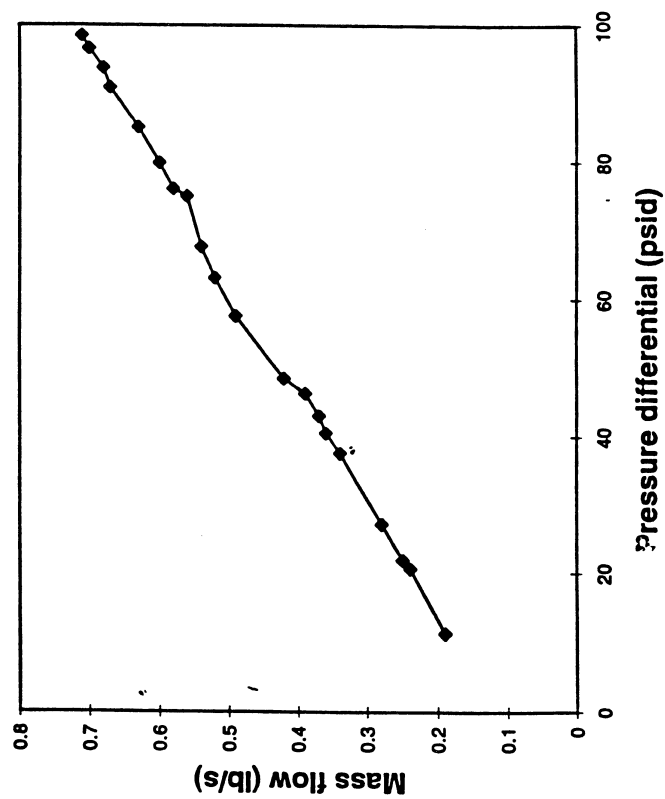
**Static Leakage
(0 RPM)**



**Dynamic Leakage
(20 psid)**

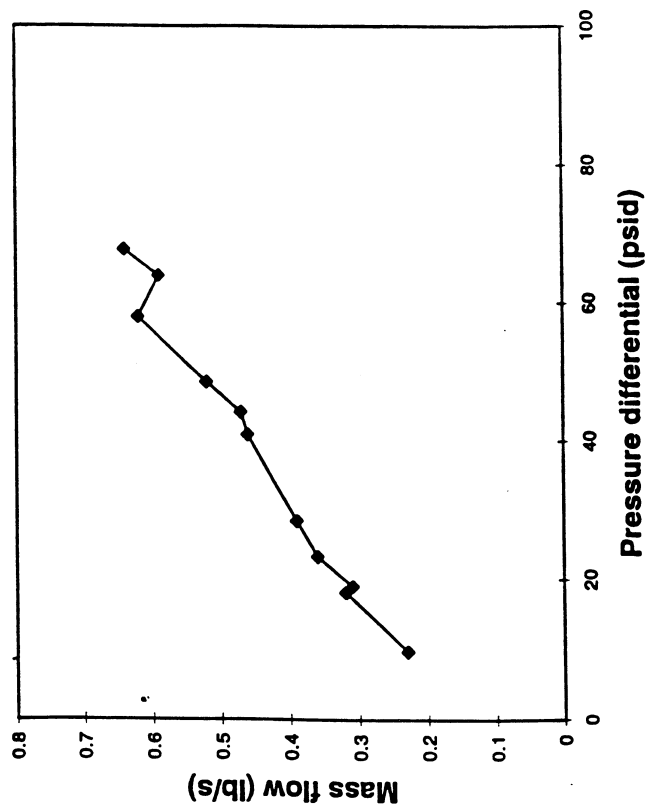
- 0.035" Labyrinth Tooth Clearance
- No Flow Deflector between Air Dam and Air Bearing
- 0.0015" seal/rotor air gap at $\Delta P < 38$ psid, Flow < 0.4 lbm/s for 0 RPM
- 0.0015" seal/rotor air gap at RPM < 1000 for $\Delta P = 20$ psid

Aspirating Seal Test Results - Static Leakage



- 0.035" Labyrinth Tooth Clearance
- Flow Deflector in place between Air Dam and Air Bearing
- 0.0015" seal/rotor air gap for entire range of pressures

Aspirating Seal Test Results - Static Leakage



- 0.085" Labyrinth Tooth Clearance
- Flow Deflector in place between Air Dam and Air Bearing
- Seal behavior is more erratic than with 0.035" labyrinth tooth clearance
- Damage to flow deflector discovered upon seal inspection.

Conclusions

36” Aspirating Face Seal testing and analysis has revealed the following:

1. Isolation of dam and air bearing flows is vital for seal performance.
2. The existing seal design seeks equilibrium 0.016” from the rotor surface.
3. Minimizing the labyrinth tooth clearance allows the seal to operate at low pressures/flows with some rotation. Rotation at elevated speeds appears to induce seal opening.
4. Positive isolation of dam and air bearing flows allows the seal to operate over full range of pressures; effect of rotation TBD.

The aspirating face seal shows potential as a replacement for labyrinth and brush seals as a durable low leakage seal after modifications to move its equilibrium position from 0.016” to 0.002”

AIR/OIL SEALS R&D AT ALLIEDSIGNAL

M. Rifat Ullah
AlliedSignal Engines
Phoenix, Arizona

TRANSCRIPT ... Air/Oil Seals IR&D at AlliedSignal

Presenter: M. Rifat Ullah, Ph.D., P.E

Date: October 16, 1997

Venue: NASA-Lewis Research Center, Cleveland, Ohio

Abstract: AlliedSignal aerospace company is committed to significantly improving the reliabilities of air/oil seals in their gas turbine engines. One motivation for this is that aircraft cabin air quality can be affected by the performance of mainshaft air/oil seals. In the recent past, coking related failure modes have been the focus of air/oil seal R&D at AlliedSignal. Many significant advances have been made to combat coke related failures, with some more work continuing in this area. This years R&D begins to address other common failure modes. Among them, carbon seal “blistering” has been a chronic problem facing the sealing industry for many decades. AlliedSignal has launched an aggressive effort this year to solve this problem for our aerospace rated carbon seals in a short (one to two year) timeframe. Work also continues in developing more user-friendly tools and data for seal analysis & design. Innovations in seal cooling continue. Nominally non-contacting hydropad sealing concept is being developed for aerospace applications. Finally, proprietary work is in planning stages for development of a seal with the aggressive aim of zero oil leakage.

CHART #1

AIR/OIL SEALS R&D AT AlliedSignal

**Presented at SEALS/SECONDARY FLOW WORKSHOP at
NASA Lewis Research Center, Cleveland --- October 16, 1997**

Contact: M. Rifat Ullah, Ph.D., P.E. (602) 231-1084

Good morning. This morning I will try to give you a feel for the work we’re doing at AlliedSignal in improving the reliability and performance of mechanical seals for aerospace applications. AlliedSignal is highly committed to improving seal reliabilities since it can impact the quality of cabin air in passenger aircrafts. That is, leaking engine seals can be a major source of customer dissatisfaction, and AlliedSignal is in the forefront of resolving these chronic problems.

CHART #2

Effect of recent R&D on coking related failures

Examples:

- 1200 Engines of TFE731 have been retrofitted with the patented Ceramic Ring Seal at 4 locations ... Chronic Odor-In-Cabin has Disappeared!
- TPE331 Compressor Seal ... B1 Life has increased by 10 times

In the past years I've indicated to you the work that we were focused on. The primary focus in recent years has been to attack seal failures related to Coking. I am pleased to tell you that many advances have been made in this area. We now have a critical understanding of how coke formation mechanism works, and more importantly, how to attack that mechanism.

I can give you at least two specific examples where our recent seal R&D efforts have resulted in major advancements in aerospace engines products. 1200 engines of TFE731 have been retrofitted with the patented ceramic ring seal at 4 locations in the mainshaft of the engine. Virtually all seals that have been put in the real world are working superbly. Bottomline: The chronic problem of Odor-In-Cabin associated with this very popular engine for business jets has disappeared.

Another example is the compressor seal in the TPE331. Results from seal thermal management R&D were used to attack the coking problem for this seal. The B1 life has increased by about 10 times, a major accomplishment.

CHART #3

1997 Air/Oil Seal Programs

<u>1997 PROGRAMS</u>	<u>COLLABORATORS w/ AS</u>
● Carbon Seal Blister Prevention	Morgan, CMU, WMU, et.al.
● Analytical Tools & Data	MSTI, ASU
● Hydropad Seal	Rexnord
● Zero Oil Leakage Concept	MSTI
● Coning Deformation Resistant Seal	(none)
● Banded Carbon Dimensional Instability	ASU

This year we have launched a number of new initiatives in air-oil seal R&D. Here is a list of the various programs we have started. The problems we are attacking are quite complex. Whenever necessary, we form strategic partnerships and collaborations to solve our seal problems. This list indicates some of our outside collaborators, such as Carnegie-Mellon University, Morgan carbon company, Mechanical Seals Technology Inc., etc. Due to the lack of time, I will not go through each of these topics that we're currently engaged in. However, I will briefly talk about one of the programs that we're working on at the moment ... namely, Carbon Seal Blister Prevention.

CHART #4

Carbon Seal Blistering Quick Background

- **Damage on Sealing Surface of Carbon; typically Face Seals**
- **Nature of Blistering studied since early 70's.**
- **Emphasis been on Industrial Seals. Aerospace seals have not been studied.**
- **Leading theory due to Strugala (1972) ... sudden expansion of oil trapped in pores can cause damage**
- **Other theories include Intense Shear, etc.**
- **In 1st Phase, AlliedSignal chose to focus on the Carbon Material itself, instead of System variables**

Here's a quick background on Carbon Blistering. First of all, "blisters" and "blister-like indications" are a kind of damage on the sealing surface of the carbon, typically evident in many mechanical face seals. In this discussion, when I say "blister" it can mean all types of indications that resemble "blisters". Here is a picture of a blistered surface ... the sealing surface looks like it has 'pot-holes' in it. Blisters at the wrong location can compromise sealing integrity, though not all seals that blister are guaranteed to leak, as far as we can tell so far.

The nature of blistering has been studied since early '70s. The seminal work was published by Strugala in '72. The emphasis so far has been on "industrial seals", for example pump seals, or refrigerant seal, etc. Aerospace seals have not yet been studied to our knowledge. The leading theory is still due to Strugala (1972), which theorizes that sudden expansion of oil trapped in pores can cause blister-like damage in carbons. The sudden expansion can be a result of engine start-up, with attendant frictional heating and temperature rise. Other theories include intense shear as a mechanism that can produce blistering.

Currently, STLE sponsored research is also ongoing at Western Michigan University, with Professor Phil Guichelaar as the PI. AlliedSignal is also among the sponsoring consortium of some 15 companies supporting that work. That work is also principally aimed at slower speed industrial seals. What we learn from that work, we're readily implementing in our own independent blistering work for aerospace seals.

In the first phase of our work (this year), we chose to focus on the heart of the problem --- the Carbon material itself; as opposed to inclusion of "system variables", meaning, everything else that works in concert with the carbon. This has been done to efficiently arrive at a practical solution to this problem.

CHARTS #5 & 6

Here are a couple of pictures showing blister damage on the sealing face of carbon-graphite.

SEM Photograph of Blistered Area of Carbon Seal

(Magnification = 510X)

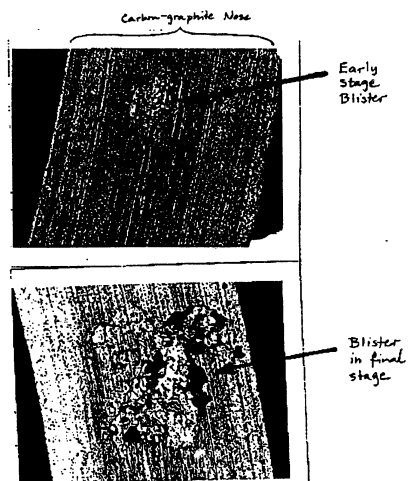
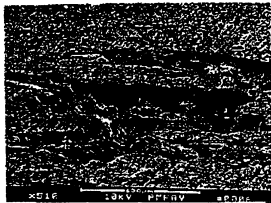


CHART #7

Carbon Seal Blistering Main Goals

In Order of Practical Importance:

- Identify and Rank Aerospace Carbon Grades
- Identify and Measure Key Carbon Properties
- Determine Mechanism(s)

The main goals of this work. In the order of practical importance:

- Identify and rank selected aerospace carbon grades
- Identify and measure key carbon properties
- Determine mechanism that causes blistering.

CHART #8

Carbon Seal Blistering ... APPROACH

PHASE-1 ... includes

- Investigate Carbon **Microstructure**
- Microdamage **Modeling** to form Hypotheses
- Determine & Measure **Key Carbon Properties**
- Fabricate Aerospace **Blister Rig**
- Rank **Blister Resistance** of selected Carbon Materials
- Define a new **Composite Property** "Blister Resistance", for Aerospace Seal Designs
- Determine **Mechanism** that causes Blisters in Aerospace Seals

In the first phase of our blistering work, the approach includes the following. We began by looking at the carbon microstructure of some common grades we use, and at seals from various engines. We also began working with Carnegie-Mellon's Professor Paul Steif on micro-damage modeling of for carbon. The aim is to arrive at plausible hypotheses to guide our work. From that we began determining some key material properties that might govern blistering. We are also constructing a special aerospace blister rig, with which we intend to perform controlled tests on selected carbon and alternative materials. We would like to rank the selection, which will be the least we will do. Based on the rest of the work, we are working on defining a new composite material property which we may call "Blister Resistance Number" for aerospace rated carbons. And finally, we aim to determine the mechanism that causes blistering in aerospace carbon seals.

CHART #9

Carbon Seal Blistering Some Inferences

PHASE-1 ... WORK IN PROGRESS

- Appears Carbon Microstructure can have strong influence
- Grain size can be important
- Size of Pores & Pore Distribution can be important
- Key Carbon Properties can include: Fracture Toughness, Permeability, etc.
- ... work in progress ...

Here are some inferences that we can tell you about, in this work that in progress. It appears that carbon microstructure can have a strong influence on this problem. For example, the nominal apparant “grain size” can be important, even though it is not easy to determine or even define a “grain” of carbon-graphite. From our modeling work, we determine that pore size and pore size distribution can be important. Also from our work we’re deducing that key carbon properties can include fracture toughness and permeability, among others. It is important to stress that when we say fracture toughness, we mean a “short crack toughness” and not the conventional K_{1c}.

CHART #10

More Collaborations Welcome

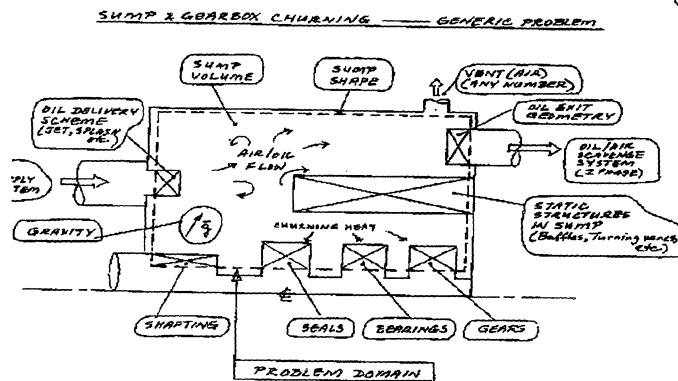
<u>1998 Work Element</u>	<u>Principal Expertise Needed (BOLD= outside collaboration needed)</u>
Carbon Blistering	Seal Rig Tests; Small-scale Bench Tests; Analytical modeling ... Applied Mechanics, Thermal sciences
Tools & Data	Seal software; Experimental Convective Heat Transfer
Hydropad Seal	Seal Rig Tests
Zero Oil Leakage Concept	Seal Innovation; Specialized Seal Rig Tests
Ceramic Face Seal Rotor	Design of Ceramic components
Banded Carbon Dimensional Instability	Analytical modeling ... Applied Mechanics, Thermal sciences
Sump & Gearbox Churning	Analytical modeling ... 2-phase/2-species CFD



As we aggressively prosecute a variety of air-oil seal problems, we welcome collaborations and strategic partnerships with qualified entities outside AlliedSignal. Here is a tentative list of air-oil seal and sump related R&D programs that we plan to work next year. Some are continuation of work already launched, while some are new program that we're considering. Again, due to lack of time here, I am not going to talk about each of these. If any one of these interests you, please contact me, and we can talk offline.

However, I am going to briefly touch on one of the new programs we're contemplating ... Sump and Gearbox Churning, a program we may engage in the near future, may be even next year.

CHART #12



PROBLEM: DEVELOP ANALYTICAL TOOLS TO MODEL
AIR-OIL FLOW BEHAVIOR IN GENERIC
SUMP AND GEARBOX. PROBLEM DOMAIN
INDICATES TYPICAL BOUNDARY CONDITIONS.

Sump and Gearbox Air-oil flow and Churning. After the oil performs its service to seals, gears, bearings in a gearbox, we need to move the oil out in the most efficient manner, so that churning is avoided. Currently, gearbox designs largely rely on past experience and rules of thumb. We use test rigs to improve performance, but that can be very expensive, time consuming, and not guarantee optimal solution. Analytical design tools are needed, that will work in parallel with experimental tools.

The generic problem statement involves analytically modeling the 3-dimensional space of a gearbox. The work can start out as a 2D problem, but the aim is to move towards 3D when possible. This figure shows the schematic of the generic problem domain with typical boundary conditions.

The boundaries of the gearbox/sump domain includes

- a liquid oil supply (such as oil jet, or splash, etc.),
- an air-oil scavenge (or drain),
- any number of air vents,
- static structures in the sump (such as baffles, turning vanes, etc.),
- rotating bodies that impart angular momentum to the air-oil fluid, such as seals, gears, bearing, and shafting
- gravity,
- etc.

Gearbox/sump volume and shape can be independent variables.

We would like to analytically predict the air-oil flow pattern/behavior in such a gearbox. Additionally, we would like to estimate churning heat generation. People with CFD expertise, especially involving 2 species (air & oil) and 2 phase flow may find this problem fascinating.

Thank you for your attention.

NASA HIGH TEMPERATURE TURBINE SEAL RIG DEVELOPMENT

Bruce M. Steinetz and Margaret P. Proctor
NASA Lewis Research Center
Cleveland, Ohio

Contributors

**G. Garrison, J. Dirkes, A. McNickle, Stein Seal
J. Flowers, Army; M. Adams, M. Tong, P. Dunlap, MTC
G. Arora, Allied Signal, J. Gardner, EG&G**

Sponsors



Air Force **E. Mayhew; A. VegBali; M. Stibich**

HSR/NASA **J. Shaw; M. Long Davis; B. Troha**

HITEMP **C. Ginty**

Turbomachinery Seal Development Objectives



- Evaluate feasibility of advanced seal concepts and materials of meeting next generation engine speed and temperature requirements.
- Complete fabrication/installation of state-of-the-art turbomachinery seal test rig capable of testing seals under known/anticipated design conditions.
- Work with industry to assess/demonstrate performance of their seals prior to test in engine.

High Temperature Turbomachinery Seal Test Rig



Test rig designed to test at speeds and temperatures envisioned for next generation commercial and military turbine engines.

Test rig is one-of-a-kind. More capable than any known test rig in existence at either engine manufacturers or seal vendors.

- **Temperature** Room Temperature thru 1500 °F
- **Surface Speed** 1500 fps at 40,455 RPM, 1600 fps at 43,140 RPM
- **Seal Diameter** 8.5" design; other near sizes possible
- **Seal Type:** Air Seals: brush, finger, labyrinth, film riding rim seal
- **Seal Pressure** 70 psi @ 1500 °F: Current
150 psi @ 1445 °F: with Hydrotest qualification of heater
- **Motor Drive** 60 HP (60,000 RPM) Barbour Stockwell Air Turbine with
advanced digital control for high accuracy/control

CD-97-76001

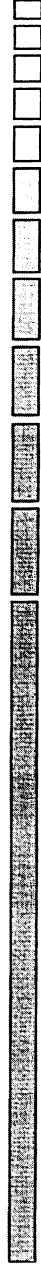
Test Parameters



- Seal flow vs. pressure, speed, temperature
(Both test rig and test seal are heavily instrumented)
- Seal performance vs. simulated ramp cycles using new digital air turbine speed controller.
Multiple speed step mission profile capabilities.
- Seal durability vs. once-per-rev rotor runout condition
- Seal durability for prescribed seal offset condition (e.g. 3 mil seal offset)
- Accelerated life tests
- Seal and coating wear

CD-97-76002

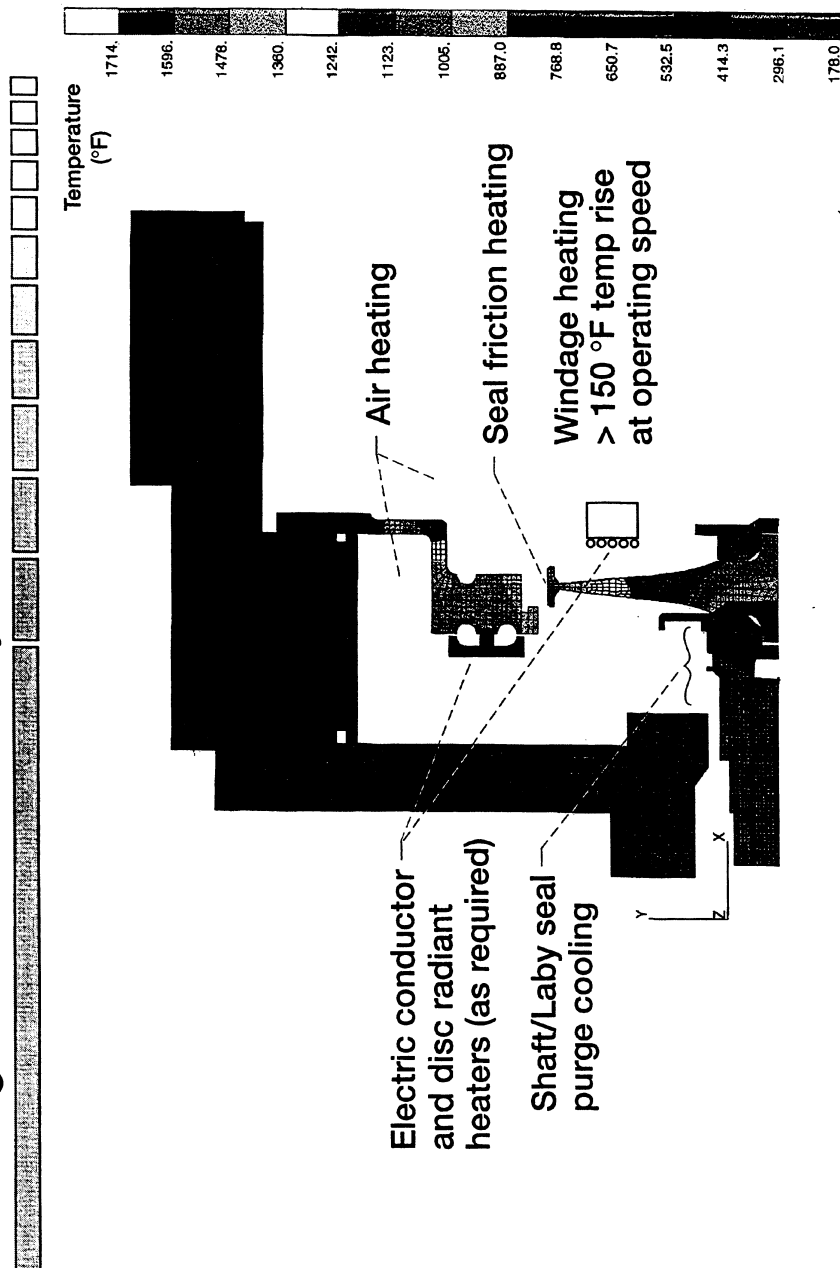
Highlights of Engineering Calculations



- MAR M-247 (Ni Co) cast rotor and seal holder meet LCF and creep life goals at 1500 °F, 1500 fps
- Tri-hub burst containment: Pressure vessel contains disc failure thru operating and overspeed conditions
- Pressure vessel sized and to be hydrotested to ASME pressure vessel code
- Squeeze film dampers damp anticipated imbalance.
Less than 0.001 in. run-out for anticipated imbalance.
- Relative seal-holder to test-rotor thermal growths acceptable thru 1500 °F operating range
- Rotor windage heating: > 150 °F at 1500 fps
- Critical fits: rotor, bearing, bearing nuts, etc., stay "tight" during maximum speed and temperature conditions

CD-97-76003

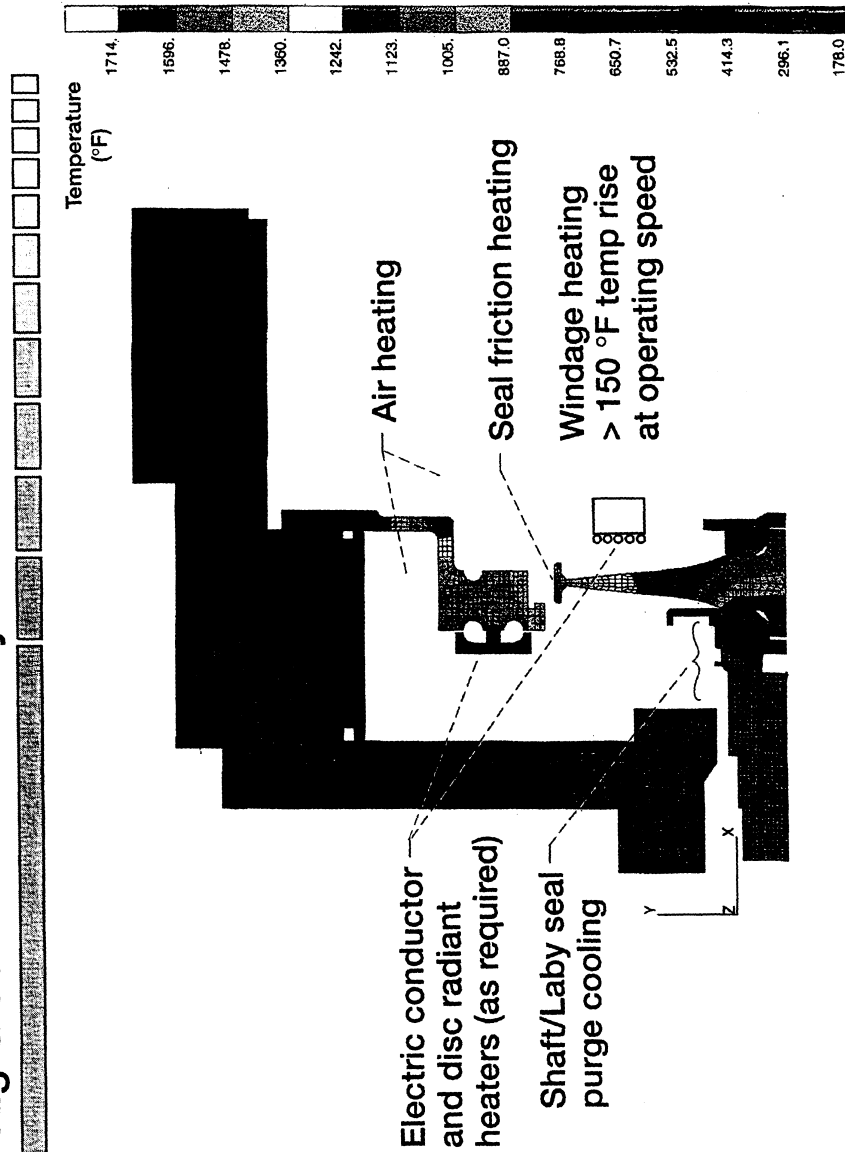
Seal Rig Global Thermal Analysis



Global thermal analysis with windage heating provides input to component stress and displacement analysis

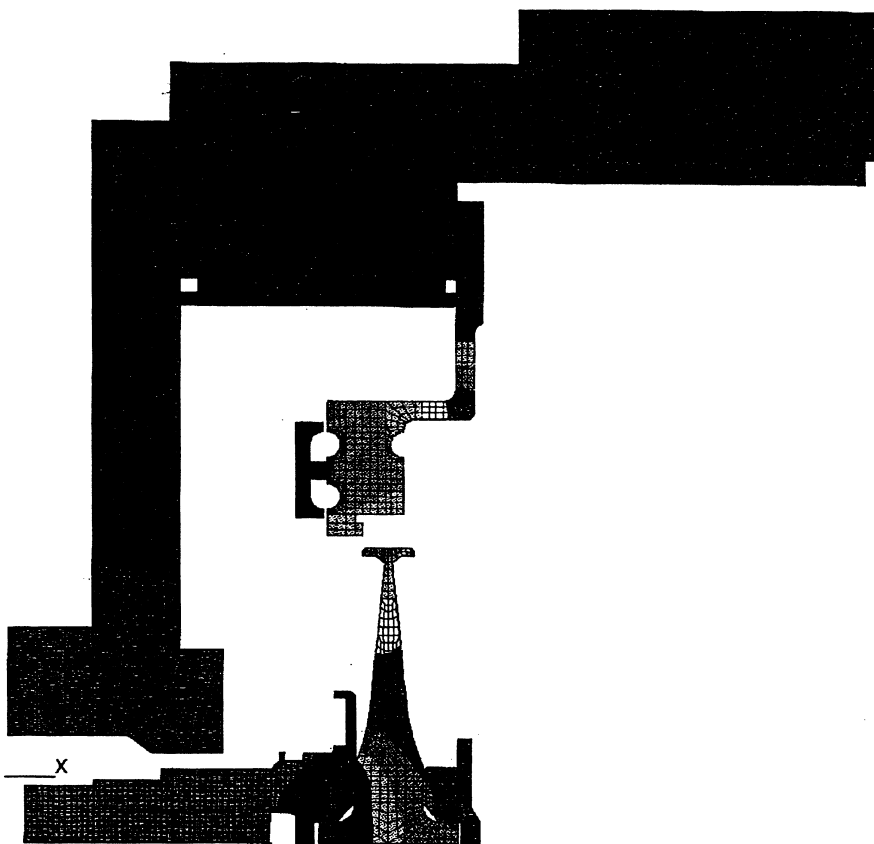
CD-97-76004

Seal Rig Global Thermal Analysis



Global thermal analysis with windage heating provides input to component stress and displacement analysis

CD-97-76004



17
15
14
13
12
11
10
88
76
65
53
41
29
17

Test Rig Status



- Engineering Calculations:
 - Rig capable of 1500 +fps/1500 °F operation
- Detailed Drawings:
- Facility/Test Cell Preparation:
 - High temperature valves/instrumentation ordered
- Complete Rig Fabrication
- Test rig ready for test

Complete

Complete June, '97

Ongoing

4thQ FY98 Est.

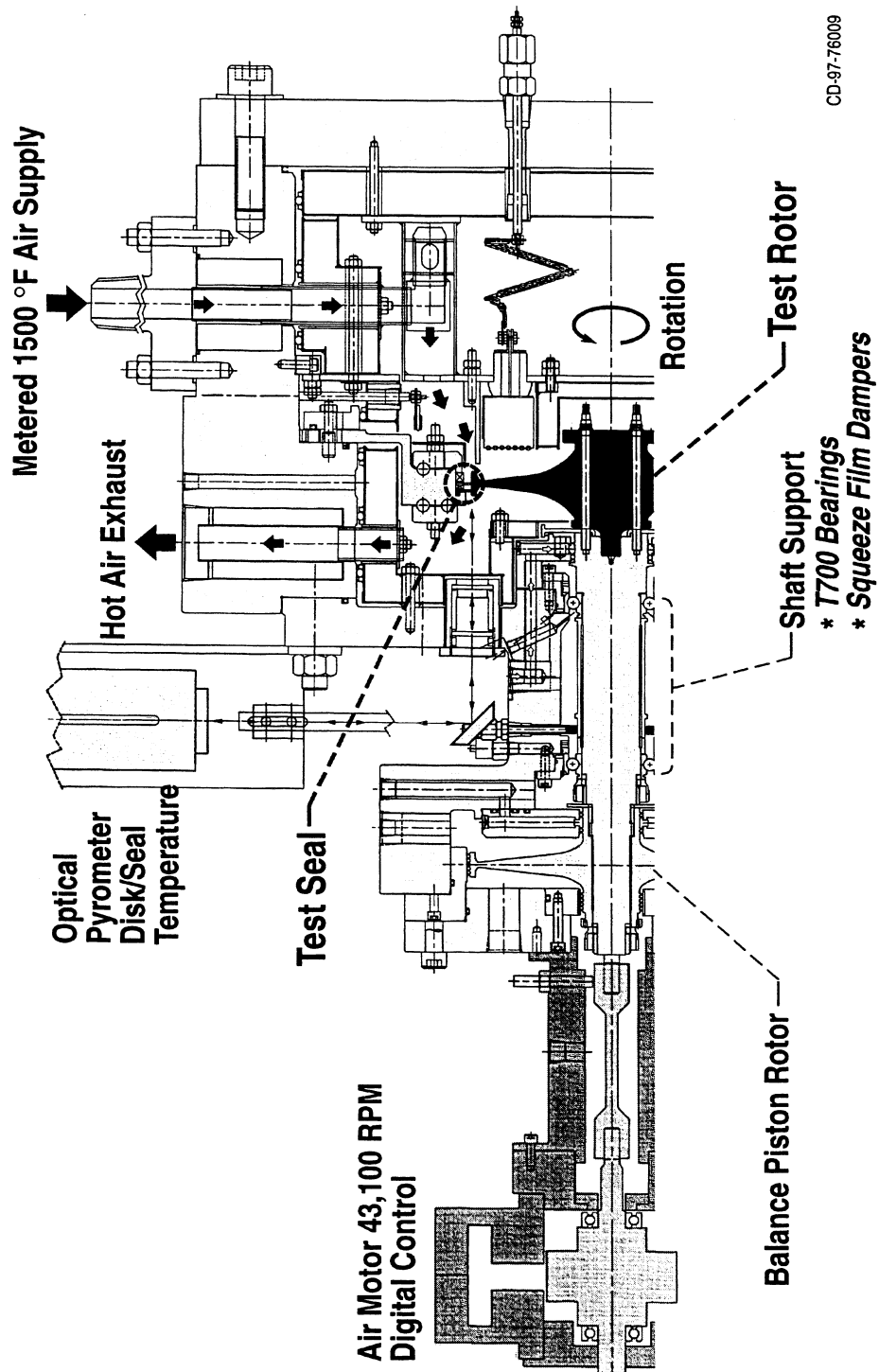
2ndQ FY99 Est.

Summary



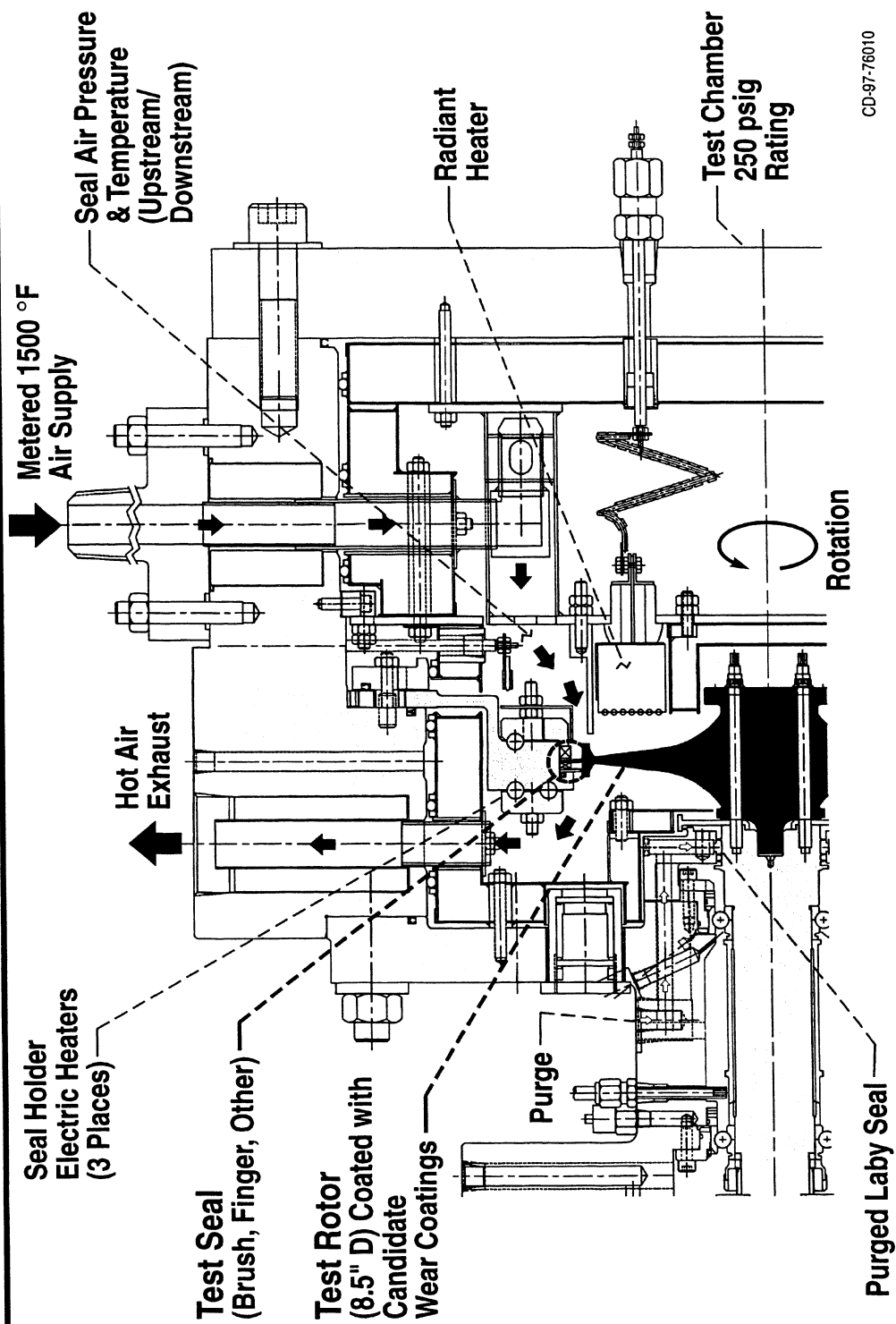
- Test rig heated by multiple conduction heaters, radiant heater and air heater to overcome significant metal heat loss permitting 1500 °F operation.
- Squeeze film dampers designed to provide smooth operation over operating range.
- MAR M-247 (Ni Co) cast alloy used for rotor and seal holder meet rotor and seal holder creep and LCF life goals.
- Test facility designed to meet anticipated IHPTET, HSR, AST seal test requirements: significant asset for the U.S. engine/seal community.

Seal Rig Schematic



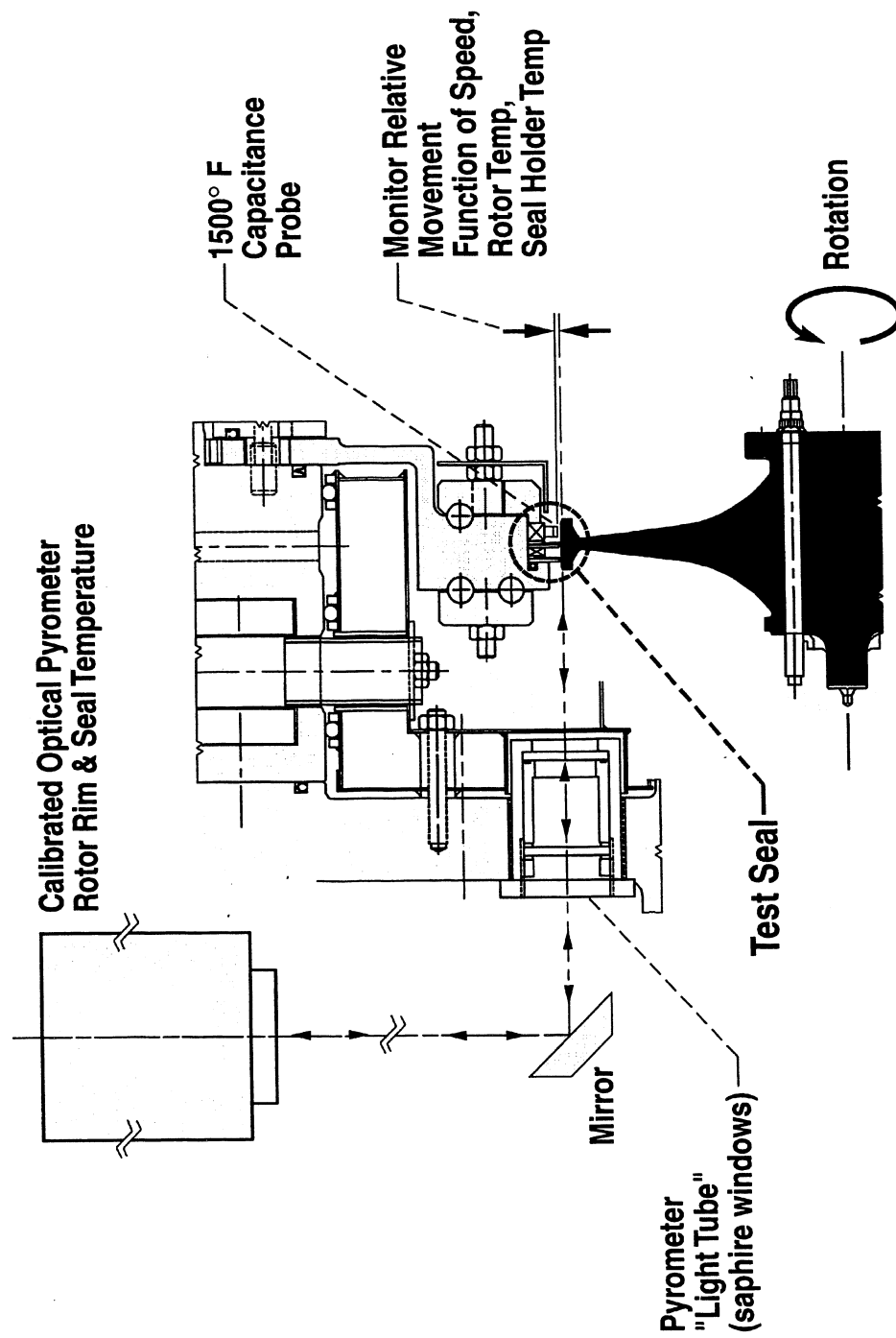
CD-97-76009

Test Chamber Enlarged View



CD-97-76010

Rig Features Unique Measurement Systems



CD-97-76011

EFFECTS OF 'COOLED' COOLING AIR ON PRE-SWIRL NOZZLE DESIGN

J.A. Scricca and K.D. Moore
Pratt & Whitney
West Palm Beach, Florida

ABSTRACT

It is common practice to use Pre-Swirl Nozzles to facilitate getting the turbine blade cooling air onboard the rotating disk with minimum pressure loss and reduced temperature. Higher engine OPR's and expanded aircraft operating envelopes have pushed cooling air temperatures to the limits of current disk materials and are stressing the capability to cool the blade with practical levels of cooling air flow. Providing 'Cooled' Cooling Air is one approach being considered to overcome these limitations. This presentation looks at how the introduction of 'Cooled' Cooling Air impacts the design of the Pre-Swirl Nozzles, specifically in relation to the radial location of the nozzles.

The current generation of engines now entering production have pushed the operating temperatures to the limits of current disk materials. Cooling air temperatures are reaching levels that challenge the capability of the airfoil designers to cool the airfoils with practical levels of cooling flow. To meet the goals of the next generation, advanced engine will require higher OPR's and operate in expanded flight envelopes which will push operating temperatures to even higher levels. Advanced materials and improved cooling technologies are being pursued to achieve these goals.

Another approach being considered to overcome these limitations is to provide 'Cooled' Cooling Air to the temperature limited components. For example, typical trade studies show that while holding metal temperature constant and cooling the cooling air temperature by 100°F would allow the combustor exit temperature to be increased 200 °F or the blade cooling air to be reduced by 15% of the uncooled cooling air level. While cycle studies incorporating these types of benefits have been done previously we are just starting to look at some of the consequences to the actual design of the engine internal flow system. Discussion of the results from these cycle studies or of specific methods to cool the cooling air will not be covered today. Rather, this presentation will look at how the introduction of Cooled Cooling Air impacts the design of the Pre-Swirl Nozzles, specifically in relation to optimizing the radial location of the nozzles.

NASA LeRC Seal/Secondary Flow Workshop

AGENDA

- Statement of the Problem
- Past Solutions
 - Commercial
 - Military
- ‘Cooled’ Cooling Air Effects
 - Redefinition of the Problem
 - Effects on Existing Engine Design
 - Proposed Solution
- Summary

LeRCTOBI.PPT

It is common practice to use Pre-Swirl Nozzles to facilitate getting the turbine blade cooling air onboard the rotating turbine disk with minimum pressure loss and reduced temperature. In today’s modern gas turbine engines the Pre-Swirl Nozzles, or ‘Pre-Swirler’ for short, is a annular vane cascade located just forward of the turbine disk. Some typical engine cross-sections are included later in the presentation. While it is intended to stick with the term “Pre-Swirler” throughout the presentation it is also noted that P&W nomenclature for the Pre- Swirler is to call it a “TOBI”, which stands for Tangential Onboard Injector.

The agenda for the presentation is outlined for you here. We will start by looking at a basic statement of the problem faced by the secondary flow analyst when designing the Pre-Swirler including a review of the factors that influence the optimum radial location. Next we will look at how these factors have influenced past designs and why the solution has been traditionally different for commercial and military applications. Introducing the ‘Cooled’ Cooling Air into the Pre-Swirler design results in some redefinition of the problem. We will look how this redefinition influences an existing engine design and then how changing the design results in an improved solution. The presentation will be concluded with a summary of the main points that were covered.

NASA LeRC Seal/Secondary Flow Workshop

Statement of the Problem

- Problem : Design Pre-Swirlers to Meet Blade Supply Pressure Requirement
- Givens : Rim Cavity Pressure, Radius of Blade Entrance , Rotor Speed, Pre-Swirlers Supply Conditions (P&T)
- Variables: Radius of Pre-Swirlers, Pressure Ratio, Pre-Swirlers Aero

LeRCTOBI.PPT

The number one requirement to meet with the design of a Pre-Swirlers is to assure that the supply pressure to the blade is always greater than or equal to the minimum level specified by the airfoil designer. As a minimum, not meeting this requirement results in higher operating temperatures, an increase in hot gas erosion and decreased airfoil life. If the pressure gets low enough then hot gas backflow into the airfoil can occur, leading to local burn-through and other conditions that dramatically decrease the airfoil's life.

In addition to the blade supply pressure requirement there are certain factors that influence the Pre-Swirlers design that are essentially outside the control of the secondary flow analyst. These are the 'Givens' in the problem and include things like the rim cavity pressure, radius of the cooling air entrance into the blade, rotor speed, and the conditions of the air supplied to the Pre-Swirlers. In conventional engines this air is usually supplied from the plenum around the combustor and inside the diffuser case. Therefore, the supply pressure and temperature are set by the high compressor exit conditions.

The variables of the problem include the radial location of the Pre-Swirlers, at least within some range governed by packaging of other hardware, etc. The pressure ratio across the Pre-Swirlers can also be varied somewhat with a minimum set by the rim cavity pressure. The aerodynamics of the Pre-Swirlers vane cascade can be varied in terms how close the air exit angle is from being tangential, velocity coefficients, etc. Keeping with good aerodynamic design practice keeps the realistic range of varying the vane cascade small.

NASA LeRC Seal/Secondary Flow Workshop

Statement of the Problem (Continued)

- Process
 - Combine the Givens with selected values for the Variables to define the Pre-Swirl Exit Velocity(V_t). This velocity sets the Blade Cooling Air Temperature ($T_{c/a}$) and results in additional Pressure Losses getting onboard the rotating structure if not matched with the Disk Speed (V_d)
- $$V_t = f(\text{Mach\#}, \text{angle}, C_v, \Delta P_t/P_t) \text{ where } \text{Mach\#} = f(P_r, T_{\text{supply}})$$
- $$T_{c/a} = T_{\text{supply}} + (V_{be}^2 - 2\eta V_d V_t) / (2g_c J c_p) \quad (\text{Reference 92-GT-378})$$
- Goals:
 - Lowest Blade Cooling Air Temperature
 - Lowest Leakage - Minimum TSFC
 - Lowest Weight
 - Maximum Piston Area for Bearing Thrust Load Control

LeRCTOBI.PPT

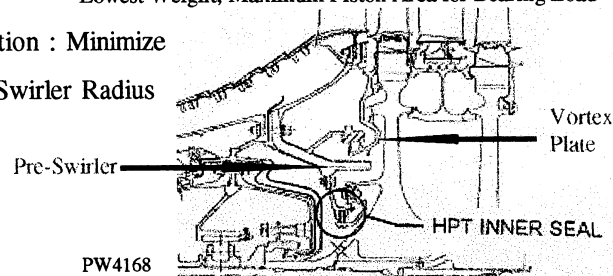
Using simple compressible flow theory the given information can be combined with selected values of the variables to define the tangential exit velocity of the Pre-Swirl. Once the velocity is known the cooling air temperature to the blade can be determined with Euler relationships. If the velocity is not matched with the wheel speed of the rotating structure, where the air is brought onboard the disk, then additional pressure losses result which must be accounted for in the analysis.

Selecting different values for variables results in a matrix of solutions that can meet the blade supply pressure requirement. Selecting the optimum solution from this matrix depends on the relative importance of several additional goals in the particular engine design. These goals include supplying the blade with the lowest cooling air temperature to minimize the blade cooling air flow rate. This cooling air temperature is a key driver in the determining the blade attachment temperatures well. Keeping the Pre-Swirl exit pressure as low as possible minimizes leakage which increases turbine efficiency and minimizes TSFC. Keeping the weight down is always a goal. Lastly, the Pre-Swirl and associated seals form a piston area that is included in the bearing thrust load calculation. For most engines, maximizing this piston area, which is done by increasing the Pre-Swirl radius, is beneficial to overall thrust load control.

NASA LeRC Seal/Secondary Flow Workshop

Past Solution - Commercial

- Primary Goals : Lowest Possible Leakage - Minimize TSFC
- Secondary Goals : Lowest Blade Cooling Air Temperature,
Lowest Weight, Maximum Piston Area for Bearing Load
- Solution : Minimize
Pre-Swirl Radius



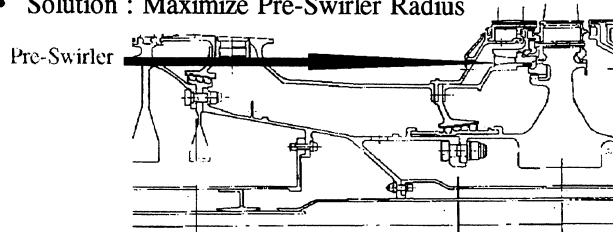
LeRC TOBI.PPT

Here is a picture of the high turbine area of a fairly typical current generation commercial engine, specifically the PW4168. It can be seen that the Pre-Swirler is located fairly far radially inward in the available space forward of the turbine disk. This type of design results when the primary goal is to have the lowest possible leakage. The Pre-Swirler exit pressure is set to a level just above the front rim cavity pressure, minimizing the ΔP across the swirler cavity seals. A vortex plate is used to allow the oversped air to vortex outward, causing an increase in pressure, before it is captured by the slots between the HPT disk and the vortex plate.

The low leakage levels possible with this type of design results in better TSFC than alternatives that place the Pre-Swirler further out in radius. However, it also results in warmer blade cooling air temperature and smaller thrust load piston areas. In essence, these goals have been made secondary. The engine is probably heavier as well, for instance, other features have to be added or made more complex to control bearing thrust loads. It should be noted that later PW4000 models have moved the Pre-Swirler out in radius because the operating temperatures reached levels that would have resulted in blade cooling air temperatures that exceeding allowable limits for the blade attachment design with this 'low radius design'.

NASA LeRC Seal/Secondary Flow Workshop
Past Solution - Military

- Primary Goals : Lowest Blade Cooling Air Temperature,
Lowest Weight
- Secondary Goals : Maximum Piston Area for Bearing Load Control,
Lowest Leakage - Minimum TSFC
- Solution : Maximize Pre-Swirl Radius



LeRCTOBI.PPT

Military engines on the other hand, have typically operated to flight Mach numbers that required the design to achieve the lowest possible cooling air temperature. Fighter engines are also more sensitive to weight than commercial engines. A design that emphasizes these goals leads to the Pre-Swirl being placed as far out in radius as possible within the available space. This engine cross-section is typical of this type of design. This design does maximize the thrust piston area but it isn't really a primary goal. Similarly, low leakage levels are desired to minimize TSFC but this will be compromised if necessary to achieve the primary goals. However, as the military adjusts to the post cold war world we are seeing TSFC concerns play more importance in design decisions.

NASA LeRC Seal/Secondary Flow Workshop
'Cooled' Cooling Air Effect on the Problem

- Problem : Design Pre-Swirlers to Meet Blade Supply Pressure Requirement
 - Givens : Rotor Speed, Rim Cavity Pressure, Radius of Blade Entrance
 - Variables : Radius of Pre-Swirlers, Pressure Ratio, Pre-Swirlers Aero
- ➡ Pre-Swirlers Supply Conditions (P&T) ← Become a Variable
- Goals :
 - Lowest Blade Cooling Air Temperature
 - Lowest Leakage - Minimum TSFC
 - Lowest Weight
 - Maximum Piston Area for Bearing Thrust Load Control

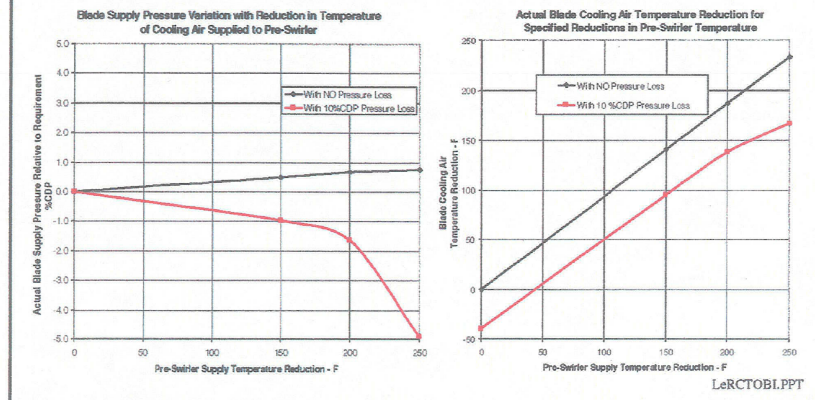
LeRCTOBI.PPT

The primary effect of adding a Cooled Cooling Air system on the design problem is that the Pre-Swirlers supply conditions are no longer a given and become a variable. Obviously the amount of temperature reduction by the system can be varied. The pressure loss through the cooling system can also be varied by designing with larger size pipes, heat exchangers and so on. Some cooling systems have even proposed auxiliary compressors to offset the plumbing losses but this is not considered likely in the near term. Therefore the supply pressure to the Pre-Swirlers is going to be somewhat reduced due to these losses.

While these supply conditions can be varied there is a direct effect on the tangential velocity of the air exiting the Pre-Swirlers. First, if nothing else changed the velocity would come down proportional to the square root of the reduction in temperature. Including the pressure losses reduces the pressure ratio and therefore the exit Mach number causing even more reduction in velocity. This new exit velocity must be compared with the speed of the rotating structure and factored back into the cooling air temperature calculation and the pressure losses getting onboard the turbine disk.

NASA LeRC Seal/Secondary Flow Workshop Results on Existing Engine Design

- 'Cooled' Cooling Air Added, Pre-Swirler Design Unchanged



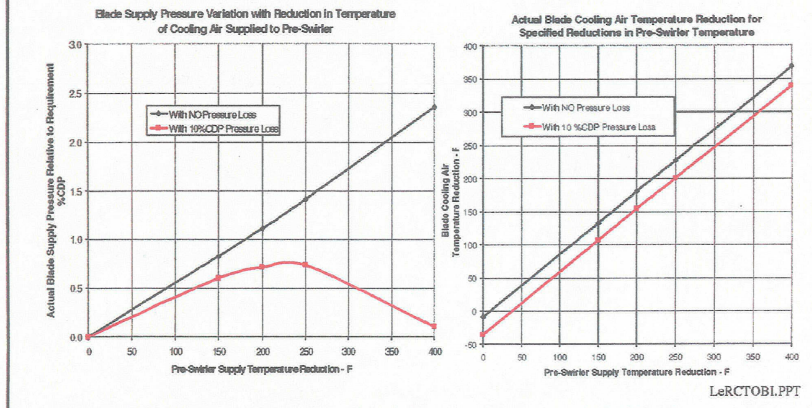
This slide shows what happens to blade supply pressure and temperature when a cooled cooling air system is added to an existing engine and no other design changes are made. Looking at the chart on the left and assuming that the cooling air system had no pressure loss (black line) it can be seen that the blade supply pressure actually rises a slight amount as the temperature is reduced. This is because the base design actually oversped the air exiting the Pre-Swirler, increasing the pressure loss getting onboard the disk, to drive the cooling air temperature to the lowest possible value. Therefore the lower velocity obtained by cooling the cooling air reduces the velocity mismatch thereby reducing the pressure loss due to it.

Including a pressure loss of 10% of the Compressor Discharge Pressure (CDP) for the plumbing losses of the cooling system gives quite a bit different result. The blade supply pressure falls gradually as the cooling air temperature is reduced up to about 175 °F. Cooling the air further causes a rapid fall in pressure because the pressure losses due to the velocity mismatch become the dominate factor in the system. This characteristic is considered to be unacceptable for an engine that has to operate over a wide range of operating conditions that is typical for a fighter engine.

The right-hand chart also reveals that the actual temperature reduction achieved at the blade entrance is significantly less than anticipated by looking at temperature reduction supplied to the Pre-Swirler. For instance, a cooling system sized to reduce the cooling air temperature by 200 °F would only achieve about 140 °F temperature reduction at the blade. Therefore, the cooling capacity of the system would have to be increased to achieve an actual 200 °F reduction at the blade entrance.

NASA LeRC Seal/Secondary Flow Workshop Proposed Solution

- Pre-Swirler Moved Radially Inward



This slide provides the same two charts on blade supply pressure and temperature for a design where the Pre-Swirler has been moved radially inward. It can be seen that blade supply pressure is fairly constant over a wide range of supply temperature reduction when the 10% CDP pressure loss is included. The maximum pressure point represents a condition where the Pre-Swirler exit velocity equals the wheel speed of the rotating structure that brings the air onboard the disk. The actual radial location of the Pre-Swirler to get this type of characteristic for any engine is then driven by achieving this zero velocity mismatch condition with the desired amount of temperature reduction.

From the right hand chart the slight temperature penalty for moving the Pre-Swirler inboard is seen with no supply temperature reduction and no pressure loss. Once again the actual temperature reduction achieved at the blade is less than the amount of supply temperature reduction. However, it is improved with the proposed design because 155 °F in blade supply temperature reduction is achieved (was 140 °F) for our example of 200 °F reduction in supply temperature.

NASA LeRC Seal/Secondary Flow Workshop

Summary

- 'Cooled' Cooling Air Reduces Pre-Swirl Exit Velocity Because of the Lower Sonic Velocity and System Pressure Losses Reducing the Pre-Swirl Pressure Ratio
- Radial Location of the Pre-Swirl Must Be Adjusted to Account for These Effects and Still Meet the Blade Supply Pressure Requirement
- Pre-Swirl Supply Temperature Must Be Overcooled to Achieve A Given Reduction in Blade Supply Temperature

LeRCTOBI.PPT

ROTATING BRUSH SEAL

S.B. Lattime, M.J. Braun, and F.K. Choy
B&C Engineering Associates, Inc.
Akron, Ohio

and

R.C. Hendricks and B.M. Steinetz
NASA Lewis Research Center
Cleveland, Ohio

ABSTRACT

The proven technology of brush seals has been extended to the mitigation of problems arising from friction and wear at the bristle-rotor interface at high surface speeds. In prototype testing, the brush is mounted on, and free to rotate with the shaft, thus providing a compliant primary seal. A face seal positioned between the backing plate of the brush seal and the housing provides a secondary seal. The purpose of this paper is to demonstrate the interaction between the brush bristles and the shaft at high surface speeds as well as introduce a numerical model to simulate the bristle behavior.

A test facility was constructed to study the effects of centrifugal forces on bristle deflection in a single rotating brush seal. The bristle-rotor interface was observed through a video camera, which utilized a high magnification borescope and a high frequency strobe light source. Rotational speeds of the rotor and the brush seal were measured by a magnetic and optical speed sensor, respectively. Preliminary results with speeds up to 11,000 rpm show no speed differential between the brush seal and rotor, or any instability problems associated with the brush seal. Bristle liftoff from the rotor is successfully captured on video.

Keywords: Hybrid brush seal, film riding face seal, turbomachinery, bristle wear, thermal loads.

INTRODUCTION

Brush seals, due to their compliance characteristics, have become a rather serious competitor for replacement of their predecessors, the labyrinth seal, in gas turbine engines. Brush seals allow axial or radial excursions of the spool shafts without suffering damage or affecting the sealing integrity. In 1988, Ferguson [1] reported that over thousands of hours of testing, brush seal leakages were, on the average, 5-10% of those allowed by equivalently sized labyrinth seals. In 1991, Chupp et al. [2] showed brush seal leakage reductions of 4.5 times that of labyrinth seals. Proctor et al. [3] tested single and double sets of brush seals in liquid nitrogen and liquid hydrogen at speeds up to 65,000 rpm and pressure drops up to 175psid per brush. The authors found leakage rates for a single brush to be 1/3 that of a 12-tooth labyrinth seal, and half that leakage rate when two brush seals, spaced about 0.25 inches apart, were used.

Although brush seals show a vast improvement in leakage performance over other seals, they can still be subject to catastrophic wear at the shaft/brush interface, through excessive thermal loads generated by the friction due to the relative differential in sliding speeds. Much of the current literature on brush seals deals with the wear characteristics and material selection. In 1992, Atkinson and Bristol [4] investigated bristle and rotor wear with two different bristle materials (cobalt and nickel based alloys) and three different coating materials (chromium carbide, tungsten carbide, and aluminum oxide). They found the brush wear to be temperature dependent. Hendricks et al. [5] reported preliminary results of brush seal testing in the fourth-stage turbine of the G.E. T700 engine. Integrity testing of a brush seal in the shroud ring of a T-700 engine was also performed. The brush seal contained 0.0028 in. diameter bristles of Haynes 25, at a lay angle between 43 to 50°. The design clearance was 0.02 to 0.05 in. The turbine was operated at 10,000 rpm and 850°F and at 20,000 rpm and 1050°F. Post test investigations showed regions of the brush seal where bristles had been pulled out and bent-over near the inlet

of the seal, snapped near the fence plate and a uniform smeared interface between the first and last axial rows. Forry [6] tested wear characteristics between Inconel X-750 and Haynes 25 bristles, both with a chrome-carbide rotor journal coating. Both brush seals were run at 23,500 rpm at approximately 900°F for 10 hours, and had an interference of about 0.03 in. with the rotor. Post test measurements indicated a wear of 0.033 in. for the X-750 bristles and 0.037 in. for the Haynes 25 bristles.

Generally, most of the activities related to the brush seal development have been experimental, with few notable exceptions. Thus Braun et al. [7], and Hendricks et al. [8], offered a bulk flow model for flow through the body of a brush, based on analytical and experimental developments concerning flow in porous media. The analytical results, when compared with experimental data showed relatively good coincidence. The maximum differential in results was observed at low flows, and was approximately 30%.

THE CONCEPT OF THE HYBRID FLOATING BRUSH SEAL (HFBS)

Attempting to utilize the improved leakage characteristics of brush seals for gas turbine applications, while eliminating the high relative surface speeds, Braun et al. [9], and Braun and Choy [10], have developed the concept of a hybrid brush seal which rotates with the shaft while riding against a non-contacting gas face seal. This arrangement is shown schematically in Figure 1. The figure depicts a longitudinal cross section through the seal test rig. The brush seal is free to rotate with the shaft while seated in between two film riding face seals. The face seals act as secondary seals while providing dynamic stability and preventing the brush seal from axial travel with the rotor. This hybrid brush seal concept was tested successfully in feasibility studies under a Phase 1 of a NASA SBIR award. The feasibility studies were run at rotor velocities of up to 5,000 rpm at room temperature. The second phase of this prototype development involves testing the seal configuration at speeds up to 40,000 rpm and temperatures up to 900°F, conditions that model actual engine conditions.

This paper presents some experimental preliminary results showing the effects of centrifugal forces on bristle displacement due to brush rotational velocities up to 11,000 rpm. An analytical predictive model based upon a simple, single beam deflection theory will be presented as well.

EXPERIMENTAL APPARATUS

The test rig is shown schematically in Figure 2. A steel shaft is supported at each end by ball bearings located in upright aluminum housings. The shaft is driven by a variable speed motor that is connected through a belt and pulley system. The pulley system allows the shaft to reach velocities as high as 15,000 rpm. The shaft's rotor is stepped to different diameters allowing different pre-loads of the brush seal bristles.

A magnetic speed sensor was positioned on the pulley end of the shaft to measure its rotational velocity. An optical speed sensor was positioned on the outer diameter of the brush seal to detect a small strip of reflective tape bonded to the outer circumference of the seal.

A video camera connected to a high magnification borescope was used to capture images at the bristle-rotor interface. The borescope was coupled to an electronic stroboscopic mechanism, which was activated by an external optical sensor that sensed the same reflective tape used by the optical speed indicator. Two additional video cameras were used along with a video mixer and a VCR to record a panoramic view of the brush seal and the two speed indicator meters. A Nikon 35mm SLR camera was used to capture, off-line, still pictures of the images recorded on videotape during the experiment.

The brush seal that was used for this analysis was designed by B&CEA and manufactured by Cross Manufacturing Ltd. (Devizes, U.K.). Figure 3 shows a schematic of the brush seal and its dimensions. The brush contains 10 rows of 0.004 in. diameter bristles made of Haynes 25. The bristles are inclined 30° in the direction of the rotor rotation. The side plates are approximately 0.1 in. thick and have inner and outer diameters of 2.88 in. and 3.7 in., respectively. The ends of the bristles make up the inner diameter of the seal at 2.78 in. The design of the brush seal came from analytic modeling of the bristle behavior, which will be described in the analytical model section of this paper.

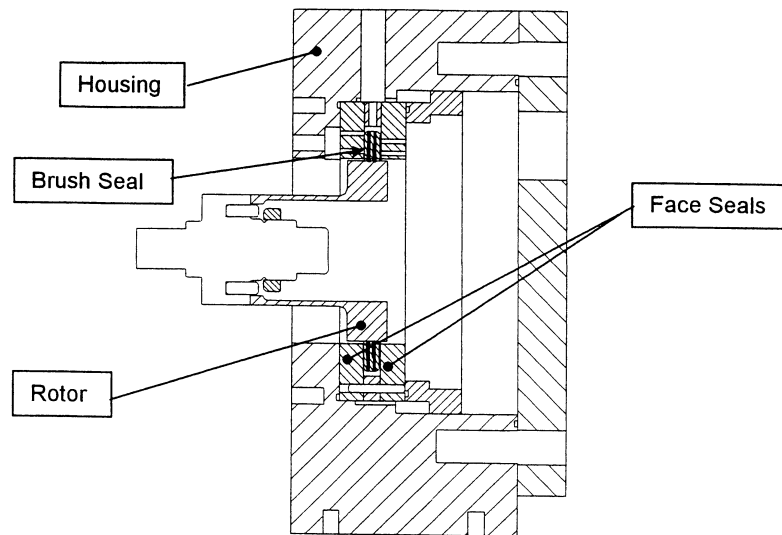


Figure 2: Cross section of hybrid brush seal assembly

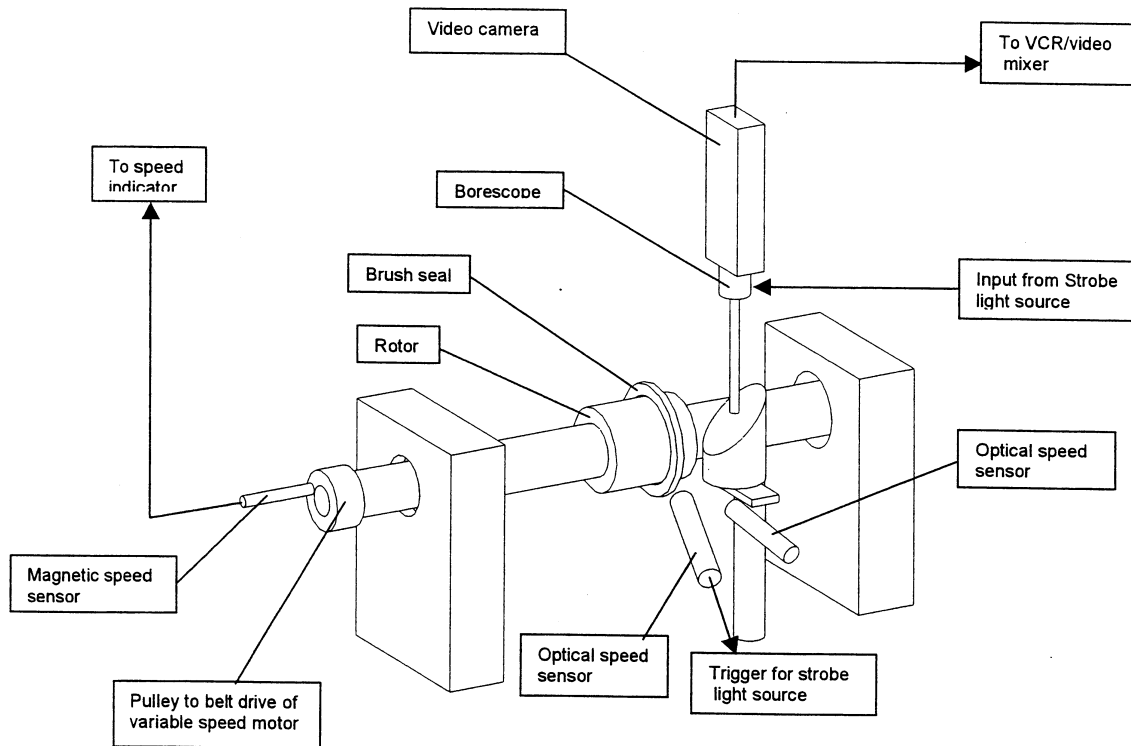


Figure 1 : Experimental apparatus schematic

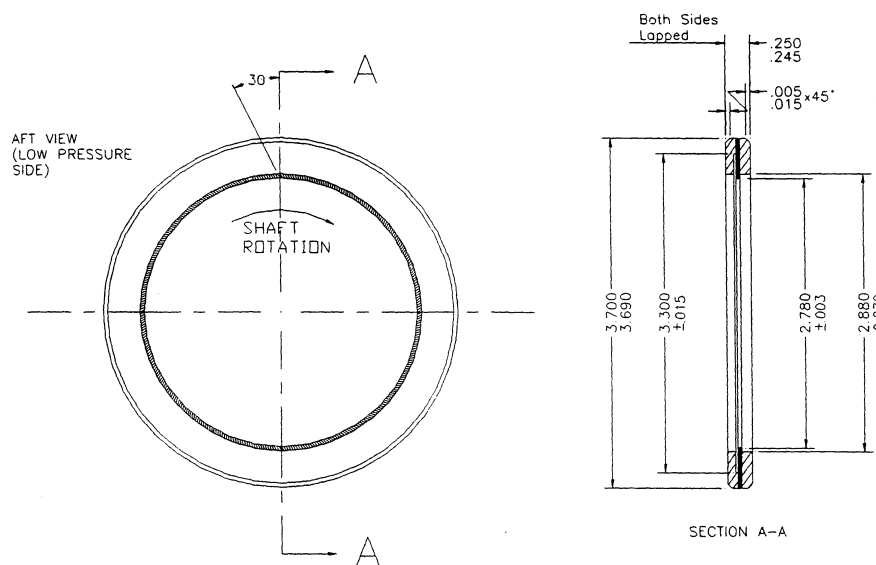


Figure 3: Brush seal

EXPERIMENTAL PROCEDURE

The brush seal was centered on a 2.788 in. diameter section of the rotor, producing 0.004 in. of radial pre-load. The optical speed sensors were positioned to face the outer circumference of the brush seal. A 0.125 x 0.5 in. strip of reflective tape had been bonded on the outside diameter of the brush seal and served as the trigger for the optical sensors. One of the optical sensors measured the speed of the brush seal. The second optical sensor triggered the light source to flash at the rotational speed of the brush seal, allowing the capture of a "frozen" image of the bristle-shaft interface through the borescope. The magnetic speed sensor was positioned to face a key at the pulley end of the shaft.

Three video cameras were used during the experiment. The first camera was attached to the borescope and positioned vertically over a 45° angled mirror, see Figure 2. The mirror allowed the camera to look in the axial direction, along the shaft, at the bristle-rotor interface. The borescope end was directed to a circumferential position of about nine o'clock on the brush seal plane. The second video camera was positioned to take a panoramic image of the backside of the brush seal. This camera was also utilized to view any strobed light of the borescope coming through the bristle pack. Penetration of such light was a clear indication of bristle lift-off from the rotor. The third camera was positioned on the speed indicator meters to view the speeds of both the rotor and the brush seal simultaneously with the other two views. A Videonics digital mixer was used to incorporate two of the three images on the same picture. This allowed the speeds of the brush seal and rotor to be captured interchangeably with the panoramic and magnified views of the brush seal.

After the system had sufficient time to warm up, the rotor was brought to 1,000 rpm and the VCR began recording images. Images were recorded of the bristle-rotor interface, with and without the speed meters, and the panoramic view of the backside of the brush seal with the speed meters. This procedure was repeated for speeds up to 4,000 rpm, in increments of 1,000 rpm. The rotor speed was then increased in increments of 200 rpm from 4,000 to 11,000 rpm, with the same sets of images being recorded.

For visual characterization of the transient behavior of the brush seal, both the bristle-rotor interface and the back plane of the brush were recorded concomitantly. The rotor was brought up from 0 to 11,000 rpm in 27 seconds and then down from 11,000 to 0 rpm in 35 seconds.

ANALYTICAL MODEL OF BRISTLE DEFLECTION

The design process of the brush seal involved parametric calculations using the geometric characteristics and material properties of the bristles. The calculations allowed the determination of the highest rotational speed at which the bristles would begin to lift off the rotor for a given bristle geometry. These properties included: a) total length of the bristles; b) length of the back and front plate; c) diameter of the bristles; d) lay angle of the bristles; e) bristle pre-load; f) bending stress of the bristles.

The eventually chosen geometric parameters were designed to assure that bristle lift off would be delayed as much as possible. This is necessary in order to assure that the brush speed tracks the shaft speed as closely as possible. The present analysis considers only two forces contributing to the bristle deflection; bristle pre-load (interference of the inner diameter of the brush seal over the outer diameter of the rotor), and centrifugal force, due to the rotation. Other influences, such as windage of the rotor and bristle packing have not been included in this analysis.

Consider the forces acting on a single bristle of length ℓ , diameter d , under a pre-load P , lay angle θ , and a rotational speed ω . The pre-load is the force applied by the rotor onto the bristle, as the O.D. of the rotor pushes the end of the bristle outward radially from its center. This is shown schematically in Figure 4. The deflection, δ_p , due to pre-load, P , is given by:

$$\delta_p = \frac{Pl^3}{3EI} \quad \text{where} \quad I = \frac{\pi d^4}{64} \quad (1)$$

The deflection, δ_w , due to centrifugal load, q , (assuming a uniform load) is given by:

$$\delta_w = \frac{ql^4}{8EI} = \frac{wl^3 \sin \theta}{8EI} \quad (2)$$

$$\text{where} \quad q = \frac{w \sin \theta}{l} \quad w = mr\omega^2, \quad I = \frac{\pi d^4}{64} \quad \text{and } m \text{ is the mass of the bristle}$$

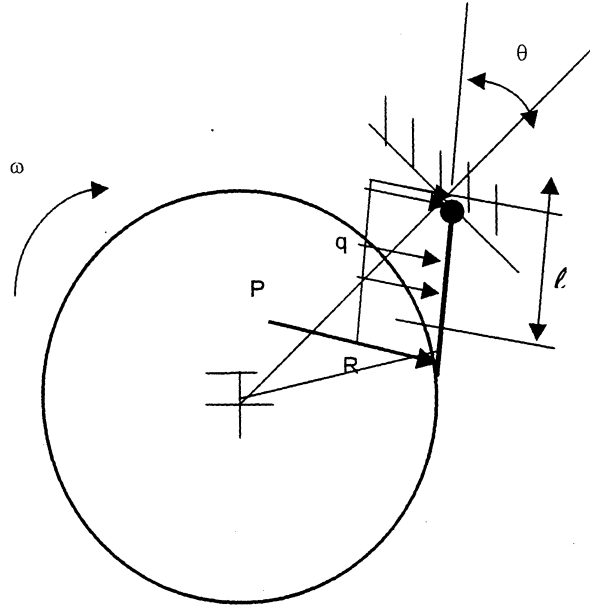


Figure 4: Single bristle under pre-load P and speed ω

Next, we analyze what happens to the bristle as it begins to rotate with the shaft. The bristle will remain in a constant state of deflection, δ , developed from the pre-load, from $\omega = 0$ until $\omega = \omega^*$, where ω^* is the speed at which the centrifugal load begins to lift the bristle off the rotor. With this in mind, we examine three cases:

- I. $\omega = 0$: $\delta = \delta_{p1} + \delta_{w1}$, but $\delta_{w1} = 0$. Thus, $\delta = \delta_{p1}$.
- II. $0 < \omega < \omega^*$: $\delta = \delta_{p2} + \delta_{w2}$. Thus, $\delta_{p2} < \delta_{p1}$ and $\delta_{w2} > 0$.
- III. $\omega = \omega^*$: $\delta = \delta_{p3} + \delta_{w3}$, but $\delta_{p3} = 0$. Thus, $\delta = \delta_{w3}$ and $\delta_{w3} > \delta_{w2}$.

Looking at the problem from this point of view, we see that as speed increases, the pre-load force decreases, and the centrifugal force increases. Proceeding along this course, we are now interested to find what speeds are attainable for a given bristle geometry and pre-load at which the bristles begin to lift off the rotor.

Using these simple equations, the brush seal design was principally controlled by the rotational speed at which the circumferential force would overcome the bristle pre-load for various bristle geometries. At this point, the bristles would begin to lift off the rotor and, presumably, the brush seal would begin to slip on the circumference of the rotor.

DISCUSSION OF RESULTS

ANALYTICAL MODEL

Table 1 presents a parametric study for bristle design, based on previously mentioned equations, used in the design of the brush seal. The table presents values for bristle diameter (d), and length (L), radius of the rotor (R), rotational speed (ω), lay angle (θ), total deflection (δ - pre-load deflection at 0 rpm), deflection due to centrifugal force (δ_w), deflection due to pre-load (δ_p), and total bending stress (σ). Rotational speeds were increased from 0 rpm until the centrifugal deflection equaled the pre-load deflection at 0 rpm. This is the speed at which the bristle would begin to lift off the rotor. Bristle diameters from 0.001 to 0.005 in., bristle lengths of 0.4 to 0.15, pre-load deflections of 0.015 to 0.002 in., and lay angles of 20 to 60° were examined. The numbers shown in the table represent some of the more physically realistic geometries.

Preliminary testing for bristle lift speed on some previously acquired brush seals, when compared to the model's predictions, showed the analytical results to be conservative. We felt at this point that the effects of bristle packing were responsible for the model's early lift off predictions. The results from the bristle deflection model and discussions with the brush seal manufacturer led to the brush seal design previously shown in Figure 3. The single brush consists of ten rows of 0.004 in. diameter bristles, 0.31 in. long, at angle of 30°. The model predicted bristle lift off after 4,155 rpm, as shown in the last entry of Table 1. The brush seal, being positioned on the 2.788 in. diameter of the rotor, produced a radial pre-load deflection of 0.004 in.

d (in)	L (in)	R (in)	ω	θ	δ (in)	δ_w (in)	δ_p (in)	σ (psi)
0.004	0.3	1.4	7010	30	0.01	0.00999	9.59E-06	26660.27
0.004	0.3	1.4	4960	30	0.005	0.005002	-1.6E-06	13334.41
0.004	0.25	1.4	10170	30	0.01	0.010005	-4.9E-06	38404.73
0.004	0.25	1.4	7190	30	0.005	0.005001	-6.9E-07	19200.66
0.004	0.2	1.4	16000	30	0.01	0.010004	-4E-06	60006.07
0.004	0.2	1.4	11310	30	0.005	0.004999	1.25E-06	29998.12
0.004	0.31	1.394	4155	30	0.004	0.003997	3.39E-06	10617.44

Table 1. Bristle Design Parameters vs. Speed

EXPERIMENTAL RESULTS

Figures 5 and 6 show a series of video images collected during the experiment. Figure 5 shows the bristle-rotor interface at rotational speeds of 8, 9, and 10,000 rpm. The bristles began to separate from the rotor around 5,000 rpm, after which the separation gap continued to grow. The gaps that are shown in the figures, between the rotor O.D. and the brush seal I.D., are about half the size that they appear to be. The rotor surface reflects the bristle ends so that a mirror image appears at the bristle-rotor interface. This reflection is seen because 45° mirror was rotated slightly outside the O.D. of the rotor surface in order to bring more light to the bristle-rotor interface. The speeds of both the rotor and brush seal are shown in all the figures. The brush kept up with the rotor to the maximum tested rotor speed of 11,000 rpm. The theory developed from the analytical model suggested that as the bristles lifted off the rotor, the brush seal would begin to slip and thus, rotate at a slower angular velocity than the rotor. The experiments showed that as the rotational speed of the brush seal increased, a critical speed ω_c was reached, after which, the bristles began to lift off the rotor. However, the brush seal did not, as our theory assumed, begin to slip after the critical speed was reached or surpassed. Figure 5 shows the bristle-rotor interface at speeds of 8, 9 and 10,000 rpm, well after bristle lift off had occurred, with no speed differential occurring between the rotor and the seal. It is apparent that an aerodynamic layer is developed between the O.D. of the rotor and the I.D. of the brush seal. This layer provides enough friction between the rotor and the bristles such that the rotational speeds of each remain synchronous. The circumferential momentum of the vortex layer is very significant since it can potentially provide sealing capabilities with no direct contact between the rotor and the brush. This phenomenon occurred throughout the experiments, even at the maximum tested speed of 11,000 rpm.

Figure 6 shows a panoramic view of the backside of the brush seal. After a rotational speed of 9,500 rpm, the light being emitted from the strobe light source can be seen coming through the bristle pack from the backside of the brush seal. This is clearly demonstrated from the series of photos in Figure 6. The light (encircled in white) is shown to grow with the rotor (brush seal) speed, at the bristle-rotor interface, at the three o'clock position on the brush seal back face. Although not shown in any of the figures, the clearance between the inner diameter of the brush seal and the outer diameter of the rotor was visually observed around the entire circumference of the rotor from speeds above 8,000 rpm. The relative speeds of both the rotor and brush seal are shown not to vary up through 11,000 rpm. The radial clearance between the rotor O.D. and the brush seal I.D. at 10,000 rpm was measured to be approximately 0.01 inches.

The transient behavior of the brush seal was observed and recorded on video. This was accomplished by bringing the rotor rapidly up to the maximum operating speed of 11,000 rpm from rest, and then shutting down the motor or bringing the speed down rapidly with the motor controller. The same clearances from bristle deflection were observed as when acquired the gradual increase or decrease of speed. The panoramic view of the brush seal showed no signs of instability in any of the tests performed. Inspection of the brush seal showed no damage to the bristles due to ramp up or shut down speed changes. This result is very important, in that, it was previously believed that rapid decreases in rotor speed could damage the bristles because the relative motion of the rotor will be against the bristle lay angle.

EXPERIMENTAL-ANALYTICAL COMPARISON

Table 2 shows a table of centrifugal deflections versus speed based on the analytical model and measurements of the captured images. The model predicted bristle liftoff after 4,155 rpm. This was fairly close to experimental observations. The bristles were observed to lift around 4,500 to 5,000 rpm. The centrifugal deflections measured from the experimental images and those predicted by the model, as shown in Table 2, do not correspond. We believe the large discrepancies in the predicted bristle deflections are due to the effects of bristle packing, which was not incorporated in the model. The model was based on a single bristle and applied to more than 190,000 bristles (10 rows at 2170 bristles per inch of bore circumference, nominal).

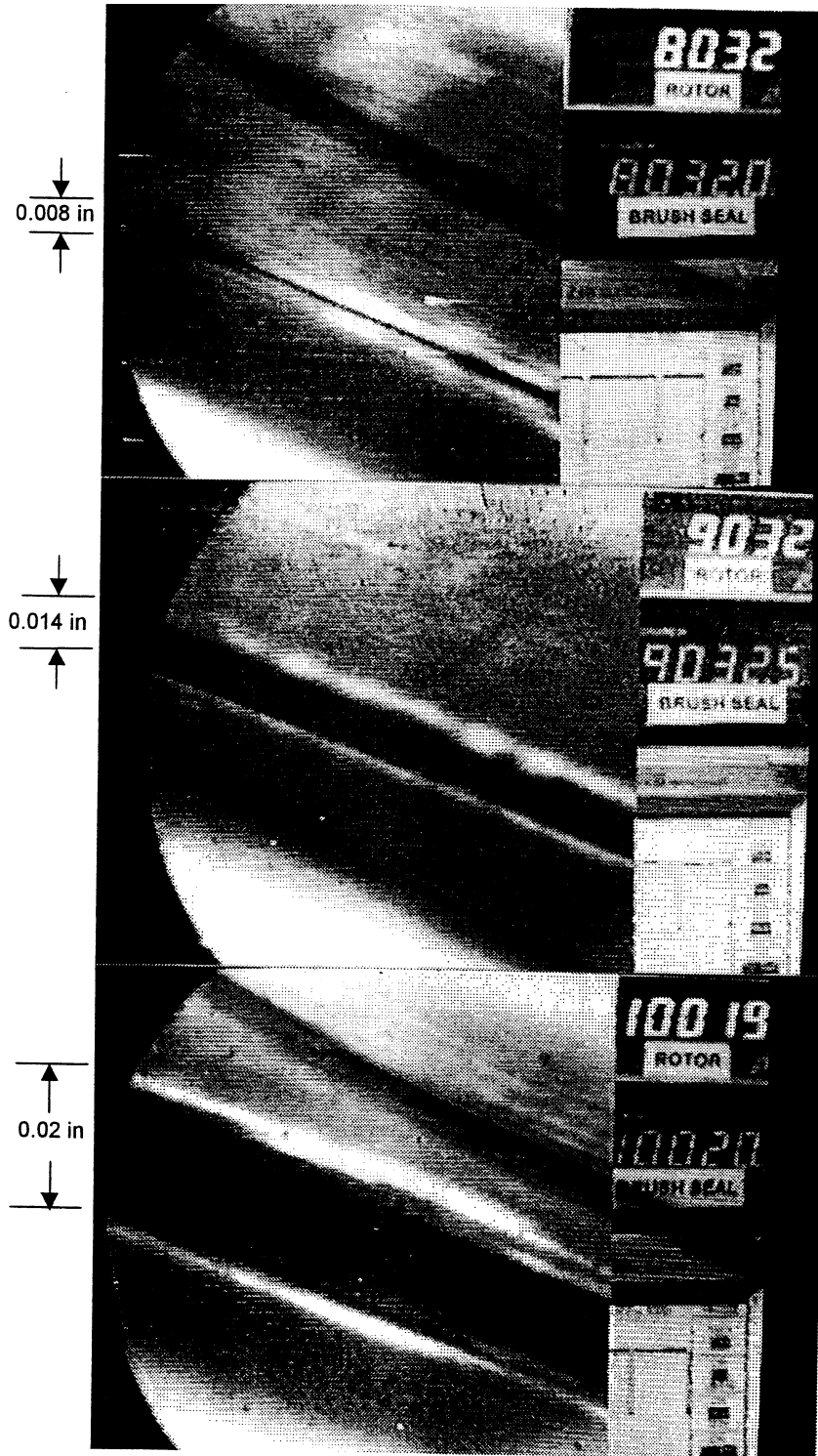


Figure 5: Bristle-rotor interface at 8, 9, and 10,000 rpm

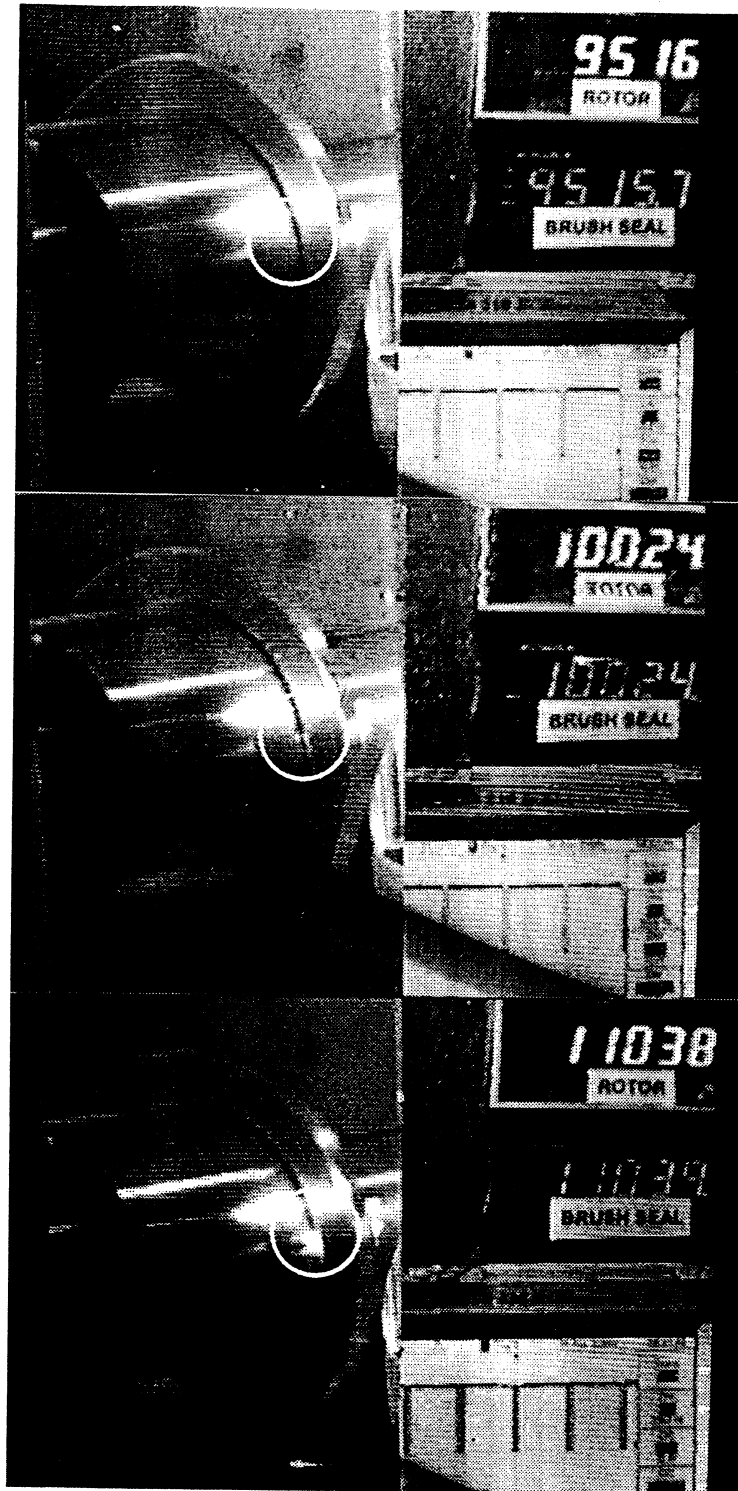


Figure 6: Backside of brush seal at 9, 10, and 11,000 rpm

ω (rpm)	δ_{Wm} (in) [model]	δ_{We} (in) [experimental]	$\delta_{Wm} / \delta_{We}$ (in)
8000	0.015	0.004	3.75
9000	0.019	0.007	2.7
10000	0.023	0.011	2.1

Table 2. Centrifugal deflection vs. speed

CONCLUSIONS

The experiments showed that the brush seal will reach a critical speed, after which, the bristles will begin to lift off the rotor. The experiments also provided the unexpected result of the bristles being entrained by an aerodynamic layer between the rotor and the bristle tips long after liftoff has occurred. The aerodynamic layer provided enough circumferential momentum to keep the brush seal rotating at the same speed as the rotor up to the maximum operating speed of 11,000 rpm. The numerical model provided some insight for the qualitative behavior of a rotating brush seal but did not correspond quantitatively to experimental results. It is believed that the effects of bristle packing and windage of the rotor must be included for a more realistic model to be developed.

REFERENCES

1. Ferguson, J.G., "Brushes as High Performance Gas Turbine Seals", *33rd ASME Gas Turbine Conference, Amsterdam, The Netherlands*, paper no. 88-GT-182, (1988).
2. Chupp, R.E., Dowler, C.A., "Performance Characteristics of Brush Seals for Limited Life Engines", *36th ASME Gas Turbine Conference, Orlando, Florida*, paper no. 91-GT-281, (1991).
3. Proctor, M.P., Walker, J.F., Perkins, H.D., Hoopes, J.F., and Williamson, G.S., "Brush Seals for Cryogenic Applications: Performance, Stage Effects, and Preliminary Wear Results in LN₂ and LH₂", *NASA Technical Paper no. 3536*, (1996).
4. Atkinson, E. and Bristol, B., "Effects of Material Choices on Brush Seal Performance", *Lubrication Engineering, Vol. 48*, pp 740-746, (1992).
5. Hendricks, R.C., Griffen, T.A., Bobula, G.A., Bill, R.C., Howe, H.W., "Integrity Testing of Brush Seal in a T-700 Engine", *NASA Conference Publication 10124, NASA Lewis Research Center Seals Workshop*, Cleveland, Ohio, pp. 117-138, (1992).
6. Forry, J.M., "High Temperature Brush Seals and High Pressure Ratio Swept Fan Program, Vol. I, High Temperature Brush Seals", *Wright Laboratory Technical Report no. WL-TR-94-2007*, (1993).
7. Braun, M.J., Hendricks, R.C., Canacci, V., "Non-Intrusive Qualitative and Quantitative Flow Characterization and Bulk Flow Model for Brush Seals", *Proceedings of the Japan International Tribology Conference, Vol. III*, pp. 1611-1616, Nagoya, Japan, (1990).
8. Hendricks, R.C., Schlumberger, J., Braun, M.J., Choy, F.K., Mullen, R.L., "A Bulk Flow Model of a Brush Seal System", *Proceedings of the 1991 ASME International Gas Turbine and Aeroengine Congress and Exposition, Paper #91-GT-325*, Orlando, Florida, June 3-6, (1991).
9. Braun, M.J., Kudriavtsev, V.V., "Hybrid Floating Brush Seal", *SBIR Phase-I, Final Report*, June, (1995).
10. Braun, M.J., Choy, F.K., 1996, Hybrid Floating Brush Seal, *Patent Pending*

EFFECTS OF COMPRESSION, STAGING, AND BRAID ANGLE ON BRAIDED ROPE SEAL PERFORMANCE

Bruce M. Steinetz
NASA Lewis Research Center
Cleveland, Ohio

and

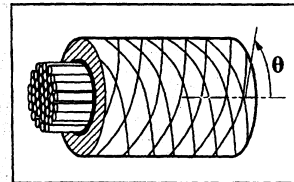
Patrick H. Dunlap, Jr. and Michael L. Adams
Modern Technologies Corp.
Middleburg Heights, Ohio

Background

- High temperature flexible packings have origins in several programs
 - Space Shuttle Thermal Protection System (TPS)
 - National Aerospace Plane (NASP) engine seals

Rope Seal Benefits

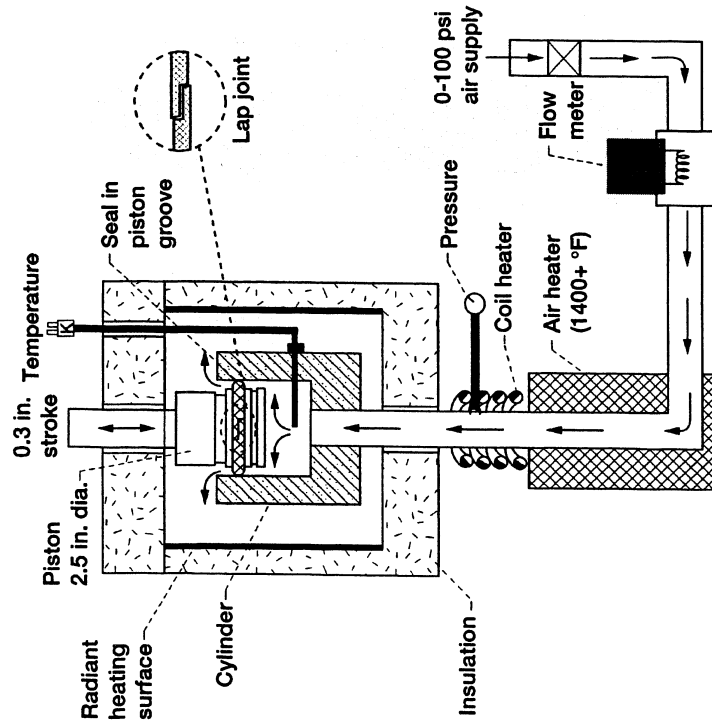
- High temperature operation (1500-2000+ °F)
 - 500-1000 °F hotter than graphite seals
- Low leakage
- Flexible: Seals & conforms to complex geometries
 - O-ring-like flexibility
- Resilient
- Allows relative thermal growth between primary/support structures
- Field joint capability
- Hybrid design resists abrasion



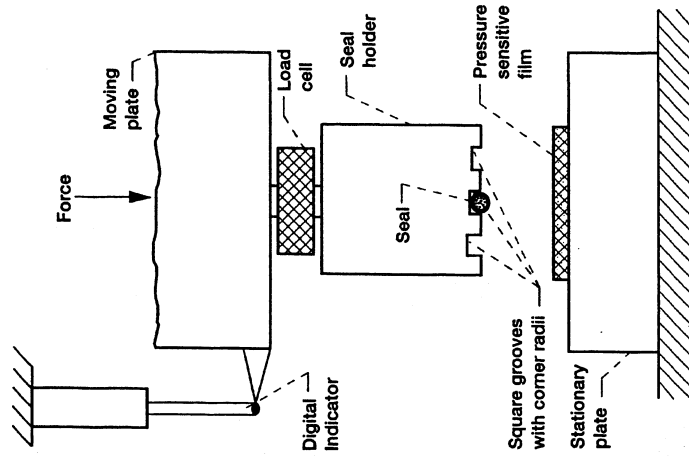
CD-97-75256

Test Fixture Schematics

Flow Fixture



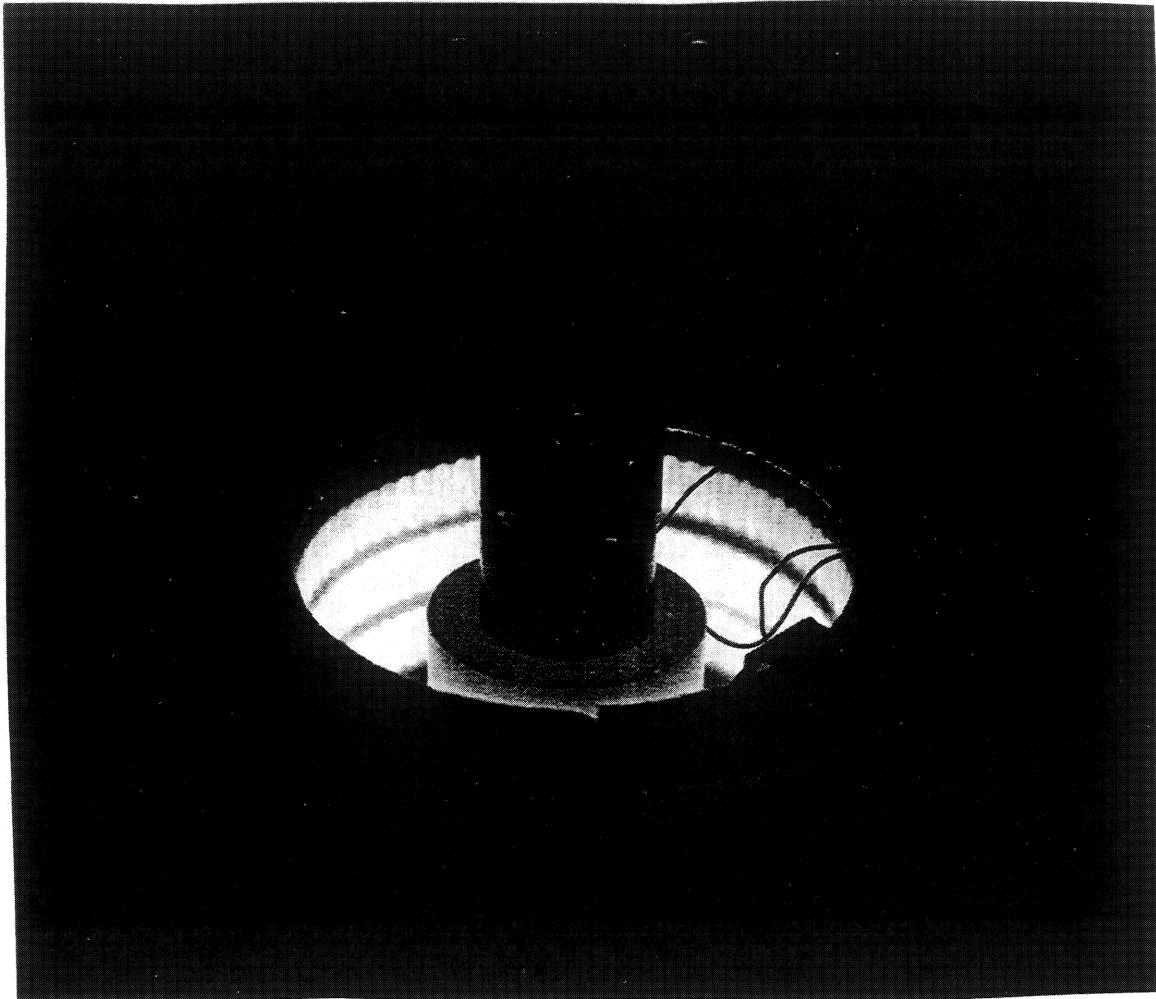
Compression Fixture



CD-97-75258

High Temperature (1500 °F)

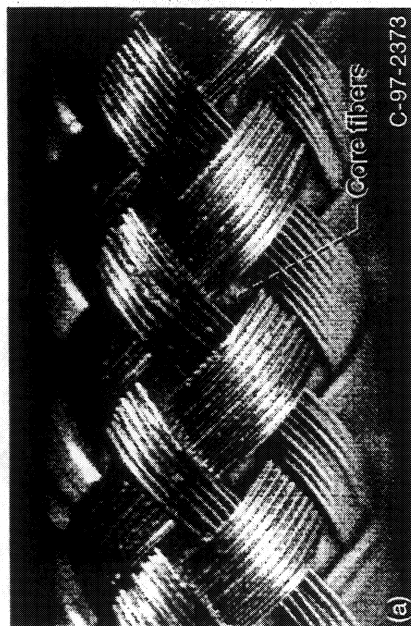
Rope Seal Test Fixture



CD-96-73172

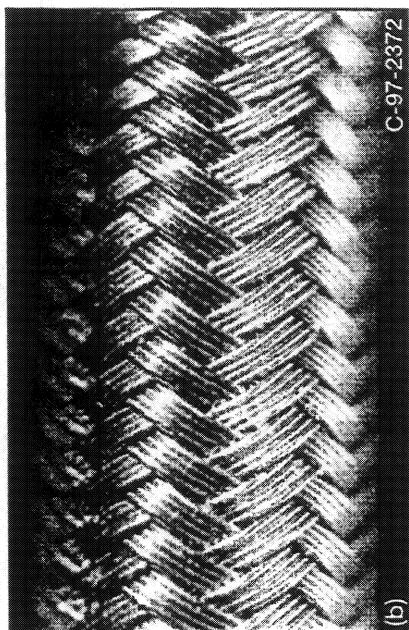
Comparison of Hybrid Seal Braid Architecture

46° Braid Angle Hybrid



Core: Nextel 550
Sheath: Haynes 188
10 wires/bundle

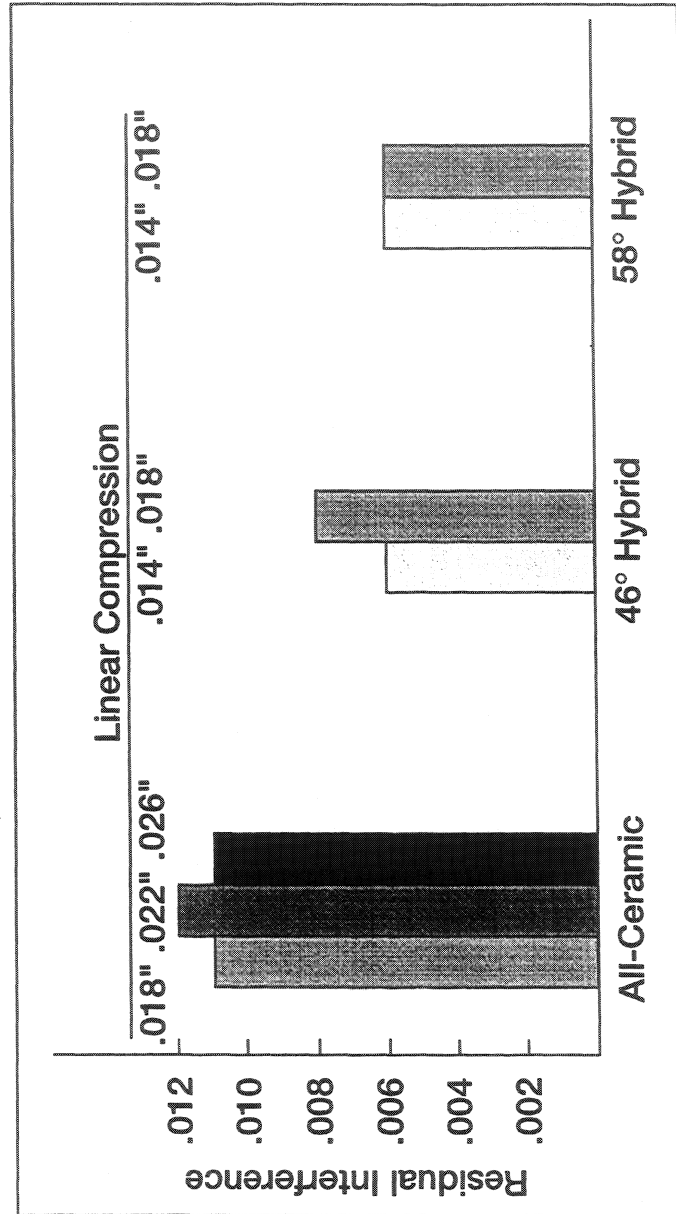
58° Braid Angle Hybrid



Core: Nextel 550
Sheath: Haynes 188
4 wires/bundle

CD-97-75266

Residual Interference After Compression Cycling

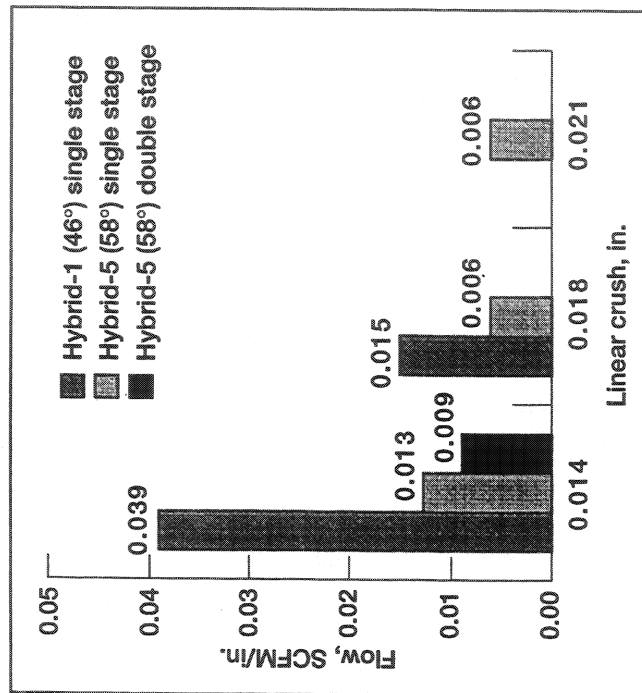


All ceramic seals exhibit more residual interference

CD-97-75265

Effect of Compression, Braid, and Staging on Seal Flow ($\Delta p = 10$ psid; $T = 1300$ °F; After Scrubbing)

Hybrid Seals (1/16")

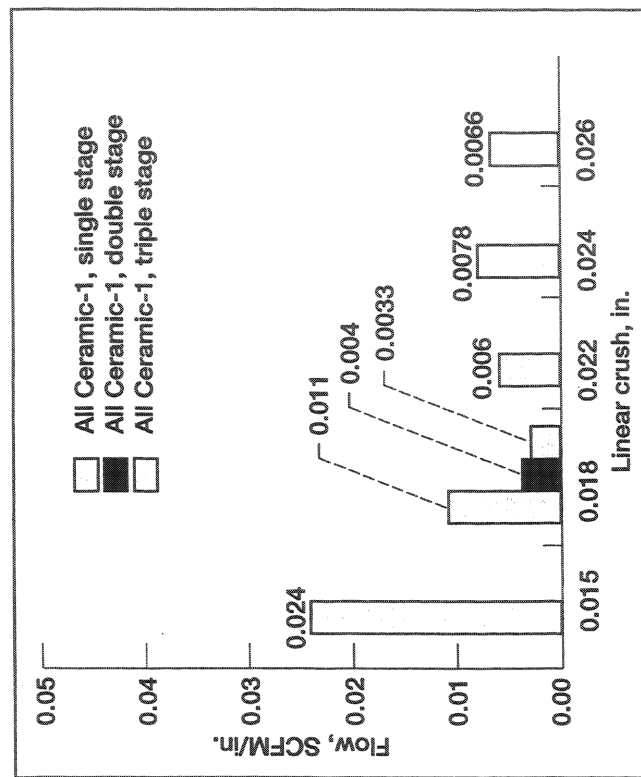


- High braid angle hybrid seal exhibited 1/2 - 1/3 the leakage of low braid angle hybrid for same linear crush, but had 6x unit pressure
- Two stage seals leaked less than single stage seals
High braid angle/high stiffness hybrid: 30+ % less

CD-97-76148

Effect of Compression, Braid, and Staging on Seal Flow ($\Delta p = 10$ psid; $T = 1300$ °F; After Scrubbing)

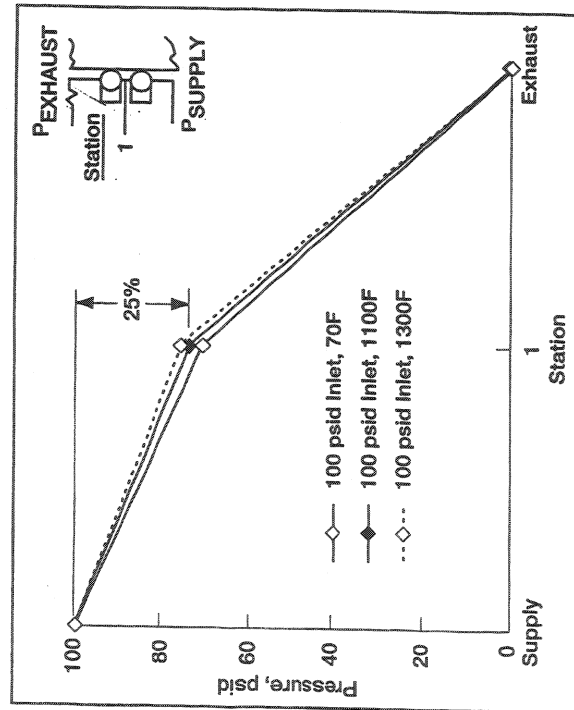
All Ceramic Seals (1/16")



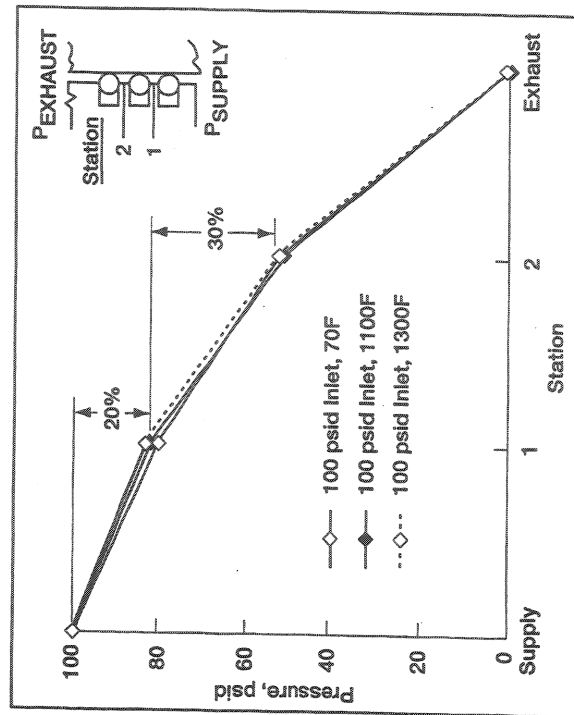
- Multiple stage seals leaked less than single stage seals
- Two stage seals: 60% less
- Three stage seals: 70% less

Effect of Staging on Seal Pressure Drop Multiple Stage Seals, After Scrubbing

All Ceramic: 2 Seals
.018" Linear Crush



All Ceramic: 3 Seals
.018" Linear Crush



CD-97-76146

Three Stage Seal Durability

After Hot Scrubbing

10 cycles x 0.13" Stroke at 1300°F



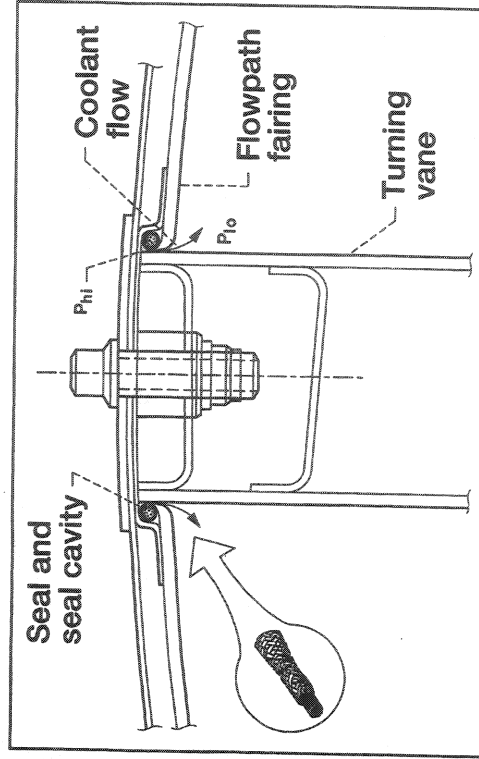
Static
Pressure
Taps
3 Places

Seals survived accelerated seal
durability cycle at temperature

CD-97-76144

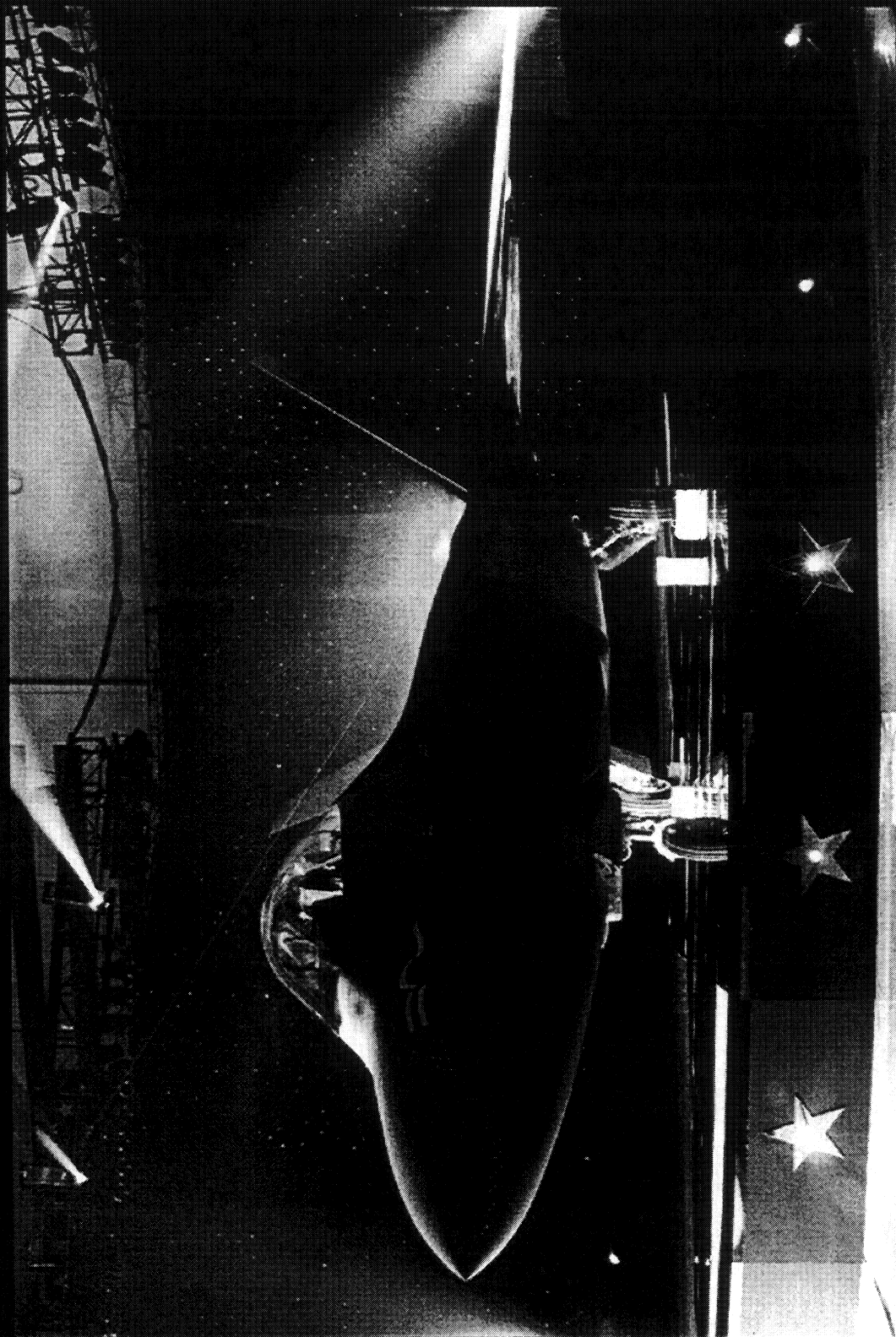
P&W Turbine Vane Seal Requirements

- Operate hot
Seal/metal temperature: 1200 °F
Gas stream temperature: last stage vane
- Exhibit low leakage – minimize cooling requirements
- Permit relative vane-to-shroud thermal growths
- Seal complex turbine airfoil geometries
- Resist abrasion in high acoustic environment
- Maintain structural integrity



CD-97-75257

Next Generation Fighter F-22 P&W F119 Engines



CD-97-75263

Summary and Conclusions

- Increasing hybrid seal braid angle and core coverage reduced leakage 1/2 -1/3rd that of conventional hybrid for same compression but increased stiffness and unit preload
- Using multiple seals, the last stage seal always resists the largest percentage of the inlet pressure
 - + Two stage seals: 1st stage resists 25%
2nd stage resists 75%
 - + Three stage seals: 1st stage resists 20%
2nd stage resists 30%
3rd stage resists 50%
- Multiple stage seals reduced leakage considerably
 - + Hybrid seals 2 stage: 30+% reduction
 - + Ceramic seals 2 stage: 60+% reduction
3 stage: 70+% reduction

Braided Rope Seals are meeting an important need arising from increased engine cycle temperature, performance, and efficiency requirements

CD-97-76153

ADVANCED METALLIC SEAL FOR HIGH TEMPERATURE APPLICATIONS

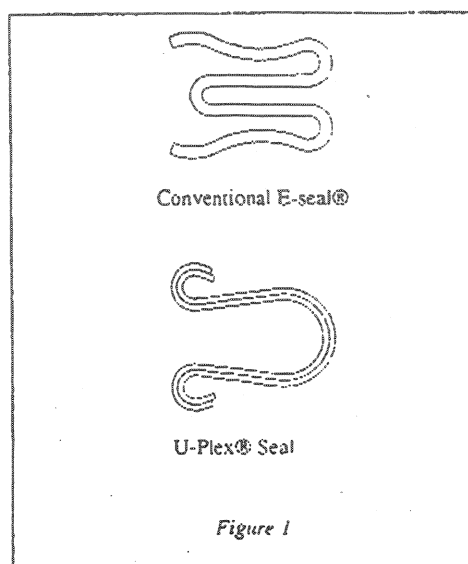
Terence Nolan, Jeff Swensen, and Jeff Layer
EG&G Pressure Science
Beltsville, Maryland

Abstract

The U-Plex® was designed to allow greater elastic deflection capability in a given gland volume than the now conventional E-seal®. Greater deflection capability with the associated lower bending stresses provides several benefits. For pneumatic duct joints, the axial free height is increased to allow sealing of flanges with weld distortions significantly in excess of what could be tolerated with E-seals®. This performance is achieved while maintaining the re-usability and ease of assembly typical of E-seal® rigid duct joints. For turbine engine air seal applications, which are quite often at temperatures where stress relaxation of metallic seals needs to be considered and significant axial cavity excursions exist, the lower stresses inherent in the U-Plex® design can provide extended seal performance, life and applicability with current, suitable materials. The development of a better "duct joint seal" led to defining seal characteristics which needed to be improved. These characteristics include increased elastic deflection, conformity to local deformations, improved pressure energization characteristics, lower force to compress (while maintaining the same level of sealing capability) and better geometric stability. These features associated with the U-Plex® design, result in both performance benefits for the seal and manufacturing benefits associated with producing the cavity for the seal to operate in.

Description

The geometry of the U-Plex® seal differs from the E-seal® in that the "legs" of the seal are incorporated in the convolution of the seal where an E-seal® has a distinct convolution and "legs". This permits the convolution radius to be significantly larger. The basic U-Plex® consists of two plies of material. The plies of material are not circumferentially welded. The end of the U-Plex® legs are tightly curled backward to provide a good sealing land area and to shield the interstitial gap between the plies from the higher pressure medium to be sealed, by facing the gaps towards the lower pressure side.

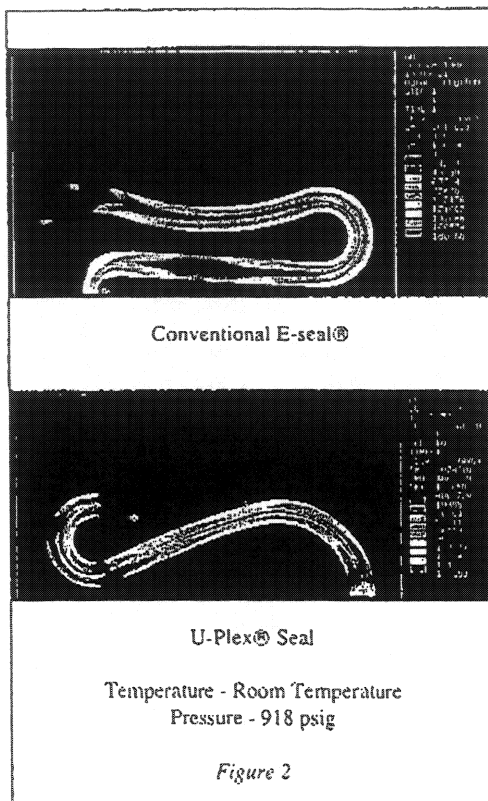


The U-Plex® design can be adjusted to accommodate different applications by varying the number of plies, ply thickness, ply material, number of convolutions, seal dimensions, and adding wear resistant coatings. Note that the individual plies could be made from different type or thickness material.

A multiple ply seal, provided all plies experience the pressure loading, allows pressure induced stresses to be evenly split between the plies. In a two ply seal, at a given pressure, the bending stresses created by deflection would be one half that of a single ply seal of the same total thickness, thus increasing the elastic deflection capability, which is key to maintaining sealing contact with the cavity surfaces.

Another aspect of the U-Plex® seal design that reduces operating stresses is the large convolution radius. The seal is designed so that compression of the seal only takes place on the seal "legs", maximizing the deflectable length of the seal. The large radius can then provide a broad area over which the bending strain is

distributed and allows pressurization to induce forces that oppose this strain, resulting in a much lower combined stress situation. This effect serves to minimize stress relaxation, which could compromise seal performance, as during the majority of time the seal is at operating temperature, it is also pressurized. E-seals® also benefit from pressurization, however, the effect is much less pronounced due to the tighter bend radii. Figure 2 is a comparison of the stress contours of the two cross sections.



In some applications, buckling of flexible metallic seals can be a concern due to the relatively low thermal inertia of the seal or transient differential movements. The geometry of the U-Plex® seal resists buckling better than the conventional E-seals since the large radius and reversed curled legs result in a higher moment of inertia in the critical plane. The reverse curl on the seal legs provides an additional benefit in segmented cavity applications; flow induced resonance has been suspected of causing occasional high cycle fatigue failures of seals, the curled legs greatly increase

the resonant frequency of the seal, thus preventing a "reed" effect. Recent testing has confirmed that the U-Plex® design minimizes seal resonance.

Pneumatic Duct Joint Applications

The U-Plex® Seal improves the integrity and robustness of Rigid Ducting Joints. Figure 3 illustrates a typical rigid ducting joint with a U-Plex® installed. All EG&G Pressure Science rigid duct joint seals, both E-seals® and U-Plex® seals, are heat treated Inconel 718.

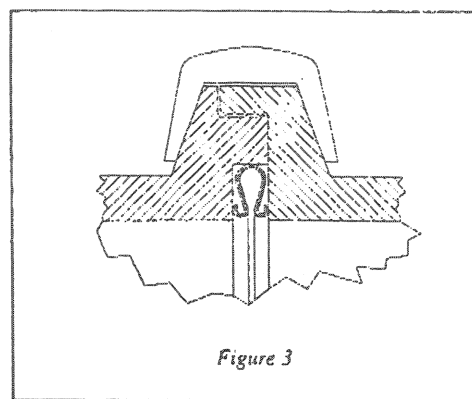


Figure 3

Testing has been performed to compare the leakage control capability between the U-Plex® seal and the conventional E-seal® in both ideal and out-of-flat conditions. The increased elastic deflection capability of the U-Plex® Seal will allow it to seal when assembled in weld distorted flanges which are as much as 2.5 to 5 times worse than those in which the convention E-seal® can accommodate. This allows relaxed flange flatness tolerance requirements and reduces rework of the ducting joint flanges. Figure 4 is a comparison of the conventional E-seal® to the U-Plex® as they relate to axial flange cavity height as specified by Aerospace Standard, SAE Document, AS 1895.

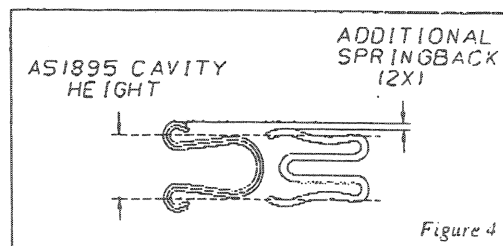
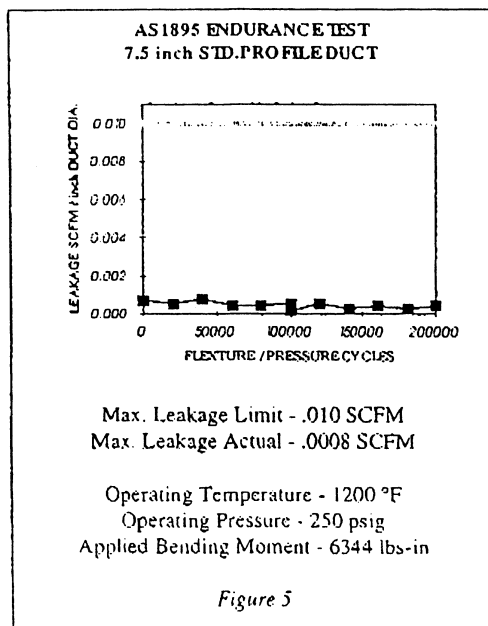


Figure 4

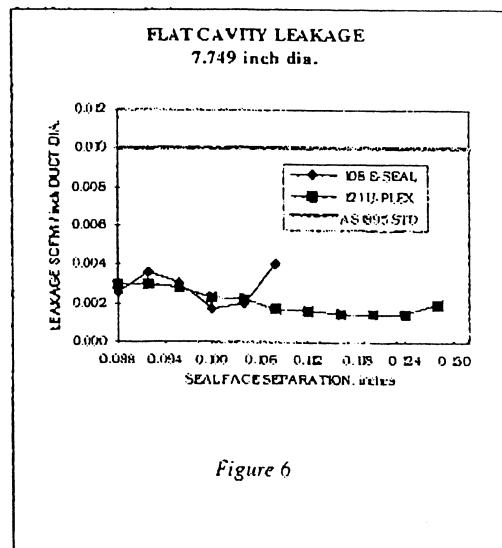
It is important to note that the U-Plex® seal, by design, stores significantly more strain energy to accommodate flange distortions and deflections. Therefore, the highly compliant U-Plex® seal can accommodate relatively large local deformations. For example, duct joints from Ø1.50" to Ø3.50" assembled with the U-Plex® seal will adequately seal flanges that are up to .011" per linear inch circumference out-of-flat. This value increases to .018" per linear inch circumference out-of-flat for diameters greater than 3.5".

The U-Plex® Seal is qualified to the Aerospace Specification for Rigid Pneumatic Joints AS1895, under section AS1895/23. A Ø7.5" U-Plex® Seal was endurance tested in a Standard Profile Rigid Duct Joint for 200,000 cycles. Each cycle consisted of pressurizing the duct and applying a bending moment to the duct while at 1200 °F. The leakage from the joint remained consistently low throughout the test.



Additionally, the U-Plex® Seal was able to pass the difficult AS1895 Safety Latch Test. This test historically has been a test that the rigid joint utilizing a conventional E-seal®, or similar sealing method, has not been able to meet in all sizes with regard to the specified leakage limit. The test involves taking a pressure loaded rigid joint and intentionally causing a

bolt failure. The intent of the test is to insure that the joint does not separate as a result of an unlikely bolt failure. The safety latch is required to keep the joint intact while a finite excessive leakage requirement is met. The conventional E-seal®, or similar sealing method, can not meet the specified leakage and is not functional subsequent to the test. The U-Plex® Seal meets the required leakage of the AS1895 Safety Latch Test and is still functional subsequent to a successful test. The ability of the U-Plex® Seal to meet this demanding requirement is due to its improved pressure energization characteristics, and lower resistance to bending. Figure 6 is a graph of leakage vs. axial cavity height. The E-seal® is not capable of sealing at cavity heights greater than the seal's axial free height. The U-Plex® seal is capable of sealing at cavity heights greater than its axial free height.

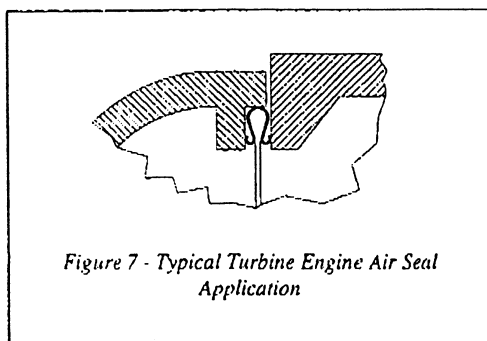


The U-Plex® Seal can achieve the leakage control capabilities of the conventional E-seal® at significantly lower contact loads. The E-seal®, qualified to AS1895, has a force-to-compress of approximately 60 lbs per circumferential inch, while the U-Plex® Seal, qualified to AS1895, has a force-to-compress of approximately 20 lbs per circumferential inch. This feature will allow the same level of sealing with less wear of the sealing surfaces. This was evident by examination of the flange sealing surfaces after the 200,000 cycle endurance test. This benefit is more applicable to the turbine engine applications where wear is a more significant issue.

Turbine Engine Air Seal Applications

Many of the features and benefits of the U-Plex® Seal identified for pneumatic rigid joint applications can be applied to turbine engine air seal applications. These features are:

- Increased elastic deflection
- Conformity to local deformations
- Improved pressure energization characteristics
- Lower force to compress
- Lower wear



Increased elastic deflection and a lower spring rate allows a larger deflection range over which the internal stresses within the cross section of the seal can remain below the elastic limit of the seal material. Since the cyclic stresses in the seals are primarily a function of axial deflection, not axially applied loads, the lower spring rate will provide a better stress profile for low cycle fatigue.

Improved pressure energization characteristics will allow better conformity in applications where the axial cavity increases during operation and in applications where stress relaxation is a concern. With any "spring loaded" face seal, the contact load will decrease as the axial cavity height increases. Since the U-Plex® Seal has better pressure energization characteristics, as demonstrated in the AS1895 Safety Latch Test, the contact load will be higher for the U-Plex®, compared to a conventional E-seal® as the axial cavity increases, and all other parameters are equal. The better pressure energization characteristics will reduce the effects of stress relaxation at high temperatures. In typical E-seal® applications where stress relaxation is an issue, the seal axial free height will approach the axial cavity height dimension during operation, thus reducing the

contact load and level of sealing. This phenomena will also occur with U-plex® Seal design, but the effects will be minimized by the pressure opposing the deflection induced strain and the fact that the better pressure energization of the seal will result in sufficient contact load as long as the seal system is designed such that line-to-line contact is maintain. For example, in the AS1895 Safety Latch Test, the axial cavity height after bolt failure is greater than the axial free height of the seal and a certain level of sealing ability is maintained.

The lower force to compress inherent to the U-Plex® design will provide better wear characteristics, while maintaining the same level of sealing. Additionally and more importantly, the U-Plex® design can accommodate more than one material type. Hence, a hybrid U-Plex® could be made from two materials, the material making up the seal contact surface would be chosen based on optimizing the tribological pairing between seal and cavity; and the other material would be chosen on material strength properties. The U-Plex® can be manufactured in any of the high temperature alloys that E-seals® are currently produced in. These materials are as follows:

- Inconel 718
- Waspaloy
- Haynes 214, 188, 242
- Rene 41
- Incoloy 909
- and new alloys as they become available

Additionally, these seals can be coated with a Tribaloy coating to provide wear resistance for the seal. The operating temperature and pressure limits for both the E-seal® and the U-Plex® are dependent on the material selection and application parameters.

To date limited testing has been done on large diameter (>Ø20") U-Plex® Seals. The U-Plex® seal will be tested in a test rig which can simulate operating temperature, pressure and differential radial movements between the seal and cavity wall. This test will also provide insight as to if the curled leg improves resistance to high cycle fatigue. One large diameter U-Plex® has been tested in this rig. This seal was split radially in one location. Large diameter E-seals® are radially split in some high pressure turbine applications to minimize the effects of mismatched thermal and/or radial restraints of the seal cavity. The split in the seal allows circumferential growth, instead of radial growth, of the seal and therefore removes the detrimental hoop loads that could induce buckling of

the seal. During previous testing of convention E-seals® in this test rig, audible high pitched noise was observed. It was hypothesized that the noise was being created by high pressure air escaping through the cavity segments over an unsupported section of the seal acting to produce a "reed" effect. In the same test set-up, the U-plex® Seal did not exhibit the same noise behavior. It is theorized that the curled legs greatly increase the resonant frequency of the seal, preventing a "reed" effect.

Further Testing and Development

For small diameter U-Plex® Seals, less than Ø7.5" and primarily for pneumatic duct joint applications, all testing is complete for qualification to AS1895/23 and tests to verify performance improvement over the conventional E-seal® is complete. Additionally, all manufacturing process development is complete.

Testing and development of the larger diameter U-Plex® seals, for turbine engine applications, will continue. A large diameter, ≈Ø30", U-Plex® seal will be tested in a test rig which can simulate operating temperature, pressure and differential radial movements between the seal and cavity wall. The testing is intended to compare/evaluate the performance benefits of the U-Plex® Seal identified above to the current performance of the E-seal®.

Conclusion

During the design process of a typical E-seal® application, where a new seal section is required, the seal cross section is usually optimized for maximum elastic deflection, lower compression loads and sufficient geometric stability. The U-Plex® Seal is, in fact, a truly optimized metallic seal cross section with additional features, such as, improved conformity to local deformation and improved pressure energization characteristics. Although first developed to "raise the bar" on performance for pneumatic duct joint seals, it is quite evident that the benefits associated with this new metallic seal cross section can be extended to improve large metallic seal technology. The U-Plex® design is a next generation product, reflecting 30 years of experience in resilient metallic seals.

DEVELOPMENT OF A THIN GAUGE METALLIC SEAL FOR GAS TURBINE
ENGINE APPLICATIONS TO 1700°F

Raymond O. England
EG&G Mechanical Components Research and Development Center
Cranston, Rhode Island

The goal of doubling thrust-to-weight ratio for gas turbine engines has placed significant demands on engine component materials. Operating temperatures for static seals in the transition duct and turbine sections, for instance, may well reach 2000°F within the next ten years. At these temperatures conventional age-hardenable superalloys lose their high strength via overaging and eventual dissolution of the γ' precipitate, and are well above their oxidation stability limit. Conventional solid-solution-strengthened alloys offer metallurgical stability, but suffer from rapid oxidation and little useful load bearing strength. Ceramic materials can theoretically be used at these temperatures, but manufacturing processes are in the developmental stages.

The development of a thin gauge metallic seal for operating temperatures up-to 1700°F is presented. The results of stress relaxation and oxidation screening tests for seven candidate alloys in strip form are discussed. Component tests using static loading in a seal chamber fixture correlate well with the stress relaxation and oxidation tests, and indicate that seals made from a new iron-based superalloy offer superior resistance to oxidation, metallurgical stability, and significant residual sealing force up to 672 h continuous exposure at 1700°F.

LM2500+ BRUSH SEAL CASE STUDY

Fred G. Haaser
GE Aircraft Engines
Cincinnati, Ohio

Abstract

The LM2500+ industrial aeroderivative gas turbine, a 25% enhanced power derivative of the LM2500 gas turbine, recently completed its development test program during the period of 5/96 - 10/96. Early in the engine program a Quality Function Deployment (QFD) process was used to determine customer needs for this product. The feedback obtained from the QFD process showed without doubt that gas turbine customers now emphasize product reliability and availability at the very top of their needs. One area of development on the LM2500+ was to investigate the use of a brush seal as a means to reduce undesirable turbine cooling leakages within the turbine mid frame in order to enhance part life. This presentation presents a case study on the factors that went into evaluating a brush seal during engine test, test results, and the ultimate decision to not implement the brush seal for cost and other reasons.

Contents

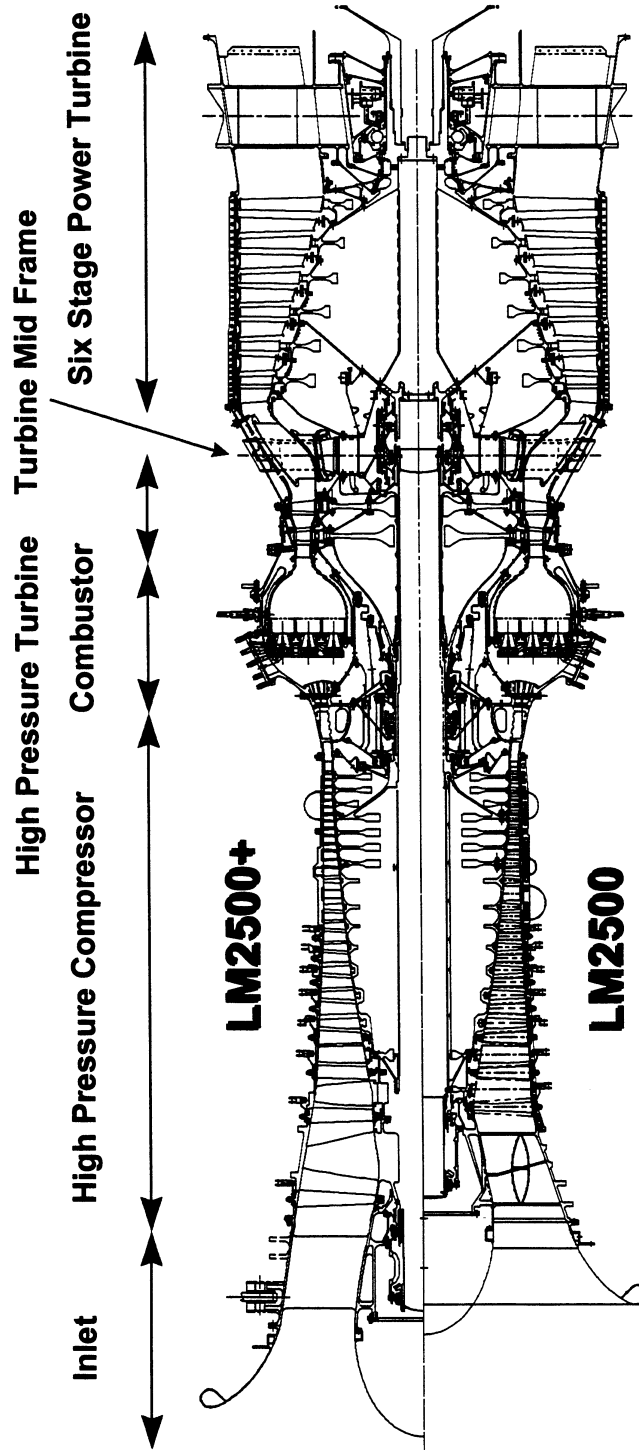
- **LM2500+ Gas Turbine Description**
- **LM2500+ Development Program**
- **Quality Function Deployment (QFD)**
- **Brush Seal Investigation**
- **Engine Test**
- **Brush Seal Case Study Summary**

LM2500+ Gas Turbine Description

- ❑ **LM2500+ is a 25% power increased (ISO conditions) version of the LM2500 gas turbine.**
- ❑ **Straight forward development of the well-proven LM2500**
 - **Total LM2500 production in excess of 1,500 engines**
 - **More than 925 marine and 575 industrial LM2500 engines delivered**
 - **Over 23,000,000 operating hours**
 - **Average installed engine time over 38,000 hours/high time engine 107,700 hours**
- ❑ **LM2500+ is available in 3 variants: Gas Generator, Gas Turbine with Six Stage Power Turbine, and Gas Turbine with Two Stage Power Turbine.**

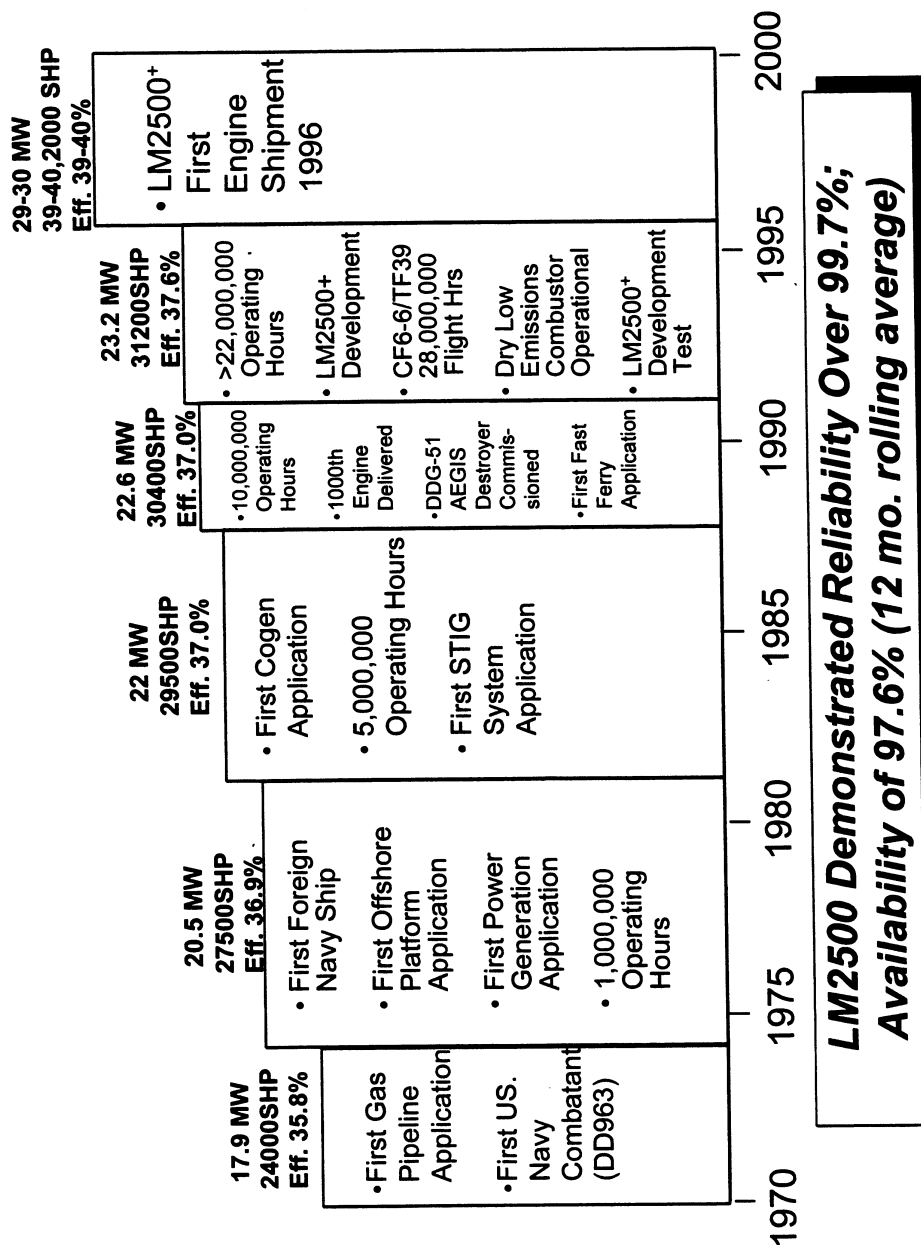
Export License TSU 10/15/97

Figure 1 - Comparison of LM2500+ to LM2500



**LM2500+ is 25% Power Enhanced LM2500
Using Zero-Staged HP Compressor**

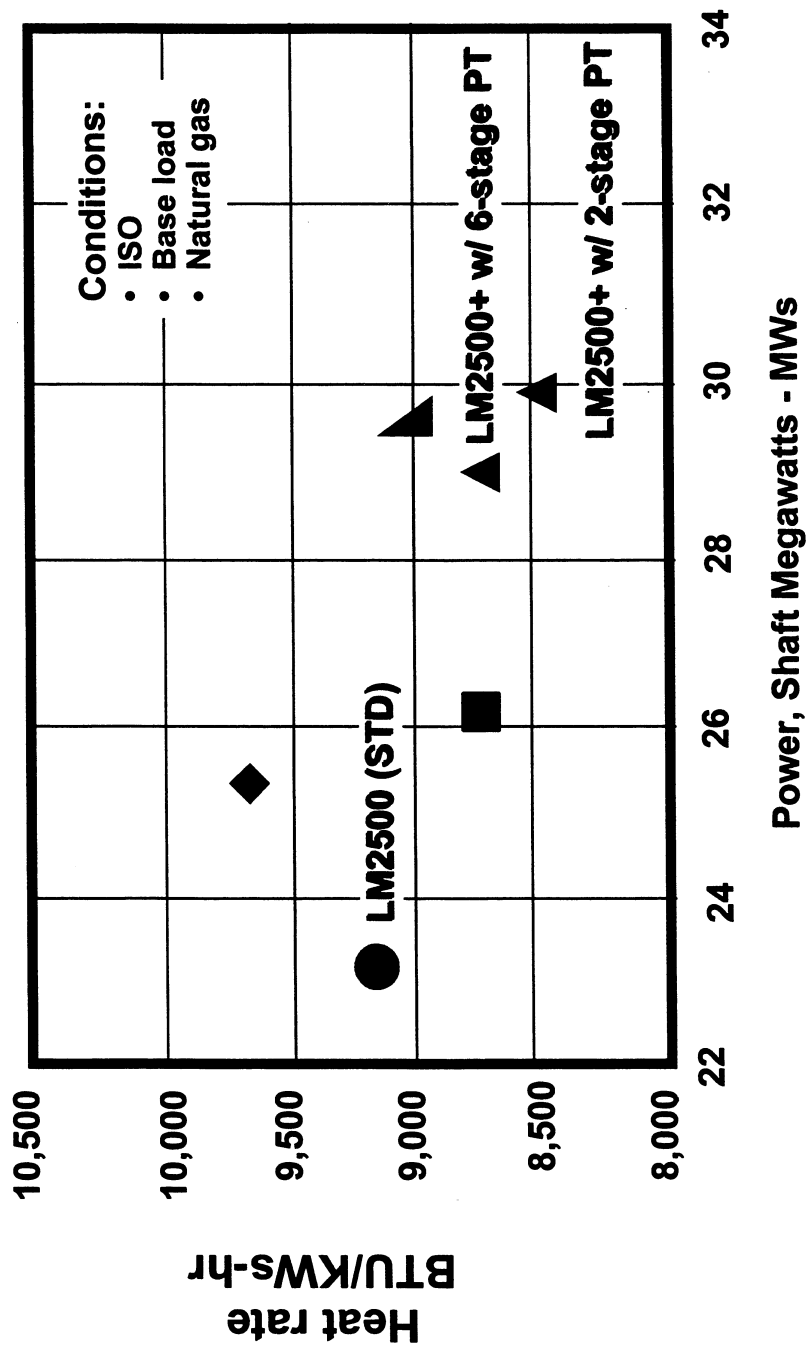
Figure 2 - Historical Synopsis of the LM2500



10/15/97

Export License TSU

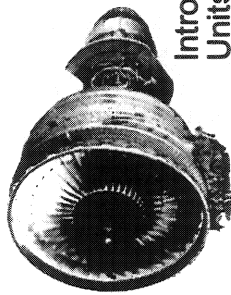
LM2500+ Performance vs. Other Products



PPT-83308-022196 (LM2500+)

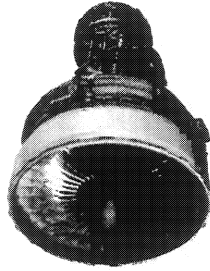
Export License TSU 10/15/97

Genealogy



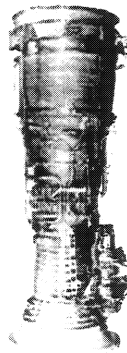
CF6-6

Introduced - 1965
Units in service - 1,152
Operating hours - 29,957,000



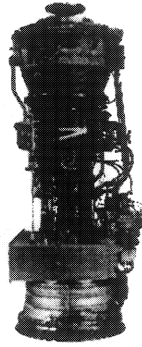
CF6-80C2

Introduced - 1985
Units in service - 2,238
Operating hours - 33,728,000



LM2500

Introduced - 1969
Units in service - 1,500
Operating hours - 23,000,000
Reliability - 99.7%
Availability - 97.8%



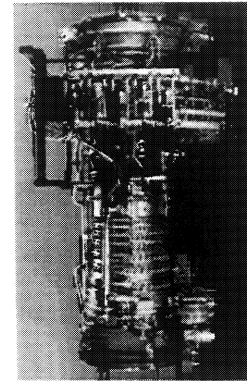
LM6000

Introduced - 1991
Units in service - 108
Operating hours - 735,000
Reliability - 99.1 %
Availability - 97.3 %



**Design
experience
& commonality**

Experience data as of 12/31/96



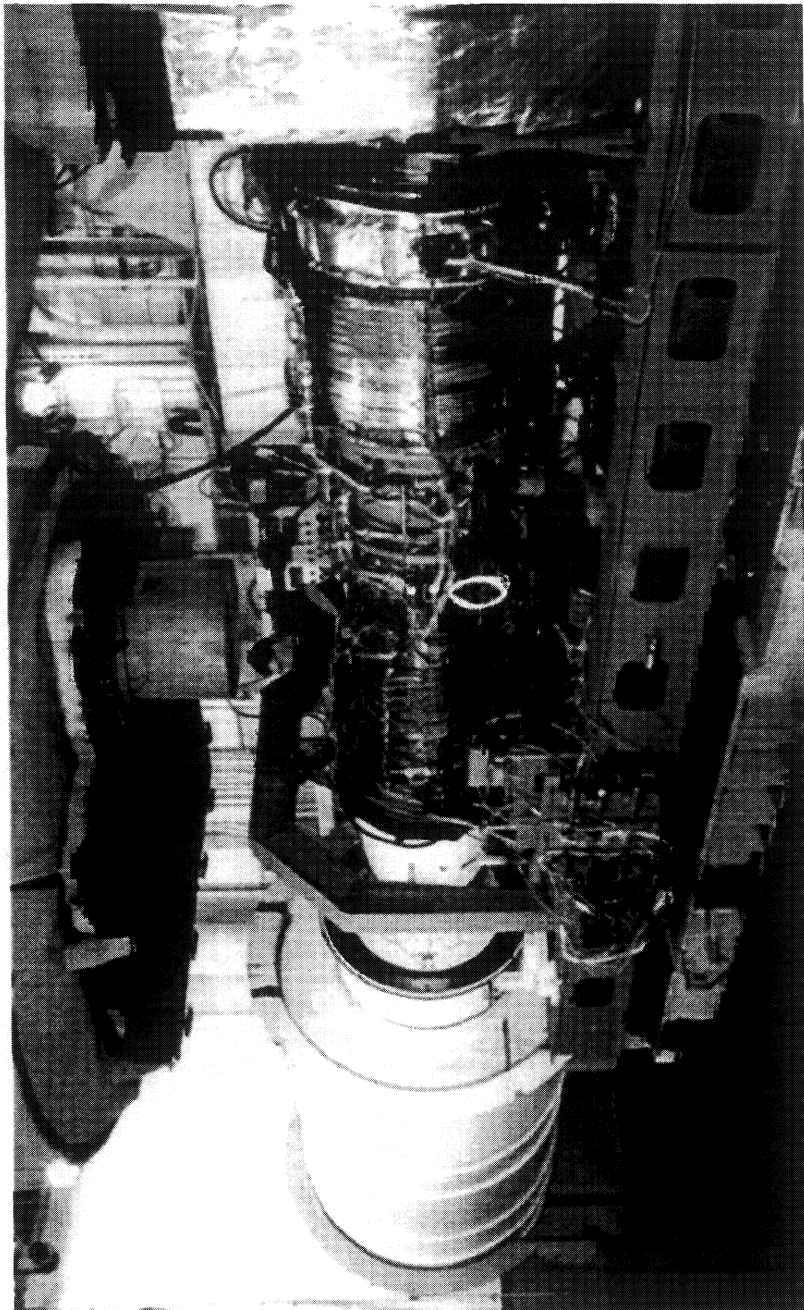
**Technology
advancements**



LM2500+ Derived from Proven Technology

10/15/97

LM2500+ Gas Turbine (Second Engine to Test)



Export License TSU 10/15/97

LM2500+ Development Program

- Program launched March, 1994 on basis that LM2500 was not as competitive as in previous years
 - competition providing larger, more fuel efficient , less costly engines
- Many best practices applied to development effort, such as critical path scheduling, target costing, risk assessment & management, scorecards, concurrent product development, and others.
- Best practice used to determine customer needs was Quality Function Deployment

Quality Function Deployment (QFD)

- ❑ ***Process where customer input is used to determine and quantify requirements for new products.***
- ❑ **Early in program the time-honored approach of verbal survey (talking) to gas turbine customers was used to obtain input on what changes to make.**
- ❑ **QFD process shows this method is no longer adequate to capture important customer needs**
 - **Time-honored approach - discussed LM2500+ new features only**
 - **QFD approach - obtain feedback on basic product needs as well as new features using written survey**

Quality Function Deployment Results

Table 1 - Comparison of Verbal Interviews vs. QFD Surveys

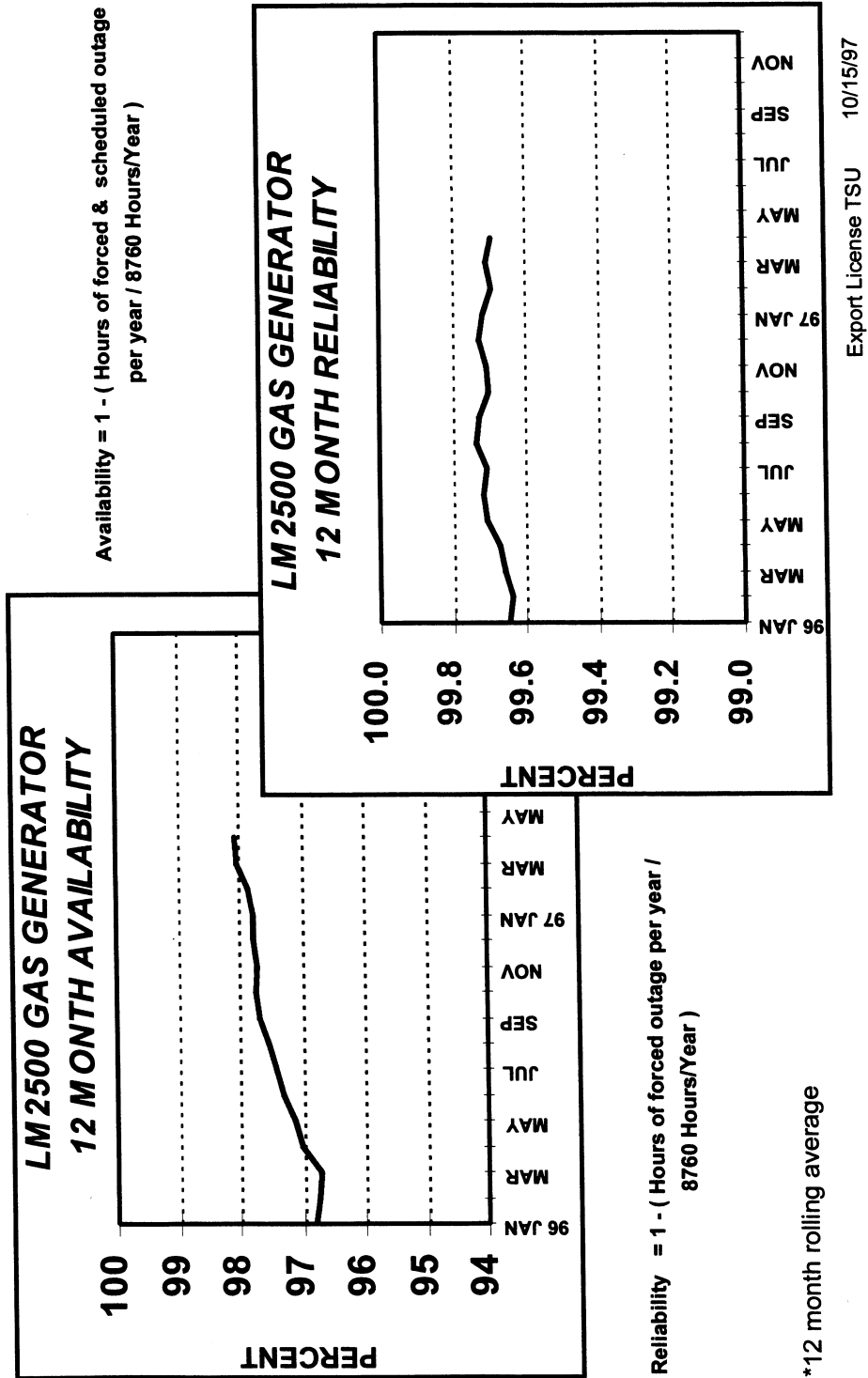
Ranking	<u>Time-Honored</u>	
	<u>Verbal Survey</u>	<u>QFD Survey</u>
1	Power	Availability*
2	Lower Price	Reliability*
3	Noise Level	Pricing*
4	Efficiency	Power
5	Length	Efficiency
6	Emissions	Emissions
7	Weight	Maintainability
		(*tied)

Key Message from Customers: Availability & Reliability are Top Quality/Design Features

Design Approach - Post QFD

- ❑ QFD survey pointed out => *customers no longer want high tech or pure power anymore they want*
 - Availability & Reliability & Pricing and then Power
 - Direct quote “Machine needs to be running when we want it to be running.”
- ❑ To achieve these requirements LM2500+ Engineering adopted the following rules:
 - only mature, demonstrated technology allowed
 - only mature materials and suppliers used
 - extra design margins imposed - above the product requirements in order to hold reliability & availability at highest possible level during LM2500+ introduction
 - Lessons Learned from the base LM2500 incorporated

LM2500 Reliability & Availability*



Brush Seal Investigation

- ❑ Both LM2500/LM2500+ Turbine Mid Frame (TMF) designs use “HP Recoup” vent air from Compressor Rear Frame to purge region between TMF casing and flowpath liner
 - to minimize hot gas ingestion into these regions
- ❑ Design goal is positive pressure drop of 0.5 psi (3447 Pa). Too little pressure drop results in flowpath ingestion and reduced casing/flange life.
- ❑ Experiences on LM2500 TMF indicated that additional pressure differential margin could improve the robustness of the frame.

Brush Seal Investigation (cont.)

- ❑ Calculation shows the LM2500 TMF total liner leakage area to be 10.59 in² (68.32 cm²).
- ❑ Program decided to test both “J” seal and Brush seal as part of the development effort.
- ❑ Significant other sealing improvements made to TMF leakage paths to reduce total leakage areas.
- ❑ LM2500+ TMF liner reduced total leakage areas to:
 - 6.45 in² (41.61 cm²) with “J” seal, or
 - 3.69 in² (23.81 cm²) with Brush seal.

Seal Cut 3 Places to Allow Easy Installation Into As-Built Test Vehicle

Back Plate Hast-X

Front Plate Hast-X

Bristles Waspaloy

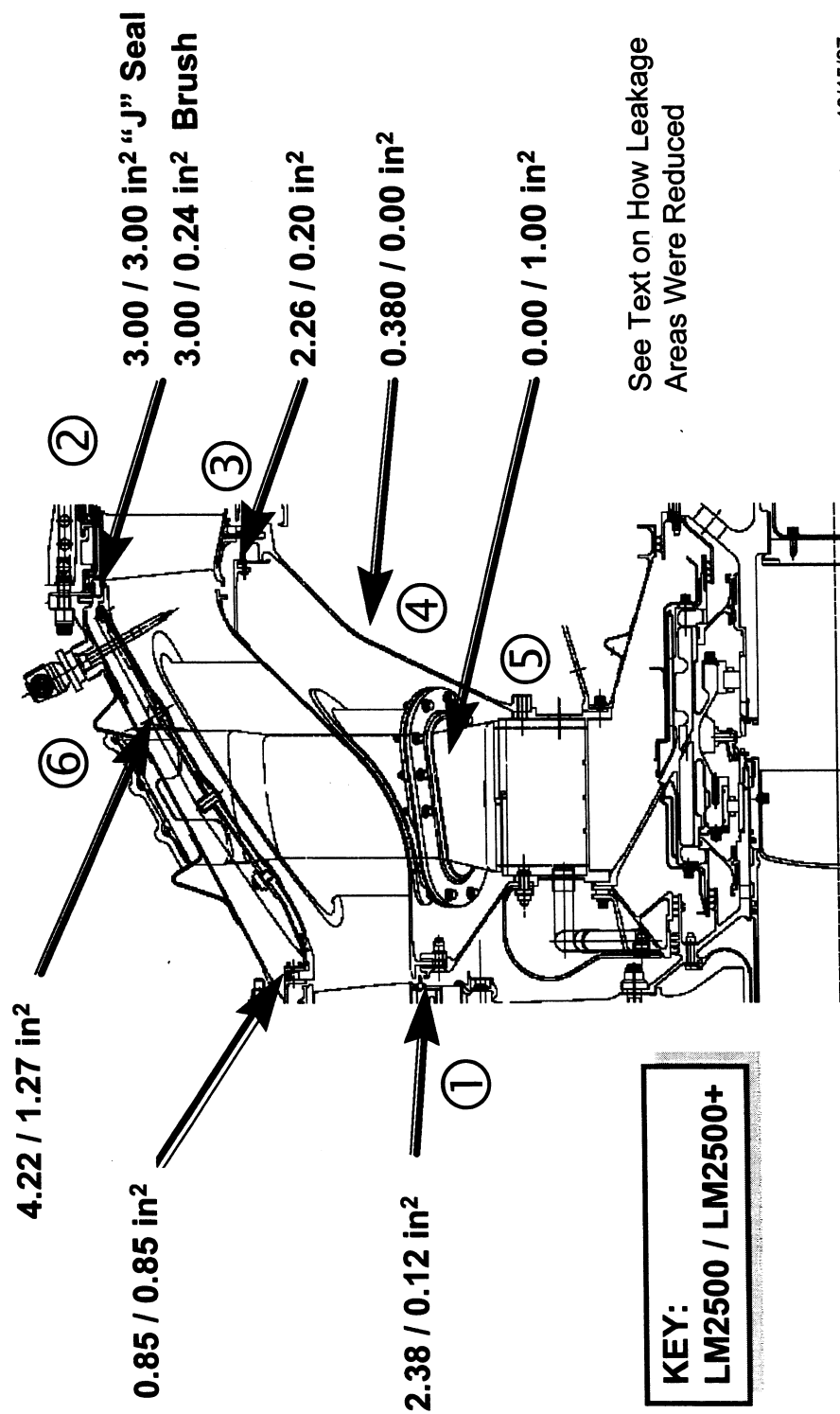
VIEW D (J6) 3 PLACES

SECTION A-A (C5)

Dimensions:

- .22 SEE NOTE 8
- .06 X CHAM [45°]
- .04 2 PLACES AS WELDED SURFACE PERMITTED
- R .04 .02
- .176 .156
- .39 .36
- .562 .532
- (1.801)
- Ø 49.624 B SEE NK
- Ø 49.614
- 47.826 Ø
- 47.811 Ø
- .03 MIN
- .06 MIN
- .85 .83
- .014 .010 WIDTH OF CUT
- A(A7)
- F
- .08 .06
- 54° 52° 11° 9°
- 60° 45° BRISTLE LAY ANGLE
- Bristles lie at 45 degree angle

Figure 4 - Turbine Mid Frame Leakage Areas



Export License TSU 10/15/97

Brush Seal Investigation (cont.)

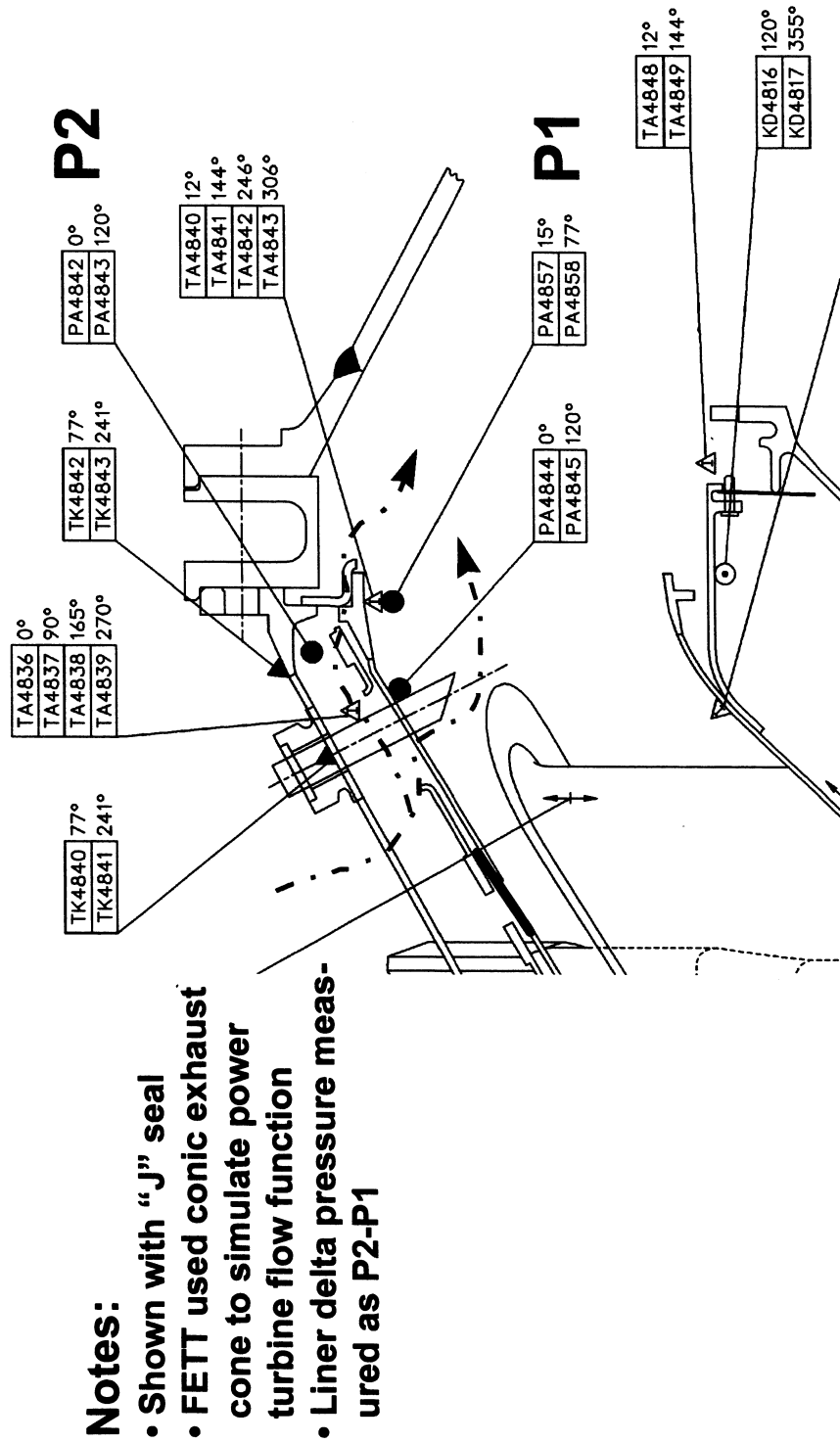
Sealing Redesign on TMF Liner & Flanges

- ① **Fwd Inner Location - Machined vs. Fabricated Joint**
- ② **Aft Outer Seal - Brush vs. “J” Seal**
- ③ **Aft Inner Seal - Leaf vs. Fish Mouth Seal**
- ④ **Aft Cavity Wall - Eliminated Fastener Lead @ 8 Loc**
- ⑤ **Fairing - Double Sliding Ring Seals Added**
- ⑥ **Flowpath Liner Probe Penetrations**
 - Reduced thermocouple flowpath probes (T48) from 11 to 8 probes
 - Probe diameter reduced 0.35 in. (0.89 cm) max to 0.28 in. (0.71 cm)
 - Reduced flowpath pressure probes from 5 to 1

Engine Test

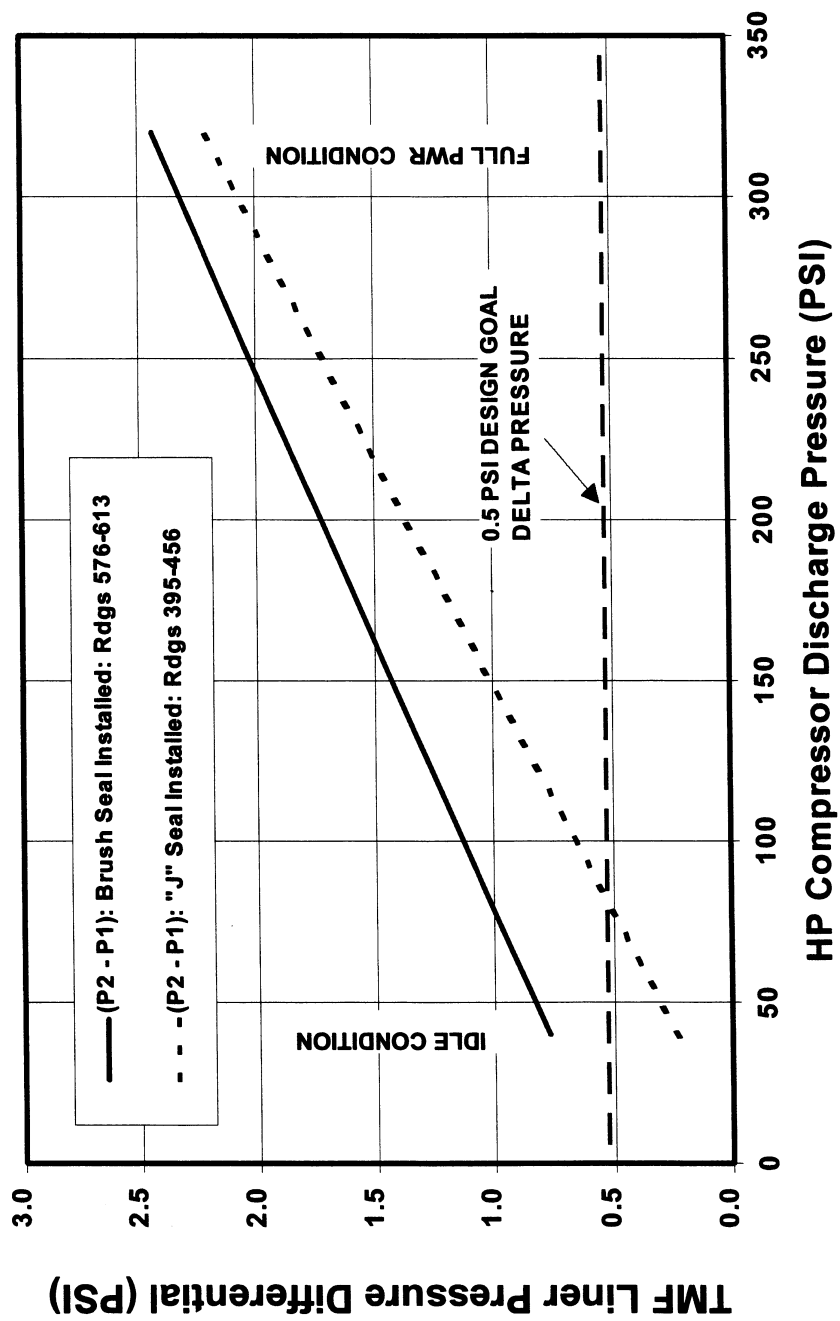
- ❑ LM2500+ First Engine to Test was heavily instrumented (Figure 5).
- ❑ Began testing first with “J” seal installed.
- ❑ Prior to test completion the turbine mid frame aft flange bolts were loosened, the “J” seal cut away, and the Brush seal installed in 3 segments.
- ❑ Pressure test data obtained therefore with “J” seal and Brush seal
 - data plotted (see Figure 6)

Figure 5 - Turbine Mid Frame Instrumentation



Export License TSU 10/15/97

Figure 6 - TMF Liner Pressure Differential Test Results



Brush Seal Case Study Summary

- ❑ Brush seal successfully installed and tested on LM2500+ First Engine to Test.
- ❑ Reduced leakage for Brush seal did reduce overall leakages vs. “J” seal, however, at power conditions the extra benefit was greater than required.
- ❑ Ultimately decided that extra cost and complexity of Brush seal not appropriate for this turbine mid frame design given the extent of other sealing improvements.
- ❑ Brush seal may still be appropriate in other situations but must account for total fluid system and heat transfer environment.

Export License TSU 10/15/97

Brush Seal Pros & Cons

Brush Seals ...

- ↑ Can significantly reduce leakage areas
- ↑ Conform extremely well to irregular surfaces
- ↑ Can easily absorb thermal motions/deflections
- ↓ Are more costly (\$7000 vs. \$650 for “J” seal)
- ↓ Are somewhat heavier than other seal types
- ↓ Suppliers are somewhat limited
- ↓ Raise concern over bristle durability and weld damage during construction

Biography: Fred G. Haaser

Current Position:

Responsible for leading all engineering efforts on the LM2500/LM2500+ family of industrial gas turbines at GE Aircraft Engines, Marine & Industrial programs. This includes integrating the engineering effort with the product line management, manufacturing, sales, and customer service organizations.

Background:

Fred Haaser received a BSME in Mechanical Engineering from the University of Notre Dame in 1976, and MS in Nuclear Engineering from the Pennsylvania State University in 1979. He worked in mechanical design for 1 1/2 years at Westinghouse's Bettis Atomic Power Lab prior to joining GE Aircraft Engines, where he has worked since 1980. A registered professional engineer and ASME member, Mr. Haaser was the Engineer Program Leader for the development of the LM6000 gas turbine, which entered production in 1992. His GE experiences prior to managing engine development programs includes managing engine secondary air systems, compressor stator design, and engine systems engineering. He is the author/co-author of four ASME papers.

ADVANCED SEAL DEVELOPMENT FOR LARGE INDUSTRIAL GAS TURBINES

Raymond E. Chupp
Westinghouse Electric Corporation
Orlando, Florida

ABSTRACT

Efforts are in progress to develop advanced sealing for large utility industrial gas turbine engines (combustion turbines). Such seals have been under developed for some time for aero gas turbines. It is desired to transition this technology to combustion turbines. Brush seals, film riding face and circumferential seals, and other dynamic and static sealing approaches are being incorporated into gas turbines for aero applications by several engine manufacturers. These seals replace labyrinth or other seals with significantly reduced leakage flow rates. For utility industrial gas turbines, leakage reduction with advanced sealing can be even greater with the enormous size of the components. Challenges to transitioning technology include: extremely long operating times between overhauls; infrequent but large radial and axial excursions; difficulty in coating larger components; and maintenance, installation, and durability requirements.

Advanced sealing is part of the Advance Turbine Systems (ATS) engine development being done under a cooperative agreement between Westinghouse and the US Department of Energy, Office of Fossil Energy. Seal development focuses on various types of seals in the 501ATS engine both at dynamic and static locations. Each development includes rig testing of candidate designs and subsequent engine validation testing of prototype seals. This presentation gives an update of the ongoing ATS sealing efforts with special emphasis on brush seals.

What is ATS ?

The Next Generation of Gas Turbine Technology

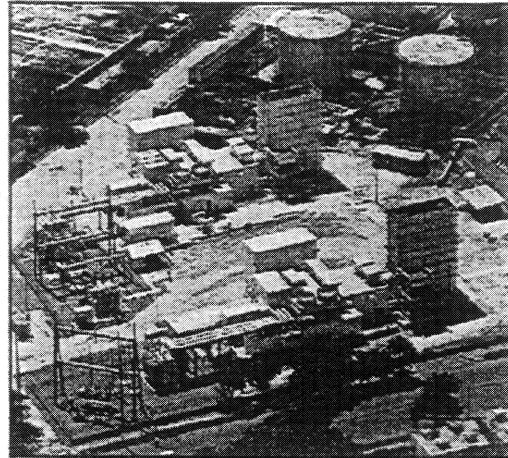
A university, utility, industry
government partnership

Lowest cost producer of
electricity

Environmentally superior

Key to Americas competitiveness
in the global electrical market

Supported by universities and
vendors throughout the
United States

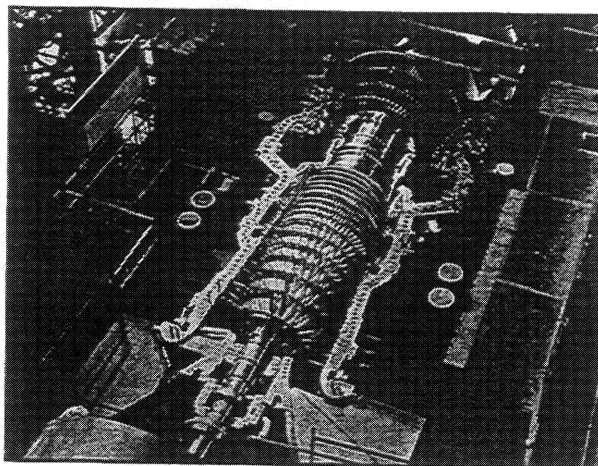


The Department of Energy's (DoE's) ATS program is a major driving force in the U.S. to improve industrial power plants. Over the last few years, large combustion turbines have evolved via integrating advanced technology into their design. Overall plant efficiencies have increased from under 40% to over 60% in the ATS plant being developed. ATS objectives address efficiency, emissions, cost of electricity, fuels, RAM, and date of introduction. They force the development to meet the major needs of the power generation industry.

Advanced Turbine Systems (ATS) Program

- Greater than 60% net plant thermal efficiency
- Less than 10 PPM NOx emissions
- Reduced cost of electricity generation by at least 10%
- Fuel-flexible design operating on natural gas with provisions for future conversion to coal or biomass fuels
- Reliability - availability - maintainability (RAM) equivalent to modern advanced power generation systems
- Commercialization in the year 2000

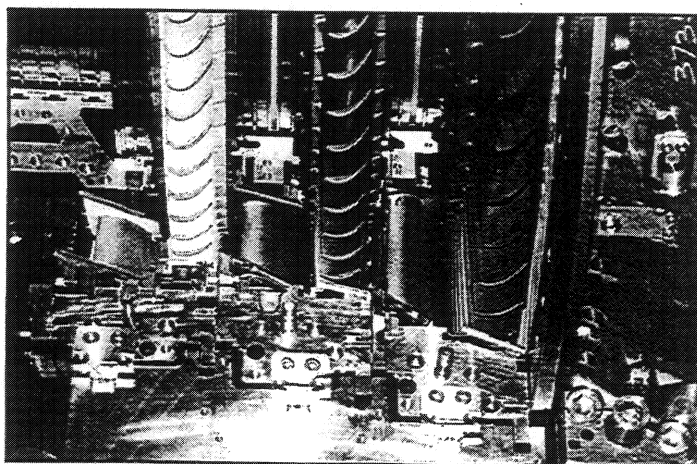
Combustion Turbine During Assembly



- Horizontal split casing
- Blades and vanes removable with rotor in place

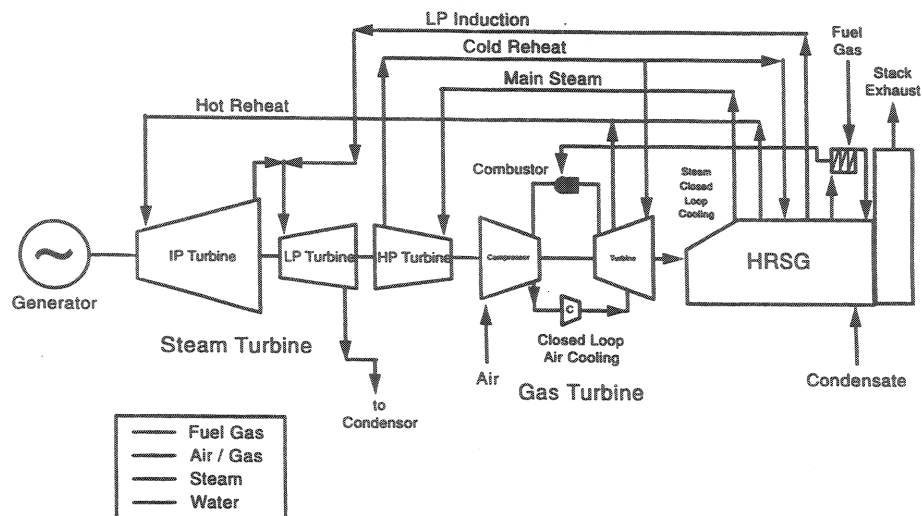
Westinghouse combustion turbines (gas turbines) have several unique design features that will be continued in the 501ATS engine. These features allow maintenance and repairs to be done on site without removing the rotor.

Turbine Horizontal Split Line Blade Ring Construction



- Turbine hardware removable with rotor in place
- Blade ring assemblies removed in two 180° sections

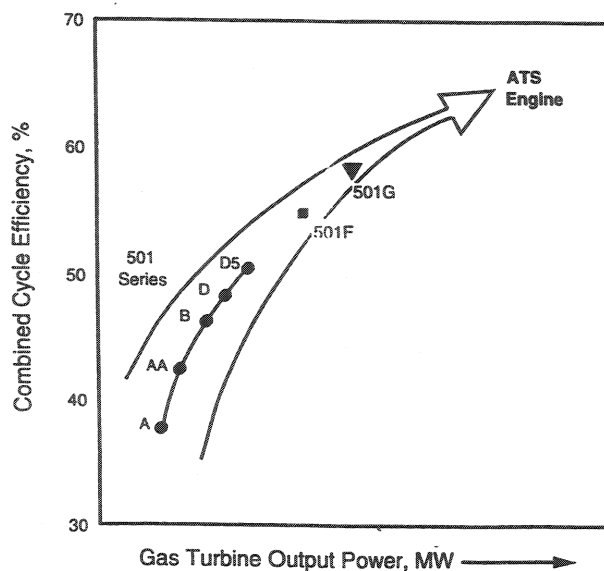
Advanced Combined Cycle Plant Layout



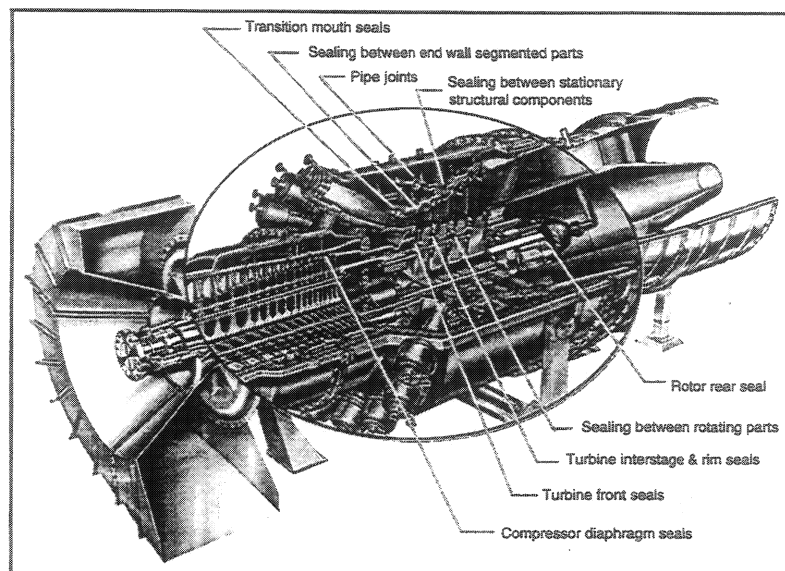
The ATS power plant combines efficient combustion turbine, steam turbine, and generator components to achieve the overall 60% efficiency goal.

Over the last few years, large combustion turbines have evolved via integrating advanced technologies into their design. Overall plant efficiencies have increased from under 40% to over 60% in the ATS.

Evolution of Large Westinghouse Gas Turbines



501ATS Sealing Focus Areas



The 501ATS combustion turbine is a derivative of current engines with improved features incorporated. Key sealing areas targeted for improvement include both static (noted in the upper part of the slide above) and dynamic (lower part) locations. Also, improved sealing is being addressed for joints between rotor cooling system circuits.

Sealing Locations

Static:

- Seam / air pipe joints
- Transition mouth
- Between large mating parts (Stein seals used for many years)

Between adjacent rotating parts:

- Joints in rotor cooling system circuits

Dynamic:

- Air sealing locations where labyrinth seals are normally used
- Rotor cooling system inlet and exit
- Shrouded and unshrouded turbine blade tips

ATS Engine Sealing Improvements

Contributes to:

- Decreased plant heat rate (improved cycle efficiency) and increased power output, e.g., for an achievable 1% decrease in leakage ==>
 - 25 + BTU/hr/KWH heat rate reduction
 - 1+% power increase
- Lower NOx emissions (via. improved static sealing at combustor transition mouth, between 1st stage vanes and in front of 1st stage rotor)
- Maintained / improved component mechanical integrity (e.g., disk cavities)

Improved sealing contributes to improve plant heat rate (efficiency) and decreased emissions. The ostensibly small performance gains are worth one to two orders of magnitude more in fuel cost savings and plant power output benefit than the increased hardware costs.

There are several opportunities/advantages in transitioning and developing improved sealing for large combustion turbines. These include: availability of advanced aero engine sealing technology, large size of combustion turbines, and primary operation at one condition.

Transitioning / Developing Improved Sealing

Motivation

- Improved sealing approaches developed for aero engines
- Large size engines - leakage may not scale up with size
- Engines run primarily at constant speed
- Fewer transient closure cycles than aero engines

Transitioning / Developing Improved Sealing

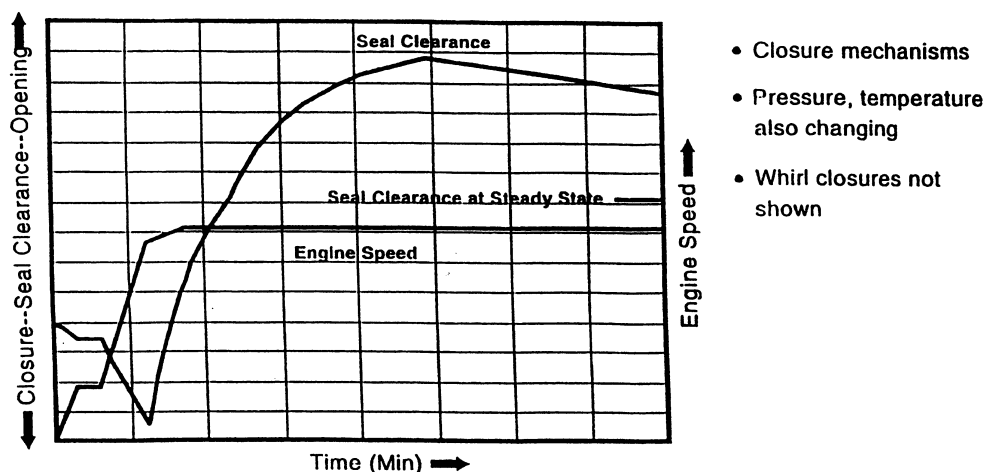
Challenges / Requirements

- Long operating life
- Large radial and axial movements during start-up / shut down
- Operate within available geometry envelope and range of environment conditions
- Moderate to aggressive leakage goals
- Segmented because of horizontal split line
- Minimum treatment of adjacent parts (e.g., coatings for brush seal runners) because of manufacturing complications / costs
- Durable for handling, field installation and operation

There are also challenges associated with applying improved sealing in these engines. These challenges include: long required operating lives, large start-up cycle relative movements, handling durability, etc.

A major challenge to improving **dynamic** sealing is the large radial closures during startup. As the engine starts rotating, the gaps between rotating and stationary parts immediately start closing up due to centrifugal growth of the rotating parts. Then, the temperature of stationary parts increases to open up the gaps. Much later, the rotating parts heat up and close the gaps down to their steady-state clearances. Unfortunately, the steady-state clearances are greater than the minimum values during start up, and this causes significant seal clearances at steady state. Clearances are also increased due to: orbiting of rotating parts as the rotor passes through critical speeds in starting up, and circumferential gap variations caused by the engine's split casing. Similar closure issues are involved with engine shutdowns.

Start-Up Cycle for Turbine Interstage Location



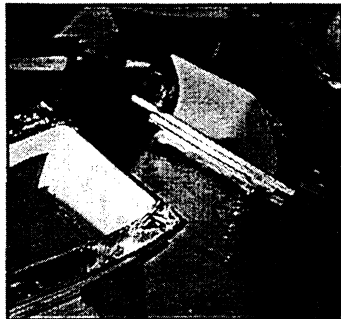
Transitioning / Developing Improved Sealing

Approach

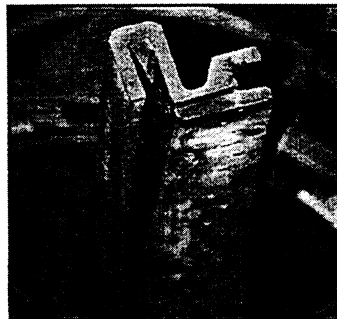
- **Address sealing areas with significant payoff in engine efficiency, emissions, mechanical integrity**
- **For static seals and seals between adjacent rotating components**
 - Incorporate proven components from current engines
 - Adapt improved sealing from aerospace applications

The ATS program includes a systematic approach to improving sealing for static locations. An example is sealing around the exit mouth of combustor transition liners. Leakage at this location is beneficial for cooling adjacent parts, but significantly increases emissions. To maintain a required rotor inlet temperature, the combustor maximum temperature must be increased by the dilution effect of leakages at the transition mouth and other locations ahead of the first-stage rotor blades. The two photographs below show how sealing is affected in current hardware. The seals in this area are made of heavy metal because of the hostile environment at this location. Also, these parts are robust to allow rugged handling. Some or all of the combustors are periodically removed for combustor and turbine hardware inspections and replacements. Challenges are the: need for robust sealing components, high temperature of gases circulating downstream of the seal, and need to provide cooling of adjacent hardware cooled by the higher leakage flows in current engines. A separate ATS development task has been launched to address improved sealing in this area.

Transition Mouth Sealing



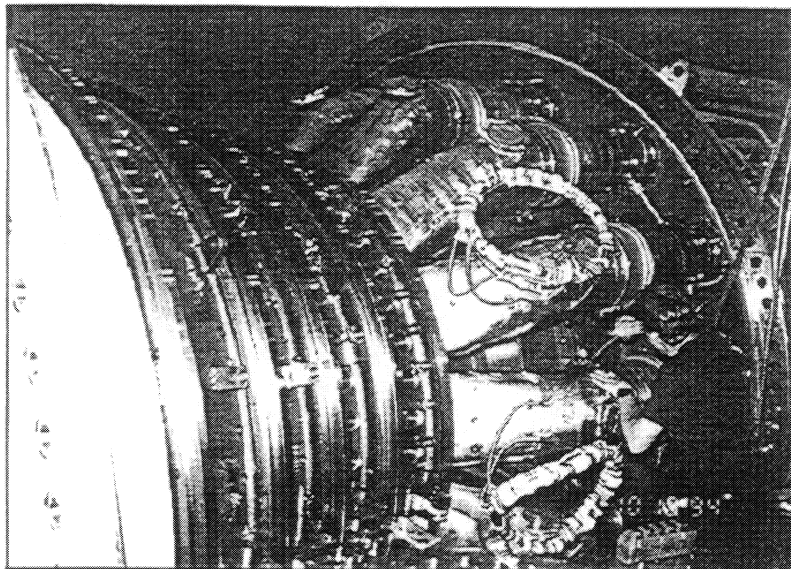
**Transition mouths with
side labyrinth seals**



**Top / bottom seal
between transition mouth
and 1st row vane endwalls**

- **Advanced transition mouth sealing must:**
 - Reduce leakage to sustain emission levels, while providing hardware cooling
 - Be robust to survive hostile thermal/vibration environment; and field installation and handling (including periodic transition removal for hardware inspections)

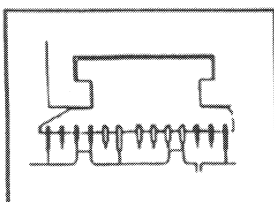
Combustion Turbine with a Transition Being Removed



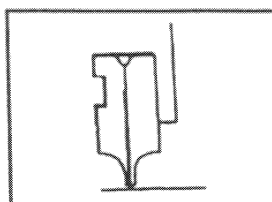
Above shows how transitions are removed. Hardware must be robust to permit on-sight removal.

Various types of dynamic seals in the 501ATS engine. Prime ones include: labyrinth seals; brush seals to replace key labyrinth seals; and a face seal at the rear of the turbine rotor. The latter is needed to meet tight sealing requirements of the closed-loop rotor cooling air system.

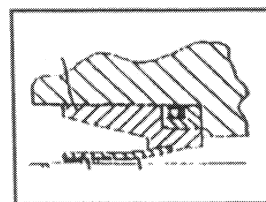
Types of Dynamic Seals



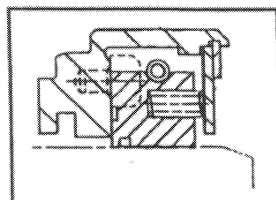
Labyrinth



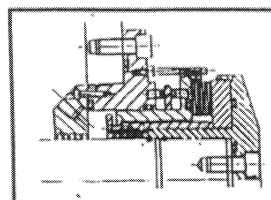
Brush



Compliant



Circumferential



Face

Transitioning / Developing Improved Sealing

Approach

- **Dynamic seals**
 - Primary focus -- replace labyrinth seals with brush seals
 - Apply face seal at ATS rotor rear location

Brush seals are a primary focus for improving dynamic sealing. Development has followed a systemic approach. It was initiated with a preliminary effort at Cross Manufacturing which demonstrated feasibility. This was followed by a series of subtask development efforts focused on individual sealing locations. EG&G has considerable experience and excellent R&D facilities to carry out the brush seal development work.

Brush Seal Development Program

- **Launched after success of preliminary effort with Cross Manufacturing**
- **Approach:**
 - 1) Potential seal locations, benefits, and required validation determined
 - 2) Focused seal development for selected engine locations
 - 3) Validation in a service engine
- **EG&G chosen for focused efforts**
(They have projects with the U.S. Air Force plus internal funding for aero-engine brush seal and manufacturing process development)

Brush Seal Development/Validation

- ◆ Define Operating Conditions
- ◆ Design Brush Seal to Meet Specific Requirements
- ◆ Rig Testing - Simulated Operating Conditions
- ◆ Design Full Scale Brush Seal Based on Rig Test Results

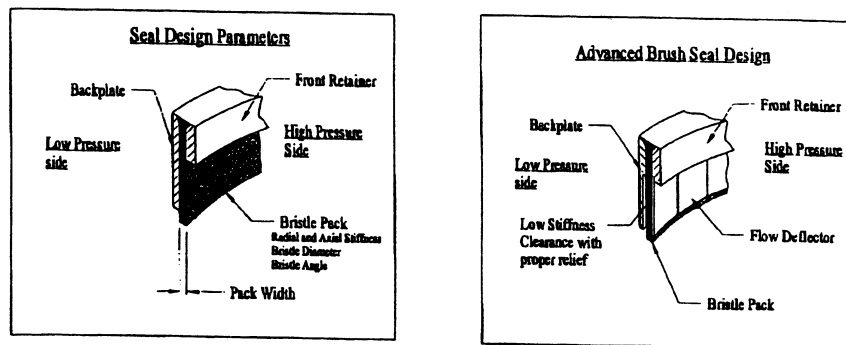
A four step approach (see above) was taken to develop and validate brush seals for each engine sealing location. The first step was to define the operating conditions and requirements (see below). Based on these data, initial brush seal configurations were determined with several bristle material options. Tribology rig tests were run for simulated engine conditions to determine the best bristle material to run against the rotating surface at the particular engine location.

Operating Conditions and Requirements

- ◆ Steady State and Transient
 - Rotor Speed
 - Environment Temperature
 - Air Pressure
- ◆ Relative Closure Time History
- ◆ Rotor Surface Condition (roughness)
- ◆ Segmented
- ◆ Durable for Handling, Field Installation, Operation

Brush Seal Design

- ◆ Design a seal which will exhibit minimal wear during interference operation, but have enough stiffness to support the required pressure drop.

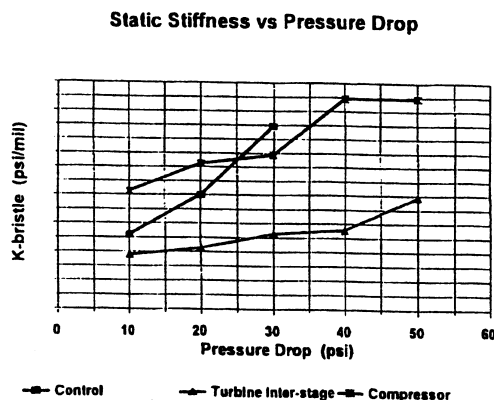


Two basic type brush seal configurations have been considered. One has a standard, generic design similar to brush seals produced by several manufacturers. The other has advanced features developed by EG&G. These features address seal hysteresis and bristle wear. Initial subscale seal testing evaluated the two brush seal configurations for the turbine interstage location. This testing demonstrated feasibility (see chart below) and the advantages of the advanced design. Consequently, only brush seals with advanced features were investigated for the other selected engine locations, i.e., compressor diaphragm, turbine front, and turbine rim.

Sub-scale Seal Testing

- ◆ Previous Testing Showed Feasibility
 - Uncoated Rotor Surface
 - High Radial Interference
 - Acceptable Wear Rates
 - Improved Sealing Performance
- ◆ Three Brush Seal Configurations - Location Specific
 - Standard design and EG&G design - Turbine Interstage
 - EG&G design - Compressor Diaphragm

Static Stiffness

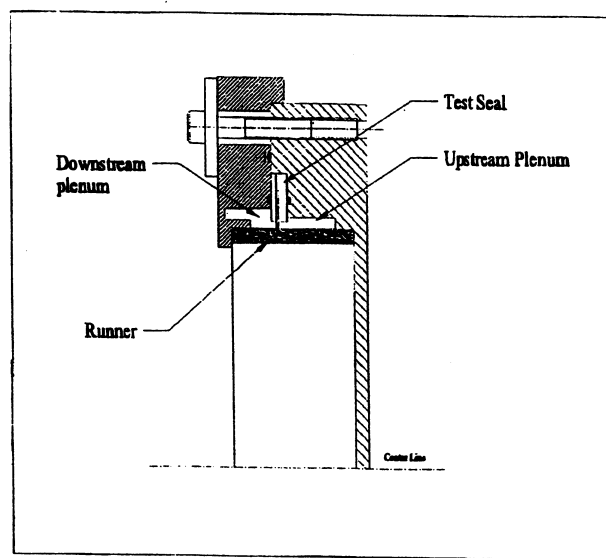


- ◆ During interference larger stiffnesses leads to higher bristle wear rates
- ◆ Seal leakage increases with start cycles

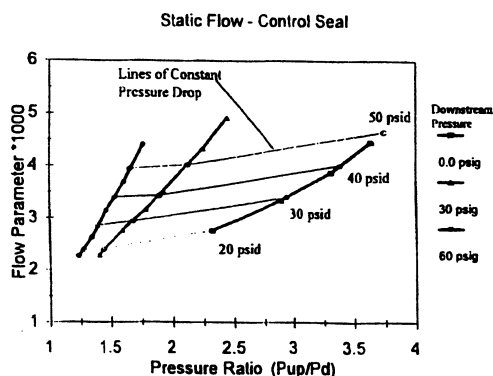
Radial stiffnesses of brush seal designs were measured statically to verify design stiffnesses and to quantify pressure stiffening as a function of pressure drop. Results above show that both advanced seal designs experienced a two-fold increase in stiffness with increasing pressure drop. The standard (control) seal had a 2 ½ times increase in stiffness over a smaller pressure drop change. The increase in stiffness affects seal wear and long term leakage performance.

Static flow data were acquired using a specially design fixture (see below). This fixture allowed seal pressure drop and pressure ratio to be varied independently via. adjusting the rig back pressure. Also, data acquired from the static flow fixture formed a database for leakage quality control of full-size segments for which only static data can practically be obtained.

Static Flow Fixture



Static Leakage Flow

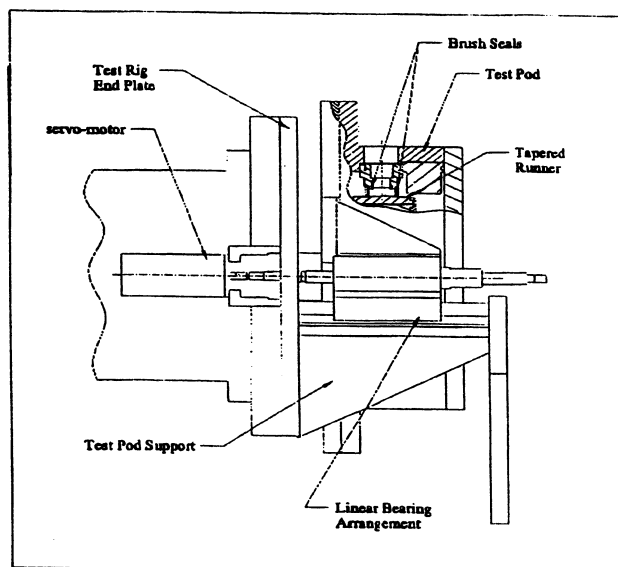


- ◆ Seal effective leakage area increased as the downstream pressure was increased for a given pressure ratio.
- ◆ Leakage flow parameter varies more with pressure drop than pressure ratio.

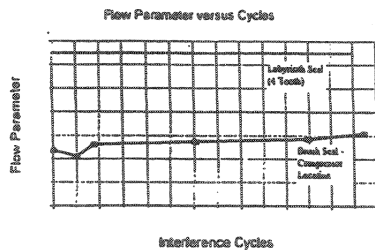
Representative results from static flow fixture tests (see above) show that pressure drop is a better parameter than pressure ratio to represent brush seal leakage.

Candidate brush seals were evaluated for wear and performance characteristics in EG&G's Aerospace Test Rig (see below). The seals were subscale size with engine pressure drop and rotor speed variations and temperature levels modeled. The rig has been updated to simulate seal closure by providing controlled axial seal movement along a tapered rotor surface.

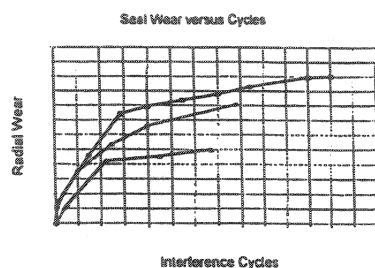
Aerospace Test Rig



Seal Leakage and Wear



- ◆ Total number of cycles representative of engine cycles between refurbishment
- ◆ Brush seal offers 60% reduction in leakage flow
- ◆ Compressor Diaphragm seal, with EG&G advanced features, exhibited less wear than the control seal

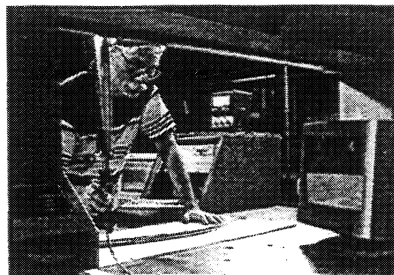
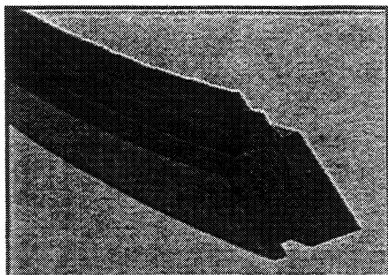


Representative data from subscale brush seal tests on the aerospace rig are shown above. The compressor diaphragm brush seal configuration exhibited superiority over the current labyrinth seal configuration even after many engine start cycles.

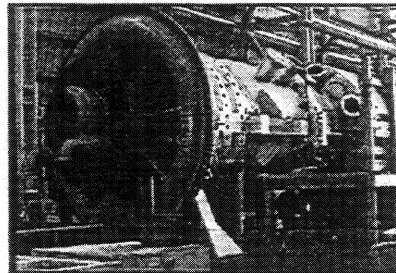
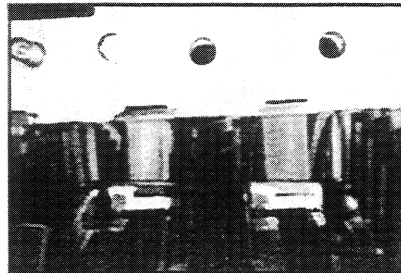
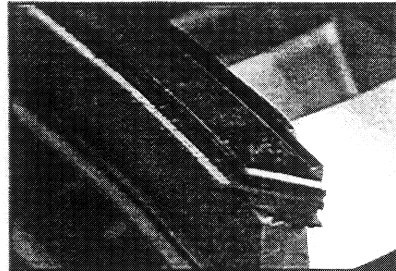
Data and lessons learned from fabricating and testing subscale brush seals led directly to defining design criteria for full-scale seals for each engine location. Below shows the 501ATS compressor diaphragm brush seal configuration and a segment being inspected.

Full-Scale Brush Seal Fabrication

- Subscale seal testing leads directly to full-scale design criteria, i.e., stiffness (bristle length, diameter, angle), fence height, advanced feature parameters
- Full-scale seal considerations
 - Segmented
 - Curvature differences
 - Large dimensions, tolerancing, centerless part inspection
 - Knife-edge profiles to minimize rub damage



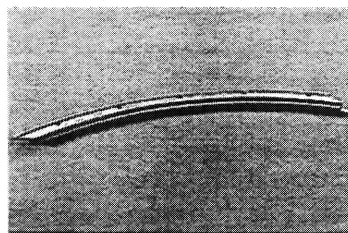
ATS Compressor Diaphragm Brush Seal Installation



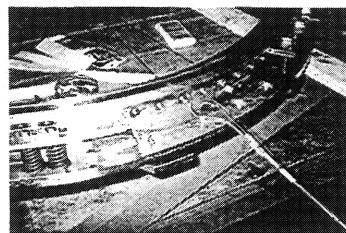
The photos above shows various stages of the brush seal segments being installed into 501ATS compressor diaphragms.

The photos below are views of full-size 501F brush seal segments and their installation. The segments have a bolted-on construction.

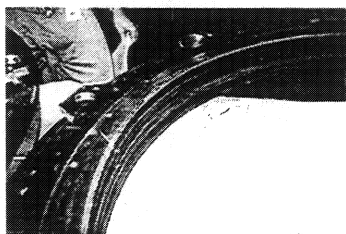
501F Turbine Interstage Brush Seal Installation



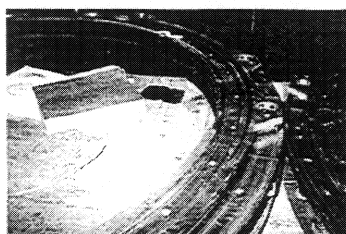
Brush seal segment (6 per row) with bolted on construction



Special instrumentation for 1st 501F unit with brush seals



One interstage with brush seal segments installed



2nd & 3rd interstages side-by-side with brush seal segments partially installed

ATS Rotor Rear Seal Development

Requirements

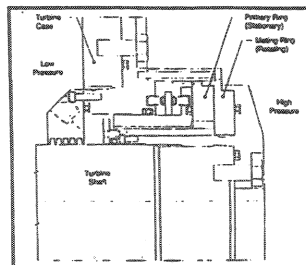
- Low leakage
- Large axial movement
- High pressure drop
- Robust, long life with part time low speed operation
- Handle particles in leakage air
- Smaller dia., not necessarily segmented

Selection:

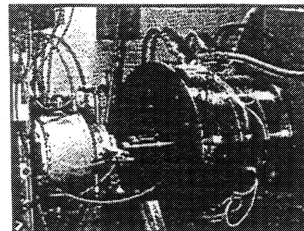
- Vendor - John Crane Inc.
- Seal - Non-contacting, dry running gas lubricated end face seal - hydrodynamic type
- Design - based on current Crane Type 28 seals with modifications to meet requirements

Evaluation:

- Long life with part time low speed operation
- Large axial movement
- Proper installation/durability capability
- Handle air contamination



Proposed rotor rear seal



John Crane test rig to simulate engine conditions

A separate development effort focused on providing very low leakage of cooled compressor discharge air (shell air) as it enters the 501ATS rotor at the rear. John Crane Inc.'s spiral groove face seal technology was adapted to this location with larger diameter and axial movement than in previous applications. Rig testing has been done to verify the seal's design and low leakage over a range of engine operating conditions.

In summary, advanced sealing components in the 501ATS combustion turbine are making significant contributions toward the overall ATS power plant goals. Advanced sealing development tasks have proceeded well and resulting sealing components will be validated in the first 501ATS engine.

Summary

- Improved sealing in utility gas turbines has significant payoffs
- ATS advanced sealing projects progressing well
- Focus on static and dynamic sealing locations with significant payoffs in plant: (1) increased efficiency, (2) reduced emissions and/or (3) maintained \ improved component mechanical integrity
- For static seals: (1) maintain/adapt proven concepts, and (2) incorporate improved sealing from aerospace/turbomachinery applications
- For dynamic seals: develop brush seals for the turbine interstages, rims, and front, and compressor diaphragms
- Focused development efforts are nearly complete for the turbine interstage and compressor diaphragm brush seals; full-scale hardware fabricated for engine/component validation testing
- Non-contact, dry-gas, hydrodynamic-lift face seal being developed for the ATS rotor rear

BRUSH SEAL ARRANGEMENT FOR THE RS-68 TURBOPUMP SET

D. Nunez, D. Ransom, and G. Prueger
Boeing
Rocketdyne Propulsion and Power
Canoga Park, California

The nature of the RS-68 turbopumps requires that the hydrogen seals separating the pump from the turbine must have extremely low levels of leakage and be contained in small packages. Conventional seal technologies are not able to reasonably satisfy such design requirements. A review of experimental measurements and analysis publications suggests that brush seals are well suited for the design requirements. Brush seals are shown to have less leakage than conventional labyrinth and damper seals and have no adverse affects on the rotordynamics of the machine. The bulk-flow analysis presented by Hendricks et al. is used as a guideline to create a spreadsheet that provides mass flow through the seal and heat generated by the rubbing contact of the bristles on the shaft. The analysis is anchored to published data for LN₂ and LH₂ leakage tests. Finally, the analysis is used to design seals for both applications. It is observed that the most important analysis parameter is the thickness of the bristle pack and its relationship to seal clearance, lay angle and pressure drop.

Agenda

- **Introduction to seal applications**
- **Concept trade**
- **Analysis methodology**
- **Design methodology**
- **Final design description**
- **Recommendations**

RS-68 Oxygen Turbopump

Pump

8,700 RPM

24,000 PSI Discharge

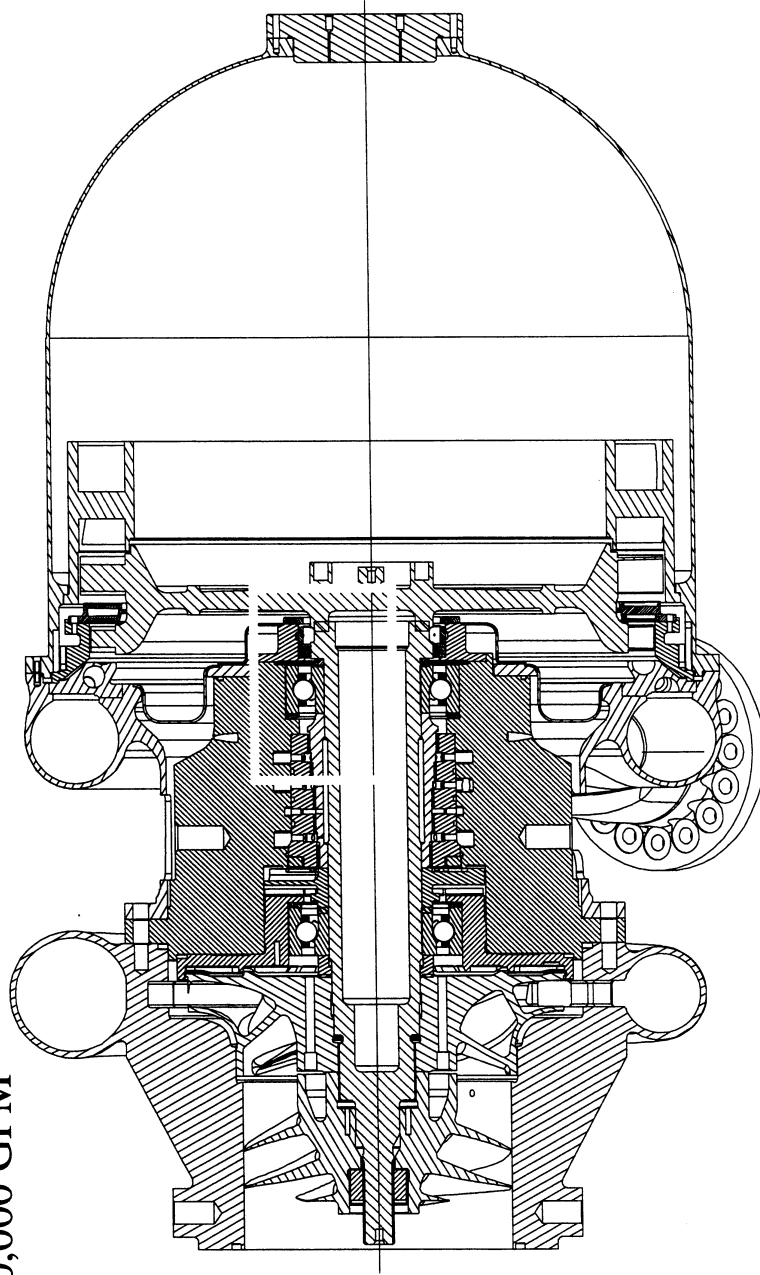
10,000 GPM

Turbine

1,400 R

715 PSI Inlet

19 lbm/sec

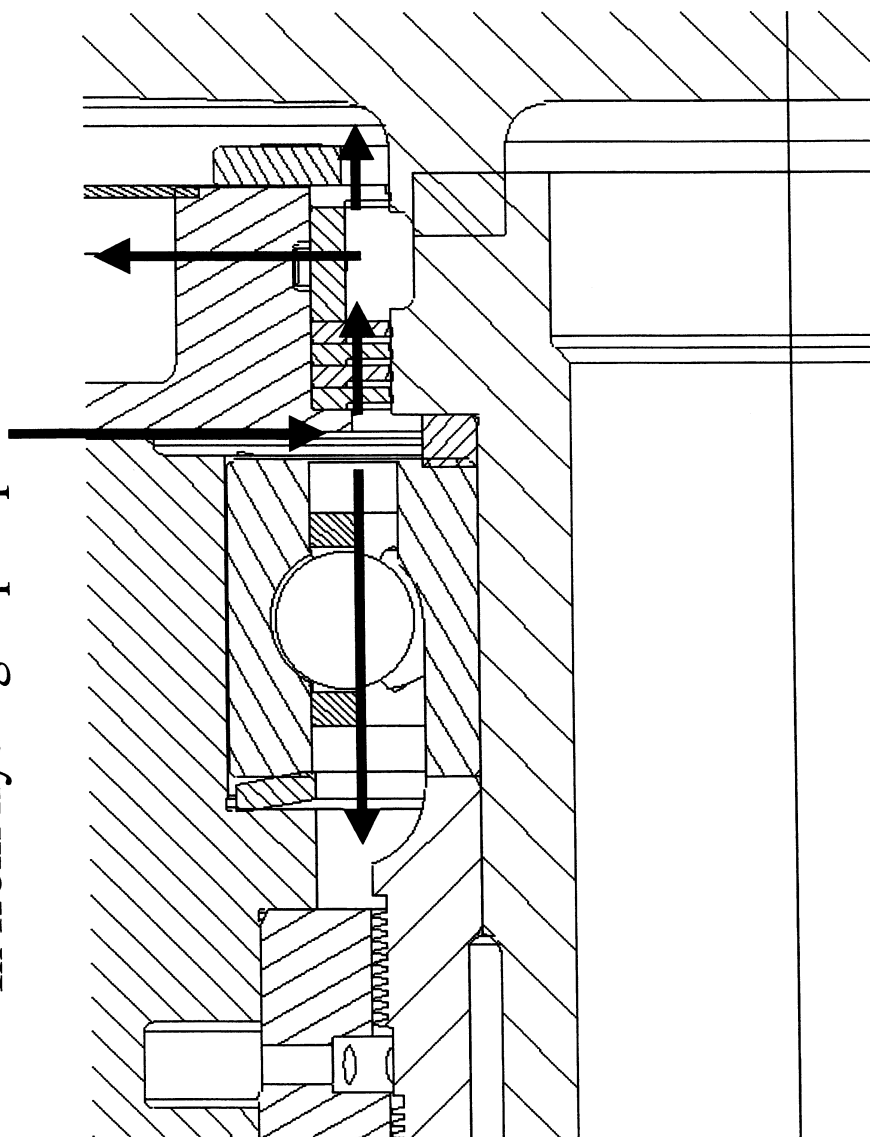


Slide 3 – RS-68 Oxygen Turbopump

This first slide is a picture of the RS-68 liquid oxygen turbopump. The LOX is pumped by the inducer and impeller located on the left end of the turbopump. The shaft rotates at 8,700 RPM producing a 24,000 PSIA pump discharge pressure and 10,000 GPM of flow. The driving turbine is on the right end of the turbopump. The turbine inlet temperature and pressure is 1,400° R and 715 PSIA respectively with a mass flow rate of 19 lbm/sec. The yellow box highlights the seal application under discussion.

RS-68 Oxygen Turbopump (Hydrogen Flow Path)

In from hydrogen pump



Slide 4 – RS-68 Oxygen Turbopump (Hydrogen Flow Path)

This picture shows the previously highlighted region of the oxygen turbopump. The hydrogen is introduced from the liquid hydrogen turbopump pump discharge and flows across the bearing (to provide cooling) and through the seal package where the majority of the flow is sent overboard and the remaining flow is used to prevent turbine gases from progressing towards the pump end of the turbopump. The amount of hydrogen that leaks into the turbine cavity must be minimized to prevent the turbine disk from cooling on the back side which will cause deformation of the disk.

RS-68 Hydrogen (Fuel) Turbopump

Pump

21,000 RPM

24,000 PSI Discharge

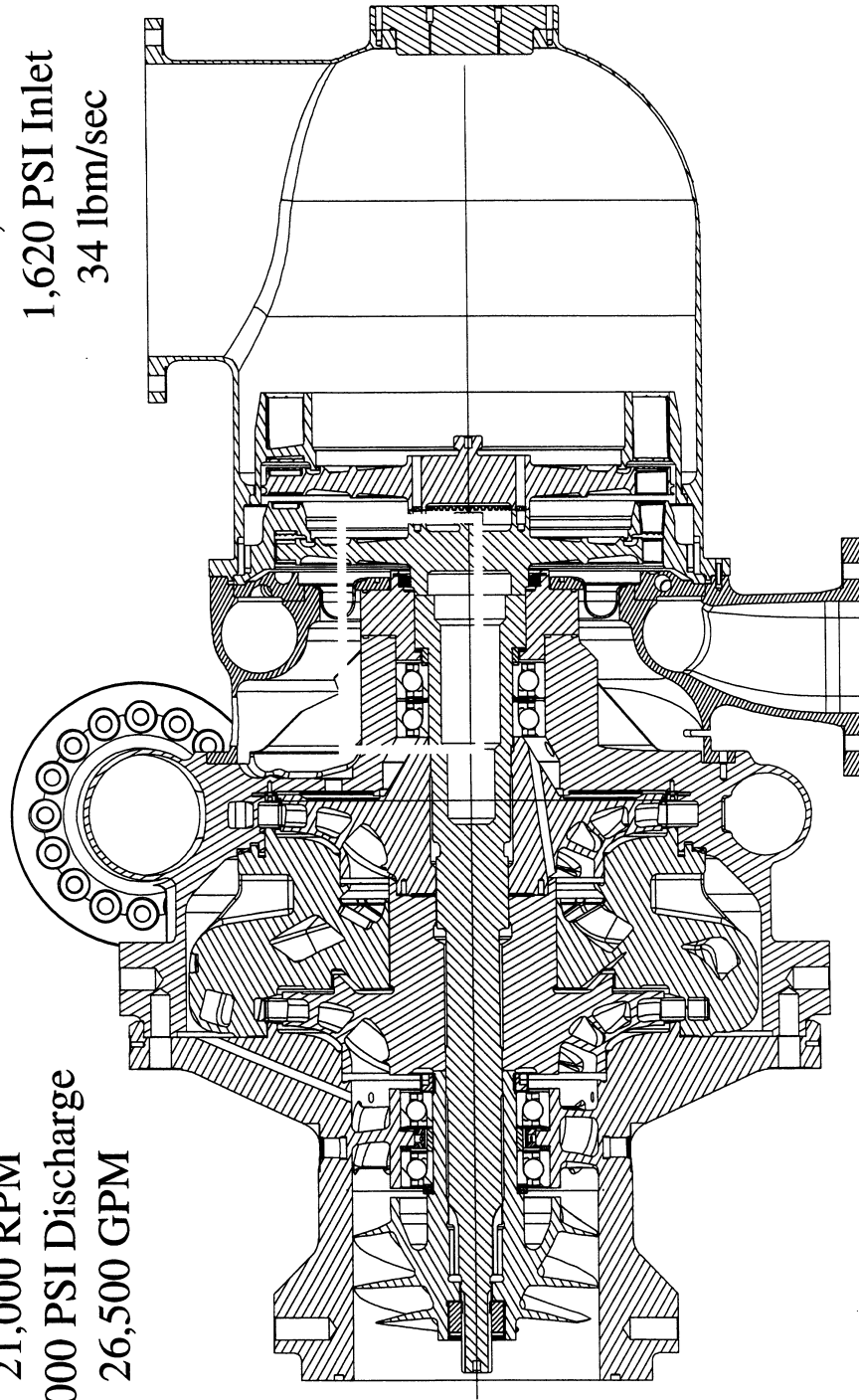
26,500 GPM

Turbine

1,400 R

1,620 PSI Inlet

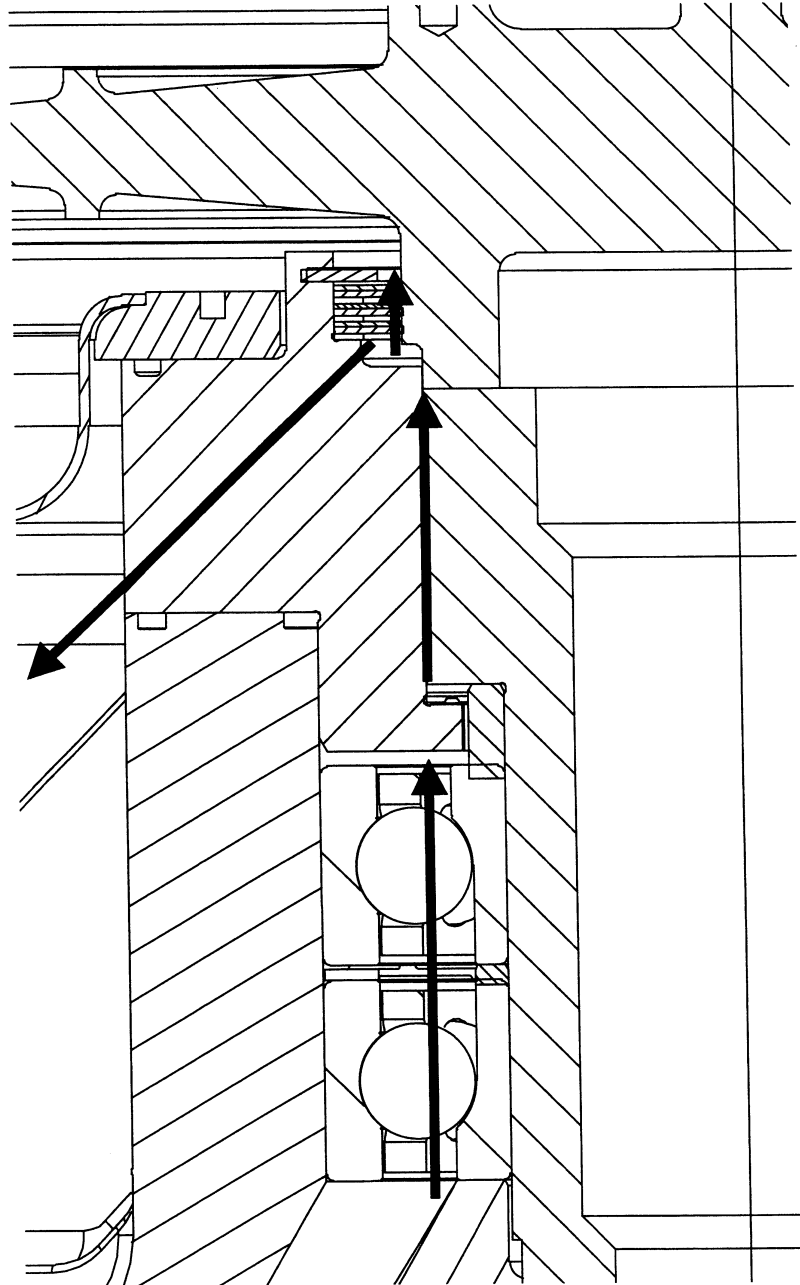
34 lbm/sec



Slide 5 – RS-68 Hydrogen (Fuel) Turbopump

This is a picture of the RS-68 liquid hydrogen turbopump. The LH₂ is pumped by the inducer and impeller located on the left end of the turbopump. The shaft rotates at 21,000 RPM producing a 24,000 PSIA pump discharge pressure and 26,500 GPM of flow. The driving turbine is on the right end of the turbopump. The turbine inlet temperature and pressure is 1,400° R and 1,620 PSIA respectively with a mass flow rate of 34 lbm/sec. The yellow box highlights the seal application under discussion.

RS-68 Hydrogen (Fuel) Turbopump (Hydrogen Flow Path)



Slide 6 – RS-68 Hydrogen (Fuel) Turbopump (Hydrogen Flow Path)

This picture shows the previously highlighted region of the hydrogen turbopump. The hydrogen passes through the ball bearings to provide cooling and then passes through a damper seal to add stability to the rotor system. Finally, a small amount is passed into the turbine cavity to prevent turbine gasses from progressing towards the pump end. The remaining hydrogen flow is dumped overboard. Again, it is important to minimize the leakage into the turbine cavity to prevent the turbine disk from deforming.

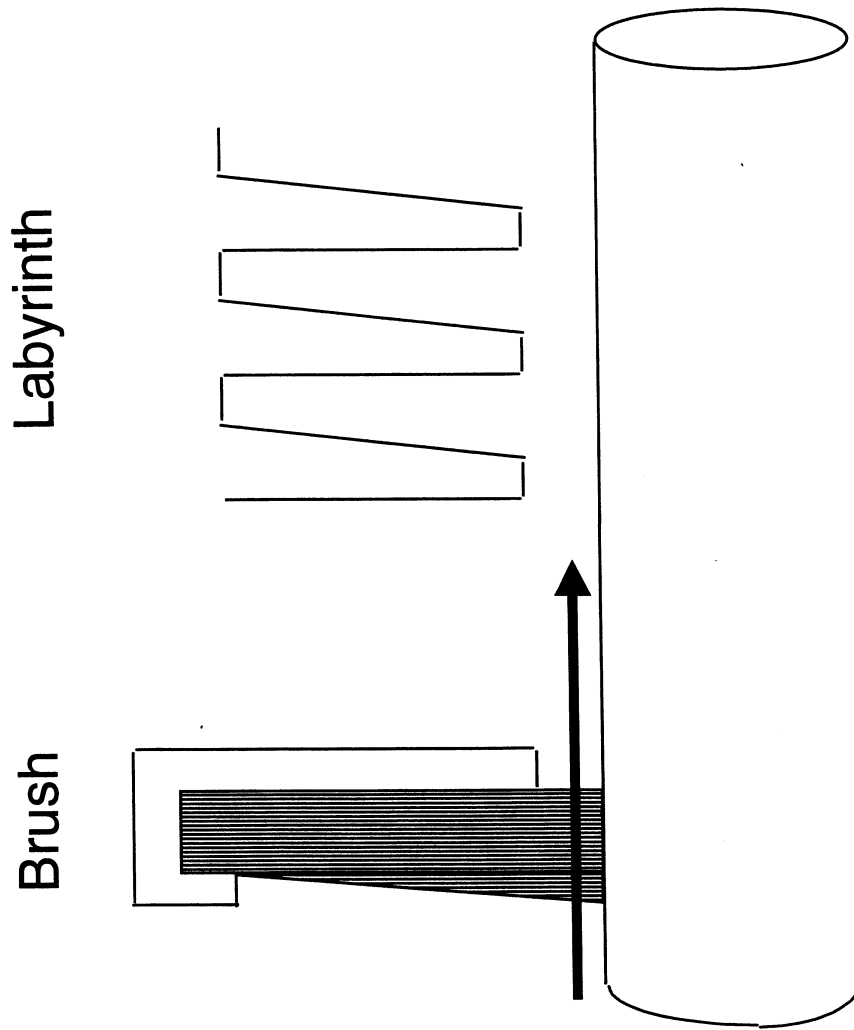
Seal Requirements for the RS-68 Turbopumps

- Hydrogen cooled turbine end ball bearing
- Low leakage into turbine cavity (less than 0.15 lbm/sec)
- Low cost, robust design
- *Liquid Oxygen Turbopump*
 - Approximately 250 psi ΔP
- *Liquid Hydrogen Turbopump*
 - Approximately 50 psi ΔP
 - Restricted axial package size

Slide 7 – Seal Requirements for the RS-68 Turbopumps

In both turbopumps, the turbine end ball bearings are cooled by liquid hydrogen. The same liquid hydrogen is passed into the turbine cavity to prevent turbine gasses from flowing towards the pump end. As mentioned before, the leakage into the turbine cavity must be minimal (less than 0.15 lbm/sec) to prevent the turbine disk from deforming. Also, the seal design used must be low cost and reliable to meet expendable vehicle cost requirements. The liquid oxygen pump requires a seal pressure drop of 250 psi. The liquid hydrogen pump requires a seal pressure drop of 50 psi and minimal axial length.

Two Annular Seal Types



Slide 8 – Two Annular Seal Types

An example of a brush seal and a labyrinth seal are shown here. The fluid flow is designated by the red arrow. As seen in the picture, the brush seal actually contacts the rotor whereas the labyrinth seal does not.

Labyrinth Seal Design for the RS-68 Turbopumps

- *Liquid Oxygen Turbopump*
 - Labyrinth seal sized for pressure drop
 - Radial clearance of 0.002 to 0.0025 inches required
 - Predicted leakage too high at 0.30 lbm/sec
 - Design clearance unreasonable due to bearing deadband
- *Liquid Hydrogen Turbopump*
 - Face riding carbon seal with labyrinth seal to control leakage
 - Added length of shaft to accommodate seal package detrimental to rotordynamic stability margins

Slide 9 – Labyrinth Seal Design for the RS-68 Turbopumps

Initially, a labyrinth seal is sized for the liquid oxygen pump application. In order to get minimum leakage, the seal clearance is set at 0.002 to 0.0025 inches radially. Since the bearing dead-band alone is about 0.001 inches, this design is not feasible and will likely result in a rub. Additionally, the leakage rate is still too high (0.30 lbm/sec) to meet the design requirements. For the liquid hydrogen turbopump, a face riding carbon seal with a labyrinth seal to control leakage is designed. The largest difficulty in using the proposed design is the axial length required for such a device. The longer shaft necessary for such a seal package is detrimental to rotordynamic stability margins.

Brush Seals Investigated (Advantages)

- Low leakage for axial length
- Application to turbopump allows for further reduction in leakage
 - Turbopump radial tolerance permits lower fence height
 - Proximity to bearing package reduces potential for fence rub
- No rotordynamic instability generated from circumferential flow
- Brush seal behaves like a swirl brake (Conner and Childs, 1993)

Slide 10 – Brush Seals Investigated (Advantages)

Brush seals have two distinct advantages over labyrinth seals, low leakage and rotordynamic stability. The low leakage is enhanced in turbopump applications because the tight radial tolerance allows for a lower fence height. In addition, the seals are located close to bearing packages so that shaft movements are minimal, thus reducing the potential for fence rub. Conner and Childs (1993) report on tests to identify the rotordynamic force coefficients of brush seals. The authors report that the seal did not exhibit any cross-coupled stiffness. Further, it is noted that the brush seal actually behaves like a swirl brake, removing the circumferential energy from the fluid that generates cross-coupled stiffness in labyrinth seals.

Brush Seals Investigated (Disadvantages)

- **Increased temperatures due to friction between bristle and rotor surfaces**
 - **Liquid hydrogen good coolant**
 - **Minimum interference of -0.002 inches reduces normal force of bristles on rotor**
- **Rubbing contact wears bristle material and rotor coating**
 - **Design life of expendable turbopump around 800 seconds**

Slide 11 – Brush Seals Investigated (Disadvantages)

Because brush seals are a contacting annular seal, heat generation and material wear are problems that must be dealt with. In the cryogenic turbopump application, the cool liquid hydrogen passing through the seal removes the heat generated by the bristles rubbing on the shaft. Also, minimizing the interference helps to reduce the magnitude of the normal force between the bristle and the shaft, thus minimizing heat generation. The minimal interference also reduces the possibility of bristle wear and particle contamination of the turbine. Finally, since the RS-68 is designed for ELV application, the design life is only around 800 seconds so that the seal does not have to last for a long duration.

Brush Seal Literature Reviewed

- **Analysis Literature**
 - **Hendricks et al. - “A Bulk Flow Model of a Brush Seal System”**
 - **Chupp et al. - “Simple Leakage Flow Model for Brush Seals”**
 - **Rhode and Pung - “Numerical Investigation of Brush Seal Bristle Lifting Phenomena”**
- **Test Literature**
 - **Proctor et al. - “Brush Seals for Cryogenic Applications”**
 - **Conner and Childs - “Rotordynamic Coefficient Test Results for a Four-Stage Brush Seal”**

Slide 12 – Brush Seal Literature Reviewed

There are three main papers reviewed concerning the analysis of brush seals. The first two are similar in that the leakage is estimated using a bulk flow analysis. However, the first paper (Hendricks et al.) models the flow through the brush seal with more sophistication and is accompanied by test data. In the second analysis, Chupp et al. intend to provide a rough but quick tool for predicting brush seal performance by lumping all of the seal parameters into an effective seal thickness, but this application requires a more thorough analysis. The third paper by Rhode and Pung appears to be too complicated for this particular analysis and is not pursued. In addition to the analysis literature, two papers are used for experimental test information. Proctor et al. present test data which is used in the analysis of Hendricks et al. to validate the analytical model. Proctor et al. measure mass flow, pressure drop and temperature for several brush seal configurations and operating conditions. Conner and Childs, as mentioned earlier, identify the rotordynamic force coefficients of several brush seals and find that the seals are dynamically stable.

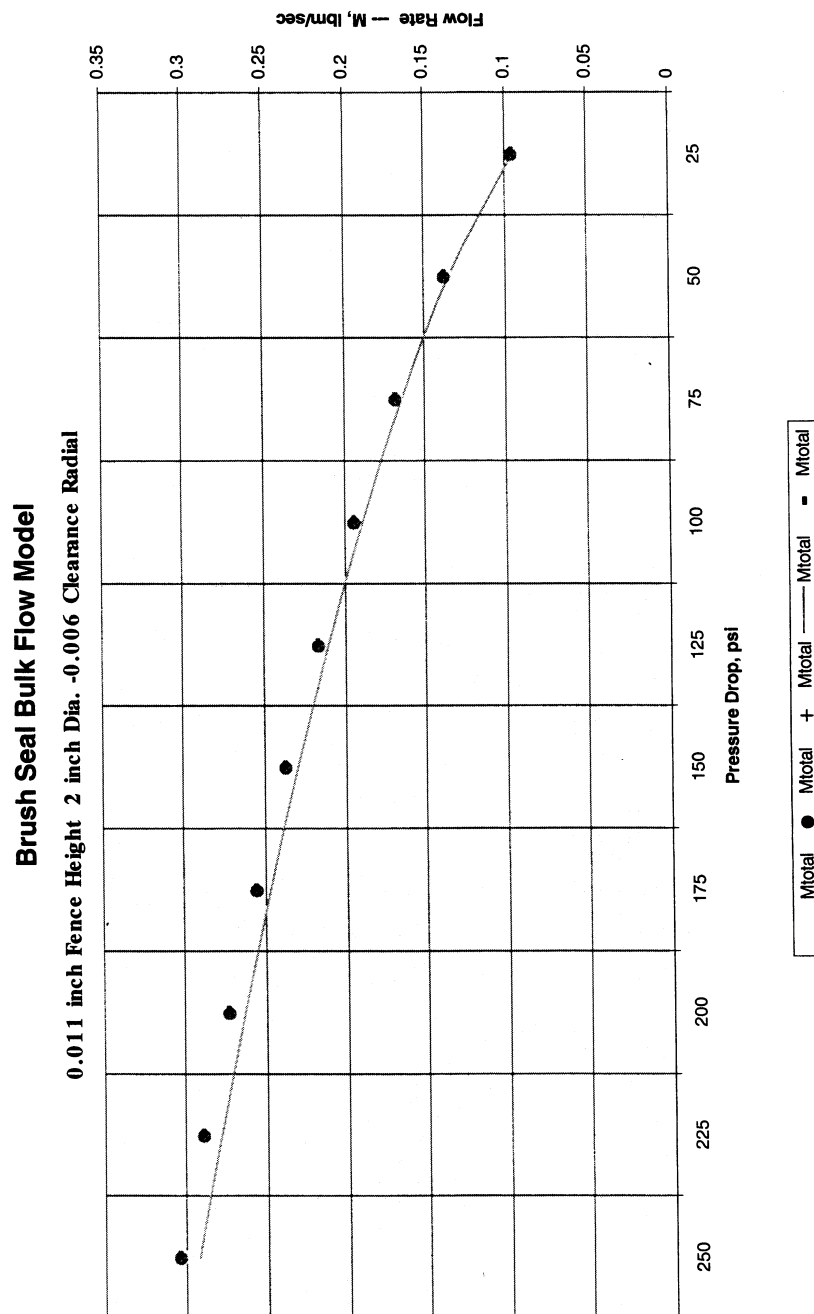
Brush Seal Bulk Flow Model Developed and Anchored

- **Hendricks model used for final analysis**
 - **More thorough analysis method**
 - **Available NASA Lewis RC test data in hydrogen**
 - **Tested brush seal geometry closer to turbopump requirements**
 - **Provides leakage estimates for the three flow paths identified in brush seal**
 - **Heat generation estimated from bristle normal force and coefficient of friction**
- **Anchored to NASA Lewis RC published test data**

Slide 13 – Brush Seal Bulk Flow Model Developed and Anchored

The model presented by Hendricks et al. is used to build an Excel spreadsheet because of the thorough analysis and the already available test data. Also, the tested seals are similar in geometry to turbopump seal requirements. The analysis spreadsheet provides leakage estimates for three flow paths; flow between the bristles, flow between the bristles and the seal dam, and flow underneath the bristles. The model also estimates heat generation from the bristle normal force and the coefficient of friction. Before it is used as a design tool, the analysis is anchored to the published test data from NASA Lewis RC.

Bulk Flow Model Validation



Slide 14 – Bulk Flow Model Validation

This chart shows how well the analytical model created in Excel compares with the LN2 experimental test data for the fence height, shaft diameter and radial clearance.

Brush Seal Design Methodology

- **Begin with parameters similar to tested seals (bristle lay-angle, bristle interference, fence height)**
 - **Decrease interference fit to reduce bristle wear and heat generation**
 - **Decrease fence height to decrease leakage**

Slide 15 – Brush Seal Design Methodology

While developing the analysis method, it is learned that the analysis is most sensitive to the bristle pack thickness. Therefore, large variations in the interference or lay angle would likely render the analysis invalid. To avoid this, the seal design is intentionally made to be similar to the already tested seals used to anchor the analysis model. The interference is decreased (from 0.005 to 0.002 inches) to avoid the possibility of wear and the fence height is lowered to decrease the seal leakage. With only these slight changes, it is expected that the analysis is still valid.

Final Design Description

Shaft Diameter	5.000 inches
Bristle Radial Clearance	-0.002 inches
Seal Fence Height	0.010 inches
Bristle Lay Angle	50°

Slide 16 – Final Design Descriptions

The final brush seal design dimensions for the two pumps are as follows; with a shaft diameter of 5.000 inches, the bristle clearance is a negative 0.002 inches radial. The fence height is 0.010 inches from the shaft radial. The bristle lay angle is 50 degrees. All of these values are subject to manufacturing tolerances so the installed dimensions may vary somewhat.

Recommendations

- **Investigate brush seal operation in liquid oxygen**
- **Investigate stability of clearance fit brush seals (generation of cross-coupled forces?)**
- **Develop eccentric operation model**

Slide 17 – Recommendations

In the interest of using brush seals on the pump side of the oxygen turbopump, it is recommended that brush seal operation in oxygen be investigated. Perhaps it is useful to use a clearance fit brush seal on the oxygen side that would only generate heat (from friction) in the event of a rub. It is also recommended that the rotordynamic stability of clearance fit brush seals be investigated since a circumferential flow could possibly develop in the clearance portion of the seal. Finally, it is recommended that a model be developed to predict brush seal behavior for eccentric operation.

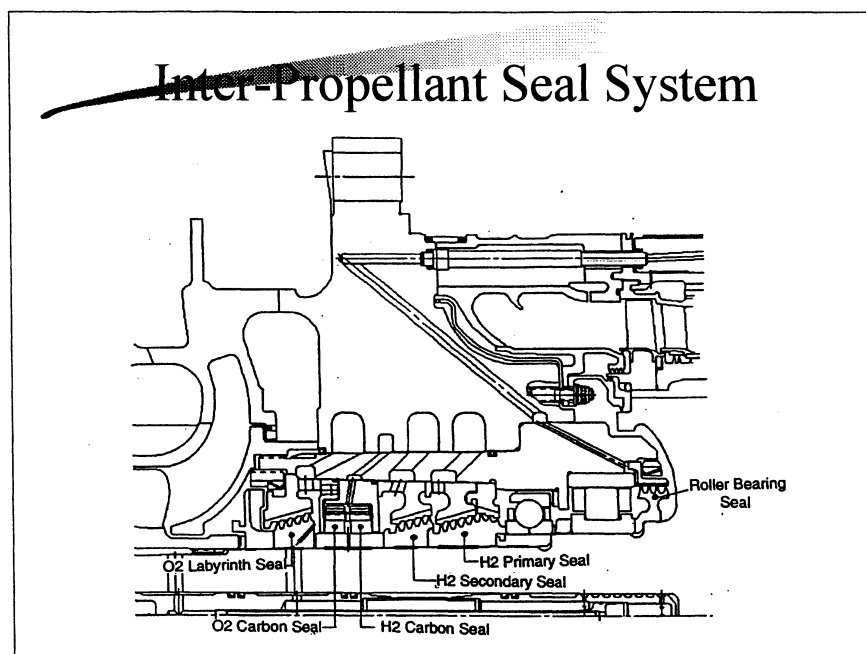
AN ADVANCED HELIUM BUFFER SEAL FOR THE SSME, ATD OXYGEN PUMP

Wilbur Shapiro
WSA, Inc.
Niskayuna, New York



NASA

- Phase I and Phase II
- Contract - NAS3-97023
- Contracting Officer - Glen Williams
- COTR - Margaret Proctor
- Stein Seal Company - Major subcontractor
for Phase II manufacture and test



The Inter-Propellant Seal System on the Shuttle Oxidizer pump separates oxygen on the pump side from Hydrogen in the turbine drive region. It consists of a series of pressure breakdown labyrinths on both the hydrogen and oxygen sides. The helium buffer seal (HBS) is located between the hydrogen and oxygen regions and pressurized helium gas prevents egress of fluid from one side to the other. The present configuration of the HBS consists of a pair of opposed carbon rings that are forced axially against their containment housing. Leakage occurs through the clearance between the rings and the shaft. Pressures on the hydrogen side are reduced by the labyrinths from 4968 psia to 31 psia, and on the oxygen side pressure is reduced from 258 psia to 19 psia.



109% RPL Operating Conditions

Buffer Fluid	Helium
Speed	24,230 rpm
Viscosity	2.8×10^{-9} lb-s/in ²
Gas Temperature	487 deg. R
Buffer Pressure	121 psig
Hydrogen Drain	14 psig
Oxygen Drain	4 psig

The 109% Rated Power Level (RPL) condition is where most of the operation will occur. Helium conditions are indicated on the table shown on slide 4.



Objectives

- Leakage of present configuration = 239 SCFM
- Reduce Helium Consumption- 50 SCFM (will result in significant increase in payload)
- Maintain Space Envelope
- Configurations- T-Seal, L-Seal

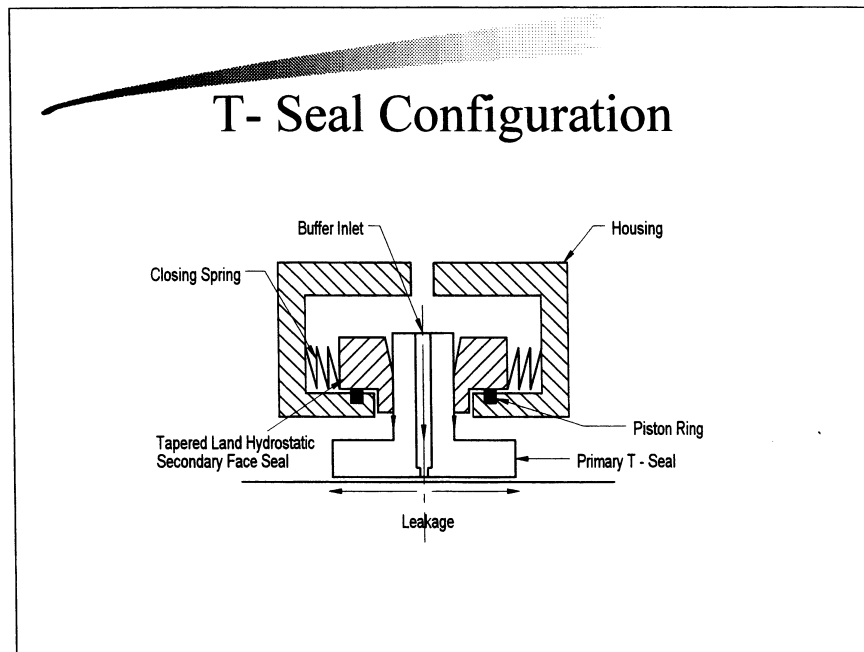
The objectives of the Phase I effort were to :

- Complete analysis and designs of helium buffer seals for the P&W alternate SSME oxygen pump that could reduce helium leakage to 50 SCFM or less.

The configurations investigated included:

- A T-seal including a secondary seal design that would eliminate high startup preload.
- Back to back L-shaped sector seals (L-Seal).

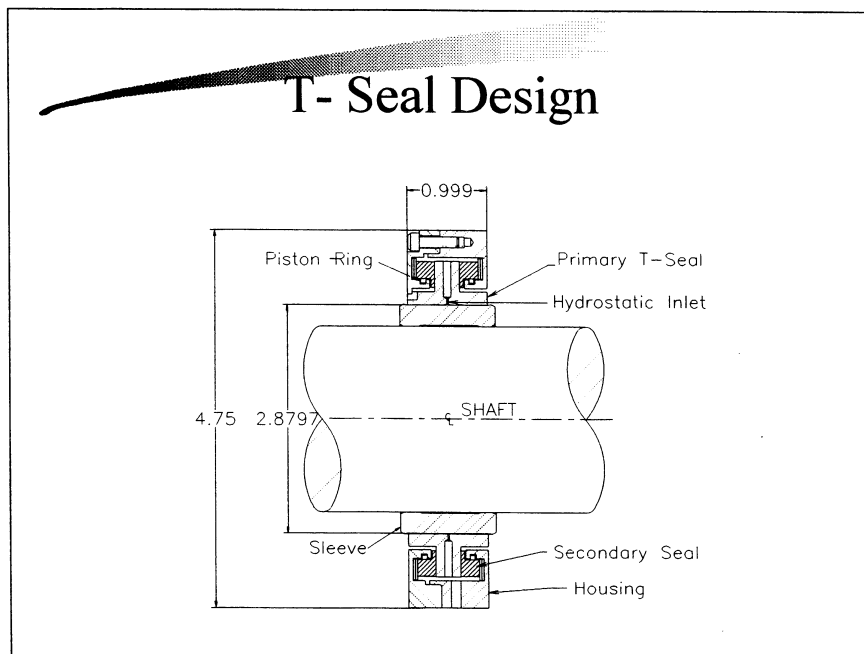
Phase II will accomplish build and test.



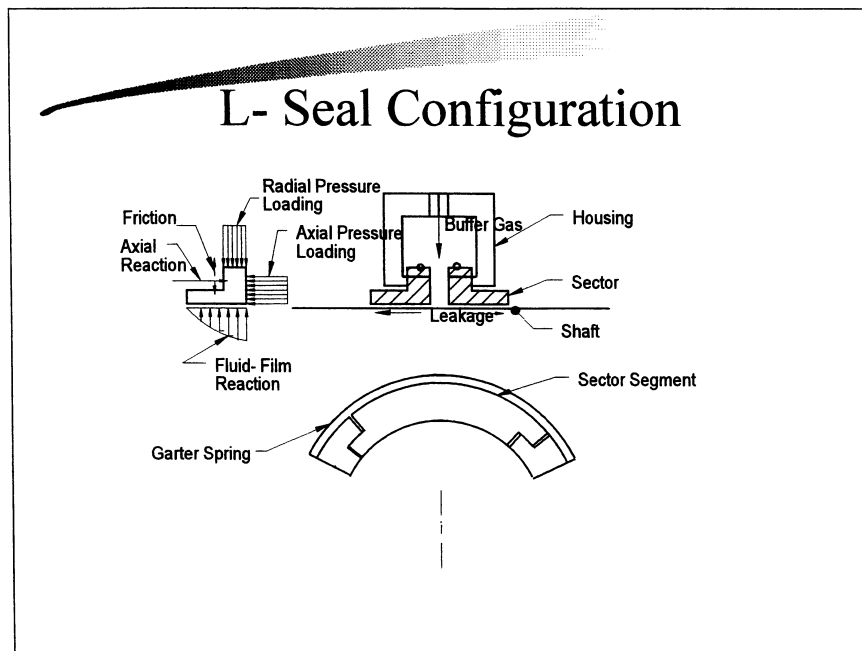
The T-Seal configuration consists of a solid carbon ring with a T-shaped crosssection as viewed at the bottom. At the mid length, 36 equally spaced inlet holes are drilled of 0.020 in. diameter to hydrostatically feed the interface clearance region between the seal and the shaft. The vertical leg of the T is sealed by two opposed hydrostatic tapered land seals that are energized by the pressure buildup in the seal cavity. Activation in this manner precludes high startup clamping loads that could prevent development of the secondary seal film.

The advantages of the T-Seal are

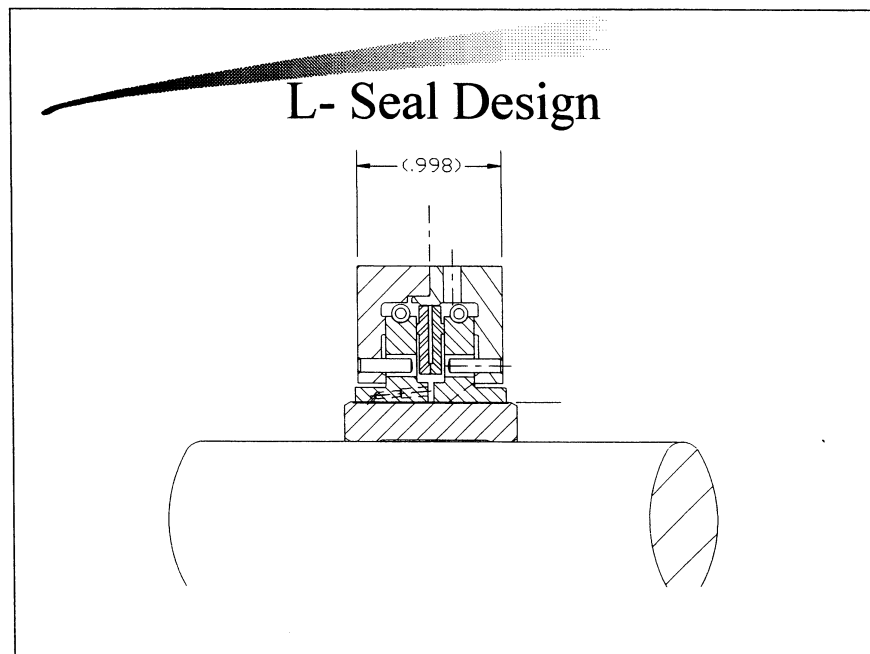
- It makes maximum use of available length.
- It conserves leakage because of the pressure drop through the orifice.
- It can track shaft excursions because of frictionless support.



The shaft sleeve diameter is 2.88 in with an overall seal length of 1 in.

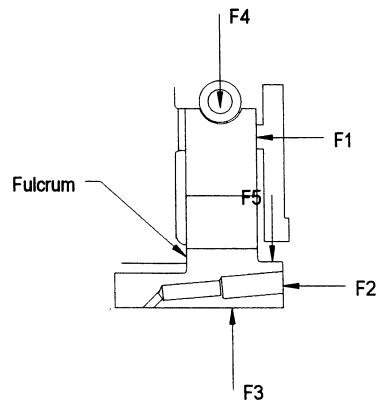


The L-Seal consists of two back-to-back sectorized circumferential seals each of which are 0.5 in. in length. The concept is shown diagrammatically on slide 8. The configuration allows added interface length because it can extend beyond the inner walls of the housing. The actual design length ends at the outer housing wall so that the seals can fit into the space provided by the existing buffer seals.



A variety of interface geometries was considered including a plain surface, taper, Rayleigh- Step and Hydrostatic. Comparative studies indicated that the best compromise was the orifice compensated hydrostatic seal. It operates well at all speeds and provides good performance at higher clearances and higher pressures. It will also act hydrodynamically at low clearance conditions and thus provide an added safety factor. Considerable effort was applied to the spring design because a comparatively heavy force was required for moment balance.

L-Seal Sector Moment Balance



To prevent an overturning moment the spring force on the sector equals 34 lbs. And the total axial load is 100 lbs. The friction force on the sector will add an additional 20 lbs to the radial load. The operating film thickness to overcome the total force will be approximately 0.1 to 0.2 mils which is considered too marginal for the application.

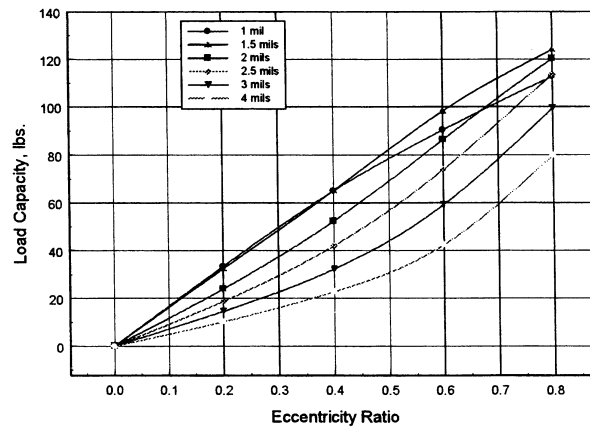


L-Seal Eliminated for Phase II

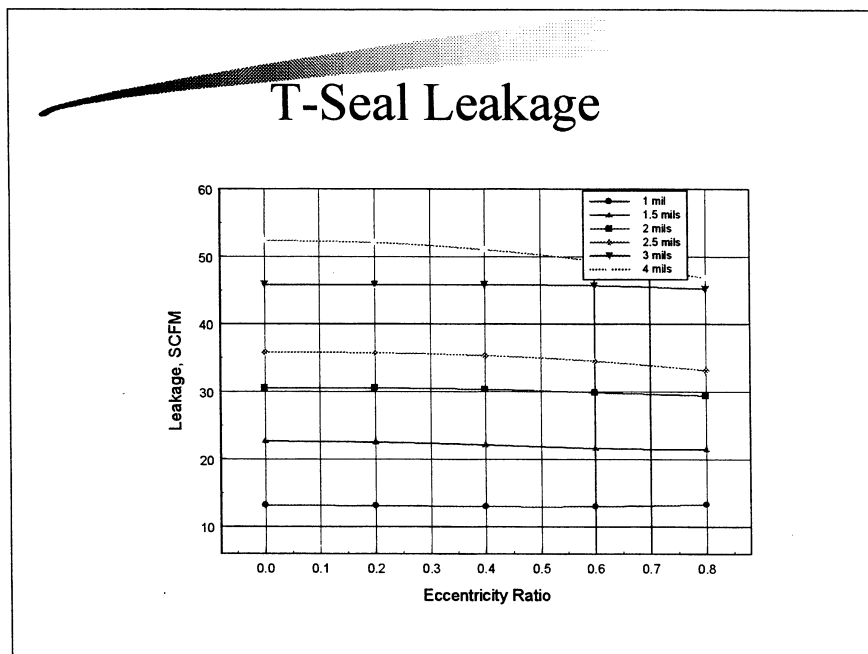
- High spring load required for moment balance
- High friction results
- Film thickness - 0.1-0.2 mils

Although designs were completed, the L-Seal was eliminated from Phase II consideration because of marginal performance and the far superior performance of the T-Seal.

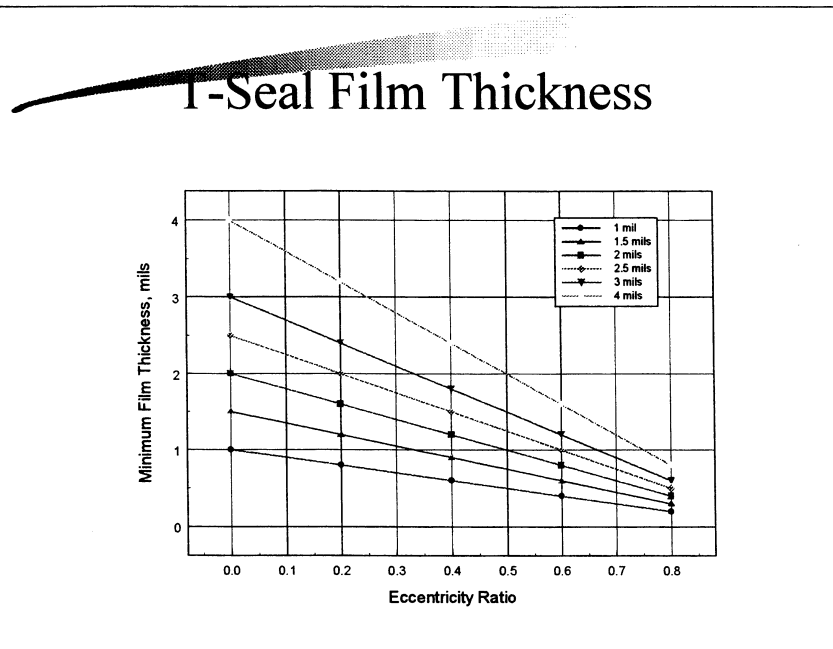
T-Seal Load Capacity



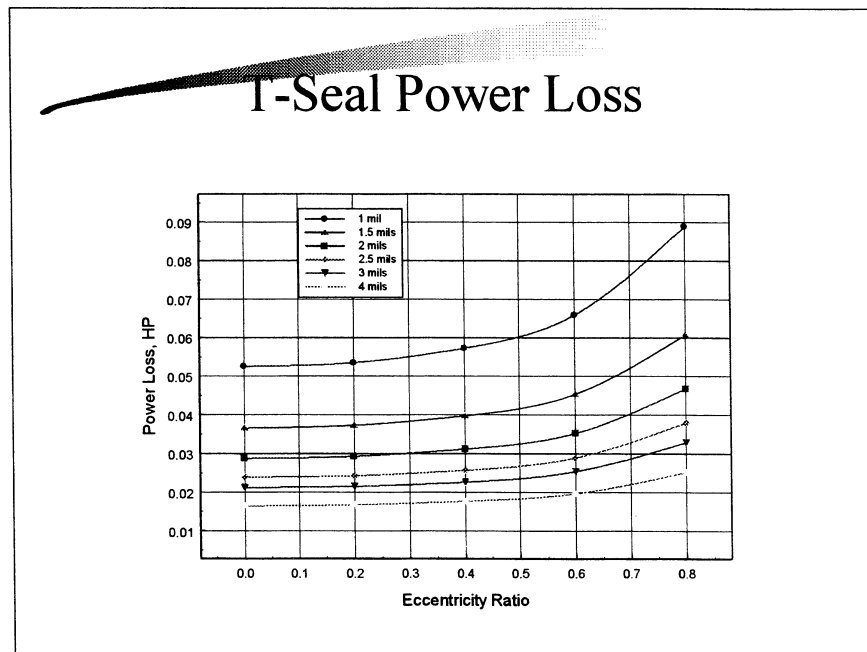
Maximum load occurs at a radial clearance of 1.5 mils and not at the 1 mil clearance that may be expected. Hydrodynamic capacity is not significant at the maximum speed of 24,230 rpm and hydrostatic action is the principal source of load capacity. At the 1 mil condition, the preload from the unloaded side reduces the net load capacity.



The target leakage of 50 SCFM is approximately 80% less than the two separate seals of the present back to back ring seals. To produce leakage less than 50 SCFM, the operating radial clearance should be no greater than three mils.

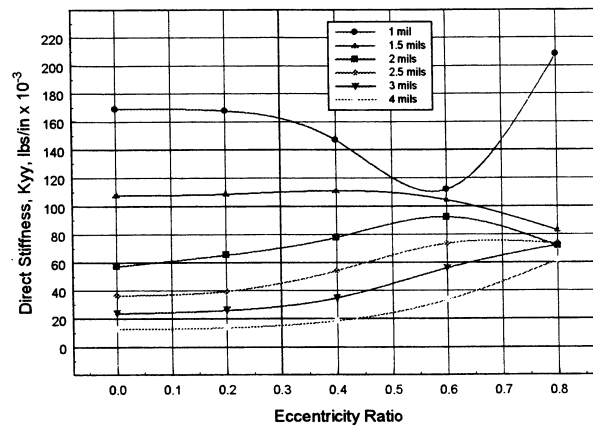


Minimum film thickness is quite adequate even at large eccentricities, because of the relatively large concentric clearances involved. It is anticipated that the seals will be operating in the concentric position because of the near frictionless support of the secondary seals.

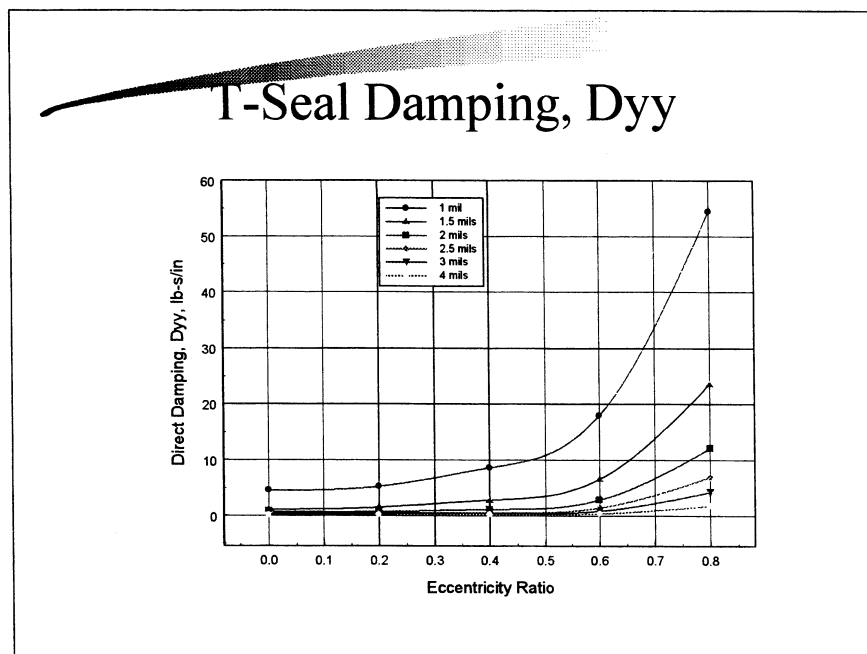


Power consumption is small, and less than 50 watts in most of the operating range.

T-Seal Stiffness, K_{yy}

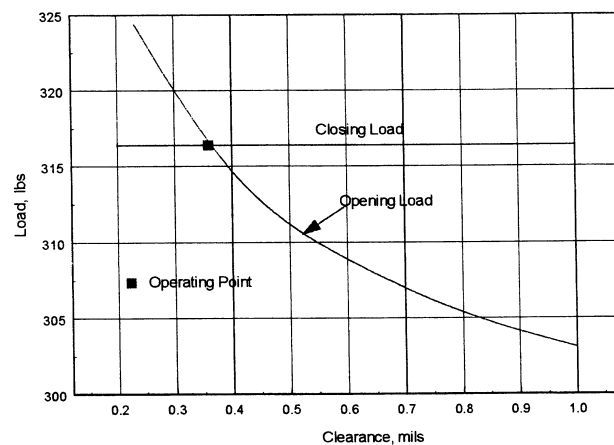


Direct stiffness curves, K_{yy} , indicate a reduction in stiffness at the one mil clearance, until an eccentricity of 0.6, and the stiffness trend reverses and markedly increases, because the hydrodynamics take hold at the lower clearance levels. At a 2.5 mil operating clearance, the stiffness is approximately 40,000 lbs/in.



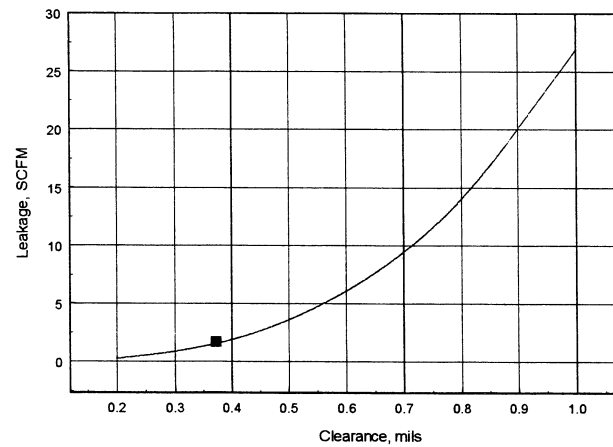
Damping increases markedly with eccentricity ratio. At 2.5 mils in the concentric position the direct damping is 0.45 lb-s/in.

T-Seal, Secondary Seal - Load



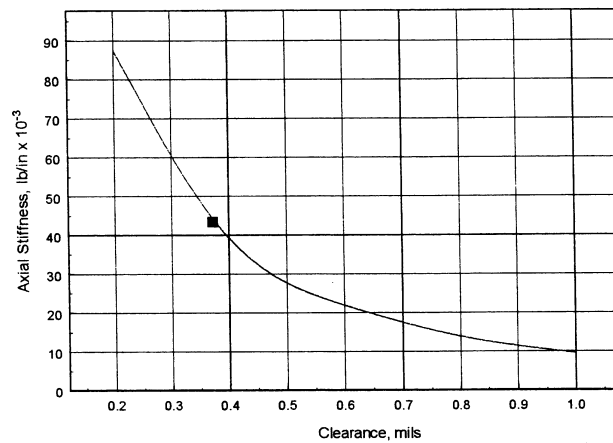
The closing load on the secondary seal was sized to provide a film thickness of about 0.37 mils. The operating film thickness can be small (0.2 to 0.4 mils) because there is no rotation between the opposed surfaces, although there can be motion due to shaft excitation.

T-Seal, Secondary Seal-Leakage



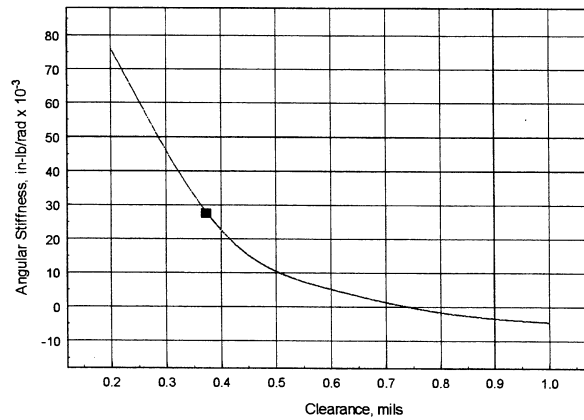
Total Leakage for the two secondary seals is less than 4 SCFM.

T-Seal, Secondary Seal- Kzz

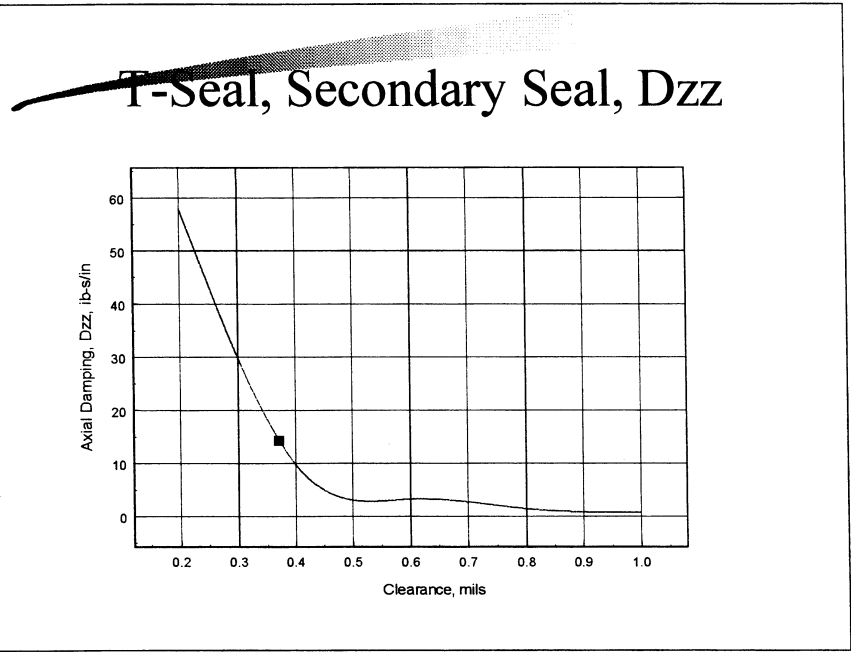


The axial stiffness is approximately 50,000 lbs/in, which is more than adequate to maintain separation during seal ring excursions.

T-Seal, Secondary Seal - Kaa

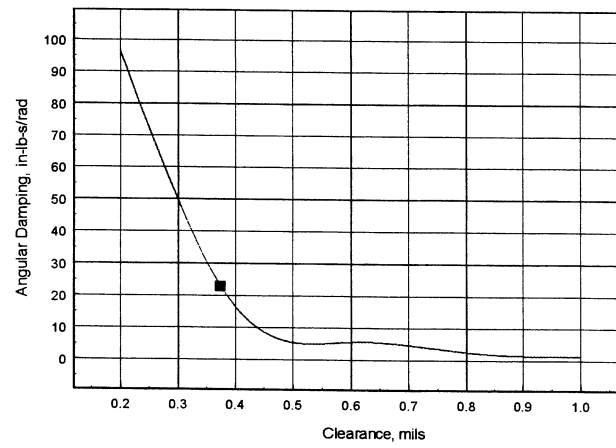


The moment, or angular stiffness remains positive for the operating range, and does not go negative until the film thickness exceeds 0.7 mils, a condition that cannot be encountered because of the hydraulic closing load. The tapered land moment stiffness remains positive at the lower operating clearances. A hydrostatic seal, that was an alternative had negative moment stiffness at lower clearances and turned positive at the higher clearances which opposite to the desired response.

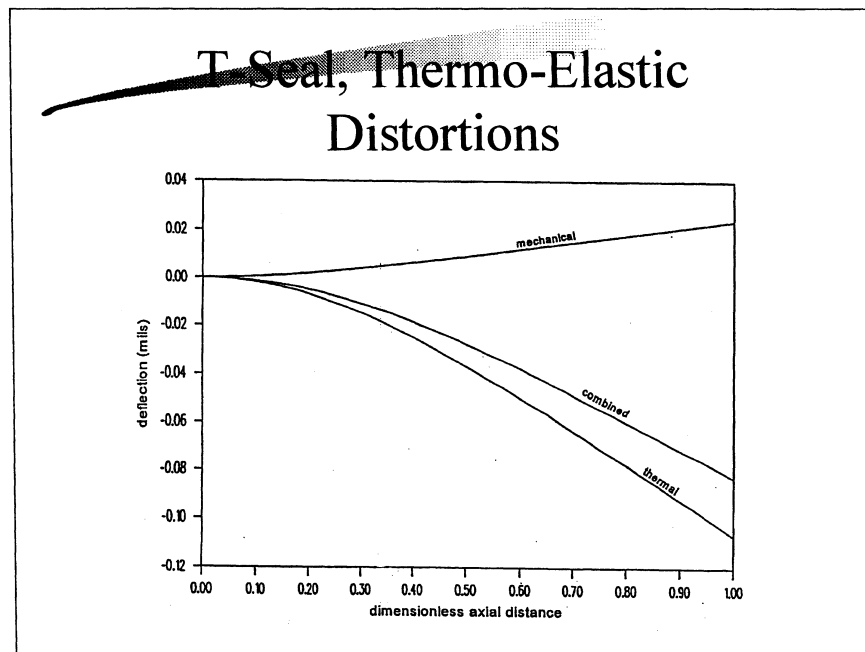


Axial damping is excellent.

T-Seal, Secondary Seal - Daa

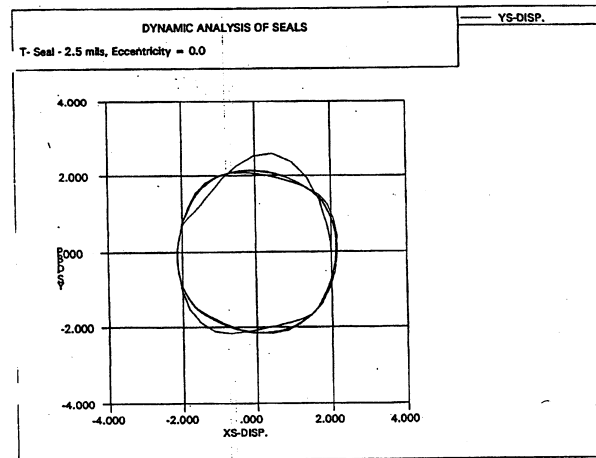


Moment damping is good.



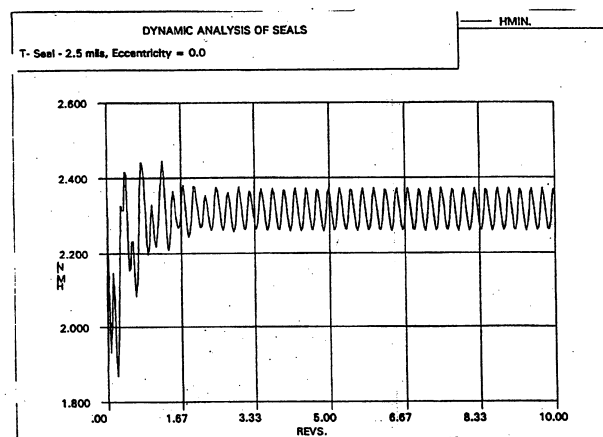
Heat generated in the film will be principally transmitted to the flowing fluid, and temperature gradients are small. The combined effect of mechanical and thermal distortion is approximately 0.1 mils, which is insignificant compared to the operating clearance. Although distortions are small, the clearance increase due to cryogenic operation has been calculated to be 1.95 mils. The manufactured clearance needed to obtain an operating clearance of 2.5 mils should be approximately 1 mil on the diameter.

T-Seal, Dynamic Orbit



Rotor excursions for the orbit shown were ± 2 mils. Results indicate excellent tracking capability. Friction of the secondary seals was accounted for.

T-Seal, Dynamic Film Thickness



The minimum film thickness is following rotor excursions. There is an insignificant reduction in film thickness to 2.3 mils.



Conclusions

- Predicted performance of the T-Seal is excellent
- Leakage less than 50 SCFM
- Safe Film Thickness of 2 to 2.5 mils
- Thermo-elastic distortions not significant
- Excellent dynamic tracking
- Phase II will accomplish hardware build and test at Stein Seal Company

An Advanced Helium Buffer Seal for the SSME, ATD Oxygen Pump

Wilbur Shapiro
WSA, Inc.

Abstract

The present configuration of the Helium Buffer Seal on the ATD oxygen pump consists of a pair of opposed carbon rings that are forced axially against their containment housings. Leakage occurs through the clearance between the rings and the shaft. The total helium leakage through both sides is approximately 239 SCFM. A reduction in leakage to 50 SCFM will result in less helium storage and consequently permit a substantial increase in payload. Under a Phase I NASA SBIR, a solid T-Ring seal was analyzed and designed that could satisfy the criteria of reducing leakage to 50 SCFM or less. The design makes maximum use of available length and employs a mid length row of hydrostatic orifices that feed buffer helium directly into a 2 to 3 mil clearance region. The flow splits into two opposite paths to buffer oxygen gas on one side and hydrogen gas on the turbine side. The seal employs opposed hydrostatic tapered land secondary seals that provide friction free support of the primary seal and allows the primary seal to follow rotor excursion and maintain concentric operating clearance. The predicted performance of the T-seal is excellent with operation at a safe film thickness of 2 to 2.5 mils and leakage less than 50 SCFM.

Introduction

The Inter-Propellant Seal System on the Shuttle Oxidizer pump separates oxygen on the pump side from Hydrogen in the turbine region. It consists of a series of pressure breakdown labyrinths on both the hydrogen and oxygen sides. The helium buffer seal (HBS) is located between the hydrogen and oxygen pressure breakdown labyrinths and pressurized helium gas prevents egress of fluid from one side to another. The present configuration of the HBS consists of a pair of opposed carbon rings that are forced axially against their containment housing. Leakage occurs through the clearance between the rings and the shaft. The labyrinths reduce pressures on the hydrogen side from 4968 psia to 31 psia, and on the oxygen side pressure is reduced from 258 psia to 19 psia. Leakage of the present configuration is 239 scfm. A reduction in leakage to 50 scfm decreases the amount of on-board helium and allows a substantial increase in payload (approximately 1000 lbs.). Thus, the objectives of the Phase I SBIR effort were:

- Complete HBS designs that could potentially reduce helium consumption to 50 scfm or less
- Maintain existing ATD space envelope

Designs were completed for two configurations:

- A solid T-seal configuration with low friction secondary seals
- Back to back L-shaped sector seals (L-seal).

The L-seal predicted performance was problematical because of moment balance considerations. The recommended configuration was the T-Seal and is what this paper will discuss. For L-seal information, refer to Reference (1).

The 109% Rated Power Level (RPL) condition is where most of the operation will occur. Helium conditions are indicated on Table 1.

Table 1 – 109% RPL Operating Conditions	
Buffer Fluid	Helium
Speed	24,230 rpm
Viscosity	2.8×10^{-9} lb-s/in ²
Gas Temperature	487 ° R
Buffer Pressure	121 psig
Hydrogen Drain Pressure	14 psig
Oxygen Drain Pressure	4 psig

T-Seal Configuration

The T-seal configuration is schematically shown on Figure 1, and a design assembly of the T-seal is shown on Figure 2. The shaft sleeve diameter is 2.88 in. and the overall seal length is 1 in. The T-seal consists of a solid carbon ring with a T-shaped crosssection as viewed at the bottom. At mid length, 36 equally spaced inlet holes are drilled of 0.020 in. diameter to hydrostatically feed the interface clearance region between the seal and the shaft. Two opposed hydrostatic tapered land seals, that are energized by the pressure buildup in the cavity, seal the vertical legs of the T. Activation in this manner precludes high startup clamping loads that prevent development of the secondary seal film.

The advantages of the T-seal are:

- Maximum use is made of available length
- Leakage is conserved because of the pressure drop through the orifice
- Shaft excursions can be tracked because of frictionless support

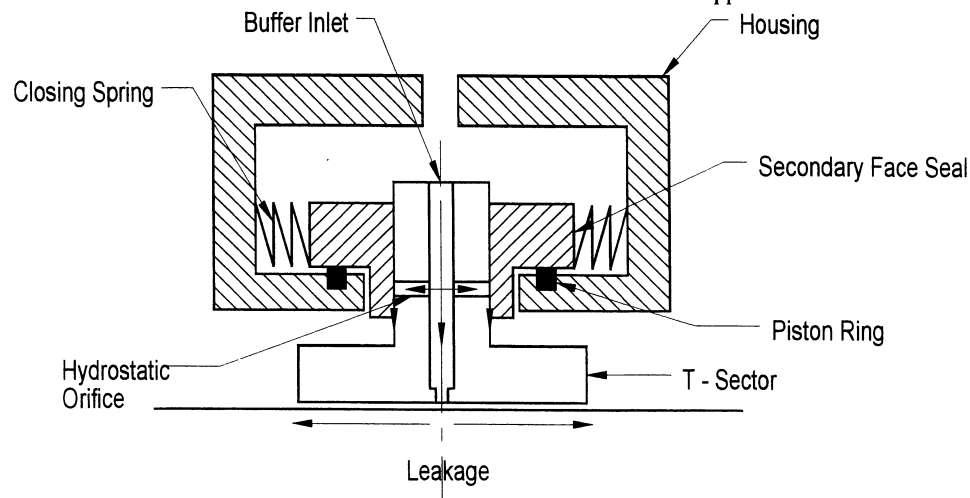


Figure 1 - Schematic of T- Seal

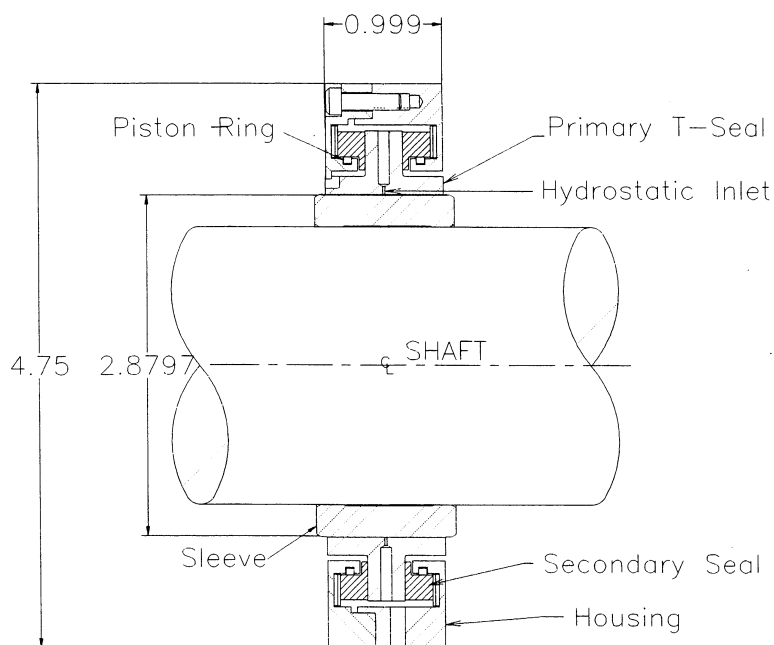


Figure 2 T-seal Assembly

T-Seal Performance

Load capacity is shown on Figure 3. Maximum load occurs at a radial clearance of 1.5 mils and not at the 1 mil clearance that may be expected. Hydrodynamic capacity is not significant at the maximum speed of 24,230 rpm and hydrostatic action is the principal source of load capacity. At the 1-mil condition, the preload from the unloaded side reduces the net load capacity. The design operating clearance was selected as 2.5 mils to accommodate thermal contraction, which occurs under operation.

Leakage as a function of eccentricity ratio and radial clearance is shown on Figure 4. The target leakage of 50 scfm is approximately 80% less than the two separate seals of the present back to back ring seals. To produce leakage less than 50 scfm, the operating radial clearance should be no greater than three mils.

Helium Buffer Seal

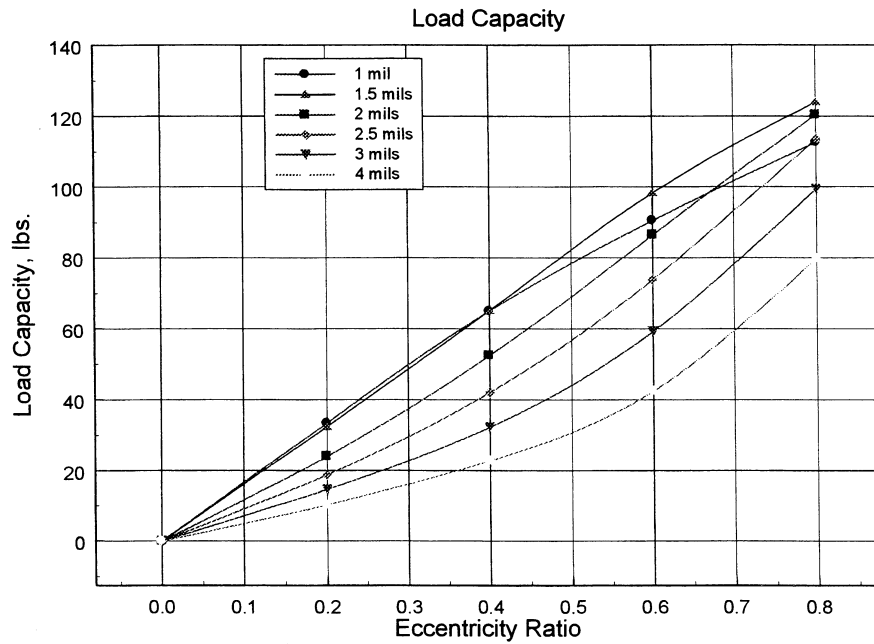


Figure 3 - T-seal Load Capacity

Helium Buffer Seal

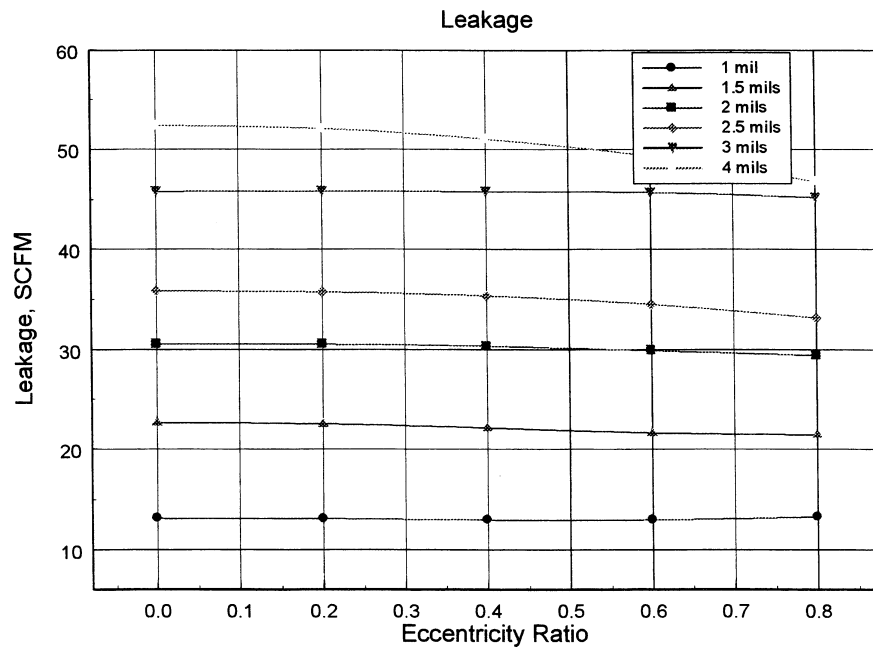


Figure 4 - T- Seal Leakage

The minimum film thickness is shown on Figure 5, and is quite adequate, even at large eccentricities, because of the relatively large concentric clearances involved. It is anticipated that the seals will be operating in the concentric position because of the near frictionless support of the secondary seals.

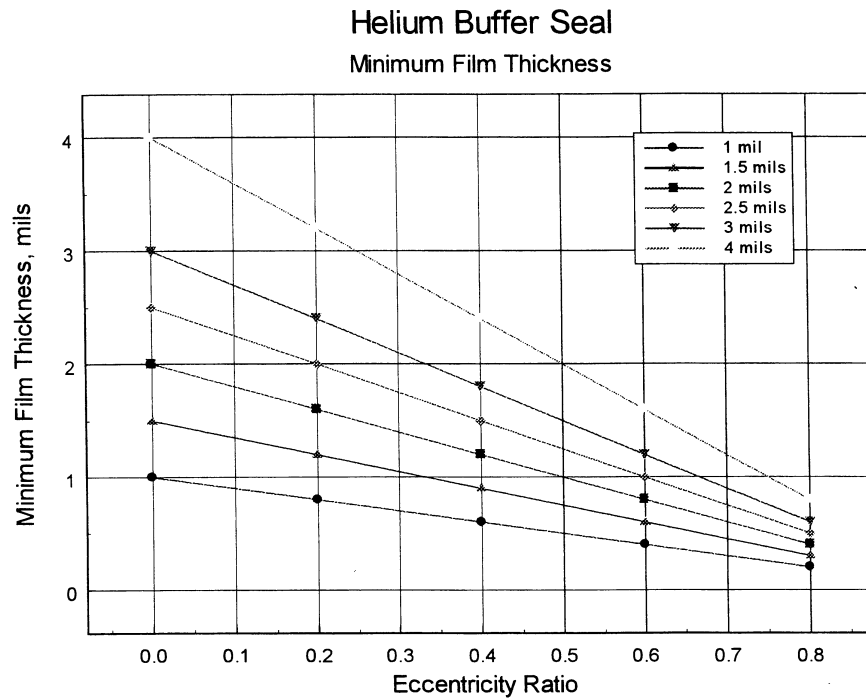


Figure 5 - T- Seal Minimum Film Thickness

Power Consumption is small and less than 50 watts in most of the operating range. Direct radial stiffness, as shown on Figure 6, indicates a reduction in stiffness, at the one mil radial clearance, until an eccentricity of 0.6, when the stiffness trend reverses and markedly increases, because the hydrodynamics take hold at the lower clearance levels. At a 2.5 mil operating clearance, the stiffness is approximately 40,000 lbs/in. Damping increases significantly with eccentricity ratio as indicated on Figure 7. At 2.5 mils, in the concentric position, the direct damping is 0.45 lb-s/in.

Helium Buffer Seal

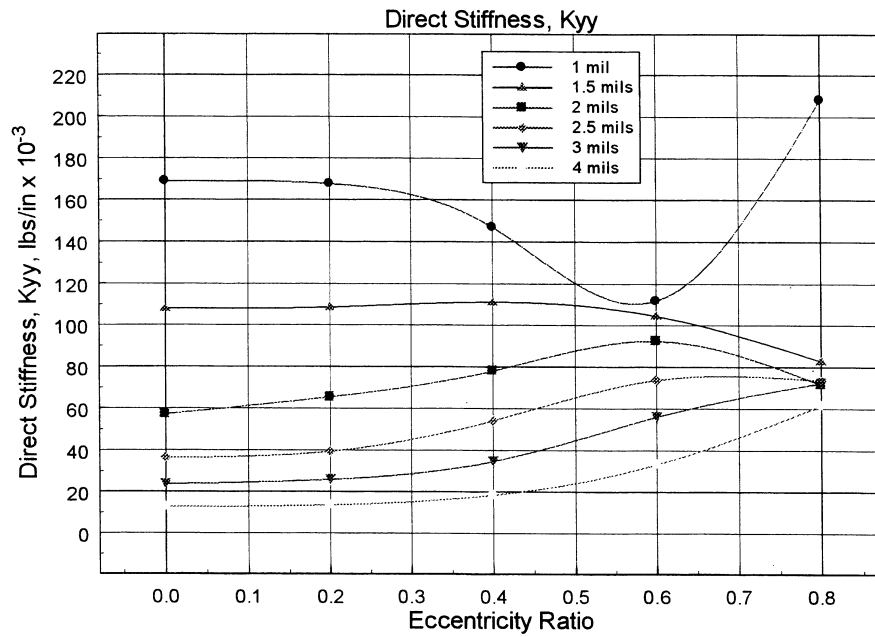


Figure 6 T-seal Direct Damping

Helium Buffer Seal

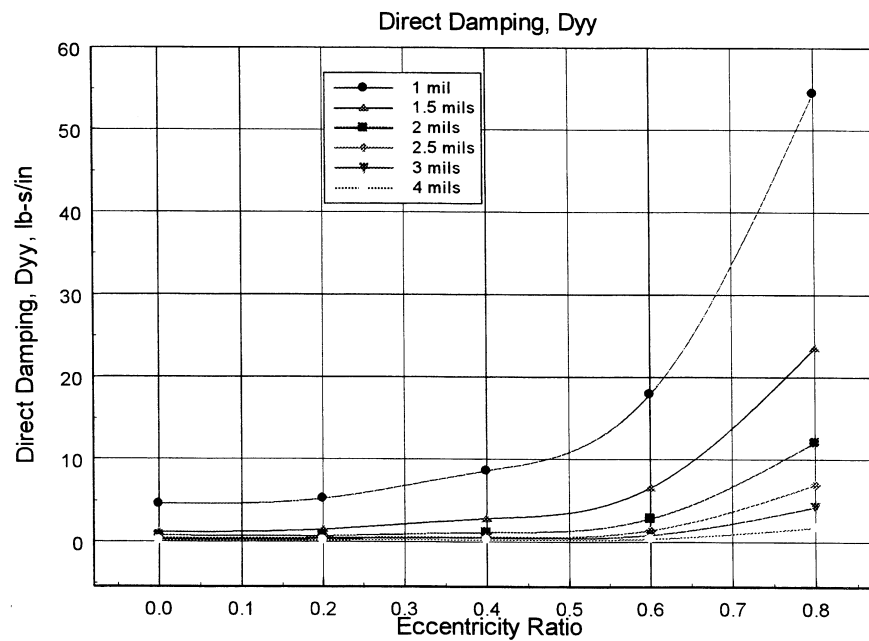


Figure 7 T-seal Direct Damping

Secondary Seal Performance

The closing load on the secondary seal was sized to provide a film thickness of about 0.37 mils. The operating film thickness can be small (0.2 to 0.4 mils) because there is no rotation between the opposed surfaces, although there can be motion due to shaft excitation. Figure 8 shows load capacity as a function of operating clearance and identifies the operating point where the closing and opening loads are in equilibrium.

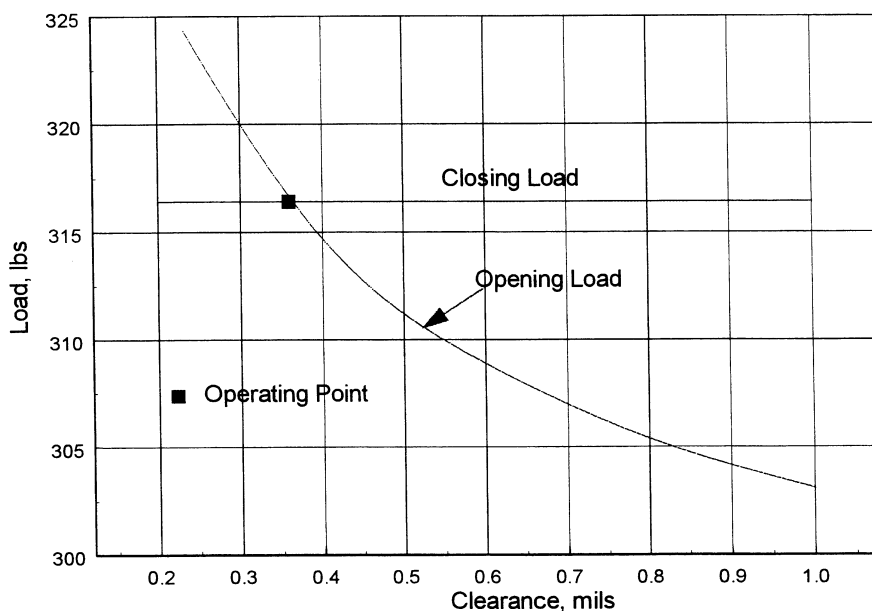


Figure 8 Secondary Seal Load Capacity

Leakage of the secondary seal is shown on Figure 9. Total leakage for the two secondary seals is less than 4 scfm. Axial stiffness is depicted on Figure 10. The axial stiffness is approximately 50,000 lbs/in, which is more than adequate to maintain separation during seal ring excursions. The moment or angular stiffness is shown on Figure 11. The moment stiffness remains positive over the operating range and does not go negative until the film thickness exceeds 0.7 mils, a condition that cannot be encountered because of the hydraulic closing load. The tapered land moment stiffness remains positive at the lower operating clearances. A hydrostatic secondary seal, that was a consideration, had negative moment stiffness at lower clearances and was not acceptable, as it would not resist overturning moments.

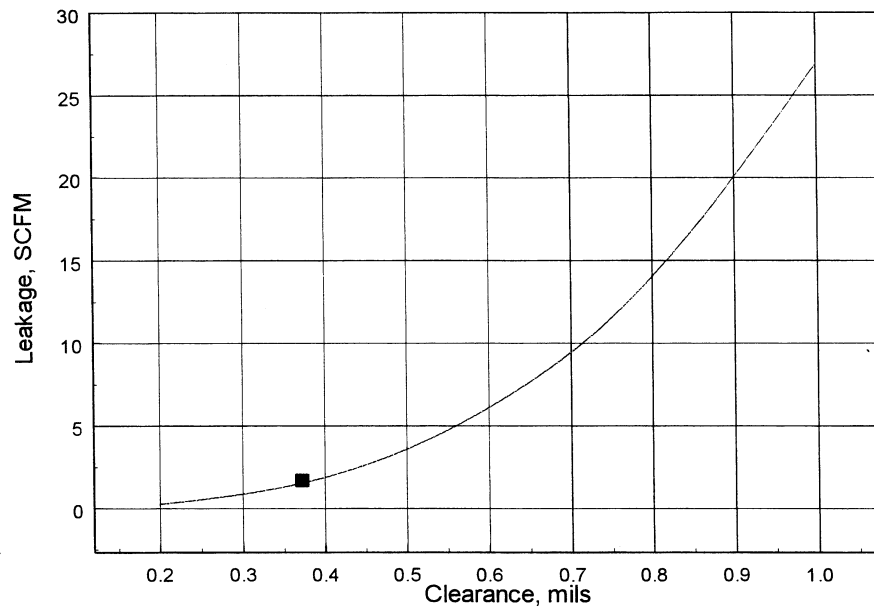


Figure 9 Secondary Seal Leakage

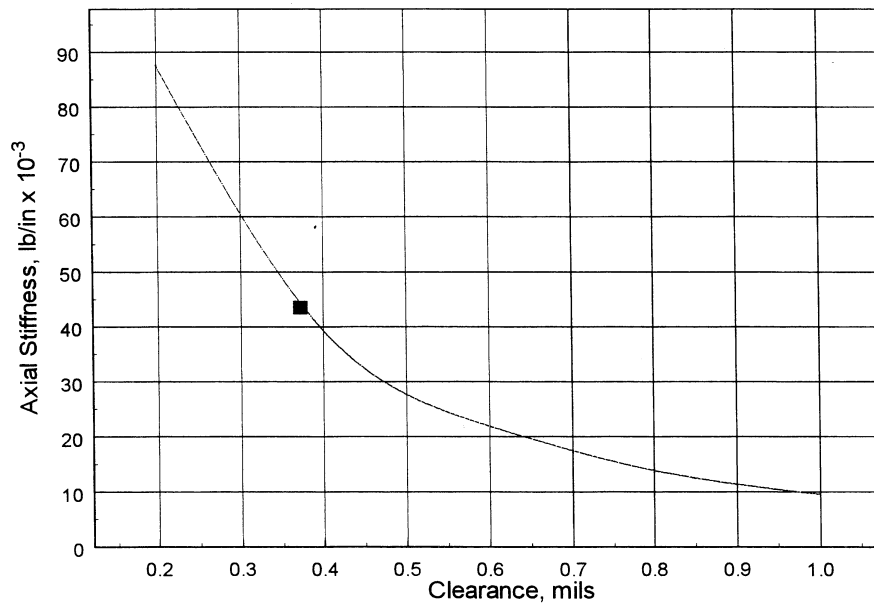


Figure 10 Secondary Seal Axial Stiffness

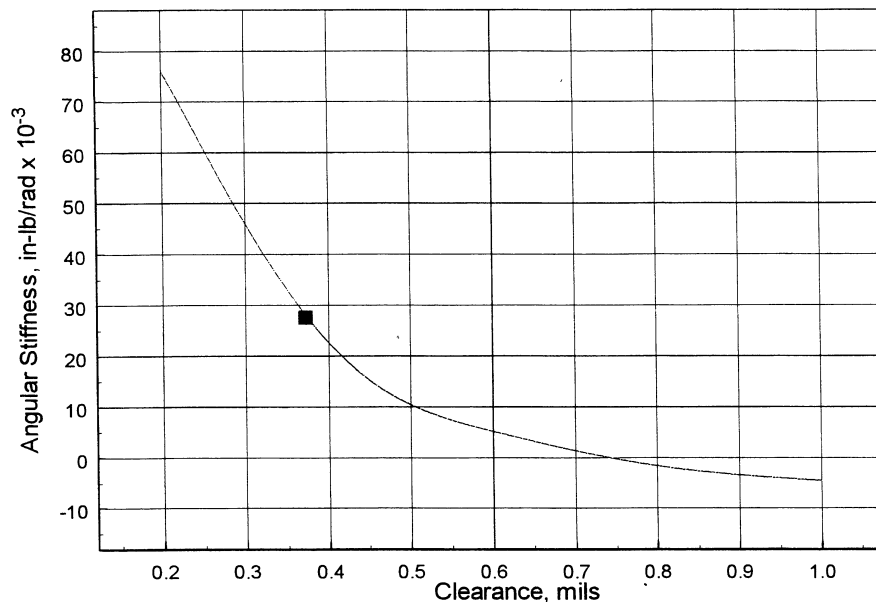


Figure 11 Secondary Seal Moment Stiffness

Thermo-elastic Distortions

Heat generated in the film will be principally transmitted to the flowing fluid, and temperature gradients are small. Figure 12 indicates distortions due to mechanical and thermal effects and the combination of the two. Pressure will tend to close off the T-seal ends and temperature will tend to open them. The combined effect of mechanical and thermal distortion is approximately 0.1 mils, which is insignificant compared to the operating clearance. Although distortions are small, the clearance increase, due to differences in material thermal expansion coefficients, at cryogenic operation has been calculated to be 1.95 mils. The manufactured clearance needed to obtain an operating clearance of 2.5 mils is approximately 1 mil on the diameter.

Dynamic Response

Dynamic analysis was also conducted to determine seal response to rotor excursions. Since the secondary seal friction is low, because of the gas film, seal tracking should be good. Indeed as shown on Figure 13, the seal is tracking rotor excursions without difficulty. A shaft orbit of 4 mils was applied and the seal is moving in unison with the shaft.

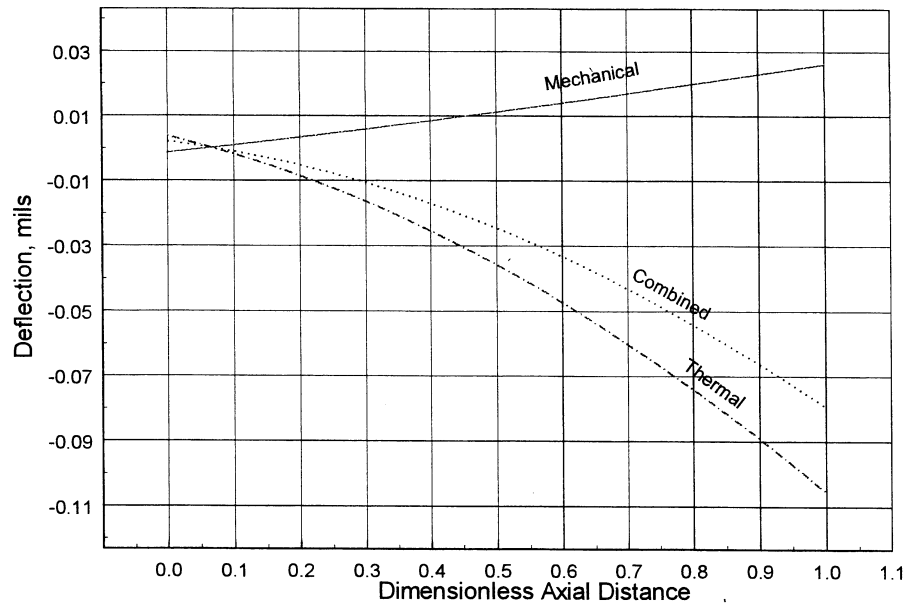


Figure 12 Thermo-Elastic Distortions

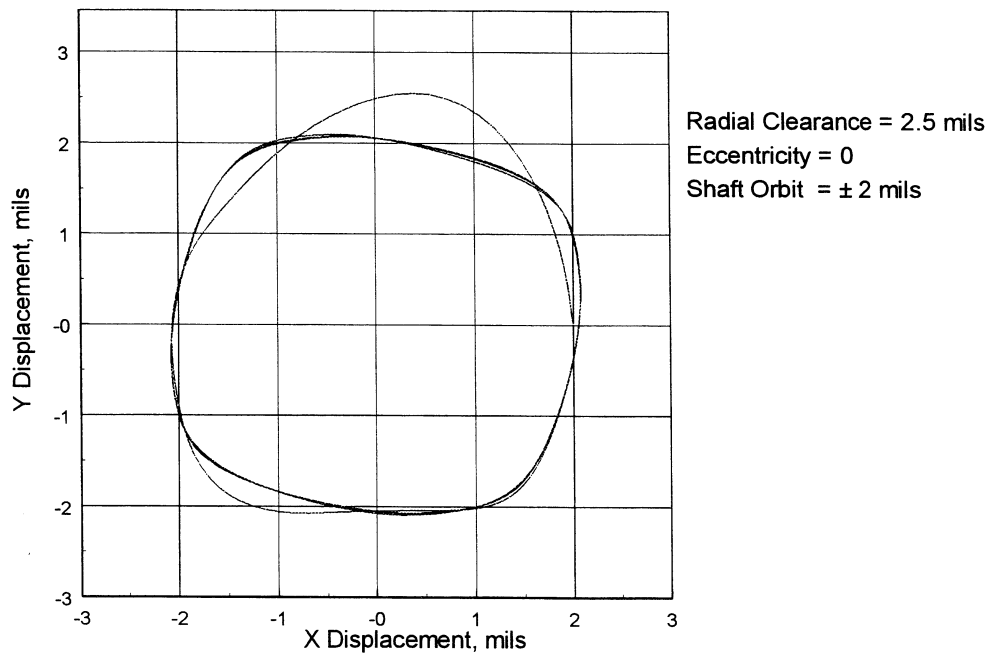


Figure 13 T-seal Dynamic Response

Conclusions

- Predicted performance of the T-seal is excellent
 - Leakage is less than 50 scfm
 - The seal operates at a healthy radial film thickness of 2 to 2.5 mils
 - Thermo-elastic distortions are not significant
 - The seal can readily track rotor excursions
- Phase II will accomplish hardware build and test at Stein Seal Company

Acknowledgements

The work was supported by a NASA contract. The contracting officer is Glen Williams and the COTR is Margaret Proctor from NASA Lewis. Their support and assistance are greatly appreciated. The cooperation of Pratt & Whitney, and in particular P. Pelfrey is recognized.

STABILITY OF THE WAVE BEARING ON AN ELASTIC SUPPORT

Florin Dimofte and Theo G. Keith, Jr.
The University of Toledo
Toledo, Ohio

ABSTRACT

Numerical computation predicts that an elastic support can substantially improve the stability of the wave bearing if the dynamic stiffness and damping of this support are in a specific range of values. To experimentally validate this prediction, the housing of a gas bearing was mounted on elastic O-rings and the threshold of sub-synchronous whirl motion was experimentally observed when the bearing runs unloaded with a rotating speed up to 30,000 RPM. The O-ring system was also dynamically characterized by measuring its stiffness and damping at various frequencies up to 500 Hz. Good correlation exists between the experimental data and numerical prediction.

1. INTRODUCTION

Fluid film bearings can experience stability problems such as whirl motions of the shaft inside the bearing. The frequency of this motion is, in most cases, equal to or less than one-half of the shaft rotational frequency and is called a "Fractional Frequency Whirl" (FFW). Unloaded plain journal bearings are very susceptible to a FFW. Gas plain journal bearings that experience a FFW usually develop an unstable motion, and wall contact generally occurs immediately after the onset of the whirl motion due to the low damping of the gas film, resulting in bearing failure. This phenomenon was observed soon after gas bearings were applied, starting in the mid-1950's. Due to its importance for bearing life FFW was thoroughly analyzed as a fluid film instability condition. Among others, Castelli and Elrod [1], and Constantinescu [2] contributed work that theoretically established when FFW occurs.

Unlike the plain journal bearing (Fig. 1a), a wave journal bearing reduces the susceptibility to FFW. A wave journal bearing [3] is a bearing with a slight, but precise, variation in the circular profile of the bearing such that a waved profile is circumscribed on the inner bearing diameter. The profile has a wave amplitude that is a fraction of the bearing clearance. Figure 1b, shows a three-wave bearing. The clearance and the wave and the wave amplitude are greatly exaggerated in Figs. 1a and 1b so that the concept may be visualized.

The wave journal bearing capacity to reduce the susceptibility to FFW was demonstrated theoretically in 1993 [3]. A parametric study indicated that the wave journal bearing offers better stability than the plain journal bearing for all operating conditions. However, the wave journal bearing performance is dependent upon the wave amplitude and performance increases significantly as the wave amplitude increases.

Experimental work on gas wave journal bearings validated numerical predictions [4]. It was also demonstrated that an unloaded journal bearing with an altered circular profile, such as a wave bearing, allows operation over a range of speeds under which the bearing can run free of FFW while the plain journal bearing is unstable.

A theoretical correlation between the bearing dynamic behavior and the wave amplitude based on a dimensionless representation of the parameters was presented in ref. [5]. In addition, this work showed that the actual region, in terms of bearing numbers, where the influence of the WAR to the bearing stability is limited. The bearing stability can be controlled well by the WAR if the bearing number, Λ , is less than 10.

However, applications of fluid film gas bearings where they should run at bearings number greater than 10 are very likely to be needed due to a continuous increasing of machine performances. Therefore, an efficient way to increase the bearing stability is to install the fluid film bearing in its housing on an elastic pad that can provide the necessary stiffness and damping in order to stabilize the bearing.

The present report analysis the possibility to further increase the wave bearing stability by using an elastic

bearing pad with dynamic stiffness and damping characteristics. The concept to use an elastic pad in order to stabilize a fluid film bearing was applied, analyzed, and discussed since middle of 60's. Thus, Lund in 1965 [6] made a theoretical analysis to investigate the stability of a symmetrical, flexible rotor supported in journal bearings. He found that when the bearing support possesses damping in addition to flexibility, the speed at onset of instability can be raised significantly above the threshold speed of a rotor in rigidly mounted bearings. Then, Powell in 1967 [7] reported that using pressurized air bearings which are supported by o-rings the speed of a dental turbine could be increased from 250,000 to 500,000 RPM. Marsh reported also 1969 [8], based on a linearized theory, that for self-acting gas journal bearings additional elements of flexibility in order to improve bearing stability is of considerable practical interest. Boffey stated also in 1969 [9], based on an analytical approach, that given the necessary values of damping and stiffness of the bearing support a self-acting gas journal bearing can run stable at all speeds. In 1971 Tondl [10] reported work on the stability of air-pressurized bearings when an elastically-suspended foundation mass is used. He found that using an elastically suspended foundation mass with damping can, for a suitable tuned foundation mass, sufficient linear foundation damping and proper ratio between the masses and moments of inertia, substantially raise the limit of spontaneous initiation of self-excited vibrations. Elrod and Glanfield presented in 1971 [11] a computer procedure for the design of flexible mounted, externally pressurized gas lubricated journal bearings. Their code predicted that a bearing support with intermediate values of damping can greatly raise the threshold of bearing instability while at large damping values this threshold drops extremely rapidly. Tatara et al. reported in 1973 [12] that whirl on-set speed of flexibly supported, externally pressurized gas journal bearing can be made very high by adequately selecting the dynamic characteristics of the bearing support in relation to the rotor and bearings. This result is also supported by the work reported by Kazimierski and Jarzecki in 1979 [13]. In addition they pointed out some discrepancies between the theory and experiments when o-rings are used as elastic bearing pads due to the evaluation process of the o-ring's dynamic stiffness and damping.

The above review of published information shows that an elastic pad definitely confirms that an elastic pad should improve the bearing stability. However, the dynamic characteristics of this pad should be selected in a specific range that needs to be found for each particular application [8, 11, and 12]. This aspect will be addressed through the following analysis that will be focused particularly on the wave bearing. O-rings were selected as elastic bearing pad. Based on [12 and 13] our conclusion was that if o-rings are used their dynamic characteristics should be evaluated over the whole range of frequency they are supposed to work and in the same working condition that is expected they will be used. Therefore, experimental results reported in a comprehensive work on o-ring characteristics such as [14] can be used only informatively with precautions and measurements should be made based on the actual application. Thus a special device was designed and made to measure o-ring dynamic coefficients. To conclude this work experimental tests were conducted to validate this theory.

2. ANALYSIS

The pressure generated in the fluid can be calculated by integrating the Reynolds equation. Assuming a compressible lubricant with isothermal behavior, the Reynolds equation has the following dimensionless form [15]:

$$\frac{\partial}{\partial \theta} \left(h^3 \frac{\partial p^2}{\partial \theta} \right) + \frac{\partial}{\partial z} \left(h^3 \frac{\partial p^2}{\partial z} \right) = 2\lambda \frac{\partial (ph)}{\partial \theta} + i 4 f \lambda \frac{\partial (p)}{\partial \theta} \quad (1)$$

where:

$$p = \frac{\bar{p}}{p_a}, \quad \theta = \frac{x_1}{R}, \quad z = \frac{x_3}{R}, \quad (2)$$

$$\tau = i \vee t, \quad (i = \sqrt{-1})$$

$$\lambda = \frac{6 \mu \Omega}{p_a} \left(\frac{R}{C} \right)^2 \quad (3)$$

The film thickness, h , is made dimensionless by dividing the film thickness equation of a wave bearing:

$$\bar{h} = C + e \cos \theta + e_w \cos [n_w (\theta + \alpha)] \quad (4)$$

by the radial clearance, C . In Equation 4 n_w is the number of waves, α is the angle between the starting point of the wave and the line of centers, and θ is the angular coordinate starting from the line of centers.

The bearing number, Λ (Eq. 3), is the main working parameter of the bearing. It includes: the dynamic viscosity of the fluid, μ , the ambient operating pressure, p_a , the rotational speed of the shaft, Ω , and the bearing main geometry parameter, (R/C) .

2.1 Bearing Steady-State and Dynamic Performance.

The bearing steady-state and dynamic performance can be determined by using the small perturbation technique on the complex form of the Reynolds equation (Eq. 1) [15]. Expanded in a Taylor series truncated to the first derivatives, the pressure can be written as:

$$p = p_0 + e_1 \exp(\tau) p_1 + e_0 \phi_1 \exp(\tau) p_2, \quad (5)$$

where p_0 is the steady-state component and p_1 and p_2 are the dynamic components of the pressure. Each component can be calculated by numerically integrating the corresponding differential equation derived from the Reynolds equation (Eq. 1).

The bearing steady-state and dynamic characteristics can be obtained by integrating the pressure components, p_0 , p_1 , and p_2 , over the whole bearing fluid film. The steady-state load capacity, F , is calculated by integrating p_0 , while both the dynamic stiffness, K_{jk} , and damping, B_{jk} ($j=x,y; k=x,y$), coefficients are calculated by integrating the dynamic pressure components, p_1 and p_2 .

2.2 Bearing dynamic reaction force.

Under dynamic conditions, the journal (shaft) center whirls in an orbit around its static equilibrium position. The corresponding bearing dynamic reaction force is actually a nonlinear function of the whirl amplitude and depends implicitly on time. In a thorough analysis it is necessary to consider the rotor and the bearing simultaneously. In most practical situations, the amplitude of the shaft whirl is, of necessity, rather small. In these cases a linearization of the bearing reaction force is permissible [15]. Then, it becomes possible to treat the bearing separately and represent the bearing reaction force components by the means of bearing dynamic coefficients:

$$F_x = -K_{xx}x - B_{xx}\frac{dx}{dt} - K_{xy}y - B_{xy}\frac{dy}{dt} \quad (6)$$

$$F_y = -K_{yx}x - B_{yx}\frac{dx}{dt} - K_{yy}y - B_{yy}\frac{dy}{dt}$$

Equation (Eq. 6) is only valid when the journal motion is harmonic, and:

$$x = \bar{x} \exp(i\omega t) = \bar{x} \exp(\tau) \quad (7)$$

$$y = \bar{y} \exp(i\omega t) = \bar{y} \exp(\tau)$$

The equation (Eq. 6) can be written in complex form as:

$$F_x = -Z_{xx}x - Z_{xy}y \quad (8)$$

$$F_y = -Z_{yx}x - Z_{yy}y$$

where:

$$Z_{jk} = K_{jk} + i \omega B_{jk} \quad (9)$$

$$j = (x, y); \quad k = (x, y)$$

are the bearing impedance coefficients. For a given bearing geometry, the dynamic coefficients are functions of the static load on the bearing and the rotor speed. The dynamic coefficients also depend on the whirl frequency, and they are actually impedances of the gas film. Note, also, that the x-axis was chosen along the direction of the steady-state load.

2.3 Bearing Stability.

In a bearing stability calculation, it is necessary to evaluate the bearing coefficients over a frequency range, usually around one half of the rotating frequency. On this basis, a stability analysis can be performed in order to calculate the critical mass. The critical mass, M_c , is used to help determine whether the bearing will run free of FFW. FFW is an instability of the fluid lubricant film of the bearing. It appears as a whirling, orbiting motion of the shaft and its frequency or speed, ω_0 , is often close to one-half the running frequency or shaft speed especially if the bearing is unloaded. This phenomenon is more likely to occur when the shaft center is close to the center of the bearing (near zero eccentricity). This frequency, ω_0 , can be much lower than one-half of the running frequency when the value of eccentricity is large [16]. To derive the equation for critical mass, in a simple manner, the rotor is considered rigid and symmetrical, and supported by two identical bearings [15]. This means that each bearing carries one-half of the rotor mass. If M is the rotor mass supported by the each bearing ($M = 1/2$ of the rotor mass) and the bearing is represented by its four impedance coefficients, $Z_{jk} = K_{jk} + i\omega B_{jk}$ ($j = x, y; k = x, y$), the motion equation can be written as:

$$\begin{bmatrix} (Z_{xx} - M\omega^2) & Z_{xy} \\ Z_{yx} & (Z_{yy} - M\omega^2) \end{bmatrix} \begin{bmatrix} x \\ y \end{bmatrix} = 0 \quad (10)$$

The threshold of instability occurs when the determinant of the matrix is zero. Noting:

$$Z = K_c + i \omega B_c, \quad K_c = M \omega^2 \quad (11)$$

the determinant equation can be solved to get:

$$Z = \frac{1}{2} (Z_{xx} + Z_{yy}) - \sqrt{\frac{1}{4} (Z_{xx} - Z_{yy})^2 + Z_{xy} Z_{yx}} \quad (12)$$

For stability calculations only the solution with a negative sign in front of the square root proves to be of interest [15]. At the threshold of instability, Z must be real. The imaginary part of Z can be evaluated over a range of frequencies to find the frequency value, ω_0 , causing the imaginary part of Z to be zero. The corresponding mass, is the mass required to make the bearing unstable under the selected working conditions and is:

$$M_c = \frac{K_{c0}}{\omega_0^2} \quad (13)$$

This critical bearing mass is a threshold and there are three possibilities: I) the critical mass is positive which means that the bearing could run stably if its actual allocated mass is less than the critical mass; ii) the threshold of instability was not found and the critical mass can be considered infinite which means that the bearing could run stably at any value of its actual allocated mass; iii) the critical mass is negative which means that the half frequency whirl instability is most likely to occur for any value of the rotor mass. The actual allocated mass is half of the rotor mass.

2.4 Effect of the bearing support stiffness and damping on bearing stability.

When bearing is supported by an elastic pad that has dynamic stiffness, K_p , and damping, B_p , and between the

bearing fluid film and the elastic support there is an intermediate mass, m_p , the motion equation (10) becomes:

$$\begin{bmatrix} (Z_{xx} - M v^2 - A_{p1}) & Z_{xy} - A_{p2} \\ Z_{yx} - A_{p3} & (Z_{yy} - M v^2 - A_{p4}) \end{bmatrix} \begin{bmatrix} X \\ Y \end{bmatrix} = 0 \quad (14)$$

where A_{p1} , A_{p2} , A_{p3} , and A_{p4} are functions of bearing impedance, Z_{ij} , the elastic pad impedance, $Z_p = K_p + ivB_p$, and the intermediate mass, m_p . If the bearing sleeve is just elastically supported the intermediate mass is the sleeve mass.

At the threshold of instability Z from expression (11) must be real. Therefore scanning down frequencies up to the value v_0 where the imaginary part of Z is vanished, the real part of Z (equation 12) becomes:

$$\begin{aligned} K_c = M_c v_0^2 = 0.5 \left[(Z_{xx} - A_{p1}) + (Z_{yy} - A_{p4}) \right] - \\ \left\{ 0.25 \left[(Z_{xx} - A_{p1}) + (Z_{yy} - A_{p4}) \right]^2 - \right. \\ \left. \left[(Z_{xx} - A_{p1})(Z_{yy} - A_{p4}) - (Z_{yx} - A_{p3})(Z_{xy} - A_{p2}) \right] \right\}^{\frac{1}{2}} \end{aligned} \quad (15)$$

and the critical mass can be again calculated by using equation (13).

2.5 Numerical Results.

Calculations were performed on the stability of a 35 mm diameter and 30 mm long gas journal bearing. The bearing radial clearance was 16 microns. The bearing was considered unloaded. Both a true circular and a three wave bearing geometry were analyzed. The wave bearing had a wave amplitude ratio of 0.3. The bearing was considered mounted on an elastic support. The support stiffness was varied from 10 to 10^7 N/m and the support damping was varied from 10 to 1000 Ns/m. The critical mass values that show the limits of bearing stability are listed in Tab. 1 and 2. The results of a rigid supported bearing are also listed in an additional column for comparison purpose.

In Tab.1 stability data of the true circular journal bearing are listed. This data shows that a true circular bearing rigidly supported is unstable at any analyzed speed from 3,000 to 30,000 RPM. Supporting the bearing into an elastic pad can help in order to stabilize the bearing if the stiffness and damping of the elastic pad are properly selected. Thus, for example, if $K_p = 10$ to 10,000 N/m and $B_p = 100$ Ns/m, the true circular bearing can run unconditionally stably up to 15,000 RPM. Both lower and higher stiffness and damping values than that listed above keep the bearing unstable.

Tab. 2 shows the critical mass value for a similar journal bearing as the true circular but this bearing had three waves with a wave amplitude ratio of 0.3. This bearing mounted rigidly, unlike the true circular bearing, can run stable if the rotor mass is less than the critical mass listed in Tab. 2 in the column called "rigid". However, this stable running condition is rotor mass depended and the threshold of stably running condition (the critical mass) is diminishing progressively while speed increases. At 3,000 RPM the critical mass is 2.12 kg while at 30,000 RPM is only .774 kg. Therefore at higher speeds the critical mass, still positive, could have very small values that has not any practical interest. Looking to all data listed in Tab. 2 it can be seen that supporting the bearing into an elastic pad with $K_p = 10$ to 100,000 N/m and $B_p = 100$ to 1000 Ns/m it can run unconditionally stably at all analyzed speeds. In other words no restriction is imposed to the rotor mass in order to run the bearing stably. Therefore supporting a wave bearing on an elastic pad with properly selected stiffness and damping make a substantial improvement in bearing overall stability.

3. EXPERIMENTAL WORKS

In order to validate the theory and to establish the procedure how to use the O-rings as an elastic bearing support experimental works were conducted in two main directions:

1. Evaluation of o-rings dynamic characteristics, and
2. Test the effect of the o-rings on bearing stability.

3.1 Evaluation of O-rings dynamic stiffness and damping.

A measuring device was designed and manufactured to measure the dynamic stiffness and damping of the o-rings for an elastic pad. This device is shown in Fig. 2a. A Piezo-shaker provided sine strokes into 1 to 5 microns amplitude range with frequencies up to 500 Hz. A dynamic load cell and a proximity probe read the load and the displacement, respectively. Small stroke amplitudes were used in order to know the o-ring characteristics just close to the moment when the instability starts. At that moment the shaft inside the bearing whirls with very small orbits. This approach makes the comparison between the theory and the experiment consistent because this theory predicts the moment when the instability starts based on "a small perturbation technique". Based on this analysis it can be known what to do to avoid a FFW and to run the bearing stably. What happened inside the bearing when the shaft is whirling with more or less large orbit could be a subject of another type of analysis such as a transient analysis.

Both load cell and proximity probe signals can be seen superposed on an oscilloscope screen. Pictures at 10 Hz and 400 Hz of this screen are presented in Fig. 2 b and c, respectively. The scope can display the frequency and the amplitude among other information. Comparing Fig 2 b and c it can be easily seen that increasing the frequency the phase between the force and the displacement increases. The displacement is after the force due to the damping of the system.

Measured stiffness and damping for various o-ring configurations are presented in Figs. 3 to 6. Measurements were performed at frequencies from 50 to 500 Hz. The used o-rings have these basic catalog dimensions: mean diameter = 2.125" (53.975 mm) and thickness = 0.070" (1.778 mm) and they are in "sealing o-ring specification". However, it was found that when they are used as an elastic gas bearing support a precompression of these o-rings from .070" to .050" is too large and makes the o-rings too stiff. Therefore, a precompression from .070" to .060" was only used.

In Fig. 3 a and b the measured stiffness and damping, respectively, for 2, 3, 4, and 5 nitril o-rings used to support the bearing sleeve are shown and difference in stiffness and damping can be seen as is expected. However, a big jump in dynamic characteristics can be observed when 5 o-rings were used compared to the other o-ring configurations.

Fig. 4 shows the dynamic characteristics of a bearing elastic pad of two nitril o-rings that have the shore hardness 50, 70, 80, and 90. The results are as expected, at an increase in shore hardness both stiffness and damping increase.

In Fig. 5 the stiffness and damping of fluorosilicone and ethylene propylene o-rings can be compared. This figure shows that same dimension and hardness O-rings but from different materials show different dynamic properties. More of this, "same" O-ring material but made by different manufacturers lead also in significant differences in O-ring dynamic properties as it is shown in Fig. 6.

Reviewing all this data the main conclusion is that the o-rings produced under a "sealing specification" should be sorted and measured for each specific application. Their dynamic properties could vary in an unacceptable range for elastic pad application if they are not sorted. Their dynamic characteristics should be evaluated by simulating all working conditions and over the whole range of working frequencies.

3.2 Test of the effect of the o-rings on bearing stability.

Experimental evaluations of O-ring effect on the bearing stability were conducted by using an experimental bearing with 35 mm diameter, 30 mm long, and 18 microns radial clearance. This bearing had three waves with 0.3 wave amplitude ratio. Fig. 7 shows the picture of this bearing. In this case, the waved bearing sleeve is mounted inside a bearing

housing. The whole bearing housing assembly has a mass of 0.276 kg. On the housing outer surface there are four grooves where the o-rings could be mounted. In order to run this bearing on the wave bearing rig, well described in references [] an adequate test bearing assembly was designed and fabricated (Fig. 8) The upper and the bottom faces of the housing (Fig. 8 #1) are supported by two thrust pressurized air bearing plates so that this housing moves freely in the horizontal plane while it is very well positioned in the vertical and angular directions. Two holes at 90 degrees made in the housing were used to fix two proximity probes that red the movement between the housing and the shaft (Fig. 7 #4). For these tests sets of two nitril o-rings were used. The o-rings shore hardness were 50, 70, 80, and 90. The shaft was turned at various speeds up to the speed when the FEW just started to install.

Typical oscilloscope screen pictures are shown in Fig. 9. The scope spot visualized the vibration of the housing, in regards to the shaft, in one direction. Pictures in Fig. 9 were made when two nitric o-rings with 50 shore hardness were used to support the bearing inside the housing. When the bearing run stably, the scope screen looks like in Fig. 9 a. Only synchronous vibration with a few microns amplitude can be observed due to a small shaft-bearing rotor runout. The frequency red by the scop (91.74 Hz) corresponded to the running speed of 5,504 RPM. At the instability threshold the scop screen started to display the changing in vibration as can be seen in Fig. 9 b. Actually, the curve started to “dance” the vibration period was doubling and the frequency red by the scop (57.47 Hz) was almost half of the synchronous frequency that corresponded to a rotation speed of 6,840 RPM.

In order to promptly observe the effect of the o-rings on bearing stability an additional test was performed. The housing (Fig. 8 #1) was provided with three radial screws that can seize the bearing (Fig. 8 #2) vanishing the o-rings effect. Thus, the shaft started rotating and the speed was increased to 1,153 RPM. The bearing was supported by two nitric o-rings with 90 shore hardness and run stably. The scope screen looked like in Fig. 10 a. Only a synchronous vibration was detected. Then, the screws were tightened and the bearing was seized solid to the housing. The FEW installed immediately with large amplitude as can be seen in Fig. 10 b This test definitely proving the o-ring effect to bearing stability.

A comparison of the experimental results to the prediction can be seen in the following table where the observed and predicted threshold speed (RPM) to unstable running condition are listed for various o-ring sets.

Shore Hardness	50	70	80	90
Observed	6,840 RPM	12,500 RPM	11,700 RPM	8,000 RPM
Predicted	6,000-9,000 RPM	9,000-12,000 RPM	9,000-12,000 RPM	9,000-12,000 RPM

The above table shows a reasonable correspondence between the experiment and the prediction.

CONCLUSIONS:

A theoretical analysis was developed to predict the effect of and elastic bearing pad, with dynamic stiffness and damping, on the bearing (fluid film) FEW instability. Then, experimental investigations were conducted in order to evaluate the dynamic stiffness and damping of various elastomer O-rings used as elastic pads. The experimental work concluded with tests of a wave journal bearing stability when it was supported by o-rings. The conclusions are:

1. The amount of the elastic support stiffness and damping that the bearing needs to run stably can be predicted. The predictions were experimentally verified.
2. The stability of a wave journal bearing can be significantly increased by using an elastic pad unlike the stability of a circular bearing that has a limited possibility to be improved by using an elastic pad. The wave bearing can run unconditional stably over a large range of speeds.

3. The elastic bearing support could be rubber, or any kind of elastomer, O-rings if the dynamic stiffness and damping of this support are in the predicted range of needed values.

4. The dynamic characteristics of the O-ring are a function of its material, manufacture, precompression and working conditions. Therefore the dynamic stiffness and damping of a specific elastic system based on O-rings have to be measured by simulating the bearing running condition.

5. A method to precisely, dynamically characterize the O-ring elastic system has developed and successfully used.

6. O-rings made in "sealing specification" can be used but with precaution. The O-rings should be sorted by material, manufacture, shore hardness, dimensions, etc, and than each lot should be measured in order to verify the O-ring dynamic characteristics.

ACKNOWLEDGMENTS

This paper reports work conducted at the NASA Lewis Research Center in Cleveland Ohio sponsored under grant NAG awarded to the University of Toledo. The author would like to express his thanks to Dr. John J. Coy, and Margaret from NASA LeRC who all kindly supported this work.

REFERENCES

1. Castelli, V. and Elrod, H.G., "Solution of the Stability Problem for 360 Deg Self-Acting, Gas-Lubricated Bearings," *Journal of Basic Engineering*, Trans. ASME, Series D, Vol. 87, 1, pp. 199-212, (1965).
2. Constantinescu, V.N., "On Hydrodynamic Instability of Gas-lubricated Journal Bearings," *Journal of Basic Engineering*, Trans. ASME, Series D, Vol. 87, 3, pp. 579-588, (1965).
3. Dimofte, F., "Wave Journal Bearing with Compressible Lubricant; Part I: The Wave Bearing Concept and a Comparison with a Plain Circular Journal Bearing", presented to STLE 1993 Annual Meeting, May 17-20, 1993, Calgary, Canada, published in *STLE Tribology Transactions* Vol. 38 1, pp. 153-160, (1995).
4. Dimofte, F., and Hendricks, R.C., "Fractional Whirl Motion in Wave Journal Bearings" presented at The Fourth Seal Code Development Workshop held at NASA Lewis Research Center in Cleveland, Ohio, on June 14-15, 1995, NASA CP 10181, pp. 337-340.
5. Dimofte, F. and Keith, T.G, Jr., "Wave Bearing Technology to Control Journal Bearing Dynamics" in Proceedings of the 7th International Symposium on Transport Phenomena and Dynamics of Rotating Machinery - ISROMAC-7, held on 22-26 Feb. 1998 in Honolulu, Hawaii, Vol 1, pp. 327-336.
6. Lund, J.A. "The Stability of an Elastic Rotor in Journal Bearings With Flexible, Damped Supports.", *Journal of Applied Mechanics*, Trans. ASME, Series , Vol. , 4, pp. 911-920, (1965).
7. Powell, J.W., "A review of the Experience of Producing over 20,000 Air Bearing Dental Turbines", Proceedings of Gas Bearing Symposium, Paper 10, University of Southampton, April 1967.
8. March, H., "The Stability of Self-Acting Gas Journal Bearings With Noncircular Members and Additional Elements of Flexibility",
9. Boffey, D.A., "The Stability of a Rigid Rotor on a Flexibly Supported Self-Acting Gas Journal Bearing", Proceedings of Gas Bearing Symposium, Paper 12, University of Southampton, April 1969.
10. Tondl, A., "The Effect of an Elastically-Suspended Foundation Mass and Its Damping on the Initiation of Self-Excited

Vibrations of a Rotor Mounted in Air-Pressurized Bearings”, Proceedings of Gas Bearing Symposium, Paper 1, University of Southampton, March 1971.

11. Elrod, H.G. and Glanfield G.A. “Computer Procedures for the Design of Flexible Mounted, Externally Pressurized, Gas Lubricated Journal Bearings”, Proceedings of Gas Bearing Symposium, Paper 22, University of Southampton, March 1971.

12. Tatara, A., Koike, H., and Iwasaki, A., “The Stability of Flexible Supported, Externally Pressurized Gas Journal Bearings”, Bulletin of the JSME, Vol. 100, pp. 1573-1579, Oct. 1973.

13. Kazimierski, Z. and Jarzecki, K., “Stability Threshold of Flexibly Supported Hybrid Gas Journal Bearings”, *Journal of Lubrication Technology*, Trans. ASME, Series F, Vol. 101, 3, pp. 451-457, (1979).

14. Darlow, M. and Zorzi, E., “Mechanical Design Handbook for Elastomers”, NASA CR 3423 - 1981

15. Lund, J.W., “Calculation of Stiffness and Damping Properties of Gas Bearings”, *Trans. of ASME, Journal of Lubrication Technology*, Series F, 90, 4, pp. 793-808, (1968).

16. Dimofte, F., “Effect of Fluid Compressibility on Journal Bearing Performance,” *STLE Tribology Transactions* Vol. 36, 3, pp. 341-350, (1993).

TABLE 1

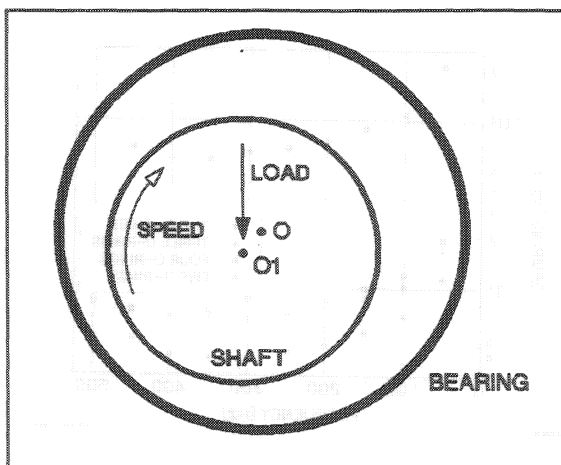
Critical Mass (kg) or Stability Criteria of a True Circular Bearing with D = 35 mm, L = 30 mm, C = 0.016 mm, Sleeve Mass=0.276 kg.										
Speed RPM	RIGID	$K_p = 10$ N/m	10	10	1,000	1,000	1,000	10,000	10,000	10,000
		$B_p = 10$ Ns/m	100	1,000	10	100	1,000	10	100	1,000
3,000	unstable	STABLE	STABLE	unstable	STABLE	STABLE	unstable	STABLE	STABLE	STABLE
6,000	unstable	unstable	STABLE	unstable	STABLE	STABLE	unstable	STABLE	STABLE	unstable
9,000	unstable	STABLE	STABLE	unstable	STABLE	STABLE	unstable	unstable	STABLE	unstable
12,000	unstable	STABLE	STABLE	unstable	STABLE	STABLE	unstable	STABLE	STABLE	unstable
15,000	unstable	unstable	STABLE	unstable	unstable	STABLE	unstable	STABLE	STABLE	unstable
18,000	unstable	unstable	unstable	unstable	unstable	unstable	unstable	unstable	unstable	unstable
21,000	unstable	unstable	unstable	unstable	unstable	unstable	unstable	unstable	unstable	unstable
24,000	unstable	STABLE	unstable	unstable	STABLE	unstable	unstable	unstable	unstable	unstable
27,000	unstable	STABLE	STABLE	unstable	STABLE	STABLE	unstable	STABLE	STABLE	unstable
30,000	unstable	STABLE	STABLE	unstable	STABLE	STABLE	unstable	STABLE	STABLE	unstable

TABLE 1 Cont.

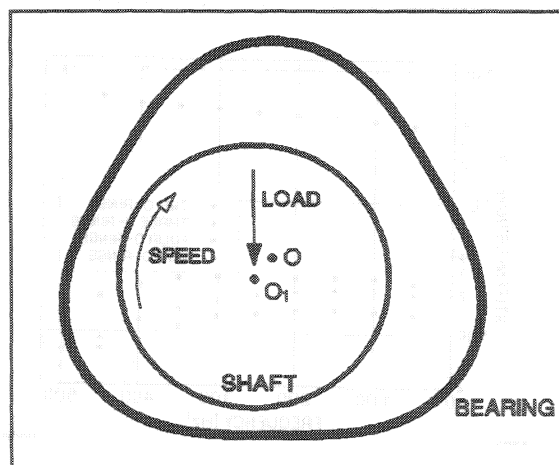
Critical Mass (kg) or Stability Criteria of a True Circular Bearing with D = 35 mm, L = 30 mm, C = 0.016 mm, Sleeve Mass=0.276 kg.											
Speed RPM	$K_p = 100,000$ N/m	100,000	100,000	1,000,000	1,000,000	1,000,000	10,000,000	10,000,000	10,000,000	10,000,000	10,000,000
	$B_p = 10$ Ns/m	100	1,000	10	100	1,000	10	100	1,000	10	1,000
3,000	unstable	unstable	STABLE	unstable	unstable	unstable	unstable	unstable	unstable	unstable	unstable
6,000	unstable	STABLE	STABLE	unstable	unstable	unstable	unstable	unstable	unstable	unstable	unstable
9,000	unstable	STABLE	STABLE	unstable	unstable	unstable	unstable	unstable	unstable	unstable	unstable
12,000	STABLE	STABLE	STABLE	unstable	unstable	unstable	unstable	unstable	unstable	unstable	unstable
15,000	STABLE	STABLE	unstable	unstable	unstable	unstable	unstable	unstable	unstable	unstable	unstable
18,000	STABLE	STABLE	unstable	unstable	unstable	unstable	unstable	unstable	unstable	unstable	unstable
21,000	STABLE	unstable	unstable	unstable	unstable	unstable	unstable	unstable	unstable	unstable	unstable
24,000	STABLE	unstable	unstable	unstable	unstable	unstable	unstable	unstable	unstable	unstable	unstable
27,000	unstable	unstable	unstable	unstable	unstable	STABLE	unstable	unstable	unstable	unstable	unstable
30,000	unstable	unstable	unstable	unstable	STABLE	STABLE	unstable	unstable	unstable	unstable	unstable

TABLE 2 Cont.

Critical Mass (kg) or Stability Criteria of a Wave BRG with WAR = 0.3, D = 35 mm, L = 30 mm, C = 0.016 mm, Sleeve Mass=0.276 kg.											
Speed RPM	$K_p=100,000$ N/m	100,000	100,000	1,000,000	1,000,000	1,000,000	10,000,000	10,000,000	10,000,000	10,000,000	10,000,000
	$B_p = 10 \text{ Ns/m}$	100	1,000	10	100	1,000	10	100	1,000	10	1,000
3,000	1.360	1.396	STABLE	2.014	2.014	2.018	2.109	2.109	2.109	2.109	2.109
6,000	0.554	STABLE	STABLE	1.613	1.616	1.666	1.893	1.893	1.893	1.893	1.893
9,000	0.337	STABLE	STABLE	1.235	1.244	1.414	1.677	1.678	1.678	1.679	1.679
12,000	0.974	STABLE	STABLE	0.925	0.945	1.322	1.465	1.465	1.465	1.468	1.468
15,000	1.890	STABLE	STABLE	0.691	0.725	STABLE	1.275	1.273	1.273	1.277	1.277
18,000	3.084	STABLE	STABLE	0.516	0.571	STABLE	1.105	1.105	1.105	1.111	1.111
21,000	4.599	STABLE	STABLE	0.386	0.469	STABLE	0.962	0.962	0.962	0.970	0.970
24,000	unstable	STABLE	STABLE	0.287	0.414	STABLE	0.840	0.841	0.841	0.850	0.850
27,000	unstable	STABLE	STABLE	0.212	0.425	STABLE	0.737	0.738	0.738	0.749	0.749
30,000	unstable	STABLE	STABLE	0.157	0.515	STABLE	0.649	0.650	0.650	0.662	0.662



a. True Circular



b. Three Wave

Fig. 1 Journal Bearing

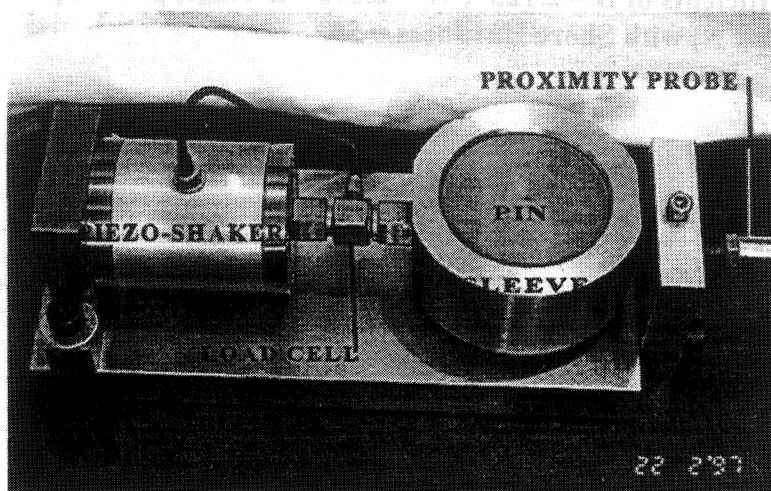


Fig. 2a Device for measuring o-ring dynamic stiffness and damping

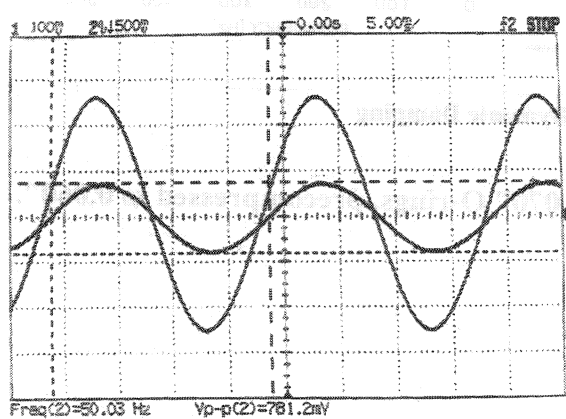


Fig. 2b Force & Displacement at 50 Hz.

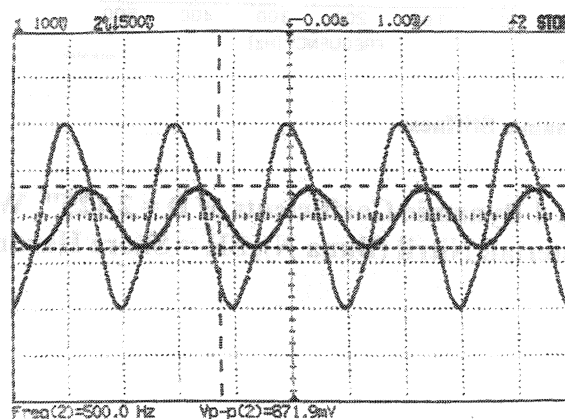


Fig. 2c Force & Displacement at 500 Hz.

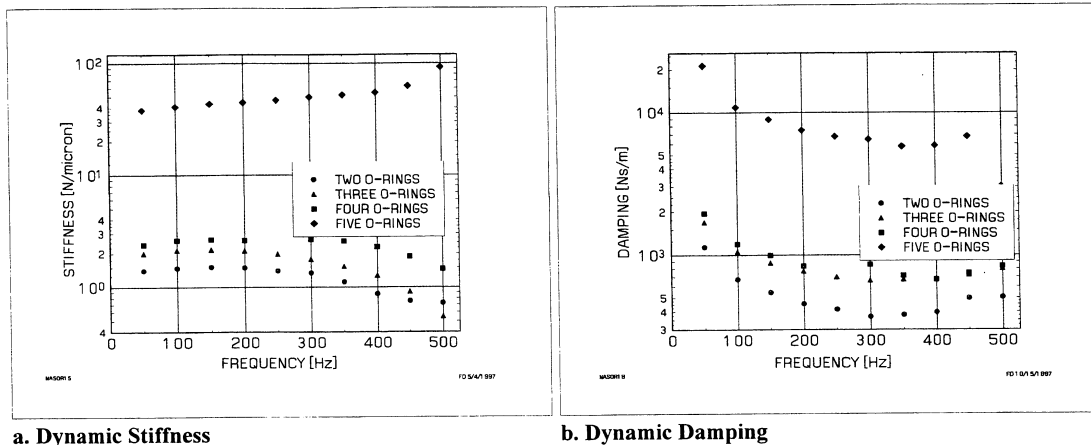


Fig. 3 Dynamic Coefficients of $D = 2.125''$, $W = 0.070''$ O-rings, precompressed to $0.060''$. Material: Nitril (Buna N) with Shore Hardness = 50.

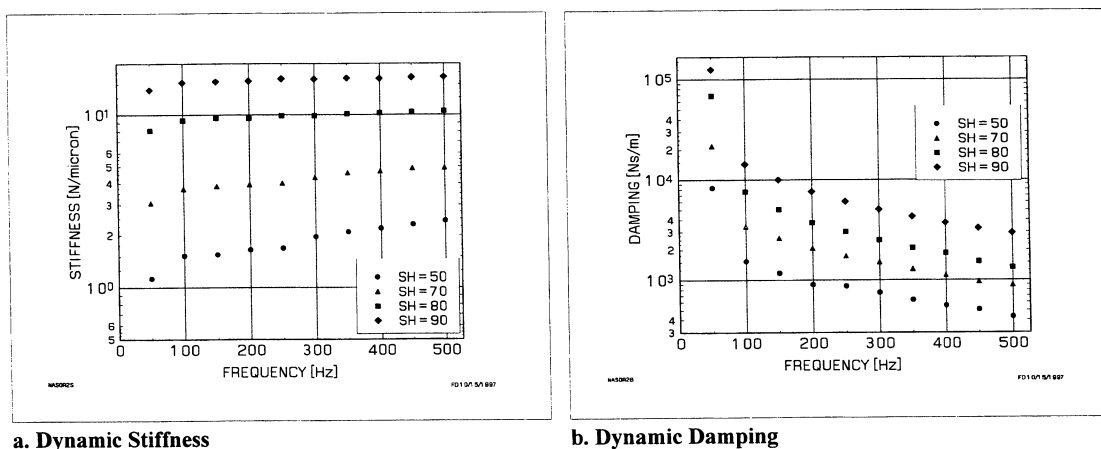


Fig. 4 Dynamic Coefficients of $D = 2.125''$, $W = 0.070''$ O-rings, precompressed to $0.060''$. Material: Nitril (Buna N), SH = Shore Hardness.

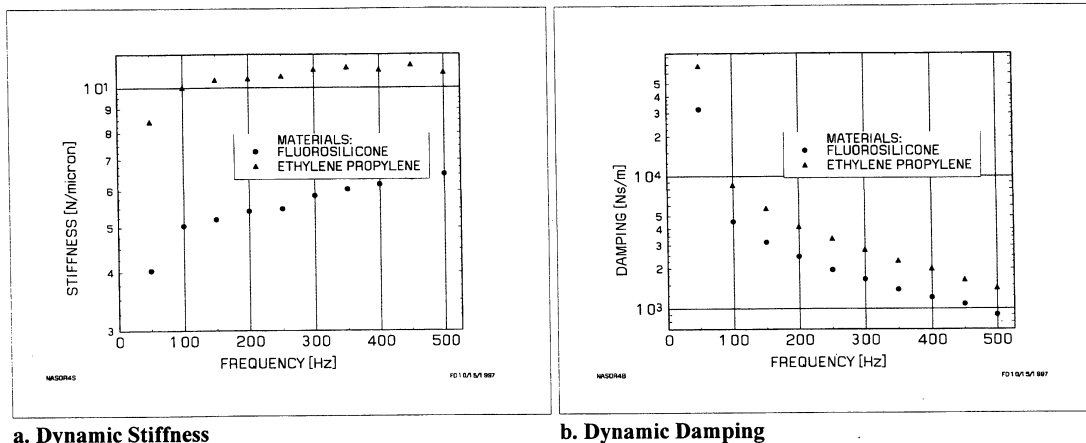


Fig. 5 Dynamic Coefficients of D = 2.125", W = 0.070" O-rings, precompressed to 0.060". Shore Hardness = 80.

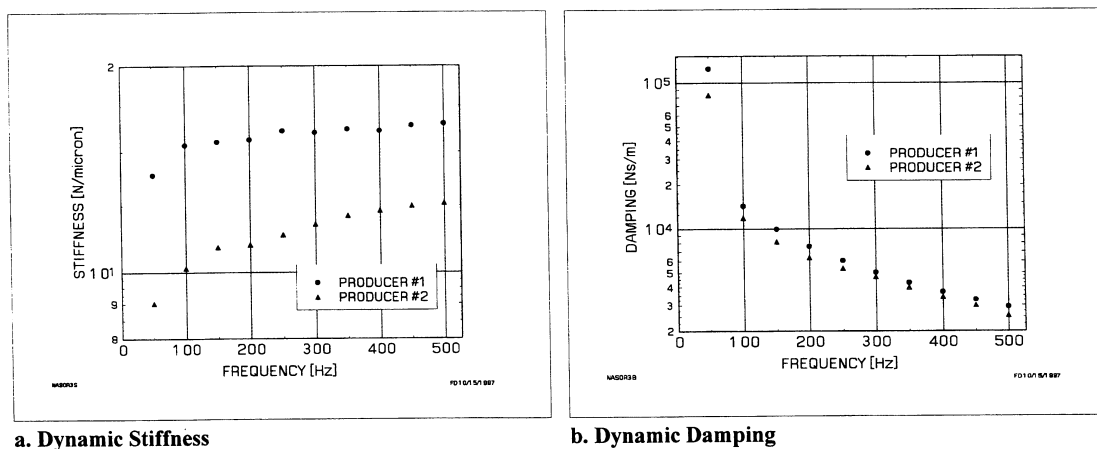


Fig. 6 Dynamic Coefficients of D = 2.125", W = 0.070" O-rings, precompressed to 0.060". Material: Nitril (Buna N), Shore Hardness = 90.

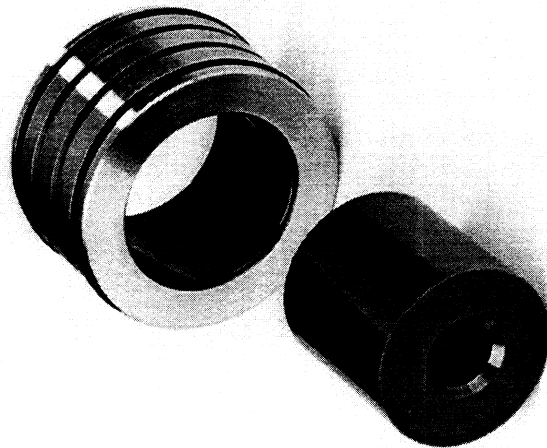


Fig. 7 Test Bearing, Rotor and Sleeve Assembly

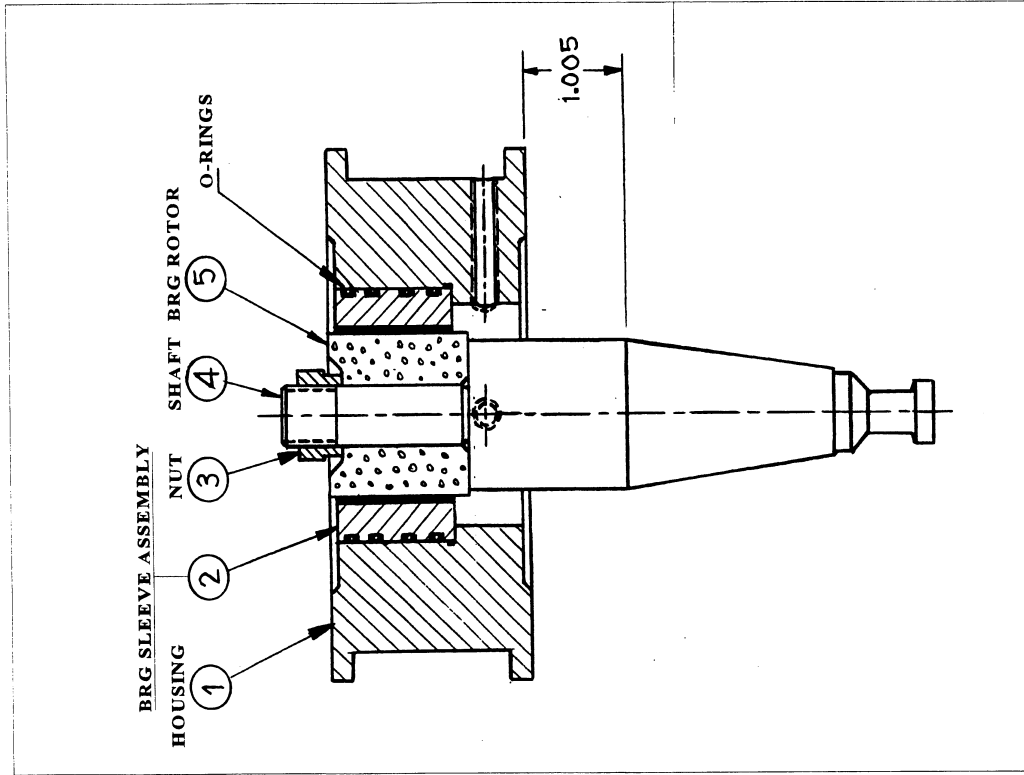


Fig. 8 Test Bearing Assembly

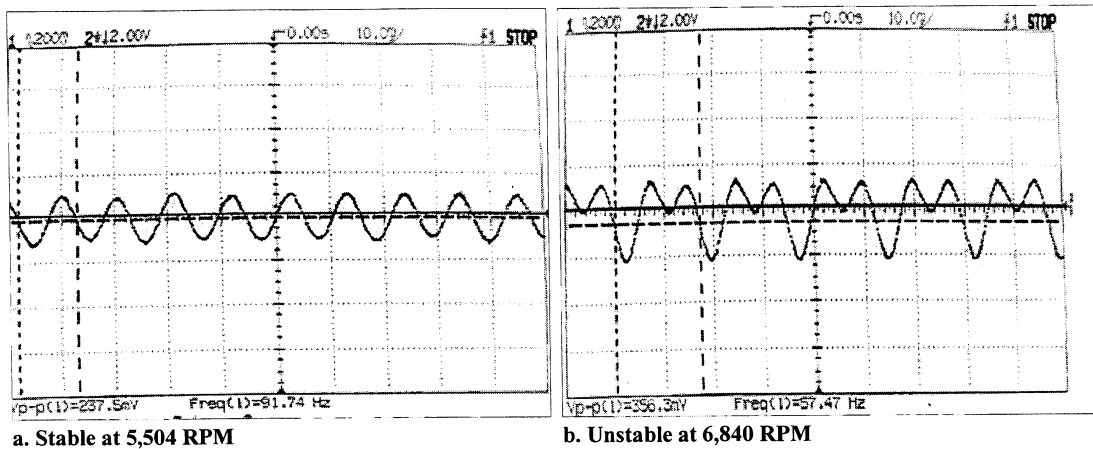


Fig. 9 Stability Threshold of the Test Bearing when It Is Supported by 2 Buna O-rings with Shore Hardness = 50.

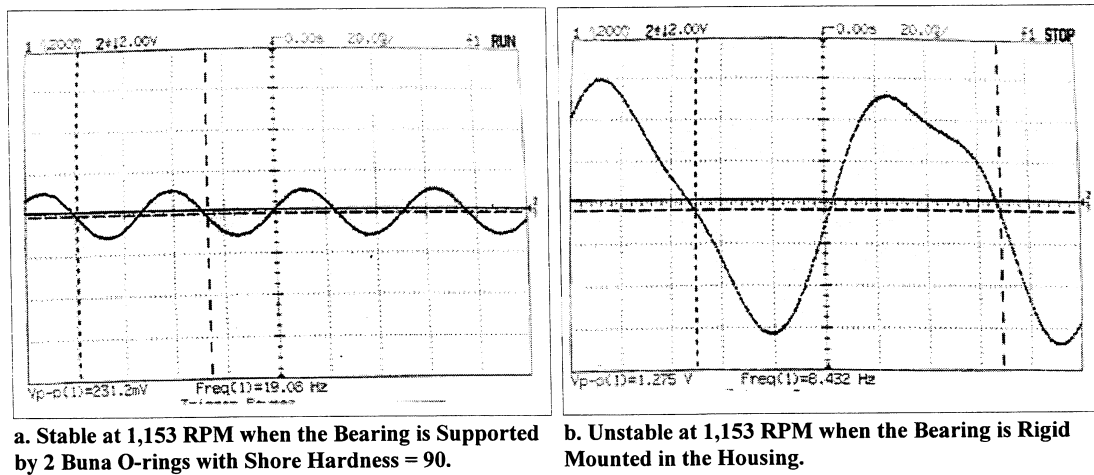


Fig. 10 Stability of a Wave Bearing when It is Supported by O-rings or It is Rigid Mounted into the Housing.

OPTIMIZATION OF TURBINE RIM SEALS

J.H. Wagner, D.E. Tew, G.M. Stetson, and J.S. Sabnis
Pratt & Whitney
West Palm Beach, Florida

ABSTRACT

Experiments are being conducted to gain an understanding of the physics of rim seal cavity ingestion in a turbine stage with the high-work, single-stage characteristics envisioned for Advanced Subsonic Transport (AST) aircraft gas turbine engines of the early 21st century. Initial experimental measurements to be presented include time-averaged turbine rim cavity and main gas path static pressure measurements for rim seal coolant to main gas path mass flow ratios between 0 and 0.02. The ultimate objective of this work is develop improved rim seal design concepts for use in modern high-work, single stage turbines in order to minimize the use of secondary coolant flow. Toward this objective the time averaged and unsteady data to be obtained in these experiments will be used to

- 1) Quantify the impact of the rim cavity cooling air on the ingestion process.
- 2) Quantify the film cooling benefits of the rim cavity purge flow in the main gas path.
- 3) Quantify the impact of the cooling air on turbine efficiency.
- 4) Develop/evaluate both 3D CFD and analytical models of the ingestion/cooling process.

AGENDA

- **Motivation**
 - **Objective**
 - **Approach**
 - **Description of Experiments**
 - **Description of Model**
 - **Initial Results**
 - **Summary**
-

MOTIVATION

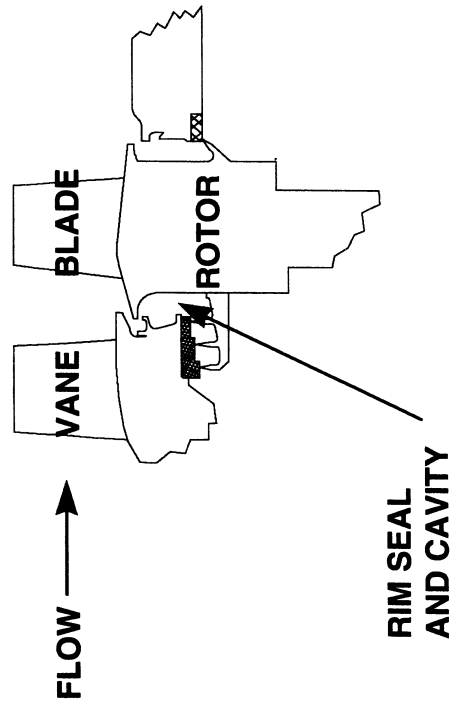
- Reduce SFC by reducing rim seal purge air required to cool cavity
 - Reduced SFC leads to
 - » Decreased DOC&I
 - » Decreased emissions
-

OBJECTIVE

- Reduce rim seal cooling air requirements by optimizing rim seal geometries

- Geometric parameters

- Platform overlap
- Radial gap
- Overlap/gap asymmetries
- Vane/blade spacing



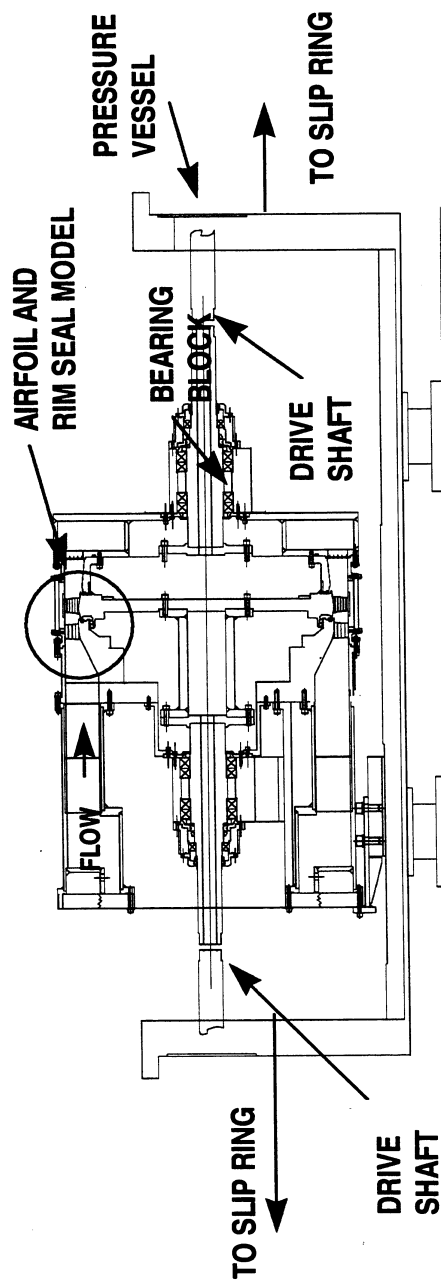
APPROACH

- **Develop understanding of rim seal ingestion process via experiments and analytical models**
 - Identify major drivers
 - Identify key design levers
 - **Develop optimized design**
 - **Evaluate new design**
-

DESCRIPTION OF EXPERIMENTS

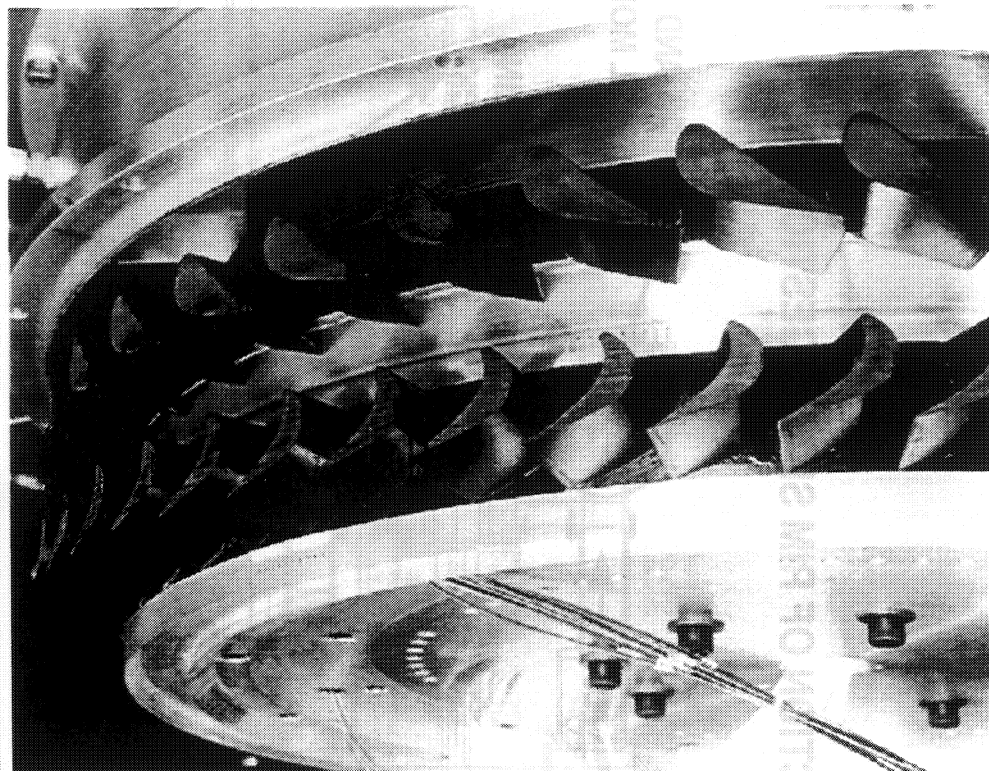
- **Facility**
- **Diagnostic Techniques**

CROSS-SECTION OF RIM SEAL INGESTION RIG



- INLET TOTAL TEMPERATURE 540 DEG R
- INLET TOTAL PRESSURE 23 PSIA
- MASS FLOW 15 LBM/SEC
- FLOW COEFFICIENT (CX/U) 0.45
- VELOCITY TRIANGLES ARE MODELED

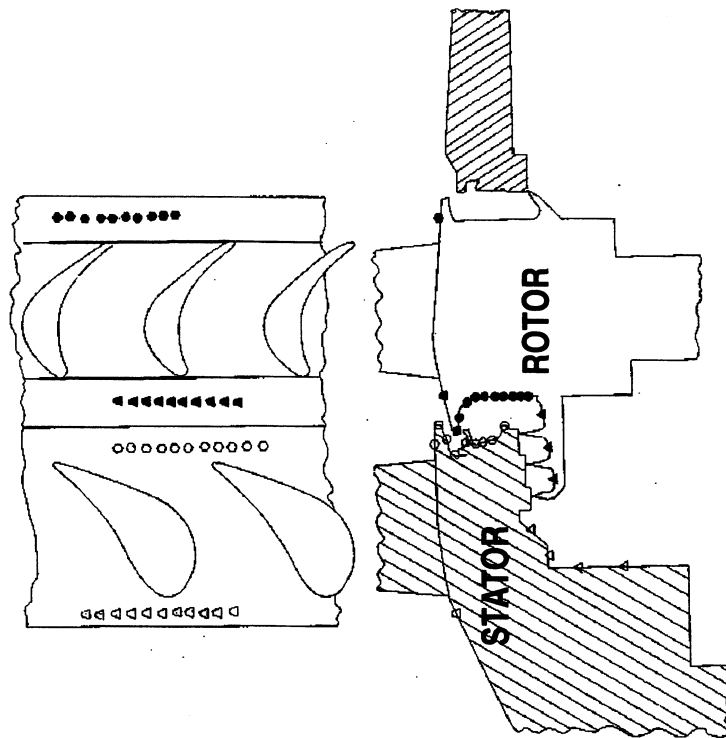
HALF-SPAN TURBINE MODEL



DIAGNOSTIC TECHNIQUES

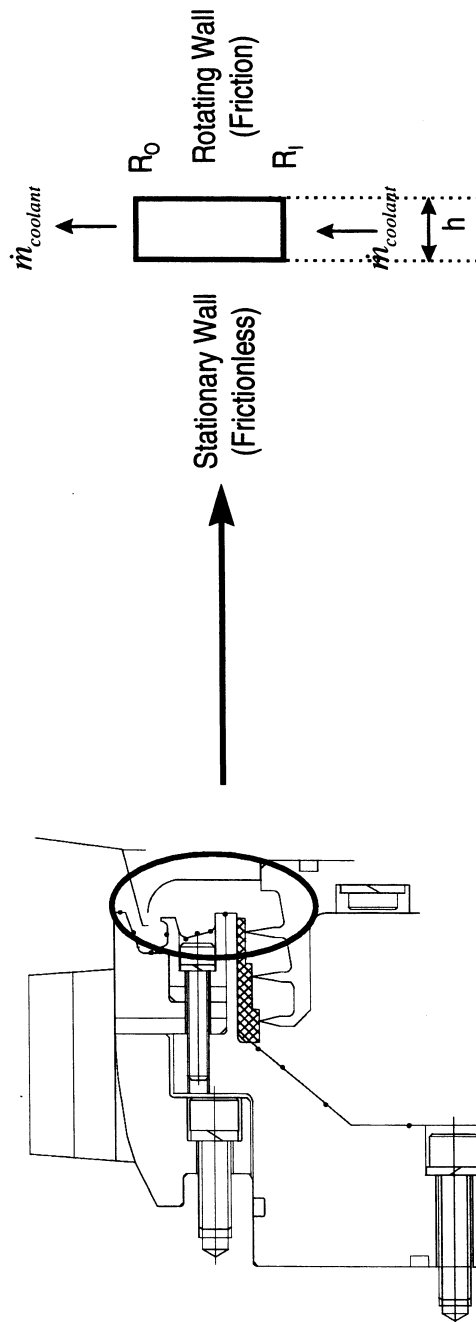
<u>Technique</u>	<u>Utility</u>
Time-Average Pressure	Evaluate CV models of cavity flow
CO ₂ Concentration	Estimate cavity ingestion(temperatures) (Sc,Pr # analogies)
Unsteady Pressure	Quantify unsteadiness of cavity flow

PRESSURE TAP LOCATIONS



DESCRIPTION OF MODEL

Control Volume Approach

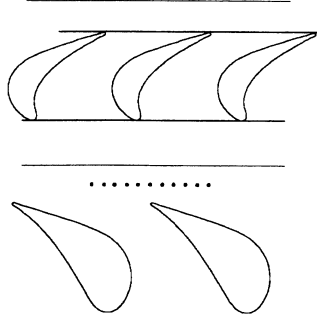


- Given
 - Re , R_i / R_o , h / R_o , $\dot{m}_{coolant}$
- Calculate
 - Radial press. dist.
 - Radial and tang. velocity dist.

IMPACT OF COOLANT ON CAVITY C_p DISTRIBUTION

- **OBJECTIVE**

- Assess impact of coolant on cavity time-average C_p distributions



$$C_p \equiv \frac{p - \bar{p}_v}{P_{t_{in}} - \bar{p}_v}$$

- **APPROACH**

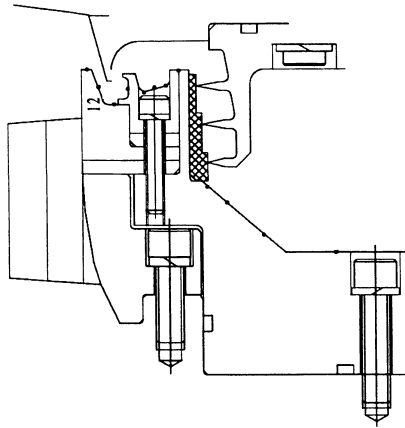
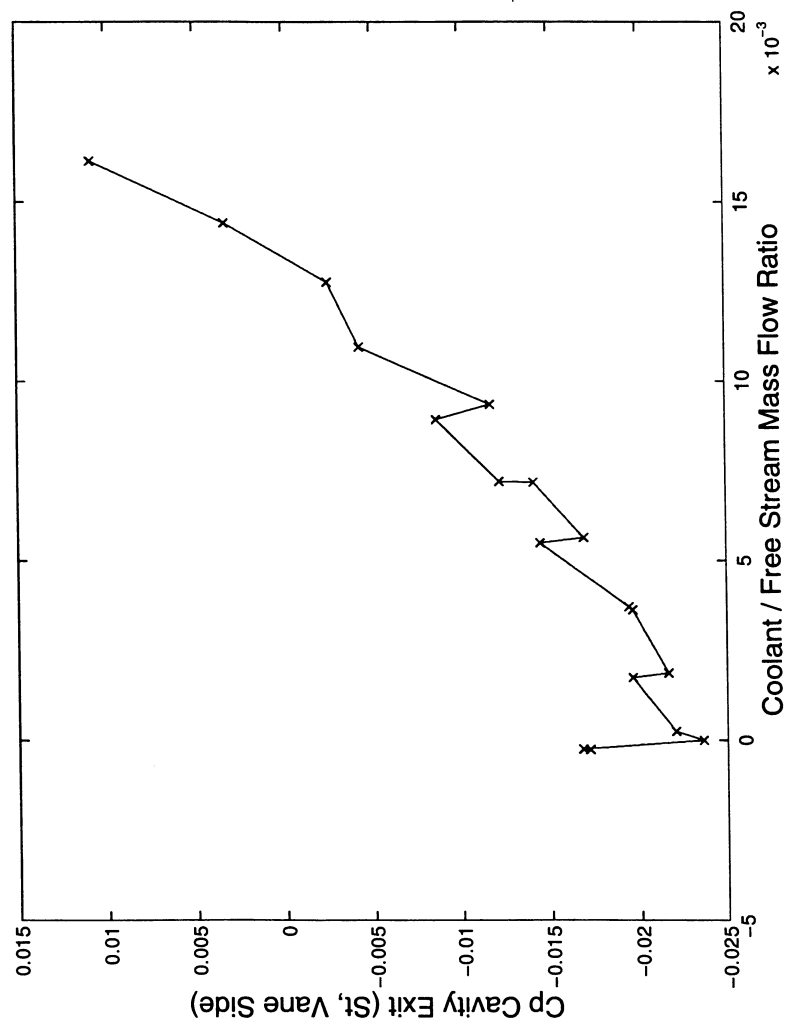
- Vary coolant to free stream mass flow ratio
- Hold flow coefficient and wheel speed constant

- **CAVEATS**

- Flow coefficient not constant (+/- 5% variation)
- Full uncertainty analysis not yet performed

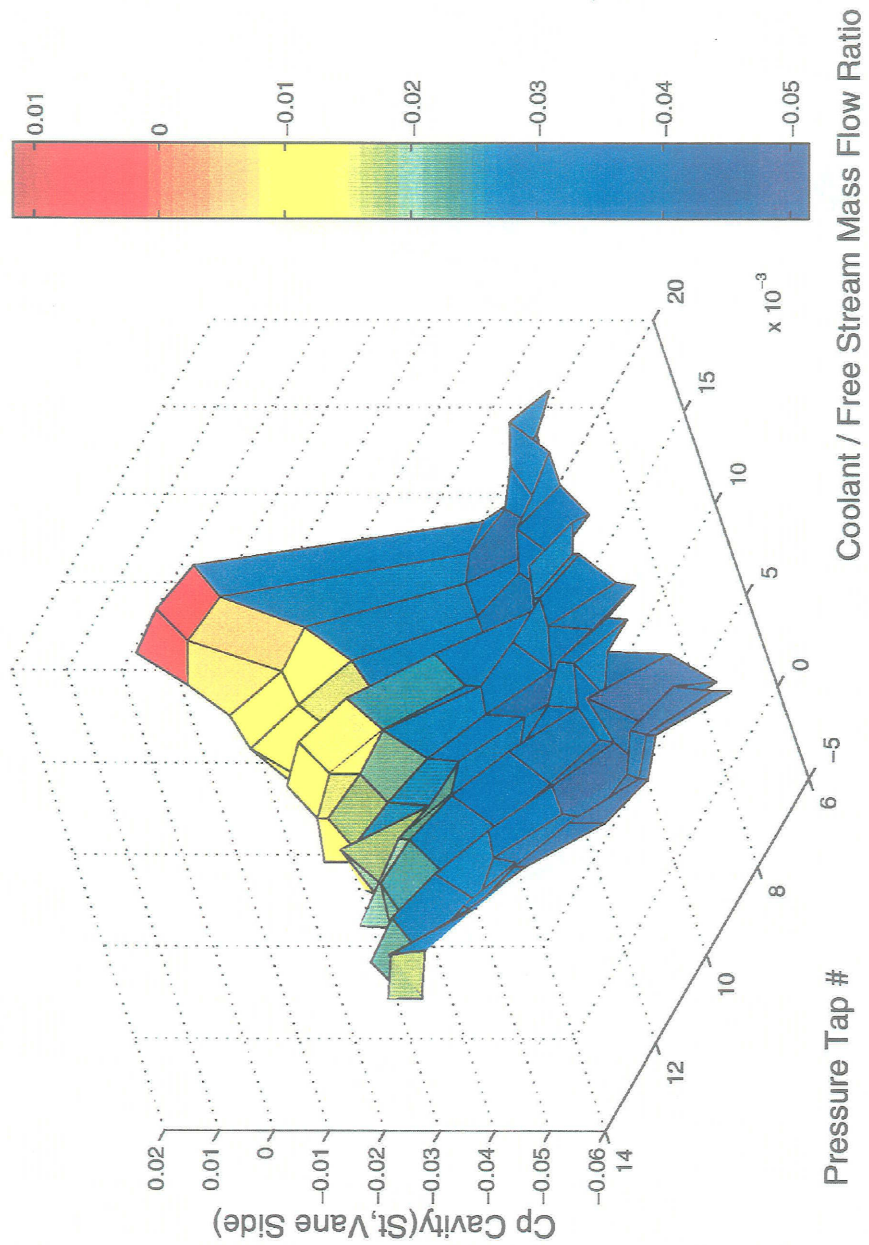
IMPACT OF COOLANT ON CAVITY Cp (DATA)

- Vane Side Cavity Exit (Tap #12)

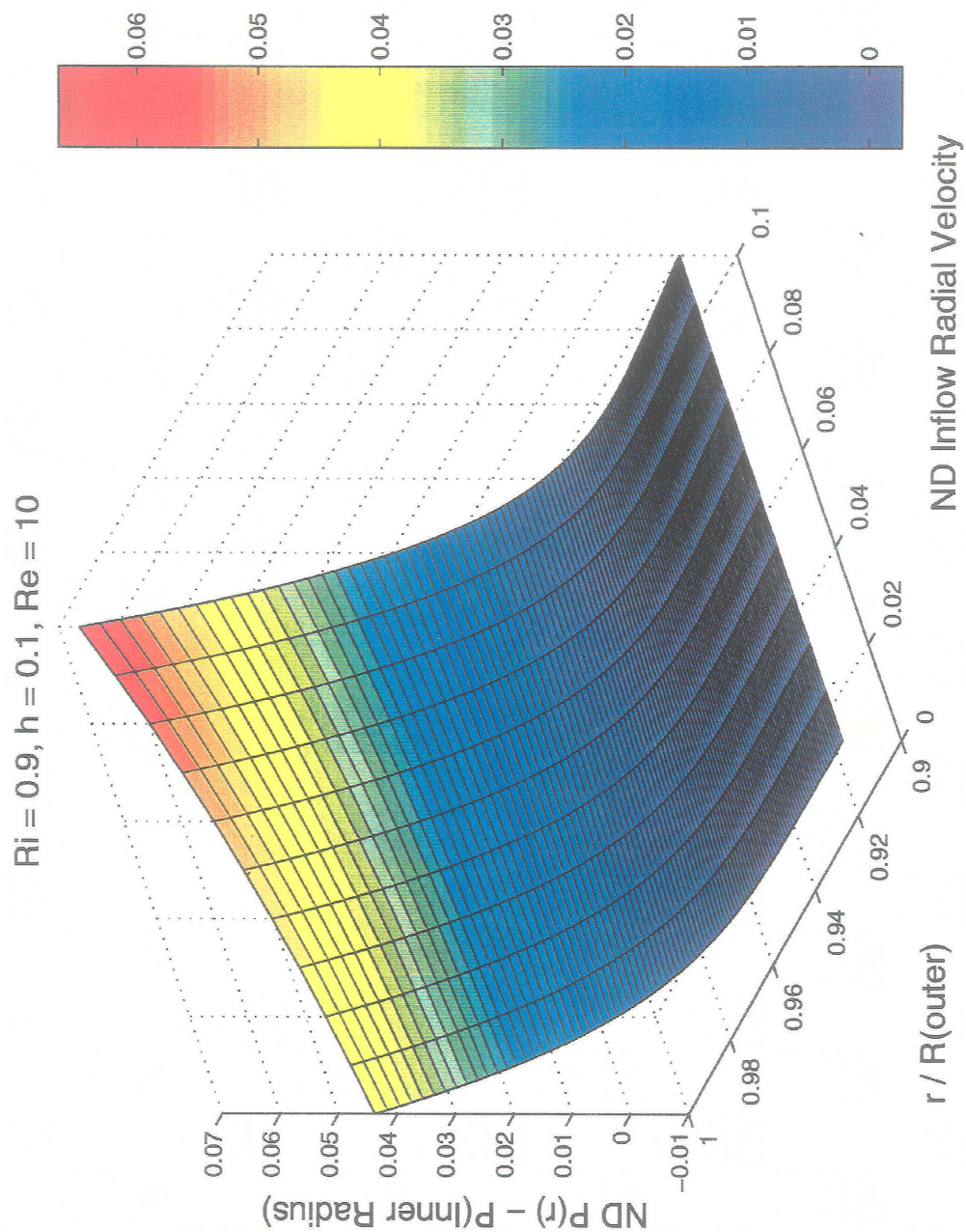


IMPACT OF COOLANT ON CAVITY C_p (DATA)

- Vane Side of Cavity



IMPACT OF COOLANT ON CAVITY PRESSURE DIST. (MODEL)



SUMMARY

- Experiments and modeling efforts directed toward reduction of rim seal purge air by optimizing rim seal geometry
 - Approach
 - 1) Understand physics of ingestion process via experiments
 - 2) Develop control volume models(design tools)
 - 3) Design optimized rim seal
 - 4) Evaluate optimized design in experiments
 - Experiments underway
 - Initial modeling results encouraging
-

NUMERICAL METHODOLOGY FOR COUPLED TIME-ACCURATE SIMULATIONS
OF PRIMARY AND SECONDARY FLOWPATHS IN GAS TURBINES

A.J. Przekwas and M.M. Athavale
CFD Research Corporation
Huntsville, Alabama

and

R.C. Hendricks and B.M. Steinetz
NASA Lewis Research Center
Cleveland, Ohio

Detailed information of the flow-fields in the secondary flowpaths and their interaction with the primary flows in gas turbine engines is necessary for successful designs with optimized secondary flow streams. Present work is focused on the development of a simulation methodology for coupled time-accurate solutions of the two flowpaths. The secondary flowstream is treated using SCISEAL, an unstructured adaptive Cartesian grid code developed for secondary flows and seals, while the mainpath flow is solved using TURBO, a density based code with capability of resolving rotor-stator interaction in multi-stage machines. An interface is being tested that links the two codes at the rim seal to allow data exchange between the two codes for parallel, coupled execution. A description of the coupling methodology and the current status of the interface development is presented. Representative steady-state solutions of the secondary flow in the UTRC HP Rig disc cavity are also presented.

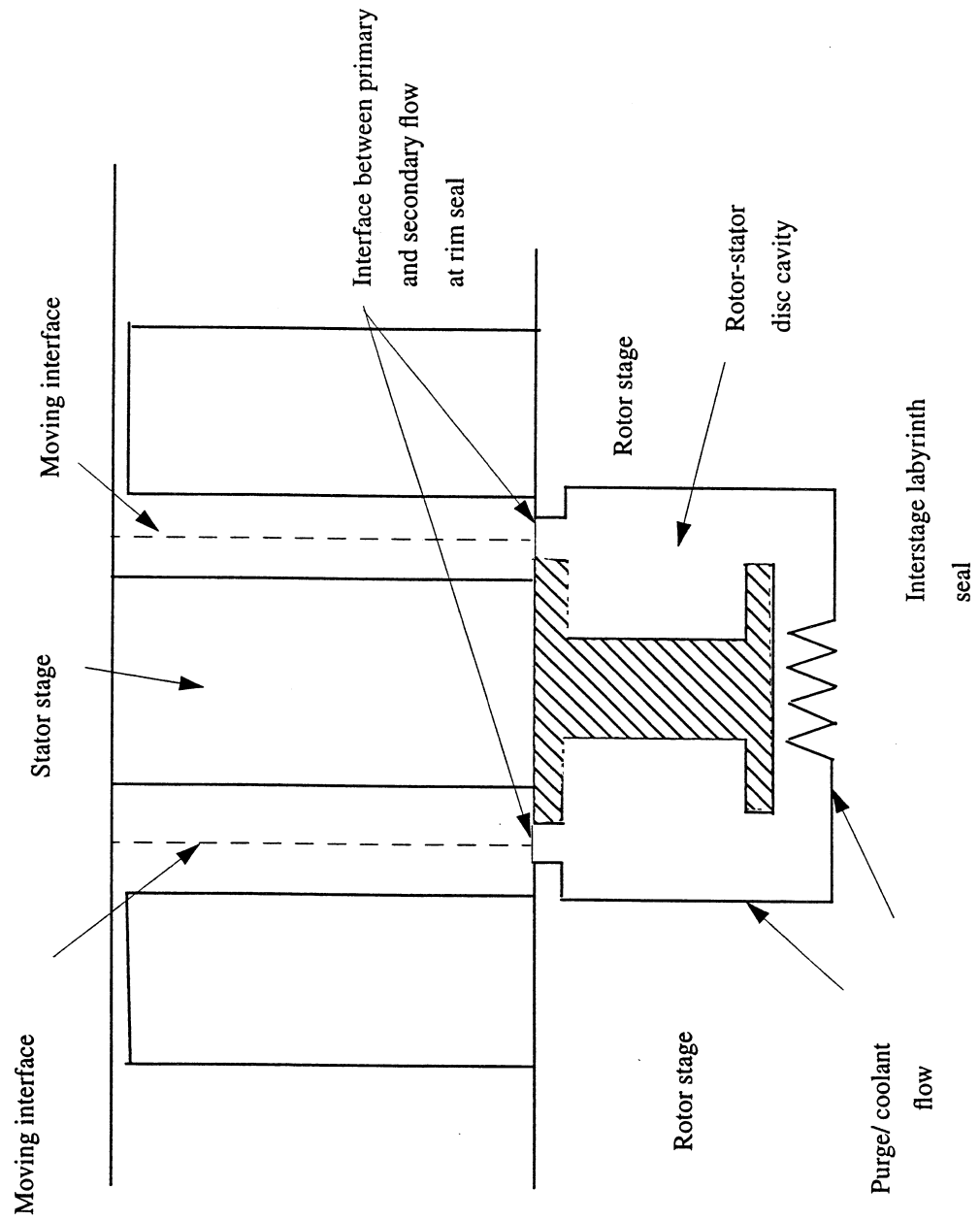
OUTLINE

- **Overview and Objectives**
- **Computational Methodology**
- **Interface Development, Status**
- **Demonstration Simulations**
- **Summary**

NEED FOR COUPLED ANALYSIS

- **Typical Gas Turbine Engine**
 - **Multi-Stage Compressor and Turbine Section with Interstage Cavities**
 - **Powerstream/Mainpath/Primary: Flow Above Blade Platforms**
 - **Secondary: Flow Below Blade Platform, Cooling Flow, Cavity Flows**
- **Powerstream and Secondary Flow Interact in Strong, Complex Manner, and Affect**
 - **Engine Power, Efficiency**
 - **Component Life (Mechanical and Thermal Loads)**
- **Drive for Higher Power/Efficiency at Reasonable Component Life**
 - **Details of Primary and Secondary Flows Needed**
 - **At Design, Off Design, and During System Transients**

PRIMARY-SECONDARY COUPLING SCHEMATIC



P-4117-8/14

NEED FOR COUPLED ANALYSIS

- **Interaction Has Different Aspects in Different Parts Compressor Section**
 - **Effect of Interstage Cavity Flows on Primary Flow**
 - **Windage Losses**
- **Turbine Side**
 - **Coolant Flow Optimization for Efficiency**
 - **Primary Gas Ingestion in Cavities Must be Prevented at All Times**
 - **Effects of Coolant Flow on Power Stream**

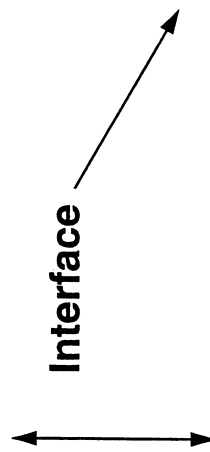
OBJECTIVES AND PROPOSED METHODOLOGY

- To Develop a Validated Set of Codes for Coupled, Transient Solutions of Primary and Secondary Flows in Multi-Stage Machines
 - Use Existing, Validated Codes for Different Streams: SCISEAL for Secondary, MS-TURBO for Primary
 - Develop Interfacing Algorithms for Coupling the Codes
 - Graphical User Interface for Ease of Use
- Use of Separate Codes
 - Widely Different Flow Physics in Primary and Secondary Flows
 - Validated Codes Available, Specifically Developed for Each Flow Stream
 - Capabilities Offered by the Combinations

COUPLED CODE METHODOLOGY

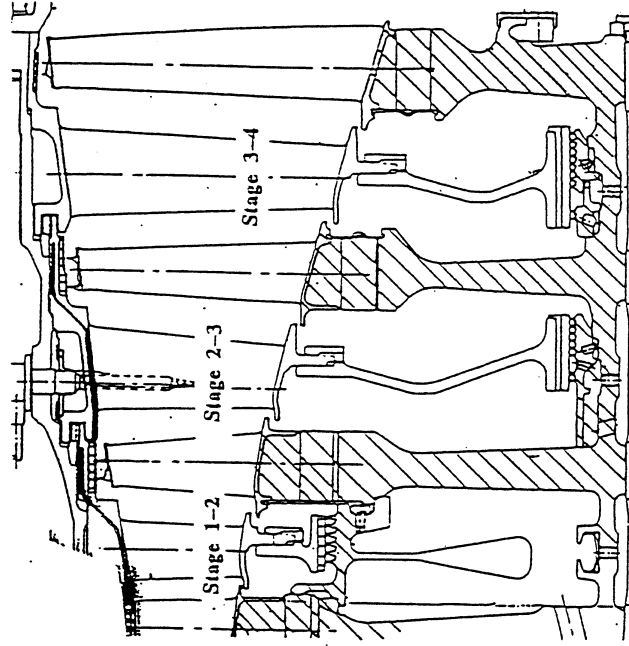
Power Stream

TURBO: density based, finite volume, structured grids, time-accurate, multiple blade rows, high speed flows



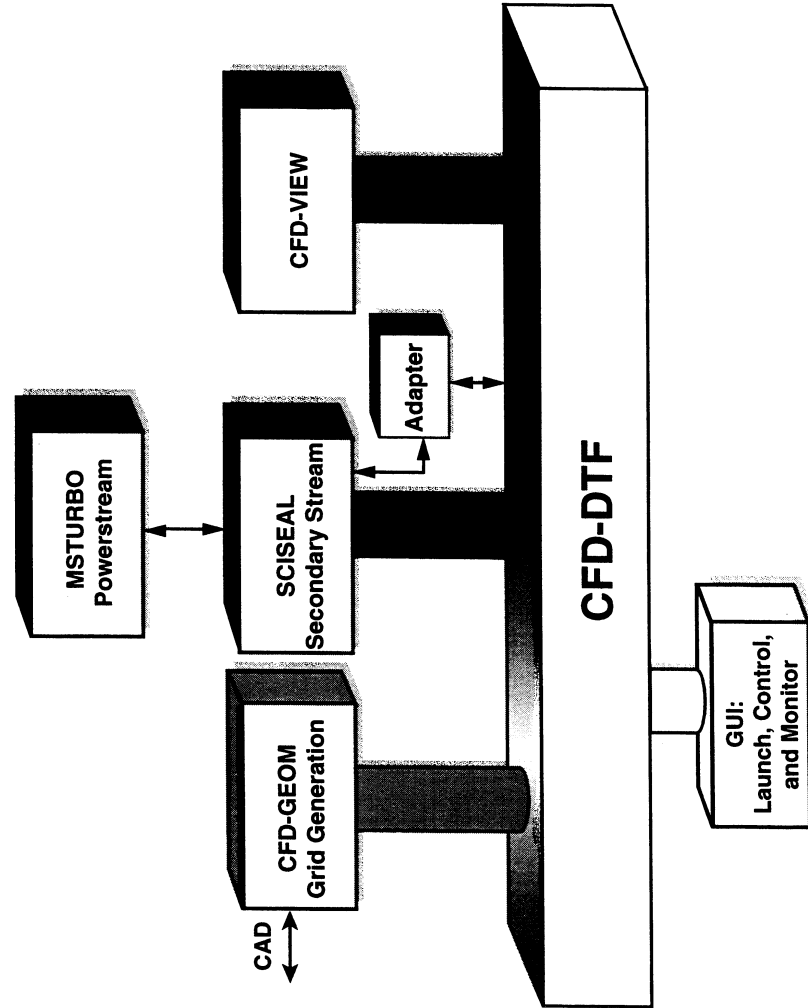
Cavity/Secondary Flow

SCISEAL-U: pressure based, finite volume unstructured, adaptive Cartesian grids, time accurate, conjugate heat transfer, turbulence, low speed flows



SIMULATION ENVIRONMENT

- **Plug-n-Play Modules Attached to DTF**



DESCRIPTION OF SCISEAL CODE

Salient Features

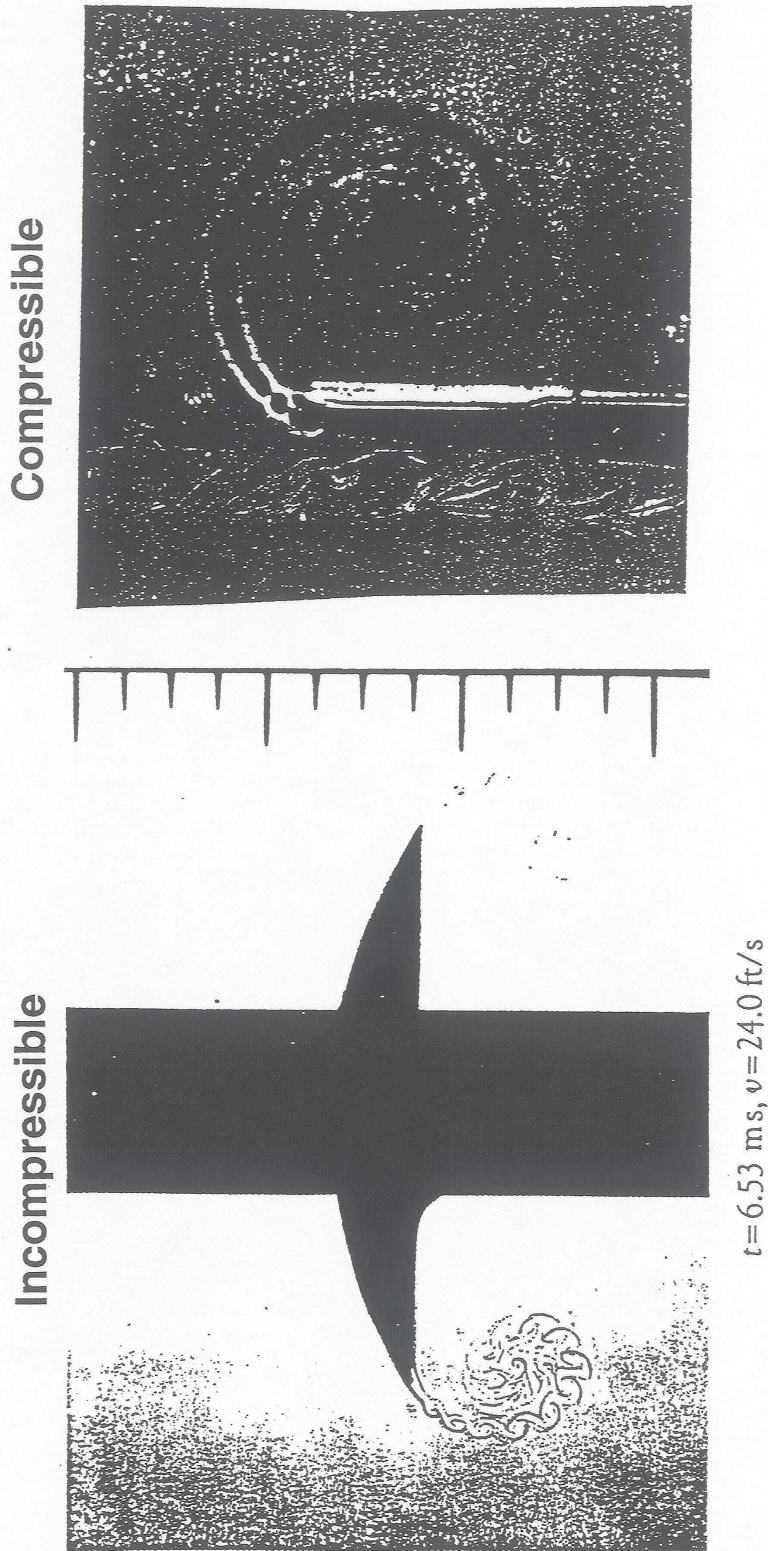
- **Unstructured Grid Topology with Mixed Elements**
- **Fully Implicit Pressure-Based, Finite Volume**
- **Cartesian Velocities, Non-Staggered Arrangement**
- **Sequential Solution Procedure with SIMPLEC-M for Velocity-Pressure Coupling**
- **Conjugate Gradient Solvers for Linear Systems**
- **Flow, Conjugate Heat Transfer, Turbulence**
- **Links with Grid Adaptor for Solution-Based Adaptation**

CARTESIAN PRISM/QUAD GRIDS

- **Conventional Unstructured Tetra**
 - Difficult to Generate Quality Volume Grids
 - Difficult to Control Clustering and Aspect Ratio for Viscous Flows Near Walls, Shear Layers, etc.
 - Require ~5x Cells than Similar Resolution Hexa
 - Non-Trivial Adaptive Remeshing, Moving Grids, etc.
- **Adaptive Cartesians**
 - Showed Remarkable Results for 3D Euler Equations Solved for Complex Configurations
 - Inefficient for N-S Equations as Very Large Number of Cells is Generated in Boundary Layer Region
- **Adaptive Cartesians-Prism/Quads**
 - Most Promising Approach for Fully Automated Simulations of Viscous, Turbulent Flows

VORTEX GROWTH AND UNSTRUCTURED ADAPTIVE GRID

- Van Dyke (An Album of Fluid Motion) examples of unsteady vortex dynamics (macro and microscales)
- Unstructured, solution-adaptive simulations

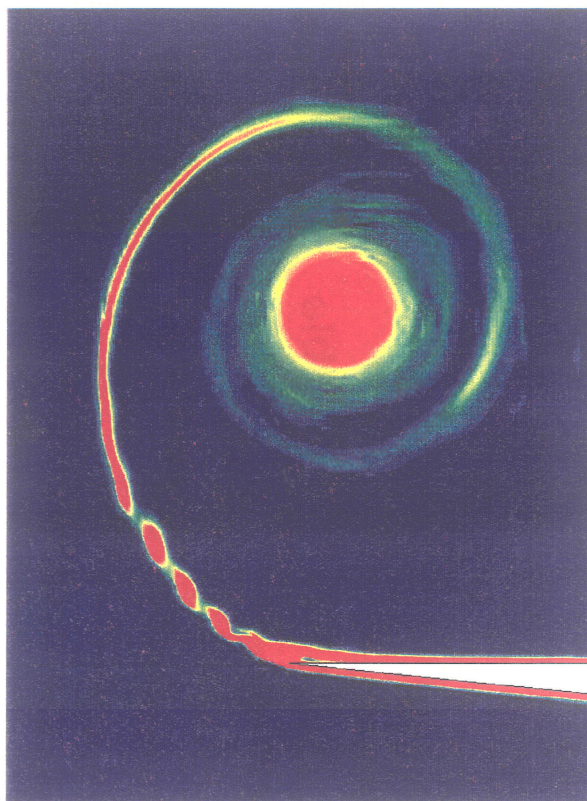
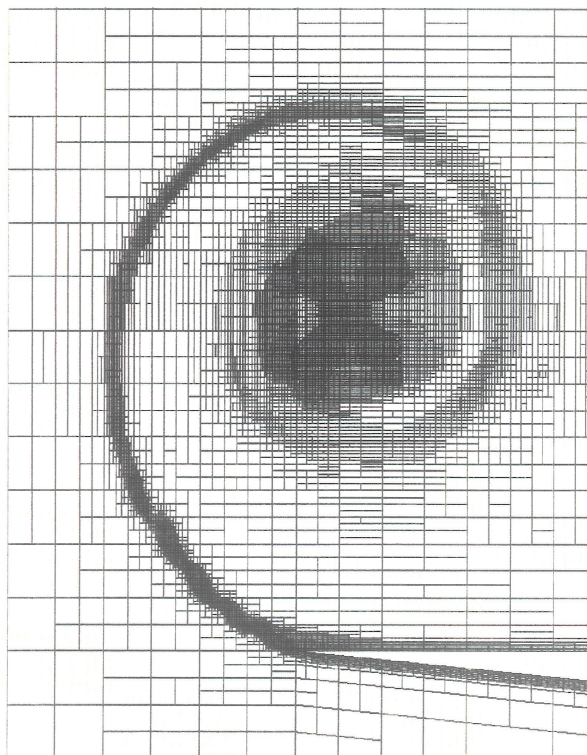


81. Growth of vortices on an accelerated plate.

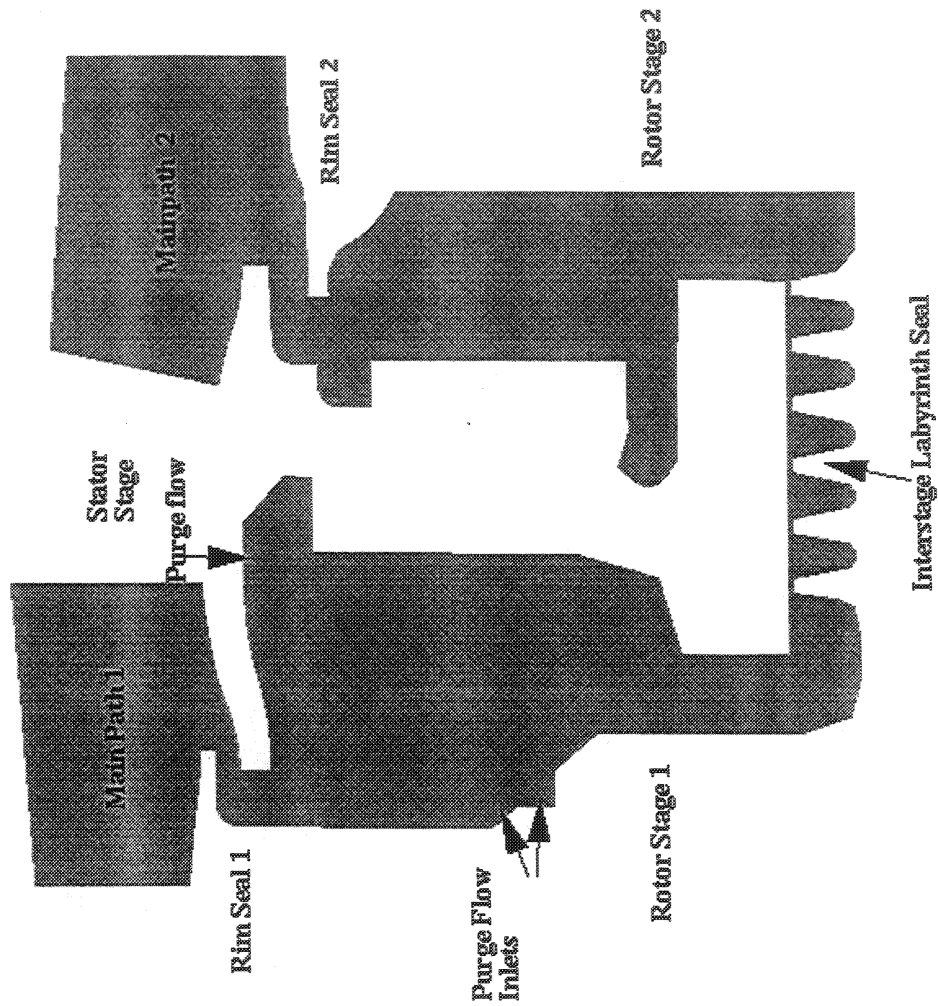
P-4117-8/4

ADAPTIVE GRIDS

- Unsteady Vortex Shedding from a Flap

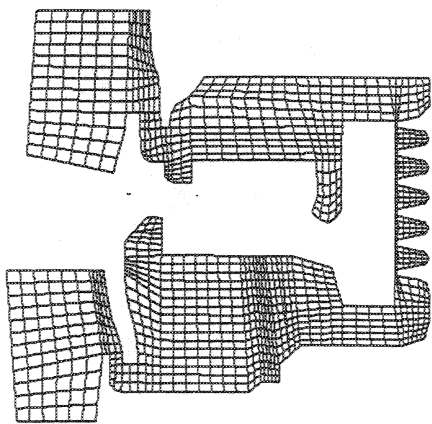


PROBLEM DEFINITION **Stage 1-2 Cavity, T56 Engine Turbine Section**

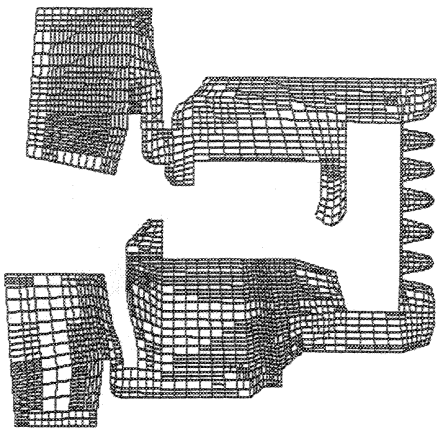


P-4117-85

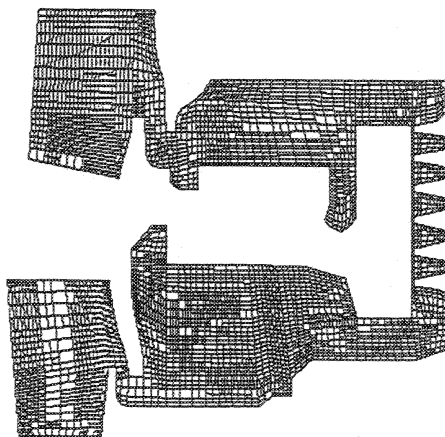
GRID STRUCTURE AT SEVERAL ADAPTATION CYCLES



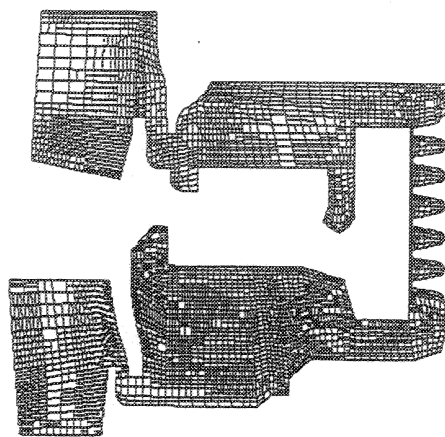
(a) Root Grid, 1180 Cells



(b) Adapted Grid, 2500 Cells

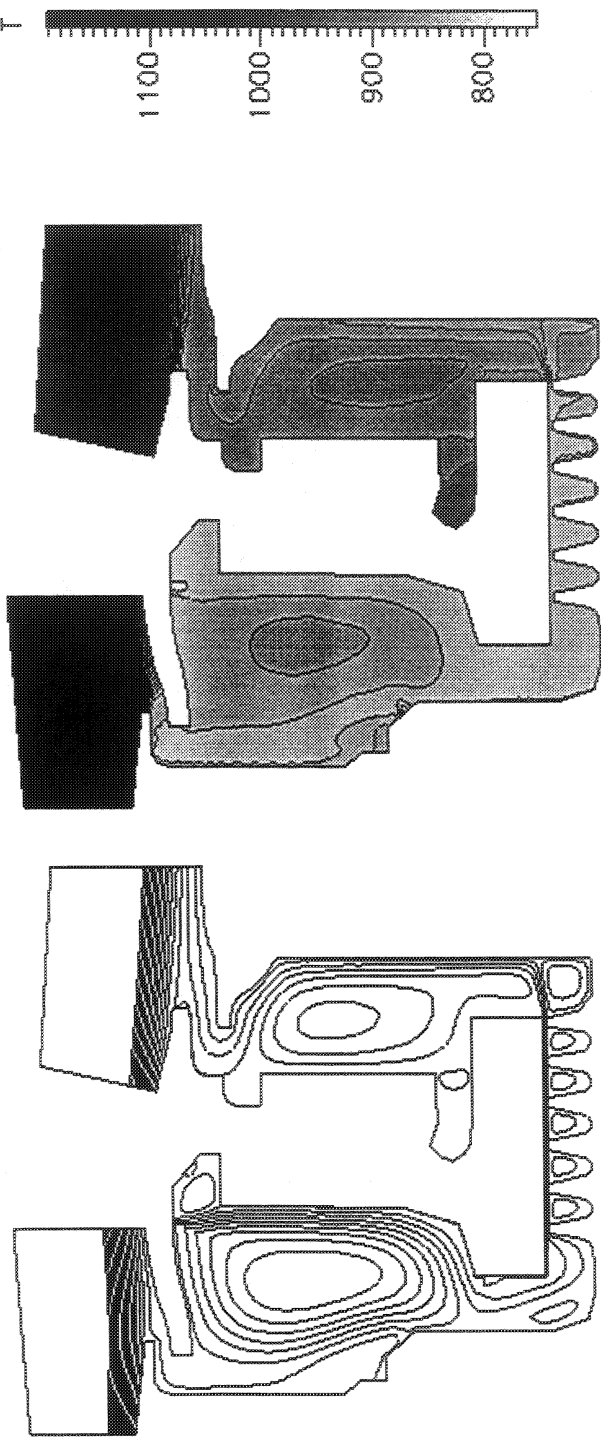


(c) Adapted Grid, 4000 Cells



(d) Adapted Grid, 5000 Cells

SOLUTIONS ON FINEST GRID **Stage 1-2 Cavity**



(a) Streamline Plot (Lines in the Main-path Have Been Suppressed). Note Outgoing Flow in Both Rim Seals

(b) Temperature Field in the Cavity

CODE COUPLING/INTERFACE ISSUES

- **Solution Methodology/Codes**
 - **Pressure or Density-Based/Primary Variables**
 - **Flux Calculation Methods**
 - **Boundary Condition Treatment**
- **Coupling Level**
 - **At Subiteration Level**
 - **Equation Level (For Continuity Equation) May be Needed**
- **Interface Placement**
 - **Location Should Minimize Grid Changes**
 - **SCISEAL Grid Fixed, TURBO Grid Time-Varying**
- **Interpolation Routines**
 - **Needed for Data Transfer from One Code to Other**
 - **Conservation of Fluxes**

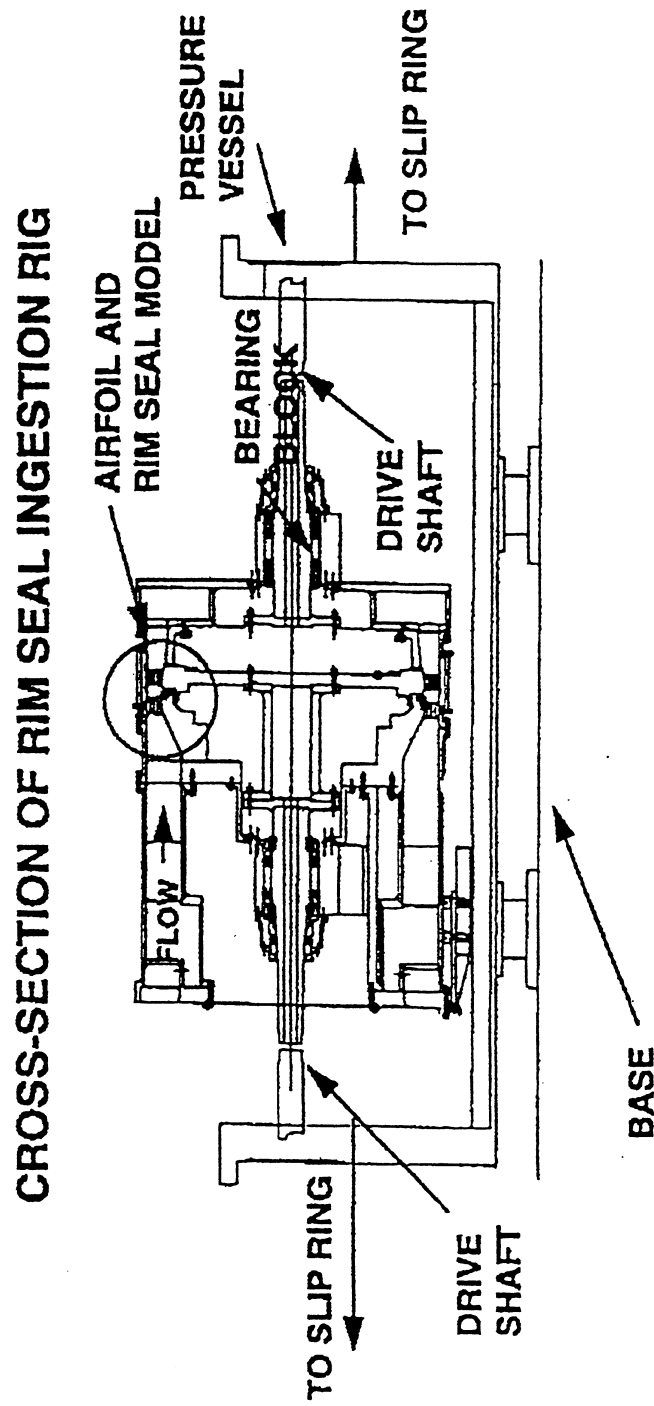
CURRENT INTERFACE STRATEGY

- **Placement of Interface Along the Rotor Hub Wall**
 - **Intersects Rim Seal Open Area**
 - **Minimizes Grid Interface Distortion**
- **Data Type to be Exchanged**
 - **Fluxes Calculated by TURBO \Rightarrow Used Directly in SCISEAL Boundary Cells**
 - **Variables from SCISEAL \Rightarrow Interpolated and Used in the Ghost Layer at Interface Boundary in TURBO**
 - **Ensures Flux Conservation**

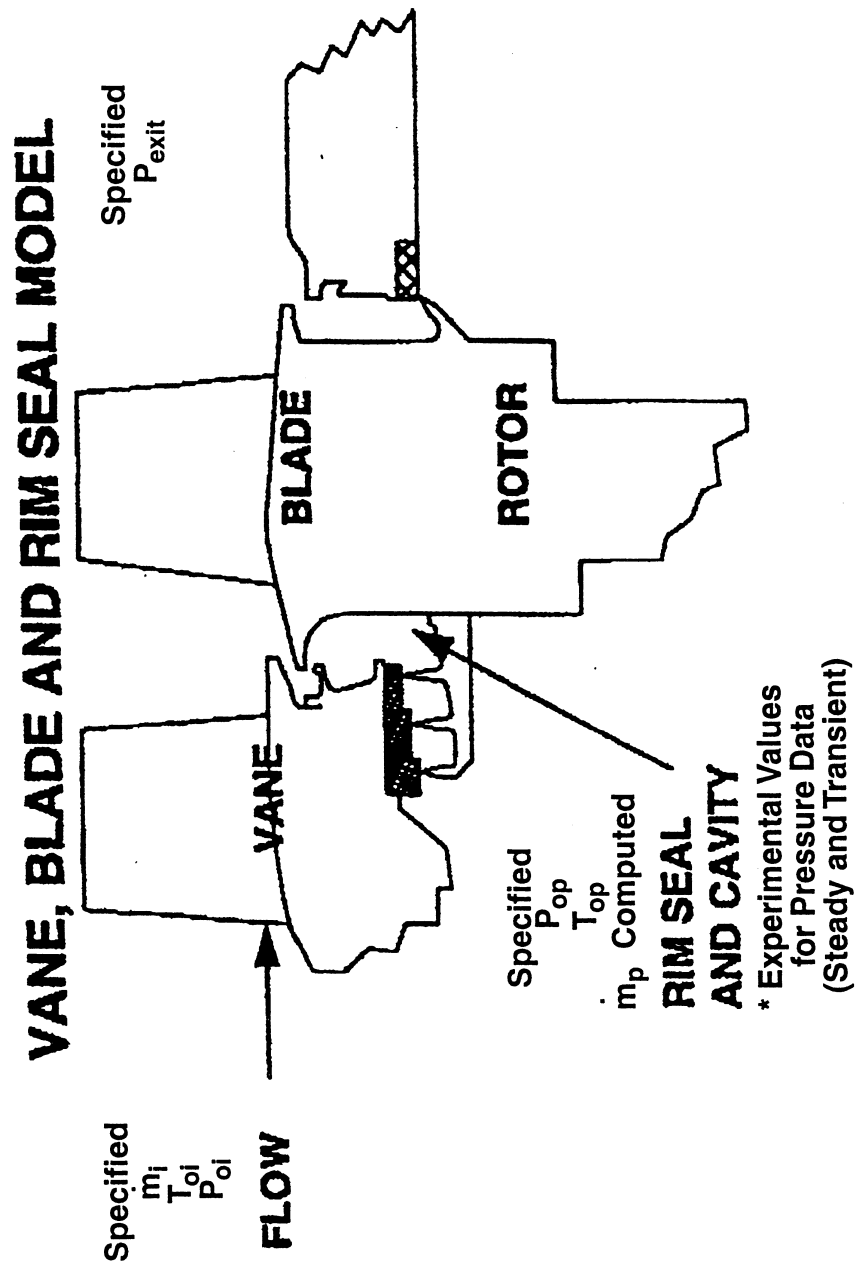
CURRENT STATUS, PLANS

- Interface Algorithm and Code Modifications are in Place
 - Debugging Completed
- Will be Used for Time-Accurate Flows in UTRC H.P. Turbine Rig
 - Stator and Rotor Plus Disc Cavity Combination
 - Experimental Data Used for Validation
- Development of a GUI Needed for Ease of Use of Unstructured Code (SCISEAL)
- Steady State Preliminary Results for UTRC HP Rig Completed

SCHEMATIC OF THE H.P. TURBINE RIG

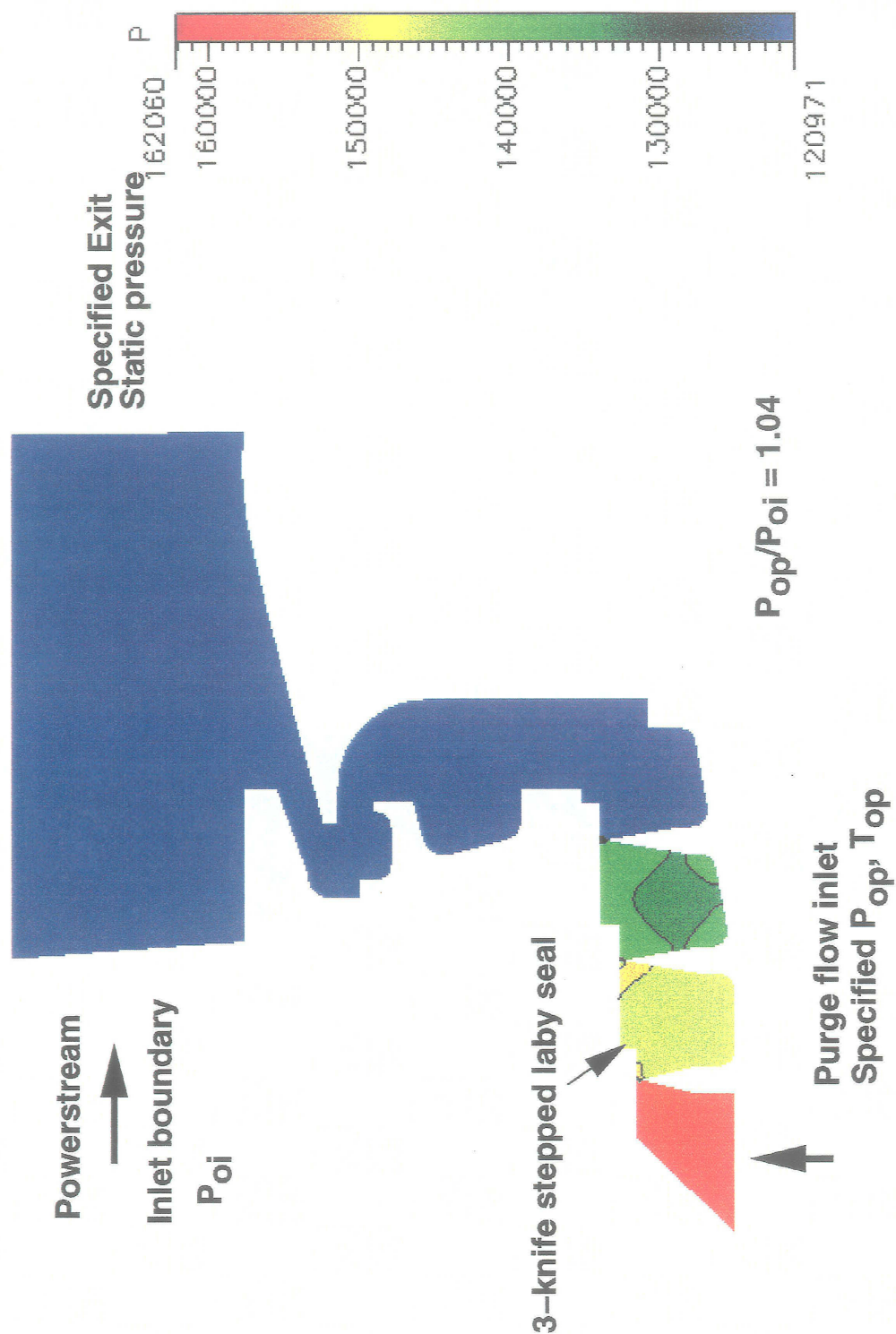


DETAILS OF THE FLOWFIELD IN H.P. RIG



UTRC H.P. Rig

Steady-State Solutions, Static pressures



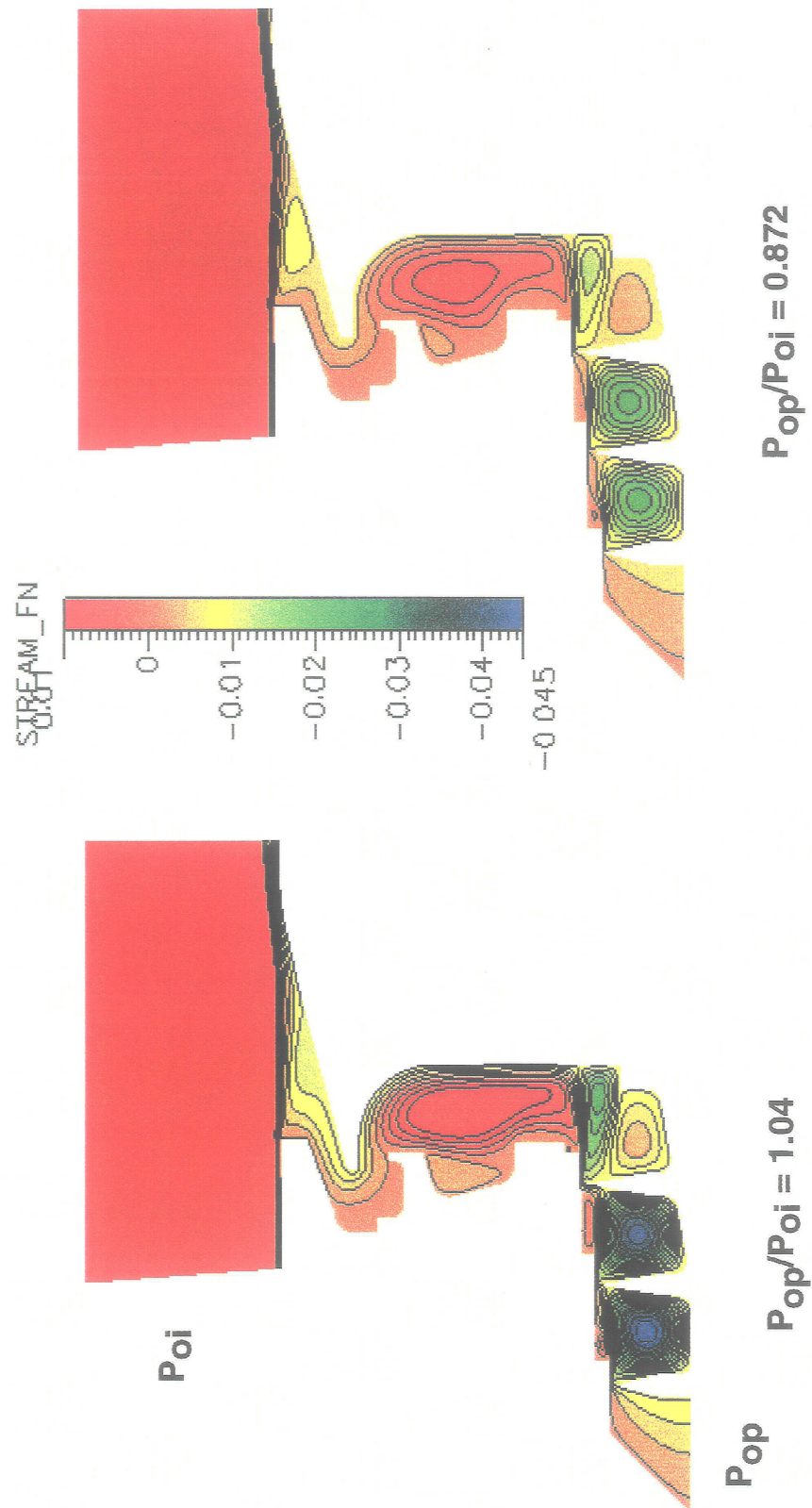
UTRC H.P. RIG

Observations

- Purge Flow \dot{m}_p Measured at Different Pressure Ratios P_{op} / P_{oi}
- Maximum Purge Flow Rate = 1.6% of Powerstream at $P_{op} / P_{oi} = 1.04$
- Minimum (0) Purge Rate $\sim P_{op} / P_{oi} = 0.85$
- 2D, Axisymmetric, Steady State Solutions Obtained
 - Several Different P_{op} / P_{oi} Values
 - Computed Purge Flow $\sim 0.95\%$ of Powerstream at $P_{op} / P_{oi} = 1.04$
 - Cutoff of Purge Flow Seen at P_{op} / P_{oi} Near $P_{op} / P_{oi} = 0.86$

UTRC H.P. Rig

Streamlines at different pressure ratios



SUMMARY

- **Interaction Between Mainpath and Secondary Flow Important; Need Detailed Information for Design and Performance Predictions**
- **A Numerical Methodology is Being Developed**
 - **Validated Codes for Two Flow Streams: SCISEAL and MS-TURBO**
 - **Interfacing Algorithms/Routines for Coupling**
 - **Validation Against UTRC Data and Other Experiments**
- **Geometries of H.P. Rig Obtained, Steady State Results in Progress**
- **Unsteady Simulations are Being Setup**
- **Plans to Give Software to OEM for Release and Eventual Incorporation in Design Cycle**

UNSTEADY ANALYSIS OF TURBINE MAIN FLOW COUPLED WITH
SECONDARY AIR FLOW

Chunill Hah
NASA Lewis Research Center
Cleveland, Ohio

Two numerical approaches are used to model the interaction between the turbine main gas flow and the wheelspace cavity seal flow. The three-dimensional, unsteady Reynolds-averaged Navier-Stokes equations are solved with a CFD code based on a structured grid to study the interaction between the turbine main gas flow and the wheelspace cavity seal flow. A CFD code based on an unstructured grid is used to solve detailed flow feature in the cavity seal which has a complex geometry. The numerical results confirm various observations from earlier experimental studies under similar flow conditions. When the flow rate through the rim cavity seal is increased, the ingestion of the main turbine flow into the rim seal area decreases drastically. However, a small amount of main gas flow is ingested to the rim seal area even with very high level of seal flow rate. This is due to the complex nature of three-dimensional, unsteady flow interaction near the hub of the turbine stage.

LIQUID ANNULAR SEAL CFD ANALYSIS FOR ROTORDYNAMIC FORCE PREDICTION

ABSTRACT

Jeff Moore and Alan Palazzolo
Texas A & M
College Station, Texas

A commercially available code developed by CFD Research Corporation (CFDRC) in Huntsville under contract by the Marshall Space Flight Center is utilized to analyze a plain and grooved liquid annular seal. These type seals are commonly used in modern turbopumps and have a pronounced effect on the rotordynamic behavior of these systems. Accurate prediction of both leakage and dynamic reaction forces is vital to ensure good performance and sound mechanical operation.

The code SCISEAL developed by CFDRC is a generic 3-D, finite volume based CFD code solving the 3-D Reynolds averaged Navier Stokes equations. The code allows body-fitted, multi-block structured grids, turbulence modeling, rotating coordinate frames, as well as integration of dynamic pressure and shear forces on the rotating journal. The code may be used with the commercially available pre and post-processing codes from CFDRC as well.

To benchmark the code, comparisons are made with recent tests by Marquette (1995) for both a plain annular and multi-grooved liquid seals. Both leakage and dynamic force coefficients (stiffness, damping, and inertia) are measured at speeds up to 24,000 rpm and pressures drops approaching 7 MPa (1000 psid) using water as the test media. The CFD results are presented along with analytical predictions using bulk-flow fluid assumptions. The results show little improvement over bulk flow with CFD for the plain annular seal but with substantially increased computational effort for CFD. On the other hand, CFD better captures the recirculating nature of the grooved seal flow field resulting in much improved prediction compared to bulk flow.

References:

Marquette, O.R., 1995, "Experimental vs. Theoretical Comparison of the Static and Dynamic Characteristics of One Smooth and Two Grooved Liquid Annular Seals with L/D of 0.457," *Turbomachinery Laboratories, Mechanical Engineering Dept., Texas A & M University, TL-SEAL-5-95*.

Presentation Overview

Introduction

Annular seals have a pronounced effect on the rotordynamic response and stability of modern high performance turbomachinery. Accurate prediction of their dynamic forces and leakage is fundamental in producing robust machinery designs with minimal risk to vibration problems operating with maximum efficiency. Using modern computational fluid dynamic (CFD) techniques, the true flow field may be captured with a minimal amount of empirical input. Labyrinth or grooved seals are especially challenging due to the complex geometry, large pressure and velocity gradients, high turbulence intensity, and large recirculations present in the flow field all of which is inherently unsteady. By generating an eccentric three-dimensional, body fitted mesh of the geometry, a pseudo-steady solution may be obtained in the rotating reference frame that is attached to the whirling rotor. The net reaction force is calculated due to the given eccentricity (definition of impedance) for different ratios of rotor speed to whirl speed (whirl frequency ratio, WFR). These impedance forces contain a component normal and transverse to the rotor displacement, obtained by integration of the static pressure and shear stress distribution around the rotor, and are curve-fitted to a linear, second order model to yield the seal's stiffness, damping, and mass force coefficients (K_{xx} , K_{xy} , C_{xx} , C_{xy} , M_{xx} , M_{xy}).

CFD Code Description

The CFD code, SCISEAL, is utilized in this study and was developed by CFD Research Corporation under a grant from NASA Lewis Research Center. The code solves the 3D Reynolds averaged Navier-Stokes equations (see equations below) for both rotating and stationary frames of reference, using cylindrical, body fitted, structured grids of multi-domains. Both compressible and incompressible flow fields may be modeled using the latest turbulence models (standard k- ϵ , low Reynolds no. k- ϵ , Baldwin-Lomax, and two-layer k- ϵ). Law of the wall formulations model the sharp velocity gradients near the wall and are used with all turbulence models with the exception of the low Reynolds number model. The two-layer model is employed in this study, which models the turbulence diffusion near the wall (inner layer) using an algebraic expression, while the turbulence kinetic energy equation is applied in both the inner and outer layers. This model relaxes the requirement of maintaining the first node from the wall outside the laminar sublayer (ie. $y^+ > 11.5$), allowing more nodes to be placed in the tight seal land sections.

The code's generality allows modeling of all variety of seals types including plain annular, labyrinth, grooved, stepped, and even geometries of varying radius (ie. impeller shrouds, etc.). Assuming concentric, circular whirling, the impedance forces for varying whirl frequency ratios are calculated, as described above, yielding the rotordynamic force coefficients.

Literature Review

Traditional modeling techniques for annular seals utilize bulk-flow assumptions (see Black, 1969, and Childs, 1983). These models assume uniform velocity distributions for the steady analysis. Harmonic variations of the flow parameters are assumed around the circumference for the dynamic analysis and removes the circumferential (theta) dependence. Turbulence is handled using empirical wall shear stresses obtained from pipe flow studies including Hirs and Moody friction factor relationships, which are a function of the local Reynolds number. These methods are quite efficient, requiring only seconds of CPU time, and are accurate for plain annular seals. Modeling seals with separation and recirculations will usually result in poor predictions, however. Modification of the bulk-flow models for grooved seals has been done using multiple control volumes using a single vortex in the cavity with empirical shear stress

LIQUID ANNULAR SEAL CFD ANALYSIS FOR ROTORDYNAMIC FORCE PREDICTION

boundary conditions at the interface (Florjancic, 1990). Again, these techniques are efficient and accurate if "tuned" for a specific set of operating conditions using empirical data. As the operating conditions and geometry differ, typically so does the resulting predictions.

More recent techniques have utilized the rapidly maturing computational fluid dynamic analysis for modeling annular seals including Dietzen and Nordman (1986) Rhode, Hensel, and Guidry (1992), and Arghir and Frene (1997). All of these authors employ a coordinate transformation relation transforming the 3D equations of the eccentric rotor into 2D axisymmetric expressions. These techniques require a zeroth order solution and first order calculations at the different whirl frequency ratios. The procedure is efficient but the coordinate transformation is only valid for constant radius seal geometries, and the analysis ignore the variation of turbulence quantities around the circumference. Furthermore, only axisymmetric seal geometries may be modeled, preventing the modeling of swirl brakes for example. The 3D whirling method used in SCISEAL, developed by Athavale, et al. (1994), is more computationally intensive but is more general in the class of problems that may be solved.

Test Rig and Grooved Seal Description

This study focuses on a high pressure, seven-grooved liquid annular seal, which was tested by Marquette (1995) in the High Speed Seal Test Rig at Texas A & M University (see Figures 1 and 2). This seal was tested to speeds up to 24,600 rpm and pressures drops over 6 MPa (900 psid) and contains a shaft radius of 38.15 mm (1.5 in), clearance of 0.11 mm (4.3 mils), and an L/D of 0.457. The equally spaced grooves have dimensions 1.587 mm deep by 3.175 mm wide.

Results of CFD Analysis of Grooved Liquid Seal

The first approach taken was to model seal geometry and use "typical" boundary conditions at the inlet for the pressure loss factor ($P_{loss}=0.1$) and the inlet swirl ratio (ratio of fluid swirl to rotor surface speed, $W_{rat}=0.45$). Results are presented for four different grid densities, striving for a grid independent solution, and are summarized in Table 1. The Coarse Grid-1 refines the circumferential grid density, the Medium Grid refines the grid density in the seal groove, the Fine Grid-1 refines the grid in the seal land (tight clearance sections), and finally the Fine Grid-2 refines both the land and the groove. The medium grid requires about 1 minute per iteration on a SGI Indigo 2 (with R10000 64 bit MIPS processor, 195 MHz), while the Fine Grid-2 requires 2.2 minutes per iteration. Since SCISEAL utilizes an iterative solver, the time per iteration is proportional to the total node number. However, convergence rates are higher for the smaller models (less iterations required). The memory requirement is roughly the number of nodes in kilobytes (eg. Medium Grid requires about 100 megabytes of memory).

The velocity vectors in the seal cavity show a large, single vortex (Fig. 5) predicted using the medium grid. A close-up of the flow field entering the seal land is given in Fig. 6. Figure 7 shows a uniform static pressure drop through the seal. The transport equations for the turbulence kinetic energy (k) and the turbulence dissipation are solved simultaneously with the Navier-Stokes equations predicting large generation and dissipation of turbulence in the jet shear layer exiting the seal land and near the seal land entrance (Figs. 8-9). Accurate calculation of the Reynolds stresses at this jet/vortex interface is necessary to accurately predict the mean velocity profiles. The isotropic assumption of turbulence, assumed by the k - ϵ model, is well known not to exist in shear layers and is one of the sources of errors of the CFD calculation.

The circumferential variation of pressure displayed using an exaggerated mesh shows the effect whirl frequency ratio in Figures 10 and 11. Figure 10 shows a harmonic distribution of pressure fluctuating

LIQUID ANNULAR SEAL CFD ANALYSIS FOR ROTORDYNAMIC FORCE PREDICTION

from low to high while proceeding clockwise from the top. This statically eccentric seal (WFR=0.0) show similar characteristics as a plain journal bearing and creates a pressure field that both opposes displacement and pushes the rotor in the direction of whirl, creating positive direct and cross-coupled stiffness coefficients (K_{xx} and K_{xy}). This cross-section was taken in the first seal groove and changes somewhat through the length of the seal. At higher whirl frequency ratios (WFR=1.5), a nearly opposite pressure field emerges creating forces in the direction of displacement and whirl. This effect will become clear in the impedance force plots. Although ignored by some seal analysis techniques, the turbulent quantities do vary circumferentially for a whirling seal as shown in Figure 12.

At the entrance of the seal, a total pressure boundary condition is assumed allowing the axial velocity to naturally develop around the circumference as shown in Figure 13. This boundary condition captures the Lamakin effect, which is a source of positive stiffness. To capture the sudden loss of pressure due to the abrupt change in cross-section entering the seal, an inlet loss factor is assumed. The pressure drop is calculated by:

$$\Delta P = \frac{\rho}{2} \bar{U}^2 (\zeta + 1)$$

Typical values of ζ range from 0.1 and as high as 0.7 (Athavale, et al., 1994).

As previously mentioned, care must be taken when choosing the node distribution to maintain the first node a proper distance away from the wall. This distance is a function of the flow field, necessitating a post-check of the non-dimensional y^+ values. Figures 14 and 15 show the y^+ values on both the rotor and cavity walls to be well within the range of the law of the wall.

Figures 16 and 17 compare the convergence rates of two different mesh densities, the Coarse Grid-1 and the Medium Grid, respectively. The coarse grid, which is half the size of the medium grid, demonstrates twice the convergence rate. Since the time per iteration is proportional to the number of nodes, the total time to convergence for the coarse grid is about 25% of the medium grid's CPU time.

Force Coefficients of Analysis I

Table 2 compares the SCISEAL computation (using medium grid) of force coefficients and leakage with both experimental results as well as the 3-control volume (3-CV) prediction of Marquette (1995) for a speed of 10,200 rpm and a pressure drop of 4.14 MPa (600 psid). The experiment measures essentially no direct stiffness with a positive cross-coupled stiffness. The CFD analysis gives reasonable prediction and much improved stiffness prediction over the 3-CV results. Direct and cross-coupled damping, however, is under-predicted by the CFD analysis as is the inertia. The whirl frequency ratio (at neutral stability), which is a measure of the stability of the seal, shows good prediction between CFD and experiment. The CFD under predicts the leakage rate by about 10%. The impedance forces from six whirl frequency ratios (0.0, 0.25, 0.5, 0.75, 1.0, and 1.5) are used to calculate the force coefficients by curve-fitting the results to a second order polynomial using the following expressions:

LIQUID ANNULAR SEAL CFD ANALYSIS FOR ROTORDYNAMIC FORCE PREDICTION

$$\bar{F}_n = \frac{F_n}{\epsilon} = -K - c\omega + M\omega^2$$

$$\bar{F}_t = \frac{F_t}{\epsilon} = k - C\omega - m\omega^2$$

where, ϵ = eccentricity
 K, C, M = direct stiffness, damping, mass
 k, c, m = cross-coupled stiffness, damping, mass

The plot of impedance versus whirl speed shows a nice curve fit by the second order functions.

To evaluate the effect of rotor speed and pressure, the force coefficients are evaluated at 24,600 rpm and 6.20 MPa (900 psi) shown in Table 3. The direct stiffness is under predicted somewhat, but the CFD results show significantly improved prediction of cross-coupled stiffness compared to the 3-CV results. Again, the damping is under predicted resulting in an over-prediction of whirl frequency ratio at neutral stability. The over prediction of 60% is still a large improvement over the 1100% error of the 3-CV. The leakage is again under-predicted by about 11%, similar to the 3-CV. The 3-CV analysis contains many "knobs" which may be adjusted (ie. jet divergence angle and shear stress parameters) to yield reasonable prediction. Marquette (1995) used a negative jet divergence angle, selected by leakage comparison, indicating the vortex deflects the jet. The opposite is predicted by CFD as shown in Figure 6.

A mesh density study is performed to verify if the preceding results are grid independent solutions. Table 4 compares the stiffness and leakage predictions for the five different mesh densities (see Table 1 for definition of each). The cross-coupled stiffness shows strong sensitivity to the number of nodes used across the seal land comparing the Medium and Fine Grid-1, then changes little with further refinement. This study shows that a mesh density at least equal to the Fine Grid-1 is required for reasonable cross-coupled stiffness prediction and now over-predicts the experimental value. Good leakage prediction is accomplished with even the coarsest grid. Table 5 shows the damping and inertial coefficients to be less sensitive to mesh density (only values up to the medium grid are computed).

Force Coefficients of Analysis II

Since the prediction of cross-coupled stiffness is a strong function of the inlet swirl ratio ($Wrat$), an upstream, axisymmetric (2D) calculation is performed in order to better quantify the flow conditions entering the seal. The upstream geometry was obtained and coupled to the 2-D model of the grooved seal. However, when using the total pressure inlet boundary condition, convergence problems were encountered due to the flow recirculation (trying to exit the domain) as shown in Figure 18. This problem was alleviated by using an inlet boundary condition (velocity specified) yielding the desired mass flow. The same exit pressure boundary condition is used; therefore, total pressure drop across the seal is predicted rather than leakage. To simulate the radial inlet supply to this upstream cavity, the radial velocity is assumed to be equal to the axial velocity and is directed inwards ($V=-U$). This boundary condition smooths out the upstream flow field and causes a large vortex in the first domain as shown in Figure 19. The swirl velocity in this inlet region is accelerated by the Couette action of the rotor and

LIQUID ANNULAR SEAL CFD ANALYSIS FOR ROTORDYNAMIC FORCE PREDICTION

steadily increases as the flow approaches the first seal land shown in Figure 20 (10,200 rpm). The swirl velocity at 24,600 rpm is shown in Figure 21 and is normalized to the same ratio of rotor surface speed as Figure 20. This plot shows the swirl velocity to develop faster and causes an increase in the inlet swirl ratio (W_{rat}) at the seal entrance.

The static pressure distribution in both the upstream section and the first seal land is plotted in Figure 22. Some of the drop is due to the increase in velocity while the remainder is due to inertial and viscous total pressure losses. Using the inlet pressure drop (ΔP) and mean axial velocity, the inlet loss factor may be calculated. The values for inlet loss factor and swirl ratio are summarized below:

Speed (rpm)	ζ	W_{rat}
10200	0.63	0.28
24600	0.7	0.36

These values were used in the total pressure boundary condition with the Fine Grid-1 mesh (without upstream region). Furthermore, the averaged values for k and ϵ were obtained from the 2D analysis and used in the 3D calculations as well. Figures 23 and 24 show how the axial and circumferential velocity distributions develop from the entrance to exit of the first seal land. Bulk flow is a reasonable assumption in this plain annular section. The axial and circumferential profiles in the center of the cavity resemble the bulk flow/pure vortex assumption used by the 3 control volume analysis. Table 6 compares the prediction of force coefficients and leakage with the experiment. The inlet swirl still appears to be under predicted indicated by the cross-coupled stiffness. The damping prediction has improved. The leakage is slightly less. The prediction at 24,600 under-predicts the direct stiffness prediction but much improved prediction of cross-coupled stiffness compared to the 3-CV method. The reason for CFD's under-prediction of the damping and inertia terms is unclear. Including the upstream fluid mass in the 3D calculation would perhaps improve the inertia prediction.

While this second analysis procedure did not yield as good as prediction as the first analysis, it is still the preferred technique in the absence of test data. The axisymmetric analysis may be obtained with low computational effort and eliminates much of the question of boundary conditions.

Conclusion

The general purpose, 3D seal code SCISEAL is validated against test data for a high speed, high pressure grooved liquid annular seal. The calculated cross-coupled stiffness is a strong function of the inlet boundary condition (ie. inlet swirl). In the absence of quality test data, an axisymmetric analysis has provide the inlet boundary conditions used in the 3D analysis. However, the swirl entering the seal appears still to be under predicted. The k - ϵ turbulence model struggles with swirling type flows and may be one of the sources of error.

Future work includes validation of other speeds and pressures. In addition, comparisons between the performance of different turbulence models will be performed.

Acknowledgement

The authors would like to thank Dr. Mahesh Athavale at CFD Research Corp. for support and expertise in the use of SCISEAL. Thanks goes to NASA Lewis Research Center for providing the funding to develop SCISEAL under the Earth-to-Orbit Propulsion program.

REFERENCES

- Arghir, M., Frene, J., 1997, "Rotordynamic Coefficients of Circumferentially-Grooved Liquid Seals Using the Average Navier-Stokes Equations," *Journal of Tribology*, **119**, pp. 556-567.
- Athavale, M.M., Przekwas, A.J., Hendricks, R.C., Liang, A., 1994, "SCISEAL: A 3D CFD Code for Accurate Analysis of Fluid Flow and Forces in Seals," Advance ETO Propulsion Conference, May, 1994.
- Black, H., 1969, "Effects of Hydraulic Forces on Annular Pressure Seals on the Vibrations of Centrifugal Pump Rotors," *Journal of Mechanical Engineering Science*, **11** (2), pp. 206-203.
- Childs, D., 1983, "Dynamic Analysis of Turbulent Annular Seals Based on Hirs' Lubrication Equation," *Journal of Lubrication Technology*, **105**, pp. 437-444.
- Dietzen, F., and Nordmann, R., 1986, "Calculating Rotordynamic Coefficients of Seals by Finite Difference Techniques," Rotordynamic Instability Problems in High Performance Turbomachinery, NASA CP No. 3026, proceedings of a workshop held at Texas A & M University, pp. 197-210.
- Florjancic, S., 1990, "Annular Seals of High Energy Centrifugal Pumps: A New Theory and Full Scale Measurement of Rotordynamic Coefficients and Hydraulic Friction Factors," dissertation, Swiss Federal Institute of Technology, Zürich, Switzerland.
- Marquette, O.R., 1995, "Experimental vs. Theoretical Comparisons of the Static and Dynamic Characteristics of One Smooth and Two Grooved Liquid Annular Seals with L/D of 0.457," Turbomachinery Research Consortium Report, TL-SEAL-5-95, Texas A & M University.
- Rhode, D.L., Hensel, S.J., and Guidry, M.J., 1992, "Three-Dimensional Computations of Rotordynamic Force Distribution in a Labyrinth Seal," *Tribology Transactions*, Vol. 36, **3**, pp. 461-469.

INTRODUCTION

- **SCISEAL** (Athavale, et al., 1994)
 - Developed by CFD Research Corp. under NASA contract
 - General 3D CFD
 - Stationary/Rotating Frames of Reference
 - Cylindrical, Body Fitted, Structured Grid
 - Compressible / Incompressible
 - Advanced Turbulence Models
 - Multi-Domain
 - Fully Integrated to Pre/Post Processors (GEOM & VIEW)
- **Solution Procedure**
 - Integrates Pressure and Shear Stresses for each Whirl Frequency Ratio (WFR) of 3-D Eccentric Mesh
 - Coordinate System Attached to Whirling Rotor
 - Impedance Forces (Normal and Cross-coupled) Found for Multiple Whirl Speeds
 - Rotordynamic Force Coefficients Determined by Fitting 2nd Order Curvefit to Impedance Forces:

$$\bar{F}_n = \frac{F_n}{\epsilon} = -K - c\omega + M\omega^2$$

$$\bar{F}_t = \frac{F_t}{\epsilon} = k - C\omega - m\omega^2$$

where, ϵ = eccentricity
 K, C, M = direct stiffness, damping, mass
 k, c, m = cross-coupled stiffness, damping, mass

THEORY

- **Reynolds Averaged Navier-Stokes Equations:**

$$U_j \frac{\partial U_i}{\partial x_j} = \frac{1}{\rho} \left(-P \delta_{ij} + 2 \mu S_{ij} - \overline{\rho u_i u_j} \right)$$

- **Eddy Viscosity Concept**

$$-\overline{\rho u_i u_j} = \mu_t \left(\frac{\partial U_i}{\partial x_j} + \frac{\partial U_j}{\partial x_i} - \frac{2}{3} \frac{\partial U_m}{\partial x_m} \delta_{ij} \right) - \frac{2}{3} \rho k \delta_{ij}$$

$$\mu_t = \rho C_\mu \frac{k^2}{\epsilon}$$

$$k = \frac{1}{2} \overline{u_k u_k}$$

- **k-ε Turbulence Model**

$$\frac{\partial k}{\partial t} + U_i \frac{\partial k}{\partial x_i} = \frac{\partial}{\partial x_i} \left(\frac{v_i}{\sigma_k} \frac{\partial k}{\partial x_i} \right) + P + G - \epsilon$$

$$\frac{\partial \epsilon}{\partial t} + U_i \frac{\partial \epsilon}{\partial x_i} = \frac{\partial}{\partial x_i} \left(\frac{v_i}{\sigma_\epsilon} \frac{\partial \epsilon}{\partial x_i} \right) + C_{1\epsilon} \frac{\epsilon}{k} (P + G) (1 + C_{3\epsilon} R_f) - C_{2\epsilon} \frac{\epsilon^2}{k}$$

- **Log Law of the Wall**

$$u^+ = y^+ \quad \text{for } y^+ < 11.5$$

$$u^+ = \frac{u_\tau}{K} \ln(E y^+) \quad \text{for } y^+ > 11.5$$

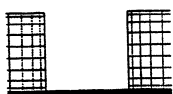
- 2-Layer Turbulence Model Used
(Std. k-ε, w/ inner layer algebraic expression for ε)

OTHER SEAL ANALYSIS TECHNIQUES

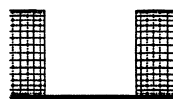
- **Bulk-Flow Techniques**
 - Assume Uniform Velocity Distributions for Steady Analysis
 - Assumes Harmonic Variation of Flow Variables in Circumferential Direction for Dynamic Analysis
 - Uses Empirical Turbulent Wall Shear Stress Relations (Blasius, Moody)
 - Efficient Solution
 - Accurate for Plain Annular Seals
 - Poor in Presence of Recirculations (labyrinth, grooved seals)
 - Black (1969), Childs (1983)
- **3 Control-Volume Technique**
 - Couples Two Bulk Flow and a Single Vortex CV's
 - Empirical Jet Shear Stress at Interface
 - Reasonable Prediction for Square Groove Cavities
 - Florjancic (1990), Marquette (1995)
- **OTHER CFD TECHNIQUES**
 - Solve Dynamic Flow Field Using Coordinate Trans.
 - Casts Eccentric Rotor into 2D Axisymmetric Coord. System
 - Dietzen and Nordman (1986), Arghir and Frene (1997)
 - Efficient, But Does Not Capture Variation of k and ϵ Around Circumference
 - Cannot Model Non-Axisym. Geometries (ie. Swirl Breaks)

Mesh Density Description for Grooved Liquid Seal

	Land	Groove	Circum.	# Nodes
Coarse Grid-2	9 X 7	15 X 17	21	45864
Coarse Grid-1	9 X 7	15 X 17	31	67704
Medium Grid	9 X 7	25 X 23	31	140399
Fine Grid-1	9 X 11	25 X 27	31	176452
Fine Grid-2	15 X 15	30 X 39	31	309690



Coarse Grid 1 & 2



Medium Grid



Fine Grid-1



Fine Grid-2

Table 1 Mesh Density Description for Grooved Liquid Seal

Force Coefficients for Grooved Liquid Seal

10,200 rpm, 4.14 MPa, Medium Grid, $W_{rat}=0.45$, $P_{loss}=0.1$

	Computation	Experiment	3 Control Vol.
K_{xx}/K_{yy} (KN/m)	19.9	-5	-130
$K_{xy}/-K_{yx}$ (KN/m)	421	740	99.8
C_{xx}/C_{yy} (KN-s/m)	2.45	4.81	4.59
$C_{xy}/-C_{yx}$ (KN-s/m)	1.57	3.63	3.16
M_{xx}/M_{yy} (kg)	1.43	5.19	3.59
$M_{xy}/-M_{yx}$ (kg)	0.46	-	-
WFR ($K_{xy} / C_{xx} w$)	0.16	0.14	0.02
Leakage (l/s)	0.72	0.82	0.82

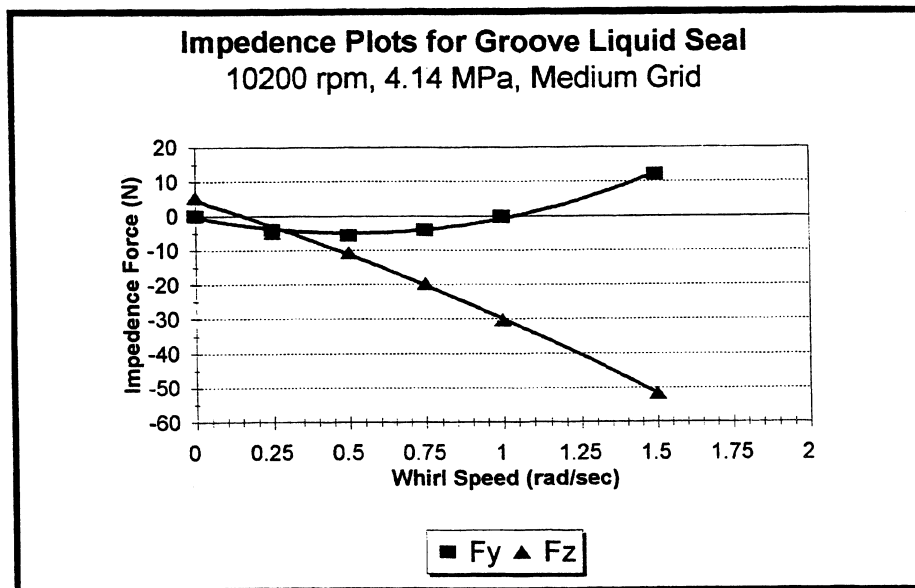


Table 2 Force Coefficients - Medium Grid, 10200 rpm, $W_{rat}=0.45$, $P_{loss}=0.1$

Force Coefficients for Grooved Liquid Seal

24,600 rpm, 6.20 MPa, Medium Grid, $W_{rat}=0.45$, $P_{loss}=0.1$

	Computation	Experiment	3 Control Vol.
K_{xx}/K_{yy} (KN/m)	-949	-2490	-3560
$K_{xy}/-K_{yx}$ (KN/m)	3740	3790	350
C_{xx}/C_{yy} (KN-s/m)	3.99	6.78	6.96
$C_{xy}/-C_{yx}$ (KN-s/m)	2.83	8.84	7.21
M_{xx}/M_{yy} (kg)	1.18	5.14	3.22
$M_{xy}/-M_{yx}$ (kg)	0.30	-	-
WFR ($K_{xy} / C_{xx} w$)	0.36	0.22	0.02
Leakage (l/s)	0.82	0.97	0.897

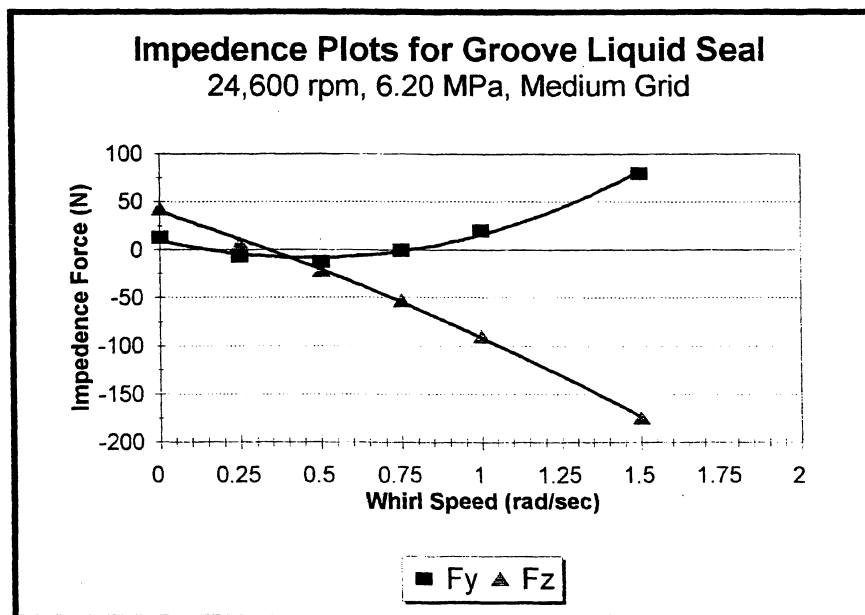


Table 3 Force Coefficients - Medium Grid, 24600 rpm, $W_{rat}=0.45$, $P_{loss}=0.1$

Mesh Density Study for Grooved Liquid Seal

10,200 rpm, 4.14 MPa, $W_{rat}=0.45$, $P_{loss}=0.1$

	K_{xx}/K_{yy}	$K_{xy}/-K_{yx}$	Leakage	# Nodes
Coarse Grid-2	302	564	0.73	45864
Coarse Grid-1	176	528	0.74	67704
Medium Grid	19.9	421	0.72	140399
Fine Grid-1	5.69	1026	0.72	171027
Fine Grid-2	174	981	0.71	309690
Experiment	-5.00	740	0.82	

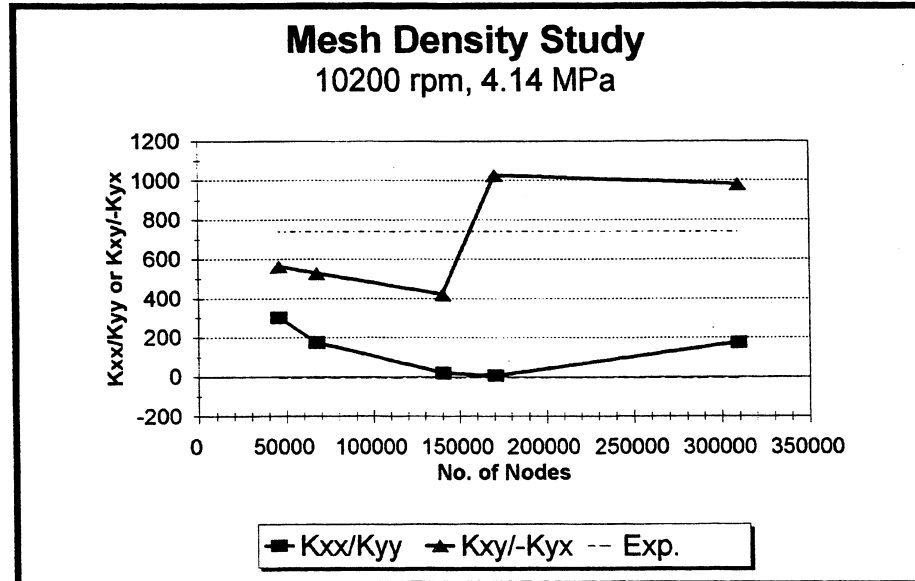


Table 4 Mesh Density Study - Stiffness Coefficients and Leakage
10200 rpm, $W_{rat}=0.45$, $P_{loss}=0.1$

Mesh Density Study for Grooved Liquid Seal

10,200 rpm, 4.14 MPa, $W_{rat}=0.45$, $P_{loss}=0.1$

	C_{xx}/C_{yy}	$C_{xy}/-C_{yx}$	M_{xx}	# Nodes
Coarse Grid-2	2.68	1.28	1.08	45864
Coarse Grid-1	2.6	1.61	1.49	67704
Medium Grid	2.45	1.57	1.43	140399
Experiment	4.81	3.63	5.19	

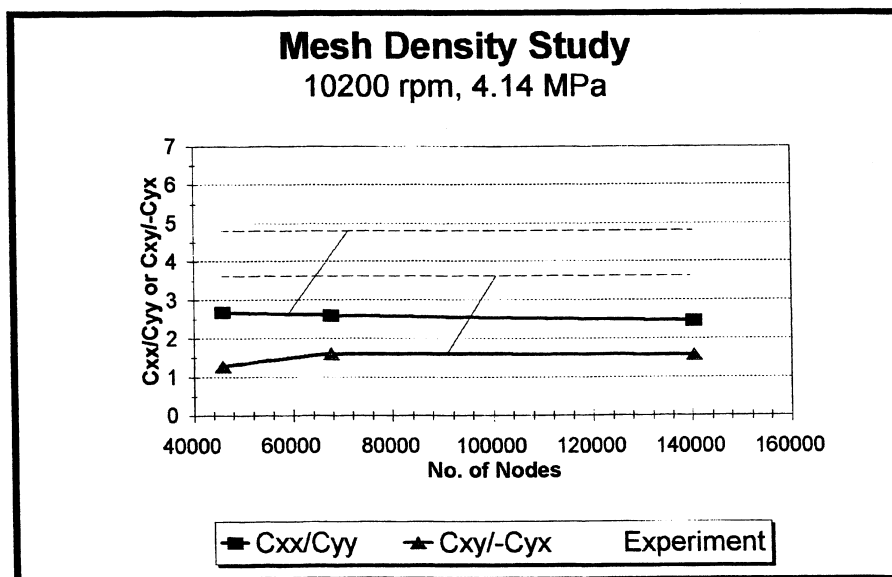


Table 5 Mesh Density Study - Damping and Inertia Coefficients
10200 rpm, $W_{rat}=0.45$, $P_{loss}=0.1$

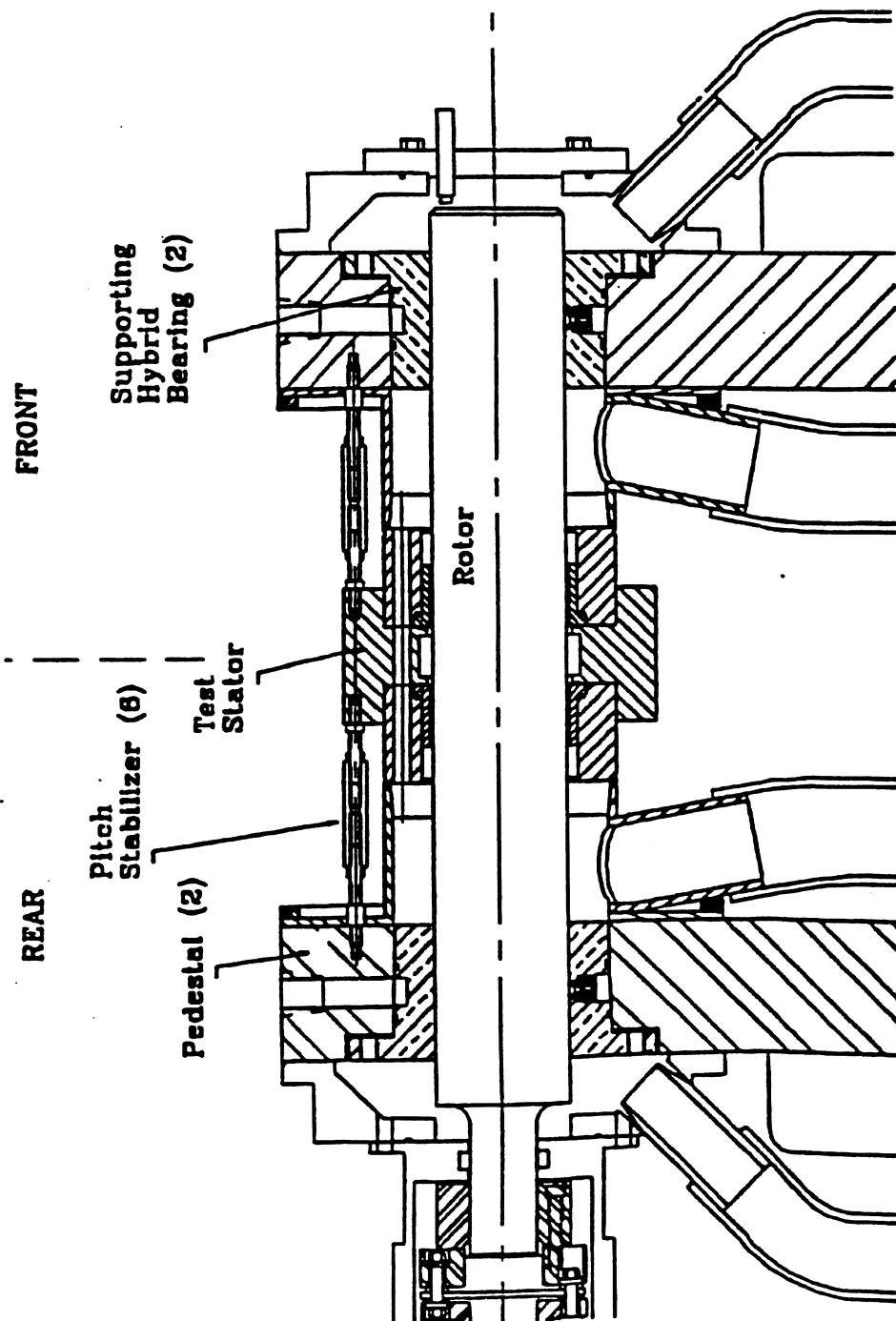


Figure 1 High Speed Seal Test Rig
(Courtesy of Marquette and Childs, 1995)

Fine Grid, 11 x 9 land, 27 x 25 groove

Rshaft = 38.15 mm, Clear.=0.11 mm

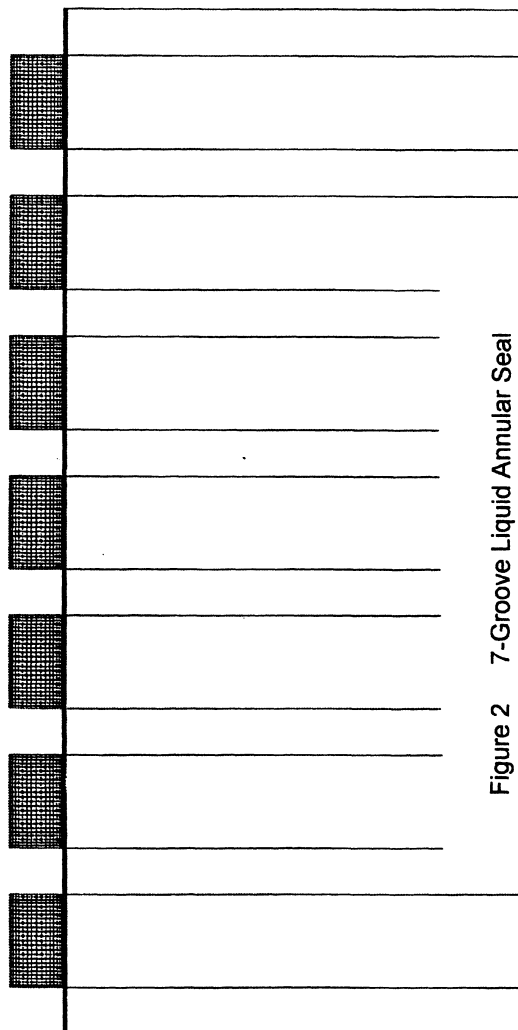


Figure 2 7-Groove Liquid Annular Seal

Fine Grid. 11 x 9 land. 27 x 25 groove

Rshoft = 38.15 mm. Clear.=0.11 mm

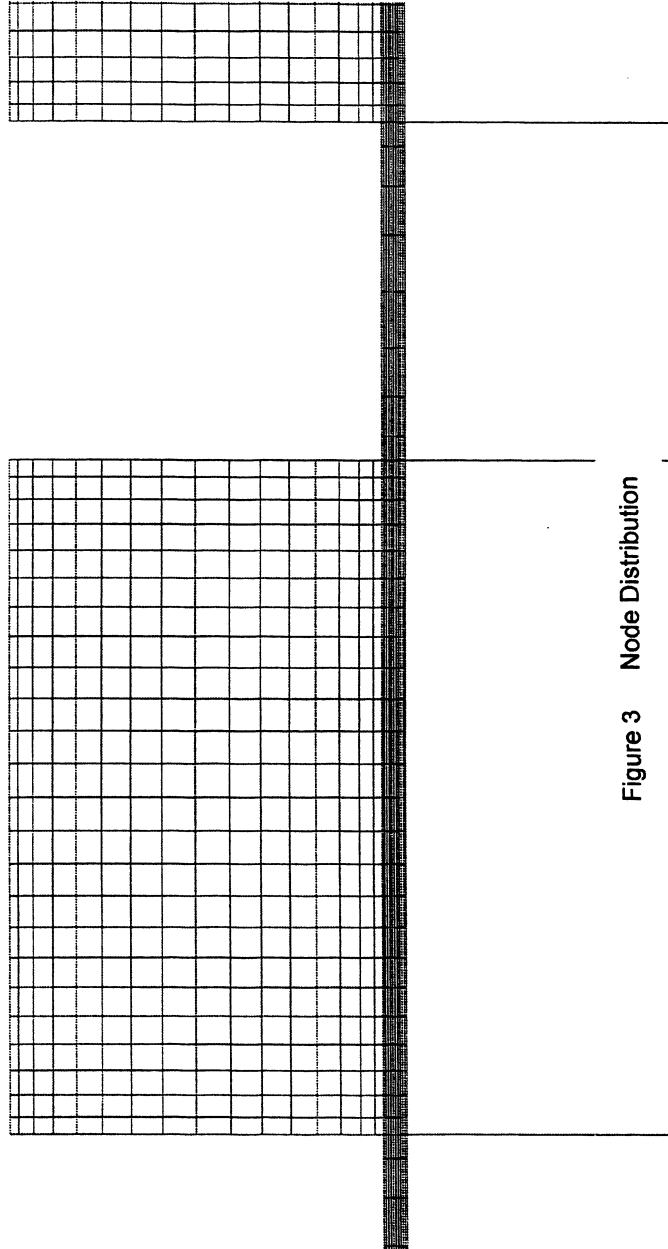


Figure 3 Node Distribution

CIRCUMFERENTIAL VELOCITY DISTRIBUTION

IN SEAL GROOVE, 10200 RPM, $\Delta P=4.18$ MPa

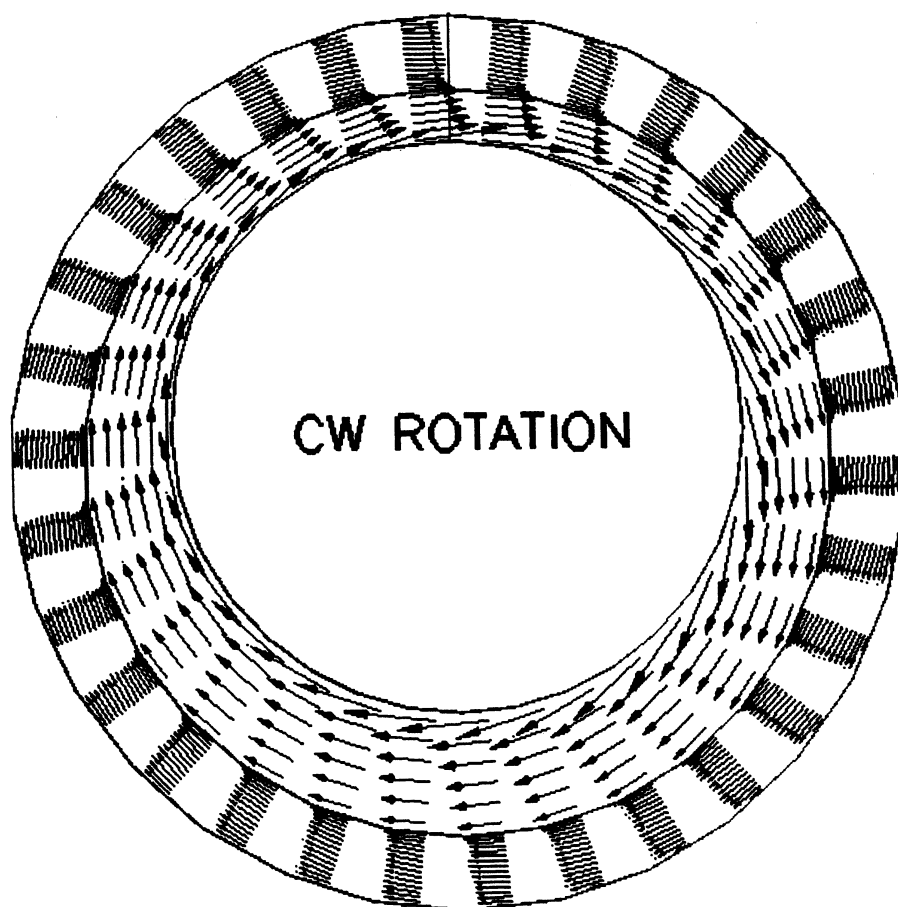


Figure 4 Circumferential Velocity Distribution

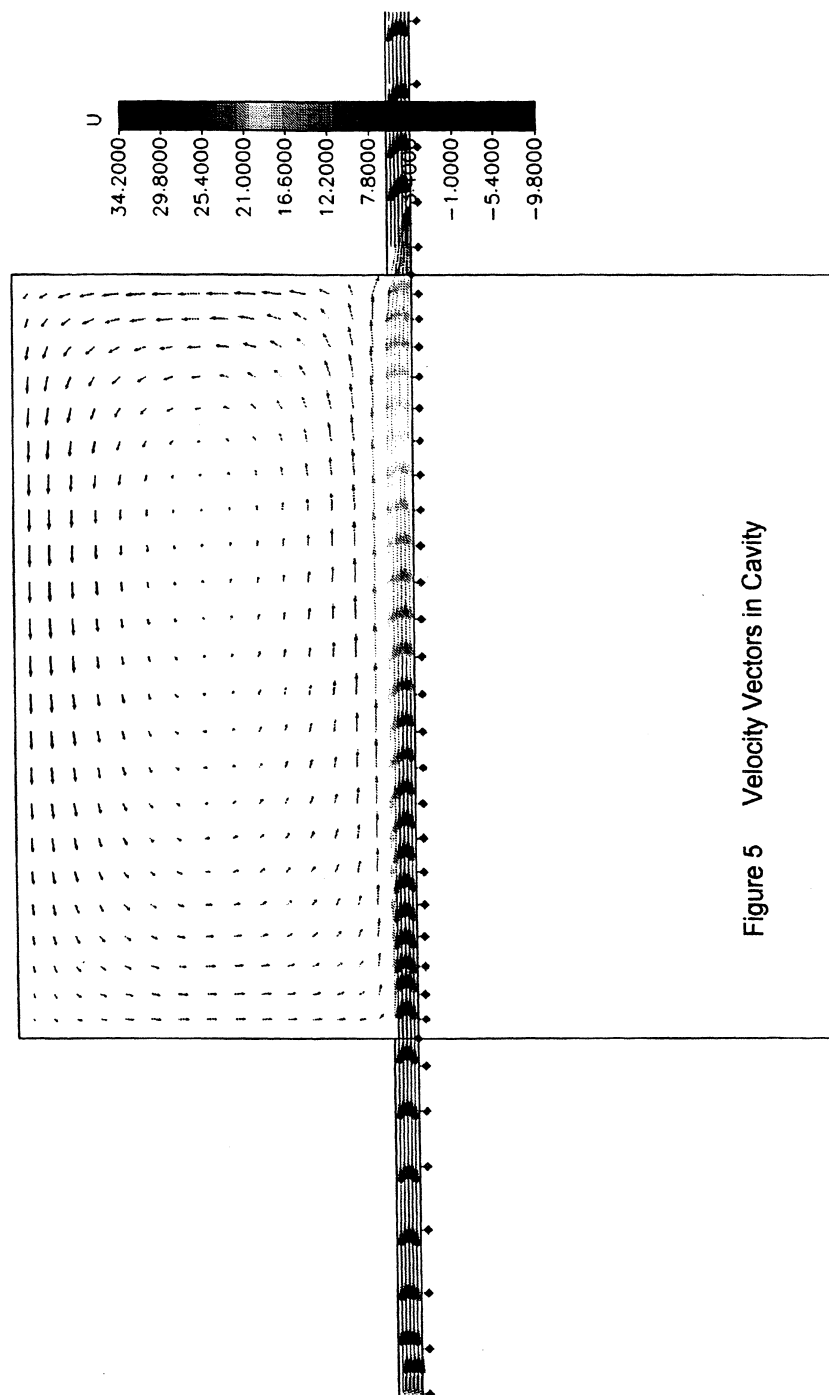


Figure 5 Velocity Vectors in Cavity

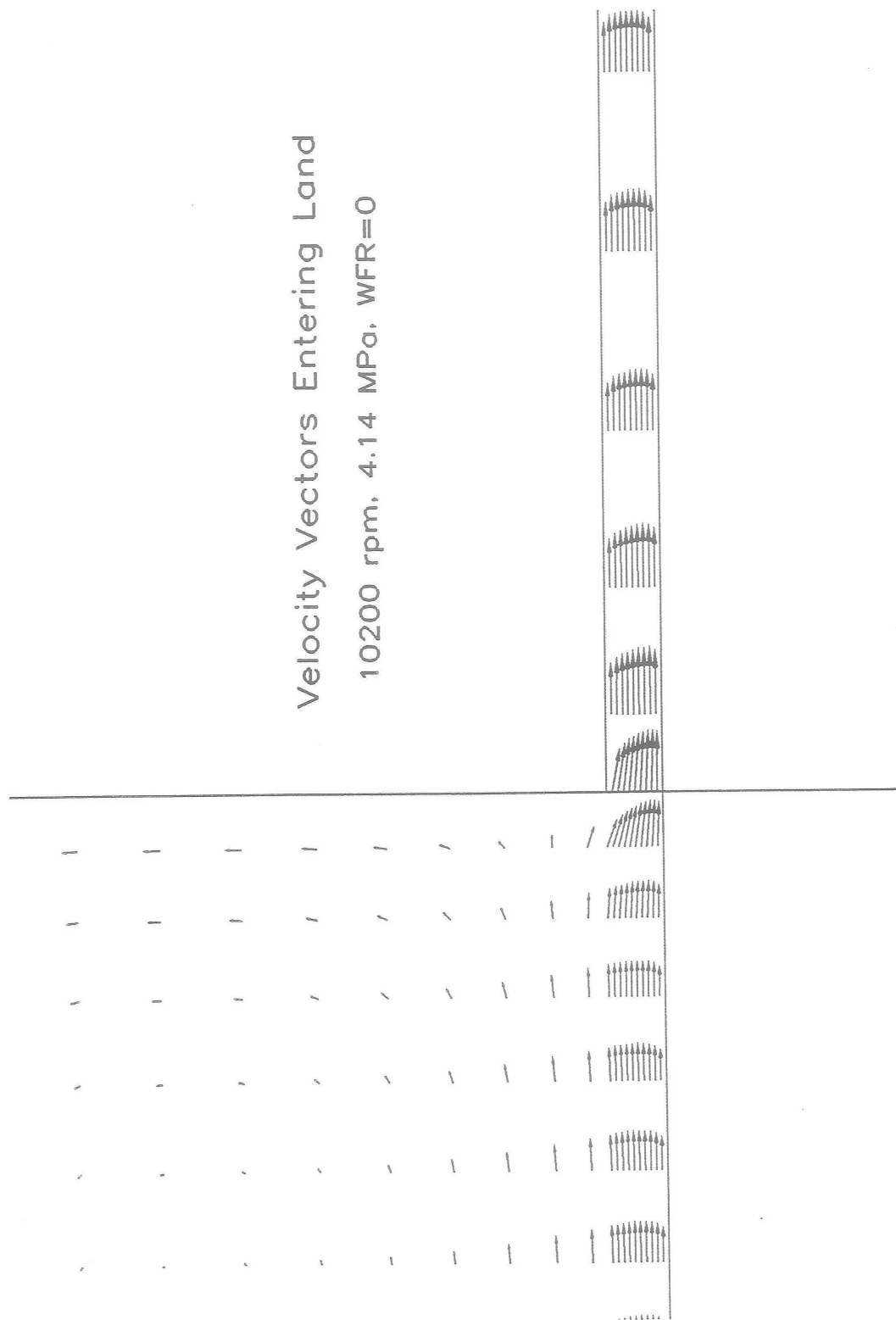


Figure 6 Velocity Vectors Entering Seal Land



Figure 7 Static Pressure Drop Through Seal

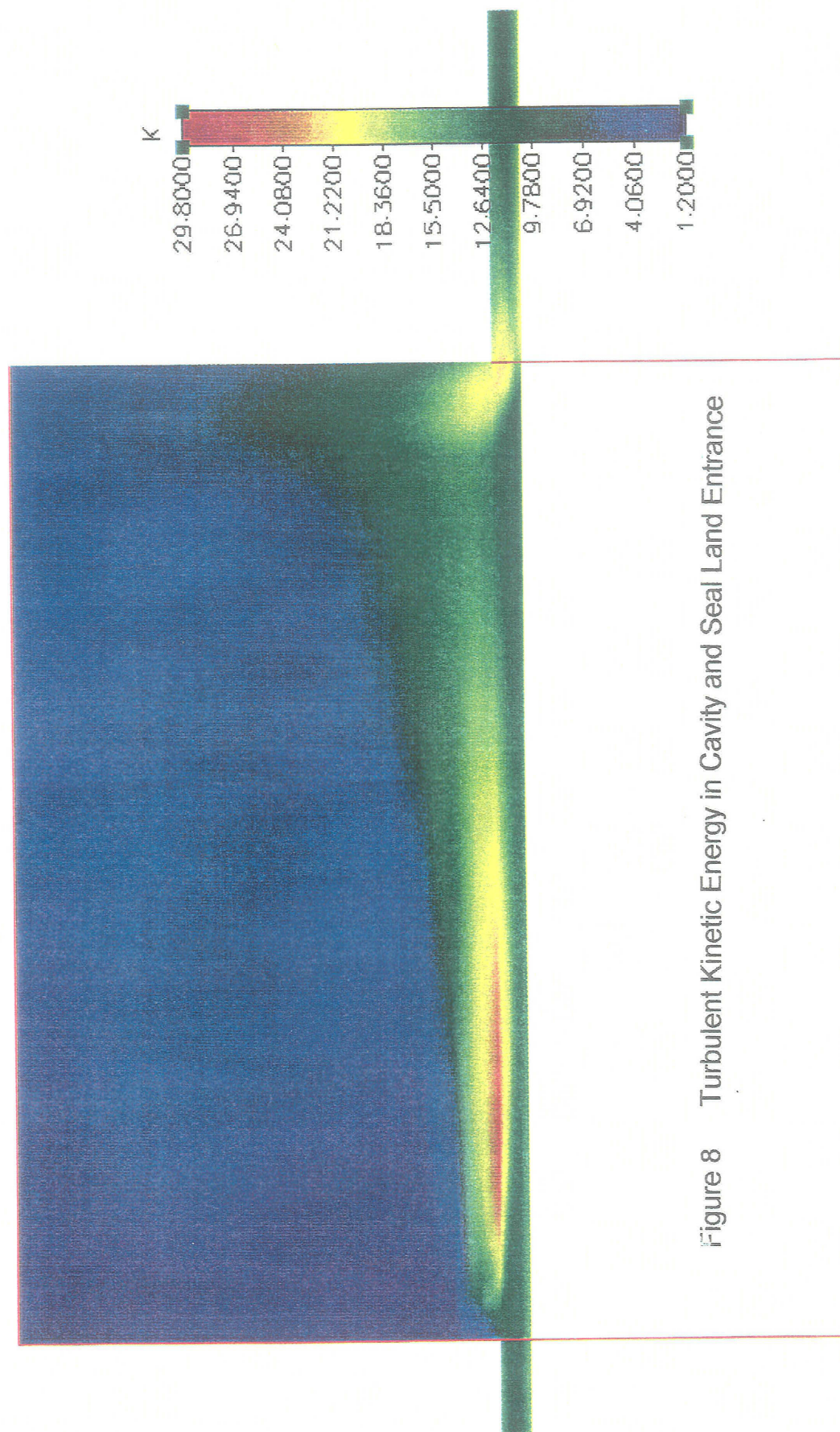


Figure 8 Turbulent Kinetic Energy in Cavity and Seal Land Entrance

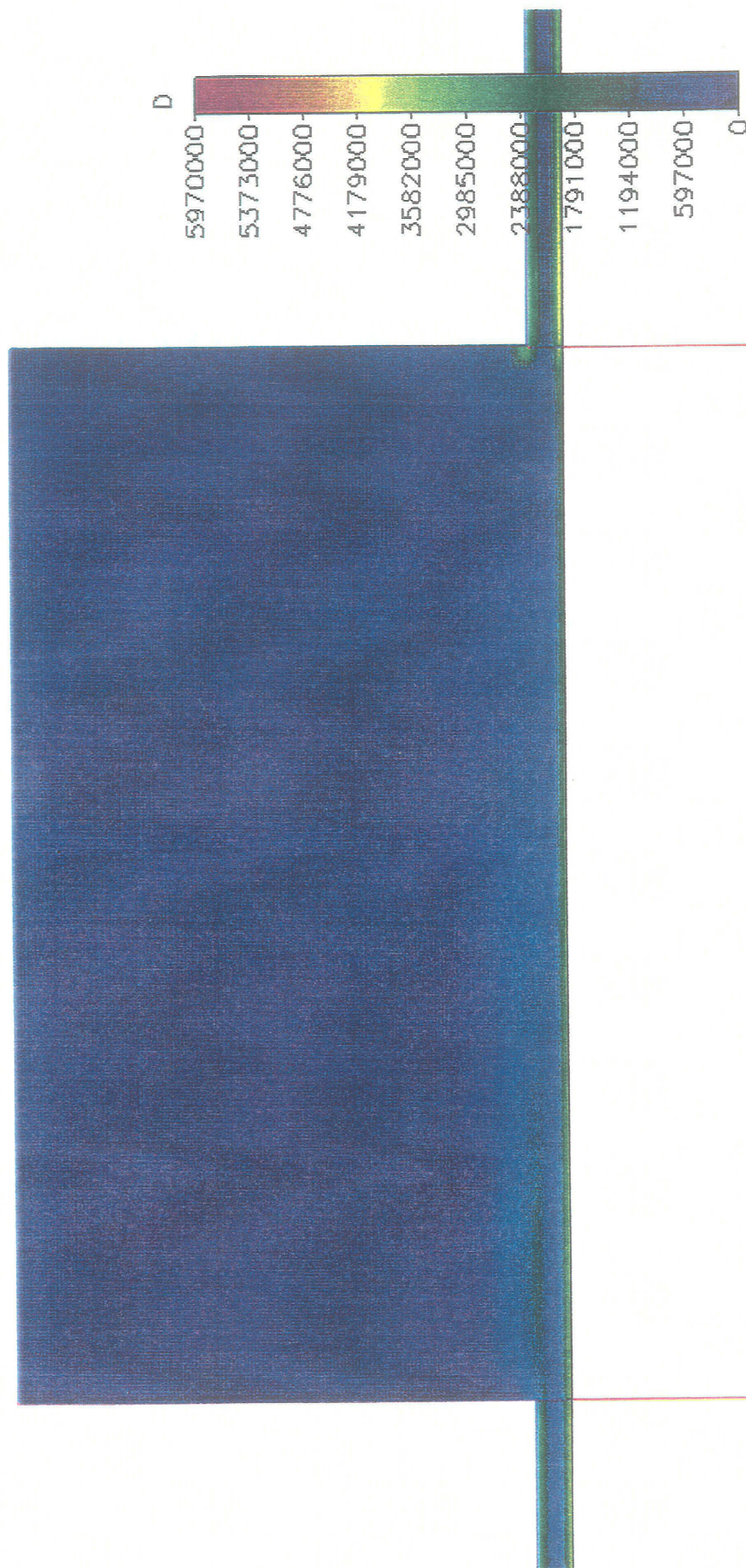


Figure 9 Turbulent Dissipation in Cavity and Seal Land Entrance

CIRCUMFERENTIAL PRESSURE DISTRIBUTION

IN SEAL GROOVE, 10200 RPM, $\Delta P=4.18$ MPa

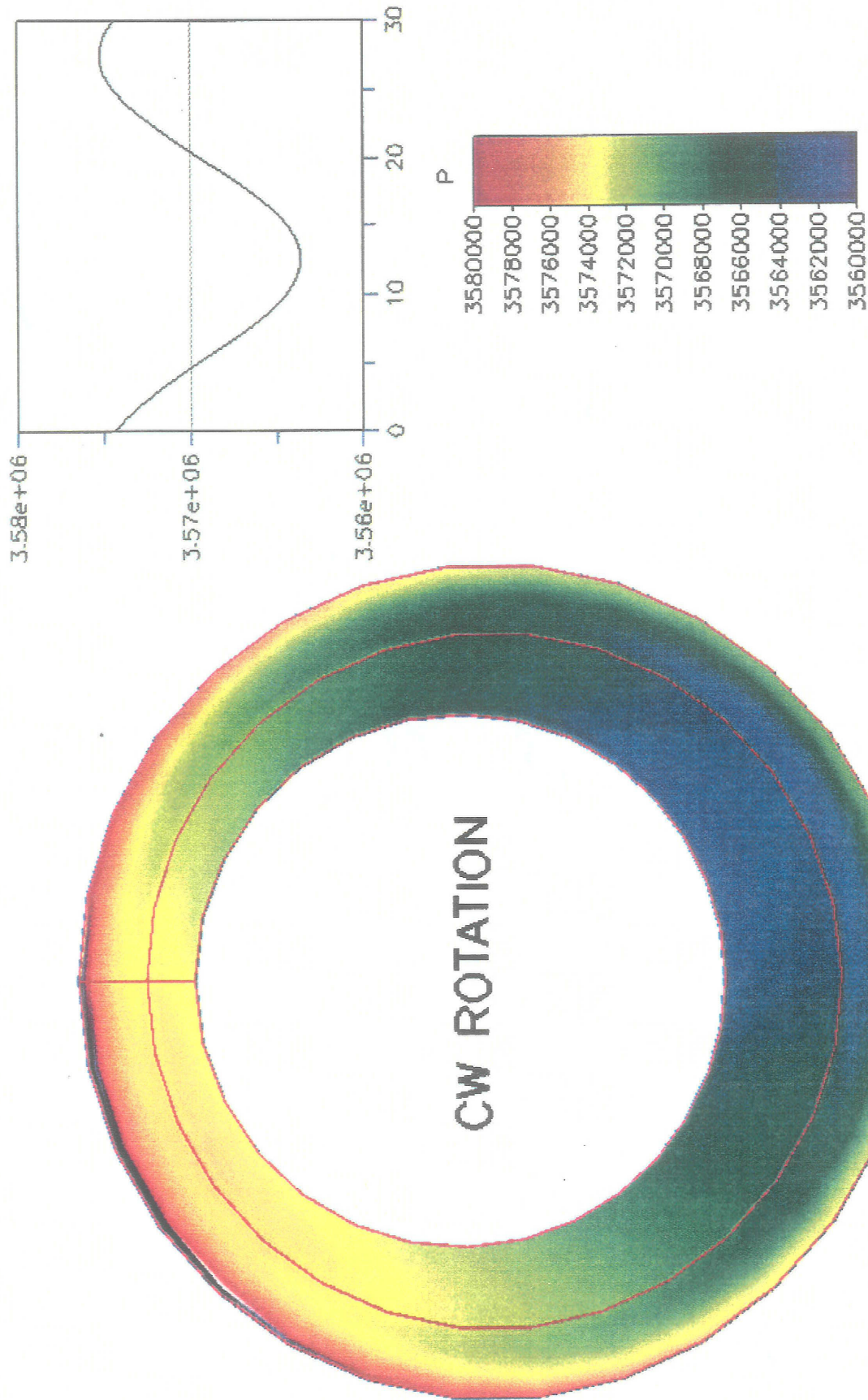


Figure 10 Circumferential Pressure Distribution, WFR=0.0

CIRCUMFERENTIAL PRESSURE DISTRIBUTION

IN SEAL GROOVE, 24600 RPM, $\Delta P=6.89$ MPa, WFR=1.5

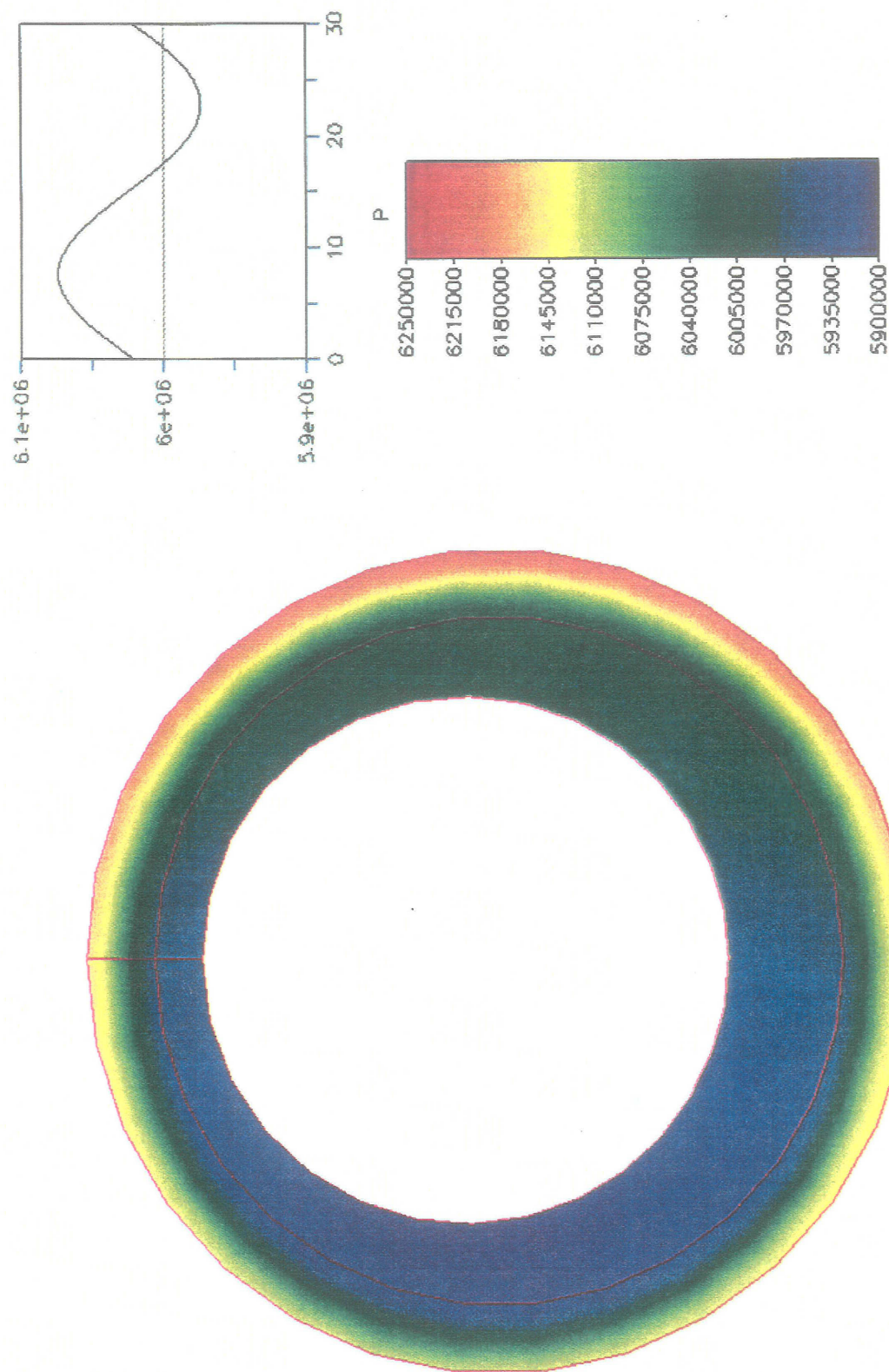


Figure 11 Circumferential Pressure Distribution, WFR=1.5

CIRCUMFERENTIAL TURB. KIN. ENERGY DISTRIBUTION

IN SEAL GROOVE. 10200 RPM. $\Delta P=4.18$ MPa

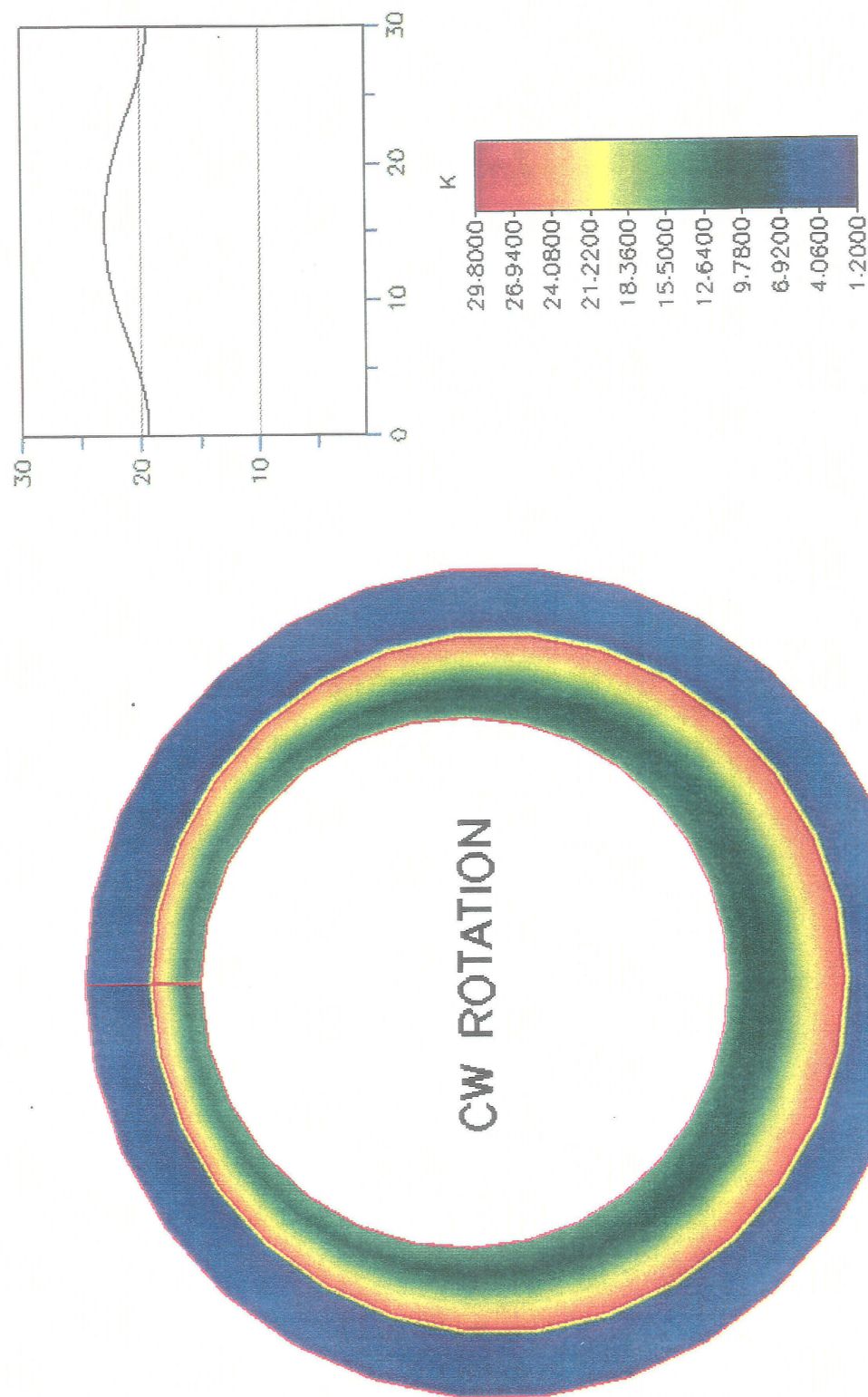


Figure 12 Circumferential Turbulent Kinetic Energy Distribution

VELOCITY AND PRESS. DISTRIBUTION AT ENTRANCE

IN SEAL GROOVE. 10200 RPM. $\Delta P=4.18$ MPa

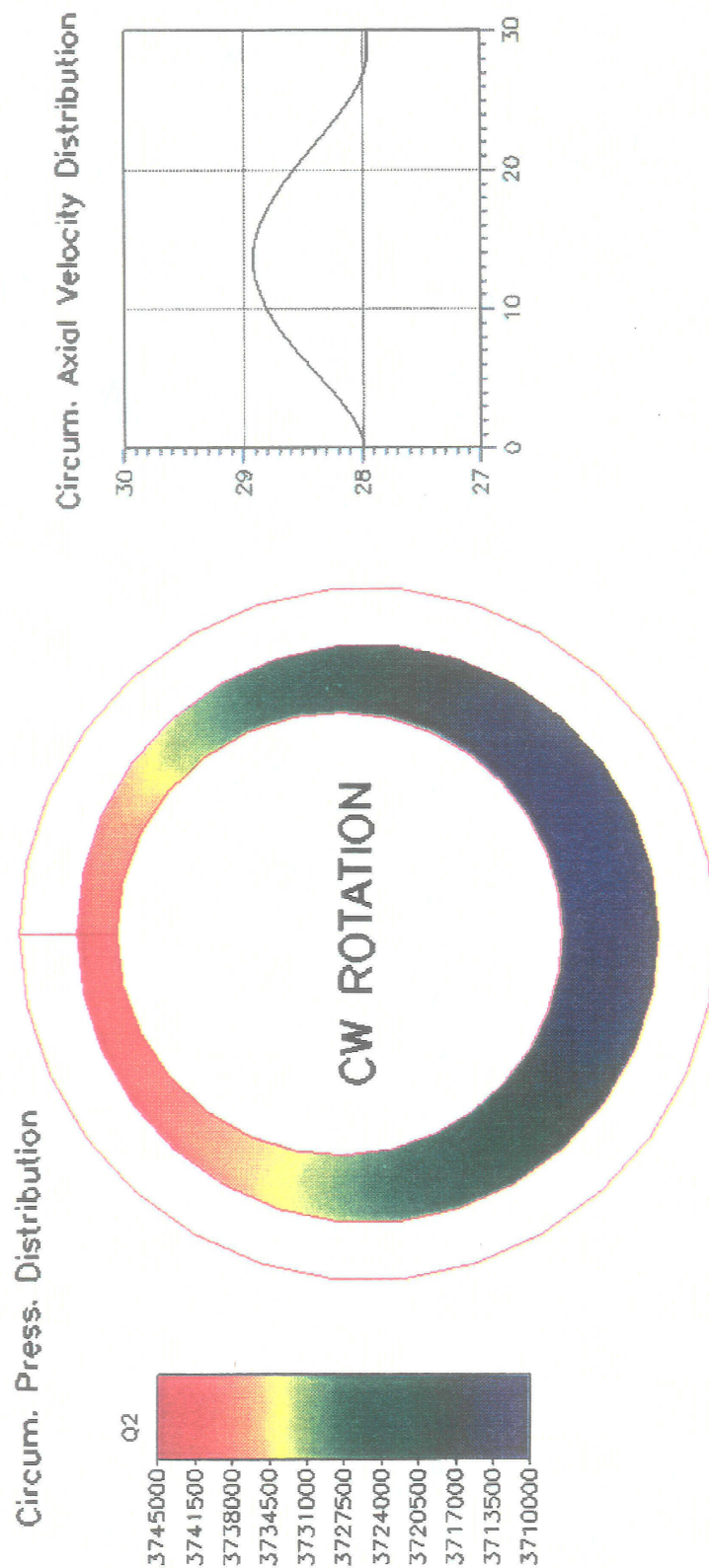


Figure 13 Velocity and Static Pressure Distribution at Entrance (Total-P BC)

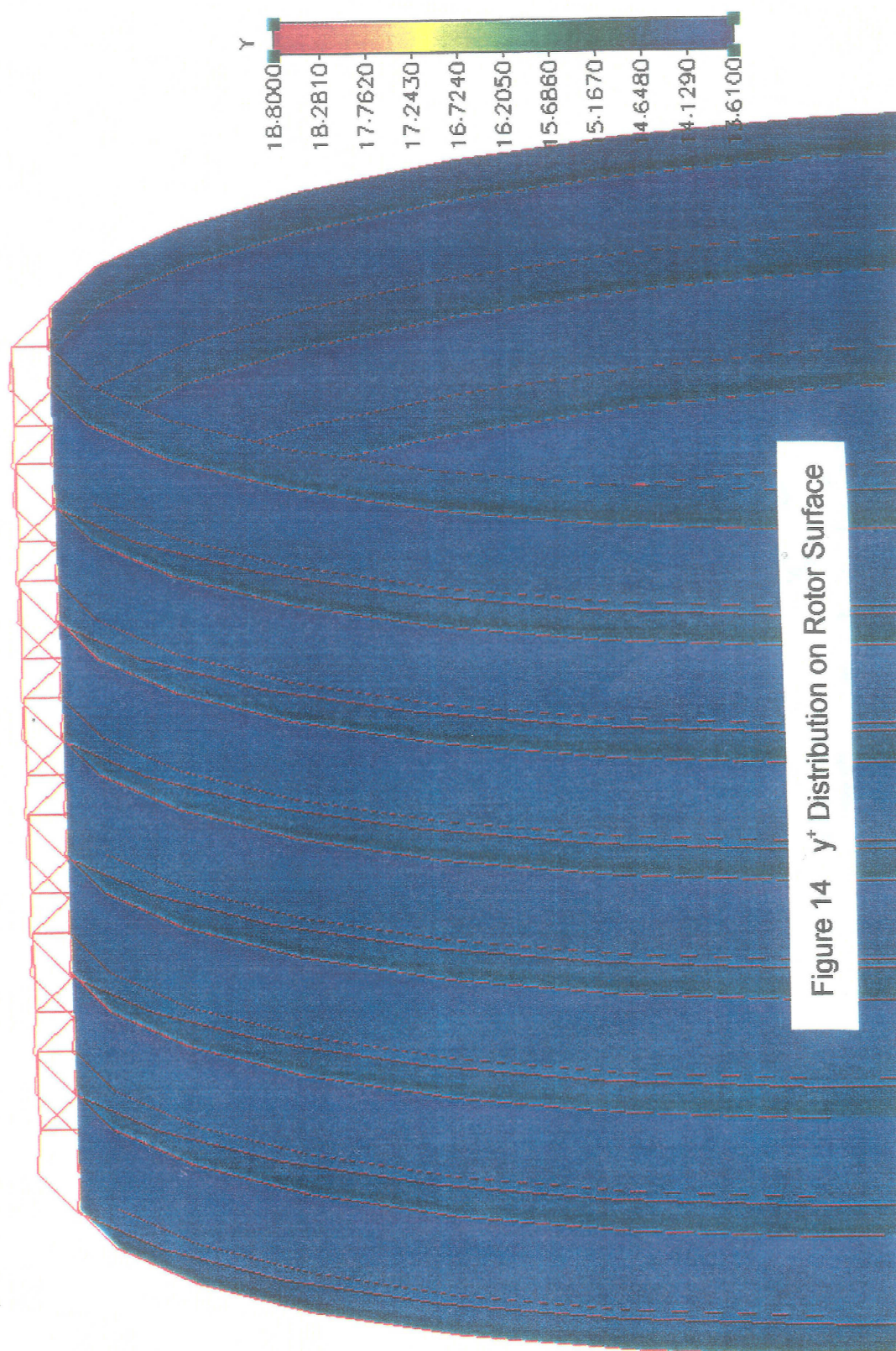


Figure 14 y^+ Distribution on Rotor Surface

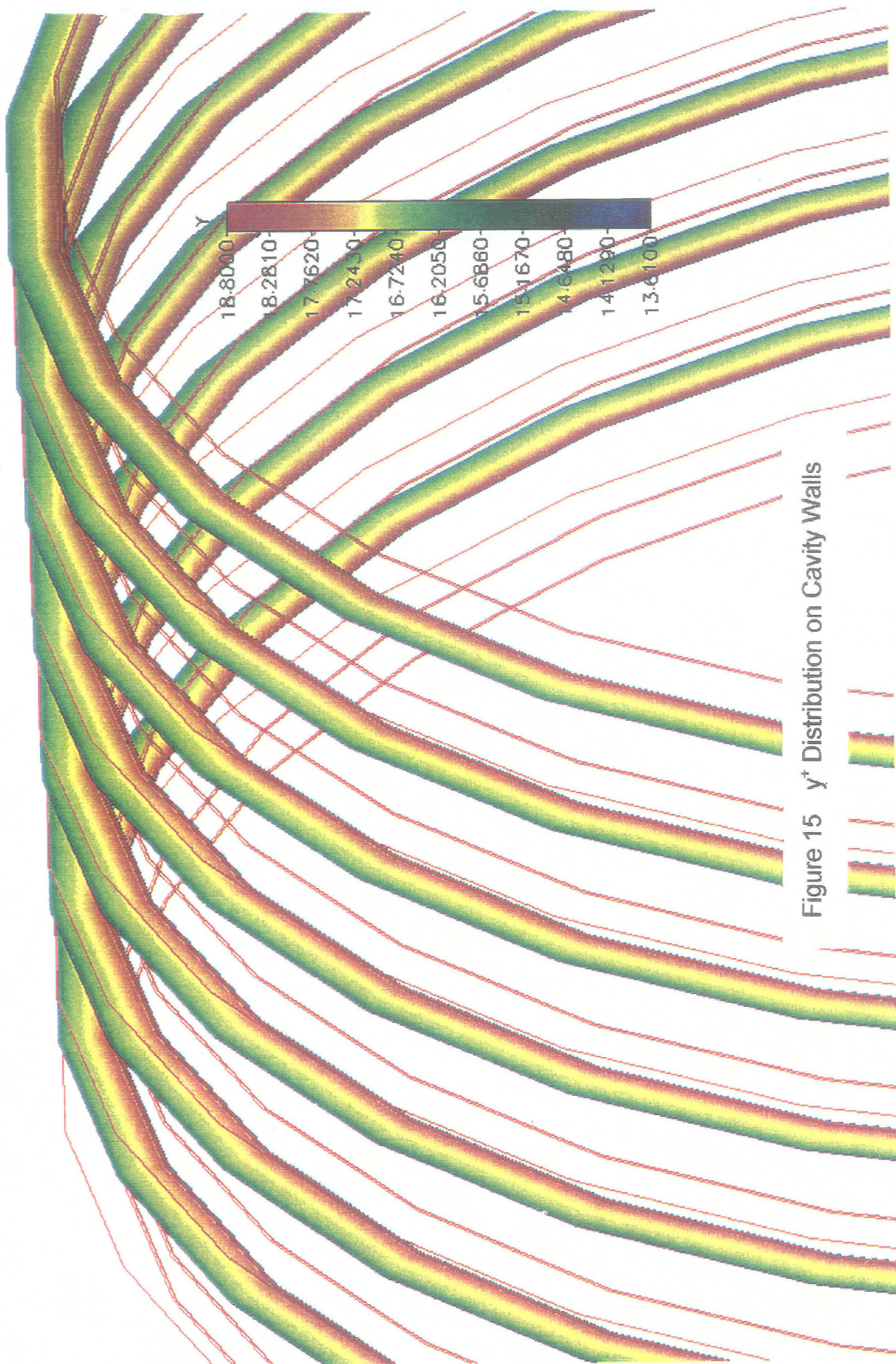


Figure 15 y^+ Distribution on Cavity Walls

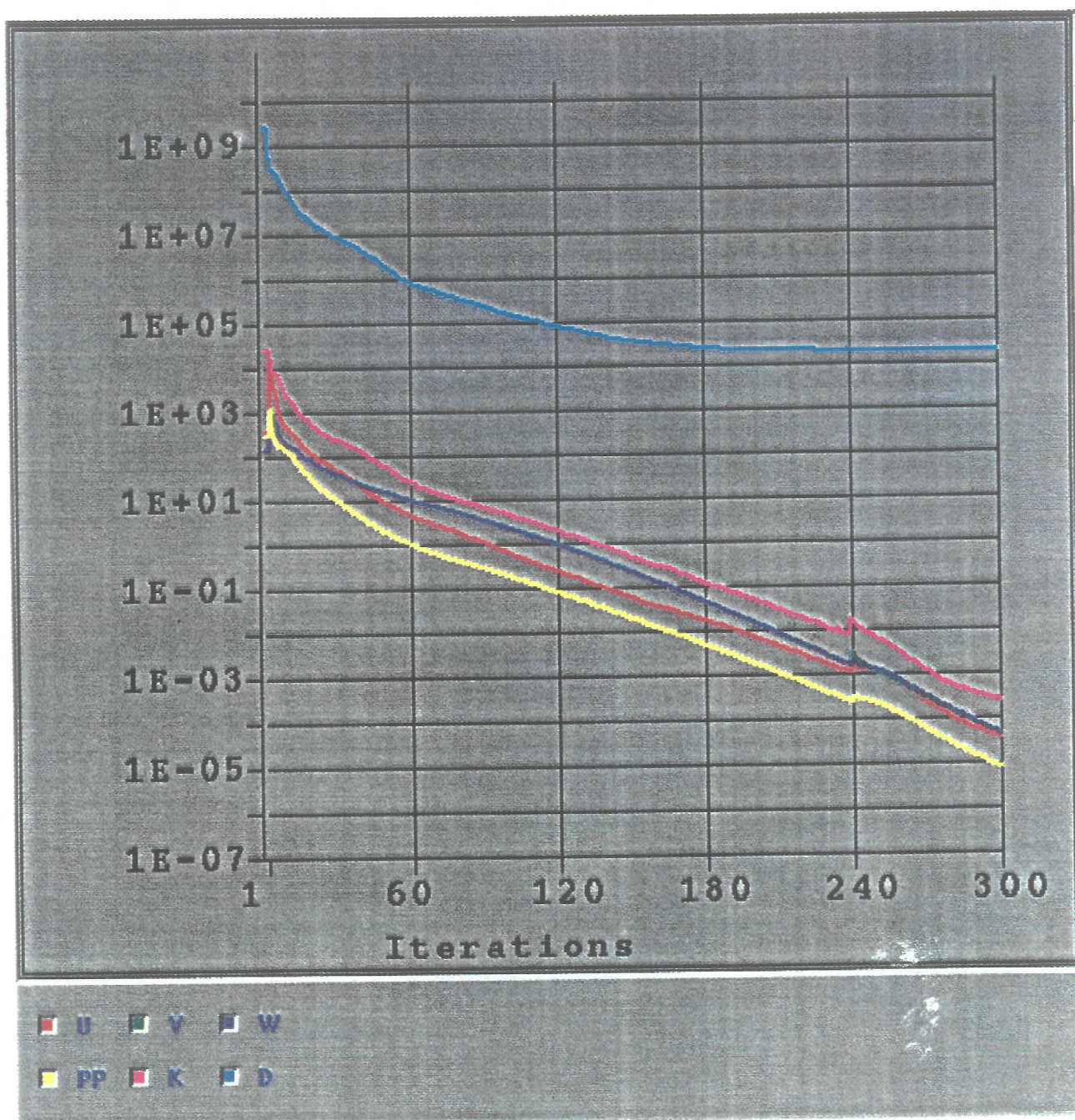


Figure 16 Residual Decay - Coarse Grid-1

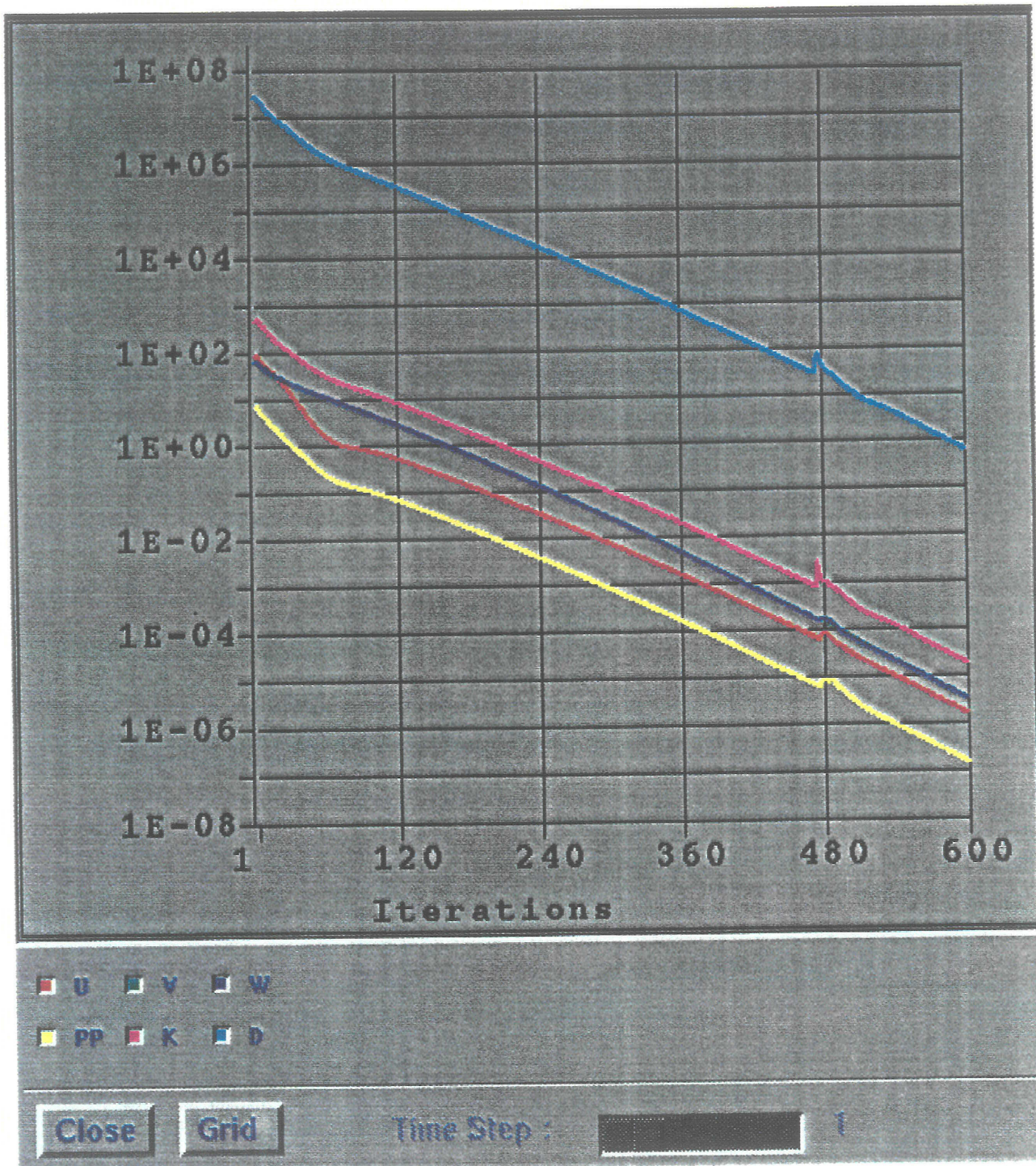


Figure 17 Residual Decay - Medium Grid

Upstream Model w/ Axial Inflow

10200 rpm, 4.14 MPa

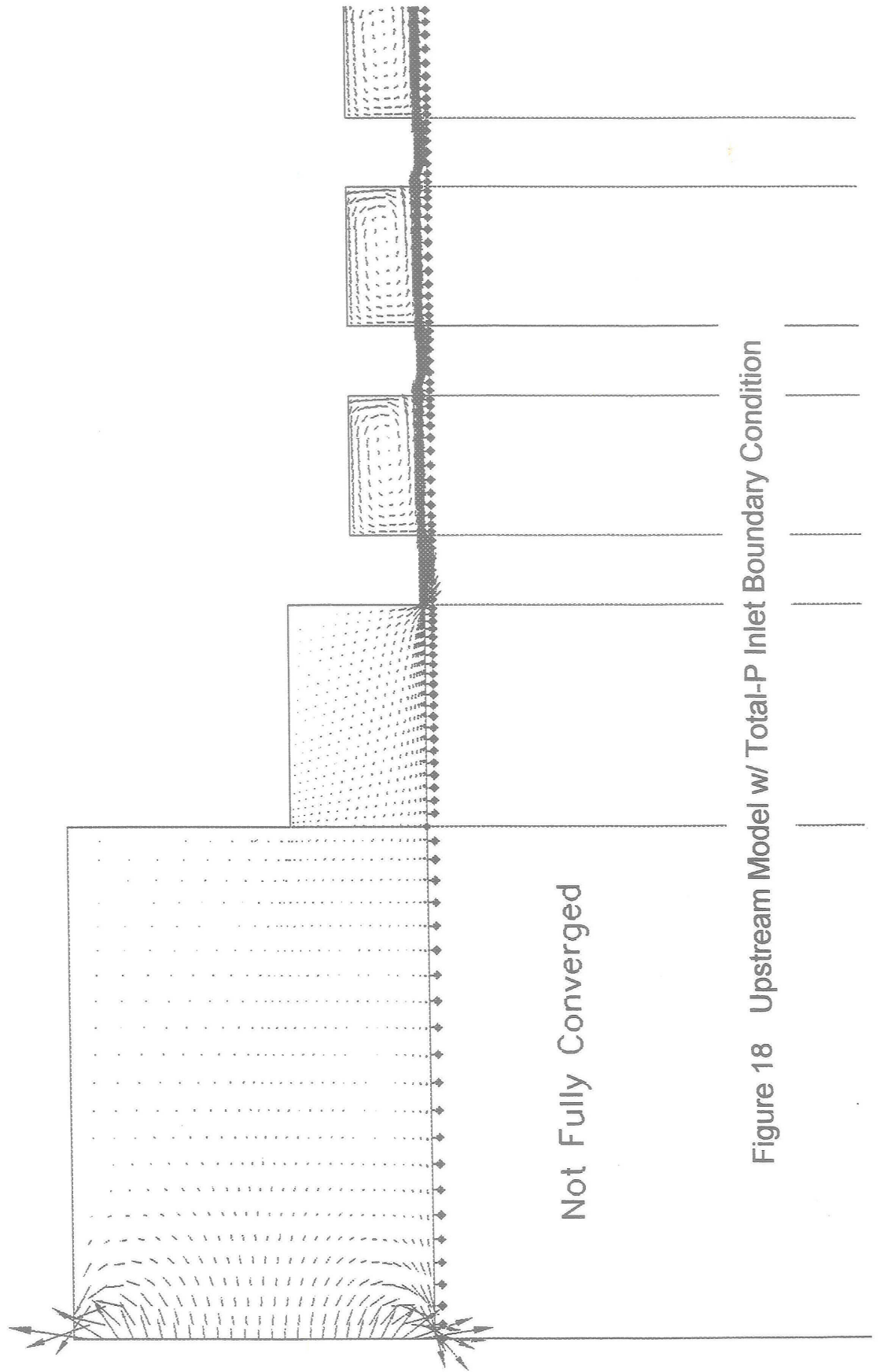


Figure 18 Upstream Model w/ Total-P Inlet Boundary Condition

Upstream Model w/ INLET Boundary Condition
 10200 rpm, 4.14 MPa, WFR=0.0

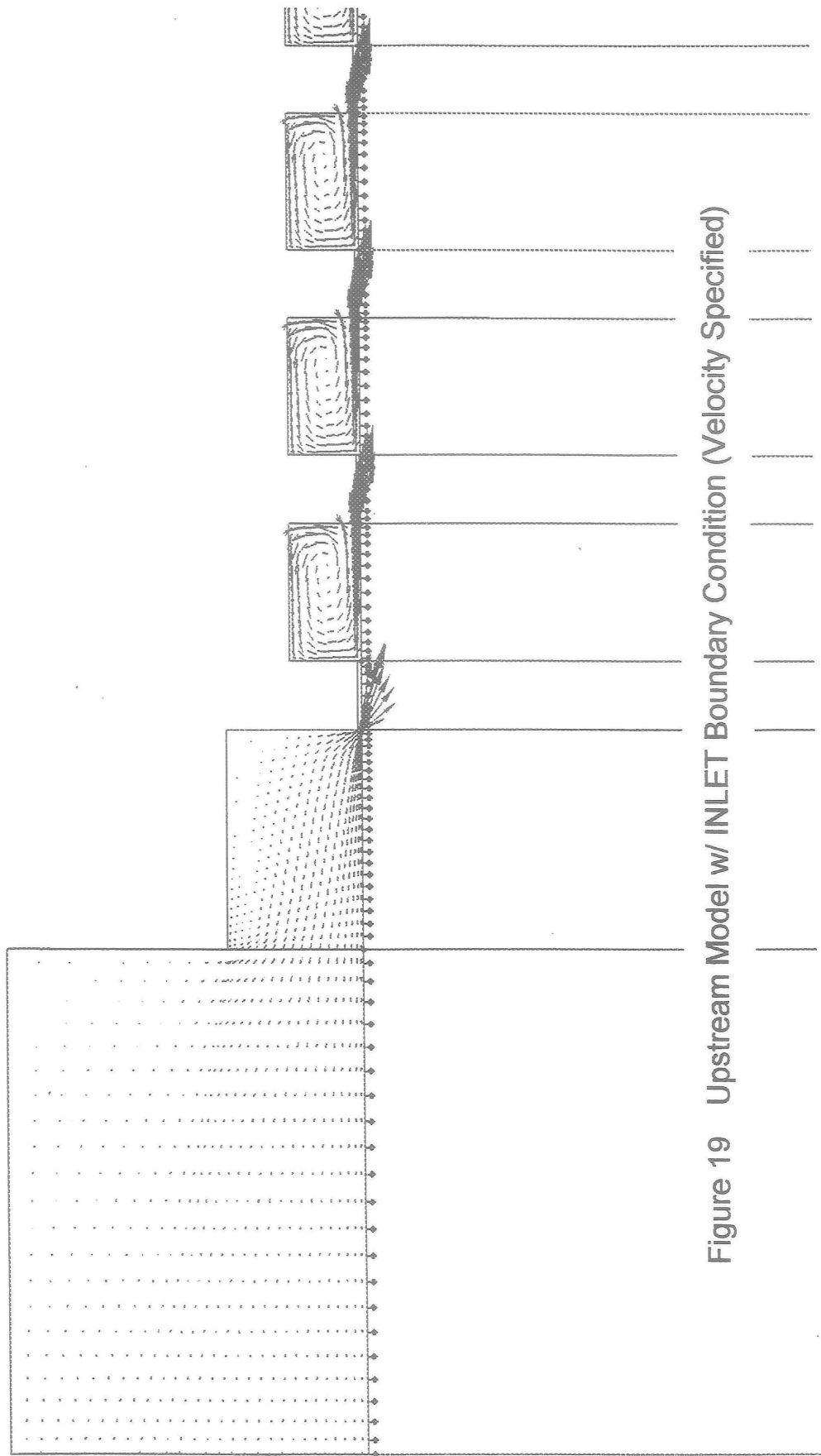


Figure 19 Upstream Model w/ INLET Boundary Condition (Velocity Specified)

Axisymmetric Upstream Model w/ INLET BC

10200 rpm, 4.14 MPa, $VJ = -UI$, Fine Up Grid

Circumferential Swirl Velocity

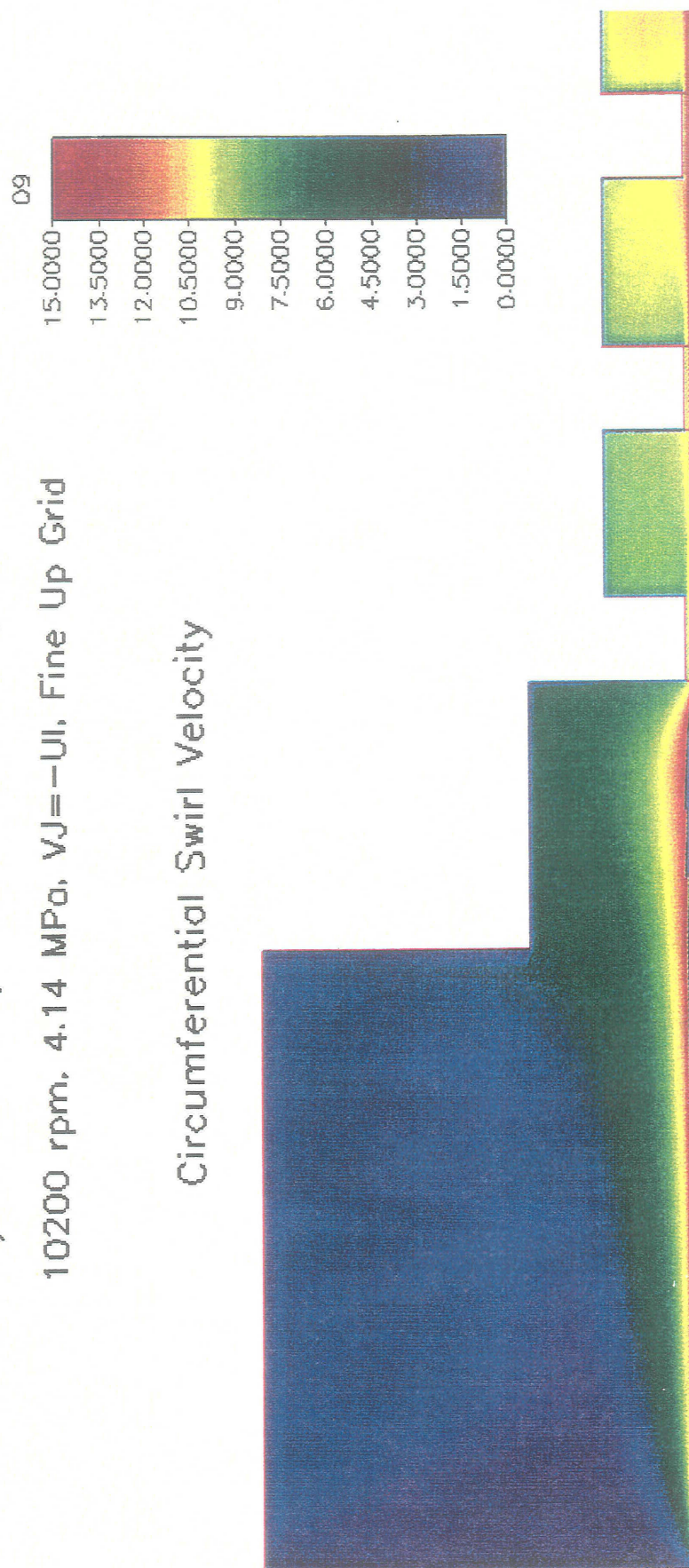


Figure 20 Development of Swirl Velocity, 10200 rpm (Normalized)

Axisymmetric Upstream Model w/ INLET BC

24600 rpm, 6.20 MPa, $VJ = -UI$, Fine Up Grid

Circumferential Swirl Velocity

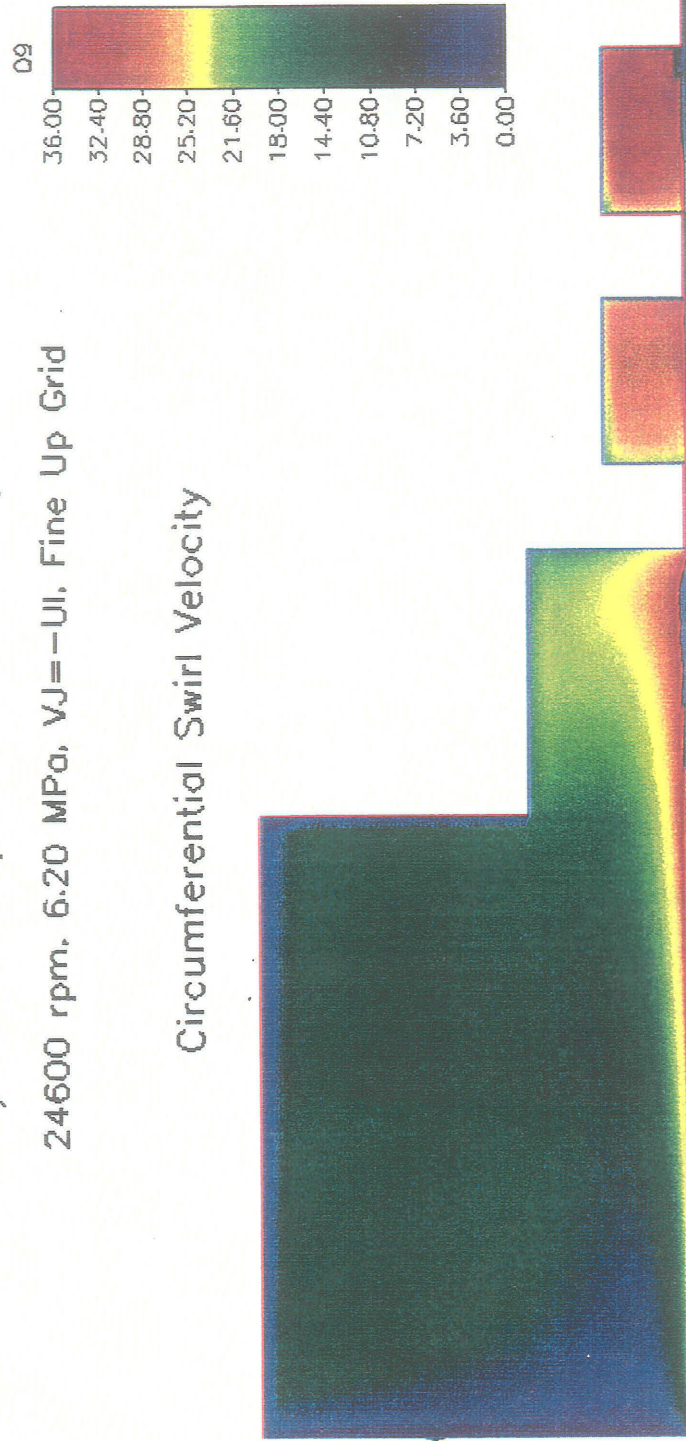


Figure 21 Development of Swirl Velocity, 24600 rpm (Normalized)

Axial Pressure Distribution Near 1st Seal Land

10200 rpm, 4.14 MPa, VJ=-UI, Fine Grid

Axisymmetric, Inlet Boundary Condition

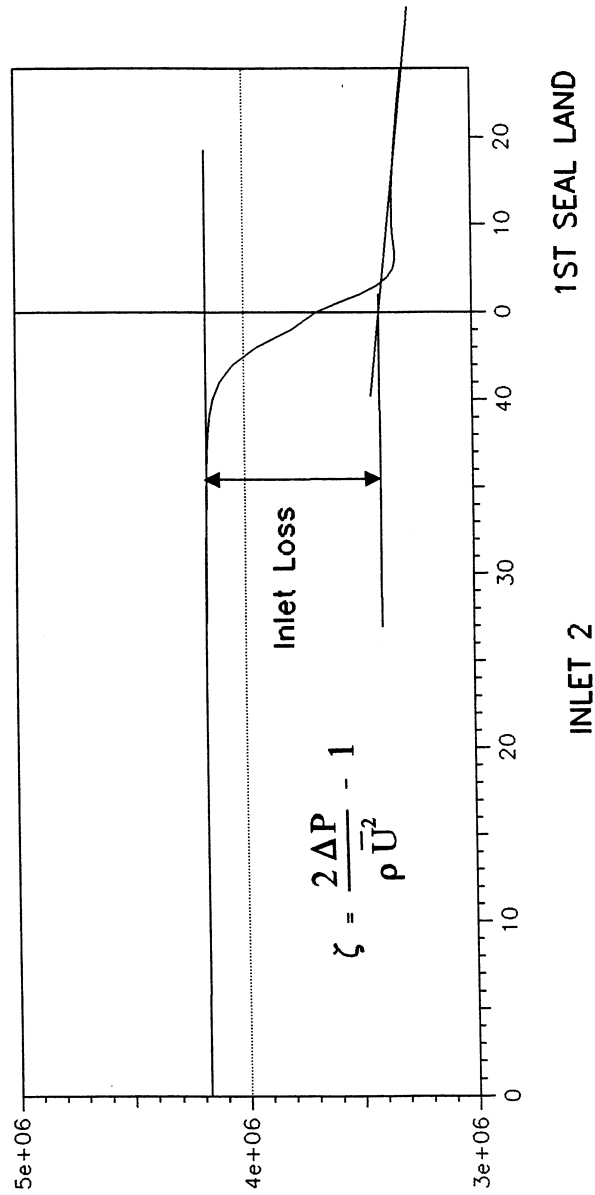


Figure 22 Inlet Loss of Pressure Entering 1st Seal Land

1st Seal Land Axial Velocity Profile

1st Seal Land w/ Fine Grid
10200 rpm, 4.14 MPa, WFR=0.0

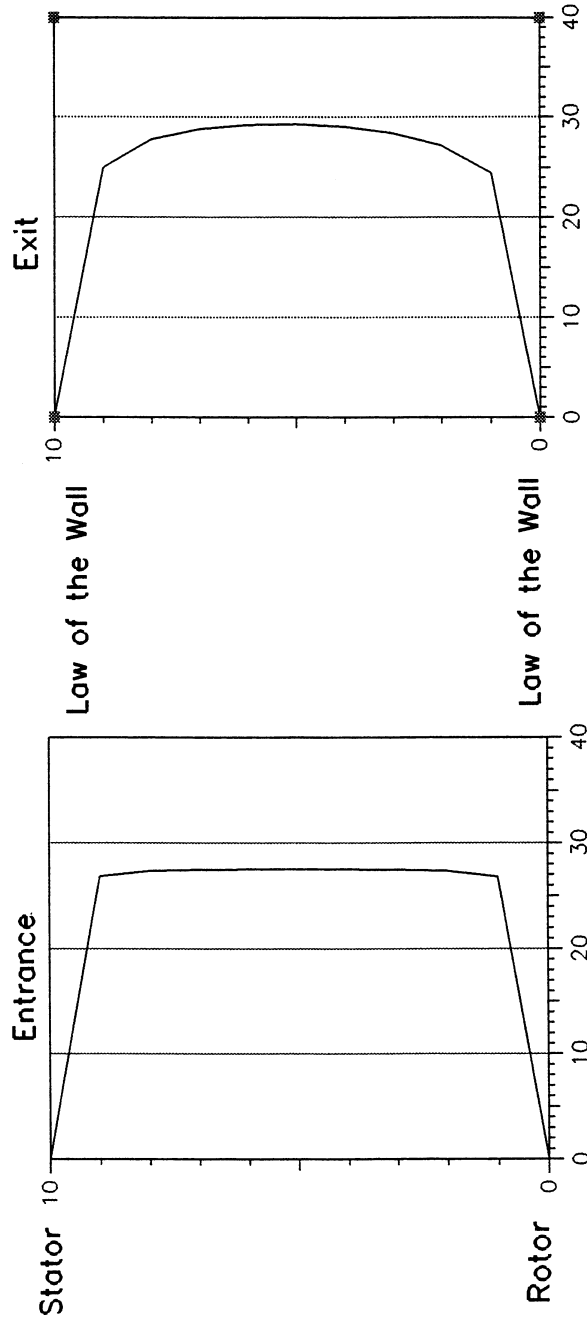


Figure 23 Development of Axial Velocity in 1st Seal Land
(Total-P BC at Seal Entrance)

1st Seal Land Circumferential Vel. Profile

1st Seal Land w/ Fine Grid

10200 rpm, 4.14 MPa, WFR=0.0

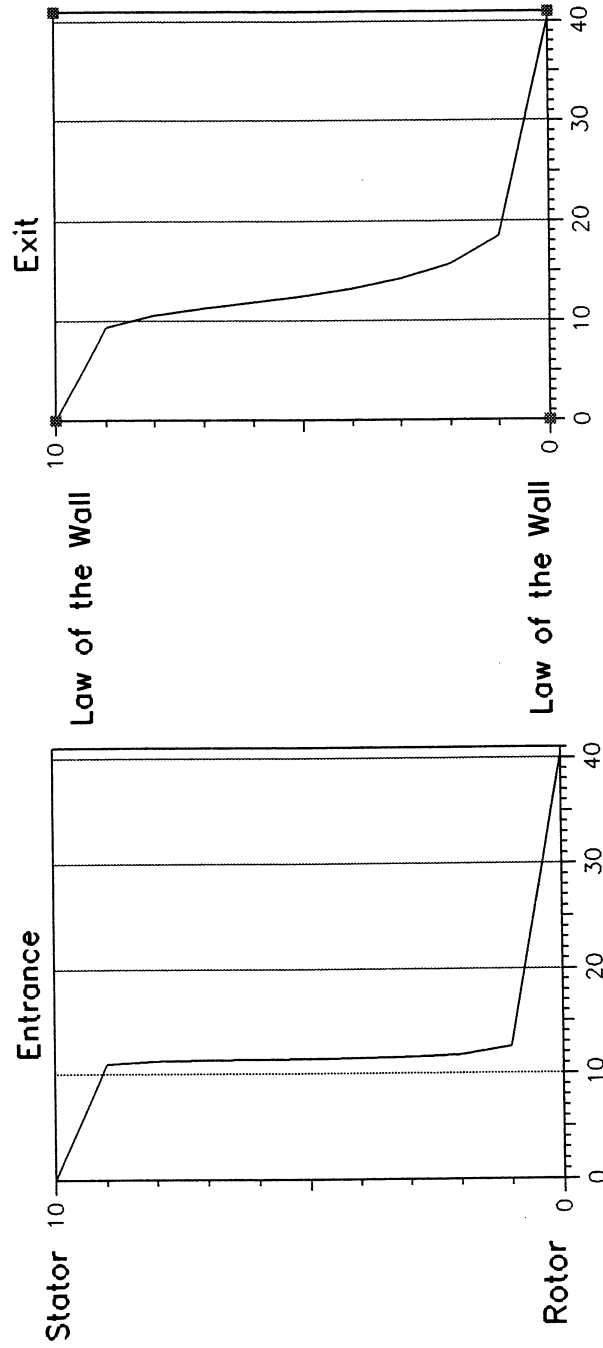


Figure 24 Development of Circumferential Velocity in 1st Seal Land (Total-P BC at Seal Entrance)

Velocity Profiles at Center of Seal Cavity

10200 rpm, 4.14 MPa, WFR=0.0

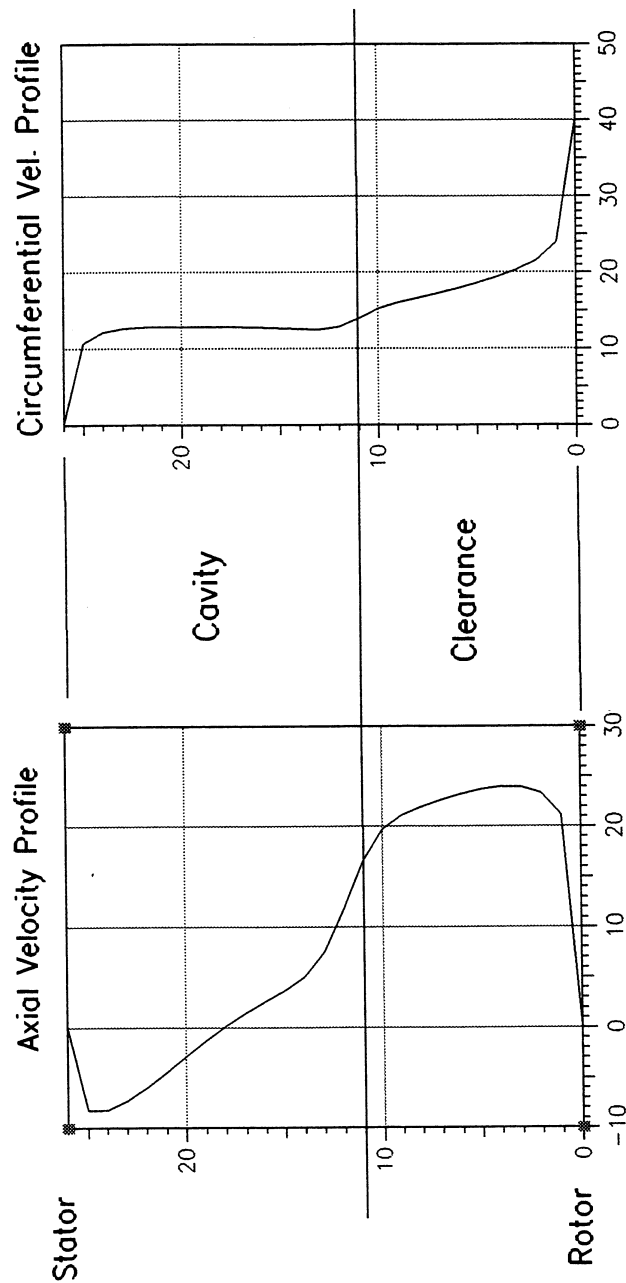


Figure 25 Velocity Distribution in Seal Cavity

Force Coefficients for Grooved Liquid Seal

10,200 rpm, Fine Grid-1, 4.14 MPa, $W_{rat}=0.28$, $P_{loss}=0.63$

	Computation	Experiment	3 Control Vol.
K_{xx}/K_{yy} (KN/m)	113	-5	-130
$K_{xy}/-K_{yx}$ (KN/m)	307	740	99.8
C_{xx}/C_{yy} (KN-s/m)	3.11	4.81	4.59
$C_{xy}/-C_{yx}$ (KN-s/m)	1.33	3.63	3.16
M_{xx}/M_{yy} (kg)	1.34	5.19	3.59
$M_{xy}/-M_{yx}$ (kg)	0.34	-	-
WFR ($K_{xy} / C_{xx} w$)	0.09	0.14	0.02
Leakage (l/s)	0.70	0.82	0.82

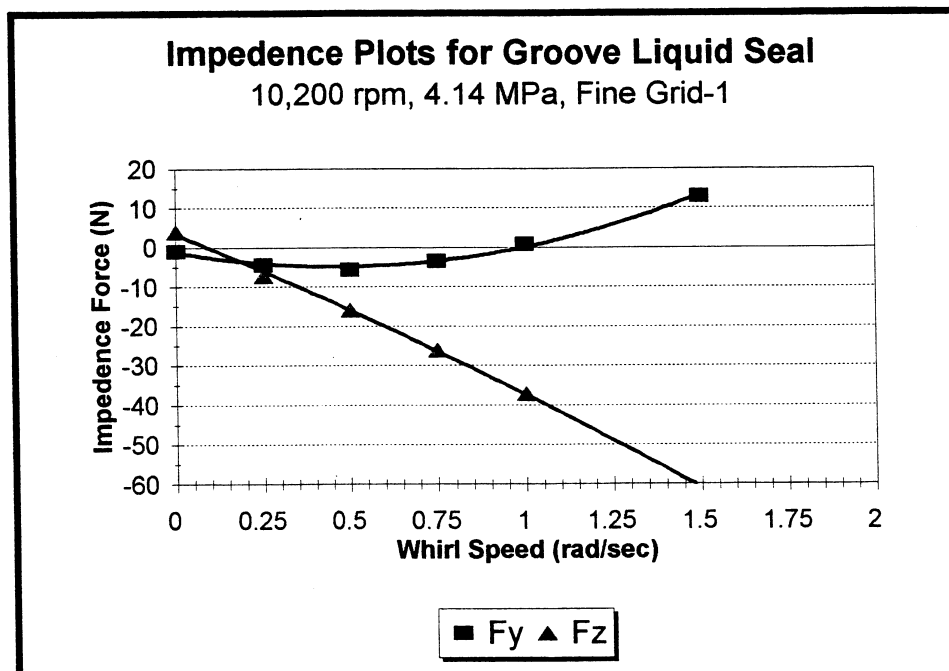


Table 6 Force Coefficients Using Boundary Conditions from Upstream Analysis
(10200 rpm, 4.14 MPa, $W_{rat}=0.28$, $P_{loss}=0.63$)

Force Coefficients for Grooved Liquid Seal

24,600 rpm, Fine Grid-1, 6.20 MPa, $W_{rat}=0.36$, $P_{loss}=0.70$

	Computation	Experiment	3 Control Vol.
K_{xx}/K_{yy} (KN/m)	-880	-2490	-3560
$K_{xy}/-K_{yx}$ (KN/m)	2028	3790	350
C_{xx}/C_{yy} (KN-s/m)	5.01	6.78	6.96
$C_{xy}/-C_{yx}$ (KN-s/m)	2.99	8.84	7.21
M_{xx}/M_{yy} (kg)	1.26	5.14	3.22
$M_{xy}/-M_{yx}$ (kg)	-0.06	-	-
WFR ($K_{xy} / C_{xx} w$)	0.16	0.22	0.02
Leakage (l/s)	0.81	0.97	0.897

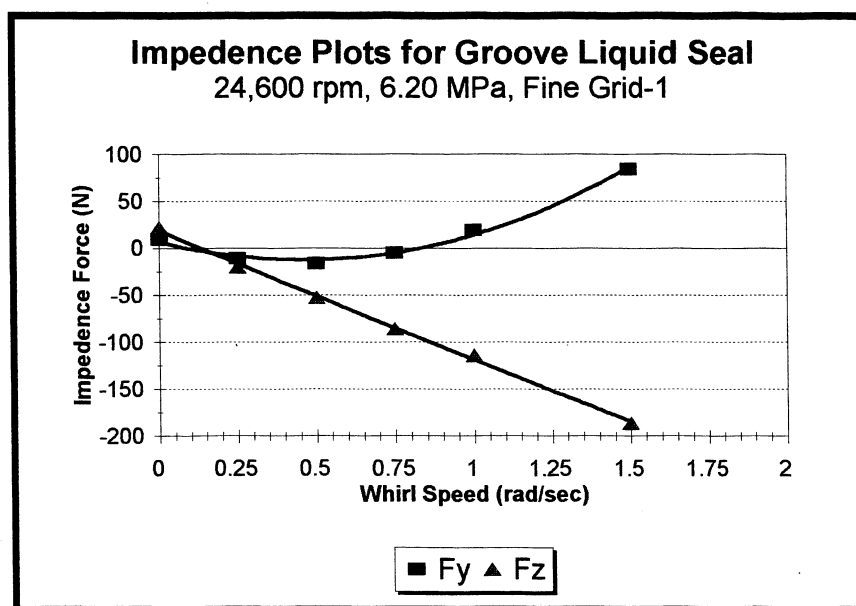


Table 7 Force Coefficients Using Boundary Conditions from Upstream Analysis
(10200 rpm, 4.14 MPa, $W_{rat}=0.28$, $P_{loss}=0.63$)

SUMMARY

- Overall, CFD Calculations Provided Improved Predictions in Stiffness over Current Modeling Techniques (Worse for Damping and Inertia)
- Cross-Coupled Stiffness a Strong Function of Both Grid Density and Inlet Boundary Conditions
- Axisymmetric Upstream Analysis Provides Means to Obtain Seal Inlet Boundary Conditions
- CFD Used as a Final Analysis Tool, Bulk Flow and Control Volume Techniques Used as a Design Tool

TURBOFAN ENGINE CORE COMPARTMENT VENT AERODYNAMIC CONFIGURATION
DEVELOPMENT METHODOLOGY

Leonard J. Hebert
The Boeing Company
Seattle, Washington

ABSTRACT

This paper presents an overview of the design methodology used in the development of the aerodynamic configuration of the nacelle core compartment vent for a typical Boeing commercial airplane together with design challenges and recommended process improvements for future design efforts.

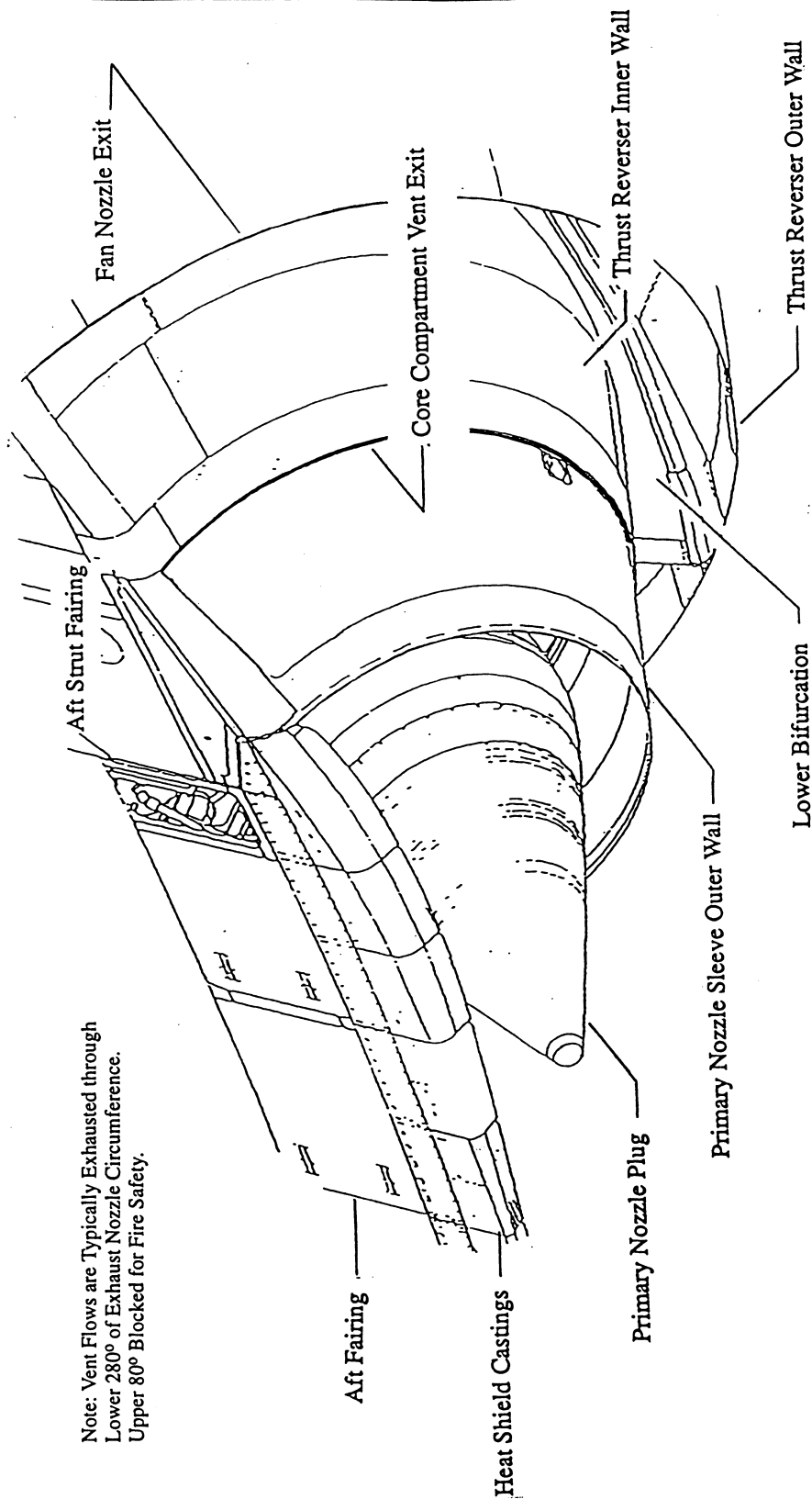
Core compartment vents exhaust engine subsystem flows from the space contained between the engine case and the nacelle of an airplane propulsion system. These subsystem flows typically consist of precooler, oil cooler, turbine case cooling, component cooling and nacelle leakage air.

The design of core compartment vents is challenging due to stringent design requirements, mass flow sensitivity of the system to small changes in vent exit pressure ratio, and the need to maximize overall exhaust system performance at cruise conditions. Typically, the vent is located on the core cowl afterbody and is sized for maximum flow rate which occurs at an icing heavy hold condition. This condition differs considerably from cruise - where thrust recovery is the objective. The afterbody pressure distribution and vent back pressure vary widely between these two conditions and must be well understood to develop a good integrated core compartment vent design.

<p>NASA Workshop 10/16/97</p>	<p>Turbofan Engine Core Compartment Vent Aerodynamic Configuration Development Methodology</p>	<p>Presentation Topics</p> <ul style="list-style-type: none"> • Typical Core Compartment Vent Geometry / Purpose. • Core Compartment Vent Design Requirements / Objectives. • Core Compartment Vent Design Methodology. • Conclusions.
---------------------------------------	---	---

Typical Exhaust Nozzle / Core Compartment Vent Geometry

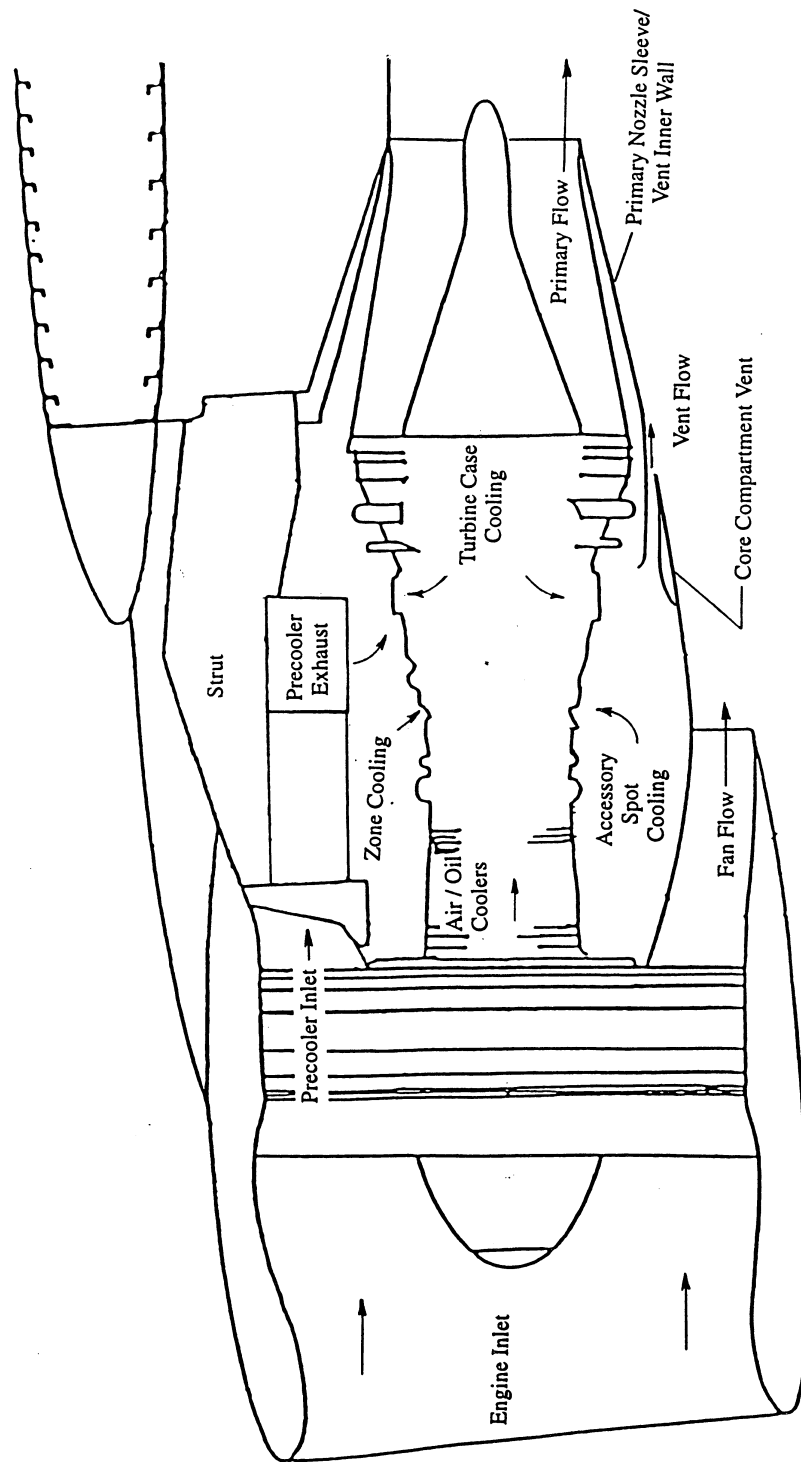
Note: Vent Flows are Typically Exhausted through
Lower 280° of Exhaust Nozzle Circumference.
Upper 80° Blocked for Fire Safety.





NASA Workshop 10/16/97	Turbofan Engine Core Compartment Vent Aerodynamic Configuration Development Methodology
	<p data-bbox="302 758 342 1388">Purpose of Core Compartment Vent</p> <ul data-bbox="500 583 1127 1724" style="list-style-type: none"> <li data-bbox="500 583 540 1724">● The Core Compartment Vent Exhausts Engine Subsystem Flows. <li data-bbox="613 1262 654 1650">● Precooler Exhaust. <li data-bbox="727 1199 768 1650">● Turbine Case Cooling. <li data-bbox="841 953 881 1650">● Engine External Component Cooling. <li data-bbox="954 1192 995 1650">● General Zone Cooling. <li data-bbox="1068 1020 1127 1650">● Engine and Gearbox Oil Cooling.

Typical Engine Subsystem Flows



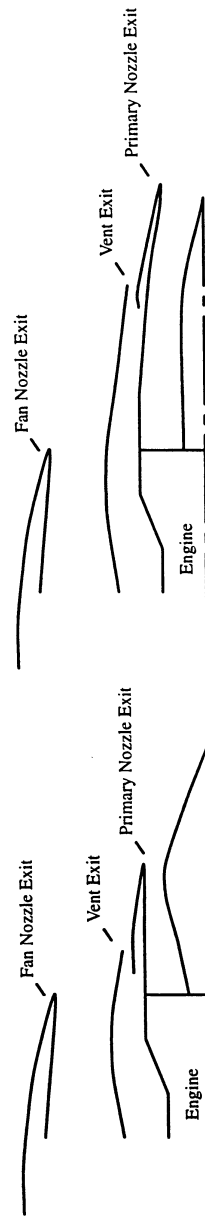
<p>NASA Workshop 10/16/97</p>	<p>Turbofan Engine Core Compartment Vent Aerodynamic Configuration Development Methodology</p> <p>Design Requirements and Objectives (Vent Sizing Condition)</p> <ul style="list-style-type: none"> ● The Core Compartment Vent is Designed in Collaboration with the Engine Company. ● The Core Compartment Vent is Sized for the Airplane Operating Condition with the Greatest Single Engine Bleed Demand / Vent Exhaust Flow. ● Typically a Single Engine Bleed, Hot Day Icing Heavy Hold Condition. ● 22,000 Feet Altitude, ISA+15 °F, 0.6+ Mach, Engine Part Power. ● Fan Flow is Subsonic. ● Maximize Core Compartment Total Pressure – Typical Limit ~ 1.3 psig. ● Results in Smallest Vent Area.
---------------------------------------	--

Design Requirements and Objectives, Continued
(Airplane Cruise Condition)

- The Core Compartment Vent is Designed to Maximize Exhaust System Cruise Performance.
- Cruise Altitude, 0.8+ Mach, Cruise Engine Power.
- Fan Flow Supersonic with Expansion / Compression Waves.
- Two to Three Times Less Corrected Vent Flow Rate than Sizing Condition.
- Maximize Core Compartment Total Pressure – Typical Limit ~ 0.8 psig.
- Maximize Vent Thrust.

Design Requirements and Objectives, Continued
(Vent Exit Location Window)

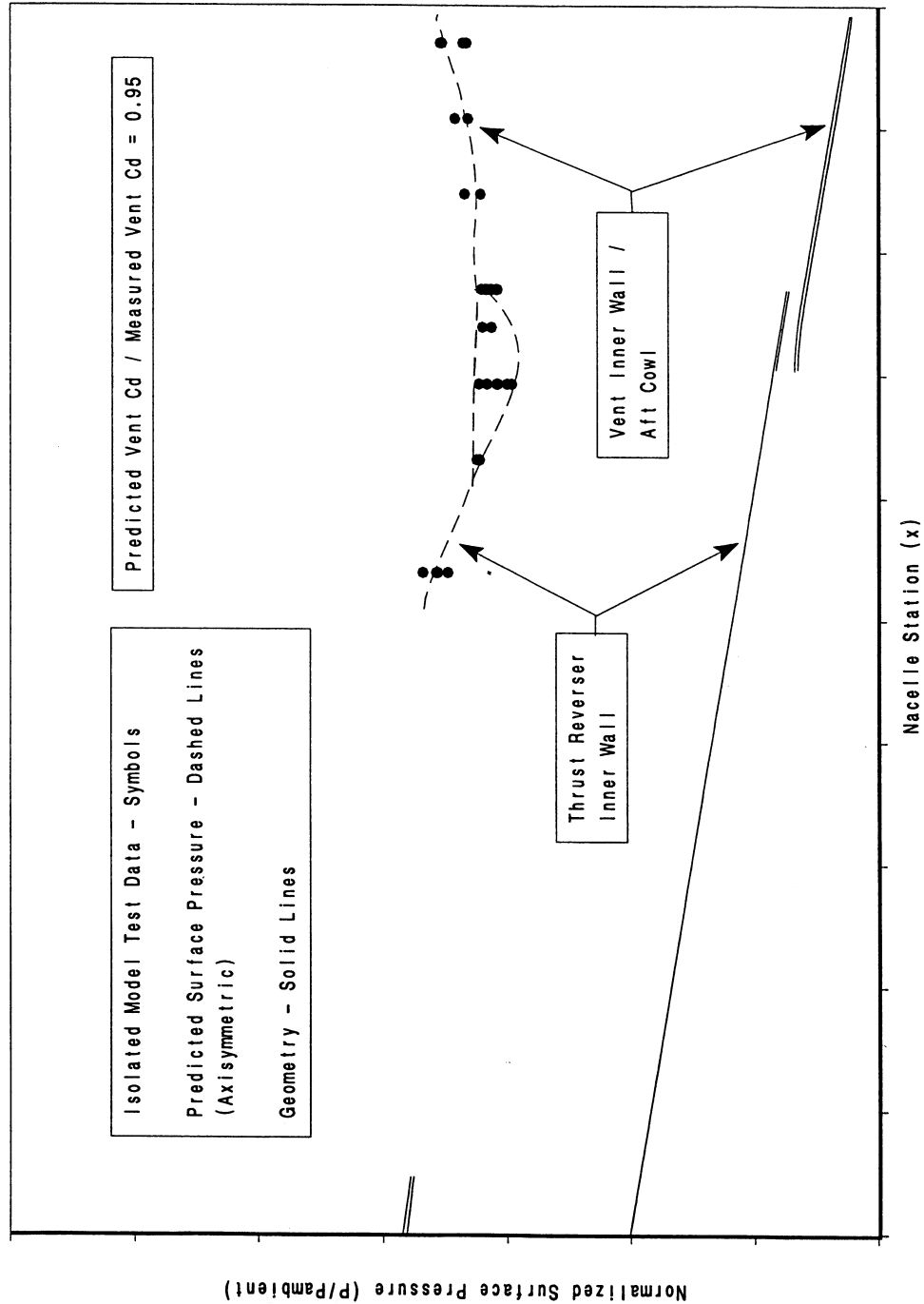
- Core Compartment Vent Exit Location Window:
- Function of Engine / Nacelle Geometry.
- Distance Between Fan Nozzle and Primary Nozzle Exits and Turbine Exit Flange Location Relative to Primary Nozzle Exit.



NASA Workshop 10/16/97	Turbofan Engine Core Compartment Vent Aerodynamic Configuration Development Methodology	
	<p data-bbox="337 667 423 1465">Core Compartment Vent Design Methodology (Analytical Tool Accuracy Requirements)</p> <ul data-bbox="558 262 748 1835" style="list-style-type: none"> <li data-bbox="558 457 602 1835">● Computational Fluid Dynamics used to Configure the Core Compartment Vent. <li data-bbox="711 262 748 1766">● Good Pressure Prediction Accuracy Required for Vent Mass Flow Prediction Accuracy. 	
	<ul data-bbox="873 331 1219 1667" style="list-style-type: none"> <li data-bbox="873 331 959 1667">● Vents Operate at Low Pressure Ratios – Mass Flow Sensitive to Variations in Local Pressure Ratio (Influence Factor up to 40:1). <li data-bbox="1089 436 1219 1667">● Local Vent Pressure Ratio is a Function of Fan Nozzle Pressure Ratio, Vent Pressure, Airplane Mach Number and External Pressure Influences of the Wing / Strut. 	

<p>NASA Workshop 10/16/97</p>	<p>Turbofan Engine Core Compartment Vent Aerodynamic Configuration Development Methodology</p>
<p>Core Compartment Vent Design Methodology (Analysis Tool / Modeling / Accuracy)</p> <ul style="list-style-type: none"> ● Navier–Stokes Code PARC2D used Primarily. ● Analyze / Design Isolated Axisymmetric Vent Geometry. ● Most Accurate / Time Effective Technology Available. ● Vent Exit Comprises ~ 280° of Exhaust Nozzle Circumference. ● Good Agreement with Isolated Model Test Pressure / Vent Mass Flow. ● Configurations Produce Positive Thrust at Cruise. 	

Pressure Prediction Accuracy
Isolated Model of Vented Exhaust Nozzle
Typical Cruise Condition

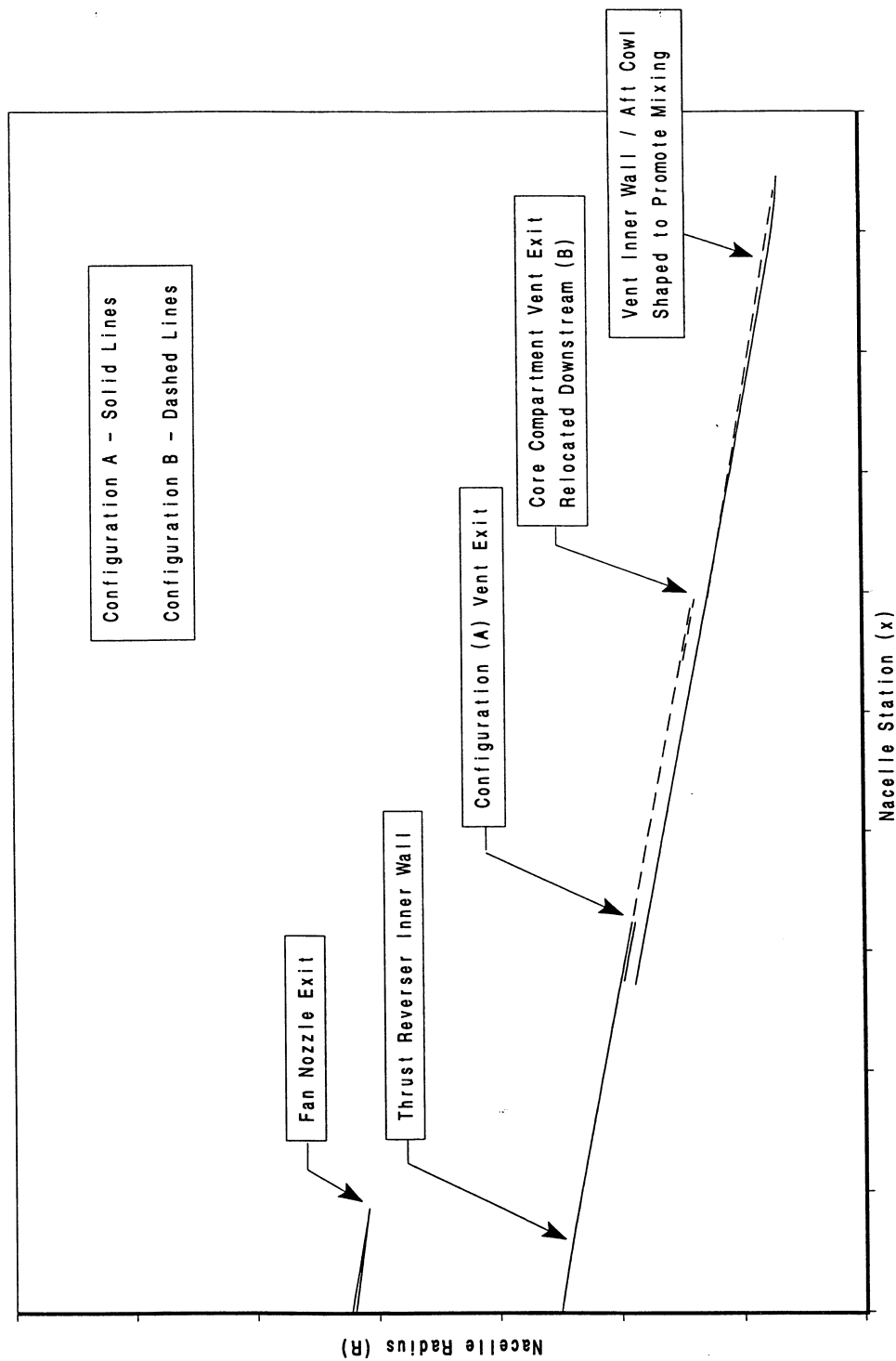


<p>NASA Workshop 10/16/97</p>	<p>Turbofan Engine Core Compartment Vent Aerodynamic Configuration Development Methodology</p>
	<p>Core Compartment Vent Design Methodology (Vent Exit Position Objectives)</p> <ul style="list-style-type: none"> ● Position Vent Exit in Cruise High Pressure Region on Thrust Reverser Inner Wall. ● Maximize Vent Flow Momentum. ● Favorable Cruise Pressure Gradient Downstream of Vent Exit. ● Maximize Nozzle Surface Pressure Recovery / Avoid Vent Flow Separation.

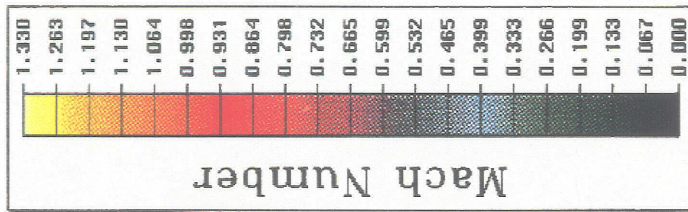
NASA
Workshop
10/16/97

Turbofan Engine Core Compartment Vent Aerodynamic Configuration Development Methodology

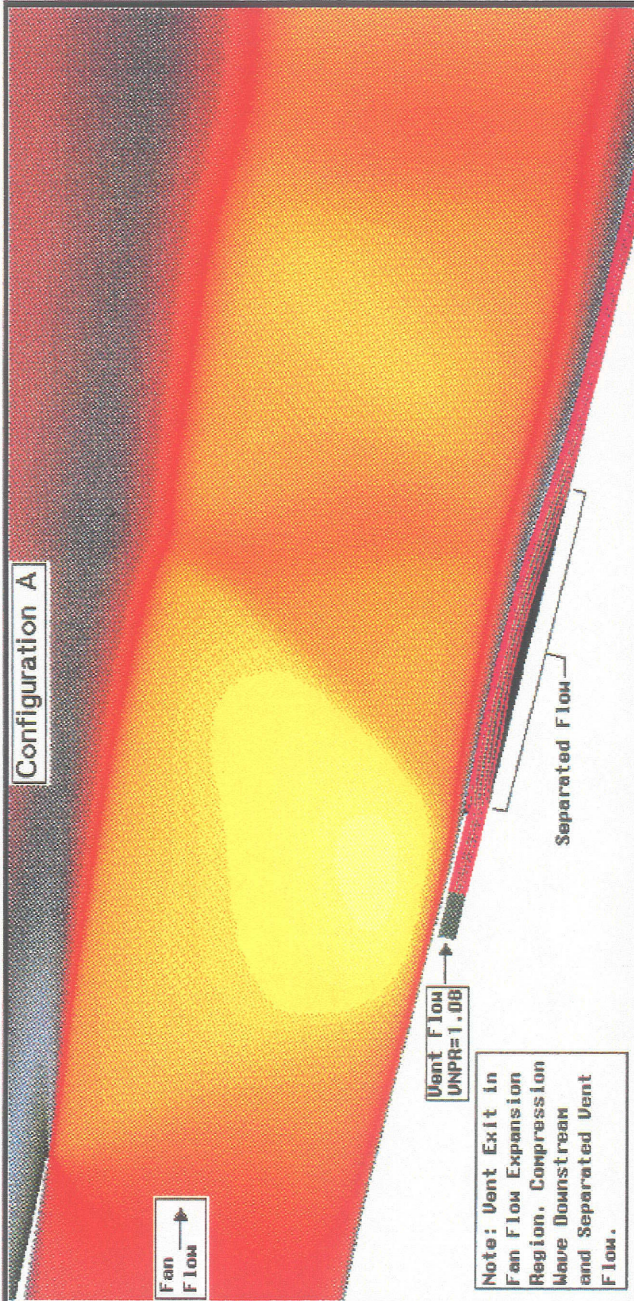
Effect of Vent Exit Location on
Exhaust Nozzle Flowfield / Performance
Comparison of Configuration A and B Geometries



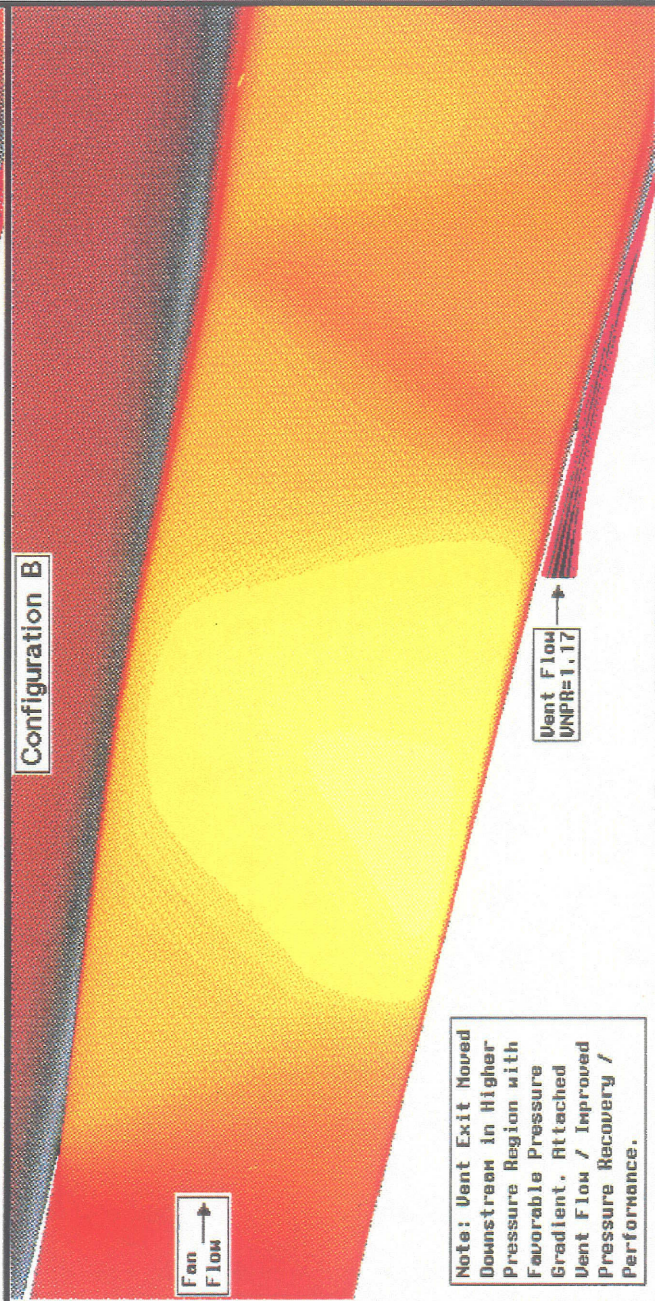
Effect of Vent Exit
Location on Vent
Flow Separation at
Cruise Conditions.



Configuration A

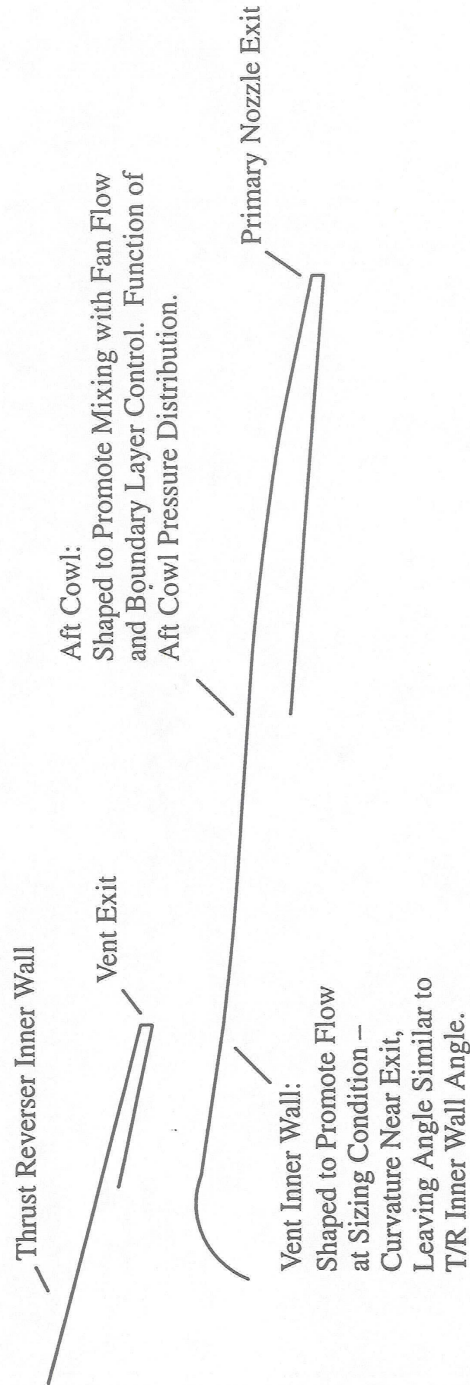


Configuration B



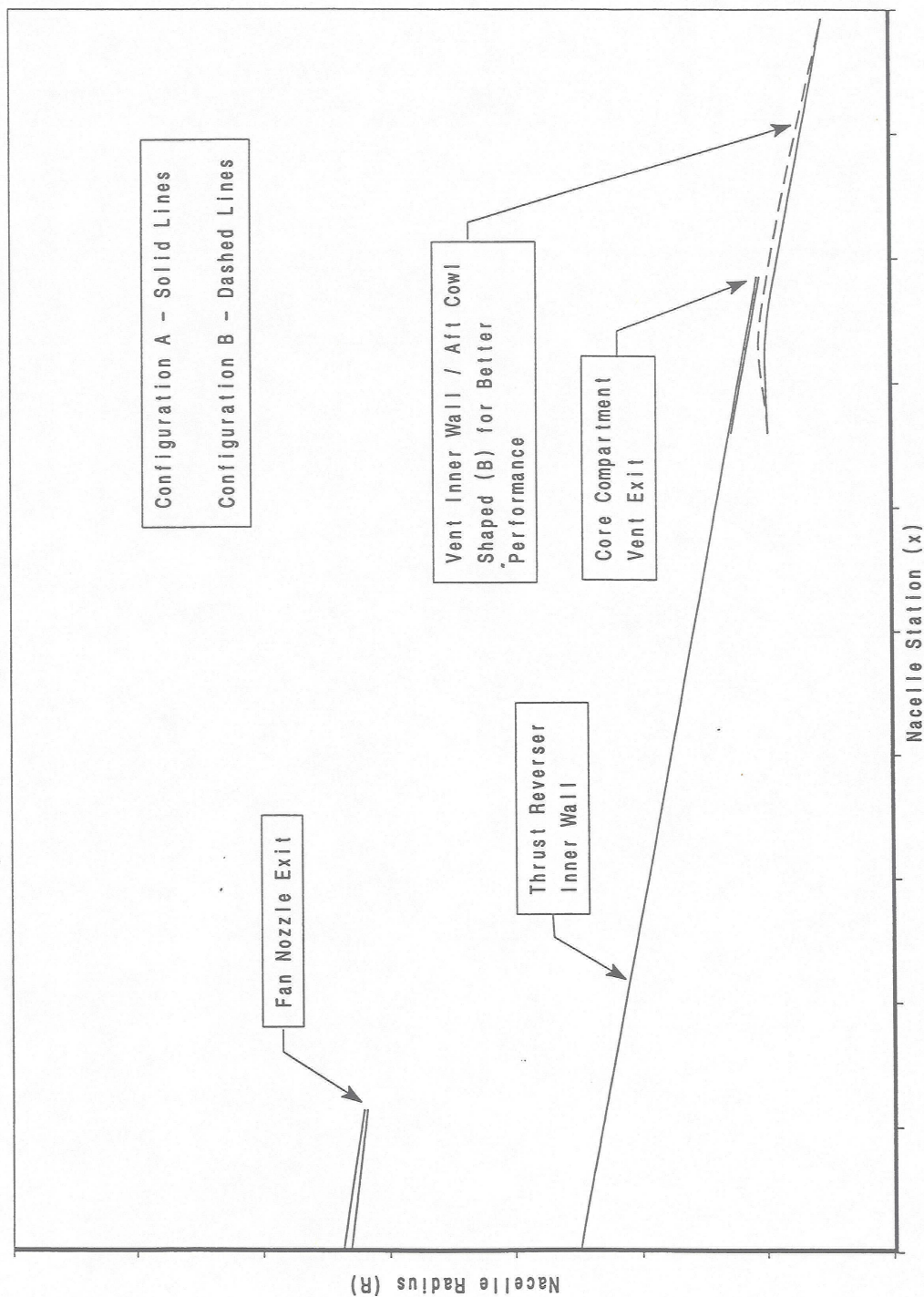
Core Compartment Vent Design Methodology
(Vent Sizing / Wall Shape Objectives)

- Size Flow Area / Shape Vent Inner Wall and Aft Cowl Wall to Accommodate Flow at Sizing Condition and Maximize Pressure Recovery at Cruise.

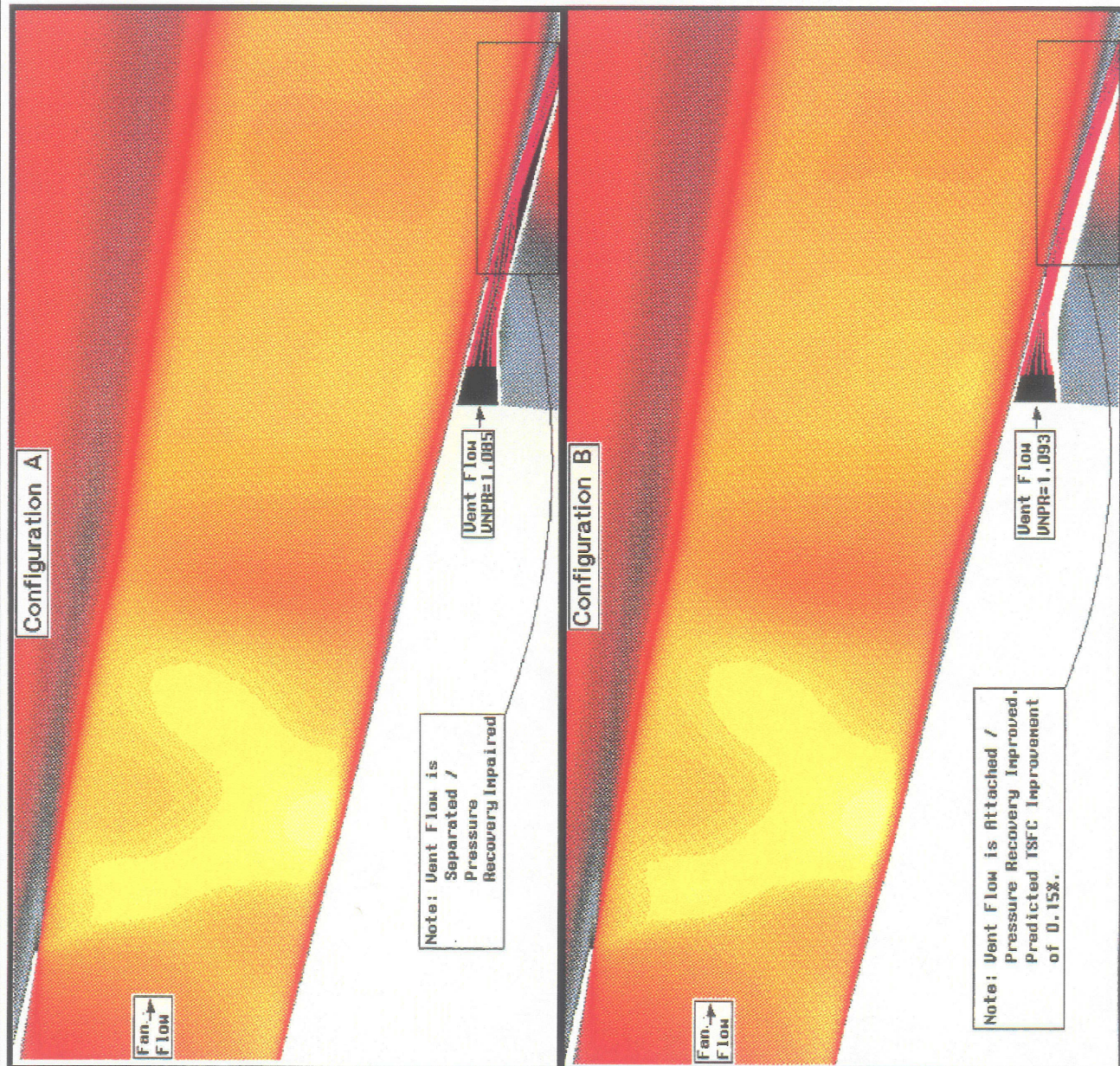
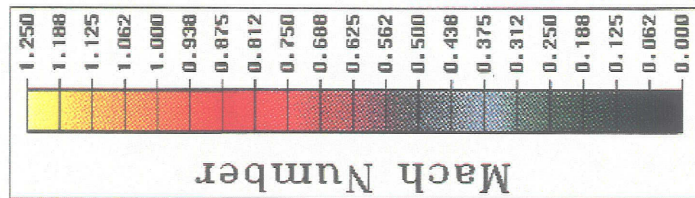


Turbofan Engine Core Compartment Vent Aerodynamic Configuration Development Methodology

Effect of Vent Inner Wall Modification on
Exhaust Nozzle Flowfield / Performance
Comparison of Configuration A and B Geometries



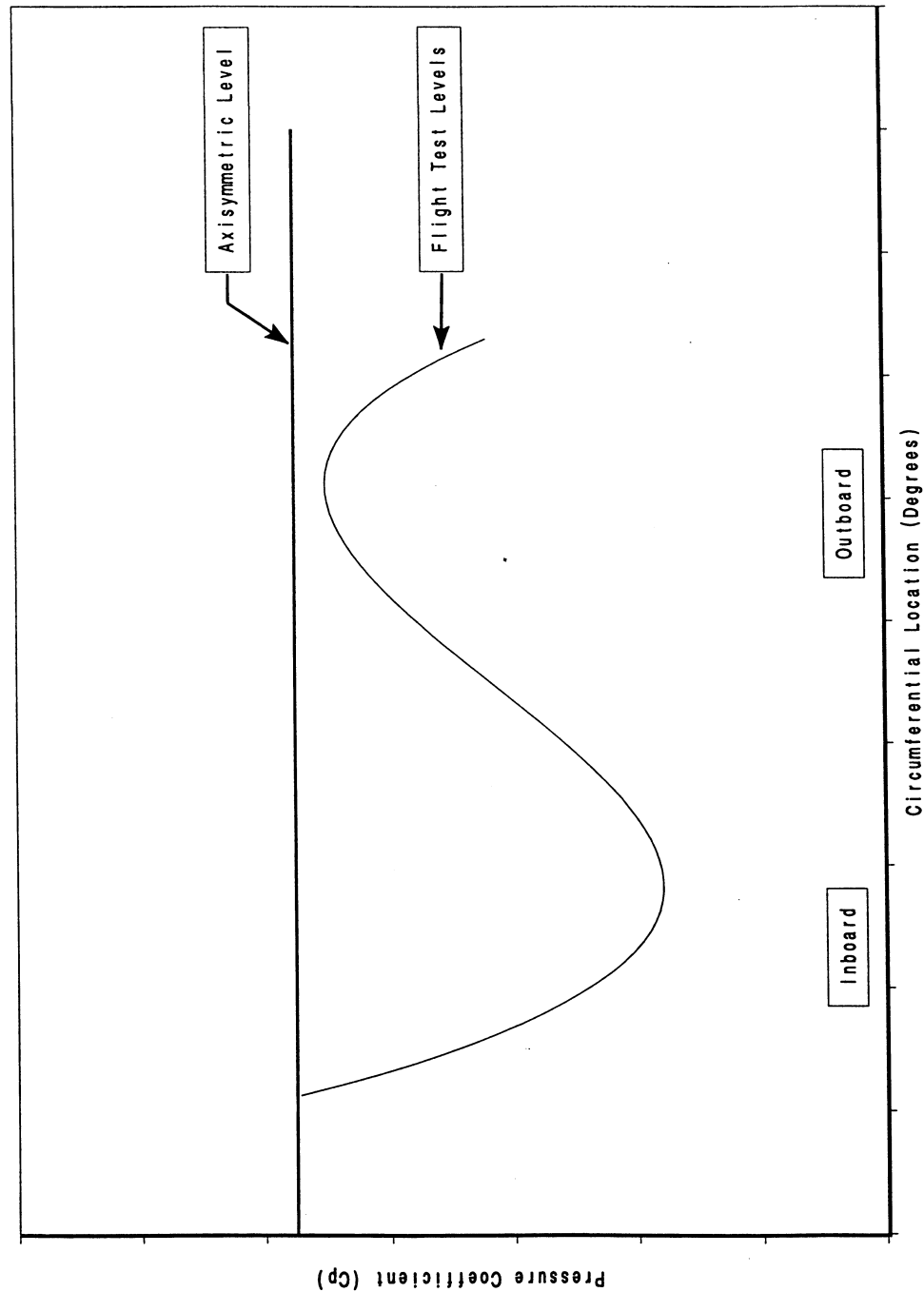
Effect of Vent
Inner Wall Shape
on Vent Flow
Separation and
Cruise
Performance



<p>NASA Workshop 10/16/97</p>	<p>Turbofan Engine Core Compartment Vent Aerodynamic Configuration Development Methodology</p>	<p>Core Compartment Vent Design Methodology (Effectiveness)</p> <ul style="list-style-type: none"> ● Flight Test Data Confirm the Effectiveness of the Designs. ● Sizing Flow Requirements Achieved. ● Positive Vent Thrust at Cruise.
---------------------------------------	---	--

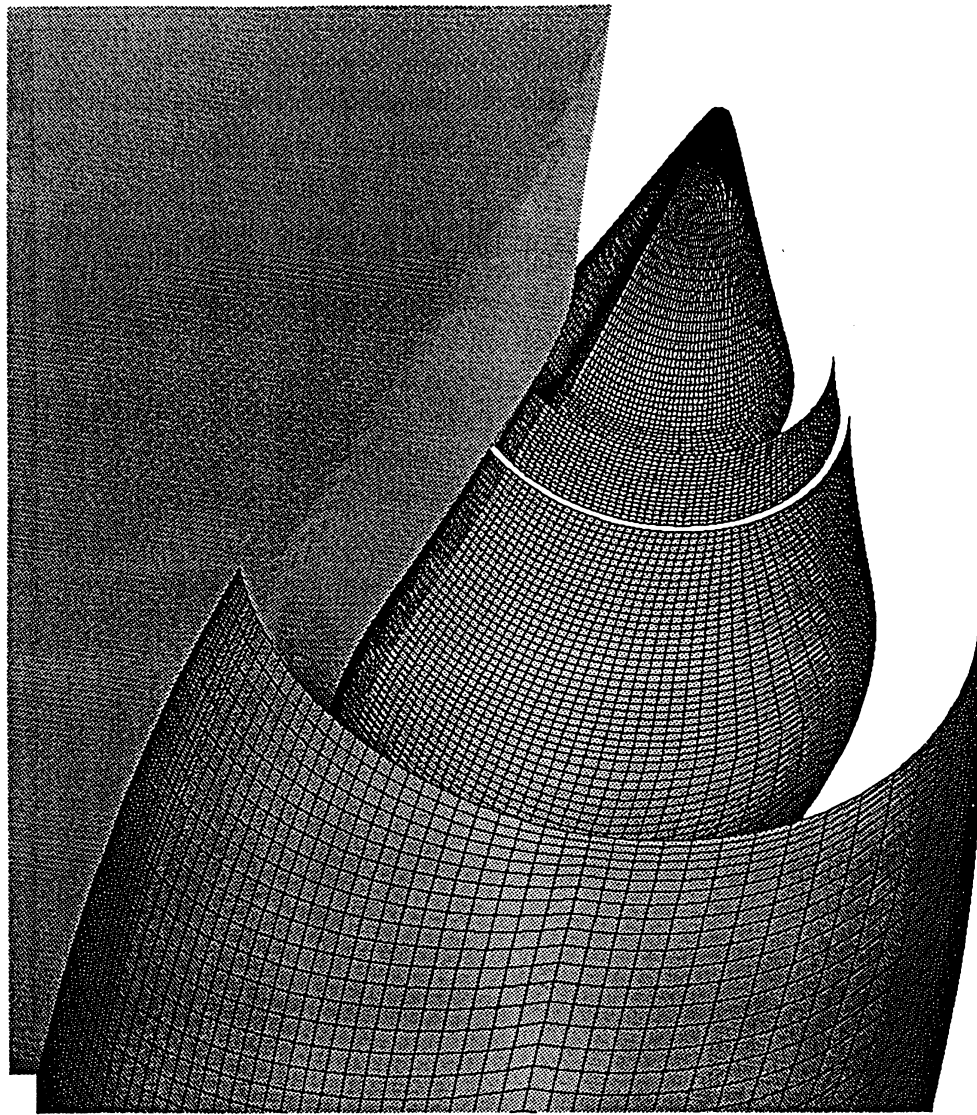
NASA Workshop 10/16/97	Turbofan Engine Core Compartment Vent Aerodynamic Configuration Development Methodology	<div data-bbox="313 604 399 1404"> Core Compartment Vent Design Methodology (Installation Effects) </div> <div data-bbox="570 287 1166 1766"> <ul style="list-style-type: none"> ● Vent Mass Flow is a Strong Function of Vent Exit Pressure Ratio (P_{tv} / P_{local}). ● Affected by Wing / Strut / Engine Installation. ● Vent Exit / Aft Cowl Pressure Magnitude and Circumferential Distribution. </div>
------------------------------	--	--

Example of Predicted and Flight Test
Vent Exit Static Pressure Levels



<p>NASA Workshop 10/16/97</p>	<p>Turbofan Engine Core Compartment Vent Aerodynamic Configuration Development Methodology</p>	<p>Core Compartment Vent Design Methodology (Improvements)</p> <ul style="list-style-type: none"> ● Three Dimensional Navier–Stokes Analysis of the Installed Nozzle could Aid the Design of Core Compartment Vent Configurations: ● Account for Installation Effects – Reduced Vent Area, Increased Vent Pressure, Greater Vent Thrust Recovery. ● Now Possible due to Improvements in: <ul style="list-style-type: none"> ● Grid Generator, Flow Solver, Computer Technology. ● Pursuing 3D Technology for Future Efforts.
---------------------------------------	---	---

Core Compartment Vent Design Methodology
(3D Grid Example)



<p>NASA Workshop 10/16/97</p>	<p>Turbofan Engine Core Compartment Vent Aerodynamic Configuration Development Methodology</p>	<p>Conclusions</p> <ul style="list-style-type: none"> • Core Compartment Vent Design Methodology Yields Configurations that: <ul style="list-style-type: none"> • Effectively Exhaust Engine Subsystem Flows. • Contribute Positive Thrust at Cruise. • Three Dimensional Viscous CFD Technology could be useful in better Designing Core Compartment Vent Configurations. <ul style="list-style-type: none"> • Account for Installation Effects. • Pursuing for Future Efforts.
---------------------------------------	---	---

ADAPTING ANALYSIS TOOLS TO ENGINE EXTERNALS ANALYSIS

Ken Dunkelberg
The Boeing Company
Seattle, Washington

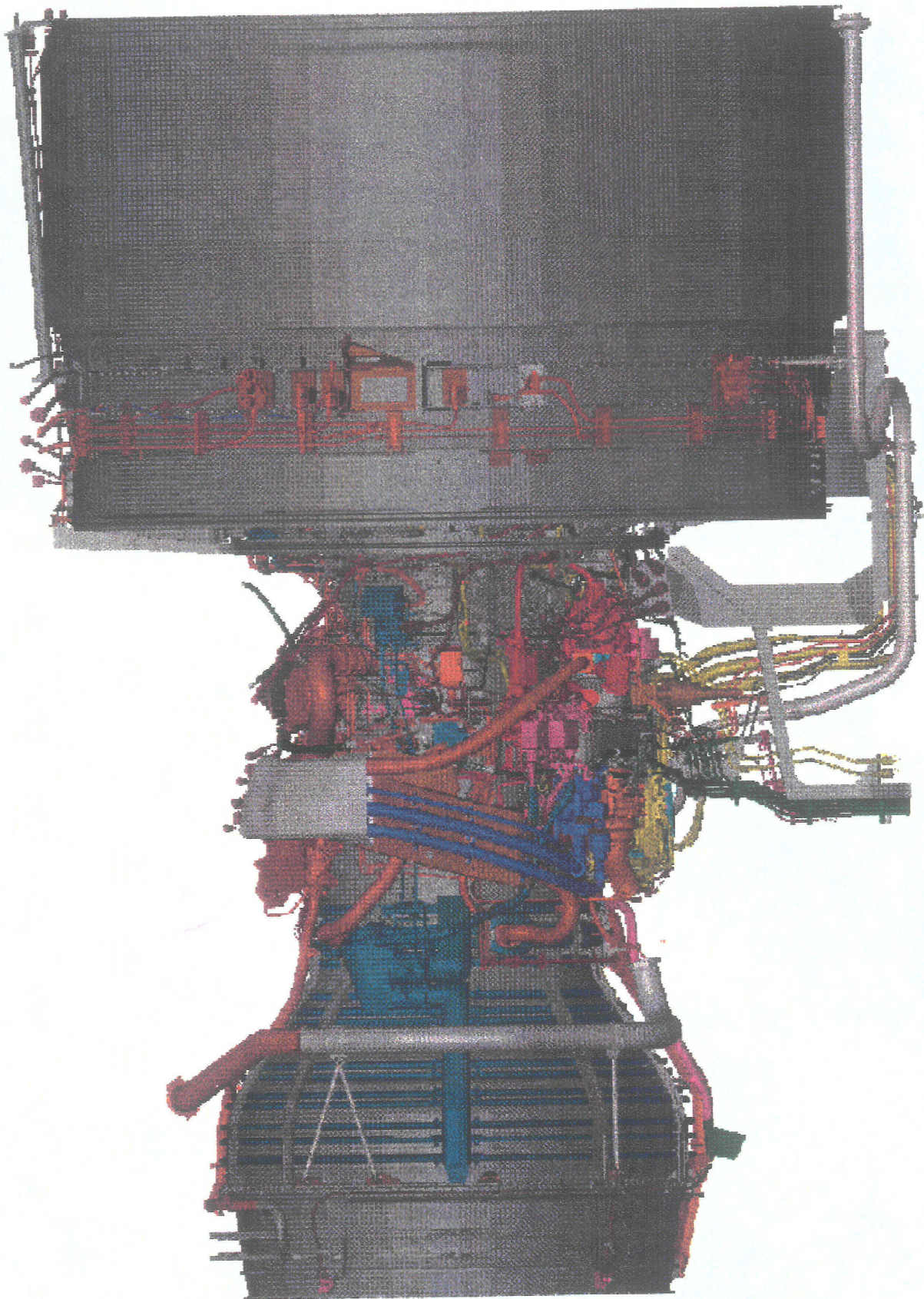
ABSTRACT

Market forces are driving industry to reduce product cycle time (the time required to conceive, design, build, test, validate and deliver a product). Application of existing tools in new areas can reduce the time required to design a new product and increase the confidence of acceptable test results later in the expensive testing and validation phase. Finite element methods, computational fluid dynamics codes and sharing of CAD datasets when applied to the design of engine externals can provide methods for product improvement and expedited delivery to the customer.

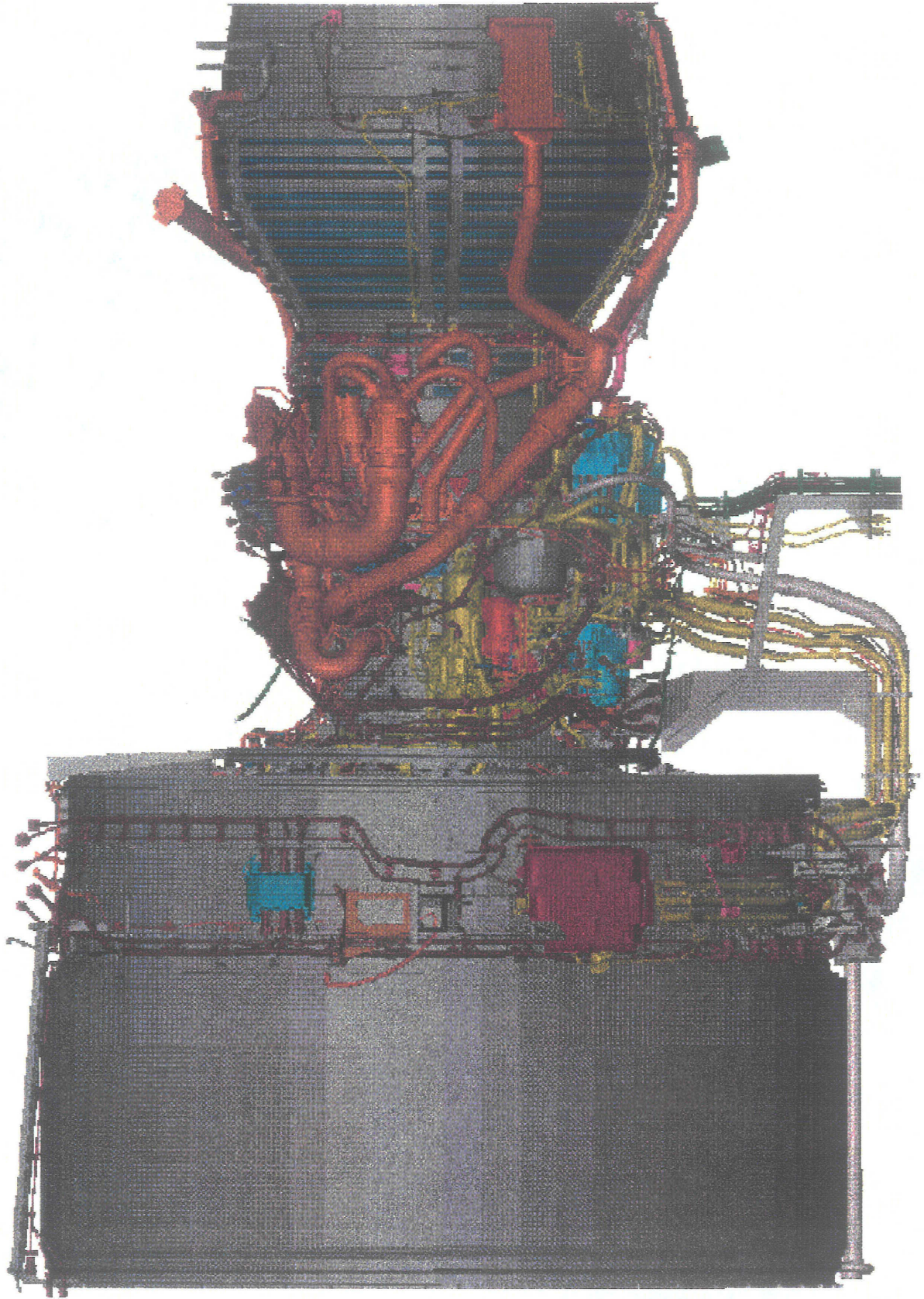
Engine Externals Provide

- **Engine**
 - Fuel
 - Lubrication
 - Control
 - Cooling
- **Airplane**
 - Pneumatic power
 - Electrical power
 - Hydarualic power
- **Flight Deck Indication**
 - Primary thrust setting parameter
 - Secondary engine parameters
 - Warnings to flight crew
 - Indications of propulsion health

PW4084 (with externals, cowlings removed)



PW4084 (with externals, cowlings removed)

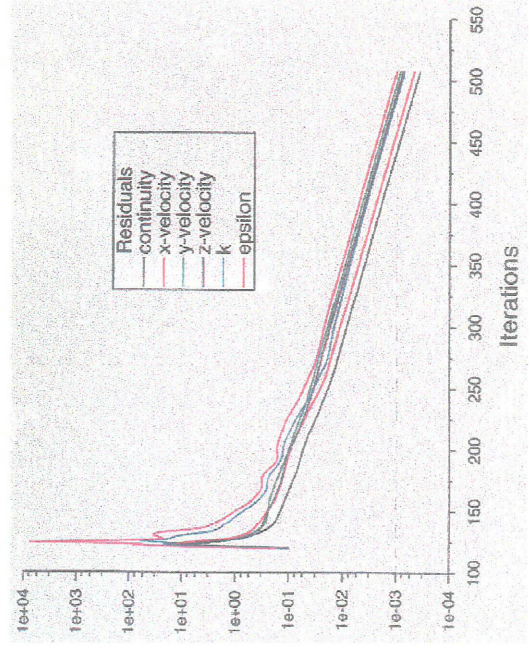
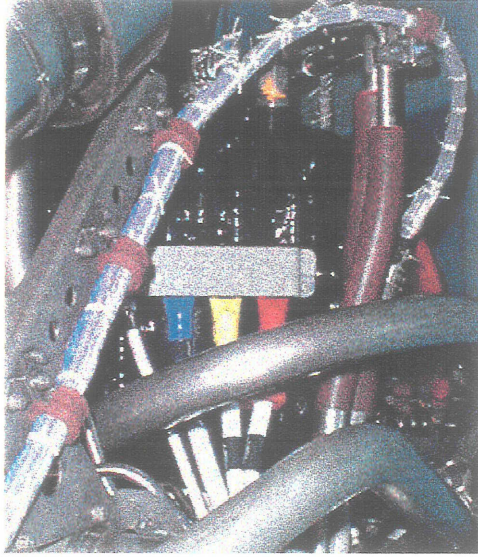


Types of engine externals analysis

- Straight forward problem solutions available for
 - Heat exchanger sizing
 - Oil cooling system performance
 - Fuel system performance
 - Pneumatic duct sizing
 - Pressure losses in ducting
 - Cooling system inlet recovery
- No straight forward problem solution available for
 - Prediction of undercowl ambient temperatures
 - Prediction of undercowl fire extinguishing agent concentration
 - Bulb seal performance

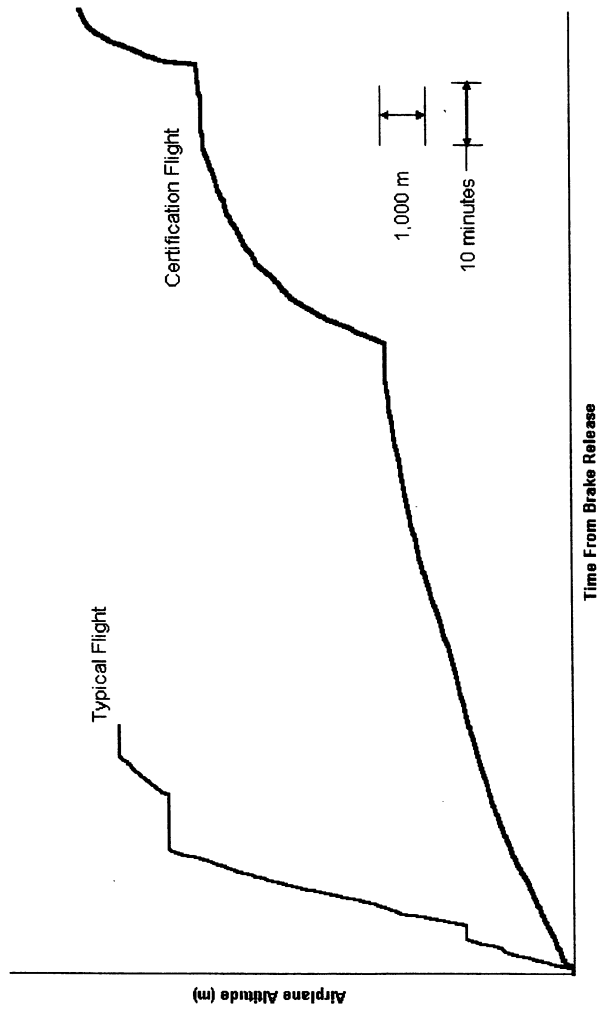
Previous reasons for not pursuing analysis

- Complex geometry unavailable to analysis software
- Lack of user friendly software
- Cost of computing (including speed)



Undercowl ambient temperatures - Requirement

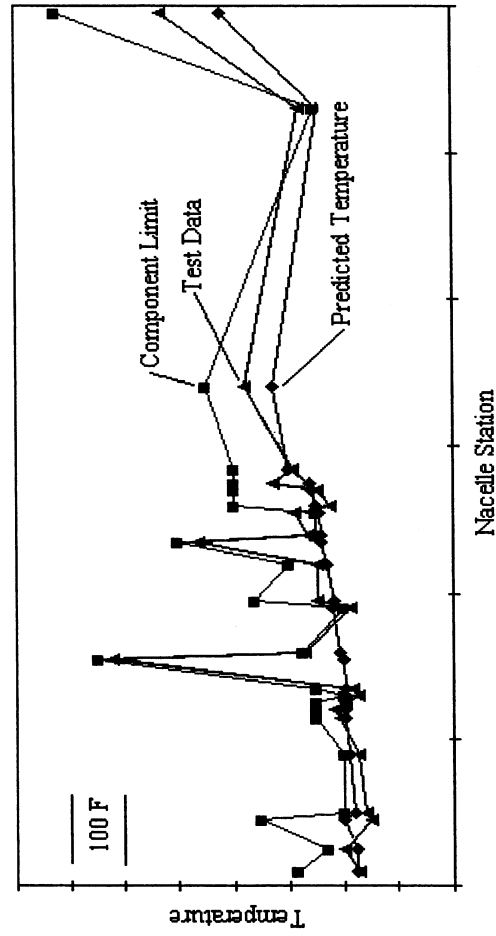
- FAA requires demonstration of cooling system performance, successful test results show that all component temperatures remain within their temperature limits during worst case airplane operating conditions.



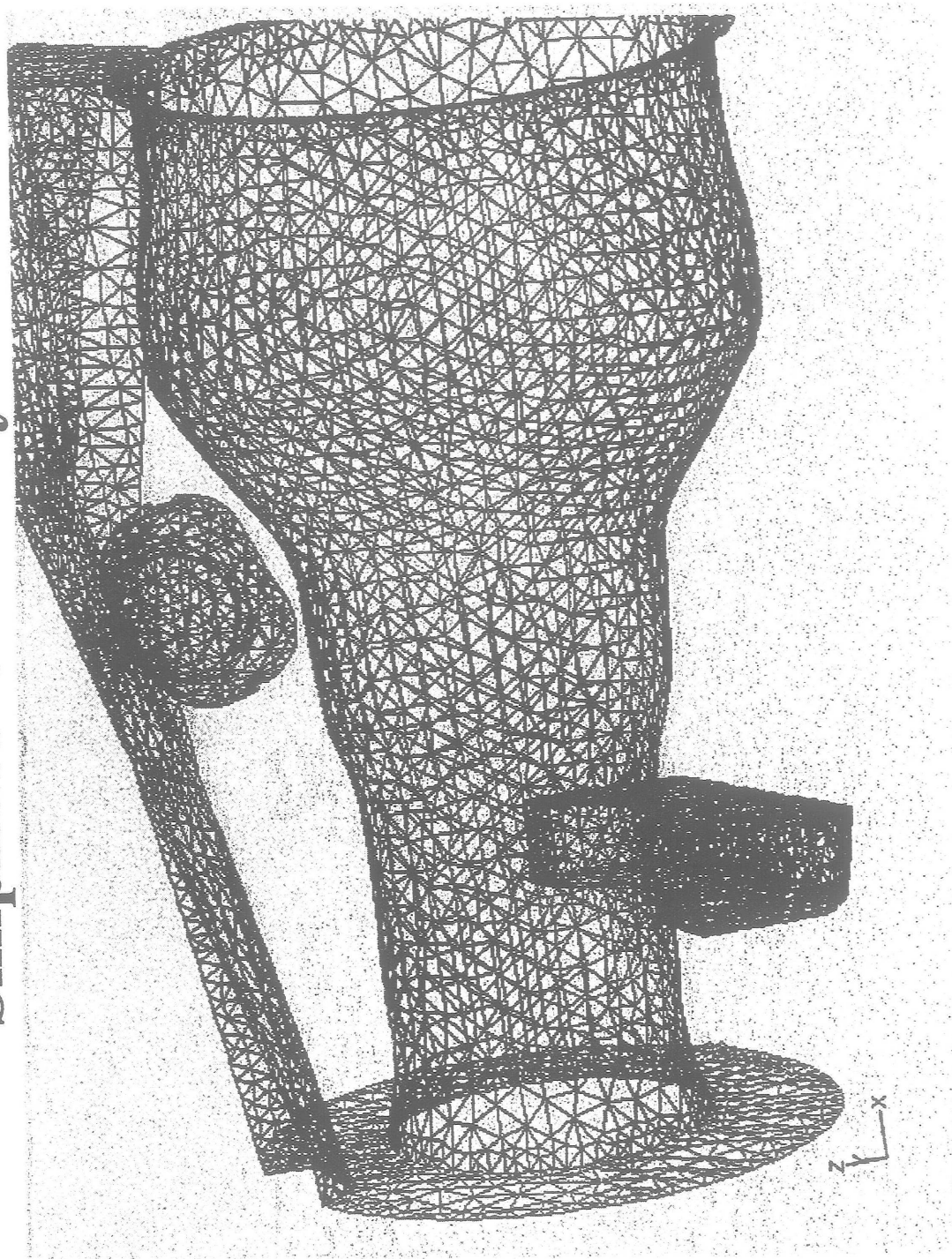
Undercowl ambient temperatures - Current Approach

- Simplistic analysis followed by test (and retest)
 - Analysis assumptions
 - One dimension analysis
 - Uniform mixing of flows
 - Hardware revisions by test (and retest)
 - Schedule disruptions
 - Increased cost

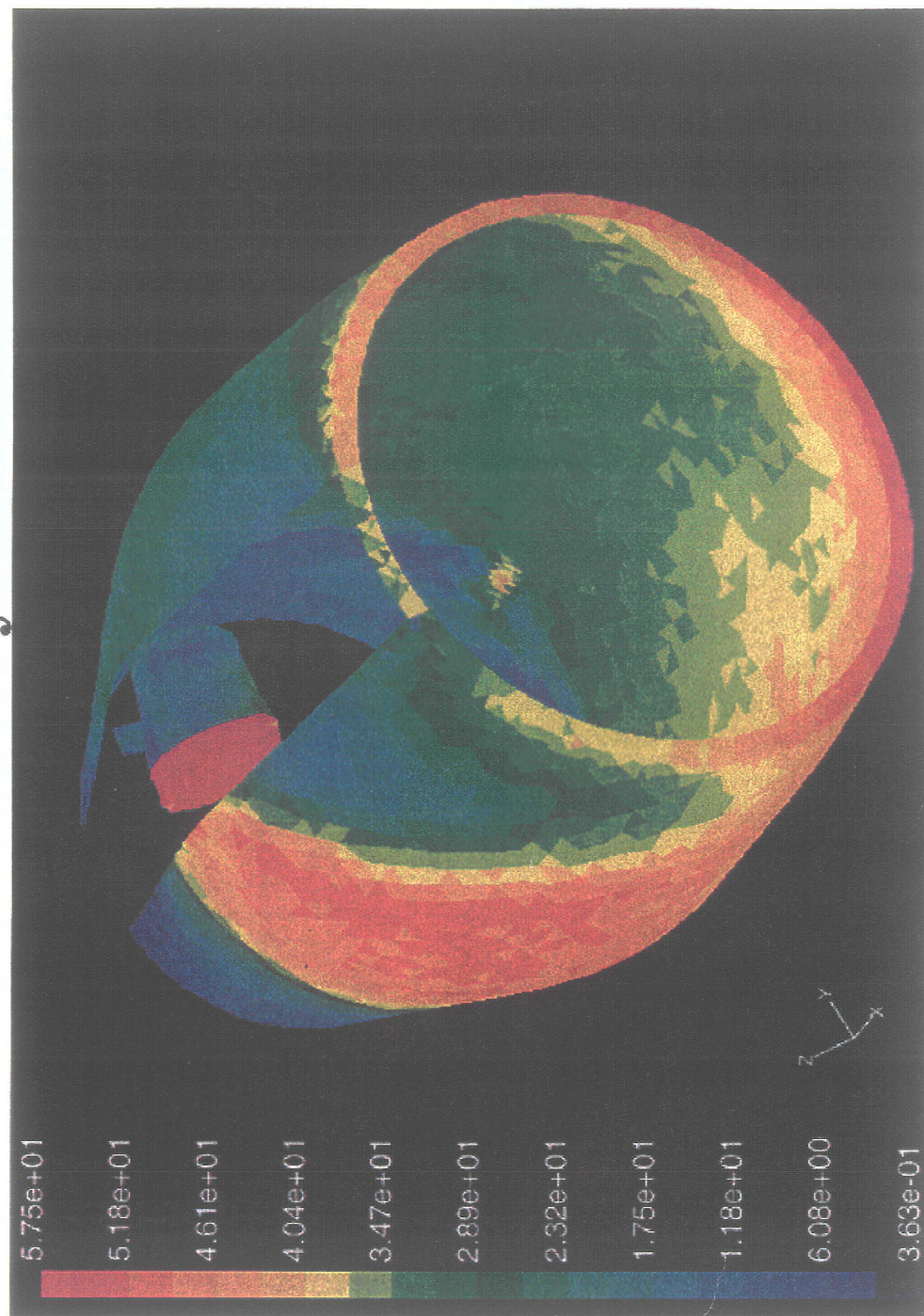
- It costs time and money, but it can be made to work



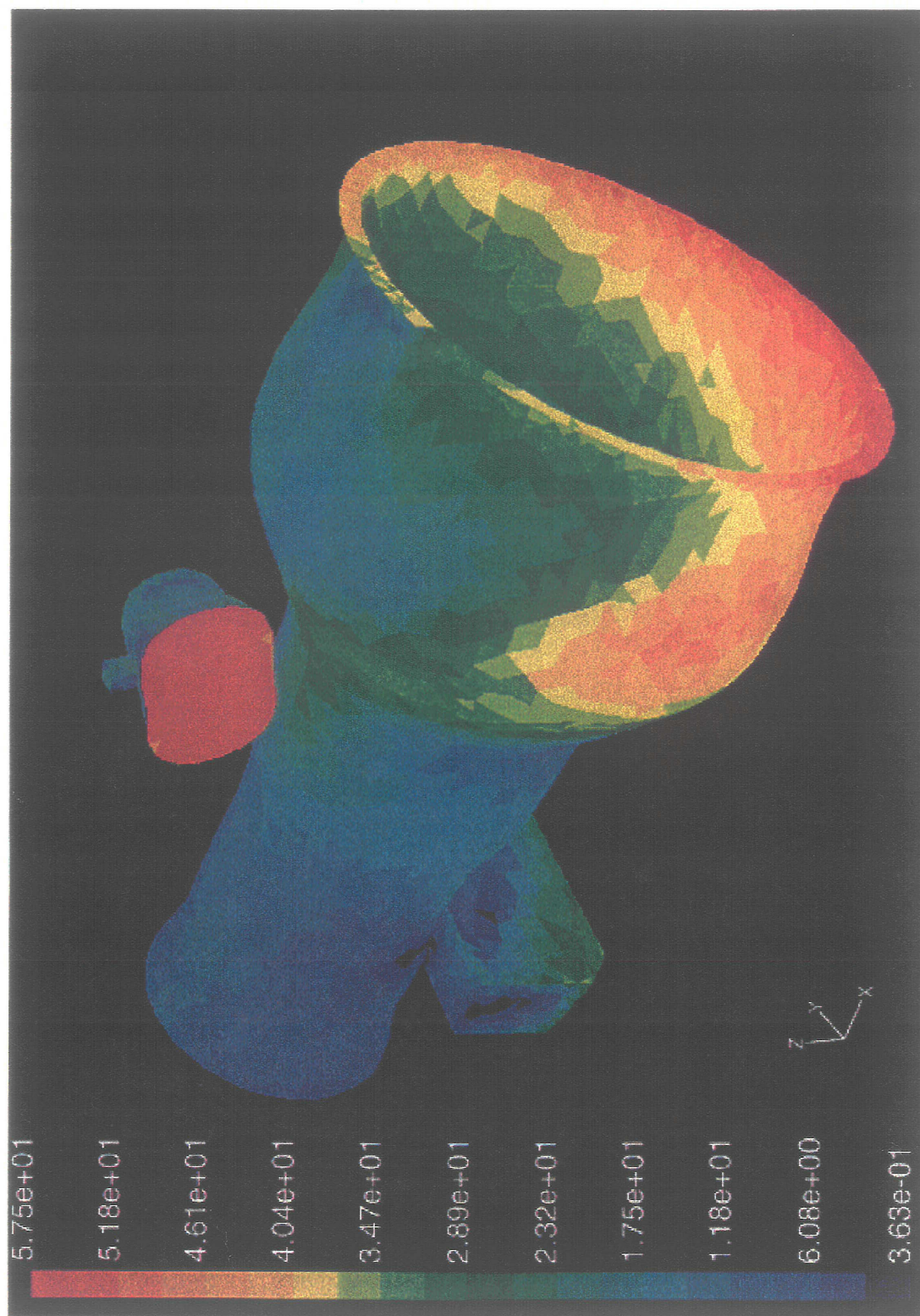
Undercowl ambient temperatures - Simplified Geometry



Undercowl ambient temperatures - Preliminary Results



Undercowl ambient temperatures - Preliminary Results

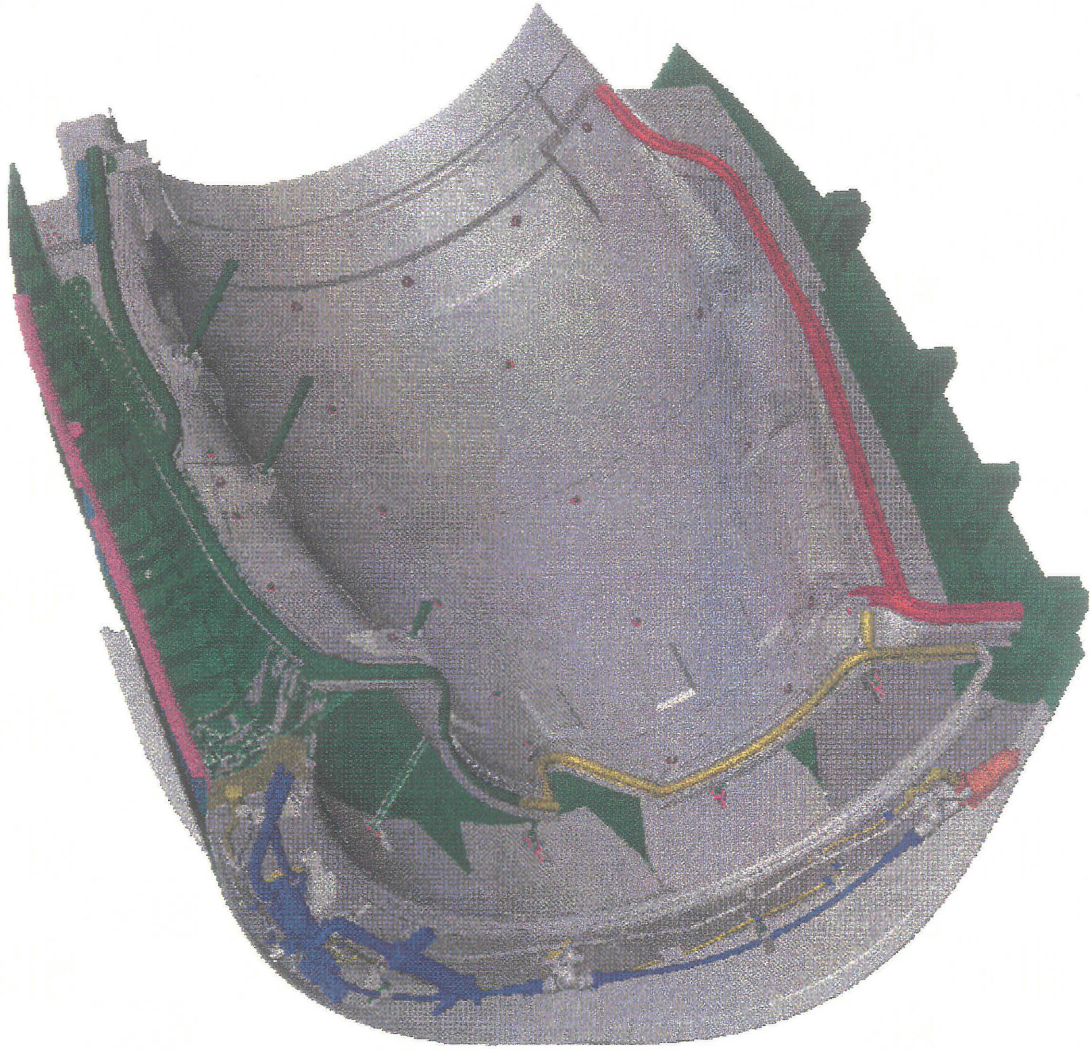


Undercowl ambient temperatures - Proposed Approach

- CFD analysis to determine airflow patterns and temperatures
- Status:
 - First stage of geometry definition complete
 - Major air sources identified and included in model
 - Preliminary adiabatic solution complete
- Future efforts
 - Refine geometry
 - Include engine case heat

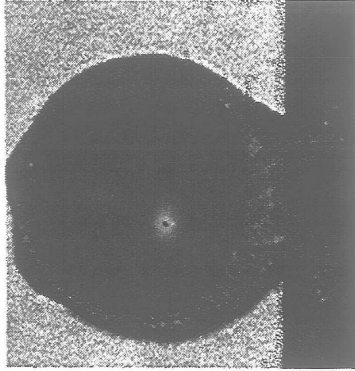
Bulb seal performance - Requirement

- FAA requires demonstration that no “hazardous quantity” of fluid pass between areas of the nacelle designated as fire zones.

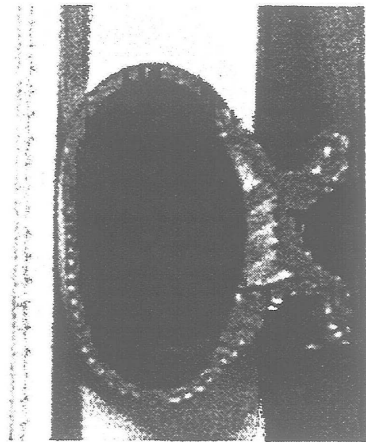


Bulb seal performance - Current Approach

- Boeing uses fireproof, elastomeric bulb seals to provide barriers between fire zones



- Main design concerns
 - Required geometry
 - Ease of manufacture
 - Design standards for seal compression



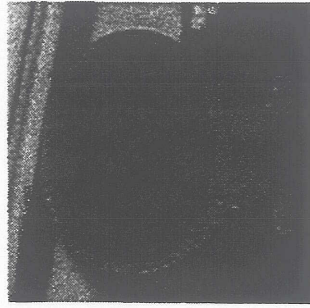
Bulb seal performance - Test Results

- Colored fluids are dumped into fire zones to demonstrate separation
- Mixed colors in the same fire zone indicate a seal leak and failure



Bulb seal performance - Failure Modes

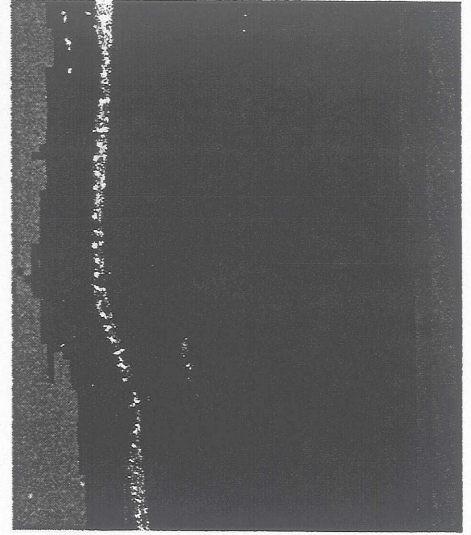
- Incomplete or inadequate seal compression



- Sliding contact (scrubbing) rather than normal compression



- Seal creased during assembly



Bulb seal performance - Proposed Approach

- Finite element modeling of seal to predict response to failure modes, complex geometry and new manufacturing methods

Conclusion

- Valuable insight to the problems of engine externals can be gained by application of analytical tools in new areas
 - Applications should be driven by current design problems that arise in test or inservice.
 - Analytical tools should be easily adapted to new classes of problems.
 - Process can be implemented now to minimize impact to customer.

COMMERCIAL AIRCRAFT MAINTENANCE EXPERIENCE RELATING TO ENGINE EXTERNAL HARDWARE

Sharon M. Soditus
United Airlines
San Francisco International Airport
San Francisco, California

Abstract

In today's business environment, airlines are extremely sensitive to the amount of dollars spent on maintaining the external engine hardware in the field. Analysis reveals that many problems revolve around a central issue, reliability. Fuel and oil leakage due to seal failure and electrical fault messages due to wire harness failures play a major role in aircraft delays and cancellations (D & C's) and unscheduled maintenance. Correcting these items on the line requires a large investment of engineering resources and manpower after the fact. Today's issues are being corrected, but only after many costly delays and cancellations, unscheduled maintenance visits and extensive upgrade programs. And in some cases there have been two or three different design improvement campaigns. In terms of maintenance and reliability of engine external hardware, there is much room for improvement. The smartest and most cost effective philosophy is to build the best hardware the first time. The only way to do that is to completely understand and model the operating environment, study the field experience of similar designs and to perform extensive testing.

Pratt & Whitney PW4000 Engine External Components

This discussion will be limited to the Pratt & Whitney PW4000 engine, one of the newest and most technically sophisticated jet engines operating today. There is over 5 years of field experience relating to the reliability and maintainability of the engine's external components in which to analyze. Presented below are the results of a reliability analysis of external engine components.

External engine components consist mostly of fuel, oil and pneumatic lines, valves, actuators, heat exchangers, gearboxes, fuel and oil pumps, fuel metering units (FMU), engine

electronic controls (EEC), wiring harnesses, sensors and switches and all the hardware necessary to support it such as brackets, clamps and nuts and bolts. All are essential to the proper operation of a jet engine. For example, external components which control the engine's secondary airflow systems are extremely important to efficient and reliable operation. It was determined during the design phase of the engine that the cost to design, test, and manufacture these systems let alone the cost of the additional weight, is greatly offset by their gain in Specific Fuel Consumption (SFC). If one of the systems has to be inop because of a component seal failure, it could mean upwards to 2% additional fuel burn. Over a long mission this additional fuel burn quickly adds up. Thus it is extremely important that all systems are operating properly.

Delays And Cancellations

One of engineering's main objective, in the airline business, is the reduction of delays and cancellations in the fleet. Over the past five years, 1157 delays and 111 cancellations were incurred due to engine related items in the PW4000 fleet for United Airlines alone. A large number of delays and cancellations are related to the reliability of the engine external components. When studying the

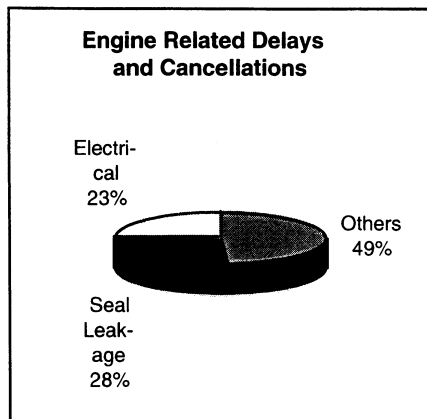


Figure 1

data in even more detail, the majority of reliability items are related to carbon, fuel and oil seal leakage followed by electrical wiring problems. See figure 1. The other category contains items such as bird strikes, hung starts, HPC compressor stalls, etc.

Seal Reliability Issue

Since the introduction of the fleet in 1991, there has been a number of seal related problems which were uncovered in service. Early on there were premature failure of fuel seals in the intercompressor bleed (2.5), stator vane actuator (SVA) and turbine case cooling (TCC) actuators. In addition, fuel leaks within the FMU began to cause a delay and cancellation situation. Later in the program carbon seal leaks appeared in the gearbox and bearing areas. Most of the premature failures resulted in a delay or cancellation which drove the need for aggressive engineering research, development and testing of new designs. In addition, line maintenance personnel was given extensive training on how to recognize leaks which could be safely deferred to the next convenient maintenance opportunity. Because of aggressive projects to replace older, less reliable hardware with newly designed hardware several thousands of revenue dollars were saved on unscheduled line maintenance resulting in on-time departures and an increase in customer satisfaction. A drop in delays and cancellations is finally being realized for in the first half of 1997, the level is one-third less than the first half of 1996. See figure 2.

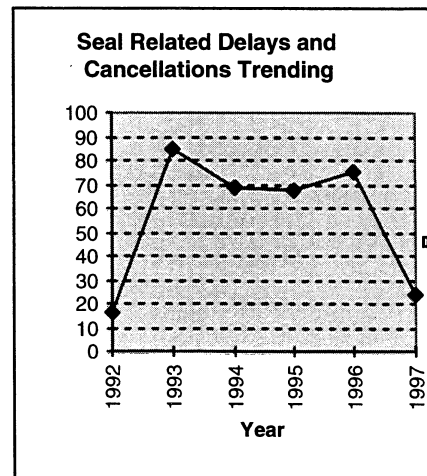


Figure 2

Electrical Reliability Issue

A similar trend can be seen for delays and cancellations caused by electrical problems. See figure 3. Early in the program, actuators also experienced internal wire harness chafing problems which resulted in component failure messages. These units were quickly replaced on the line with units which contained a more robust wire harness design. At the same time, problems with engine wire harnesses and connectors surfaced. Since this is one of the first FADEC engines, both, the manufacturer and end user, had some lessons to learn about how important it was to have a robust harness system. From a manufacturing standpoint the harness design was not robust enough. The aluminum backshells used for the connectors proved not to be durable in service. All backshells were speedily replaced with stainless steel backshells.

Electrical problems with the permanent magnet alternator (PMA) also began to surface. As it turns out, the environment in which this unit is placed was not well understood during the design phase. The original design could not handle the heat and vibration and would fail prematurely. A large amount of engineering effort is now going into developing a more durable unit for the future. As with the leakage problem, additional line training has gone far to reduce the delays and cancellations. Personnel were trained to better troubleshoot and identify electrical issues and how to solve them on the line. What can be seen in

the figure 3 below is all the effort in engineering and education that is paying off with the reduction of

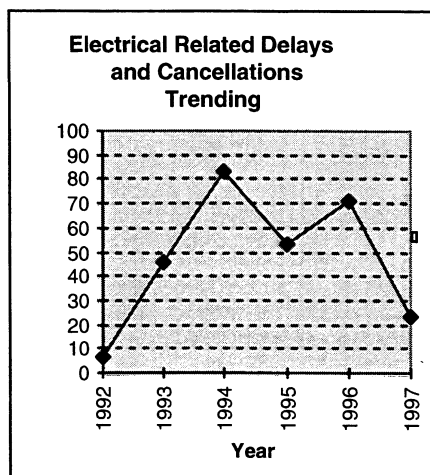


Figure 3
delays and cancellations. The first half of 1997 is also one-third less then the first half of 1996.

Delay's And Cancellations Are Not The Only Story

The delays and cancellations caused by component failure are relatively easy to tabulate. However, component failures have an even greater impact on the system as a whole. A large amount of money is spent on unscheduled maintenance, removal of components and occasionally removal of engines that are damaged by an external component failure. Additionally, there are numerous campaigns to replace older, less reliable hardware with newly upgraded hardware. On the PW4000 engine, the actuators (2.5 bleed, SVA and TCC) alone have had their share of reliability issues from wire management problems to seal failures. From 1992 through 1995 there have been 113 unscheduled component removals due to these problems. Although these failures did not caused a delay or cancellation, they did interrupt the normal engine maintenance schedule.

In order to accomplish the upgrades on these units, over half a million dollars was spent by the airline alone on projects to replace older hardware with upgraded hardware. And then some units were upgraded two and three times

since their introduction in service. Factor in the cost to engineer, manufacture and test new components, it can be clearly seen that an opportunity for substantial cost savings exists. It is here where the airlines and the engine manufacturers can save money in the long run by investing in good research during the design phase of the program.

Engine Performance Is Affected By Reliability

FAA regulations allow an engine to operate with only the minimum essential equipment. The definition of essential equipment is negotiated by the FAA, the engine manufacturer and the airline before engine certification and spelled out in a document call the Minimum Equipment List (MEL). Many of the secondary airflow systems controlled by the external engine hardware is listed in the MEL since they are systems which are not necessary for the safe operation of the engine. And so these systems can be inopted before flight if there is a problem. These systems are mainly used to fine tune the performance of the engine. When one of these systems is inopted, the result is higher fuel burn, lower engine efficiency, and higher exhaust gas temperature (EGT). In this situation, fuel burn can increase anywhere from 0.3 to 2.0 %. The impact of this additional fuel burn on a long mission is serious. Not only will there be the extra cost in fuel but a flight may be weight restricted, thus leaving passengers at the gate or causing an expensive fuel stop at a remote location in the world. The latter two can affect customer trust and comfort in the airline. There is no way to put a price tag on the cost to the airline in this situation.

The Ultimate Goal

The PW4000 engine itself is a robust and reliable engine. A typical engine will operate on wing on an average of 14,000 hours or 4 years between overhauls. What is also expected is that the external components and their systems operate reliably for the same amount of time or longer between overhauls. Once an engine is removed from wing and shipped to the shop for overhaul, all the external components are removed and sent out for complete overhaul. The units are disassembled, cleaned, inspected, reworked, repaired, replaces with new internal parts and assembled with all new seals. Much of the work is

done within United so the component engineers are able to see first hand the condition of the external components after years of service. After assembly, the units are then acceptance tested and made serviceable for use on the production floor or on the line.

Once an engine is overhauled in the shop, the external components assembled on that engine have all been overhauled. The intent is to have these components perform flawlessly in the field until the next engine overhaul. Some components are extremely reliable and some are still less than reliable. The ultimate goal of the component engineer at United is to get closer to 100% reliable performance out of each and every component. This is being done right now by reviewing chronic components of removal from service, completing reliability modifications which directly improve performance of the component and partner with suppliers to United in meeting or exceeding performance goals of each component.

Summary

United Airlines has operated the Pratt & Whitney PW4000 engine for over 5 years. This amount of time has built a good database of experience. Serious study of the data can be very enlightening and reveal opportunities for improvement in current and future component designs. A large amount of time and money is consumed in the field maintaining, repairing, and replacing external engine component due to premature failure.

Today reliability of external engine components and systems are of most the importance. The opportunity exist to have a great impact in the operating cost to airlines by reducing delays and cancellations, improving engine performance, reducing unscheduled maintenance and improving customer thrust and satisfaction. It must start at the design phase. Better modeling of the engine external operating environment will lead to more robust components. This is the challenge for all current and future hardware.

HOW UNITED SERVES THE WORLD TODAY

- AVERAGE 200,000 TO 250,000 PASSENGERS A DAY
 - AVERAGE 2000 TO 2500 FLIGHTS A DAY
 - AVERAGE TURN TIME FOR A DOMESTIC FLIGHT IS 55 MINUTES
 - AVERAGE TURN TIME FOR A SHUTTLE FLIGHT IS 30 MINUTES
-

ReCAT

RELIABILITY IS VERY IMPORTANT

- DELAYS AND CANCELLATIONS
 - UNSCHEDULED MAINTENANCE
 - HIGHER FUEL BURN
 - EXPENSIVE UPGRADE PROGRAMS
-

ReCAT

RELIABILITY IS VERY IMPORTANT

- PW4000 ENGINE PROGRAM ALONE
- DURING 1992 - 1995
 - 1157 DELAYS AND 111 CANCELLATIONS ARE ENGINE RELATED
- AVERAGE OF ONE D & C PER 0.9 DAYS
- MAJORITY OF THESE ISSUES ARE EXTERNAL COMPONENT

ReCAT

SIMILAR ISSUES ARE SHARED ACROSS THE FLEET

- ACTUATOR SEALS LEAK
- GEARBOX CARBON SEALS LEAK OR COKE
- SENSORS AND FEEDBACK SYSTEMS GIVE ERRONEOUS MESSAGES
- HARNESES WILL CHAFE

ReCAT

THE IMPACT IS GREATER

- 1992 - 1995
 - 113 UNSCHEDULED ACTUATOR REMOVALS ALONE
 - OVER \$0.5M SPENT IN UPGRADE CAMPAIGNS

- UP TO 2% INCREASE IN FUEL BURN
-

ReCAT

THE GOAL

- AVERAGE ENGINE OPERATES FOR 14,000 HOURS OR 4 YEARS

- BRING EXTERNAL COMPONENT RELIABILITY UP TO 100%
- COMPLETE RELIABILITY MODIFICATIONS
- PARTNER WITH SUPPLIERS TO MEET GOAL

ReCAT

LEARN FROM EXPERIENCE

- RELIABLE COMPONENTS ARE IMPORTANT TO EFFICIENT OPERATION
- BETTER MODELING DURING DESIGN PHASE
- STUDY OF THE CURRENT DESIGNS AND THEIR RELIABILITY
- PARTNER WITH THE CUSTOMER TO LEARN FROM THEIR EXPERIENCE

ReCAT

United Airlines Engine Condition Monitoring System

United Engine Data Acquisition

United utilizes a automated data collection system to acquire on-wing engine data that is to be used for engine condition monitoring. With the exception of a few airplanes, United's airplane fleet uses the Aircraft Communication Addressing and Reporting System (ACARS) either through pilot input or by automated data acquisition equipment.

Once data is transmitted from the airplane, the Aeronautical Radio Incorporated (ARINC) network receives and processes the message and transmits the message to the United ground station at CHICAGO. The message at the ground station is then processed by a number of UAL software applications. The data is then databased for a period of 6 months. Airplane message data is then used by other software applications for engine parameter trending (ECMII), engine fuel consumption guarantees, airplane aerodynamic guarantees, engine reduce thrust statistics, etc...

United Engine Condition Monitoring (ECM)

United Airlines engine condition monitoring program consists of a number of software application tools to monitor on-wing engine health. Engine problems transparent to the pilot can be identified using certain data analysis techniques. The use of these techniques allow United Airlines to identify and correct engine problems before an operational penalty is encountered. The software tools that allow these techniques to work are summarized below.

- On-Board Monitoring Equipment:

Some of United's airplanes utilize Digital Flight Data Acquisition Unit (DFDAU) and Aircraft Monitoring System (ACMS) equipment to monitor engine conditions. This equipment uses real time software to monitor data parameters for given engine conditions. When a given engine condition exists, a message is compiled and transmitted through ACARS. Routine reports used by United Airlines include engine start, takeoff, and stable cruise. In addition, abnormal engine conditions are monitored continuously for aborted takeoff, in-flight engine shutdown, engine limit exceedance, engine stall, N1 overboost, etc...

- Fault Analysis Alerts:

When an airplane message is received, corrected and/or raw parameters are compared to expected minimum, maximum, or difference between engine values, redundant instrumentation (e.g. TAT and T2), engine control schedules (e.g.. N2 vs VSV position, etc...). If the transmitted data parameters fall outside of the expected window, a Fault Analysis Alert message is sent to the applicable engineering group.

- ECM Manual Message Table:

When an airplane is required to be closely monitored, this table allows the applicable engineering group to specify the airplane, departure station, and/or airplane messages that need to be seen. When the airplane meets the input requirements an ECMMSG message is sent to the applicable engineering group. This allows the group to monitor engines to confirm a given engine condition or troubleshooting fix.

United Engine Condition Monitoring (ECM) continued

- Electronic Engine Control (EEC) and Vibration Monitoring Unit (AVM) Status Alerts:

Under normal operating conditions, the configuration of the input and output to the EEC/AVM is known. Data on the EEC/AVM configuration is provided in messages transmitted from the advanced technology airplanes (757, 767, 747-400, A320, etc...). Tables are set up to identify inputs and normal EEC/AVM configuration for routine messages. Data from the airplane message is compared to the table data. If differences occur which would identify an abnormal configuration, an EEC/AVM Status Alert is sent to the applicable engineering group. The status alert identifies the suspect input/output component so that troubleshooting action can be taken. This application provides the ability to replace the correct FADEC system component therefore reducing EEC unconfirmed removals.

- ECM On-Line Database:

As data is received by the ground station, collection of data is stored in a database. The data stored is accessible on-line for view and electronically for ad hoc applications for engine troubleshooting and performance studies. In addition, other software applications use this database to acquire data for their use.

- Pratt and Whitney ECMII:

This software provide basic trend monitoring for primary engine parameters for short and long term trending. Airplane collected during the day is processed daily. Output from this application is used for engine failure prevention, troubleshooting, and engine removal planning and repair requirements.

- Pratt and Whitney Engine Fleet Ranking Report:

This software uses stable cruise data to determine an Exhaust Gas Temperature (EGT) index that is used to rank engines from worst performance to best. Output from this application is used for engine failure prevention, troubleshooting, and engine removal planning and repair requirements.

- Pratt and Whitney TEAMIII:

A product of Pratt and Whitney Diagnostics Systems Group and supports PW products such as the PW4084 and IAE V2500 engine. This software uses takeoff and stable cruise data to determine a broad diagnosis of the engine health. Output from the program provides information on engine primary parameter trends, internal pressure and temperature parameter trends, engine module performance analysis (FAN, LPC, HPT, and LPT), and engine instrumentation analysis. Output from this application is used for engine failure prevention, troubleshooting, and engine removal planning and repair requirements.

- Engine Reduce Thrust Statistics

The software provides United Airlines to trend how many reduce thrust takeoffs are performed and the amount of reduced thrust for each aircraft fleet.

- Fuel Consumption Guarantee

Each engine manufacturer provides a fuel consumption guarantee. The collection of engine stable cruise data and processing through ECMII is the base for administration of the guarantee.

Other United Airlines Applications

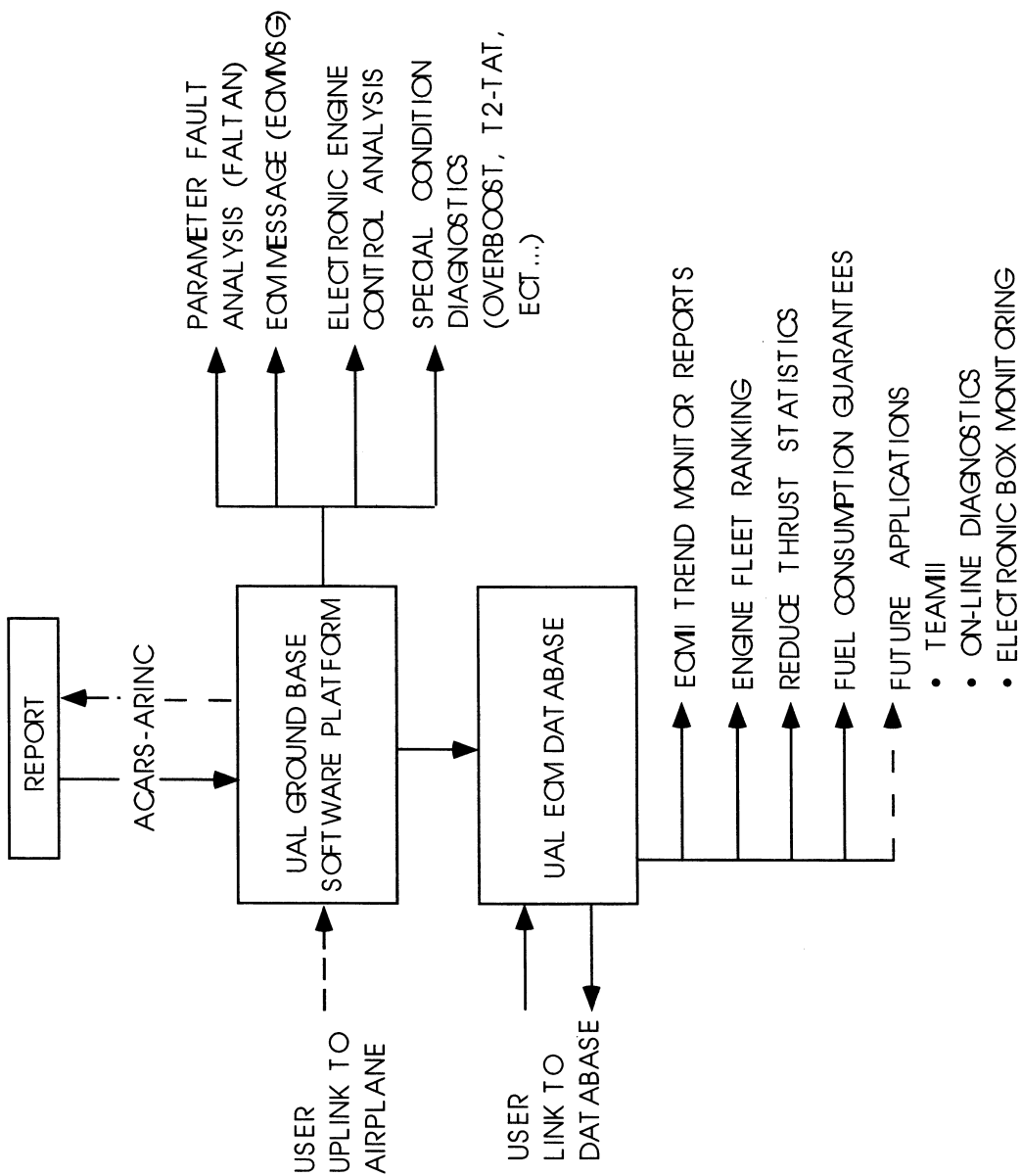
- Aircraft Performance Monitoring

Stable cruise data collected in flight is processed through Uniteds Cruise Data Survey to determine specific range for each operating aircraft. Output from this application is applied to the fuel load planning to ensure fuel loads are adequate for a given flight. On newer generation aircraft Airplane Performance Reports are generated for input into this application; other aircraft use data from the engine reports. This application is equivalent to the Boeing and Airbus airplane performance software.

- Other Reports Transmitted and Used

Auxiliary Power Unit (APU) Reports
Environmental Control System Reports
Autoland Reports
Weather Reports

UAL DATA FLOW SCHEMATIC



737/CFM56-7 AIRCRAFT ENGINE SYSTEMS

Steve Wright and Justin Shiosaki
The Boeing Company
Seattle, Washington

ABSTRACT

The configuration of the propulsion system engine externals must meet many airplane requirements such as cost, thrust, weight, range and systems power extraction. On the 737-700 several program requirements also played a major role in the development of the engine externals. These program goals were increased range, same cost as a 1994 737-300, 15% reduction in maintenance costs from the 737-300, and a propulsion package that appeared as if it was designed by one company.. This presentation will show how these requirements shaped the design of the engine externals for the 737-700/CFM56-7B.

Engine Installation



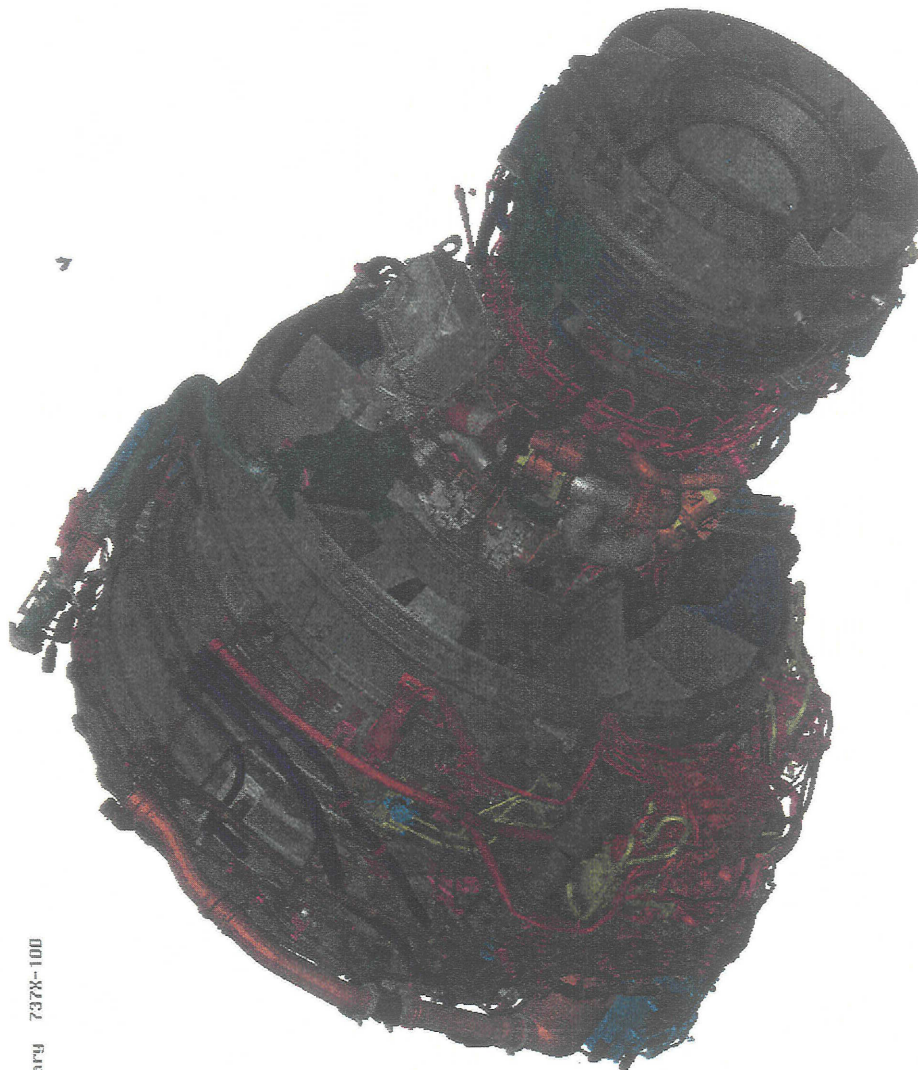
Boeing



Boeing Designed Systems

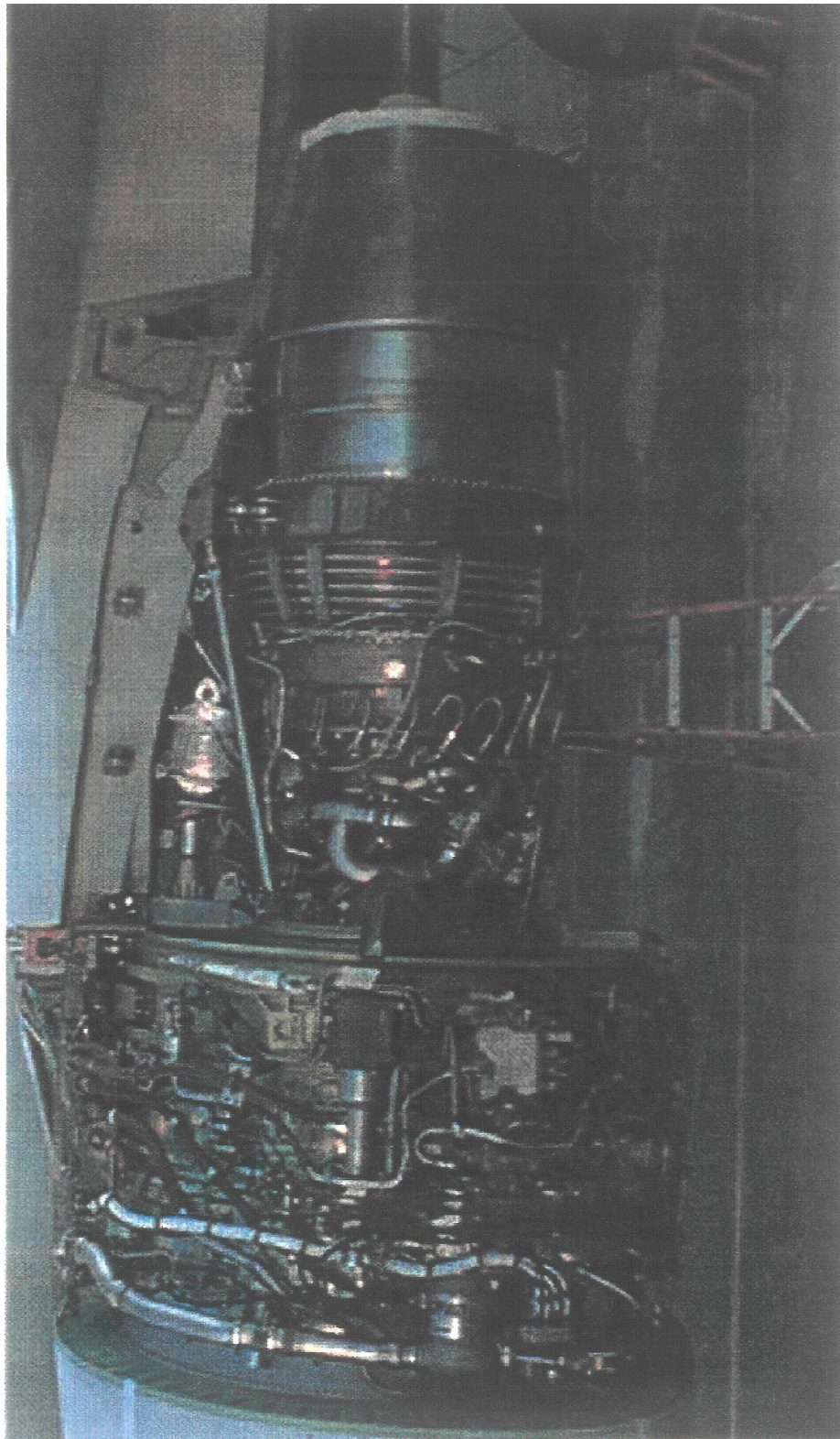
- Pneumatics - ducting, valves, controllers, precooler
- Starting - ducting, valve
- Integrated Drive Generator (IDG) - power feeder cables, cooling
- Cowl Thermal Anti-Ice (CTAI) - ducting, valve, controller
- Fire Protection - fire detectors, drains, extinguishing
- Fuel Line
- Hydraulics - hoses, tubes, case drain filter

CFMII and Boeing

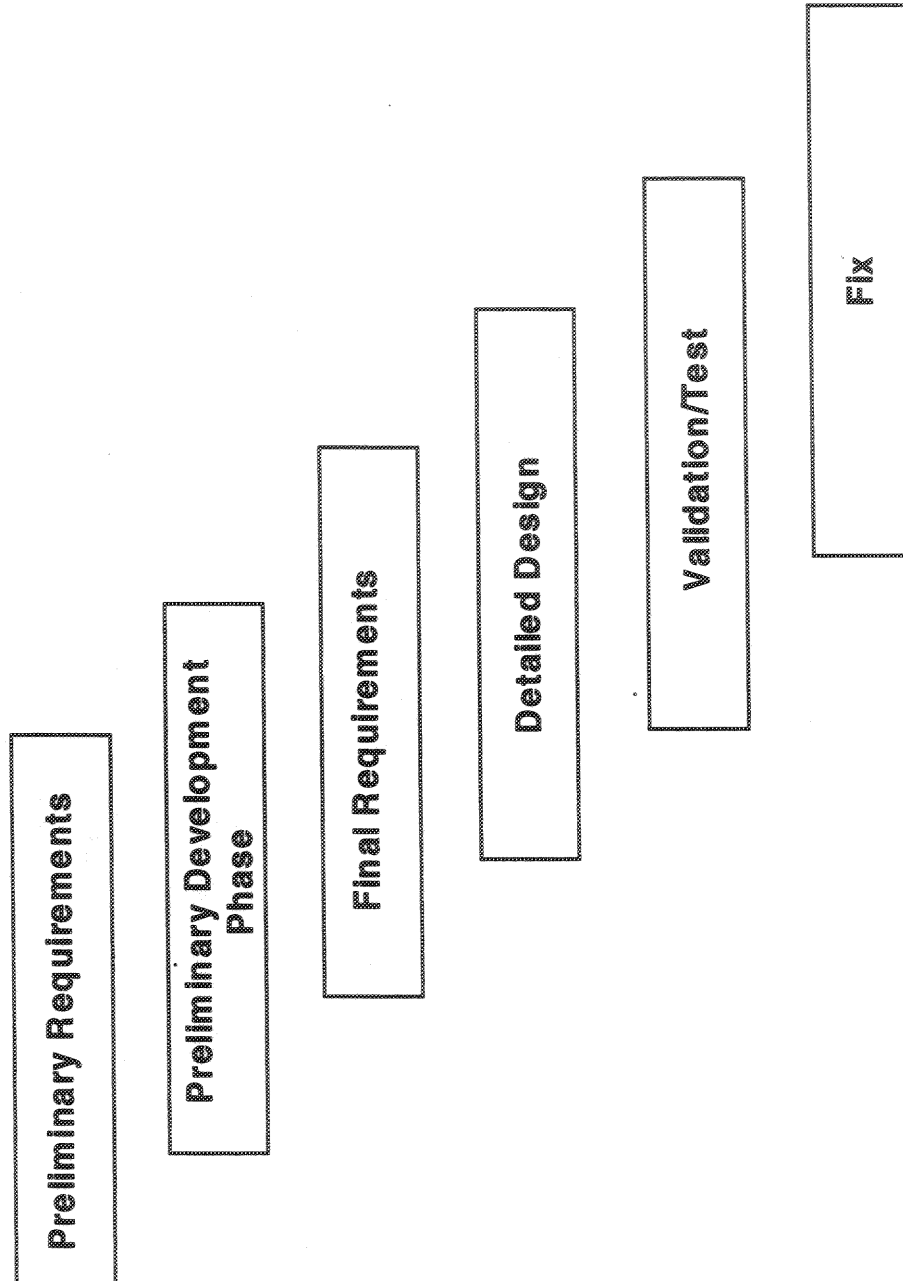


ary 737X-100

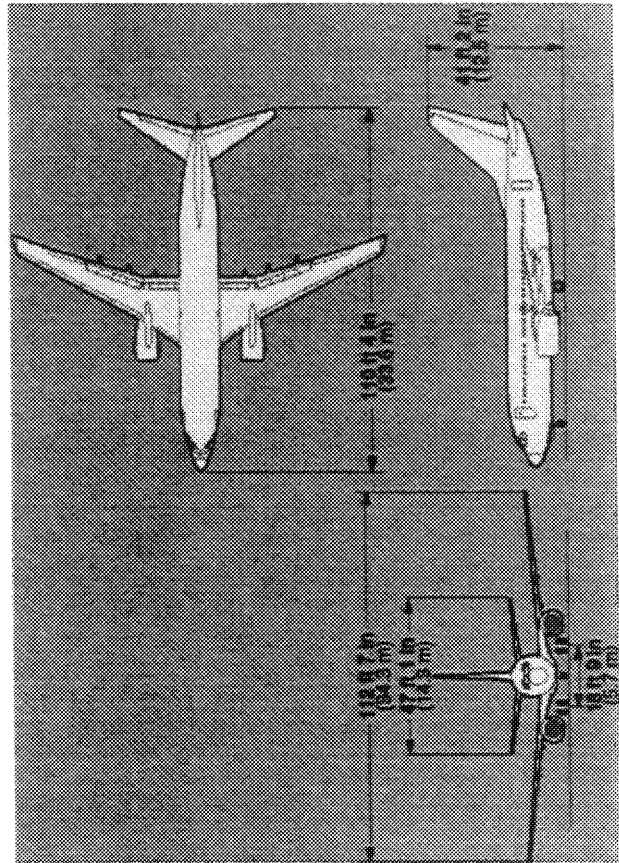
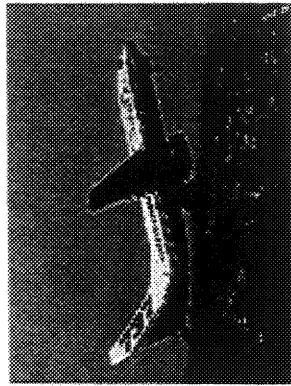
Engine Without Cowl



How We Ended Up With This Configuration



737-700



737NG AIRPLANE FOCUS

- **Past**
 - **Fly It**
 - **Higher**
 - **Farther**
 - **Faster than competition**
 - **Boeing's Economics**
- **Present**
 - **Emphasize Airline's Economics**
 - **And Fly It**
 - **Farther**
 - **Faster**
 - **Higher than current 737**

737NG ENGINE FOCUS

- **Decrease**
 - Noise - Stage 3 minus 4 db
 - Fuel Burn - 7.7% lower SFC than CFM56-3C-1
 - Maintenance - 15% less maintenance cost than CFM56-3C-1
 - Cost - same price as today's 737
- **Increase**
 - Thrust - up to 26,400 lbs
 - Reliability/Time on Wing

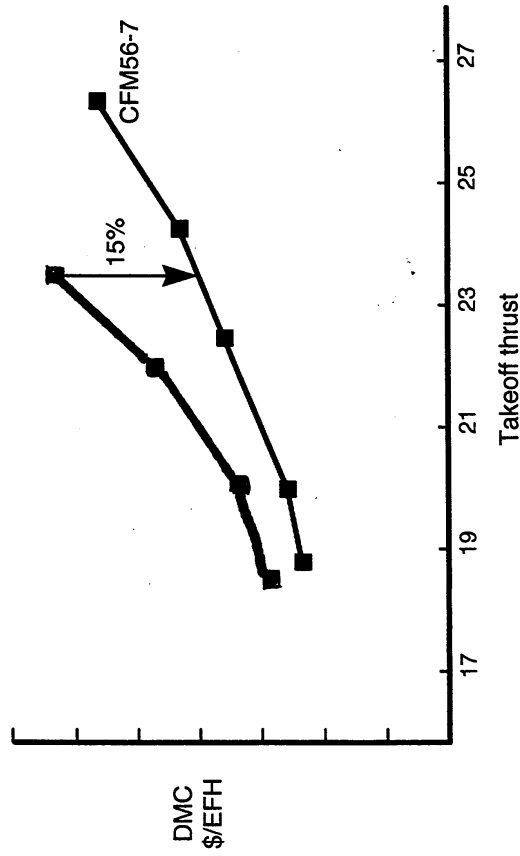
737NG EBU FOCUS

- **Decrease**
 - **Maintenance**
 - **Fuel Burn (indirectly)**
 - Minimize weight, cooling air**
 - **Cost**
 - Recurring and Non-Recurring**
- **Increase**
 - **Reliability/Time on Wing**

*** RELIABILITY AND MAINTAINABILITY WERE KEY
DESIGN INFLUENCES**

Reduced Maintenance

- **15% Reduction in Total Direct Maintenance Cost from 737-300**
- **Get Customer Input Early**
 - **Ease of component removal was a primary focus**
 - Digital verification for all LRU's by design engineers
 - Physical validation by airline mechanics



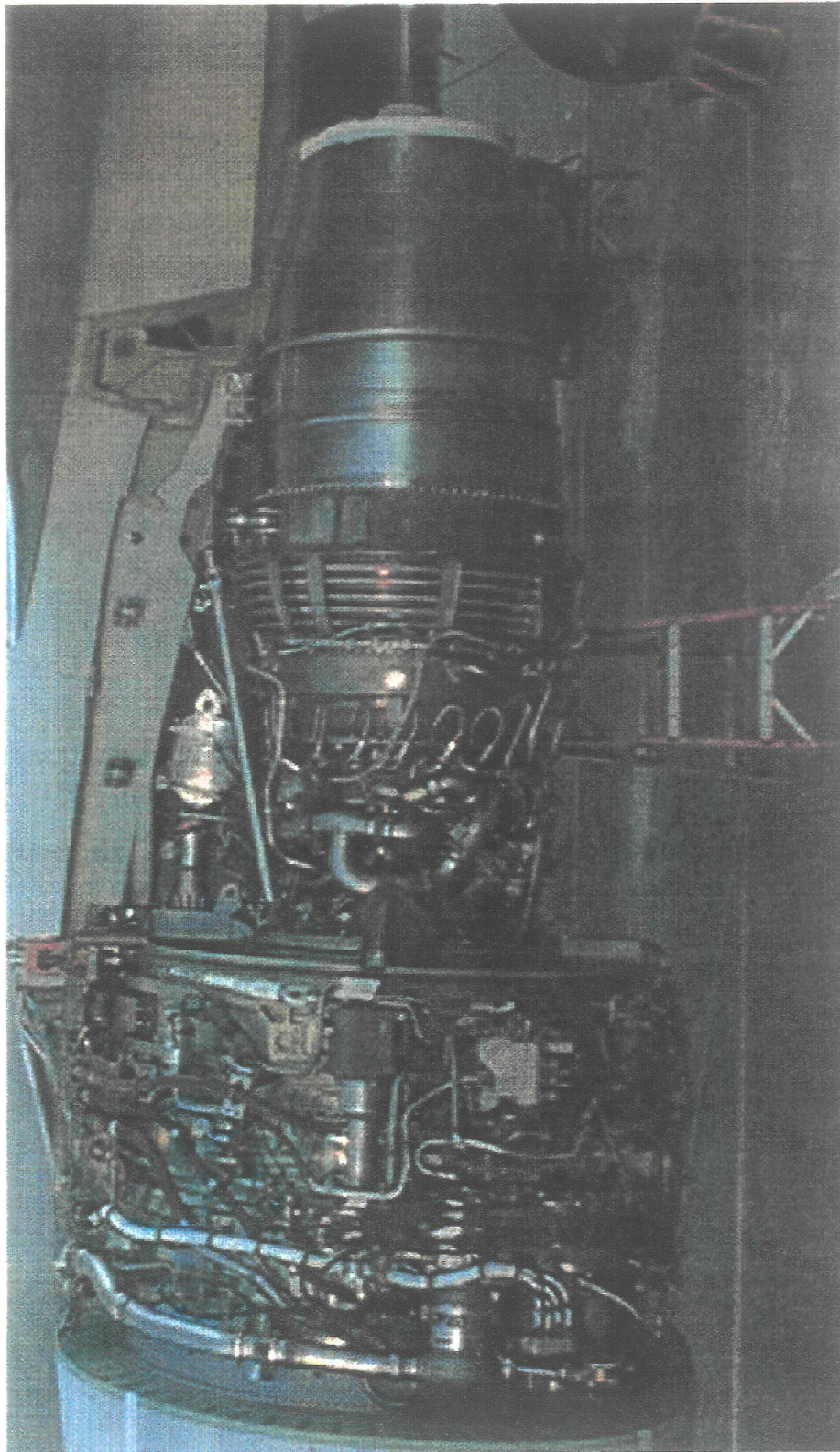
Improved Reliability

- **Use Existing Components if Reliable**
 - **Bleed Air Valves and Regulators**
- **Lessons Learned Incorporated From Other Programs**
 - **CTAI Valve, Starter, IDG, Fire Detectors**
- **New Technologies Must Be Proven Out**
 - **Precooler Control Valve**
- **Extensive Testing to Validate Designs**
 - **Complete EBU package on all engine tests (goal)**

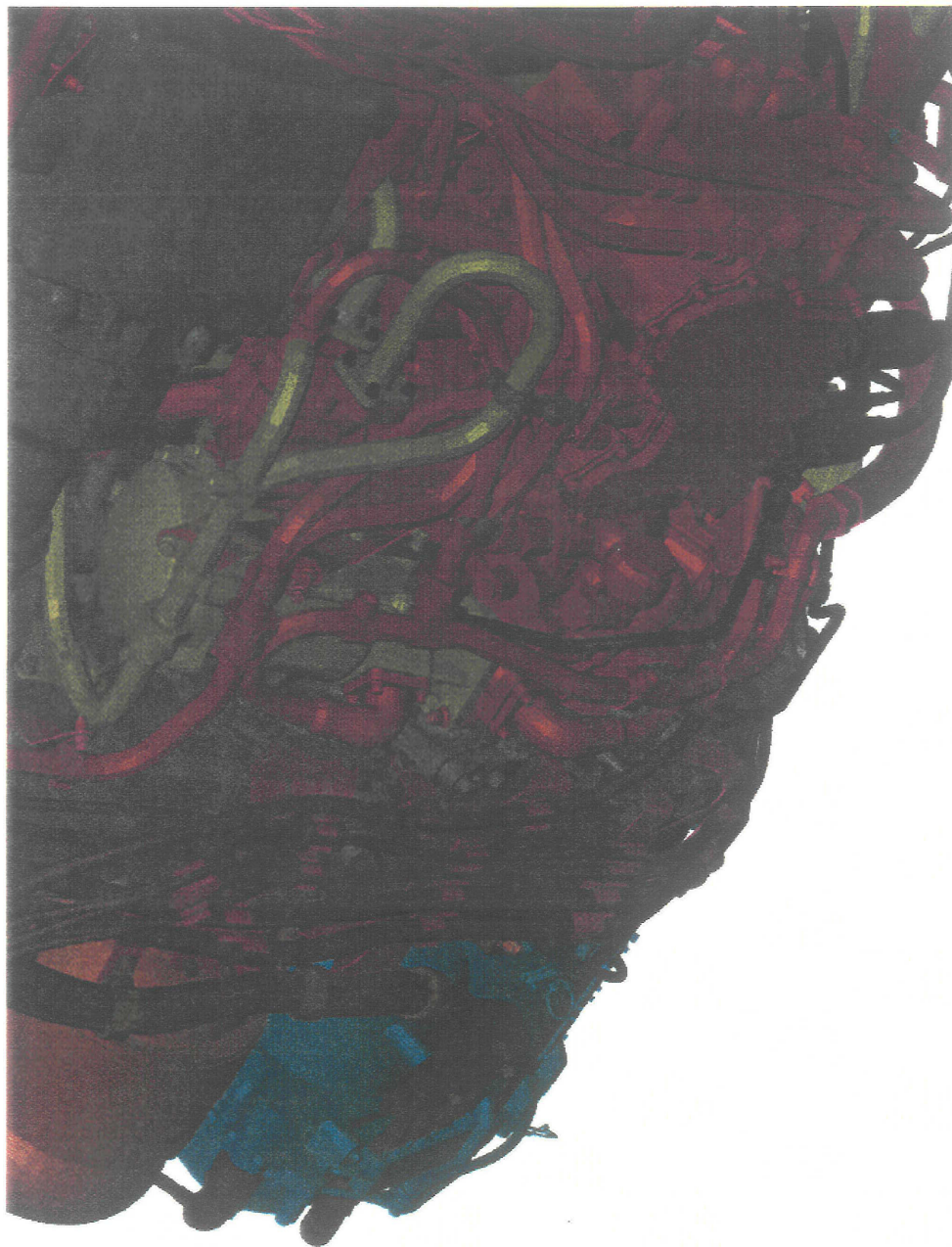
INTERNAL EQUIPMENT BASIC REQUIREMENTS

- **PERFORM INTENDED FUNCTION**
- **CAN BE INSTALLED ON THE AIRPLANE**
- **BUILDABLE**
- **WITHSTAND INSTALLATION ENVIRONMENT**
 - Vibration
 - Fatigue - Last the Life of the Airplane
 - Temperature
 - Fluid Resistance
- **MEETS FAR'S**

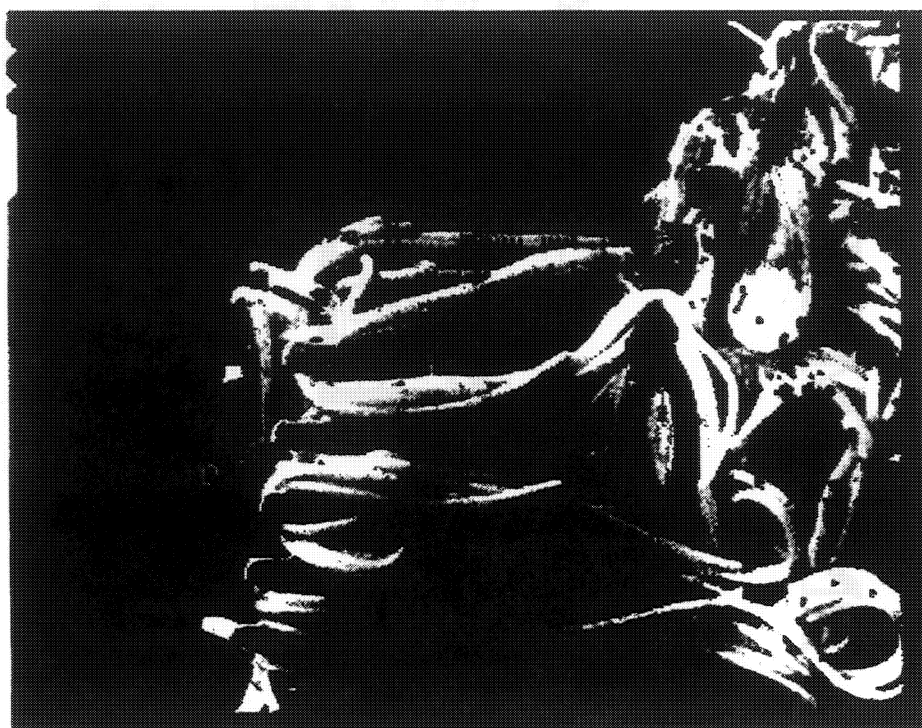
Engine Without Cowls



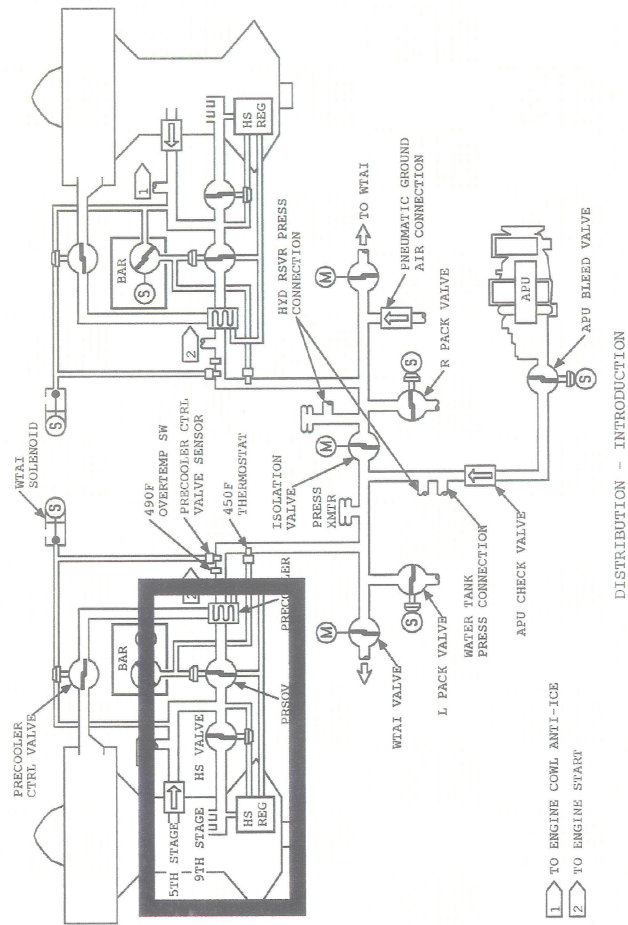
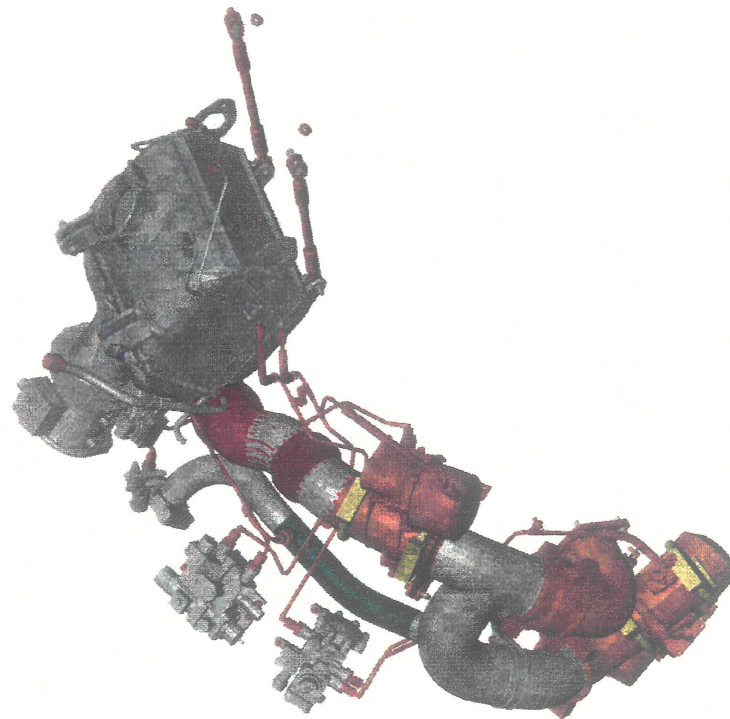
SPAGHETTI



SPAGHETTI

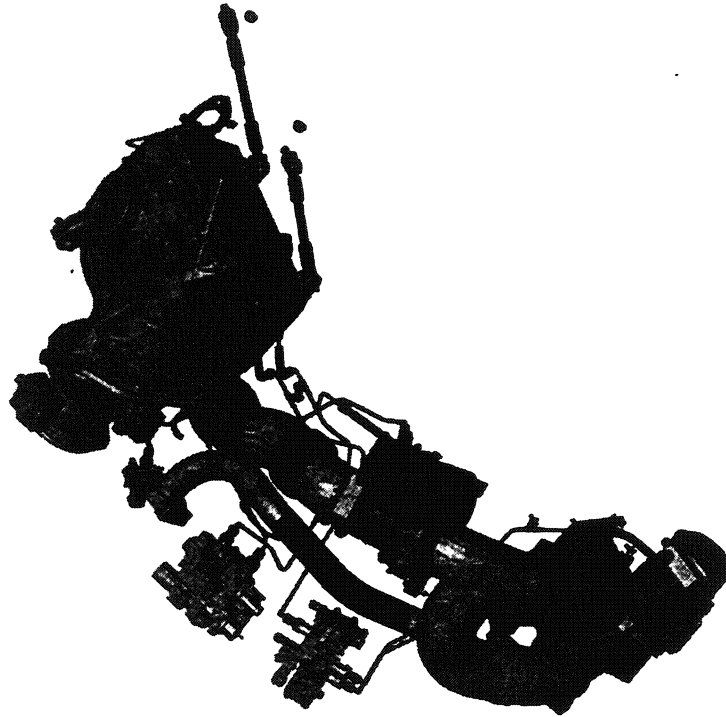


PNEUMATICS

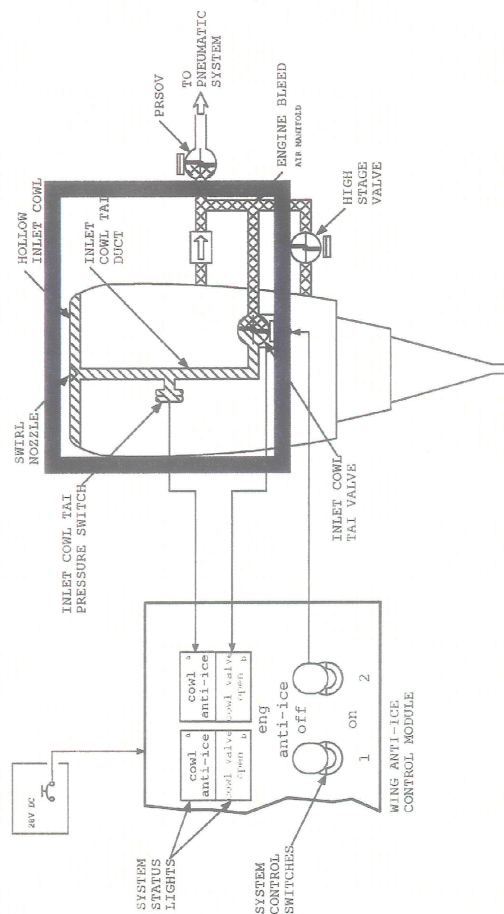


PNEUMATICS

- Responsibilities
 - Ducting
 - Flex Joints
 - Flanges
 - Valve Installation
 - Controller Installation
 - Precooler Installation
- Requirements
 - Pressurize the Airplane
 - Temperature Control
 - Pressure Relief
 - Nacelle Cooling / Engine Case Distortion
 - Equipment Removals
 - Pressure Loss
 - MTBUR



CTAI



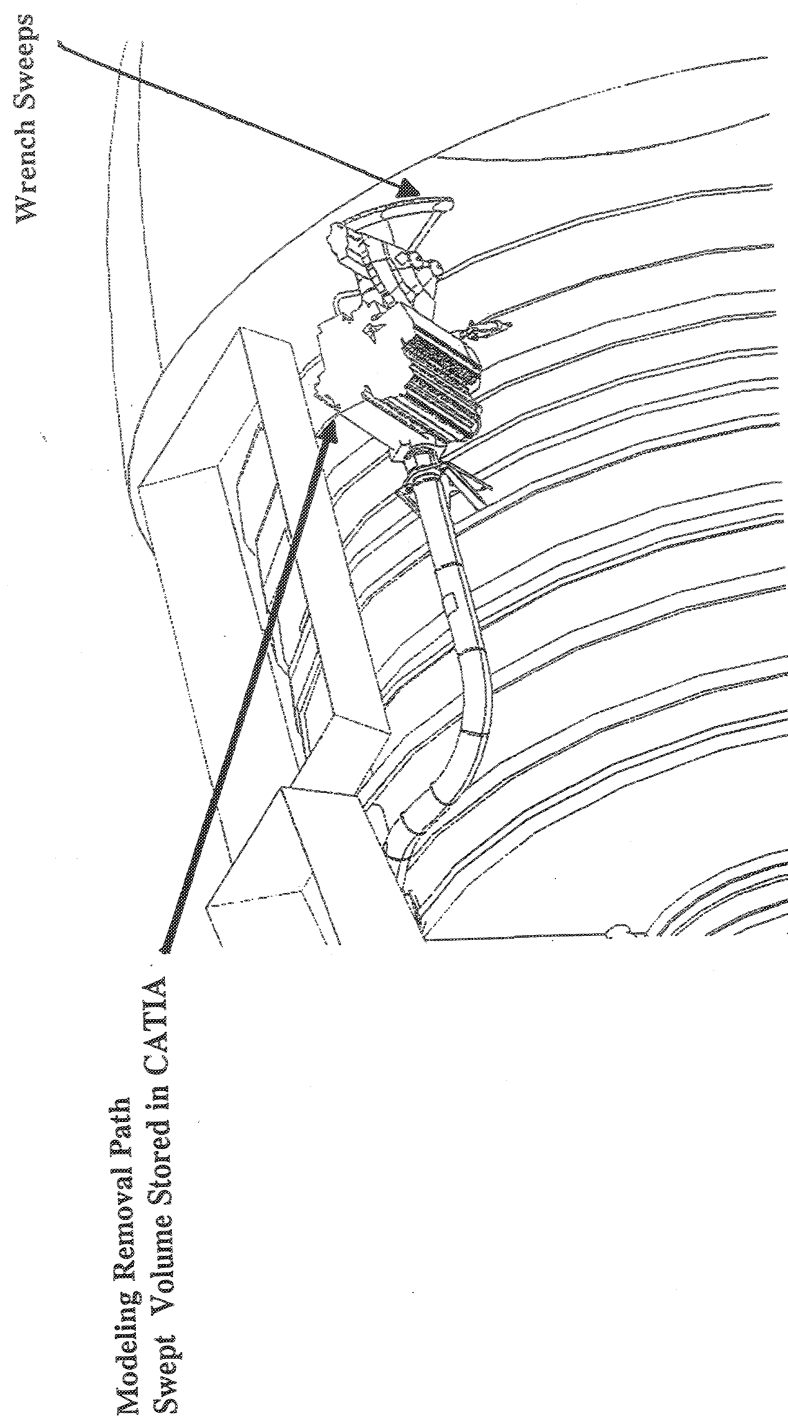
INLET COWL ANTI-ICING SYSTEM - INTRODUCTION

CTAI

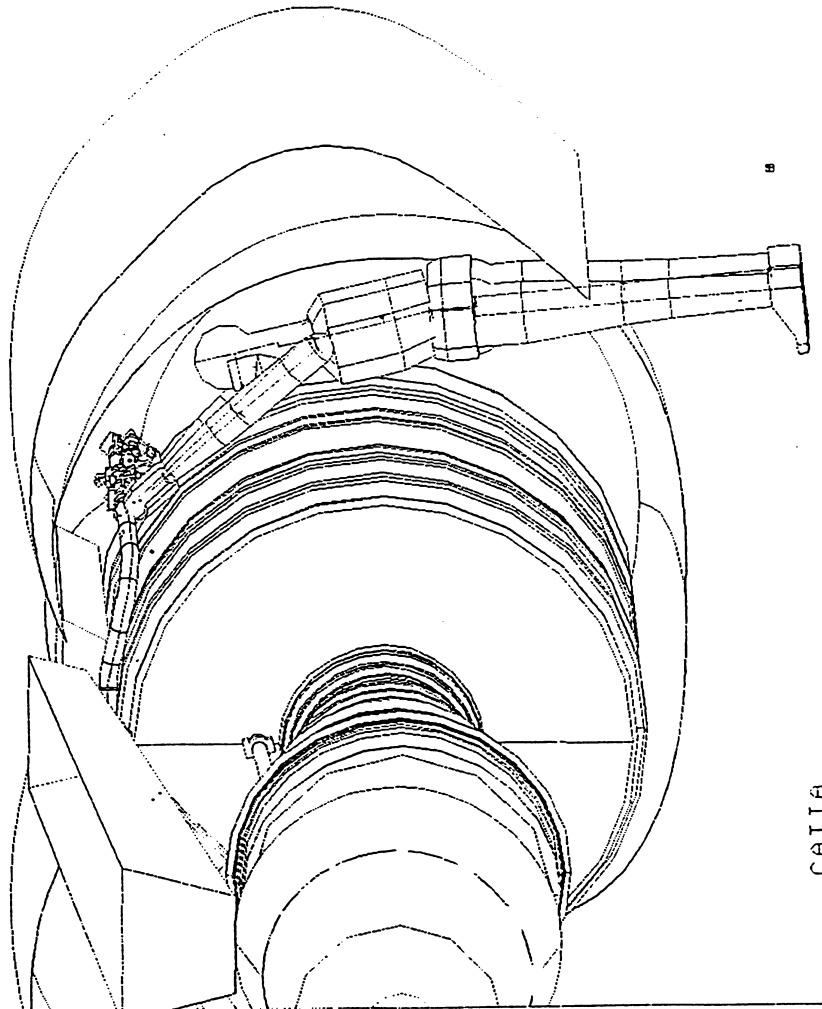
- Responsibilities
 - Ducting
 - Flanges
 - Valve
 - Pressure Sensor Installation
- Requirements
 - Anti-Ice Engine Inlet
 - Pressure Drop
 - Heat Rejection into Fan Compartment
 - Valve Removal
 - MTBUR



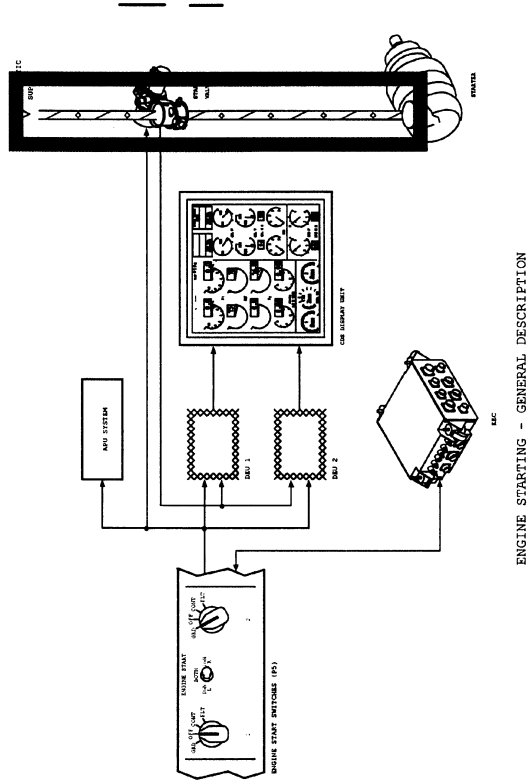
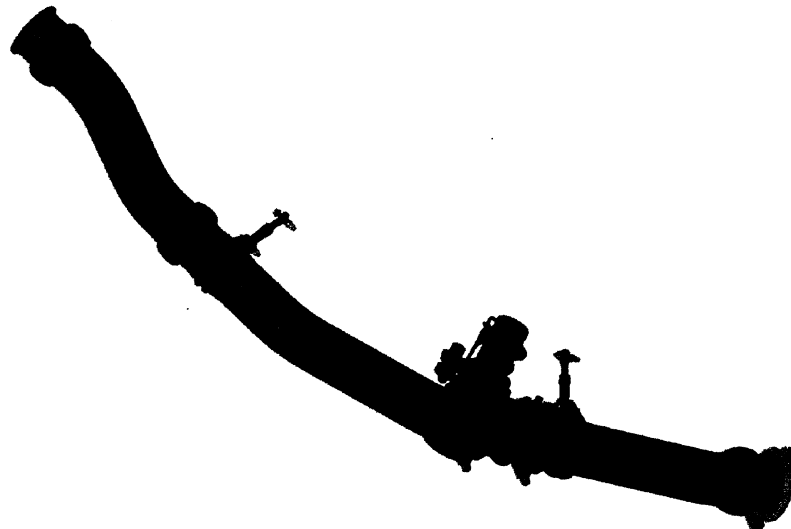
PNEUMATICS MAINTENANCE



PNEUMATICS MAINTENANCE



STARTER



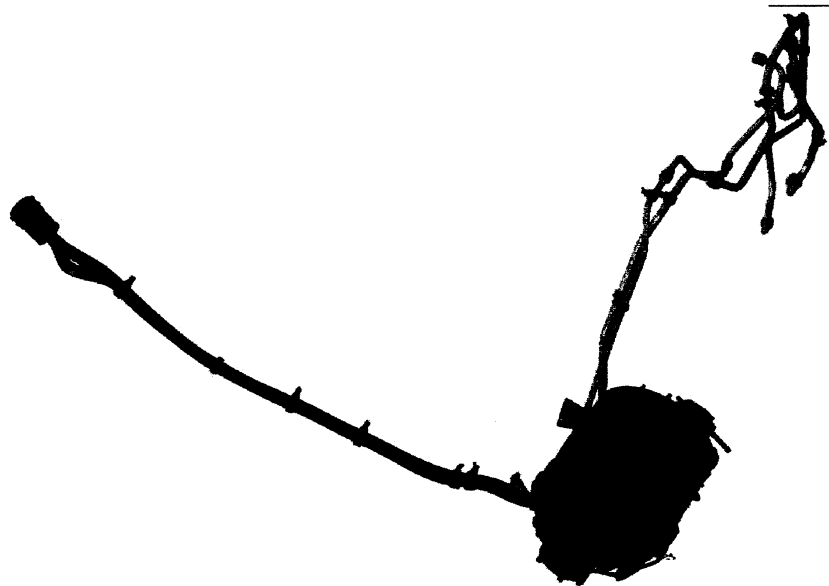
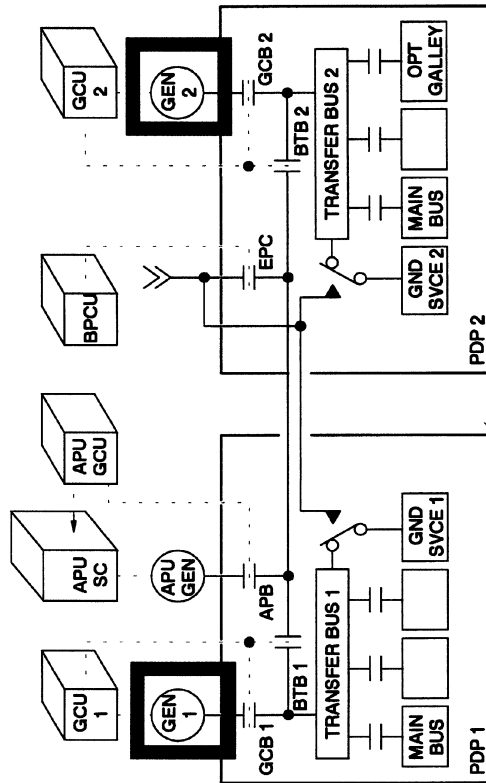
Change identifier in View - Header and Footer

STARTER

- Responsibilities
 - Ducting
 - Flex Joints
 - Flanges
 - Valve Installation
- Requirements
 - Supply Air to the Starter
 - MTBUR
 - Valve Removal

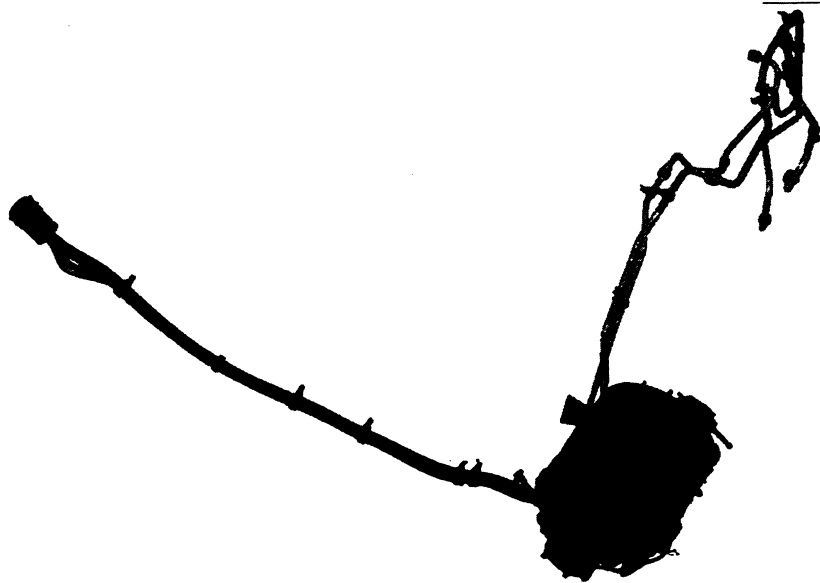


IDG



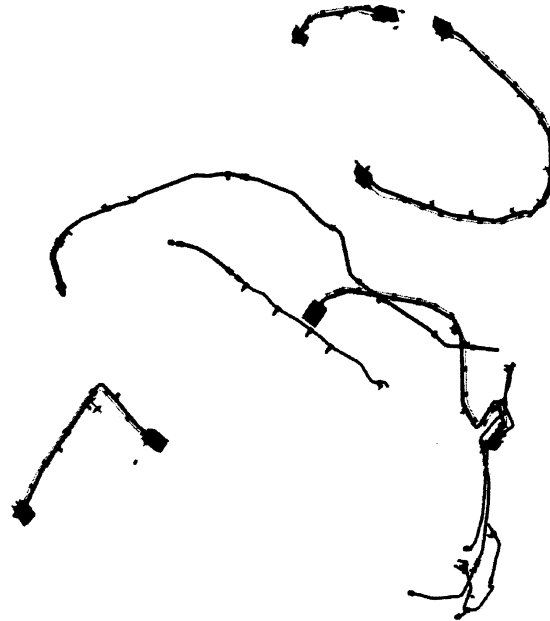
IDG

- Responsibilities
 - Power Feeder
 - Oil Cooling Lines
 - Air/Oil Cooler
 - IDG Installation
- Requirements
 - Engine/Gearbox Deflections
 - Pressure Drop
 - IDG Retention for Blade Out
 - IDG Removal
 - MTBUR
 - Fire Safety

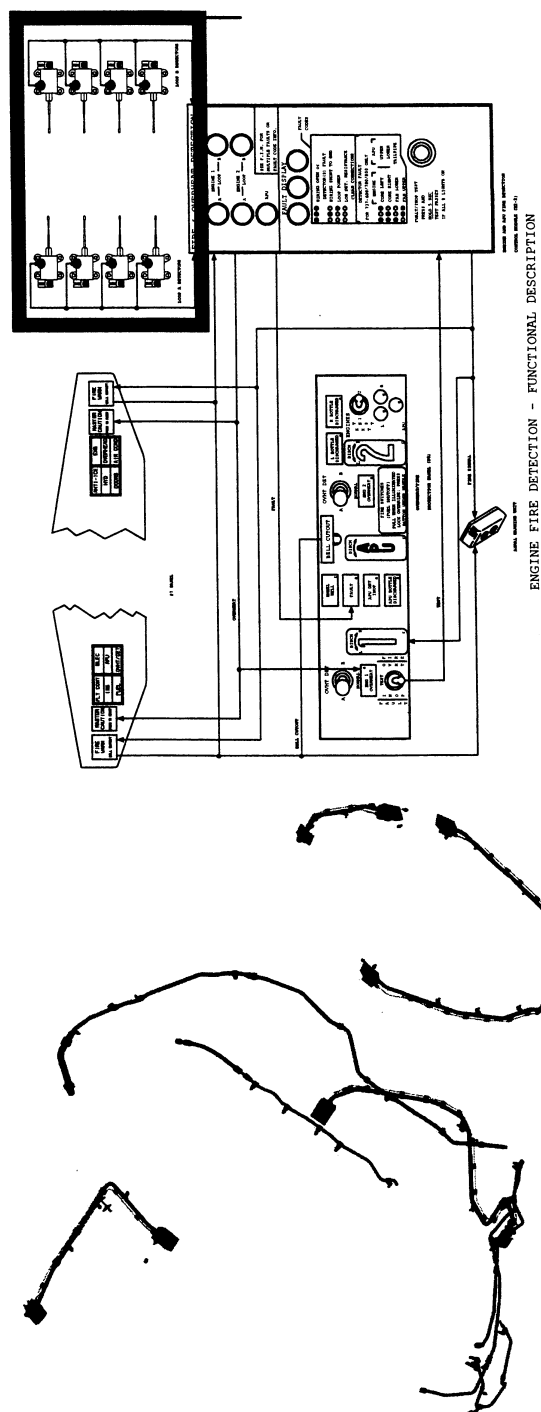


FIRE PROTECTION

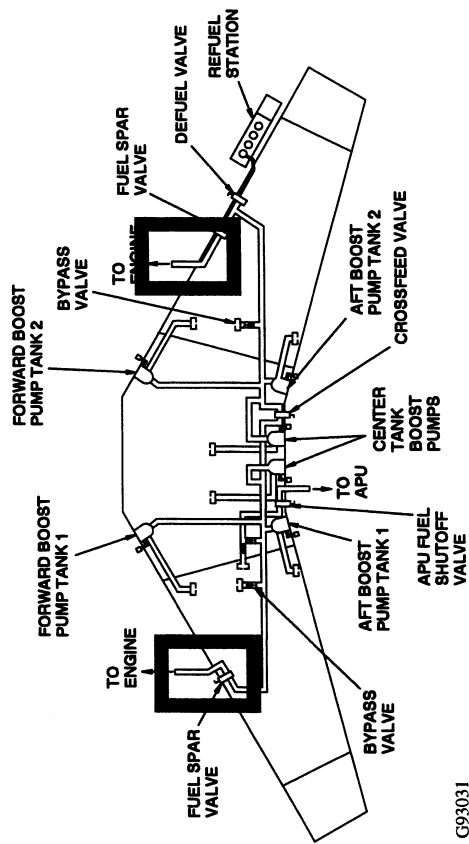
- Responsibilities
 - Fire Detectors
 - Fan Case Drains
 - Firex Tubes
- Requirements
 - Down Hill Drains
 - Overheat Detection
 - Fire Detection
 - Fire Detector Removal
 - MTBUR



FIRE PROTECTION

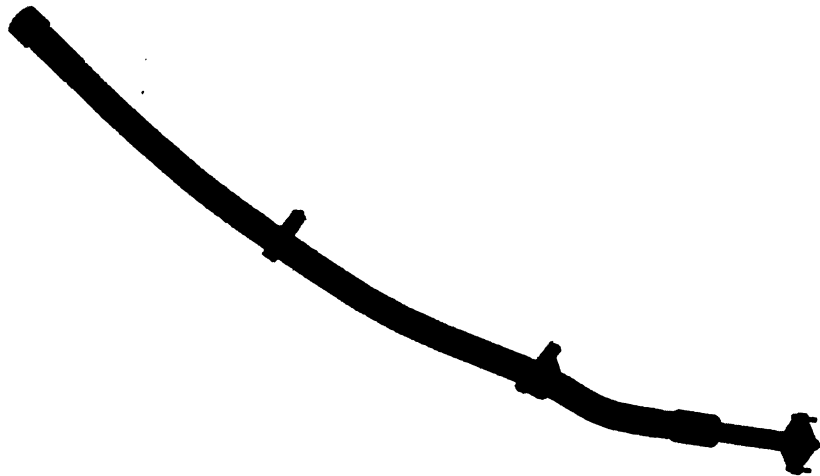


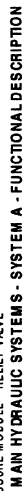
FUEL



FUEL

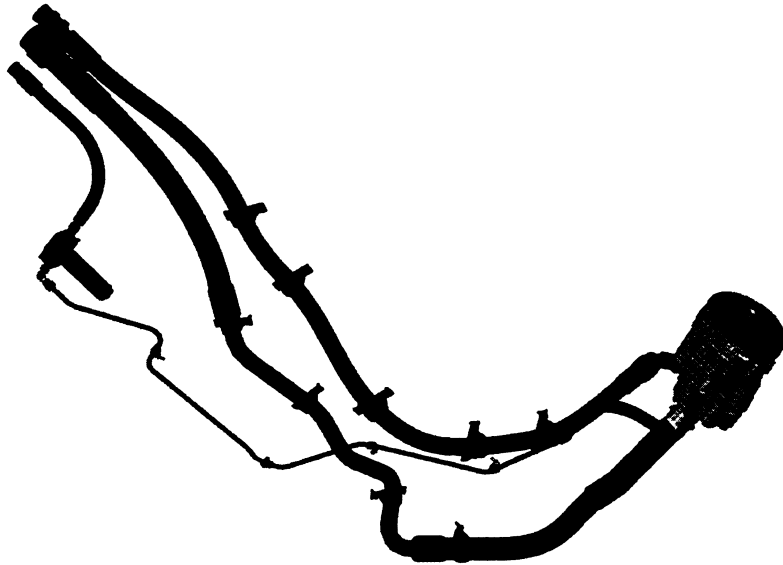
- Responsibilities
 - Fuel Hose
- Requirements
 - Strut/Engine Deflections
 - Pressure Drop
 - Fire Safety





HYDRAULICS

- Responsibilities
 - Hoses
 - Tubes
 - Case Drain Filter Installation
 - Pump Installation
- Requirements
 - Pressure Drop
 - Fire Safety
 - Strut/Engine Deflection
 - Engine/Gearbox Deflection
 - Pump Removal
 - MTBUR



BRACKETS



BRACKETS

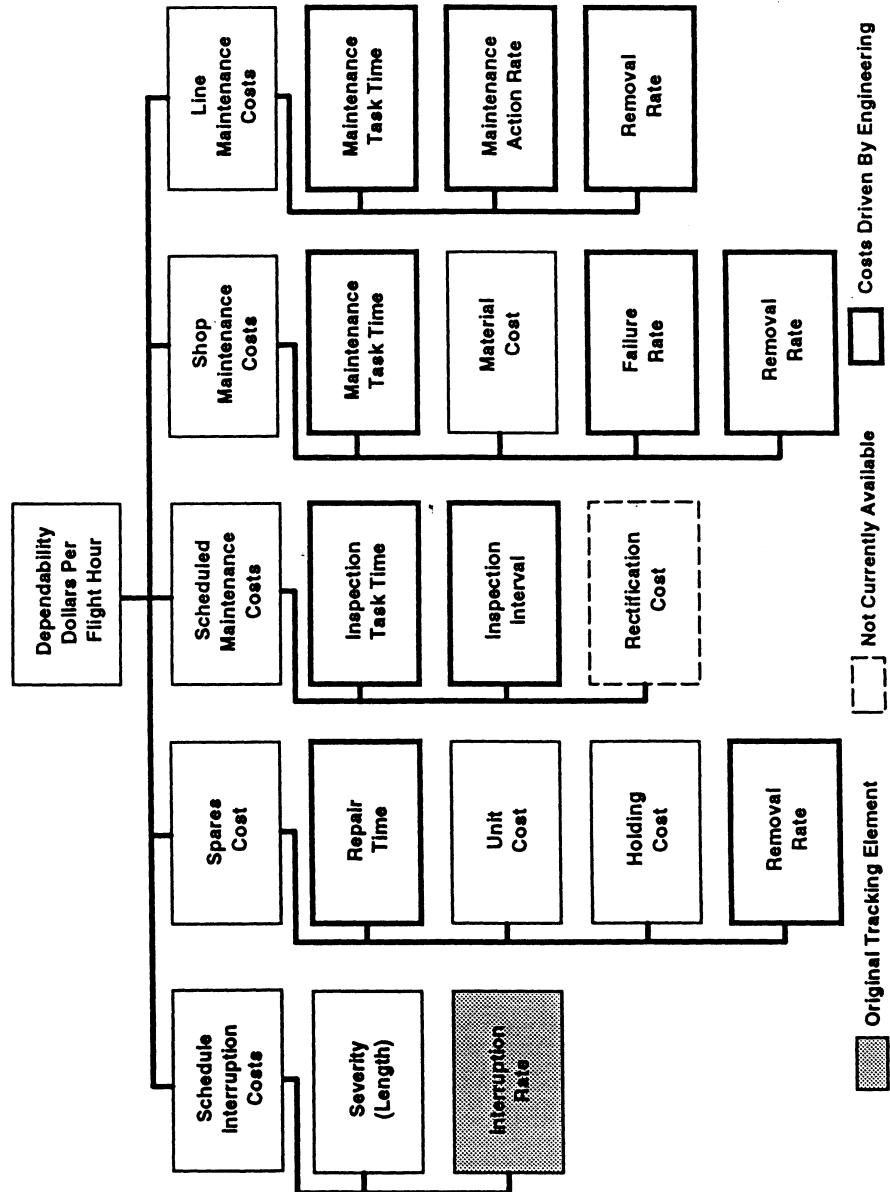
- Responsibilities
 - Brackets
- Requirements
 - Retain Systems and Components



[illegible][illegible]

Dependability

AIPLANE DEPENDABILITY COST ELEMENTS



Conclusion

- **EBU Systems are the Power Source for the Airplane.**
- **Five Basic Requirements Are the Major Focus.**
 - **Function**
 - **Installation**
 - **Production**
 - **Environment**
 - **FAR's**
- **EBU System is a Small Portion of the Airplane Systems.**
- **One System can Effect Numerous Systems.**
- **Each System has Unique Requirements.**

THE IMPORTANCE OF ENGINE EXTERNAL'S HEALTH*

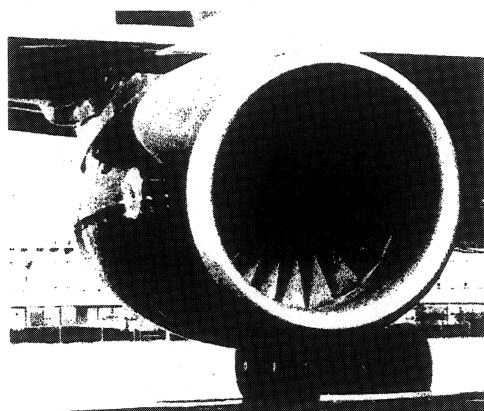
Barry L. Stoner
Pratt & Whitney
East Hartford, Connecticut

ABSTRACT

Engine external components include all the fluid carrying, electron carrying, and support devices that are needed to operate the propulsion system. These components are varied and include: pumps; valves; actuators; solenoids; sensors; switches; heat exchangers; electrical generators; electrical harnesses; tubes; ducts; clamps and brackets. The failure of any component to perform its intended function will result in a maintenance action, a dispatch delay, or an engine in flight shutdown. The life of each component, in addition to its basic functional design, is closely tied to its thermal and dynamic environment. Therefore, to reach a mature design life, the component's thermal and dynamic environment must be understood and controlled, which can only be accomplished by attention to design analysis and testing. The purpose of this paper is to review analysis and test techniques toward achieving good component health.

Keywords: Engine, External, Components, Thermal, Vibration and Durability

Figure 1. Engine on wing



1. INTRODUCTION

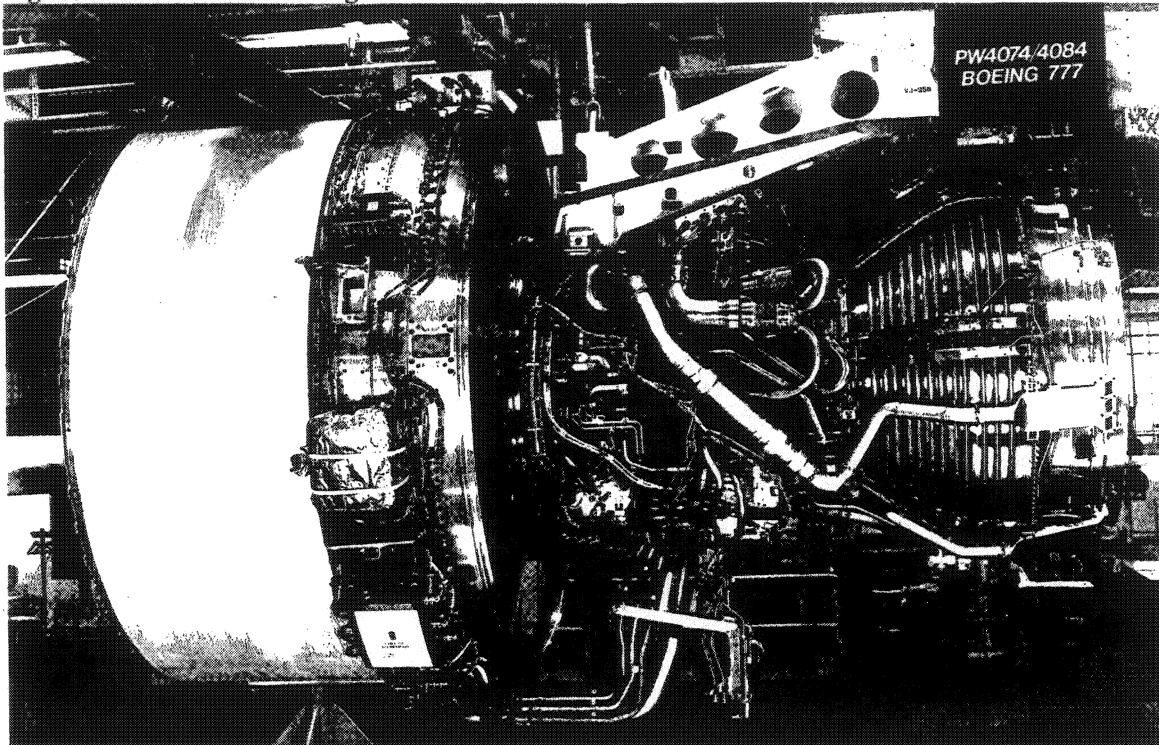
Aircraft engines are not unlike their automotive counterparts in that they are connected with many components such as pumps, tubes, wires, and controls to perform the many operational functions required of aircraft or automobiles in addition to providing propulsion. A look underneath the fan cowl or the core cowl of a modern aircraft gas turbine engine is as bewildering as a look beneath the hood of your car with all the electrical and mechanical gadgets needed for engine control, environmental protection, and passenger comforts. The engine provides power by converting chemical energy from fuel into mechanical and electrical energy for propulsion of the aircraft and control of the many systems beneath the cowls and within the fuselage. Engines produce heat and create vibrations as a result of these energy conversion processes which influence their own design,

*Paper presented at the Seventh International Symposium on Transport Phenomena and Dynamics of Rotative Machinery (ISROMAC-7) in Honolulu, Hawaii, on Feb. 22-26, 1998.

the design of external components, the design of the aircraft, and the design of the systems needed to accommodate passengers.

The objective of this paper is to address the thermal and dynamic aspects of the external components to achieve acceptable in service component life. Analysis and test techniques will be discussed that have been used successfully by the Nacelles, Externals, and Controls Component Center at Pratt & Whitney (P&W) in designing propulsion systems for modern commercial aircraft. While specific terms are used in the industry to describe components such as the nacelle (inlet, fan cowl, thrust reverser, core cowl, nozzle and plug), engine build up (EBU - components needed to operate systems on the aircraft), and engine externals & controls (components needed to operate the engine), for the purpose of this paper the terms "components" and "externals" will be used as generic terms to describe all the components outside the engine case and within the nacelle. The passenger seldom sees any engine components except the fan blades when looking into the inlet or at the nacelle structure. Figure 1 shows the typical view as seen by the passenger. For a look at the complex externals beneath the cowls, Figure 2 shows the engine's left hand side externals and Figure 3 shows the right hand side prior to nacelle installation.

Figure 2. Left hand side of engine

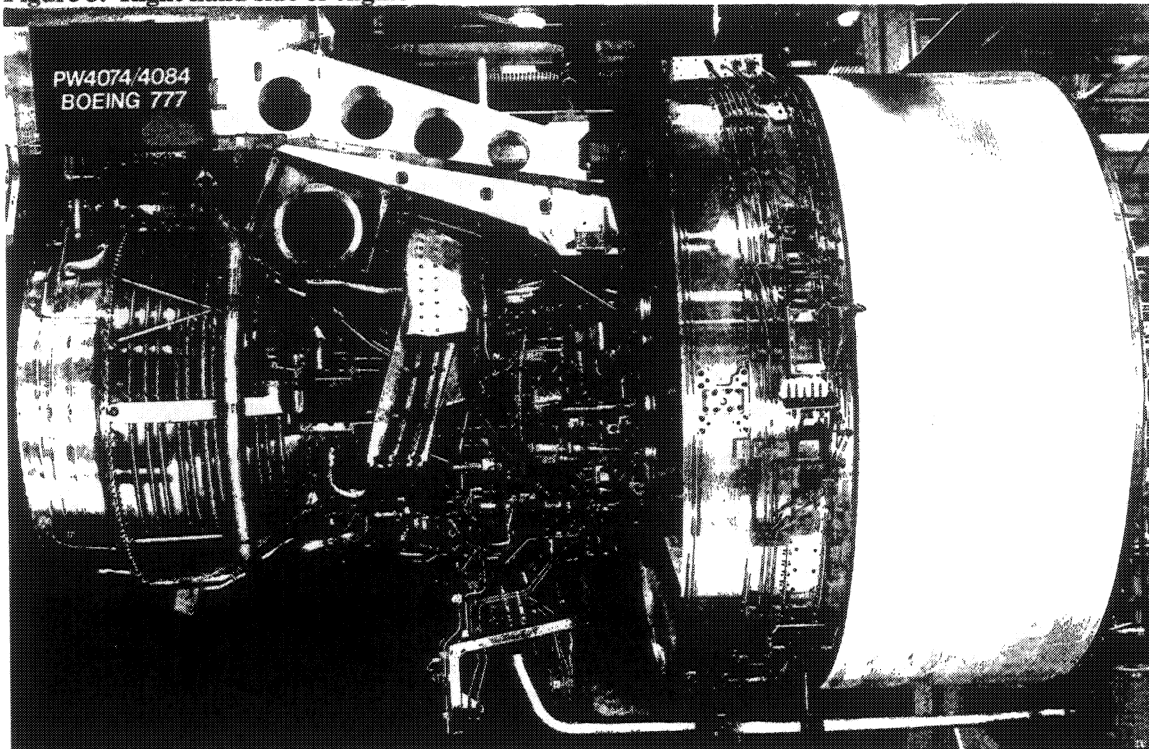


The customer requirement for extended range operation with two-engine airplanes (ETOPS) demands high component reliability. Whenever a commercial twin engine airplane is more than one hour from an adequate airport, FAA regulations require that the aircraft be ETOPS certified. Demonstrated design and in service reliability is necessary to achieve this certification. The most modern twins, like the B777, were designed to achieve ETOPS at "entry into service" (EIS). To earn ETOPS certification at EIS, the FAA imposed Special Conditions which "raised the bar" for component reliability [1,2].

The importance of good externals health is as critical as the health of the engine because the externals and the engine work together to provide the complete propulsion package. Redundancy and/or long life is designed into each critical system and component of the propulsion system. However, some components will fail because of wear or other causes which will result in a maintenance action, a schedule delay, or an in flight engine shutdown. Each of these actions costs

time and money to the airline operator and to travelers not to mention the loss of good will. Therefore, it is imperative that the engine and the externals be designed as a completely reliable propulsion package.

Figure 3. Right hand side of engine



2. THERMAL CONSIDERATIONS

Heat transferred through the engine cases is the primary heat source contributing to external component temperatures. The externals receive this heat via each of the three fundamental modes of heat transfer - conduction, convection, and radiation. The engine cases range in temperature from inlet air temperature at the face of the fan to well over 650C in the engine hot section (high speed compressor, burner and turbines). The hot cases transfer heat to the adjacent external air which then transfers heat to the externals. If the components are mounted to the cases or if the components are in close proximity to the cases, heat is readily transferred by conduction and radiation. Typically, the engine hot section cases form the inner boundary for the core compartment which is covered by the core cowl. The fan case provides the inner boundary for the fan compartment which is covered by the fan cowl.

The majority of externals are mounted in the same region as the engine gearbox although many other components are mounted where there is adequate space or near the point of their use to minimize the weight of the installation. The placement of externals can be a complex problem as space is often limited, and hot temperatures often dictate the placement of some components in cooler regions for reliability. Other sources of heat can result from engine flange leakage; from hot oil, air, and fuel tubes; from heat exchanger exhaust; and from electrical heating.

Two primary variables - environmental air conditions and engine power conditions - affect the engine case heating which, in turn, influences the external component temperatures. Environmental air conditions range from extreme cold to hot in the atmospheric transition from ground level to the highest flight altitude. The engine breathes this air to burn the fuel and produce power. To fly the airplane, the engine must produce power to meet the requirements for taxi, take off, climb, cruise,

decent, approach, landing, and stoping(thrust reverse.) During any commercial flight profile or mission, the engine typically experiences two thermal cycles while meeting these power requirements, one for the take off, climb, cruise, and descent, and one for the thrust reverse. Finally, the components are affected by the shutdown phase of the engine when internal heat is transferred outside the engine while cooling, called “soak back.”

3. DYNAMIC CONSIDERATIONS

The vibration inputs to the externals result primarily from the engine rotors. Other inputs can result from noise and from fluid mechanics associated with tubes, ducts, inlets, vents, valves and pumps. The engine rotor speed inputs are readily available from the engine performance predictions whereas the other inputs tend to be more subtle. Each of these inputs needs evaluation during the engine and component test phases to assure design accommodation.

Engine rotors are carefully balanced within production acceptance limits prior to shipping. Each engine has vibration pickups to monitor rotor imbalance. This monitored information is sent to the onboard maintenance computers for maintenance evaluation. As the engine operates between start up and the maximum rotor speeds, imbalance will be transmitted as a forced vibration to the external components, which could cause some components to resonate at their natural frequency or other harmonic. The aging of an engine usually increases the dynamic inputs to the externals. For good durability, components must be designed to tolerate rotor imbalance and to have resonance frequencies outside the engine speed range and away from engine rotor harmonics.

4. COMPONENT DESIGN

The careful identification of a component's functional requirements, and the precise execution of its design to meet these requirements are the keys to good component performance and durability. To meet Pratt & Whitney's goals for superior on-wing component performance and durability, P&W has created the generic document, PPS2000 - purchase performance specification - and a second document, the “specific” PPS [3]. Together these documents define the requirements a supplier must meet when producing any component. In addition, the FAA has defined a 36 point checklist that each component must complete to satisfy the airworthiness requirements for certification. The thermal and the dynamic requirements are spelled out in these documents.

The materials selected for a component must accommodate its intended function while taking into consideration the component's environment. For example, if the component's function is to generate electricity, then certain materials common to generators such as winding and bearing materials are likely to be chosen. The housing, on the other hand, may provide a choice from aluminum, titanium, or steel. If the generator uses electronics for control, these devices generally have a limited choice of materials with severe temperature limitations. Electronics typically require special cooling in order to survive the heat generated within the unit, as well as the heat from the environment.

The specific placement of the component on the engine influences the severity of its environment. If the component is placed in a hot region of the engine compartment it may need cooling; however, if a cool region is selected, passive cooling may suffice. So why not place all components in a benign thermal or dynamically quiet region? Although desirable, limited space often prohibits the placing of all components in the same region, and those components requiring mechanical power to operate such as pumps and generators must be mounted on the engine's gearbox. The choice of gearbox location, either on the fan or engine core, is the result of a complex rationalization of aerodynamic, structural, thermal, weight, and cost considerations that will not be discussed here. However the result sets the stage and limits the design choices available for component placement (most P&W installations use the core mounted gearbox).

The thermal preference for component placement is in or near the forward compressor region, away from the hotter turbines, or on the sides or bottom of the engine, away from the hotter top region of the compartment. The dynamic preference is to mount components rigidly to the case; but again space, available attachment points, and thermal considerations may not permit this. To accommodate the need to mount components, many are placed on brackets attached to the limited

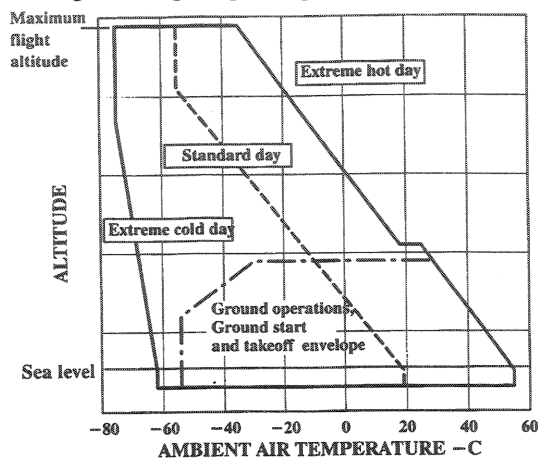
case attachment points. These brackets will separate the component from the hot cases and provide thermal isolation but must be designed with appropriate stiffness to meet the dynamic requirements.

The life requirement for a component is usually specified in the PPS. While it is desirable to have each component last the life of the engine or the airplane, the state of the art in component design has not reached this level for all components and thus life limits are specified for those components. It should be noted that some components can experience early life failures or have infant mortality. This characteristic is totally unacceptable and P&W requires that components be designed and tested and the manufacturing processes demonstrated to avoid this shortfall prior to entry into service.

5. THERMAL REQUIREMENTS AND ANALYSIS

The fundamental environment for an aircraft engine is the atmosphere. An example of the typical atmospheric temperature extremes is shown in Figure 4 as a function of altitude.

Figure 4. Engine operating envelope



A component must operate within these temperature extremes. Since material life/component life is a function of its time exposure to temperature and other loads, the definition of the aircraft flight profile must also be specified.

Figure 5 shows a typical flight profile for a commercial airplane. The engine temperatures and the subsequent component temperatures stem from the

Figure 5. Flight profile

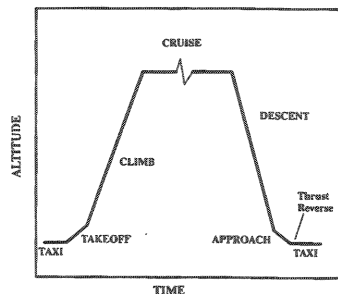
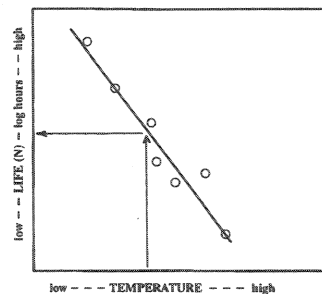


Figure 6. Material life vs Temperature



engine power conditions associated with the aircraft flight profile and the atmospheric conditions. MIL-STD-810C describes generic requirements for addressing a component's high and low temperatures and thermal shock [4]. To satisfy these requirements, the component's temperature environment is calculated according to its physical placement within the engine compartment at each flight segment. These temperature predictions are obtained primarily from test data or calculations as necessary. Since daily temperatures are infinitely variable, a simplified model is used based on an analysis of the atmosphere and the flight profile. Component temperatures are calculated assuming that 85% of the thermal exposure is at standard day atmospheric conditions, 15% at maximum hot day conditions, and 1% at minimum cold day conditions. To complete this time exposure calculation, the time at each flight segment must be determined from the flight profile. This information is then used to determine the component's exposure to temperature. This method of determining a component's temperature exposure is obviously more complex than just identifying the component's maximum temperature - a method that is sometimes used, but insufficient.

For many materials, a life curve can be plotted on a temperature versus time basis to indicate a locus of failure points. These curves are generated by testing the material at temperature and load conditions until the material fails (see Figure 6). Failure of the material is defined according to its use: creep limit, weight loss, tensile strength, dielectric strength and deformation. Since materials in jet engines experience a wide range of temperatures distributed over a flight mission, the cumulative loss of life due to the distributed temperature exposures can be accounted for by application of the linear cumulative damage rule known as Miner's Rule [5]. This rule, which applies to many common aerospace materials, is presented as:

$$R = \sum_{i=1}^m \frac{\mathfrak{S}_i}{L_i} \qquad \text{Life} = \frac{\sum \mathfrak{S}_i}{R}$$

R is the portion of life consumed at the conditions (1 is 100%); L_i is the life of the material at temperature i as derived from the life curve (Figure 6), and \mathfrak{S}_i is the time spent at temperature i .

Consider the following example. A part spends 400 hours at 200C and 200 hours at 260C. A life curve for the part material indicates that its life at 200C is 800 hours and its life at 260C is 600 hours. The calculations are shown as :

$$R = \frac{400}{800} + \frac{200}{600} = 0.83 \qquad \text{Life} = \frac{400 + 200}{0.83} = 723 \text{ hours}$$

These calculations show that 83% of the life was consumed at the conditions and that the life was 723 hours. If this calculated life does not meet the specified life requirements, then a redesign would be necessary.

This method of accounting for a material's thermal life, which sometimes can be extended to the component itself, has been found to be quite useful [6].

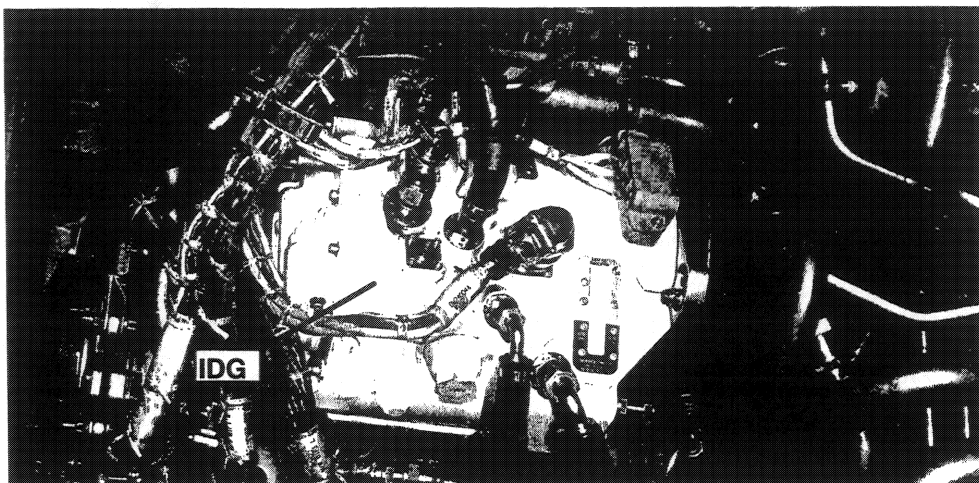
6. DYNAMIC REQUIREMENTS AND ANALYSIS

The vibration environment, used for design and development testing of a component, is also defined in MIL-STD-810C. The component, when exposed to this environment, must survive without structural damage or wear beyond service limits over the component's life. The test item is vibrated along each of the three orthogonal axes at the four most significant resonances found from a resonance search. Resonances are defined as output over input greater than two. The input level at the mounting point is usually 20G at frequencies up to 3000 Hz. The mounting of the component must duplicate the installation on the engine; i.e. brackets, clamps, etc.

Tubes, brackets, and clamps perform seemingly ordinary functions, but the design of these components to withstand the loads and thermals of the aircraft engine can be quite challenging.

These components cannot be designed as separate entities. They must be designed integral to the systems they support meeting the stiffness requirements to avoid resonances within the engine speed range, while avoiding unacceptable thermal stresses yet satisfying fatigue strength requirements, as well as static stress limits.

Figure 7. Generator (IDG) installation on engine



Electrical wires must also be routed and retained to avoid failures due to dynamics, this includes wires external and internal to the component. The best way to clear wire vibration problems is to shake the component in the three orthogonal directions over a range of frequencies and accelerations specified in the PPS and monitor the wires for motion. During the exposure to this environment, the wires must not vibrate in any manner that may lead to eventual damage when extrapolated over the component's life.

7. COMPONENT COOLING REQUIREMENTS

Initially, a component's temperatures are predicted based on an analysis of its environmental conditions or from test measurements for similar installations scaled to the maximum environmental design conditions. Two requirements are then considered when determining if dedicated cooling is needed. The first is the need to meet the component's design life and the second is based on the need to have adequate thermal margin to pass certification flight tests. If the temperatures are predicted within 28C of a passively air cooled component's maximum design temperature, then cooling is applied. Because weak and variable flow fields exist within the core compartment, experience has demonstrated that air cooled component temperatures are often difficult to predict accurately (this is an area where more sophisticated analysis tools are needed) [7]. However, the use of the 28C margin has produced excellent certification results and has resulted in improved component thermal lives. For fuel or oil biased components, the temperature variability is not as great; therefore, an 11C margin is used as the criteria for determining cooling needs. For fan compartment mounted components, where the temperatures are not as hot or variable, an 11C margin is also used as the determining factor for all components.

8. ENGINE TEST VERIFICATION

The successful completion of component rig tests and engine tests is a very important part of the design process. It is this testing that provides the confidence and verification to insure that design requirements for each component have a high probability of being achieved. The component rig test requirements are defined in the PPS and MIL-STD-810C, and the engine test requirements are defined in FARs Parts 25(Certification Flight Test) & 33(Certification Engine Test.) Prior to these certification tests, P&W conducts some very important design tests - the engine shake rig tests and the engine endurance tests.

The engine shake rig is basically an engine case structure that receives input from an electrodynamic exciter [8]. This rig is built with "all" the externals and with accelerometers and strain gauges. The externals are then excited with twice the rotor imbalance throughout the appropriate frequency range. The accelerometers will show whether the component vibration levels are acceptable and the strain gauges will record the stress levels as a result of the vibration. Typically vibratory stress levels below 35 mega Pascals will insure infinite life. Design modifications are employed as necessary.

The engine endurance tests are the most difficult tests and expose the externals to all the engine's characteristics. The engine endurance tests are designed to put time on the externals at the maximum operating conditions - temperature, pressure and rotor speeds. The build of these engines is with all the externals operational. One important dynamic feature P&W adds to these tests is to conduct them with twice the rotor imbalance of the production acceptance limit. The external components are fitted with thermocouples and dynamic probes, but the primary purpose of these tests is to determine if any remaining flaws exist prior to entering certification. To meet the special conditions for ETOPS, the components must also pass a 3000 cycle engine test and a 1000 cycle flight test - a cycle refers to the excursion between idle and high power.

9. FINAL REMARKS

The engine externals encompass a huge number of components that are designed and demonstrated through testing to have the high reliability needed for modern commercial aircraft. Parts counts reach into the hundreds for tubes, hoses (400) and brackets (700). About one hundred control system's components are needed and EBU and nacelle components add a few hundred more. Each of these components are secured with thousands of fasteners. Needless to say, this is a formidable task to design and qualify each of these parts which demands the working together of many aircraft, customer, engine and supplier engineers to achieve the design goals and satisfy the certification requirements.

As a result of this paper, it is hoped that the importance of the external's component reliability, being as critical as that of the engine, is better understood and that the attention to design and test detail is the key to controlling the thermal and dynamic environments needed for high component reliability.

REFERENCES

1. *FAA Advisory Circular, AC 120-42A, Extended Range with Two-Engine Airplanes (ETOPS)*, 12/30/88.
2. *ETOPS Special Condition No. 25-ANM-84*, 7/1/94.
3. *Pratt & Whitney Purchase Performance Specification No.2000B*, 9/21/93(restricted).

4. MIL-STD-810C, Environmental Test Methods, 3/10/75.
5. Minor, M.A., *Journal of Applied Mechanics*, September 1945.
6. Ellis, R.L., Calculation Of External Thermal Mission, *7th Annual United Technologies Engineering Conference and Technology Exposition*, 5/2/96(available).
7. Nacelle Component Cooling Analysis Tools Meeting, Boeing Propulsion, 3/12/97.
8. Tolman, S. E., Private communication - Shake Rig Testing, 4/10/97.

NOMENCLATURE

<i>R</i>	The fraction of life consumed at the conditions.
\sum_i	The time spent at temperature <i>i</i> .
<i>Li</i>	The life of the material at temperature <i>i</i> .
<i>i</i>	An individual temperature.
<i>m</i>	The last individual temperature.

ENGINE DEVELOPMENT DESIGN MARGINS BRIEFING CHARTS

Chuck Bentz
Universal Technology Corporation
Dayton, Ohio

CHART 1 comments: ENGINE DEVELOPMENT DESIGN MARGINS

BACKGROUND: New engines experience durability problems after entering service. The most prevalent and costly is the hot section, particularly the high-pressure turbine. The origin of durability problems can be traced back to: 1) the basic aero-mechanical design systems, assumptions, and design margins used by the engine designers, 2) the available materials systems, and 3) to a large extent, aggressive marketing in a highly competitive environment that pushes engine components beyond the demonstrated capability of the basic technology available for the hardware designs. Unfortunately the user must operate the engine in the service environment in order to learn the actual hot section life. Development testing in ground based facilities can point to some early durability problems with the hot section hardware but the actual thrust loading and the time at max effort take-off conditions used in service are needed to determine the hot section life.

Several hundred thousand hours of operational service will be required before the demonstrated reliability of a fleet of engines or the design deficiencies of the engine hot section parts can be determined. Also, it may take three to four engine shop visits for heavy maintenance on the gas path hardware to establish cost effective build standards. Spare parts drive the operator's engine maintenance costs but spare parts also makes lots of money for the engine manufacturer during the service life of an engine. Unless competition prevails for follow-on engine buys, there is really no motivation for an OEM to spend internal money to improve parts durability and reduce earnings derived from a lucrative spare parts business.

If the hot section life is below design goals or promised values, the OEM might argue that the engine is being operated beyond its basic design intent. On the other hand, the airframer and the operator will continue to remind the OEM that his engine was selected based on a lot of promises to deliver spec thrust with little impact on engine service life if higher thrust is used intermittently. In the end, a standoff prevails and nothing gets fixed.

This briefing will propose ways to hold competing engine manufacturers more accountable for engine hot section design margins during the entire Engine Development process as well as provide tools to assess the design temperature margins in the hot section parts of Service Engines.

PURPOSE: The purpose of this briefing will be to define a methodology of interaction between the customer and the competing engine manufacturers during the entire engine development process to achieve desired or promised levels of hot section durability. This briefing will also outline the Development of Design Margins for the Hot Section Components which will include the Combustor and the High and Low Pressure Turbines.

Temperature margins are absolutely needed in the hot section during engine development to reduce the durability problems and performance demands that a new engine type will face as it enters revenue service for the commercial operators or operational service for the military.

ENGINE DEVELOPMENT DESIGN MARGINS

PURPOSE

Define a methodology for customer/developer interaction during the entire engine development process to achieve desired hot section durability.

- Component development
- Engine development
- Service assessments

Chuck Bentz
Universal Technology Corporation
Dayton, OH

CHART 2 comments: SCOPE

This briefing is divided into two sections.

The first section is a discussion of engine degradation in service, the impact of usage rates (flight hour/cycle) and flight legs, the sensitivity of engine life to thrust derate and thrust uprating. Comments will be made concerning the origin of durability problems.

Real engine data will be shown to illustrate the impact of engine component degradation on service life as well as the impact of take off thrust rating used in service on engine life.

The second section discusses a proposed methodology for Engine Development Design Margins for hot section parts. Some comments will be made on the value of System Engineering during engine development in terms of reducing overall Life Cycle Cost. Customer involvement is a key element of the engine development process as well as accomplishing independent assessments of critical component designs such as the high-pressure turbine. As higher levels of engine performance are being demanded, higher gas temperatures will be used in the engine cycles which puts greater demands on the accuracy of design systems used by the engine designers for the hot section parts as well as the available materials systems. By tracking the demonstrated progress of component and engine development tests, the customer will be in a better position to judge the potential life of a new engine before it selected and enters service.

Working with several engine manufacturers during an engine development encourages more accountability among the viable competitors but represents an additional workload to evaluate the progress of the hardware development to design intent. However, design deficiencies can be discovered during component testing if sufficient test instrumentation are used and the tests are conducted at temperature levels representative of engine conditions. In full scale engine testing, hot section design deficiencies may be more difficult to analyze because of the lack of high temperature instrumentation and sufficient coverage of the critical areas such as the temperature profiles exiting the high-pressure combustor and entering the exit guide vane and the first stage turbine.

SCOPE

BACKGROUND

- ENGINE DEGRADATION IN SERVICE
- IMPACT OF USAGE RATES AND FLIGHT LEGS
- SENSITIVITY TO THRUST DERATE AND THRUST UPGRATING
- ORIGIN OF DURABILITY PROBLEMS

ENGINE DEVELOPMENT DESIGN MARGIN METHODOLOGY

- PROPOSED APPROACH FOR HOT SECTION PARTS
- LCC CONSIDERATIONS DUE TO DURABILITY ISSUES
- CUSTOMER INVOLVEMENT IN ENGINE DEVELOPMENT PROCESS
- TRACKING DEMONSTRATED PROGRESS
- COMPETITION ENCOURAGES MORE ACCOUNTABILITY

CHART 3 comments: Background

It is important to understand the impact of engine component degradation as well as the flight environment (length of flight leg and flight hours/N1 Cycle) on engine time on wing. Engine degradation is caused in part by the loss to the tip seals and airfoil shapes plus more peaked temperature profiles exiting the high-pressure combustor. Engine time on wing is reduced for various other reasons to include: 1) the more frequent use of lower derate (higher thrust settings), 2) the flight legs result in fewer flight hours/N1 Cycle or 3) the engine is uprated ("Throttle Pushed") to satisfy the operators need for more thrust. Thus, one user of a given engine type may achieve higher time on wing because his average flight legs are longer. On the other hand, another operator may experience less engine time on wing for the same flight legs than another operator for the reason that his average take off derate thrust settings are much lower which requires higher cycle temperatures resulting in accelerated hot section distress. The origin of the problem may also be that the engine hardware is operating at higher gas temperatures to produce the desired take off thrust than the design intent of the hot section. As the loss in gas path seals increase the tip clearances in both the compression system and the turbines forcing the engine cycle run hotter to produce the same engine pressure ratio, the peaked gas temperatures exiting the combustor may exceed the basic materials capability of the hot section parts. Exposure to prolonged high gas temperatures will result in severe oxidation/erosion on the leading edges and trailing edge tips of the first stage high-pressure turbine blade resulting in increased scrape rate or total replacement of the T1 Blade Stage.

When a high bypass turbofan as shown in **CHART 4** reaches 0 °C EGT Margin (defined as the Redline Temperature minus the Measured EGT measured at station 6), the engine must be scheduled for a shop visit to accomplish heavy maintenance to restore the gas path hardware performance. Otherwise, serious over-temperature to the high-pressure spool parts will result and increase the scrape rate of the vane and blades. Thus, engine time on wing is influenced by the average engine derate used in service, the average length of the flight legs, and the flight hours/N1 Cycle. One N1 Cycle is equivalent to engine idle to max RPM and return to idle. Sometimes the number of partial N1 Cycles are counted at intermediate RPM's and divided by four to increase the total accumulated N1Cycles. Counting the partial cycles may be more important to the military user than the commercial operator.

CHART 5 is provided to clarify some of the terminology commonly used in engine maintenance. Logisticians and maintainers use these metrics to forecast spare parts and workload requirements as well as judging the quality of the maintenance work performed. The concept of computing the SVR using the Shop Visit Factor (SVF) times the ERR was developed to estimate the time between heavy maintenance. Dividing TBO into the overall refurbishment cost of an engine provides the maintenance cost per engine flying hour. SVF is a function of 1 minus the fraction of engines removed by management decision or Returned to Wing for no fault and/or minor repairs. Each user has a different RTW percentage based on the condition of engine hardware in service and the prevailing maintenance policy at the military unit or commercial operator.

BACKGROUND

UNDERSTANDING THE ISSUES:

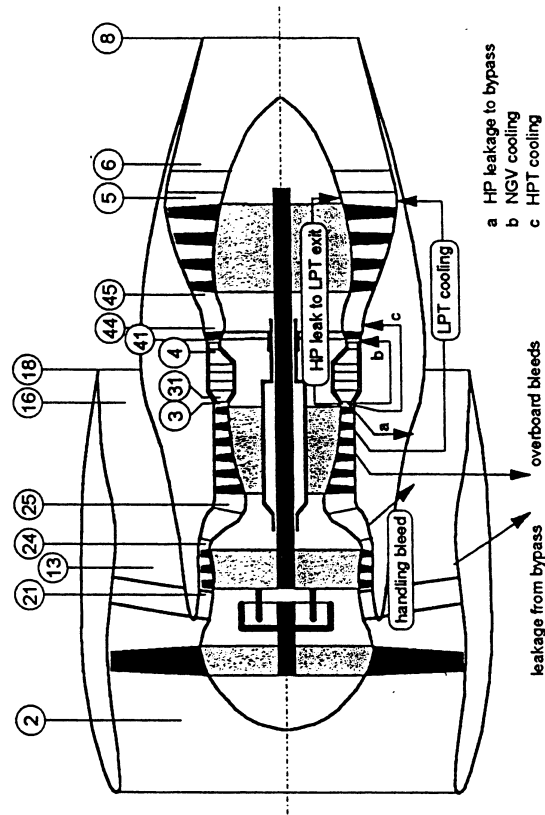
DEGRADATION

MISSION ENVIRONMENT

ENGINE DURABILITY

ORIGIN OF THE PROBLEM

UNMIXED FLOW TURBOFAN



TERMINOLOGY CLARIFICATION

ERR = SER + UER

SVR = SVF X ERR

Where:

SVF (Shop Visit Factor)

ERR (Engine Removal Rate)

SVF = 1 - %RTW/100

SER (Scheduled Engine Removal)

RTW (Return to Wing)

UER (Unscheduled Engine Removal)

ERR, SER, UER AND SVR are reported as 12 mo. rolling averages for the Entire Fleet. Dimensional Units (EVENTS/1000 EFH) (i.e. 0.09/1000 EFH)

Categories

SER's: Forced Inspections, Convenience or Planned Removals

UER's: Ground or Flight Anomaly, FOD, Hardware Failure, Leaks, etc.

TBO = Ave. Total Accumulated Cycles X Fleet Ave. EFH's/Cycle

SVR = 1000/TBO TBO refers to a Heavy Maintenance Action

CHART 6 comments: Engine Degradation in Service

New engines as well as refurbished engines are built to established standards by the maintainers. The level of EGT Margin for a new engine delivery is set by the customer whether the military or commercial operators. The engine will not be accepted unless the EGT Margin is above an established level of EGT Margin. During the refurbishment cycle, new parts are installed to restore the gas path performance but the engines can not be economically restored to New Engine condition. The important point of this chart is that the new or rebuilt engine goes through an Initialization and Wear in Period that decreases the available EGT Margin. Initialization occurs during the first 50 to 100 N1 Cycles whereas the Wear in Period is generally completed after 300 to 400 N1 Cycles depending upon the levels of engine derate used by the operator. During Steady State, a New Engine or a refurbished engine will provide the same rate of EGT Margin degradation as shown on the graph. If the base material capability of the T1 blades is marginal at the end of the service life, the rapid deterioration of the T1 blade surfaces will occur causing the more Rapid Deterioration Rate of the EGT Margin.

CHART 7 comments: Flight Leg Impact of TBA

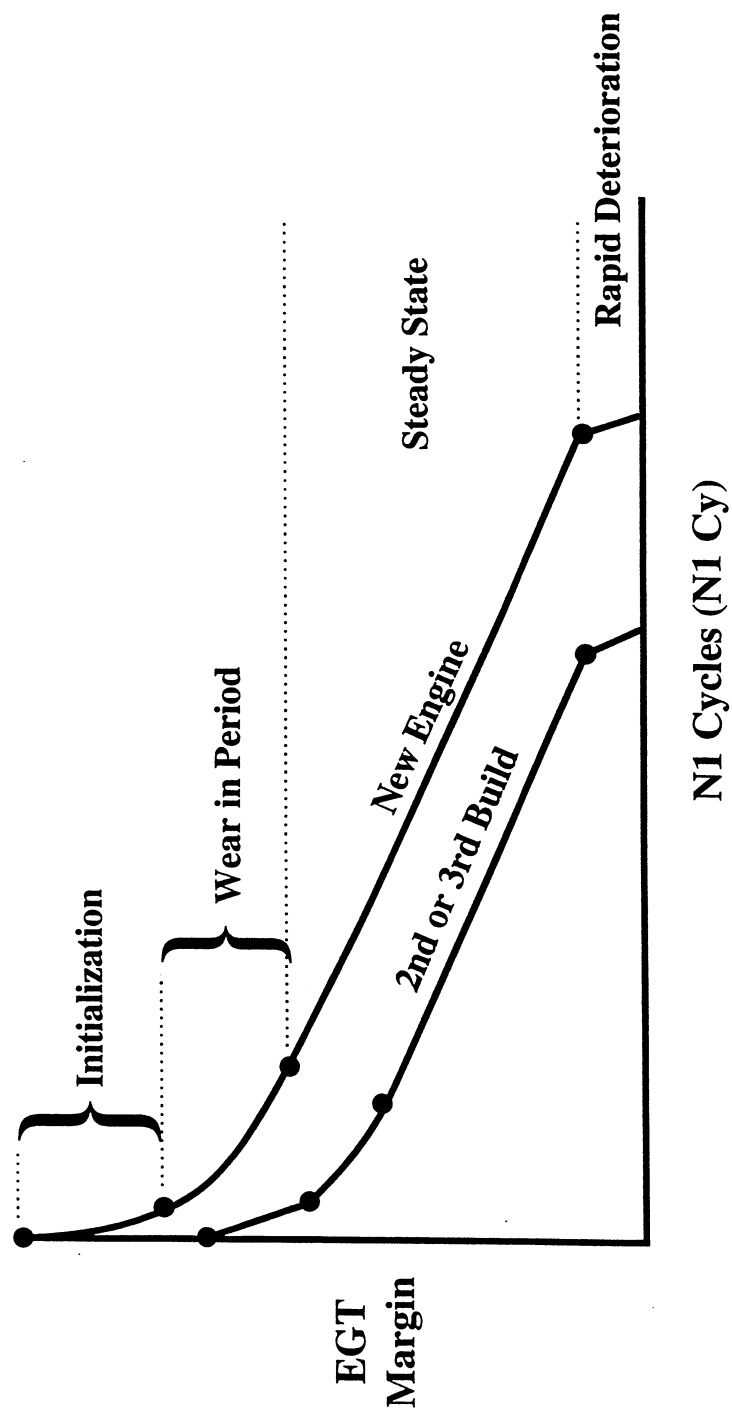
This chart provides an insight of the impact of the flight leg on engine time on wing. Commercial operators will fly long and short haul routes but accumulate only 1 N1 Cycle/Takeoff and Landing. Whereas, a military transport will fly a 3.5 hour mission and accumulate 0.7 to 3.5 EFH/N1 Cycle. High power usage accelerates engine deterioration. N1 Cycles count the number of events the Hot Section is exposed to high gas temperatures.

There is a misconception that may create some confusion, if not some targeted disinformation. The Time on Wing of an engine that experiences fewer N1 Cycle may be misleading. For instance, the build standard for a 9000 EFH engine may be around 1000 N1 Cycles if the engine flies a 9 hour flight leg. Whereas the build standard for an engine flying a 1.9 hr flight leg will be around 5000 N1 Cycles to achieve 8400 EFH's of service. The ERR of the long haul engines are generally lower than the short haul engines. The disinformation is created when certain marketing imply that the long ERR can be achieved for the short haul application. To avoid any confusion, the average flight leg should be provided for the Engine Removal Rates (ERR) that are stated to sort out the long haul engine durability from the short haul engine durability. Compare like flight leg ERR's between various engine offerings. Adjust the ERR for the same flight leg before judging the time on wing of competing engine offerings.

CHART 8 comments: EGT MARGIN SENSITIVITY

This chart indicates the sensitivity of EGT Margin loss for a 1% loss in engine component efficiency for a high pressure ratio engine cycle with a Bypass Ratio of 6. The most notable is the High Pressure Turbine (HPT) with a -26.2 °C. loss in EGT Margin. Depending on the level of distress from oxidation and erosion, the loss in component efficiency could be greater than 1.5 to 2%. See Comments:

ENGINE DEGRADATION IN SERVICE



FLIGHT LEG IMPACT ON TBO

- VARIOUS OPERATORS FLY A MIX OF FLIGHT LEGS AND ROTATE AIRCRAFT AND ENGINES TO MAXIMIZE TIME ON WING
- COMMERCIAL AIRLINES FLY CERTAIN AIRCRAFT TYPES ON SHORT AND LONG HAUL ROUTES AT 1 CYCLE/TAKE OFF AND LANDING
- MILITARY TRANSPORTS WILL FLY 3.5 EFH/MISSION BUT AVERAGE CYCLE RATES WILL RANGE FROM 0.7 TO 3.5 EFH/CYCLE
- A 1000 CYCLE Build on a 9 HR Flt Leg will achieve 9,000 EFH before a Heavy Maintenance. A 5,000 CYCLE Build flying a 1.9 HR FLT LEG will achieve around 8,400 EFH before EGT Margin forces engine off wing.
- High Power Usage accelerates Engine Deterioration. N1 CYCLES count events the Hot Section is exposed to high gas temperatures.
- "High time engines" generally experience fewer N1 CYCLES. Beware of Low ERR Marketing unless Ave. Flight Leg is provided. Short Haul durability may be considerably worse than a competitor's engine.

EGT MARGIN SENSITIVITY

(1% LOSS IN ENGINE COMPONENT EFFICIENCY)

<u>COMPONENT</u>	<u>MARGIN LOSS</u>	<u>COMMENTS:</u>
• FAN	- 3.2 °C.	< 1/2 % ON A FULL RUN ENGINE
• LPC	- 2.4	< 1/2% UNLESS HIGH EROSION
• HPC	- 10	> 1 to 1.5%, HIGHER WITH SEVERE BLADE EROSION
• HPT	- 26.2	> 1.5 to 2%, DEPENDING ON DISTRESS (OXIDATION AND EROSION)
• LPT	- 16.5	< 0.1 to 0.2%, UNLESS SEVERE LOSS OF TIP SEALS

COMMENTS: CORE FLOW DECREASE FROM GAS PATH DETERIORATION
WILL INCREASE MARGIN LOSS FOR THE HPC AND HPT.

CHART 9 comments: CAUSES OF DETERIORATION

This chart is self-explanatory and identifies the causes for component deterioration for the compression system, the combustor and the high and low-pressure turbines.

CHART 10 comments: NON-ATTRIBUTION STATEMENT

Real engine data are used to describe the impact of flight leg, EFH/N1 Cycle and thrust derate on engine time on wing and illustrate the need for development design margins. Since these analyses were performed, the T1 Blades for the military and commercial versions of the same engine type have been replaced with upgraded cooling designs and coating systems. The upgraded blade design should be independently reviewed at a future date (circa 1998-9) in order to determine the demonstrated improvements in operational service.

CHART 11 comments: IMPACT OF INCREASED THRUST RATING (Same Hardware)

This chart shows the accelerated rate of EGT Margin reduction when a 37.5K take off thrust rated engine (Baseline Engine) is operated at a 40K (Throttle Push) take off thrust rating. The fleet of 37.5K commercial engines uses an average derate of 19 to 21% based on a 40K thrust rating whereas the 40K rated engine used an average derate of 5 to 8%. The rate of deterioration increased from 10 °C/1000 N1 Cycles to a range from 14-16 °C/1000 N1 Cycles. The Initialization and Wear in Period for the engines operating at the higher thrust rating occurred at lower levels of N1 Cycles than the 37.5K rated engines.

CHART 12 comments: PW2037 EGT MARGIN DEGRADATION

This chart shows the degradation rate of several first time out commercial engines with an average flight leg of 2.7 EFH. All engines were removed for T1 blade distress or performance deterioration. The wear in drop was around 19-23 °C at 700 N1 Cycles. The rate of EGT Margin Degradation for four engines ranged from 10.5 °C/1000 N1 Cycles over a range from 700 to 2000 N1 Cycles to 9.2 °C/1000 N1 Cycles from 2000 to 3200 N1 Cycles. It was notable that rapid degradation (33-55 °C/1000 N1 Cycles) occurred around 8-10 °C EGT Margin remaining. Microstructure analyses indicated leading edge metal temperatures exceeded 2150 to 2250 °F. Severe loss of material on the blade tips due to oxidation and erosion was noted from the blade mid span back to the trailing edge. Loss of material on the blade tips reached 70 to 80 mils on most blades at the trailing edge.

CAUSES OF DETERIORATION

- **COMPRESSION SYSTEM**
 - LOSS OF TIP SEALS AND AIRFOIL TIP EROSION
 - SECONDARY FLOW LEAKAGE (MINOR)
- **COMBUSTOR**
 - PEAKED EXIT TEMPERATURE PROFILE
 - OXIDATION AND EROSION IN THE DOME REGION
 - WARPAGE OF EXIT GUIDE VANES
- **HIGH AND LOW PRESSURE TURBINES**
 - INCREASED TIP CLEARANCE
 - COATING SYSTEM LOSS AND OXIDATION/EROSION
 - DEEP TIP SCHRLOUD RUB AND/OR LOSS OF CERAMIC MATERIAL
 - SOME BLADE WARPAGE OR UNTWIST
- **GRADUAL LOSS IN CORE AIRFLOW AND PRESSURE RATIO**

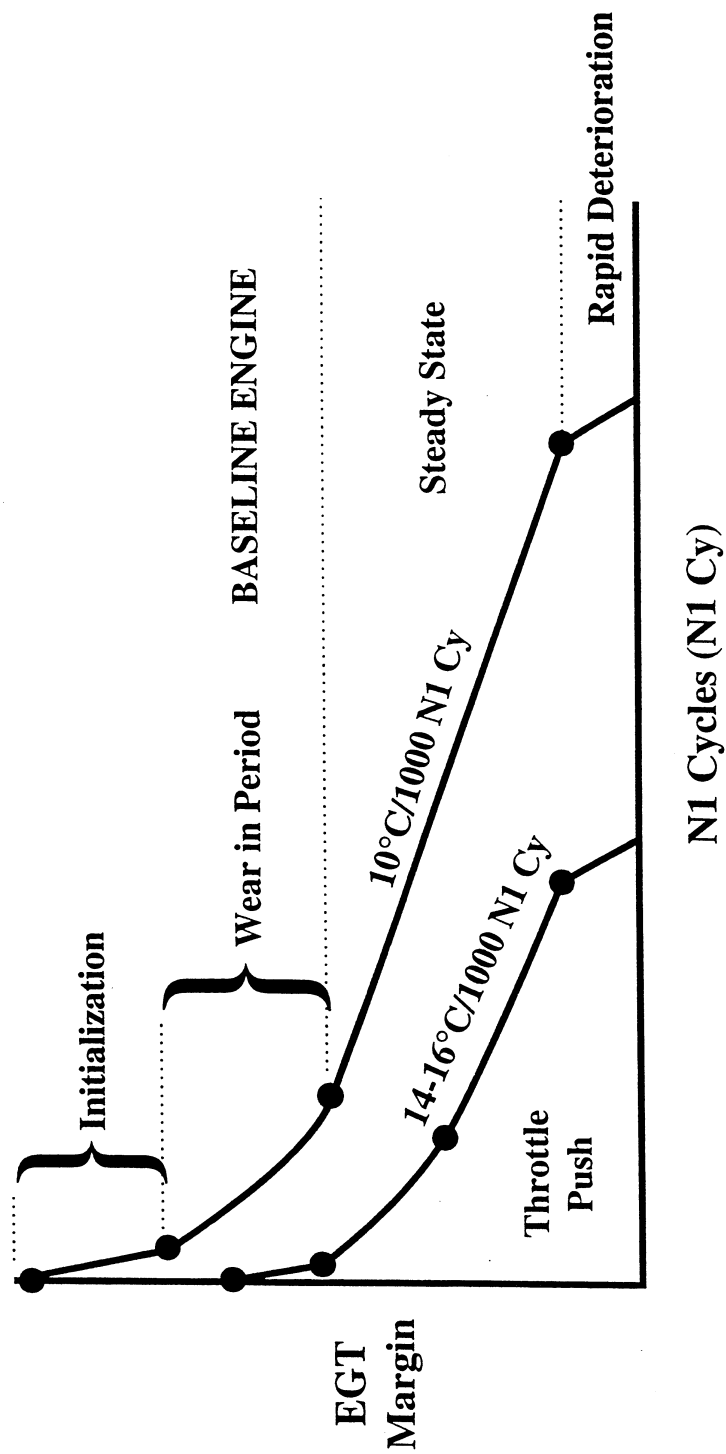
NON-ATTRIBUTION STATEMENT

ENGINE COMPONENT PERFORMANCE DETERIORATION AND THRUST UPRATE CAN SERIOUSLY IMPACT HOT SECTION DURABILITY

COMMERCIAL AND MILITARY DATA ARE PRESENTED FOR THE SAME ENGINE TYPE WITH DIFFERENT TAKE OFF THRUST RATINGS AND CYCLE USAGE RATES. OPERATING ENVIRONMENT ALSO A FACTOR.

REAL ENGINE DATA ARE USED TO ILLUSTRATE THE NEED FOR DEVELOPMENT DESIGN MARGINS

IMPACT OF INCREASED THRUST RATING (SAME HARDWARE)



PW2037 EGT MARGIN DEGRADATION

FIRST TIME OUT COMMERCIAL ENGINES

10-12% AVE. DERATE (37.5K F_n RATED T.O.)

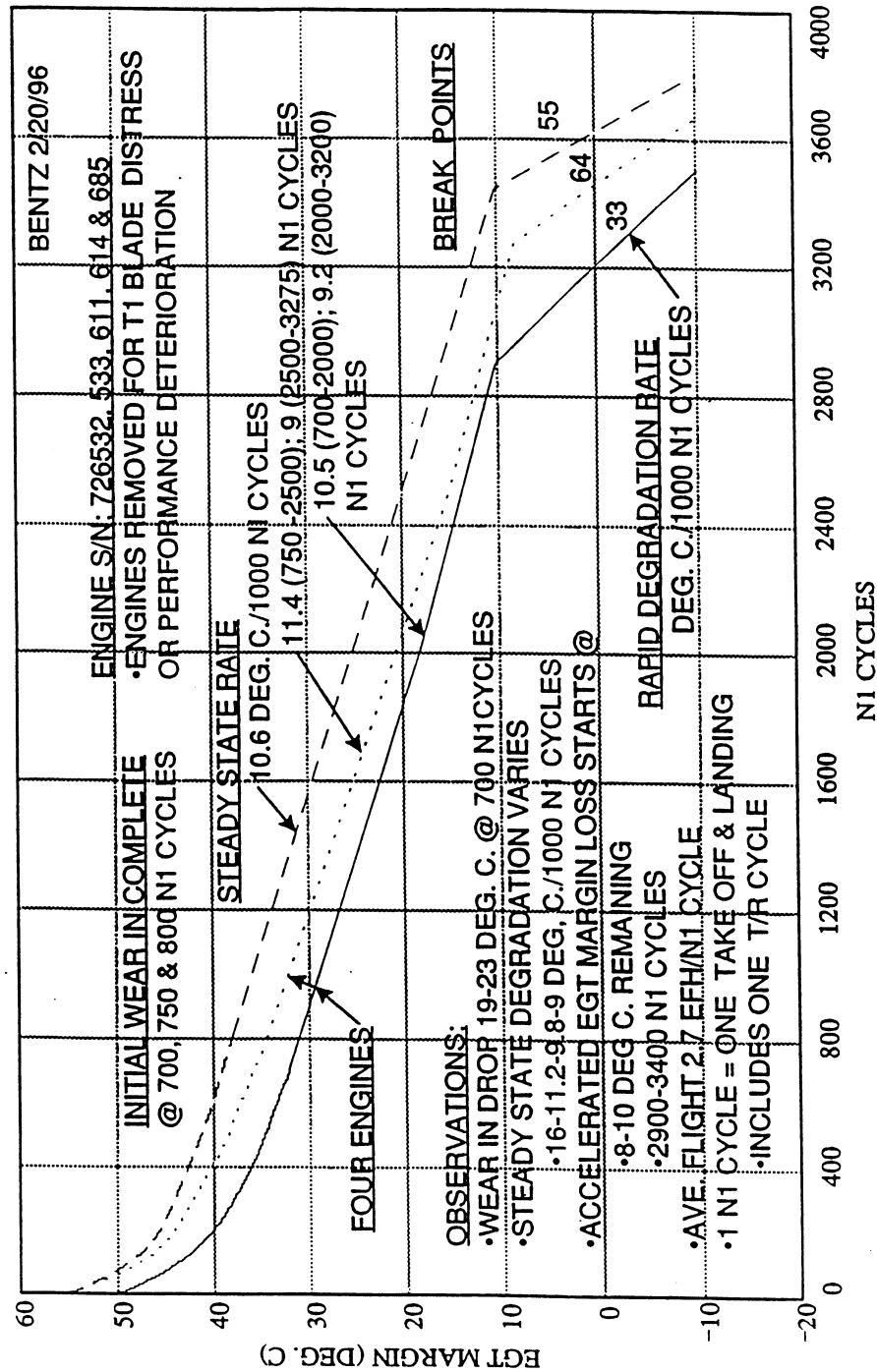


CHART 13 comments: DURABILITY OF NEW BLADE DESIGN (Same engine type)

This chart shows the impact that a 10% lower engine derate (higher thrust usage) has on the engine time on wing before T1 Blade distress drive the engine off the wing. The other difference was that Operator B had more Max Effort climb outs during take off. As noted, both Operators have an average flight leg of 1.94 hours however Operator B has lower Time on Wing and lower N1 Cycles before a heavy maintenance is required. The T1 blades on these engines had TBC coverage on the blade platforms only.

CHART 14 comments: F117 DO-1 EGT MARGIN DEGRADATION

An independent assessment of seven engines was accomplished circa early CY96. It was determined from the data analyzed that the average engine degraded at a rate of 14.5 °C/1000 N1 Cycles. The average take off derate was 12 to 16%. Max take off thrust was used during 7 to 20% of the take off conditions for the engines analyzed. Rapid degradation also occurred at around 8 to 10 °C EGT Margin remaining. **CHART 15 (COMMENTS ON ENGINE USAGE)** discusses some of the noted trends in the engine data analyzed for “average” type engine usage. The LIGHT DUTY and HARD-PRESSED Engine Usage curves were estimated based on all the data analyzed.

CHART 16 comments: DEGRADATION CHARACTERISTICS COMPARED

This chart summarizes the differences in several engine metrics between the commercial and military versions of the same engine type. The military version is operated at a 40K take off rating while the commercial version is rated at 37.5K thrust. The average engine usage is shown on the lower portion of the chart. The commercial version has only one max take off per month whereas max take off thrust is used in the range from 7 to 20% on some of the military engines. The other notable difference is the partial N1 Cycles per flight. The commercial engine has one partial cycle during each landing when the thrust reverser is deployed. The military engine can have 4 to 8 partial N1 Cycles on the ground and/or in flight performing one or more of the mission scenarios.

CHART 17 comments: INDEPENDENT ASSESSMENT

This chart summarizes the impact of uprating a commercial engine for military use, which is usually a more severe environment due to the various mission profiles, and austere operating conditions. “Throttle Push” is usually needed to offset increased drag and airframe weight or to provide for increased payload and range. However, “Throttle Push” will reduce engine life as noted by the analyses performed in the foregoing charts. The OEM must upgrade the hot section parts to provide acceptable engine time on wing and manage the durability problems of fielded engines.

DURABILITY OF NEW BLADE DESIGN

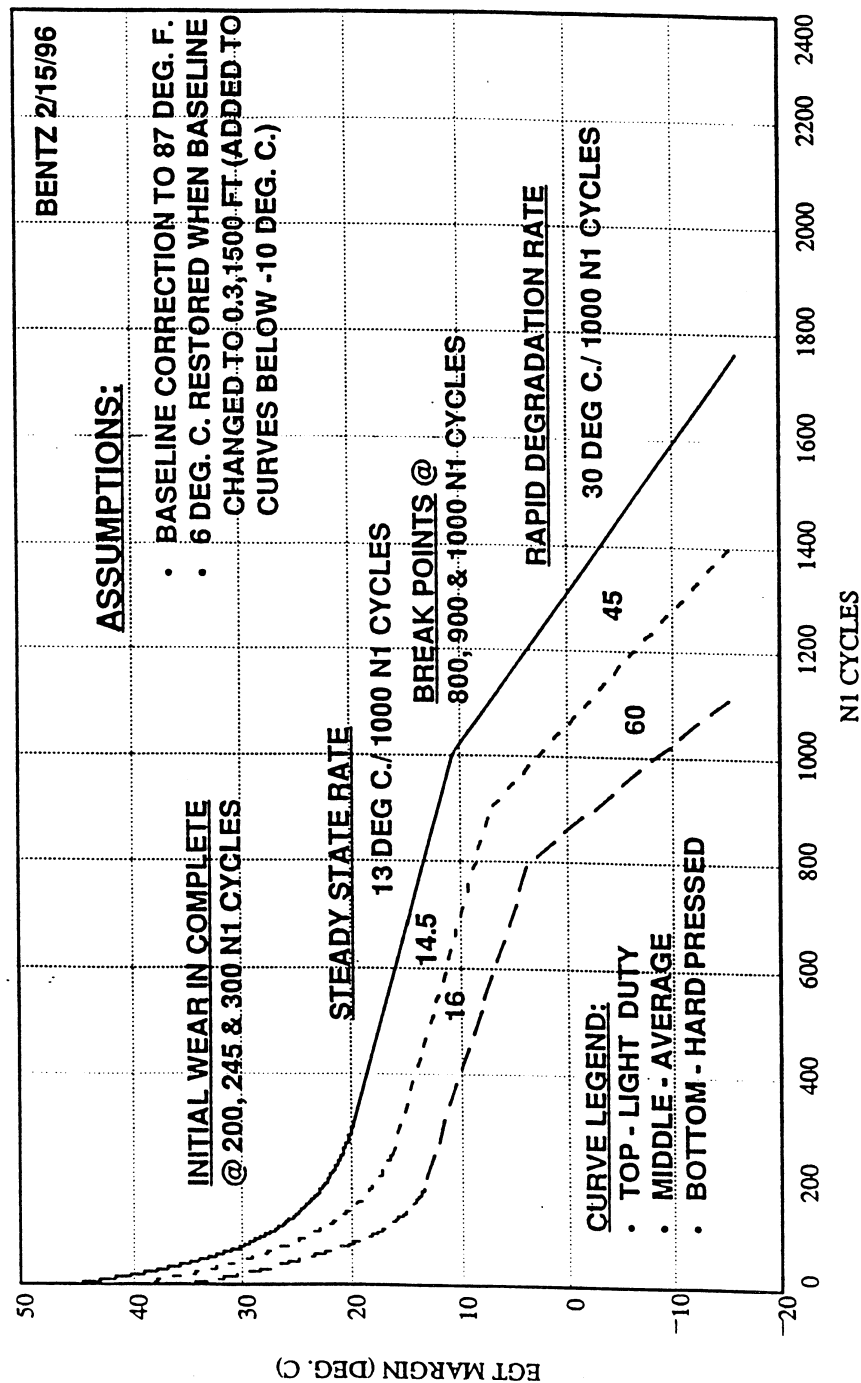
(SAME ENGINE TYPE)

<u>METRICS</u>	<u>OPERATOR A</u>	<u>OPERATOR B</u>
EFH'S	8200 - 9200	6100 - 6400
DERATE	19 to 21%	9 to 11%
CLIMB OUT	Throttle Retard for Noise Abatement	Many Max. Effort
AVE. FLT LEG	1.94 Hours	1.94 Hours
N1 CYCLES BEFORE HEAVY MAINTENANCE	4200 - 4700+	3100 - 3300
T. O. CONDITIONS	Some High Alt. Moderate Temp. Clean Runways	Many High Alt. Hotter Climate More Debris

F117 DO-1 EGT MARGIN DEGRADATION

P9, 10, 13, 14, 16, 17 & 18 ENGINES THRU JAN 96

(INDEPENDENT DATA ASSESSMENT)



COMMENTS ON ENGINE USAGE

F117 DO-1 EGT MARGIN DEGRADATION

<u>TYPE USAGE</u>	<u>% AVE DERATE</u>	<u>% @ MAX T.O. F_n</u>
LIGHT DUTY	16 TO 20	1 TO 7
AVERAGE	12 TO 16	7 TO 20
HARD PRESSED	8 TO 12	20 TO 35

NOTED TRENDS IN GO-81 DATA: (LAST 10 PTS. AVERAGED EACH REPORTING PERIOD):

- SOME ENGINES OPERATED AT HIGHER % @ MAX T.O. F_n DURING WEAR IN PERIOD WITH NO IMMEDIATE IMPACT ON EGT MARGIN DROP.
- LOWER AVERAGE DERATE INCREASES WEAR IN DROP AND STEADY STATE DEGRADATION RATES.
- AFTER 300 N1 CYCLES, THE AVERAGE % @ MAX T.O. POWER INCREASED AROUND 4 TO 8% WHILE THE AVERAGE DERATE REMAINED FAIRLY CONSTANT. AVERAGE DERATE ON SOME ENGINES INCREASED BY 3 TO 5%.

DISCLAIMER:

- THE ABOVE RANGES FOR % AVE DERATE AND % @ MAX T.O. F_n WERE DERIVED FROM ALL DATA THRU JAN 96 AND REFERRED TO AS THE AVERAGE ENGINE. THE LIGHT DUTY AND HARD PRESSED TRENDS WERE ESTIMATED USING LOWER AND HIGHER DEGRADATION RATES DURING ENGINE WEAR IN AND STEADY STATE OPERATION.

DEGRADATION CHARACTERISTICS COMPARED

F117 DO-1 VERSUS COMMERCIAL PW2037

<u>ITEM</u>	<u>F117 DO-1</u>	<u>PW2037</u>
WEAR IN DROP (DEG. C.)	24 - 32	19 - 23
ACCEPTANCE EGT MARGIN (DEG. C.)	45 - 55 (ENG)	55 (A/C)
START STEADY STATE RATE (DEG. C.)	13 - 21	32 - 36
@ N1 CYCLES	200 - 300	700 - 800
DEGRADATION RATE (DEG. C./1000 N1 CYCLES)	13 - 16	9 - 11.4
START RAPID DEGRADATION (DEG. C.)	8 - 10	8 - 10
@ N1 CYCLES	800 - 1000	2900 - 3400
<u>AVERAGE ENGINE USAGE</u>		
% DERATE @ TAKE OFF	12 - 16	19 - 21 (A)
% @ MAX T.O. THRUST	7 - 20 (B)	1
EST. PARTIAL N1 CYC PER FLT/GRND OPER.	4 - 8 (C)	1

LEGEND: (A) DERATE BASED ON F117 T.O. RATING
 (B) TIME AT HIGH POWER ACCELERATES TURBINE BLADE DISTRESS
 (C) NOT ALL PARTIAL CYCLES SHOULD BE COUNTED AS A MAJOR CYCLE

INDEPENDENT ASSESSMENT

- **FREQUENT HIGH POWER TAKE OFF AND CLIMB OUT ACCELERATES HOT SECTION DISTRESS**
- **THRUST UP RATING DEMANDS INHERENT GROWTH MARGIN IN HOT SECTION COMPONENT PARTS ESPECIALLY THE HIGH PRESSURE TURBINE**
- **HIGHER PROFILE FACTOR AND REDUCED BLADE COOLING PERFORMANCE LEADS TO HIGHER BLADE METAL TEMPERATURES**
- **MICROSTRUCTURE ANALYSES VERIFIED ANALYTICAL PREDICTIONS, BLADE SURFACE TEMP. EXCEEDED DESIGN INTENT BY +150 TO +200°F**
- **"THROTTLE PUSH" TO OFFSET INCREASED DRAG AND AIRFRAME WEIGHT OR PROVIDE INCREASED PAYLOAD/RANGE WILL IMPACT ENGINE LIFE**
- **THE OEM MUST RESPOND BY UPGRADING THE HOT SECTION DESIGN AND MANAGE THE CURRENT ENGINE DURABILITY PROBLEMS**

CHART 18 comments: A CRITICAL OBSERVATION

This chart reiterates the fact that new engines will experience durability after entering service. The most prevalent and costly to fix are the HPC, Combustor and the HPT Blades. The origin of engine durability problems is outlined again for review. Something can be done to reverse the trends but will take informed and dedicated Systems Engineering and the disciplined use of **DEVELOPMENT DESIGN MARGINS**.

CHART 19 comments: DEVELOPMENT DESIGN MARGINS

This chart summarizes the various topics to be covered in this section of the briefing.

CHART 20 comments: DESIGN MARGINS APPROACH

This chart covers the basic approach of establishing and tracking Development Design Margins. It outlines a Systems Engineering Approach that requires analytical work to be accomplished independent of the engine manufacturer. Preliminary estimates of T1 Blade leading edge temperatures are made independent of the engine designer based on assumed state of the art component characteristics. Design deficiencies are determined from component and engine testing. The customer must determine the source of the deficiencies that were determined through component or engine testing. These deficiencies may be a direct result of the design system or the component assumption used by the engine designer. The customer must also perform independent microstructure analyses of hot section parts to verify the max temperature exposure. The engine designer should be made aware that the customer will be conducting independent analyses of the hot section designs. Algorithms and design templates will be provided to accomplish the independent analyses.

CHARTS 21 and 22 comments: LCC CONSIDERATIONS and ROI BENEFITS

These two charts attempt to show the LCC impact of Hot Section problems and the benefits of performing dedicated Systems Engineering during an engine development. If an engine hot section were to provide only half the goal life for a fleet of 400 engines and effective System Engineering were applied to successfully achieve the goal life, then the ROI in maintenance cost reductions is estimated to be 1000.

CHART 23 comments: MORE AFFORDABLE APPROACH

This chart outlines a Systems Engineering Approach for use by the government and a more affordable approach for commercial operators. Specialized consulting could also be considered to accomplish some or all of the analyses.

A CRITICAL OBSERVATION

- New Engines Experience Durability Problems after Entering Service
- Most Prevalent and Costly to Fix: HPC, Combustor and HPT Blades
- Origin of the Problem
 - Basic Aero-Mechanical Design Systems, Assumptions and Design Margins
 - Available Seals and High Temperature Materials Systems
 - Development Testing Does Not Simulate Actual Service Environment
 - Aggressive Marketing in a Highly Competitive Environment
 - Evolving Mission Usage Changes (Cycles Rates and Flight Legs)
 - Voluntary Uprate Beyond Demonstrated Hot Section Durability Limits
 - Engine Choice Based on Criteria other than Sound Engineering Data
 - User Needs a New Aircraft to Replace an Aging Fleet
 - Airframer/OEM Advocacy, Keep Design Teams Busy and Production Steady
- Durability Short Falls Revealed during First Run Time in Service

DEVELOPMENT DESIGN MARGINS

PROPOSED APPROACH

LCC CONSIDERATIONS

MARGINS TEMPLATE

CUSTOMER INVOLVEMENT

TRACKING PROGRESS

COMPETITION AND ACCOUNTABILITY

DESIGN MARGINS APPROACH

Calculate Engine Cycle Performance for Candidate Engine Configurations

- Request Cycle Pressure Ratios, Bypass Ratio, Max. Turbine Inlet Temperature
- Use Design Point Component Efficiencies, Pressure Drops, Core Airflow at Sea Level Static and Cruise Conditions

Establish Demonstrated Performance Baseline for all Engine Components

- Determine Combustor Pattern and Profile Factors from Low & High Pressure Rig Tests. (Were Test Rigs Full Scale and when were tests conducted?)
- Obtain design assumptions for Overall Blade Cooling Performance (Were these levels demonstrated in both a Component Rig and Engine Test?)
- Request or Estimate Stage Cooling Flows for the Exit Guide Vane and the High Pressure Turbine (Use Increased Levels of Cooling as Required.)

Participate in Preliminary and Final Hot Section Design Reviews

- Compare independent results with Hot Section Designers Interface Control Document and the Blade Leading Edge Metal Temperature Requirements
- Evaluate the Results of Rig and Engine Tests. Sufficient Test Time at Max. Gas Temperature is Important. Obtain Blades for Microstructure Analysis.

Encourage OEM to Update Hardware Design, Assumptions and Practices

- Continue to Track Development Work to Correct Identified Deficiencies

Request all Design Assumptions for Proposed Engine Design and Results of Engine Development Testing (Data should not be guarded by OEM.)

LCC CONSIDERATIONS

(ASSUME 25 YEARS SERVICE LIFE)

ASSUME THE FOLLOWING CATEGORIES IN LIFE CYCLE COST:

- DEVELOPMENT PROGRAM: \$5 TO 10B (Estimate) OR NO COST IF CFE
- ENGINE COST: \$8 TO 20M EACH PLUS INITIAL SPARES PROVISIONING
- MAINTENANCE COST: \$1.5 TO 2M FOR EACH HEAVY MAINTENANCE WITH 8 TO 15 REQUIRED BUILDS DEPENDING ON DURABILITY AND LIFE LIMITS
- FUEL BURNED: FUEL PRICES WILL ESCALATE, \$0.90 TO 1.50/GAL.

ASSUME THE FOLLOWING BREAKOUT OF TOTAL LIFE CYCLE COSTS:

- ENGINE ACQUISITION: 20 TO 25%
- MAINTENANCE COST: 25 TO 35%
- FUEL BURNED: 40 TO 60%

IMPACT STATEMENT: If the HOT SECTION provides only HALF the GOAL LIFE, then the MAINTENANCE COST will increase by \$5B (Est.) for a Fleet of 400 Engines. Military pays CATALOG PRICE for COMMERCIAL PARTS whereas Commercial Customers demand and get prorated CREDITS for all WARRANTED PARTS and EXCESS FUEL BURNED.

ROI BENEFITS

IF 40 M/Y'S OF SYSTEM ENGINEERING WERE DEDICATED TO TRACKING ENGINE DEVELOPMENT TO INSURE THAT DURABILITY GOALS WERE ACHIEVED BEFORE DOWNSELECT, THE COST WOULD BE AROUND \$5M. (Assumed \$125K/MY)

THE ROI IN MAINTENANCE COST REDUCTIONS = 1000

FUEL BURNED INCREASES AS GAS PATH COMPONENTS DEGRADE, ESPECIALLY PERFORMANCE RETENTION IN THE HPC AND HPT.

A 5% INCREASE IN FUEL BURNED WOULD COST AROUND \$0.6 B. THE ROI WOULD INCREASE IN THE RANGE FROM 1120 TO 1200.

THE ROI FOR IMPROVED PERFORMANCE RETENTION = 120 TO 200

MORE AFFORDABLE APPROACH

System Engineering Requires Parttime and Full Time Specialists in each of the Component Areas before Engine Down Select

- Program Manager for each Engine Manufacturer
- Performance Analysts
- Dedicated Development Engineers for each Engine
- Materials and Structures Specialists
- Test Engineers

A More Affordable Approach is Possible for Commercial Operators

- Establish a Performance and Durability Analyst Position for Current and New Engines in the Propulsion Maintenance Facility
- The Program Manager for each Engine in Service, New Engines or Upgrades could request a technical assessment on Durability Issues.
- Empower the Analyst to obtain the necessary design information from the Engine Manufacturer(s) for the internal analyses.
- Explain that Future Business Opportunities would be contingent upon their full cooperation and commitment to fix deficiencies

Specialized Consulting could also be considered as needed

CHART 24 comments: DESIGN MARGINS TEMPLATE

This chart summarizes the four major elements of establishing and tracking Development Design Margins. They are: 1) Establish and track engine component performance parameters, 2) Establish State of the Art Values for the Performance Coefficients that affect blade and vane metal temperatures (Phi, CPF, PF, Coatings Systems, etc.), 3) Calculate the Vane and T1 Blade Metal Temperature Requirement (use T_{bm}r equation), and 4) Calculate metal temperature sensitivity for a range of Pattern and Profile Factors (PF) and the Overall Cooling Performance (Phi). Note: CPF is Combustor Pattern Factor used for the vane while PF is the Profile Factor used in the calculation for the T1 Blade. It is important to use degraded values for gas path component efficiencies, Pressure Ratio's and Core Airflow at the end of the service interval when calculating the gas path temperatures and the Calculated Blade Surface Temperature on the leading edge of the blade. It is also important to compare independent calculations with the design intent of the engine designer. As Component Rig and Engine Test Data are available, compare with estimates and design intent. Urge designer to correct any deficiencies and determine when the next design iteration will be tested. Obtain vanes and blades for microstructure analyses. The materials will indicate the level of high temperature exposure and eliminate some of the smoke and mirrors!

CHART 25 comments: TRACK COMPONENT PERFORMANCE

This chart attempts to show critical parameters of the gas path that must be tracked during the development process. The differences between the Desired and the Demonstrated values for component efficiencies and Pressure Ratio can cause a lot of error in the design temperatures of the hot section parts. Unfortunately the turbine blade design is a long lead item and any changes to the cooling design and blade castings are difficult to correct in a timely manner. Temperature Margins are important early in an engine development program to protect the design life of the hot section. Estimated values component efficiency reduction are provided for use in cycle calculations.

CHARTS 26-28 comments: ESTIMATING T1 BLADE MAXIMUM SURFACE TEMPERATURE

The next three charts plus the appendix entitled **DERIVATIONS** outline the general equation for estimating the maximum surface temperature on the leading edge of the first stage turbine blade. The **DERIVATIONS** Appendix contains the same derivation for the Vane. These equations are first order approximations of the surface temperature on the leading edge of the vane and blade airfoils.

DESIGN MARGINS TEMPLATE

Establish and Track Engine Component Performance Parameters

- Demonstrated Baseline at each Engine Manufacturer
- Establish Desired Levels for Proposed New Engine Centerline
- Determine Reduction in Efficiency, Pressure Ratio and Core Airflow at the end of a Service Interval

Establish State of the Art Values for Performance Coefficients that Affect Blade and Vane Metal Temperatures (Phi, CPF, PF, Coating Systems, etc.)

- Set Reasonable Levels for Degraded State at end of a Service Interval

Calculate Vane and T1 Blade Metal Temperature Requirement (Tbmr Eq.)

- Use Degraded Engine Component Efficiencies at End of Service Interval
- Compare with Design Intent, Rig and Engine Test Data

Calculate Metal Temperature Sensitivity for a Range of Pattern and Profile Factors and Overall Cooling Performance

- Use Sensitivity Curves to Determine Demonstrated Levels of CPF, PF and Phi using data from highly instrumented Developmental Engine Test
- Microstructure Analyses will provide Actual Metal Temperature Exposure

TRACK COMPONENT PERFORMANCE

<u>Component</u>	<u>Demonstrated Efficiencies</u>	<u>Desired Efficiencies</u>	<u>Degraded State (Estimated)</u>
• Fan	____%	____%	- 1/2%
• LPC	____%	____%	- 1%
• HPC	____%	____%	- 1%
• Combustor	____%	____%	- 3%
• HPT	____%	____%	-1 1/2%
• LPT	____%	____%	-1/2%

<u>Demonstrated</u>	<u>Desired</u>	<u>Degraded State</u>
• Fan	____PR	____PR
• LPC	____PR	____PR
• HPC	____PR	____PR
• Combustor	____ Δ P/P	____ Δ P/P
• HPT	____PR	____PR
• LPT	____PR	____PR
• Corr. Wa	____Core	____Core

ESTIMATING T1 BLADE MAXIMUM SURFACE TEMPERATURES

The general equation for estimating the maximum surface temperature on the leading edge of the first stage turbine blade is:

$$T_m = (1 - \Phi) / RF [PF(T_4 - T_3) + T_{41}] + \Phi(T_3 + \Delta T_p)$$

Definition of Coefficients:

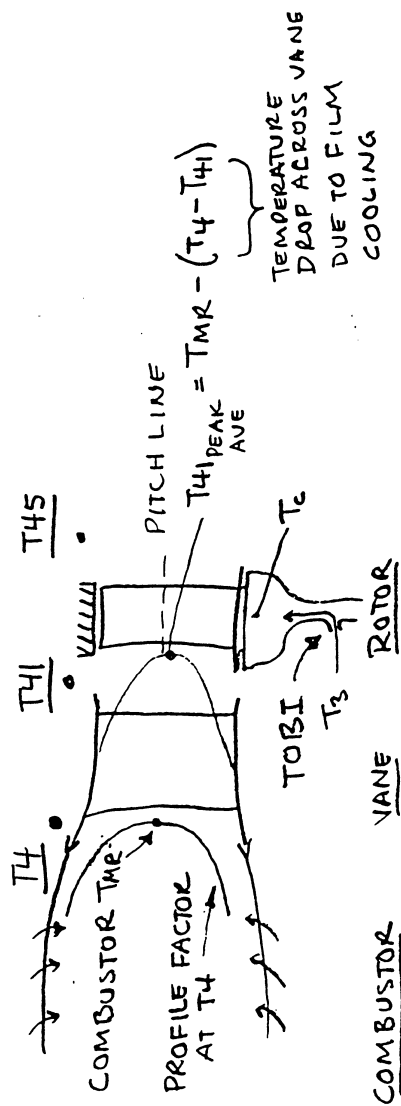
Phi	Overall Blade Cooling Performance used in the blade design
RF	Relative Rotor Factor used to calculate the relative rotor temperature
PF	Combustor Profile Factor used to estimate the maximum mean radial temperature entering the turbine stage
Tp	Delta temperature rise of the cooling air T3 due to disk pumping

Comments:

The above equation is a first order approximation of the surface temperature on the leading edge of the first stage turbine blade at the pitch line.

$$T_m = T_{cbs} \quad \text{Calculated Blade Surface Temperature}$$

COMBUSTOR EXIT TEMPERATURE PROFILE



$$(PF) \text{ COMBUSTOR PROFILE FACTOR} = \frac{T_{MR} - T_4}{T_4 - T_3}$$

$$(TRR) \text{ T RELATIVE ROTOR} = \frac{T_{41}}{\text{ROTOR FACTOR}}$$

$$(Phi) \text{ OVERALL COOLING PERFORMANCE} = \frac{T_{RR} - T_M}{T_{RR} - T_c}$$

$$T_c = T_3 + \Delta T_{\text{pumping}}$$

$$T_{MR} = \text{MEAN RADIAL TEMPERATURE}$$

FROM GAS TURBINE COMBUSTION

BY ARTHUR H. LEFEBVRE

142 GAS TURBINE COMBUSTION

Thus, it is highly desirable that rig work on the improvement of temperature traverse quality should be carried out at the maximum engine pressure, since this corresponds to maximum heat-transfer rates to nozzle guide vanes and turbine blades.

Another difficulty in the assessment of pattern factor or temperature traverse quality stems from lack of confidence in the reliability of the experimental data. Because of the time and cost involved, temperature surveys are necessarily based on a limited number of thermocouple readings or gas samplings, and a very small change in the location of a probe can make all the difference between recording and failing to record a "hot spot" in the exit-temperature traverse. Owing to the inherent variability, it is highly desirable to examine data obtained from three or four chambers, all built to the same standard, when defining a typical pattern.

The most important temperature parameters are those that affect the power output of the engine and the life and durability of the hot sections downstream. As far as overall engine performance is concerned, the most important temperature is the turbine inlet temperature T_4 , which is the mass-flow-weighted mean of all the exit temperatures recorded for one standard of liner. Since the nozzle guide vanes are fixed relative to the combustor, they must be designed to withstand the maximum temperature found in the traverse. Thus, the parameter of most relevance to the design of nozzle guide vanes is the overall temperature distribution factor, which highlights this maximum temperature. It is normally defined as

$$\text{Pattern factor} = \frac{T_{\max} - T_4}{T_4 - T_3} \quad (4.42)$$

where T_{\max} = maximum recorded temperature

T_3 = mean inlet air temperature

T_4 = mean exit temperature

The temperatures of most significance relative to the turbine blades are those that constitute the average radial profile. They are obtained by adding together the temperature measurements around each radius of the liner and then dividing by the number of locations at each radius, i.e., by calculating the arithmetic mean at each radius. A typical radial temperature profile is shown in Fig. 4.27. The expression used to describe the radial temperature distribution factor, also known as the *profile factor*, is

$$\text{Profile factor} = \frac{T_{mr} - T_4}{T_4 - T_3} \quad (4.43)$$

where T_{mr} = maximum circumferential mean temperature

The pattern factor and profile factor, as defined above, are best suited for situations in which a perfectly uniform exit-temperature distribution would be considered ideal. However, in modern high-performance engines, which employ extensive air cooling of both nozzle guide vanes and turbine blades, the desired average radial distribution of temperature at the combustor exit plane is far from flat; instead, it usually has a profile that peaks above the midheight of the blade, as

AERODYNAMICS 143

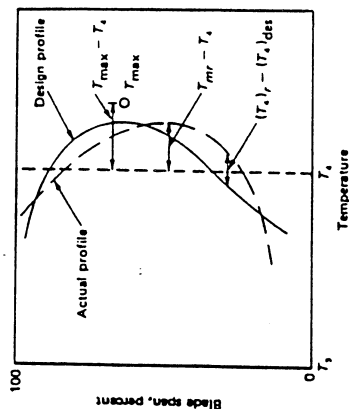


FIG. 4.27 Explanation of terms in exit temperature profile parameters.

illustrated in Fig. 4.27. A parameter that takes the design profile into account is the *turbine profile factor*, defined as

$$\text{Turbine profile factor} = \frac{(T_{4,r} - T_{4,des})_{\max}}{T_4 - T_3} \quad (4.44)$$

where $(T_{4,r} - T_{4,des})_{\max}$ is the maximum temperature difference between the average temperature at any given radius around the circumference and the design temperature for that same radius.

Statistical methods are sometimes used to describe the temperature distribution at the combustor outlet. Their main application is in combustor development, where they are used both in analyzing the key factors governing the temperature distribution of any given combustor, and in helping to identify the causes of differences in measured temperature distribution among combustors of nominally the same design [48 to 50].

Dilution-Zone Design

At this stage in the design process, the amount of air available for dilution purposes will have been established, using charts of the type illustrated in Fig. 4.28, along with estimates of liner diameter and liner pressure-loss factor. The principal dilution-zone design variables are the number and size of the air-admission holes and the zone length. To ensure a satisfactory temperature profile at the chamber outlet, there must be adequate penetration of the dilution air jets, coupled with the correct number of jets to form sufficient localized mixing regions. Now the penetration of a round jet is a function of its diameter [see Eq. (4.27)]. If the total dilution-hole area is spread over a large number of small holes, penetration will be inadequate, and a hot core will persist through the dilution zone. At the other extreme, the use

CHART 29 comments: BLADE TEMPERATURE SENSITIVITY TO COMPONENT PERFORMANCE COEFFICIENTS

This chart is provided to show the range of performance degradation that can be expected for the performance factors shown. It should be pointed out that the levels for the Overall Cooling Performance (Phi) are very optimistic. The New Engine Phi should be in the range of 0.55 to 0.5 rather than 0.75 to 0.7. These later values were used in an advanced study. The importance of using degraded values for the Performance Factors and the Advanced Coating Systems is to insure that the condition of the hot section parts at the end of each service interval are serviceable and have a low scrape rate. Otherwise, the cost to refurbish the high-pressure turbine will be extremely high. The Relative Rotor Factor is a function of the vane and blade stage design and difficult to calculate but must be considered. The engine designer must declare a development pad for the T1 Blade to accommodate unforeseen development problems and for a "Throttle Push" that may be needed to provide more engine thrust later in the program. Upgrading the engine should not result in a corresponding decrease in engine time on wing. The OEM should provide a new T1 Blade design for the upgraded engine especially if the current blade design is not meeting engine life goals.

CHART 30 comments: PROPOSED EQUATION FOR ESTIMATING T1 BLADE METAL REQUIREMENTS

The equation to calculate the Base Metal Requirement (Tbmr) for the T1 Blades contains eight terms that are described under Definition of Terms. The bracketed terms are referred to as the component sensitivity factors that take into consideration the additional temperature margin that has to be accounted for at the end of the service interval in order to avoid any distress on the first stage blades and allow repair. Use of this equation will be demonstrated in **CHART 33**. A more detailed discussion of the rationale for each of the terms in the equation is contained in a report prepared for the Turbine Engine Division of the Air Force Propulsion and Power Laboratory at WPAFB, OH.

CHART 31 and 32 comments: MIXED FLOW TURBOFAN and SAMPLE GASTURB CALCULATION (Joachim Kurzke www.gasturb.de)

A cross section of the an mixed flow turbofan engine is provided in **CHART 31** to understand the sample cycle calculations made by GasTurb for Windows shown in **CHART 32**. A baseline cycle calculation is made using the proposed component efficiencies, pressure drops and design pressure ratio's at the select design point. GasTurb calculates Tcbs in the Composed Values for different levels of Overall Cooling Performance (Phi). It can be noted that a Phi of 0.5 provides a 243 °F higher Tcbs than a blade design using a Overall Cooling Performance of 0.7. This large increase in blade surface temperature for a small reduction in cooling performance sounds the alarm to verify the overall cooling performance in the engine rather than a component rig test.

BLADE TEMPERATURE SENSITIVITY TO COMPONENT PERFORMANCE COEFFICIENTS

<u>Performance Factors</u>	<u>Range of Performance</u>
Overall Cooling Performance	New Engine 0.75 to 0.7 End of Service Life 0.6 to 0.5
Combustor Profile Factor	New Engine 0.25 to 0.28 End of Service Life 0.28 to 0.32

Note: End of Service Life refers to End of Service Interval

Advanced Coating Systems 1 st Generation	New Engine 200 °F. End of Service Life 100
2 nd Generation	New Engine 300 °F. End of Service Life 100
3 rd Generation	New Engine 400 °F. End of Service Life 100

Note: Current TBC Systems initially provide 50 to 75 °F of protection on the blade depending on thickness, but due to erosion on the leading edge down to the base material, TBC provides no protection of the base material near the end of the Service Interval and all blades must be scrapped due to oxidation. The assumed 100 °F. protection at the end of a Service Interval is within the inspection capability of flight line boroscopes since erosion or spallation will expose the base material on some of the blade leading edges. It is also difficult to maintain uniform thickness of TBC on the blade leading edge within 1 to 2 mills.

Rotor Factor	New Engine 0 °F. (1.15 Baseline)
Development margin	N2 speed changes +/- 20 °F.
Tm Pad for "Throttle Push"	Need more thrust +50 °F.

Note: The assumed +50 °F. Pad provides for engine growth with components that have achieved their design efficiency and pumping goals.

PROPOSED EQUATION FOR ESTIMATING T1 BLADE METAL REQUIREMENTS

$$T_{bmr} = T_{cbs} - T_{tbp} + T_{gmr} + [T_{dec} + T_{ltp} + T_{lcp} + T_{hpf}] \pm T_{rrf}$$

Note: The bracketed terms, $[T_{dec} + T_{ltp} + T_{lcp} + T_{hpf}]$, are referred to as the component sensitivity factors.

Definition of Terms:

T_{bmr} Base Metal Requirement for the T1 Blades.

T_{cbs} Calculated Blade Surface Temperature using the baseline assumptions for the blade design. In this study, $\Phi=0.7$, $PF=0.25$, $RF=1.15$ and a delta temperature rise of 156 °F for disk pumping of the cooling air, T3.

T_{tbp} Thermal Barrier Protection of TBC Systems.

T_{gmr} Assigned Growth Margin Reserve.

T_{dec} Degraded Engine Component Efficiencies. Assumes pumping capacity of the Fan, LPC and HPC and the turbine work coefficient have all been achieved.

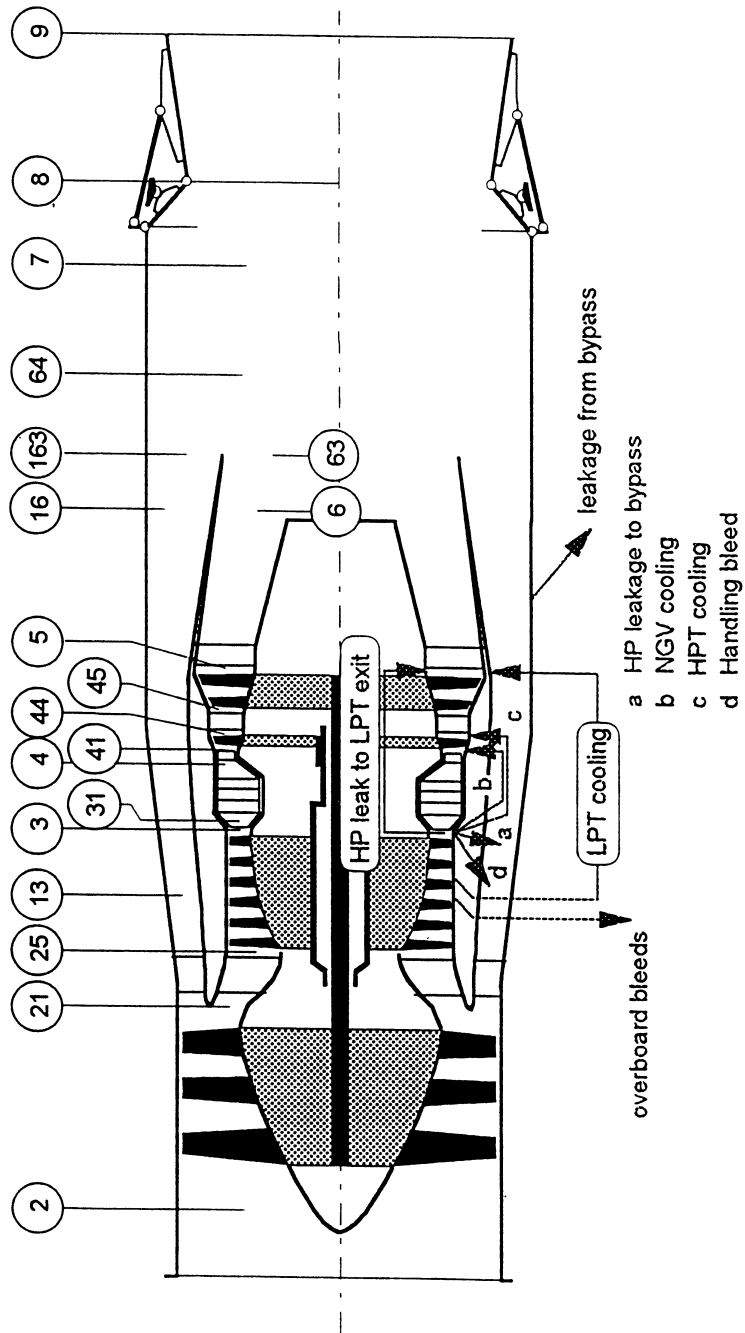
T_{ltp} Loss in Thermal Protection for TBC system due to erosion and/or spallation.

T_{lcp} Lower Overall Cooling Performance demonstrated than design intent and from deterioration during operational use.

T_{hpf} Higher Combustor Profile Factor than design intent and/or from deterioration during operational use.

T_{rrf} Relative Rotor Factor.

MIXED FLOW TURBOFAN WITH VARIABLE EXHAUST NOZZLE



SAMPLE GASTURB CALCULATION

File: C:\GTB WIN\LAST_MTF.CYM - modified
Date: Jun2497
Time: 10:06

mixed Turbofan Alt=60000ft / Mn=3.00 ISA

T4=4121.8°R., T3=2460, 2X Cooling, Degraded Comp. Perf., Phi=0.7, 0.6, 0.5

Station	W	T	P	WRstd	FN
amb		389.97	1.040		= 8068.83
2	156.571	1091.92	30.902	108.035	SFC = 1.5387
13	37.005	1402.24	66.008		WF Burner= 3.4488
21	119.565	1552.69	91.070	33.383	BPR = 0.3095
25	119.565	1552.69	91.070	33.383	P25/P21 = 1.0000
3	117.174	2459.83	486.311	7.711	Core Eff = 0.6390
4	105.677	4121.80	463.844	9.439	Prop Eff = 0.7866
41	115.242	3994.91		10.133	P3/P2 = 15.737
45	120.025	3152.20	134.357	32.365	P16/P6 = 1.05011
5	122.416	2677.29	59.291	68.936	A64 = 772.08933
6	122.416	2677.29	58.106		A63 = 689.61064
16	37.005	1402.24	61.017	A163 = 82.47869	
64	159.422	2402.75	58.453	XM63 = 0.18263	
8	159.422	2402.75	58.453	XM163 = 0.32351	
P2/P1 = 0.8088			P4/P3 = 0.9538	A8 = 257.62282	
Efficiencies:	isentr	polytr	RNI	P6/P5 = 0.98000	
Outer LPC	0.7929	0.8124	0.60	P16/P13 = 0.92440	
Inner LPC	0.7879	0.8153	0.60	W NGV/W25 = 0.08000	
HP Compressor	0.8832	0.9042	0.98	WHcl/W25 = 0.04000	
HP Turbine	0.8748	0.8565	1.04	WLcl/W25 = 0.02000	
LP Turbine	0.8862	0.8752	0.45	WBLD/W21 = 0.00000	
Mixer	0.9900			WBLD/W25 = 0.00500	
Con-Di Nozzle:				PWX = 0	
A9* (Ps9-Pamb)			7.648	A9/A8 = 5.99000	
				XM9 = 3.20704	
				CV9 = 0.97388	

Composed Values:

Fn/W2	=	51.53469	
0.635*T3+0.0652*T4+0.261*T41+109.2	=	2982.60327	$\phi = 0.7$
0.513*T3+0.087*T4+0.348*T41+93.6	=	3104.31665	(2523°F)
0.391*T3+0.1087*T4+0.435*T41+78	=	3225.61719	(2644°F)
P8qamb	=	56.19679	(2766°F)
			0.6
			0.5

CHART 33 comments: SAMPLE CALCULATION OF THE TURBINE BASE METAL REQUIREMENT

The end of the service interval calculations must be accomplished to determine the temperature increases that must be accounted for when the engine components degrade. A baseline cycle calculation is used to determine the delta increase in the Tdec. Loss in Thermal Protection, Leading Edge Phi and Higher Profile Factor are determined for each of the design points. The examples shown are for the SLS and M3/60K Cruise operating points. It is noted that the estimated Tbm_r of 2583 °F at SLS is beyond current materials capabilities. Current materials start to oxidize and erode above 2050 °F and melt at around 2400 °F. The loss in thermal barrier protection is caused by erosion that decreases the TBC thickness and cannot be avoided. Limited exposure to fine particles on the ground or in the air can cause a sudden drop in EGT Margin and a corresponding increase in Turbine Inlet Temperature to maintain the same engine thrust which will destroy the T1 Blades.

CHART 34 and 35 comments: T_m SENSITIVITY TO COOLING PERFORMANCE and T_m SENSITIVITY TO PROFILE FACTOR (Both at SLS Conditions)

If Cooling Performance (Phi) decreases from 0.7 to 0.5, T_m will increase by 200 °F at a T4 of 3460 °R. At 4070 °R, T_m would increase approximately 325 °F. A Profile Factor change from 0.25 to 0.35 would result in approximately 36 °F increase in T_m at a T4 of 3460 °R. Overall Cooling Performance provides a significant change to T_m as noted. It is extremely important that advanced high temperature cycles use realistic and attainable levels of Phi. These levels should be based on engine testing rather than component rig or coupon tests as the scale of turbulence, air density and configuration differences will result in a poorly executed cooling system design and negative temperature margins.

CHART 36 comments: CUSTOMER INVOLVEMENT

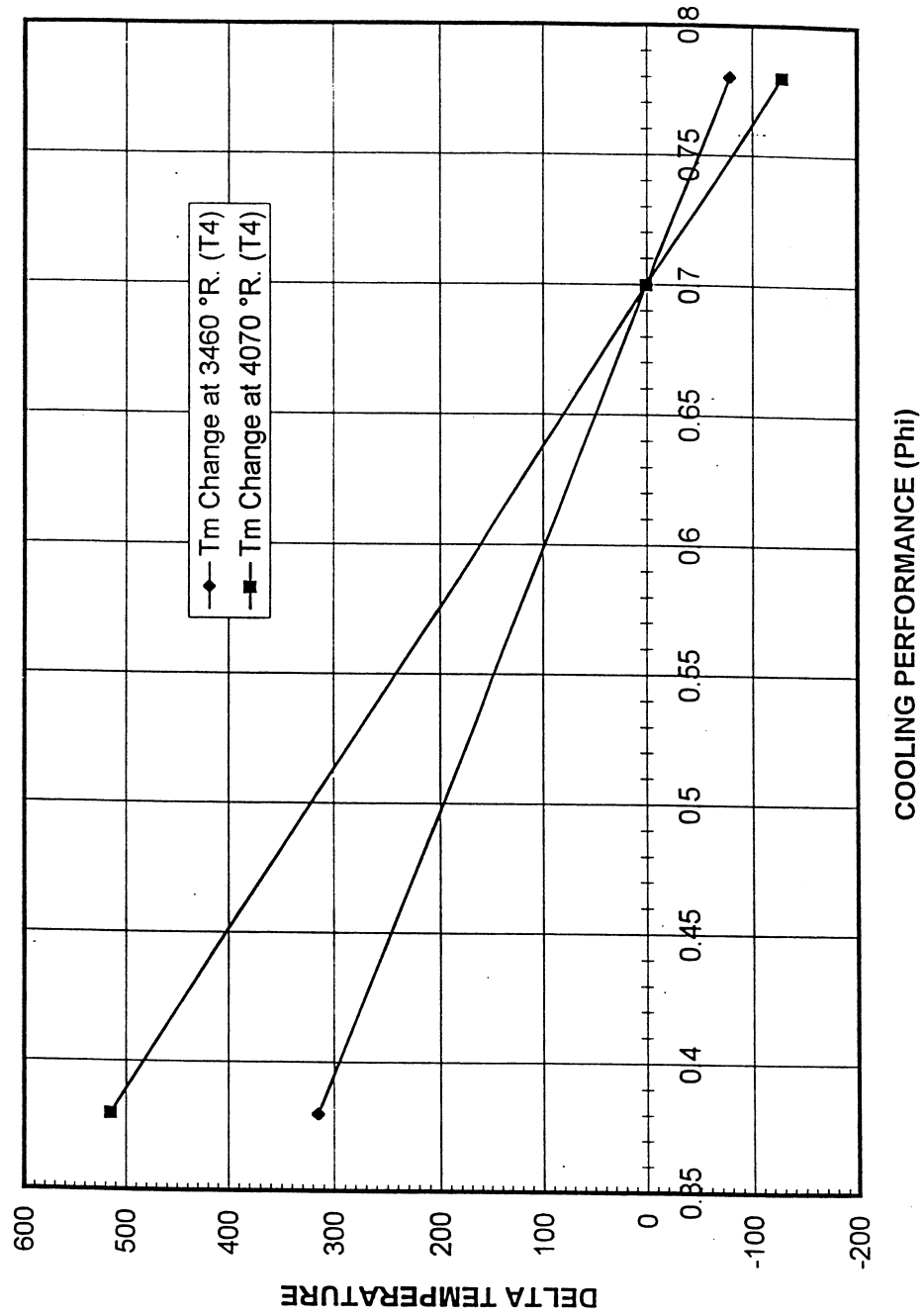
This chart is self-explanatory. Get involved. Obtain responsible design information and development data from all tests. Insure design stability of the gas path components. Nothing is more frustrating for a turbine designer than to have the design temperature increased with no available temperature margins or time for a complete redesign of the blade and cooling schemes. The other important point is to participate in conceptual, preliminary and final design reviews. Do your homework and come to the meeting prepared with good questions. Expect to get slow rolled or isolated! Microstructure analyses of distressed hardware will determine who is right!

SAMPLE CALCULATION OF THE TURBINE BASE METAL REQUIREMENT

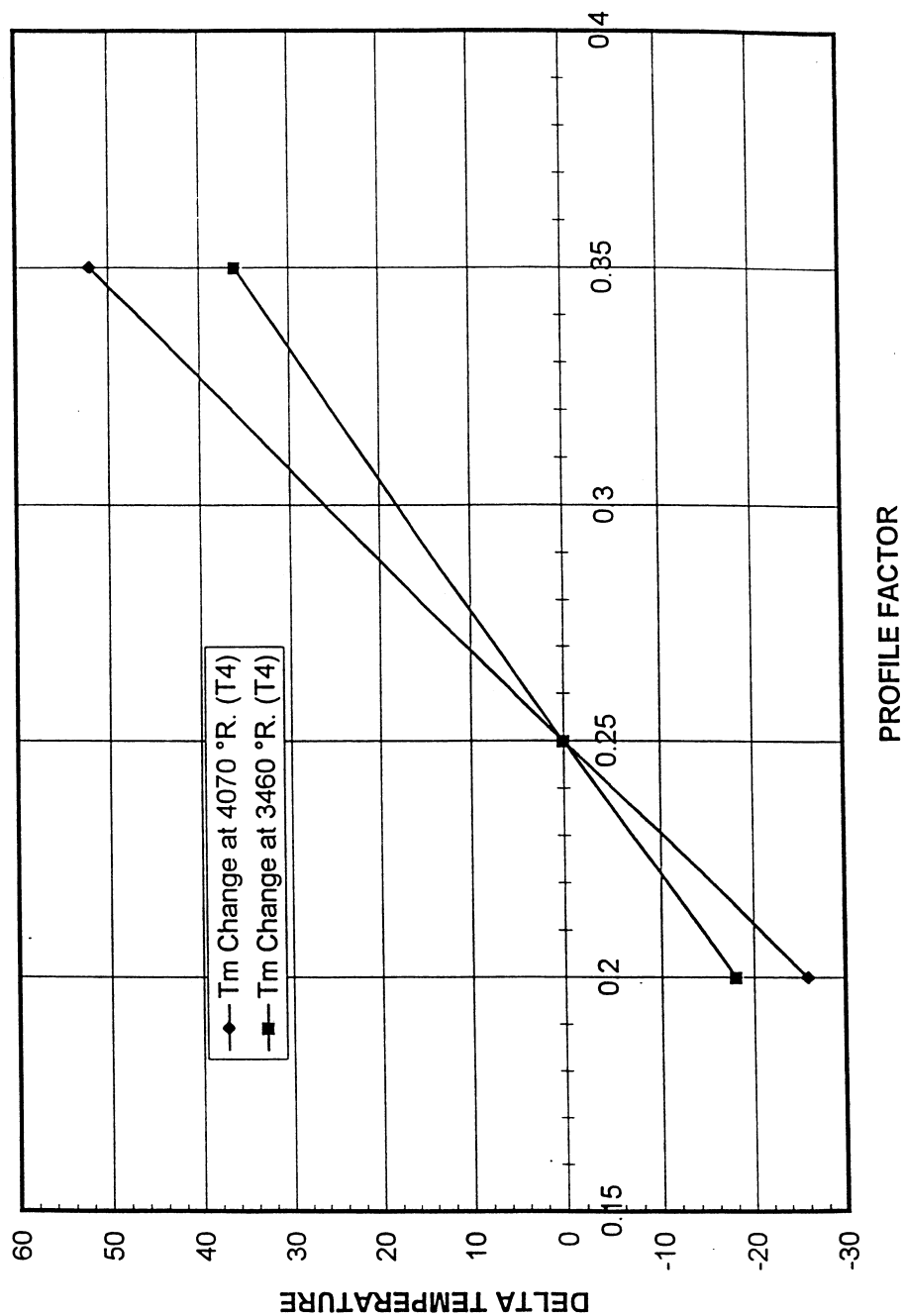
Factor (°F.)	Comments/Assumptions	SLS 50K Fn	M3/60K Cruise
Tcbs	T4=4240 °R. SLS T4=4122 °R. M3/60K (no efficiency degradation) 2 nd Generation TBC	2285 °F.	2523 °F.
Ttbp	Fn Growth and Reserve	-300 °F.	-300 °F.
Tgmr	Combined Efficiency Loss	+50 °F.	+50 °F.
Tdec	Loss in Thermal Protection during Service Interval	+31 °F	0
Tltp	Leading Edge Phi=0.55 (End of Service Interval)	+200 °F.	+200 °F.
Tlcp	Higher PF=0.32 (End of Service Interval)	+279°F. (310-31)	+182 °F. (182-0)
Thpf	Estimated RF=1.13 to 1.17	+38 °F.	+30 °F.
Trtf		+/- 20 °F.	+/- 20 °F.
Tbmr	Base Metal Requirement (Estimated)	2583 +/- 20 °F. at SLS	2685 +/- 20 °F. at M3/60K Cruise

Comments: A seasoned engine designer will argue that the above base metal requirements for the T1 Blades are too one sided. The analysis should have considered a random Monte Carlo distribution in selecting the performance degradations for the various "Component Sensitivity Factors".

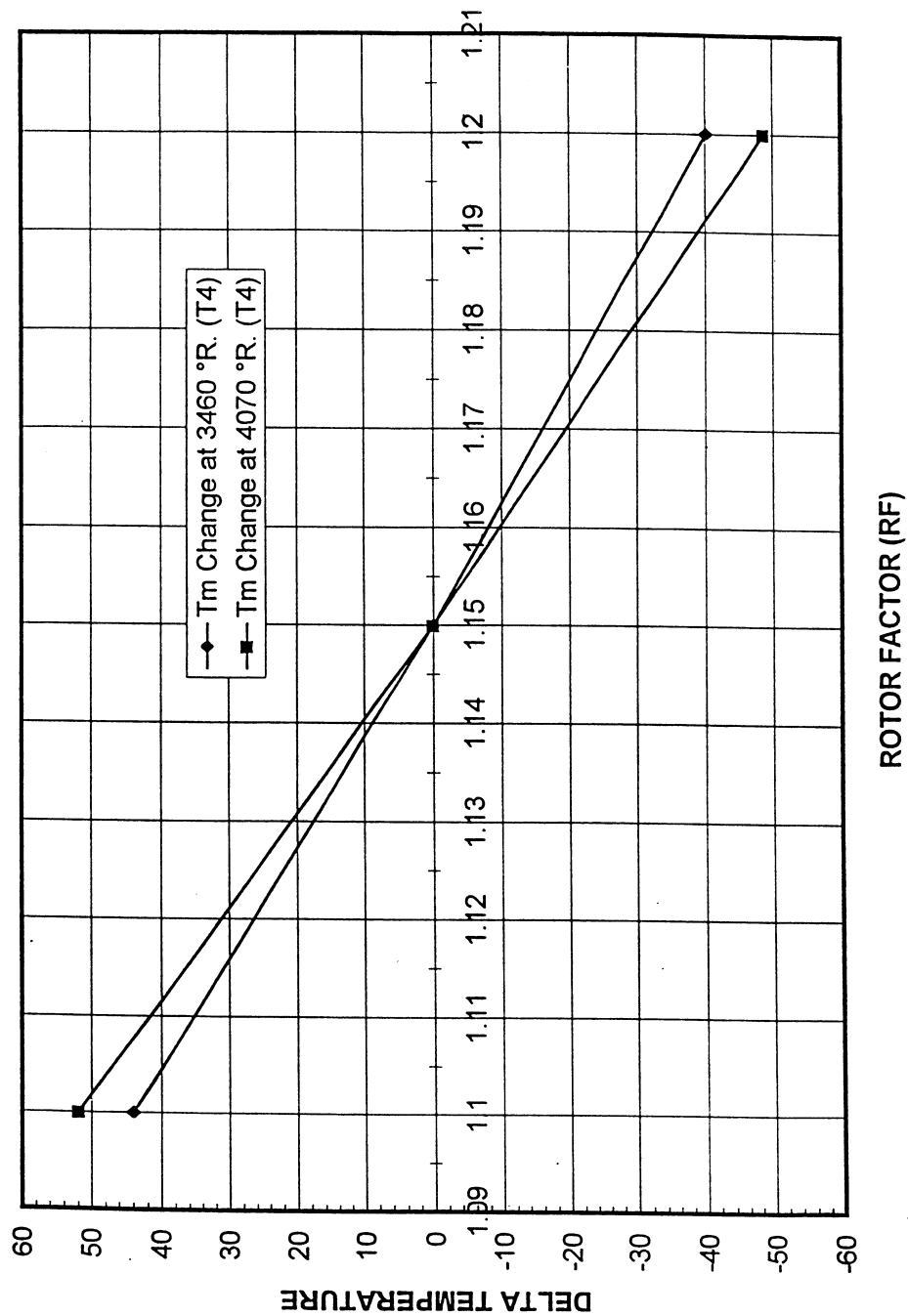
T_m SENSITIVITY TO COOLING PERFORMANCE SEA LEVEL STATIC CONDITIONS



T_m SENSITIVITY TO PROFILE FACTOR SEA LEVEL STATIC CONDITIONS



T_m SENSITIVITY TO ROTOR FACTOR (RF) SEA LEVEL STATIC CONDITIONS



CUSTOMER INVOLVEMENT

Obtaining Responsible Design Information and Development Data will be a Major Challenge

- Don't be lulled into accepting Optimistic Design Assumptions in an Aggressive Advanced Engine Design. Hot Section Life will Suffer.
- Purpose to interact with the Component Designers and Development Engineers in side meetings rather than Top Level Marketing Information
- Current Operational Engines and Advanced Development Engine Hardware will provide many insights if not a lot of concerns!

Insure Design Stability of the Gas Path Components

- Vanes and Blades will run hotter than designed if the Compressor, Combustor and the Overall Cooling Performance goals fall short of the design intent.
- Hot Section Parts require long lead design and development intervals
- 1/4 to 1/2X Blades will Cost the User lots of money. Warranty Guarantees are purposely structured to protect the OEM yet make money on spare parts.

Participate in Conceptual, Preliminary and Final Design Reviews

- Do your homework. Come prepared to asked informed questions based on independent analyses. Expect to get Slow Rolled or Isolated!
- Don't be alarmed if your analyses are not in agreement with the designers.
- Microstructure analyses of distressed hardware will determine who is right!

CHART 37 and 38 comments: TRACKING PROGRESS and COMPETITION AND ACCOUNTABILITY

Independent analyses will create a greater appreciation and understanding of the accomplishments of the engine manufacturer and the areas for improvement. Continue to remind the competitors that Positive Design Margins for the Hot Section Parts are absolutely essential. Always question the Design Practices and Procedures plus the engine design assumption when distressed hot section parts result after an engine test. Use the Cooling Performance and Profile Factor Sensitivity curves prepared for the engine design to debate whether the correct Phi and PF were used in the blade design and/or were the engine component efficiencies lower than design requirements. The benefits and liabilities of TBC Systems must be continually evaluated for affordability and reparability.

Competition is key in having the option to procure the most durable engine type that meets the performance requirements of the airframe. Independent analyses will encourage more accountability from the engine manufacturers in the competition. Continue a relentless pursuit. Operational and Maintenance Budgets will benefit.

CHART 39 comments: SUMMARY

In conclusion, become more involved in all phases of the engine design and development process. Use the tools suggested in this briefing. Conduct independent analyses of all component designs. Compare "Hard Pressed Hardware" test results with the design intent. Understand and assess the technology baselines of all components at each engine manufacturer. Evaluate the Design Systems and Best Practices at each engine company. Microstructure analyses of hot section parts are essential to pass judgment. Make sure that the parts that are analyzed have been exposed to sufficient hot time at high power engine design temperatures.

Engine Design Margins are required to successfully field an engine with acceptable durability, survive component degradation and low derate operation in service. Design Margins will allow some thrust uprate as needed to satisfy system requirements.

Always balance risk with reasonable levels of conservatism.

Pursue excellence in Engine Development. Operational and Maintenance budgets will benefit.

TRACKING PROGRESS

Independent analyses will create a greater appreciation and understanding of accomplishments and areas for improvement.

- Let OEM's know that independent analyses will be conducted
- Keep a "Pearl Harbor File" of Design Intent and Demonstrated Capability
- Monitor Redesign work and Development Tests. Re-evaluate results.

Continue to remind competitive engine manufacturers that Positive Design Margins for the Hot Section Parts are absolutely essential

- Achievable levels of Combustor Pattern and Profile Factors and Overall Cooling Performance are encouraged in the Hot Section Design
- Question the Design Practices and Procedures when distress is noted on Hot Section Parts. Were the engine design conditions under-estimated?
- Use the Cooling Performance and Profile Factor Sensitivity Curves to debate whether these design factors are below design intent or the gas path airflow and component efficiencies are below gas path design requirements.

The Benefits and Liabilities of Thermal Barrier Coating Systems and Blade Casting Technologies must be continually evaluated for affordability and repairability. 2 to 3X Blades are desirable. 1X Blades are a "Cash Cow".

COMPETITION AND ACCOUNTABILITY

Competition is key in having the option to procure the most durable engine type that meets the performance requirements of the airframe.

Competition will allow the customer to have access to data to conduct independent analyses and remain involved in the development process.

The drawdown in Defense spending will stretch out the development of "Cutting Edge Technologies". New engines or derivatives may have to depend on component improvements for commercial engines.

New high temperature materials are needed to design high performance engines. These programs are conducted at company expense over an extended period of time. Progress is slow and guarded.

Independent analyses of Hot Section Design Development Margins will encourage more accountability from the engine manufacturers in a competition. Continue a relentless pursuit. O & M Budgets will benefit.

SUMMARY

- **Become more involved in all phases of the Engine Design and Development Process**
 - Conduct independent analyses of all component designs
 - Compare "Hard Pressed Hardware" test results to design intent
 - Understand and assess the technology baselines of all engine components
- **Evaluate the Design Systems and Best Practices of each Manufacturer**
 - Microstructure analyses of Hot Section Parts are essential to pass judgement
 - Sufficient Hot Time at High Engine Design Temperatures are required
 - Total engine run test time only is not a good measure of durability in service
- **Engine Design Margins are required to successfully field an engine with acceptable durability, survive component degradation and low derate operation in service and provide adequate run times after thrust uprate.**
- **Balance Risk with Reasonable Levels of Conservatism**
- **Pursue Excellence in Engine Development. O & M Budgets will benefit.**

DERIVATIONS

T1 Blade Leading Edge

Exit Guide Vane Leading Edge

VANE LEADING EDGE SURFACE TEMPERATURE

BENTZ CE
30 JUL 97

1/2

DERIVATION:

$$\text{COMBUSTOR PATTERN FACTOR} = \frac{T_{\text{MAX}} - T_4}{T_4 - T_3} \quad (1)$$

SEE p162 & 163 OF REFERENCED REPORT

$$T_{\text{MAX}} = \text{CPF} (T_4 - T_3) + T_4 \quad (2)$$

$$\text{OVERALL COOLING PERFORMANCE} (\phi) = \frac{T_{\text{MAX}} - T_M}{T_{\text{MAX}} - T_C}$$

$$T_C = T_3 \quad T_M = T_{\text{CVS}} \quad \text{CALCULATED VANE SURFACE TEMP. ON LEADING EDGE}$$

$$\phi (T_{\text{MAX}} - T_3) = T_{\text{MAX}} - T_{\text{CVS}} \quad (3)$$

$$T_{\text{CVS}} = T_{\text{MAX}} - \phi (T_{\text{MAX}} - T_3)$$

$$T_{\text{CVS}} = (1 - \phi) T_{\text{MAX}} + \phi T_3 \quad (4)$$

$$= (1 - \phi) [(1 + \text{CPF}) T_4 - \text{CPF} T_3] + \phi T_3$$

$$= (1 - \phi) (1 + \text{CPF}) T_4 - (1 - \phi) \text{CPF} T_3 + \phi T_3$$

$$T_{\text{CVS}} = (1 - \phi) (1 + \text{CPF}) T_4 - [(1 - \phi) \text{CPF} - \phi] T_3$$

$$\text{OR } T_{\text{CVS}} = (1 - \phi) (1 + \text{CPF}) T_4 + [\phi - (1 - \phi) \text{CPF}] T_3 \quad (5)$$

CALCULATED VANE SURFACE TEMPERATURE
ON THE LEADING EDGE.

EQ'S (2) & (4) CAN BE USED TO ACHIEVE
THE SAME RESULTS.

BENTI CE
12 MAY 97

T METAL EQUATION DERIVATION

$$PF = \frac{T_{MR} - T_4}{T_4 - T_3} \quad (1) \quad PF = \text{COMBUSTOR PROFILE FACTOR}$$

$$T_{MR} = PF(T_4 - T_3) + T_4 = (PF+1)T_4 - PF T_3$$

$$T_{41} \xrightarrow{\substack{\text{PEAK AVE} \\ \uparrow \text{PA}}} = T_{MR} - (T_4 - T_{41}) \quad (2) \quad \xleftarrow{\substack{\text{TEMP DROP ACROSS VANE DUE} \\ \text{TO COOLING AIR ADDITION}}}$$

$$T_{41} \text{ PA} = (PF+1)T_4 - PF T_3 - (T_4 - T_{41})$$

$$= PF T_4 + T_4 - PF T_3 - T_4 + T_{41}$$

$$T_{41} \text{ PA} = PF(T_4 - T_3) + T_{41} \quad (3)$$

$$T_{RR} = \frac{T_{41} \text{ PA}}{RF} \quad (4) \quad RF = \text{COMPUTED RELATIVE ROTOR FACTOR BASED ON TURBINE DESIGN GEOMETRY AND ROTOR SPEED}$$

$$T_{RR} = \frac{1}{RF} [PF(T_4 - T_3) + T_{41}] \quad (5)$$

$$\phi = \frac{T_{RR} - T_M}{T_{RR} - T_c} \quad (6) \quad \phi = \text{BLADE COOLING PERFORMANCE}$$

$$\phi (T_{RR} - T_c) = T_{RR} - T_M$$

$$T_M = T_{RR} - \phi (T_{RR} - T_c)$$

$$T_M = T_{RR} (1 - \phi) + \phi T_c$$

$$T_M = \frac{1}{RF} [PF(T_4 - T_3) + T_{41}] (1 - \phi) + \phi T_c \quad (7) \quad T_c = T_{\text{COOL}}$$

$$T_c = T_3 + \Delta T_p \quad (8) \quad \Delta T_p = \text{TEMP RISE FROM PUMPING IN TURBINE DISC}$$

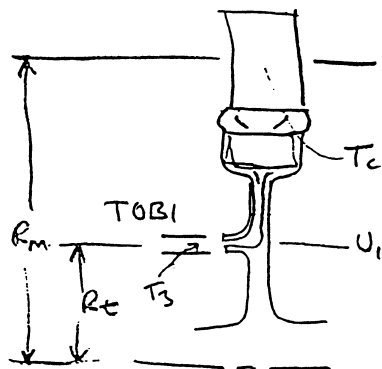
$$T_M = \frac{1}{RF} [PF(T_4 - T_3) + T_{41}] (1 - \phi) + \phi (T_3 + \Delta T_p) \quad (9)$$

T METAL EQUATION DERIVATION (Cont'd)

HIGH PRESSURE SPOOL. T_c pumping Temp rise (ΔT_p)

INITIAL DESIGN: $N_2 = 21,335 \text{ RPM}$
 $U_{\text{Tip comp}} = 1631' / \text{sec}$

ASSUME: $U_T \cdot \text{HPT} \approx 2000' / \text{sec}$
 $R_t = 0.895'$ $R_m = 0.875'$ $U_m = 1940' / \text{sec}$



$$U_i \approx 0.46 U_m$$

$$U_i = 893' / \text{sec}$$

ASSUME $\delta = 1.3266$
 FOR $T_3 = 2077^\circ \text{R}$

$$\frac{R_t}{R_m} \approx 0.46$$

$$T_c = T_3 + \Delta T_{\text{pumping}}$$

$$\Delta T_p = \frac{\delta-1}{\delta} \cdot \frac{1}{R_g} \left[\frac{U_m^2}{2} - U_i^2 \right] \quad (10)$$

$$= \frac{0.3266}{1.3266} \cdot \frac{1}{(53.3)} 32.2 \left[\frac{1940^2}{2} - 893^2 \right]$$

$$= \frac{0.3266}{2.277 \times 10^3} \left[\frac{3.764 \times 10^6}{2} - 0.797 \times 10^6 \right]$$

$$1.085 \times 10^6$$

$$= 0.1556 \times 10^3$$

$$\underline{\Delta T_p = 156^\circ \text{F}}$$

T METAL EQUATION DERIVATION (Cont'd)

IF $\phi = 0.5$ (0.7) BASELINE

PF = 0.25

RF = 1.15 $\Delta T_p = 156$

$$T_M = \frac{(1-\phi)}{RF} [PF(T_4 - T_3) + T_{41}] + \phi(T_3 + \Delta T_p)$$

$$= \frac{0.5}{1.15} [0.25(T_4 - T_3) + T_{41}] + 0.5(T_3 + 156)$$

$$= 0.1087 T_4 - 0.1087 T_3 + 0.435 T_{41} + 0.5 T_3 + 78$$

$$T_M = 0.3917 T_3 + 0.1087 T_4 + 0.435 T_{41} + 78 \quad (11)$$

IF $\phi = 0.6$

$$T_M = \frac{0.4}{1.15} [0.25(T_4 - T_3) + T_{41}] + 0.6(T_3 + 156)$$

$$= 0.08695 T_4 + 0.513 T_3 + 0.348 T_{41} + 93.6$$

$$T_M = 0.513 T_3 + 0.087 T_4 + 0.348 T_{41} + 93.6 \quad (12)$$

IF $\phi = 0.7$

$$T_M = \frac{0.3}{1.15} [0.25(T_4 - T_3) + T_{41}] + 0.7(T_3 + 156)$$

$$= 0.0652 (T_4 - T_3) + 0.261 T_{41} + 0.7 T_3 + 109.2$$

$$T_M = 0.635 T_3 + 0.0652 T_4 + 0.261 T_{41} + 109.2 \quad (13)$$

REPORT DOCUMENTATION PAGE			Form Approved OMB No. 0704-0188	
Public reporting burden for this collection of information is estimated to average 1 hour per response, including the time for reviewing instructions, searching existing data sources, gathering and maintaining the data needed, and completing and reviewing the collection of information. Send comments regarding this burden estimate or any other aspect of this collection of information, including suggestions for reducing this burden, to Washington Headquarters Services, Directorate for Information Operations and Reports, 1215 Jefferson Davis Highway, Suite 1204, Arlington, VA 22202-4302, and to the Office of Management and Budget, Paperwork Reduction Project (0704-0188), Washington, DC 20503.				
1. AGENCY USE ONLY (Leave blank)		2. REPORT DATE August 2006		3. REPORT TYPE AND DATES COVERED Conference Publication
4. TITLE AND SUBTITLE Seals/Secondary Fluid Flows Workshop 1997			5. FUNDING NUMBERS WBS 732759.03.01.02.15	
6. AUTHOR(S) Robert C. Hendricks, editor				
7. PERFORMING ORGANIZATION NAME(S) AND ADDRESS(ES) National Aeronautics and Space Administration John H. Glenn Research Center at Lewis Field Cleveland, Ohio 44135-3191			8. PERFORMING ORGANIZATION REPORT NUMBER E-15561-1	
9. SPONSORING/MONITORING AGENCY NAME(S) AND ADDRESS(ES) National Aeronautics and Space Administration Washington, DC 20546-0001			10. SPONSORING/MONITORING AGENCY REPORT NUMBER NASA CP-2006-214329-VOL1	
11. SUPPLEMENTARY NOTES Proceedings of the Seals/Secondary Fluid Flows Workshop 1997, sponsored by Glenn Research Center, Cleveland, Ohio, October 15-16, 1997. Responsible person, Robert C. Hendricks, organization code R, 216-977-7507.				
12a. DISTRIBUTION/AVAILABILITY STATEMENT Unclassified - Unlimited Subject Categories: 07 and 37 Available electronically at http://gltrs.grc.nasa.gov This publication is available from the NASA Center for AeroSpace Information, 301-621-0390.			12b. DISTRIBUTION CODE	
13. ABSTRACT (Maximum 200 words) The 1997 Conference provided discussions and data on (a) program overviews, (b) developments in seals and secondary air management systems, (c) interactive seals flows with secondary air or fluid flows and powerstream flows, (d) views of engine externals and limitations, (e) high speed engine research sealing needs and demands, and (f) a short course on engine design development margins. Sealing concepts discussed include, mechanical rim and cavity seals, leaf, finger, air/oil, rope, floating-brush, floating-T-buffer, and brush seals. Engine externals include all components of engine fluid systems, sensors and their support structures that lie within or project through the nacelle. The clean features of the nacelle belie the minefield of challenges and opportunities that lie within.				
14. SUBJECT TERMS Seals; Secondary air flows; Rotordynamics; Gas turbine; Aircraft; CFD; Testing; Turbomachinery			15. NUMBER OF PAGES 513	
			16. PRICE CODE	
17. SECURITY CLASSIFICATION OF REPORT Unclassified	18. SECURITY CLASSIFICATION OF THIS PAGE Unclassified	19. SECURITY CLASSIFICATION OF ABSTRACT Unclassified	20. LIMITATION OF ABSTRACT	

